



UNIVERSITAT DE  
BARCELONA

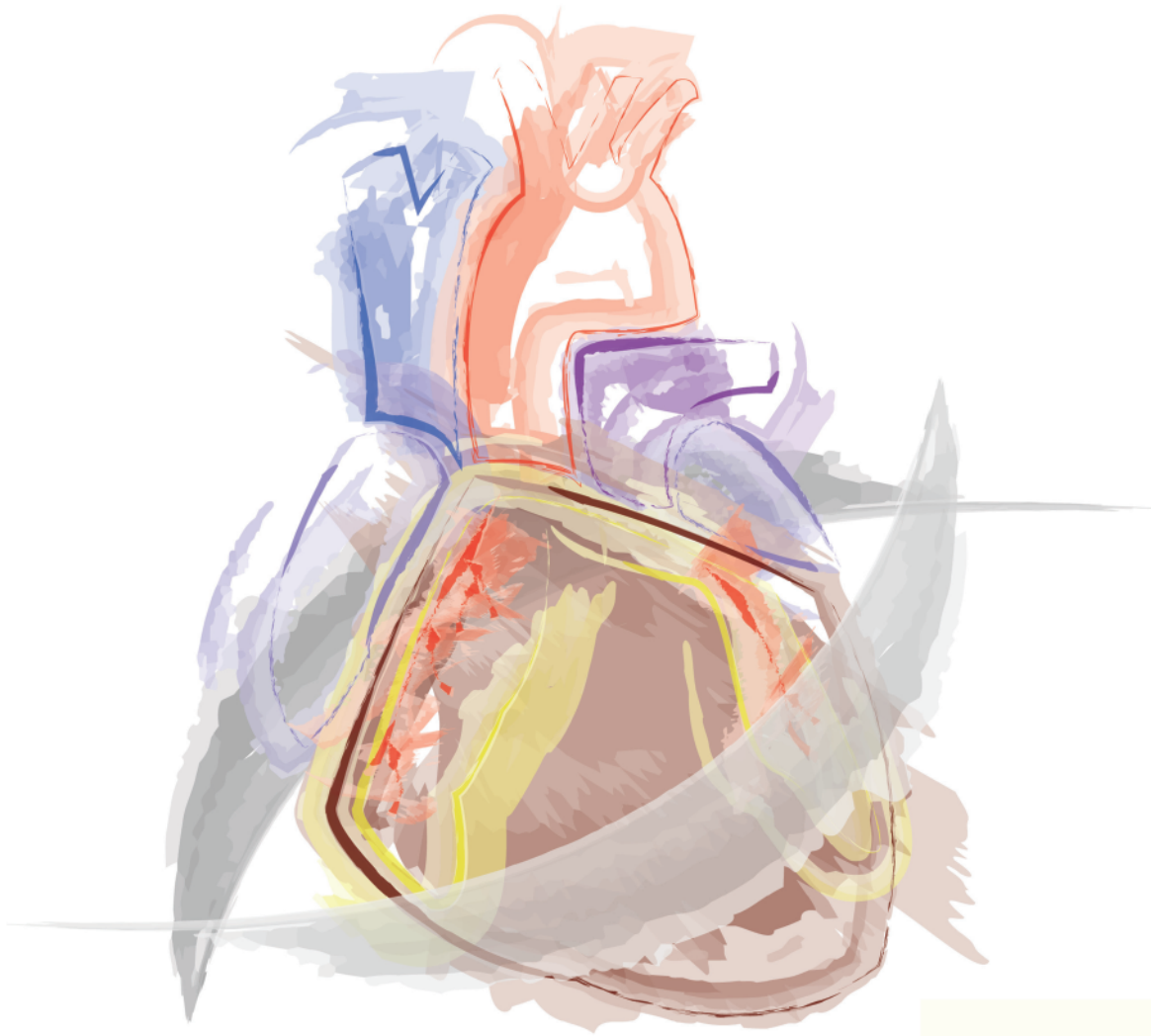
## Cell-enriched engineered cardiac grafts improve heart function and promote cardiac regeneration: a novel therapy for myocardial infarction

Isaac Perea Gil

**ADVERTIMENT.** La consulta d'aquesta tesi queda condicionada a l'acceptació de les següents condicions d'ús: La difusió d'aquesta tesi per mitjà del servei TDX ([www.tdx.cat](http://www.tdx.cat)) i a través del Dipòsit Digital de la UB ([diposit.ub.edu](http://diposit.ub.edu)) ha estat autoritzada pels titulars dels drets de propietat intel·lectual únicament per a usos privats emmarcats en activitats d'investigació i docència. No s'autoritza la seva reproducció amb finalitats de lucre ni la seva difusió i posada a disposició des d'un lloc aliè al servei TDX ni al Dipòsit Digital de la UB. No s'autoritza la presentació del seu contingut en una finestra o marc aliè a TDX o al Dipòsit Digital de la UB (framing). Aquesta reserva de drets afecta tant al resum de presentació de la tesi com als seus continguts. En la utilització o cita de parts de la tesi és obligat indicar el nom de la persona autora.

**ADVERTENCIA.** La consulta de esta tesis queda condicionada a la aceptación de las siguientes condiciones de uso: La difusión de esta tesis por medio del servicio TDR ([www.tdx.cat](http://www.tdx.cat)) y a través del Repositorio Digital de la UB ([diposit.ub.edu](http://diposit.ub.edu)) ha sido autorizada por los titulares de los derechos de propiedad intelectual únicamente para usos privados enmarcados en actividades de investigación y docencia. No se autoriza su reproducción con finalidades de lucro ni su difusión y puesta a disposición desde un sitio ajeno al servicio TDR o al Repositorio Digital de la UB. No se autoriza la presentación de su contenido en una ventana o marco ajeno a TDR o al Repositorio Digital de la UB (framing). Esta reserva de derechos afecta tanto al resumen de presentación de la tesis como a sus contenidos. En la utilización o cita de partes de la tesis es obligado indicar el nombre de la persona autora.

**WARNING.** On having consulted this thesis you're accepting the following use conditions: Spreading this thesis by the TDX ([www.tdx.cat](http://www.tdx.cat)) service and by the UB Digital Repository ([diposit.ub.edu](http://diposit.ub.edu)) has been authorized by the titular of the intellectual property rights only for private uses placed in investigation and teaching activities. Reproduction with lucrative aims is not authorized nor its spreading and availability from a site foreign to the TDX service or to the UB Digital Repository. Introducing its content in a window or frame foreign to the TDX service or to the UB Digital Repository is not authorized (framing). Those rights affect to the presentation summary of the thesis as well as to its contents. In the using or citation of parts of the thesis it's obliged to indicate the name of the author.



***Cell-enriched engineered cardiac  
grafts improve heart function and  
promote cardiac regeneration: a novel  
therapy for myocardial infarction***

Isaac Perea Gil  
Badalona, July 3rd, 2017







UNIVERSITAT<sub>DE</sub>  
BARCELONA

**Faculty of Medicine**

**PhD in Biomedicine**

**Biomedical Engineering program**

Isaac Perea Gil

Badalona, July 3rd, 2017

Thesis to opt for the PhD degree with International Mention by  
the University of Barcelona





UNIVERSITAT DE  
BARCELONA



## Faculty of Medicine

### PhD in Biomedicine

### Biomedical Engineering program

Report presented by Isaac Perea Gil to qualify for the PhD degree with International Mention by the University of Barcelona.

The present work has been done in the ICREC research group (Insuficiència Cardíaca i REgeneració Cardíaca), at Fundació Institut d'Investigació en Ciències de la Salut Germans Trias i Pujol in Badalona, and directed by doctors Antoni Bayés Genís and Cristina Prat Vidal.

#### PhD candidate

Isaac Perea Gil

#### Directors

Dr. Antoni Bayés Genís    Dr. Cristina Prat Vidal

#### Tutor

Dr. Ramon Farré Ventura

Badalona, July 3rd, 2017





## Acknowledgments

---



És tanta la gent a qui he d'agrair haver format part d'aquesta tesi, que espero no deixar-me a ningú pel camí. Igualment, per si un cas algú se'm passés per alt, em disculpo per avançat amb tot aquell a qui em pugui descuidar.

Primer de tot, vull començar agraint als meus directors de tesi, en Toni i la Cris, per tot el que han hagut d'aguantar. Perquè sempre m'han sabut aconsellar, donar-me ànims quan semblava que no ens en sortiríem, per totes les correccions i comentaris que tant han ajudat a millorar aquesta tesi, i per tot el coneixement que m'han proporcionat. No només això, sinó que en tot moment han sabut dirigir-me i motivar-me en cada moment. Recordo encara una frase que em va dir al començament del doctorat: "quan acabis, seràs una persona completament diferent a la que va començar fa 4 anys". En aquell moment no sabia en quina classe de "monstre" em podria convertir. Ara sé que m'heu portat pel bon camí. I us n'estic eternament agraït. Moltes gràcies. Gràcies Toni, pels consells, pel teu coneixement, la capacitat d'apagar focs, i la mà esquerra per solucionar problemes que jo n'era incapaç (encara recordo la trucada a la Jennifer...). Cris, gràcies per aguantar-me dia a dia, per la teva paciència i per ensenyar-me tot el que sé. Gràcies per confiar en mi, tot i l'entrada triomfal en veure el primer pericardi, fent-li un petó de benvinguda al terra. Poc a poc, he anat superant l'adversió a la sang (curiós...). Gràcies, a tots dos. No he pogut aprendre de dos millors directors.

A la resta de membres del grup ICREC, que han estat com una segona família per a mi, passant en determinats moments més temps amb ells que a casa. Gràcies a tots i cadascun de vosaltres, els que hi sou, i els que ja no, per fer-me sentir un més des del primer moment i fer tan fàcil el poder treballar, estant disposats a ajudar en tot moment. No només m'heu ajudat a millorar a nivell professional, sinó que també ho heu fet a nivell personal. Al Santi, pel seu humor, el seu coneixement, i els seus "astupendus" mates a les "pachangas" de professionals del bàsquet que som; a la Carol (rossa), per ser l'experta en tincions i ensenyar-me que es pot ser de l'Espanyol i sobreviure; a la Carol (morena), per ensenyar-me a treballar des de l'ordre i la tranquil·litat; a la Paloma, pels seus consells gastronòmics i nutricionals, i la seva capacitat per solucionar marrons; a l'Oriol, per la seva mà amb les complicades iPSCs

i per ensenyar-me que es pot combinar la poesia amb la ciència (molta sort!); i a l'Elena, per ocupar-me la meua poietat ;), però sobretot, per ser tan constant (tants ELISA ho demostren). No em vull deixar aquells que han emprès un nou camí i ja no hi són: la Laura, per la seva eficiència, calidesa, i amabilitat amb temes tan agradables com factures, rescabaments i pressupostos; a l'Aida, per ser un mirall d'on aprendre i la companyia en hores intempestives; i a l'Àlex, que tot i ser breu, sempre hi ha estat quan se l'ha necessitat (menys en el bàsquet...). A tots vosaltres, gràcies!

Gràcies a la gent del Clínic, en especial, al Dr. Navajas, al Dr. Farré, a en Juanjo (també doctor, enhorabona!) i a l'Ignasi. He après molt d'una disciplina molt diferent (i complicada), i m'heu fet sentir com a casa meua des del primer moment, acompanyats en tot moment de l'AFM, company inseparable durant llargues tardes. Gràcies!

I would also like to thank Dr. Wu for accepting me to stay at Stanford for 6 months, and specially, Dr. Karakikes, for being so patient with me (and my English), for teaching me all what I know about the iPSCs, and for facilitating my stay there (really good barbeques!). Also, thanks to the rest of Dr. Wu lab members, for being so kind, helpful, and considerate with me from the very beginning. I had a really good time there, and I hope we can meet again soon!

Agrair als meus amics de tota la vida, l'Adri (i l'Alícia), el Floren i en Moya. Ells han estat al meu costat en tot moment, s'han preocupat, m'han animat, i sempre han estat allà per fer un sopar o una cervesa/aigua quan més ho necessitava. També donar les gràcies a l'Iris, la Montse, la Mònica, en Dídac, la Dèbora, la Cris, en Toni, la Patri, l'Irmina, en David i en Marcos, per preocupar-se en tot moment, per ajudar-me, animar-me, i fer-me preguntes que m'han fet pensar i donar-li una volta més al que estava fent. Menció especial per la "tita" Toñi, la proveïdora oficial de cors, moltes gràcies! Agrair també a la Sheila, l'Àngel, l'Àlex, la Laura i l'Hèctor, per estar sempre al meu costat i animar-me a continuar endavant. I finalment, a en Josep i l'Erica. A ell per, tot i la distància, haver-se preocupat en tot moment i ser un suport molt important per a mi; i a ella per tota la comprensió i ajut durant tants i tants anys.

Gràcies a l'Elena, l'Ana, el José, el Pepe, l'Elena i en Marc, pel seu suport,  
X

recolzament i constant ajut. Teníeu raó, al final vaig acabar fora (contra la meua voluntat!). Gràcies per cuidar-me'ls mentre era fora, no els podia deixar en millors mans.

Agrair també als meus tiets Manuel i Paca, i els meus cosins Àlex (i Valentina) i Maica pel seu suport durant tot aquest temps.

Gràcies als meus tiets Carmen i Jordi, als meus cosins Kim, Saray (i Diego), Àlex i Ariadna, i a la iaia Chelo, la millor pastissera que he conegut mai. Per tots els dissabtes que tant m'agrada que arribin, pels bons moments que em feu passar i els que ens queden per endavant, per tenir paciència amb mi mentre comptava "bolitas azules o agujeros", però sobretot, per haver estat sempre al meu costat. Sense vosaltres, la tesi no seria una realitat! I mai millor dit, la il·lusió i voluntat amb que organitzeu el càtering m'ha donat/em dóna encara més força.

A la meua germana, la Ham, i en Manel, dissenyadors de la portada, que m'encanta! Per recolzar-me, pels sopars, per les sessions de pel·lícules que valen la pena, pels restaurants amb senyores que ballen a la boca, les nits d'Eurovisión, i per tants i tants riures. Crec que perfectament podríeu fer una tesi doctoral sobre "Libre albedrío y otras conspiraciones sobre la libertad de decisión". Aneu dissenyant portada...

Als meus pares, perquè en tot moment m'han donat totes les facilitats per continuar estudiant, per confiar en mi i ajudar-me en tot moment, per escoltar-me, per educar-me i per ser un model a seguir en tot moment. Sento que molts cops no us he pogut agrair suficient tot el que heu fet per mi gràcies a la meua "facilitat de paraula", però sense vosaltres, aquesta tesi no seria una realitat. Papa, hi ha títols que no es donen a les universitats, però no et calen. Ets el millor mestre que puc tenir. Mama, gràcies per deixar-me triar el meu propi camí, però amb la teua mà propera per ajudar-me a aixecar tants cops com he caigut. Gràcies per tot el que feu per mi, espero poder-vos-ho retornar com us ho mereixeu.

Al petit Sora, que des del moment que va arribar a casa ara fa dos anys, va omplir la casa d'(encara més) alegria. Per induir-me "voluntàriament" a descansar

quan t'asseies al teclat, per obligar-me a estirar les cames quan volies sortir a la terrassa, i per estirar-te al costat de l'ordinador per veure l'esclau treballar. Però sobretot, per la companyia que m'has fet dia i nit, adormit a sobre meu mentre treballava, i per no separar-te del meu costat. Potser no té gaire sentit que t'escrigui perquè no ho entendràs, però si vas aprendre el "sienta", potser això també!

I finalment, a la persona més important. El meu percentatge de contribució a la tesi hauria de ser compartit al 50% amb ella... bé, millor deixem-ho en 10%/90% per ella. Per aguantar-me dia i nit, dia i nit, dia i nit... i així fins avui. Per consolar-me, per confiar en mi més que ningú, per escoltar-me i preguntar-me un i altre cop "¿QUÉ ES UNA ENZIMA?". Per estar sempre al meu costat, pel teu positivisme, per haver-me fet tan fàcil haver estat fora. Per ser cadascuna de les frases d'aquesta tesi. Per haver tingut més fe que jo mateix. Perquè amb tu al meu costat, tot ha estat més fàcil. Sol no hauria fet. Gràcies, Núria. Per ser el meu suport incondicional, la meva fan número 1, l'alumna avantatjada que fa preguntes preexposicions. Gràcies per ser la meva companya inestimable en aquest llarg camí anomenat doctorat, i en un altre encara més llarg que tot just comença anomenat vida. Recordo una frase d'una pel·lícula que et va agradar: "Bueno sí, soy doctor, pero no esa clase de doctor. Tengo un doctorado pero no es lo mismo". Crec que finalment ho he aconseguit. Gràcies a tu. IO!

## Index

---





<b>ACKNOWLEDGMENTS .....</b>	<b>VII</b>
<b>INDEX .....</b>	<b>XIII</b>
<b>ABBREVIATION LIST .....</b>	<b>XIX</b>
<b>INTRODUCTION.....</b>	<b>1</b>
1. History of circulatory system: long story short.....	3
2. In the heart of circulatory system .....	7
2.1. Heart layers.....	11
2.1.1. The heart wall .....	11
2.1.2. The pericardium.....	12
3. The embryonic development of the heart.....	14
3.1. Key pathways and proteins in heart formation.....	16
4. Cardiovascular diseases (CVDs): a real burden .....	19
4.1. Myocardial infarction (MI).....	22
5. Current therapies in the MI context .....	24
5.1. Anti-ischemic drugs .....	25
5.2. Antithrombotic therapy.....	26
5.3. Fibrinolytic/thrombolytic agents.....	28
5.4. Percutaneous coronary intervention (PCI).....	29
5.5. Surgical procedures .....	30
6. Research strategies for cardiac regeneration: current status .....	31
6.1. Cardiac gene therapy.....	36
6.1.1. Strategies for gene delivery .....	36

6.1.2. Gene transfer vectors .....	37
6.1.3. Target genes of interest .....	40
6.2. Cardiac cell therapy .....	42
6.2.1. Cell sources for cardiac cell therapy .....	43
6.2.2. Cell delivery routes .....	50
6.3. Cardiac tissue engineering .....	52
6.3.1. Cardiac tissue engineering strategies .....	53
6.3.2. Scaffold materials .....	58
6.3.2.1. Natural materials .....	59
6.3.2.2. Synthetic materials .....	65
6.3.3. Final considerations regarding scaffold requirements .....	68
<b>HYPOTHESIS AND OBJECTIVES .....</b>	<b>73</b>
<b>REPORT ON THE PHD CANDIDATE’S PARTICIPATION IN THE ARTICLES PRESENTED IN THE THESIS .....</b>	<b>77</b>
First article: Preclinical evaluation of the immunomodulatory properties of cardiac adipose tissue progenitor cells using umbilical cord blood mesenchymal stem cells: a direct comparative study .....	82
Second article: <i>In vitro</i> comparative study of two decellularization protocols in search of an optimal myocardial scaffold for recellularization .....	83
Third article: Online monitoring of myocardial bioprosthesis for cardiac repair .....	84
Fourth article: A cell-enriched engineered myocardial graft limits infarct size and improves cardiac function. Pre-clinical study in the porcine myocardial infarction model.....	85
Fifth article: Head-to-head comparison of two engineered cardiac grafts for	

myocardial repair: a pre-clinical myocardial infarction swine model.....	86
Sixth article: <i>In vivo</i> experience with natural scaffolds for myocardial infarction: the times they are a-changin' .....	87
<b>RESULTS SUMMARY .....</b>	<b>89</b>
1. Immunomodulatory properties of cardiac ATDPCs .....	93
2. Generation of cardiac acellular scaffolds and recellularization using cardiac ATDPCs .....	105
3. <i>In vivo</i> effects promoted by the engineered cardiac grafts for cardiac regeneration post-MI .....	147
4. Collection of <i>in vivo</i> conducted work using natural scaffolds for treating MI: a current review .....	219
<b>DISCUSSION .....</b>	<b>247</b>
1. Immunomodulatory properties of the cardiac ATDPCs.....	249
2. Generation of cardiac acellular scaffolds.....	253
3. Repopulation of the decellularized cardiac scaffolds .....	260
4. <i>In vivo</i> effects exerted by the engineered cardiac grafts for cardiac recovery	266
<b>CONCLUSIONS.....</b>	<b>275</b>
<b>BIBLIOGRAPHY.....</b>	<b>283</b>



## **Abbreviation list**

---



**AAV:** adeno-associated virus/viral

**ACE:** angiotensin-converting enzyme

**ADP:** adenosine diphosphate

**AFM:** atomic force microscopy

**APOLLO:** AdIPOse-derived stem cells in the treatment of patients with ST-elevation myocardial infarction

**ATDPCs:** adipose tissue-derived progenitor cells

**ATP:** adenosine triphosphate

**AUGMENT-HF:** A randomized, controlled study to evaluate ALGisyl-LVR™ as a Method of Left ventricular augmentation for Heart Failure

**AVN:** atrioventricular node

**βARKct:** beta-adrenergic receptor kinase C terminus

**BMP:** bone morphogenetic protein

**BMSCs:** bone marrow-derived stem cells

**BOOST:** Bone marrow transfer to enhance ST-elevation infarct regeneration

**CABP:** coronary artery bypass

**CADUCEUS:** Cardiosphere-Derived autologous stem cells to reverse ventricular dysfunction

**CPCs:** cardiac progenitor cells

**cTnl:** cardiac troponin I

**cTnT:** cardiac troponin T

**CVD:** cardiovascular disease

**Cx43:** connexin43

**DAPI:** 4',6-diamidino-2-phenylindole

**DNA:** deoxyribonucleic acid

**ECM:** extracellular matrix

**EMG:** engineered myocardial graft

**EPG:** engineered pericardial graft

**ESCORT:** transplantation of Embryonic Stem Cell-derived progenitors in severe heart failure

**ESCs:** embryonic stem cells

**FGF:** fibroblast growth factor

**FHF:** first heart field

**FISH:** fluorescence *in situ* hybridization

**GATA4:** GATA binding protein 4

**GP:** glycoprotein

**Hand:** heart- and neural crest derivatives-expressed protein

**HCN4:** ion channel protein hyperpolarization-activated cyclic

nucleotide-gated channel 4

**HGF:** hepatocyte growth factor

**ICD-10:** International statistical Classification of Diseases and related health problems 10th revision

**IFN- $\gamma$ :** interferon-gamma

**IGF:** insulin growth factor

**iPSCs:** induced pluripotent stem cells

**Isl1:** insulin gene enhancer protein 1

**IsoB4:** isolectinB4

**LMWH:** low molecular weight heparin

**LVEF:** left ventricular ejection fraction

**LVESV:** left ventricular end-systolic volume

**MAGIC:** Myoblast Autologous Grafting in Ischemic Cardiomyopathy

**MAGNUM:** Myocardial Assistance by Grafting a New bioartificial Upgraded Myocardium

**MEF2:** myocyte enhancer factor 2

**Mesp1:** mesoderm posterior 1 protein

**MI:** myocardial infarction

**MSCs:** mesenchymal stem cells

**NHLBI:** National Heart, Lung, and Blood Institute

XXII

**Nkx2.5:** NK2 transcription related factor 5

**PCI:** percutaneous coronary intervention

**PCL:** polycaprolactone

**PCTA:** percutaneous coronary transluminal angioplasty

**PEG:** polyethylene glycol

**PLA:** polylactic acid

**PLGA:** poly(lactic-co-glycolic) acid

**SAN:** sinoatrial node

**Sca-1:** stem cell antigen-1

**SEISMIC:** Safety and Effects of Implanted (autologous) Skeletal Myoblasts (myocell) using an Injection Catheter

**SERCA2:** sarco/endoplasmic reticulum Ca<sup>2+</sup>-ATPase

**SHF:** second heart field

**SMA:** smooth muscle actin

**Tbx:** T-box transcription factor

**TGF- $\beta$ :** transforming growth factor beta

**TNF- $\alpha$ :** tumor necrosis factor-alpha

**TOPCARE-AMI:** Transplantation Of



Progenitor Cells And REcovery of left ventricular function In patients with Acute Myocardial Infarction

**TXA<sub>2</sub>**: thromboxane A<sub>2</sub>

**UCBSCs**: umbilical cord blood stem cells

**UFH**: unfractionated heparin

**VEGF**: vascular endothelial growth factor

**Wnt**: wiggless integrated

**YAP/TAZ**: Yes-associated protein/transcriptional coactivator with PDZ-binding motif



## Introduction

---



## 1. History of circulatory system: long story short

The earliest notions about a system in charge of distributing and nourish the whole organism arrived in the Ancient Egypt. An old Egyptian papyrus dated from 1500 BC, the *Ebers Papyrus*, showed the correlation between pulse and humans health. More than one thousand years later, during the Ancient Greek, Hippocrates and his pupils accurately drew the nature of blood flow, the vessels and the valves, as well as they identified the heart as a muscle. A bit later, Aristotle thought of the heart as the physiological center, given the animal dissection he carried out, but in a philosophical manner: he considered it the soul source from where the vessels originated. A step forward was made by Praxagoras, when he identified two types of blood vessels, the arteries and the veins. However, as stated by Erasistratus, who also identified and named the semilunar heart valves, it was wrongly believed that the arteries contained air, instead of blood, and that liver was considered the primary or secondary mechanical pump and main source of human blood vessels (Garber and Livingston, 2008).

It was not until the second century AD, five hundred years later, that the methodologies and studies conducted by the physician Aelius Galen, better known as Galen of Pergamon, led to reject some of the previous inherited dogmas regarding circulatory system, postulating new ones. Galen found that the arteries were filled with blood and not with air as it was believed until then. By arteriotomy in living animals, he also correctly inferred a dual circulatory system: the venous, somehow nutritionally relevant; and the arterial, related to body heat maintenance. Nevertheless, he also proposed some false statements and ideas that would take long time until they got refused. He suggested that both circulatory systems were interconnected by pores, the anastomoses, in the interventricular septum; besides, he also introduced some mysticism with the idea of a pneuma (the spirit or soul) flowing through the vessels and being distributed throughout the body, or determined the liver as the central organ and origin of all veins (Garrison, 1931).

During the long period of the dark and middle ages (500-1400 AD), no further

knowledge was acquired and the old statements were not questioned. Most of the experiments done during this era were driven to reconfirm or teach the findings that were passed down. Only Ibn al-Nafis, in 1242, provided few insights into the pulmonary circulation and small connections (pores) between arteries and veins, discarding the porous interventricular septum, although he only mentioned it for pulmonary vessels. Unfortunately, his theories were lost during centuries, and they were not recovered till the 16th century, when the majority of his proposals were already demonstrated (Aird, 2011).

In the Renaissance (1400s AD), this setting started to turn over, when new discoveries were achieved. Leonardo Da Vinci first provided precise heart drawing, and he also identified the atherosclerotic coronary arteries, and the atria as heart chambers (Aird, 2011). This was only the beginning of a really fruitful period, with remarkable findings reached along the 16th century AD: Michael Servetus correctly described the pulmonary circulation, from the right ventricle to the lungs, and he refused Galen's thought of pores bored into the interventricular septum (Servetus, 1553); Andreas Vesalius detailed the atrioventricular valve and named it 'the mitral valve', as well as supported Servetus' non-perforated septum conception. The pulmonary circulation was finally defined in more detail by Renaldus Columbus in a posthumous publication in 1559, gathering his own experiments and the advances made until then (Columbus, 1559). At this point, when most of the Galen's view began to be obsolete, Andreas Caesalpinus, in 1571, contributed to describe heart valves function and to confirm the blood flow course, from the right ventricle to the lungs, and then back to the left ventricle, finally substituting the porous interventricular septum conception; and turned down the liver as the blood pump, conceived in the Ancient times (Caesalpinus, 1571). Finally, in 1574, Fabricus ab Acquapendente examined venous valves and attributed to them the function to prevent blood outward movement from the heart towards the periphery, contrary to what Galen initially said (Acquapendente, 1603). Throughout this era, even though some advances were made, the main Galen's theories were not completely refused, and these new discoveries were introduced as little corrections or refinements of Galen's established dogmas.

But it was William Harvey who finally refused the rooted false views about the cardiovascular system, establishing the basis for modern cardiovascular medicine. In 1628, his published book *Exercitatio Anatomica de Motu Cordis et Sanguinis in Animalibus*, collected all the new findings Harvey did. The most important was the explanation of the correct cyclic blood circulation, from the heart to the lungs, then back to the heart, pumped out to the body, and back from the periphery through veins, placing the heart as the mechanical pump; but lacking the link between arteries and veins though (he postulated vessel porosities). Many other remarkable contributions he made were: apex beating; heart fibers possibly spirally-arranged; heart-beat mechanism; pulse as an expression of heart pumping action; the relation of cardiac pumping with arterial blood pressure; stroke volume estimations; and some notes about vasoconstriction and vasodilation, among others. Received with skepticism at first, the scientific community finally accepted these new ideas, replacing the old and wrong dogmas (Harvey, 1628). In 1661, Marcello Malpighi discovered the missing connection between arteries and veins, the capillaries, then eventually closing the blood circulatory continuous circuit (Malpighi, 1661) (**Figure 1**).

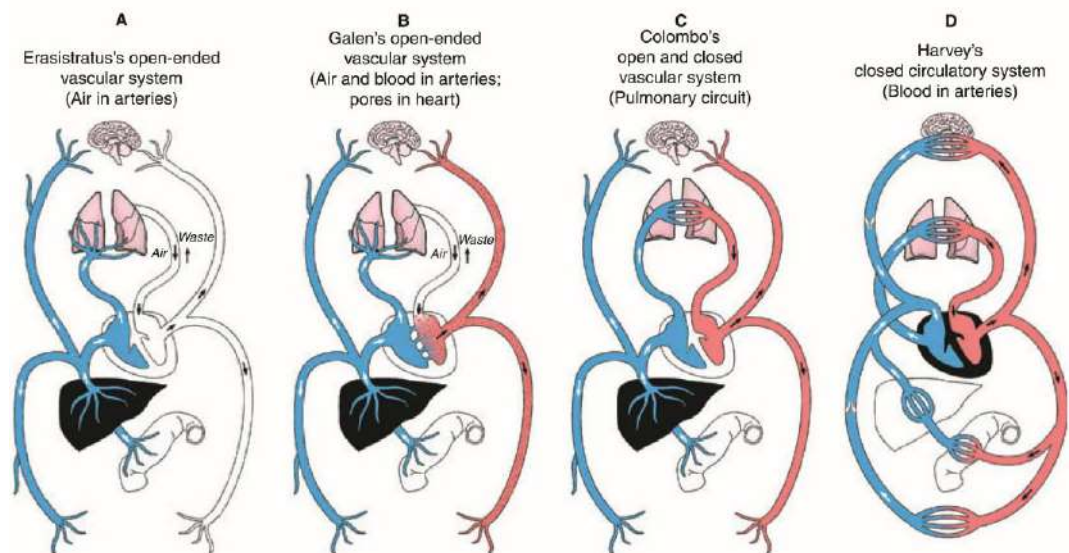


**Figure 1. Cardiovascular system conception over time.** (A) Erasistratus' vision of the cardiovascular system, where arteries contain air and veins blood. Food is taken through the intestines and reaches the liver, where it is transformed into blood and distributed throughout the body. Some blood is diversified to the right ventricle and sent to the lungs. Here, air is taken up and transferred back to the heart left ventricle, where it will be driven to the periphery within arteries. (B) Galen's open ended vascular system. Arteries contain blood, and blood contained within the heart passes from left to right ventricle through interventricular septum pores. The liver still remains as the primary source of veins. (C) Columbus' particular description of the circulatory system. Here, he defined the pulmonary circuit: from right ventricle to the lungs, then back to the left ventricle to be distributed throughout the body by arteries. However, it was wrongly preserved the liver as the main vein source, and the blood flow direction inside the veins: from the liver to the rest of tissue and organs, with little of it entering the heart. (D) Harvey's closed circulatory system. The heart was confirmed to be the source of veins and main mechanical blood pump, and the correct blood flow direction was established, with the description of vein valves function (two of them represented in white) being primordial for such affirmation. Blood transfer from arteries to veins was not solved yet, proposing anastomoses or pores in the flesh. The diagrams have been reproduced from [Aird, 2011](#).

These previous milestones in the cardiovascular physiology and anatomy opened the way for new discoveries in the forthcoming years. In 1658, Jan Swammerdam observed and identified for the first time the red blood cells within the blood, the erythrocytes ([Swammerdam, 1737](#)); and ten years later, John Mayow ascertained that the only difference between arterial and venous blood was the chemical erythrocyte composition ([Mayow, 1668](#)). In 1695, in Leeuwenhoek's publication *Arcana naturae detecta*, he first described cardiac muscle showing a



certain structural similarity to the ordinary striated muscle ([van Leeuwenhoek, 1695](#)).

Following initial Harvey's hypothesis, in 1852, Hermann F. Stannius started to unravel the mechanism under the atrioventricular rhythm, when he applied a ligature to the sinoauricular junction of frog heart and observed beating blockage ([Stannius, 1852](#)). Later on, new contributions were made with the discovery of the atrioventricular bundle in 1893 by His and Kent ([His, 1893](#); [Kent, 1893](#)), and culminated with the sinoauricular node discovery by Keith and Flack in 1907 ([Keith and Flack, 1907](#)). Regarding the electrical heart conduction, in 1838, Carlo Matteucci demonstrated electrical activity in the heart using a galvanometer ([Matteucci, 1842](#)); in 1841, Jakob Henle discovered the vasomotor nerves ([Henle, 1841](#)); and in 1845, Johannes E. Purkinje described for the first time the ventricular Purkinje fibers, subendocardial cells specialized in electrical conduction ([Purkinje, 1845](#)). Almost forty years later, the experiments of Engelmann and Gaskell confirmed the myogenic view of the heart, observing the own contractile activity of isolated cardiac muscle strips ([Engelmann, 1875](#); [Gaskell, 1882](#); [Gaskell, 1883](#)).

The most recent advances in technology during the last century helped to the refinement and corroboration of the misleading points. One of them was the new and detailed view of the capillary circulation performed independently by Dale, Krogh and Lewis, during the 1920s, by using the capillary microscopy ([Dale and Richards, 1918](#); [Krogh, 1919](#); [Lewis, 1926](#)). In these last years, the application of catheterization has enabled to acquire a more complete understanding not only of heart anatomy and physiology, but also of the different pathologies threatening cardiovascular system function.

## **2. In the heart of circulatory system**

The circulatory system, also called the cardiovascular system, responds to the evolutionary necessities of higher animals to transport and distribute blood

throughout the body, covering larger distances, carrying oxygen, hormones, immune cells and nutrients, as well as waste metabolic products for their elimination. To that end, the circulatory system is composed of blood vessels connected to the heart, the organ which acts as a mechanical pump, sending out through the vasculature the blood it receives (Pocock *et al.*, 2013). With a central role on circulatory system, the heart is a hollow, cone-shaped muscular organ located in the middle of the thoracic cavity, the mediastinum, composed primarily of cardiac myocytes and support cells tissue arranged in a three-dimensional circumferential orientation. The intrinsic heart automaticity or autorhythmicity capacity enables the generation of its own electrical signals, without neural or hormonal stimulation. These stimuli are propagated through a specialized cellular conduction machinery, the nodal system, towards the contractile cardiomyocytes, promoting in response their contraction and driving blood pumping out (Gavaghan, 1998; Iuzzo, 2009).

Anatomically, the heart is divided into four chambers: left and right atria, which are responsible for collecting blood from the lungs and the rest of the body, respectively, and transfer it to the corresponding ventricle; and left and right ventricle, whose function is to pump the blood to the whole body and to the lungs, respectively. To ensure one-way pumped blood flux and avoid reflux, two valves are present in-between atria and ventricles; and two more at the lumen

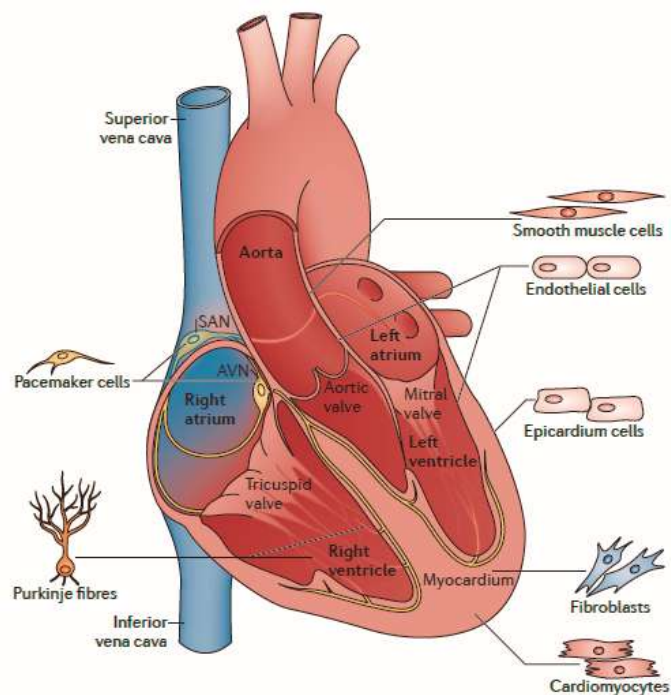


**Figure 2. Heart anatomy and cell types.** This picture displays the four-chambered heart with the valves, the nodes and the main vessels, indicating the representative specialized cell types for each. SAN: sinoatrial node; AVN: atrioventricular node. Image obtained from Xin *et al.*, 2013.

entrance of the two main arteries: pulmonary and aorta. Thus, the atrioventricular valves tricuspid and bicuspid or mitral permits correct blood flow only from atria to ventricles, with no backward flux; whereas the semilunar valves, pulmonary and aortic, assures blood flow through both pulmonary and aortic arteries with no return to the ventricles (Milnor, 1990; Weinhaus and Roberts, 2009) (Figure 2).

Blood circulation cycle starts with the deoxygenated blood from the systemic circuit arriving at the right atria from both the superior and inferior vena cava and filling up the empty chamber. The right atria contracts and blood passes through the tricuspid valve to reach the right ventricle, where it is pumped into the pulmonary circuit flowing through the pulmonary artery to exchange carbon dioxide for new oxygen. The reoxygenated blood is conducted from the lungs to the left atria by the pulmonary veins to reenter the cardiac circulation. Upon blood atria filling, this is pumped through the mitral valve to the left ventricle, which in turn, contracts and pushes out the oxygenated blood via aorta to be distributed to the body (Martini *et al.*, 2014) (Figure 3).

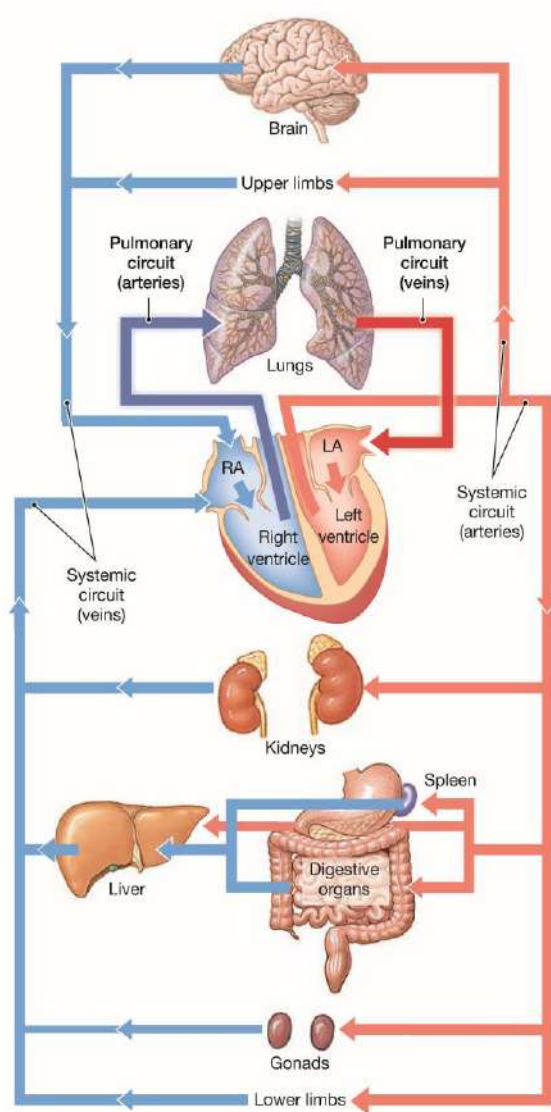


**Figure 3.** Blood circulation cycle diagram. The schematic image was taken from Martini *et al.*, 2014.

Synchronous cardiac contraction requires electrical impulses that, in the end, cause cardiomyocyte depolarization and subsequent atrial and ventricular timely contraction. Initially, this action potential is generated within the sinoatrial node (SAN), located in the right atrium wall. The generated electrical signal is driven to the

atrioventricular node (AVN), which lies in the atrium-ventricle junction, by an electrical signal conducting heart muscle cells pathway, the internodal tract. Along the way to the AVN, the stimulus spreads across the atrial wall, which ultimately leads to atrial muscular cells stimulation and contraction. Once the electrical impulse enters the AVN, it travels to the interventricular septum inside the bundle of His, another collection of specialized cardiac cells for stimuli conduction. Then, the signal follows its way inside two bundle of His derived branches, each directed to the corresponding ventricle. These ramifications terminate in Purkinje fibers which directly transmit the signal to the ventricular cells, depolarizing them and activating ventricular contraction (Katz, 2011; Martini *et al.*, 2014) (Figure 4).

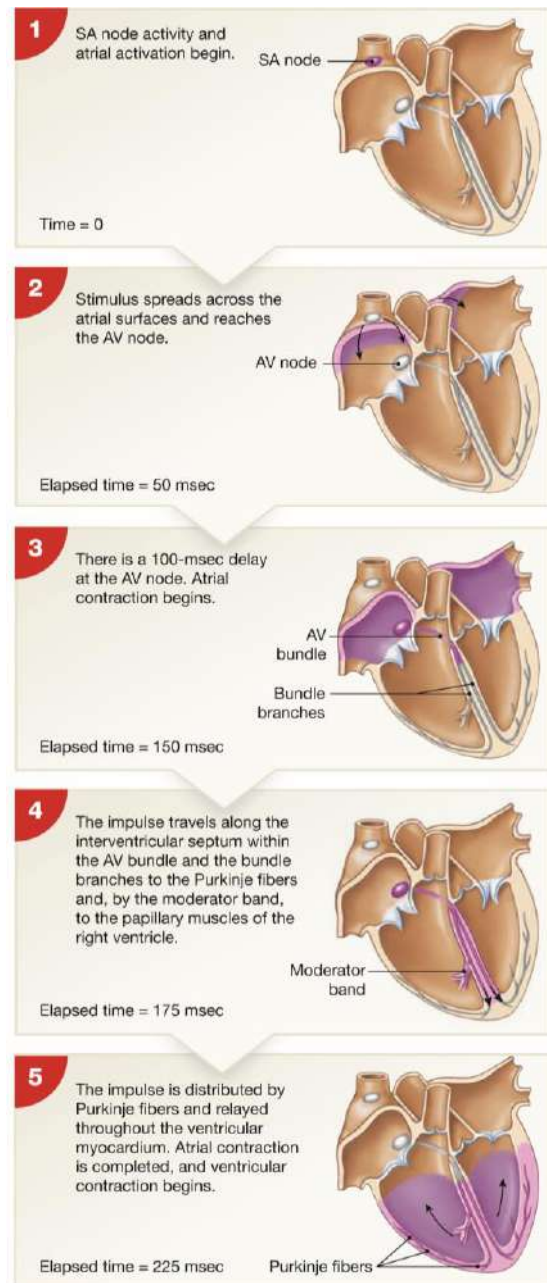


**Figure 4.** Electrical conduction system throughout the heart. Phases of electrical signal transmission, from its generation inside the SAN to the resulting ventricular cell contraction. Images reproduced from Martini *et al.*, 2014.

## 2.1. Heart layers

### 2.1.1. The heart wall

Three differentiated cardiac layers constitute the heart wall, each of them with a specific function and cell composition. These heart layers, illustrated in **Figure 5**, are listed from inner to outer:

- The innermost layer, **the endocardium**, is a slim sheet of endothelium (squamous epithelium) which rests over a thin areolar connective tissue layer that joins with the myocardium. The endocardium covers the fibrous skeleton of cardiac valves, as well as it is in intimate contact with incoming and outgoing heart blood vessels endothelium in each of the four heart chambers. This layer is composed mainly of endothelial and Purkinje cells placed beneath the endocardium, in a space called subendocardium. The endothelial cells-secreted peptide endothelin might have a role regulating contraction, although its function is still under scrutiny (Marieb and Hoehn, 2006; Drawnel *et al.*, 2013).
- The middle layer, **the myocardium**, is the thickest and main layer making up the atrial and ventricular heart wall. It is integrated essentially of involuntary, striated cardiac muscular tissue and, to a lesser degree, nerves and blood vessels. This muscular tissue is composed of cardiomyocytes, specialized cells tightly connected to each other by intercalated discs, forming a cardiac syncytium, that facilitates electrical signal transmission. Cardiomyocytes contain myofibrils, organelles consisting of long repeating chains of sarcomeres, fundamental for contraction. The cardiac muscle draws a distribution following a spiral organization pattern, disposed over a dense connective tissue network, providing a strong fiber anchor and reinforcing internal structure. This swirling organization facilitates the efficient cardiac muscle contraction to pump out blood volume.

- **The epicardium**, also referred as visceral pericardium, is the outermost membrane that covers heart external surface. This serous layer is composed of mesothelium bound to an underlying areolar loose connective tissue which, in turn, maintains the attachment to the myocardium. Importantly, blood vessels and nerves irrigate the underneath myocardial tissue through the epicardium (Marieb and Hoehn, 2006).

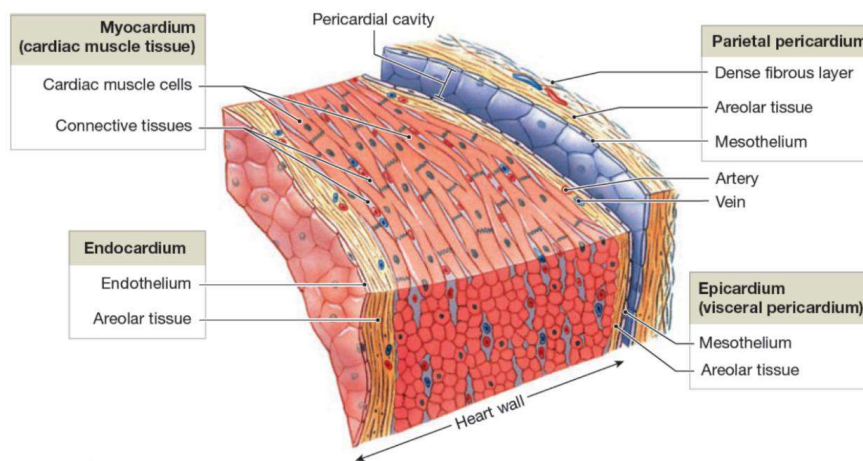


**Figure 5. Heart layers.** A cross section of the heart wall and pericardium showing each of the cardiac layers. Image from Martini *et al.*, 2014.

### 2.1.2. The pericardium

The heart is enclosed within a double-walled sac, the pericardium, a fibrous-serous membrane whose main function is to protect the organ, as well as stabilize its position within the mediastinum. It is bound to the diaphragm through the pericardiophrenic ligament, and it presents in its outer face vascularized adipose islets, while the inner face corresponds to the serous laminae. The pericardium is a well-vascularized membrane, with the arterial supply coming from the pericardiophrenic and musculophrenic branches of the internal thoracic artery and the descending thoracic aorta, and the venous drainage provided by the pericardiophrenic veins, either directly or mediated via the superior intercostal veins and internal thoracic veins into the brachiocephalic veins. Regarding innervation, the parasympathetic nerve supply of the pericardium comes from the vagus and left

recurrent laryngeal nerves, as well as branches from the esophageal plexus, while the sympathetic innervation is derived from the first dorsal ganglion, stellate ganglion and the aortic, cardiac and diaphragmatic plexuses. On the other hand, the phrenic nerve provides sensory fibers to the pericardium (Rodriguez and Tan, 2017).

Structurally, the pericardium is divided into two discernible membranes (Figure 5):

- The inner **serous pericardium**, which in turn, is subdivided into the **visceral pericardium** or epicardium, lining with the myocardium; and the outer **parietal pericardium**, a mesothelial cell monolayer separated from the visceral pericardium by the pericardial cavity and in close contact with the second pericardial membrane, the **fibrous pericardium**. Both layers remain separated by the pericardial cavity, which contains the pericardial serous fluid (between 20 and 60 mL), an ultrafiltrate of plasma that lubricates the heart and prevents its graze with the adjacent structures.
- The **fibrous pericardium**, the outermost layer placed over the parietal pericardium, is a conical sac made of a dense collagen and elastin interconnected framework. Its last mission is to protect the cardiac organ against excessive ventricular distention and external agents, and to fix heart position in the thoracic cavity through tight bonds to the sternum (LeWinter and Samer, 2005; Rodriguez and Tan, 2017).

Surrounding the pericardium, adipose flaps of mediastinal origin can be found allocated in two differentiated locations: the epicardial adipose tissue, placed on the great vessels and coronary arteries roots; and the pericardial adipose tissue, distributed on top of the outer surface of the fibrous pericardium. Recently, epicardial adipose tissue has become of great interest as it has been described as a reservoir of a novel stem cell population, the cardiac adipose tissue-derived progenitor cells (ATDPCs), with a cardiac-like phenotype and an elevated immunosuppressive capacity (Bayes-Genis *et al.*, 2010). These cells have been properly isolated and expanded to be used throughout this thesis project.

### 3. The embryonic development of the heart

Heart is the first organ to become fully functional during vertebrate embryonic development, after a complex embryonic process involving several steps that lasts for ten weeks in humans (**Figure 6**). Its formation starts at week 3 of gestation, during early gastrulation occurring in the primitive streak. Herein, there is a cell migration phenomenon from the upper layer to both cranial sides of the embryonic disc to form the three differentiated embryonic layers: endoderm, mesoderm and ectoderm. The cardiac progenitor germ line, localized in this newly-formed mesoderm, moves from the two cranial lateral plates to the cranial border of the embryonic disc, where they join at the midline to define a cardiac primordium, named the cardiac crescent or first heart field (FHF). At this point, there are two different cell population subsets present within the cardiac crescent: a first group of cardiac progenitors with the potential to become cardiomyocytes and eventually give rise to the myocardium; and a second subpopulation of cardiac crescent cells that will trigger the development of two lateral endocardial tubes, by means of the vasculogenesis process, that will define the endocardium (Schleich, 2002; Moorman and Christoffels, 2003; Abu-Issa and Kirby, 2007). Moving into the fourth gestation week, the cranial and lateral folding of the embryo causes the fusion of both tubes along with the myocardial progenitor cells, to form the primitive heart tube. Both cell layers composing the primitive heart tube, the myocardium and the endocardium, are separated by the cardiac jelly, a thick extracellular matrix (ECM) layer secreted by the myocardium (Sylva *et al.*, 2014).

During the fourth week, the tubular heart experiences concomitant looping and elongation through the addition of new differentiated cardiomyocytes from the second heart field (SHF), a second pool of cardiac progenitors located in the mesoderm, at either end of the tube (Dyer and Kirby, 2009). Progressive tube extension and proper heart looping promotes a series of expansions and constrictions (*sulci*) that subdivides the primordial heart into the primitive heart chambers. From the inflow end, the developed structures are the left and right horns of the sinus venosus, the primitive atrium, the primitive ventricle, the *bulbus cordis* and the



outflow tract. Accordingly, the *bulbus cordis* mostly forms the right ventricle; while the primitive ventricle is responsible for constituting the left ventricle. The outflow tract or *conotruncus* will set up the *conus arteriosus* and the *truncus arteriosus*. These two new-formed structures will eventually split up to become the outflow regions of the ventricles, as well as the ascending aorta and the pulmonary trunk (Schoenwolf *et al.*, 2009). Additionally, at this development stage, a group of epicardial precursor cells, derived from the extracardiac embryonic tissue proepicardium, starts to surround the forming myocardium surface and will end up constituting the outer epicardium (Wessels and Pérez-Pomares, 2004).

Throughout the fifth and sixth week, the septation process takes place to form the four final heart chambers. A pair of septa, the *septum primum* and the *septum secundum*, start to grow to build up the wall which separates both left and right atria, perforated by a pair of foramina that permit right-to-left blood correct shift. Meanwhile, the *bulbus cordis* maintains its growth to, in the end, form the right ventricle. During the sixth week, a new anatomical wall arises, the muscular ventricular septum, which partially divides both ventricles. It is after the eighth week when the outflow tract has completed septation and division processes, becoming the final outflow regions of both ventricles, the ascending aorta and the pulmonary trunk; afterwards, remodeling process happening in the *conus arteriosus* will place the aortic and pulmonary valves in the corresponding aortic and pulmonary arteries, respectively. Finally, the septation is completed by means of a three-septa fusion, between the muscular interventricular, conotruncal and atrioventricular septa (Sylva *et al.*, 2014).

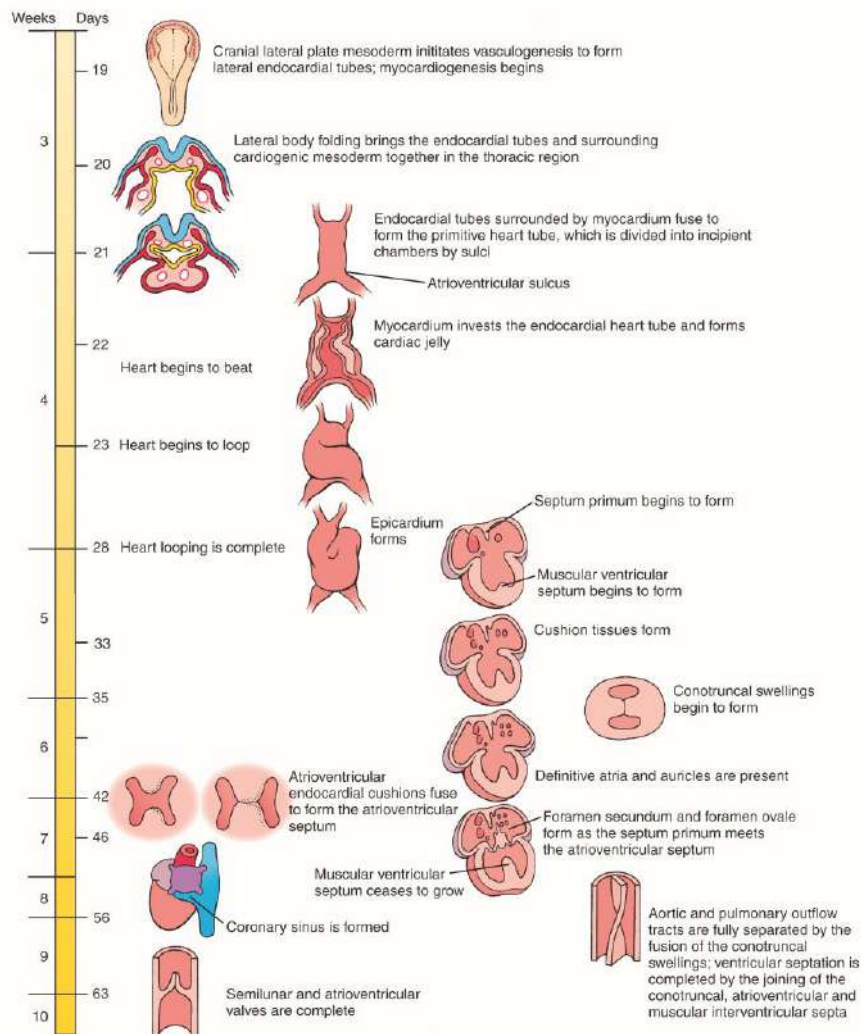


**Figure 6.** Human heart embryonic development timeline. Main events during cardiac development. Diagram extracted from Schoenwolf *et al.*, 2009.

### 3.1. Key pathways and proteins in heart formation

For the correct progress through the different steps of the cardiac embryonic development that will eventually lead to the mature heart formation, it is necessary a comprehensive interplay among major developmental signaling pathways, involving the expression of both transcription factors and cardiac-committed proteins. These signaling cascades are directed to guide and differentiate the pluripotent stem cells towards each of the heart cell types during the embryonic process (**Figure 7**).

The induction of mesoderm formation following gastrulation, from where the initial cardiac progenitors will arise, is namely conducted by three pathways acting over the initial embryonic pluripotent stem cells: the canonical wingless integrated (Wnt), the bone morphogenetic protein (BMP) and the transforming growth factor beta (TGF- $\beta$ ), with the specific participation of the Activin and the Nodal protein signaling. Once the mesoderm has been developed, it is necessary further regulation for cardiac reprogramming of the resident progenitors. The primordial cardiovascular precursors, which express mesoderm posterior 1 protein (Mesp1), receive incoming cues from the BMP and TGF- $\beta$  pathways, along with new signals from the fibroblast growth factor (FGF) and the non-canonical Wnt pathways; while the canonical Wnt signaling network is gradually inhibited after gastrulation by the Dickkopf1 and the frizzled-related protein 2 expressed by the adjacent endocardium (Nosedá *et al.*, 2011). Altogether, this signaling crosstalk leads to the appearance of the cardiac precursor lineage within both the FHF and the SHF.

At this point, two different cardiac-committed genetic profiles can be distinguished among the cardiac precursor populations following the signaling cascade: in the FHF, cells express NK2 transcription related factor 5 (Nkx2.5) and GATA binding protein 4 (GATA4) transcription factors, together with the heart- and neural crest derivatives-expressed proteins 1 and 2 (Hand1 and Hand2), the ion channel protein hyperpolarization-activated cyclic nucleotide-gated channel 4 (HCN4) and the T-box transcription factor 5 (Tbx5). On the other hand, SHF cardiac precursors displayed expression of cardiogenic genes myocyte enhancer factor 2 (MEF2), insulin gene enhancer protein 1 (Isl1), Tbx1, Fgf8 and Fgf10, in addition to the mentioned Nkx2.5 and GATA4 transcription factors and the Hand1 and Hand2. All these genes are indispensable in the subsequent myocardial differentiation from both cell populations (Buckingham *et al.*, 2005; Srivastava, 2006; Vincent and Buckingham, 2010).

The final cardiac specification and maturation of heart precursors is determined by the signaling modulation exerted by the BMP, FGF, Nodal, Hedgehog and Notch pathways, the retinoic acid and non-canonical Wnt5 and Wnt11 contribution, and the inhibition of the canonical Wnt signaling cascades. The

sequential integration of all of them activates a downstream signal transduction that triggers the differential pattern expression of a set of genes depending on the cell type specification, its position and function (Sahara *et al.*, 2015). For instance, the ventricular myocytes show expression of connexin43 (Cx43) and sarco/endoplasmic reticulum Ca<sup>2+</sup>-adenosine triphosphate (ATP)ase (SERCA2), among others; whereas the atrioventricular nodal cells differentially express connexin30.2 or Tbx3, as an example (Später *et al.*, 2014).

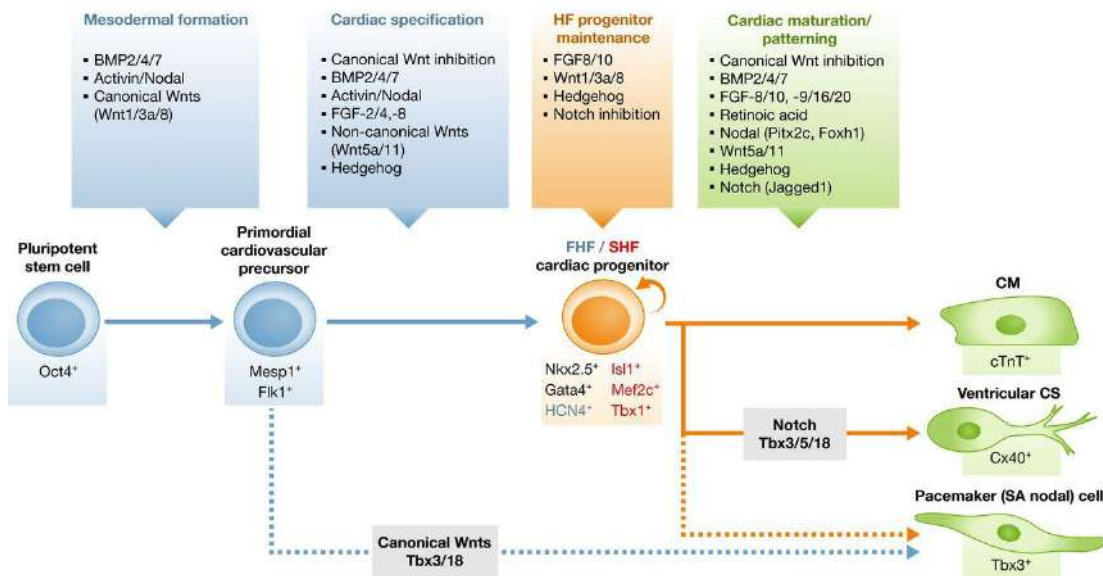


**Figure 7.** Signaling pathways driving cardiac cell reprogramming during human heart embryogenesis. Main signaling networks and regulators/modulators at each step of the cardiac differentiation process. The embryonic stages represented are the mesodermal formation, the cardiac specification, the heart field progenitor maintenance, and the cardiac maturation/patterning. In blue are indicated the first heart field (FHF) markers, and in red the ones for second heart field (SHF), respectively. This flow chart was reproduced from Sahara *et al.*, 2015.

The mature cardiomyocytes, the main and most important cellular subunit of the heart, display a cardiac-specific profile of proteins, the cardiac markers, which are solely expressed within this cellular subset and allow its identification (Figure 8). Some of these markers will be of special interest throughout this work, as they will permit the detection of the cardiac population arising from progenitor cell lineage. Briefly, these key proteins are:

- From the contractile apparatus: **cardiac troponin I (cTnI) and T (cTnT).**

- From the gap intercellular junctions: **Cx43**.
- **SERCA2**, a calcium ATPase pump.
- Transcription factors required for complete cardiac differentiation: **MEF2 and GATA4**.

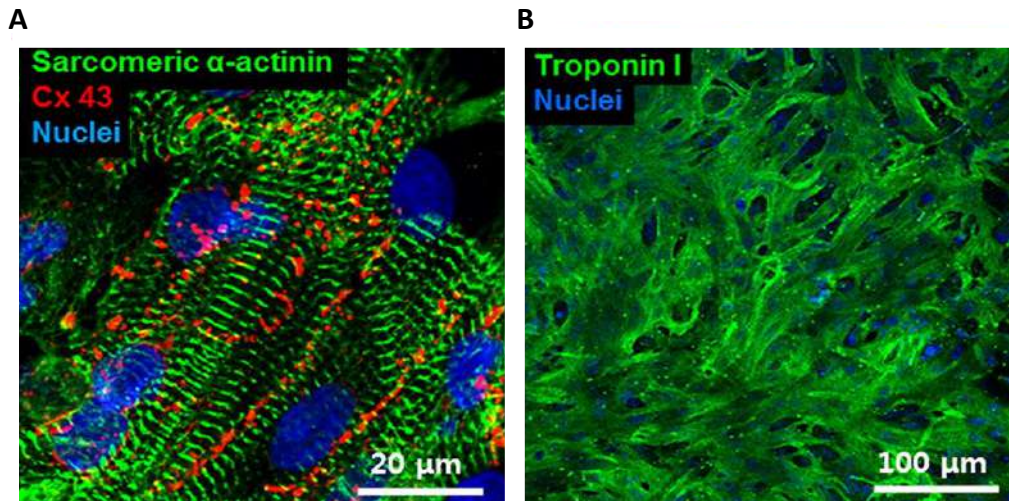


**Figure 8.** Neonatal rat ventricular cardiomyocyte markers. (A) Immunostaining against the cardiac markers sarcomeric  $\alpha$ -actinin (green), Cx43 (red) and (B) Troponin I (green) of neonatal rat ventricular cells. Nuclei were counterstained with 4',6-diamidino-2-phenylindole (DAPI) in blue. Both microscopy photographs were reported in *Shin et al., 2013*.

#### 4. Cardiovascular diseases (CVDs): a real burden

The cardiovascular diseases (CVDs) account for more than 30% of deaths worldwide, surpassing other global pandemics such as cancer, respiratory diseases or diabetes mellitus, and positioned as the top-ranked disease causing mortality ([World Health Organization webpage](#)) (**Figure 9**). The CVDs prevalence is significantly higher among the elderly, since almost half of the affected population is estimated to be over 60 years (*Mozaffarian et al., 2016*). As a group of diseases so extended around the world, it represents not only a drastic reduction in their quality of life, but also an increasing economic burden in terms of direct costs for governments and health systems to fight the CVDs threat; and indirect costs derived from these illnesses, such

as the loss of human productivity due to the caused mortality. As an example, in 2011 and according to Mozaffarian and collaborators, the sum of direct and indirect costs related to CVDs in the United States was calculated to be of 317 billion of dollars. Even worse, an estimation of the CVDs total cost for the next fifteen years has placed the maximum expenditure around 1200 billions of dollars in 2030; and the CVDs prevalence will shift from the 35% in 2012 to the 44% in 2030 (Mozaffarian *et al.*, 2016), drawing a worse outlook for the upcoming years.

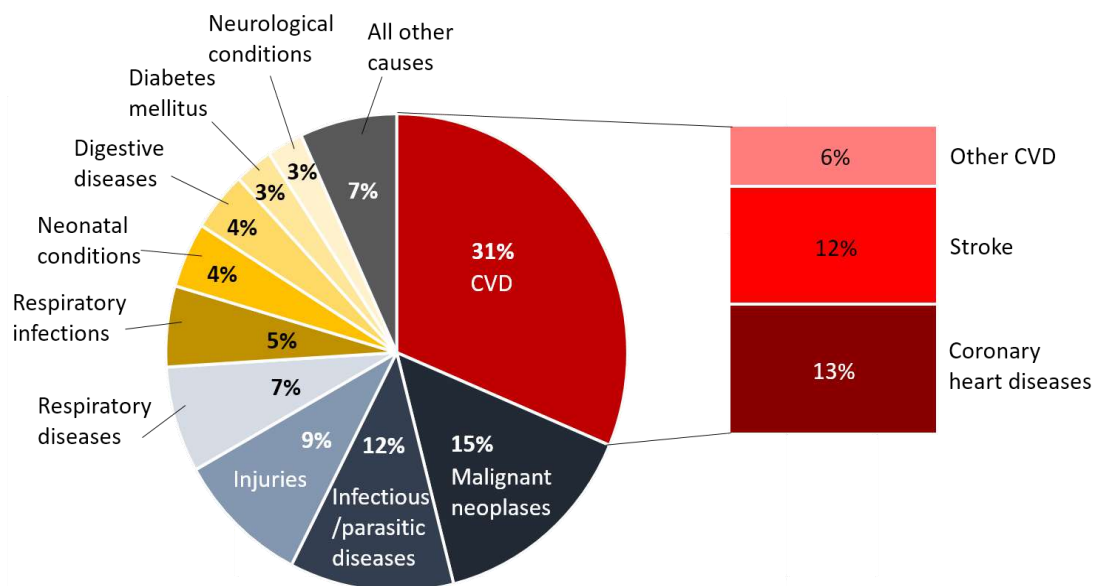


**Figure 9. Major causes of death worldwide.** Percentage of mortality attributable to different diseases and adverse conditions. The CVDs group has been broken down in three categories to represent the contribution of each individual CVD to the global CVDs percentage burden. This graph was elaborated using the data published on the [World Health Organization webpage](#).

The CVDs can be classified in two different categories based on the anatomical location of the illness, dividing them in diseases of the vessels and diseases of the heart; the involvement of atherosclerosis; or the World Health Organization classification system with the International statistical Classification of Diseases and related health problems 10th revision (ICD-10). Following this latter criterion, below is a brief description for the CVDs that affect and damage heart, in a direct or indirect manner, with a higher interest:

- **Acute rheumatic fever:** a severe infection caused by the *Streptococcus*

*pyogenes* or the group A *Streptococcus* bacteria, which can cause pericarditis, myocarditis or endocarditis.

- **Chronic rheumatic heart diseases:** recurrent or persistent infections, i.e. mitral, aortic and tricuspid disorders, such as stenosis; and chronic rheumatic pericarditis, myocarditis and endocarditis.
- **Hypertensive diseases:** disorders associated with a too high blood vessel pressure, such as the hypertensive heart disease.
- **Ischemic heart diseases (or coronary artery diseases):** the most common heart disease in which a blood clot, generally an atheroma plaque, occludes the coronary arteries and impedes normal blood flow towards the heart, for instance, angina pectoris, acute myocardial infarction, aneurysm or chronic ischemic heart disease.
- **Pulmonary heart disease and diseases of pulmonary circulation:** includes all that illnesses derived from high blood pressure, occlusion or damage in the lung blood vessels. Cor pulmonale, pulmonary embolism or aneurysm of pulmonary artery are classified within this category.
- **Other forms of heart disease:** all other diseases non-specified previously or some of the described illnesses with different etiology. For example, non-rheumatic pericarditis, non-rheumatic valve disorders, atrial fibrillation and arrhythmias, cardiomyopathies, cardiac arrest and some types of heart failure.
- **Cerebrovascular diseases:** vascular diseases where the arteries supplying the brain with oxygen are affected. For instance, the subarachnoid hemorrhage, intracerebral hemorrhage, cerebral infarction or the stroke.
- **Diseases of arteries, arterioles and capillaries:** damage, occlusion or other disorders in other peripheral arteries.
- **Diseases of veins, lymphatic vessels and lymph nodes, not elsewhere classified:** disorders within peripheral veins and the lymphatic system, such as embolism or varicose veins.

- **Other and unspecified disorders of the circulatory system:** hypotension or some postprocedural disorders of the cardiovascular system.
- **Congenital malformations of the circulatory system:** problems in the heart structure and anatomy developed during embryogenesis and present at birth. Representative examples of this group are the congenital malformations of cardiac chambers and connections, cardiac septa, valves and blood vessels, either great arteries and veins, or peripheral vessels.

#### **4.1. Myocardial infarction (MI)**

Myocardial infarction (MI) is the coronary artery disease with the highest incidence among population, with an estimation of new 550,000 and 200,000 recurrent MI cases in the United States, and a mortality rate close to 15% (Mozaffarian *et al.*, 2016). Clinically, the MI is a pathology that occurs after the lumen of a coronary artery has been occluded, usually as a result of vessel wall narrowing due to a high pressure or the formation of an atherosclerotic plaque. Consequently, the volume of blood flowing through the blocked artery is highly reduced, thus limiting the amount of oxygen and nutrients supplied to the heart (Figure 10A). If the obstruction of blood circulation to the cardiac muscle is prolonged over time, it leads to a massive loss of cardiomyocytes and the formation of a characteristic necrotic collagen scar that hampers normal blood pumping cardiac activity because of abnormal loading conditions (Pfeffer and Braunwald, 1990). Ultimately, these adverse events trigger the MI expansion along the ventricular wall, and as a last physiological response to stop MI progression and send enough blood volume to the rest of the body, the heart starts a maladaptive process known as adverse ventricular remodeling. This phenomenon induces ventricular wall dilatation and narrowing, leading to changes in the ventricle shape, switching to a more spherical form, and resulting in cardiac hypertrophy. Finally, the dilated chambers are submitted to a systolic exertion with higher oxygen consumption, and the heart is unable to pump out enough blood to fulfill body necessities, which in some cases derivate in the irreversible end-stage



heart failure (Jessup and Brozena, 2003) (Figure 10B).

Endorsed by the European Society of Cardiology last guidelines, the MI diagnosis is based on the rise and/or fall of cardiac biomarkers values (preferably, troponin) and with at least one of the following additional conditions: symptoms of ischemia; new significant ST-T changes or new left bundle branch blockage; pathological Q waves in the electrocardiogram; evidence of viable myocardial tissue loss or abnormal wall mobility through imaging; or identification of an intracoronary thrombus by using angiography or autopsy (Steg *et al.*, 2012).

During the last years, with special emphasis within the last 20, the MI mortality has experienced a significant and gradual drop in developed countries (Reikvam and Hagen, 2011; Orozco-Beltran *et al.*, 2012; Smolina *et al.*, 2012; Nichols *et al.*, 2014; Mozaffarian *et al.*, 2016). Despite the latest advancements that have led to this progressive death cases fall, the definitive therapy to reverse MI still remains elusive. The only current treatment which enables a complete recovery following MI is heart transplantation; however, this procedure is notably hindered by donor availability limitation and immune rejection issues of the receptor patient (Colvin *et al.*, 2017). Therefore, it exists a real necessity for developing new and more effective therapies to fight against MI.

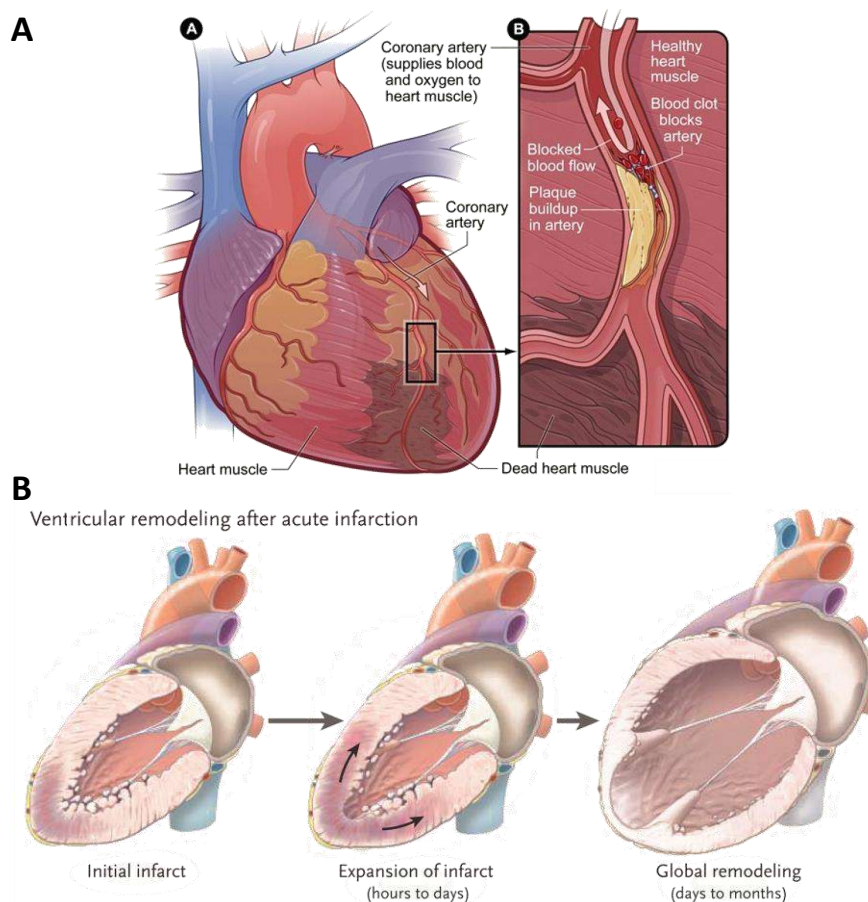


**Figure 10. Myocardial infarction and ventricular remodeling overview.** (A) Left panel: Heart muscle showing the damaged coronary artery during MI. Right panel: Detailed coronary artery cross section with the atheroma plaque blocking blood flow to the heart. Images obtained from the [National Heart, Lung, and Blood Institute \(NHLBI\)](#). (B) Ventricular remodeling following MI. Initially, there are no clinically relevant changes when the infarction has begun. Within days, the infarcted area expands and the ventricular wall becomes thinner. Eventually, the global remodeling takes place, resulting in ventricular dilation, diminished systolic function, mitral valve dysfunction and aneurysm formation. Diagram reproduced from [Jessup and Brozena, 2003](#).

## 5. Current therapies in the MI context

Nowadays, treatments administered to the patients suffering from MI are mainly directed to reperfuse or recover the blocked coronary artery blood flow, as rapidly as possible, with the goal of ameliorating clinical manifestations and prevent fatal

cardiac arrest caused by arrhythmias, especially ventricular fibrillation. Regarding the best time window of action, it is of vital importance to reperfuse the occluded coronary artery during the first 60 minutes following MI onset to avoid mortal arrhythmias happening before hospitalization. During this span, known as golden hour, coronary artery successful reperfusion correlates with a lower associated mortality (Berger *et al.*, 1999; Armstrong *et al.*, 2009). For instance, thrombolysis treatment applied after 70 minutes represented an increase in mortality from 1.2% to 8.7% (Weaver *et al.*, 1993). Unfortunately, in a long-term basis, these treatments are only indicated for improving patient quality of life and alleviate MI symptoms, since none of the current options available in the clinics results in a complete reversion of the MI damage and progression, as well as a total functional salvage post-MI, except for the aforementioned heart transplantation.

The current therapies can be subdivided into anti-ischemic drugs, antithrombotic therapy, fibrinolytic/thrombolytic agents, percutaneous coronary intervention (PCI) and surgical procedures. These options, in some cases, are not discriminatory, and they may be administered using combinations of them. For example, antithrombotic and fibrinolytic/thrombolytic drugs are given concomitantly to potentiate thrombus lysis and size reduction.

### **5.1. Anti-ischemic drugs**

This class of drugs can either reduce oxygen myocardial demand (by slowing down heart rate, reducing preload, or decreasing muscle contractility) or increase the oxygen supply to the myocardium through vasodilatation induction. The most common drugs found within this group are:

- **Nitrates:** they act as a vasodilator, easing oxygen supply to the myocardium and relieving chest pain by decreasing preload and ventricular volumes. The most common compound here is the nitroglycerine.
- **$\beta$ -adrenergic blockers:** competitive antagonist to the  $\beta$ -adrenergic receptor,

thus preventing adrenaline or noradrenaline binding. Consequently, they reduce cardiac rate and diminish blood pressure widening blood vessels, alleviating oxygen consumption. Some examples contained in this group are metoprolol, carvedilol or bisoprolol.

- **Calcium channel blockers:** these antagonists impede the normal calcium ion transit along the channels, resulting in a dilation of vessels. Verapamil or diltiazem are just some calcium channel blockers used routinely.
- **Ranolazine:** it inhibits the late inward sodium current in cardiac muscle, which in turn leads to reduce intracellular calcium levels. This lower calcium concentration lowers blood pressure and oxygen requirements.
- **Angiotensin-converting enzyme (ACE) inhibitors:** these agents are administered to widen blood vessels, retrieving normal oxygen flow to the myocardium. The ACE inhibitors mechanism of action is focused on the renin-angiotensin-aldosterone system, by blocking the conversion of angiotensin I to the vasoconstrictor angiotensin II, thereby promoting vasodilation and decreasing blood pressure. The maximum exponent here is enalapril.
- **Statins:** these drugs aid to reduce cholesterol content, the primary lipid constituting the atheroma plaque that obstructs the coronary artery lumen. Atorvastatin and simvastatin are two examples of widely employed statins.

## ***5.2. Antithrombotic therapy***

The successive thrombotic mechanisms occurring after early plaque disruption are pivotal to trigger thrombosis and coronary artery occlusion. Here, platelet accumulation plays a key role, given that initial platelet formation at the site of plaque breakdown further amplifies platelet aggregation and hastens thrombus formation. Moreover, the higher the number of activated platelets present, the more dormant platelets will activate through thrombin cascade, which in turn will produce more fibrin mesh that stabilizes the thrombus (Van de Werf, 2009). Therefore, the

antithrombotic treatments should be directed to inhibit activated platelets and platelet clumping, or to specifically block thrombin coagulation signaling pathway branch to limit thrombus progression (Figure 11). At present, and based on the mechanism of action, the most used antithrombotic treatments are divided into antiplatelet drugs and anticoagulant drugs:

- **Antiplatelet drugs:** encompasses the therapeutic agents that modulate the platelet activation pathway at diverse points, to directly block platelet stimulation and recruitment, thus limiting its aggregation. This family can be subclassified into the following groups:

- **Aspirin:** or acetylsalicylic acid, specifically blocks

thromboxane A<sub>2</sub>

(TXA<sub>2</sub>), a protein necessary for platelet

aggregation.

Thus, while the inhibition is sustained, platelet aggregation capacity is drastically reduced during platelet lifetime. Besides, aspirin has also a vasodilator effect.

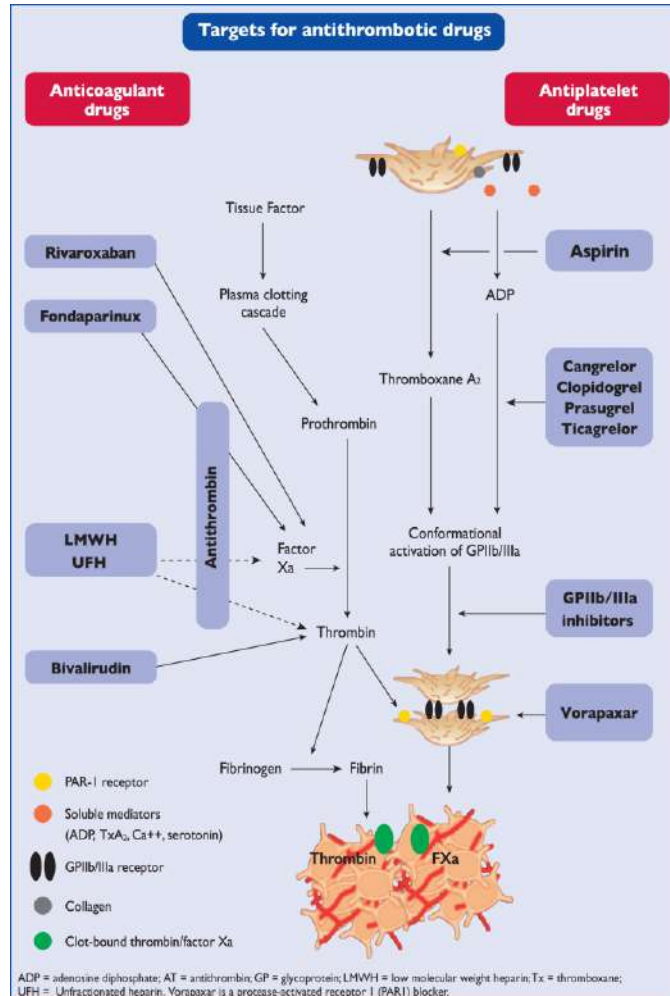


**Figure 11.** Therapeutic targets of the antithrombotic drugs. Coagulation cascade diagram and the action points targeted by the antithrombotic agents. ADP: adenosine diphosphate; GP: glycoprotein; LMWH: low molecular weight heparin; TXA<sub>2</sub>: thromboxane A<sub>2</sub>; UFH: unfractionated heparin. The image was taken from Roffi *et al.*, 2016.

- **P2Y<sub>12</sub> receptor inhibitors:** P2Y<sub>12</sub> receptors, a subtype of adenosine diphosphate (ADP) chemoreceptors, are found on the platelet surface, and are also involved in platelet aggregation. Their blockage prevents further platelet accumulation and blood clotting. The four more representative drugs in this category are clopidogrel, ticagrelor, cangrelor and prasugrel.
  - **Glycoprotein (GP) IIb/IIIa receptor inhibitors:** the GP IIb/IIIa receptor is an integrin complex located in platelets that interacts with fibrinogen and von Willebrand factor, both related to platelet crosslinking and interconnection. Its proper inhibition limits platelet aggregation and thrombus progression. For example, abciximab, eptifibatid or tirofiban are administered intravenously or through infusion during hospitalization.
- **Anticoagulant drugs:** comprises those drugs that act specifically inhibiting thrombin synthesis within the coagulation cascade, such as inhibition of thrombin or factor Xa. Anticoagulants act reducing thrombin-associated fibrin formation, which stabilizes the platelet-rich thrombus, slowing down clot formation. Also, platelet gathering is hampered as a downstream consequence of thrombin inhibition. Here can be included the heparin, direct thrombin inhibitors (bivalirudin), direct factor Xa inhibitors (fondaparinux) or coumarins.

### ***5.3. Fibrinolytic/thrombolytic agents***

This kind of drugs is primarily employed with MI indications to dissolve and break down the formed thrombus and restore the blood flow through the occluded coronary artery. To that end, it can be distinguished between fibrinolytic agents or thrombolytic agents, depending on whether they only dissolve fibrin, or they lysate the whole blood clot, respectively. The main example within this group would be the

tissue plasminogen activators family, which catalyzes the conversion from plasminogen to plasmin, major responsible for dissolving blood clot. Other options included here would be the anistreplase, the urokinase or the streptokinase.

#### **5.4. Percutaneous coronary intervention (PCI)**

The PCI is a non-surgical, minimally invasive procedure, generally performed by an interventional cardiologist aimed to treat narrowing of the coronary arteries found in coronary artery disease. Recently, its implementation has remarkably increased at the expense of thrombolytic agents, due to the PCI higher effectiveness, as assessed by the results provided by the revision of 23 randomized trials ([Keeley \*et al.\*, 2003](#)). As an example, in the United Kingdom, the percentage of MI patients undergone to PCI has switched from almost 0% in 2003 to approximately 90% in 2013, while the thrombolytic therapy accordingly dropped from 100% to 10% ([Royal College of Physicians, 2013](#)).

The PCI requires of catheterization, the introduction of a catheter tube through the radial or femoral artery to reach the obstructed coronary artery via the aorta, guided with the help of a contrast dye. In the most extended practice, the percutaneous coronary transluminal angioplasty (PCTA), a temporary balloon is administered using a second catheter to the affected artery, and inflated to reach a fixed size enough to widen blood vessel walls. Additionally, if it is necessary to permanently maintain the artery opened, a small wire mesh tube, the stent, can be placed in the artery to keep it dilated. When the stent has been fixed, the balloon is deflated and removed from the patient's body, while the stent remains within the vessel lumen (**Figure 12**). Comparatively, the stent displays the lowest restenosis percentage when compared to PCTA and fibrinolytic drugs, with a 5%, 15% and 30%, respectively, for each of the therapeutic options ([Wilson \*et al.\*, 2001](#)).

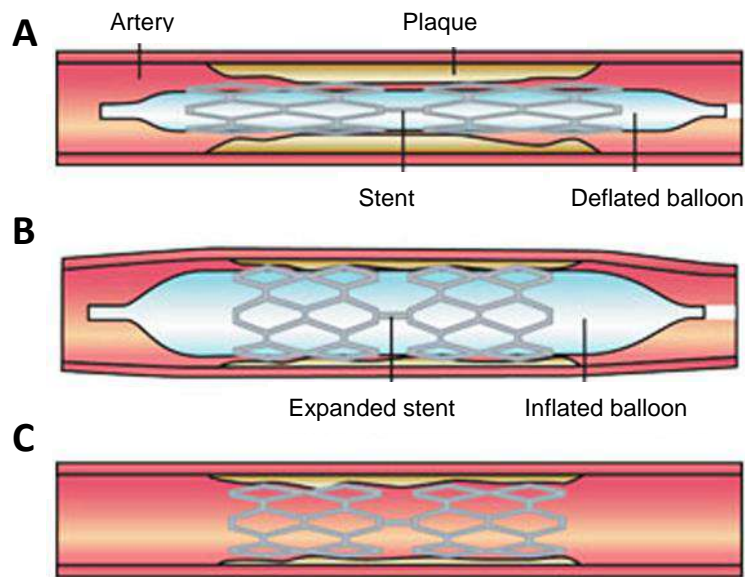


**Figure 12. Stent implantation procedure.** (A) Catheter introduction with the deflated balloon and the closed stent inside the coronary artery damaged by the atheroma plaque. (B) When the catheter reaches the correct position, the balloon blows up to widen the vessel lumen. At the same time, the stent opens along with the balloon. (C) The temporary balloon deflates again and is removed from the artery, while the implanted stent continues compressing the atherosclerotic plaque outwards against the vessel walls. This allows the recovery of at least part of the initial and normal blood flow that circulated through the coronary artery. Schematic images were obtained from the [University of Southern California resources](#).

### 5.5. Surgical procedures

If none of the exposed treatments improved MI clinical symptoms, the last option to heal MI are the surgical procedures, with the major associated drawback of being highly invasive for the patient. Within this category, two different options can be classified:

- **Coronary artery bypass (CABP):** the CABP is the surgical intervention in which a patient artery or vein is grafted between the obstructed coronary artery and the aorta artery, creating a new blood flux pathway to overpass or bypass the coronary injury. Routinely, the saphenous vein is the vessel chosen as the graft to generate the new conduit; albeit the internal mammary arteries have also shown good outcomes, with even better long-term patency rate and improved survival for the vessel graft ([Raja et al., 2004](#)).



- **Heart transplantation:** it consists in the removal of the recipient's heart, affected from a severe MI that in most cases derived to heart failure, to implant a functional donor heart into the recipient's body. Patients undergone to a heart transplantation experience an improvement in their quality of life, with a median life expectancy of twelve years after transplant. Despite the positive effects derived from heart transplantation, latest data published in 2017 indicate that the donor limitation, the increasing recipient waiting list and the need of immunosuppression, restrict this option to very few cases (Colvin *et al.*, 2017).

## 6. Research strategies for cardiac regeneration: current status

Despite existent therapeutic possibilities to reperfuse the infarcted coronary artery, myocardial reperfusion is not always achieved and oxygen flow supply is not fully restored in most cases, highly restricted by adverse side effects and reperfusion injuries derived from the treatment. This might result in a successful artery flow recovery, but perfusion in the infarcted zone remains compromised by two main reperfusion associated effects: microvascular damage and reperfusion injury. The microvascular damage results from the formation of new microthrombi derived from the original thrombus embolization, followed by the release of different substances from the activated platelets, thus leading to the microvascular spasm (Ito *et al.*, 1996). On the other hand, the reperfusion injury causes cellular edema, free radical formation, calcium overload and a substantial acceleration of cellular apoptosis (Carden and Granger, 2000). Besides, it has been reported that neoatherosclerosis can develop in the implanted stent itself, limiting blood flow through the vessel (Nakazawa *et al.*, 2011). Moreover, the no-reflow phenomenon can occur: when a coronary artery remains occluded, some detrimental changes modify the capillaries and arterioles microvasculature. Upon occlusion relief by means of reperfusion techniques, the normal blood flow to the ischemic myocardium may still be impeded

and insufficient (Rezkalla and Kloner, 2002). In this scenario, and with all these factors restricting reperfusion treatment application, new therapeutic strategies are under research with the ultimate objective of regenerating myocardium after MI.

The heart was firstly defined as a terminally differentiated organ with no capacity to self-regenerate the injured area. Recently, this paradigm has changed in the light of new advances in the field. First evidences of myocardial regeneration were demonstrated in newt, when deoxyribonucleic acid (DNA) synthesis was observed in myocytes after undergoing a small excision of the left ventricular wall (Oberpriller and Oberpriller, 1974). Also, evidences of cardiomyocyte renewal were observed in rat atria with left ventricle infarction, suggesting cardiomyocyte turnover under injury conditions (Rumyantsev, 1974). In zebrafish, a robust capacity for cardiac self-repair has been extensively described (Poss *et al.*, 2002; Raya *et al.*, 2003), where the dormant resident cardiomyocytes reactivate and reenter the cell cycle (Jopling *et al.*, 2010). Interestingly, two weeks after apex amputation, the percentage of new cardiomyocytes increased by tenfold from the initial value for undamaged heart of 3%; and one month later, it remained as high as 20% (Poss *et al.*, 2002). Also in mice, a similar autoregenerative capacity was found, although to a lesser extent (Soonpaa and Field, 1997; Porrello *et al.*, 2011; Senyo *et al.*, 2013). In humans, the number of adult cardiomyocyte renewal per year, although low, is also present, ranging from 0.04% to 1.6% depending on the study (Bergmann *et al.*, 2009; Mollova *et al.*, 2013). The main cell populations that contribute to this intrinsic heart regenerative activity have been broadly determined. The cardiomyocytes themselves; the resident cardiac stem cell niche, source of new cardiomyocytes through differentiation; and the extracardiac stem cells are the three main sources for the generation of *de novo* cardiomyocytes (Finan and Richard, 2015) (Figure 13). These cell lines have been clearly identified, and enough evidence of their

contribution to cardiac endogenous renewal capacity has been determined through the following findings: the cardiomyocyte active mitosis, the presence of a cardiac stem cell niche within the heart, and the cardiac chimerism, respectively.

The first experiments to proof intrinsic cardiomyocyte mitotic activity were conducted by Bergmann and collaborators with their isotopic studies. Herein, the  $^{14}\text{C}$  generated during the Cold War integrated into the DNA to establish the cardiomyocyte age. As a result, it was reported that the annual cardiomyocyte turnover ranges from 0.3% to 1 % during human lifespan, with less than 50% of total cardiomyocytes experiencing renewal during lifetime (Bergmann *et al.*, 2009). Furthermore, cardiomyocyte proliferation seems to be more active in humans during youth, with high levels of dividing cardiomyocytes in mitosis and cytokinesis. Mitotic cardiomyocytes dropped at the age of 20, whereas the cardiomyocyte cytokinesis stopped being evident (Mollova *et al.*, 2013). Altogether, this supported the hypothesis of a low, limited-proliferating activity within adult heart. Therefore, in mammals, unlike what occurs in zebrafish, cell cycle reentry of cardiomyocytes is not the primary source of endogenous repair, but stem or progenitor cells are the principal players (Hsieh *et al.*, 2007).

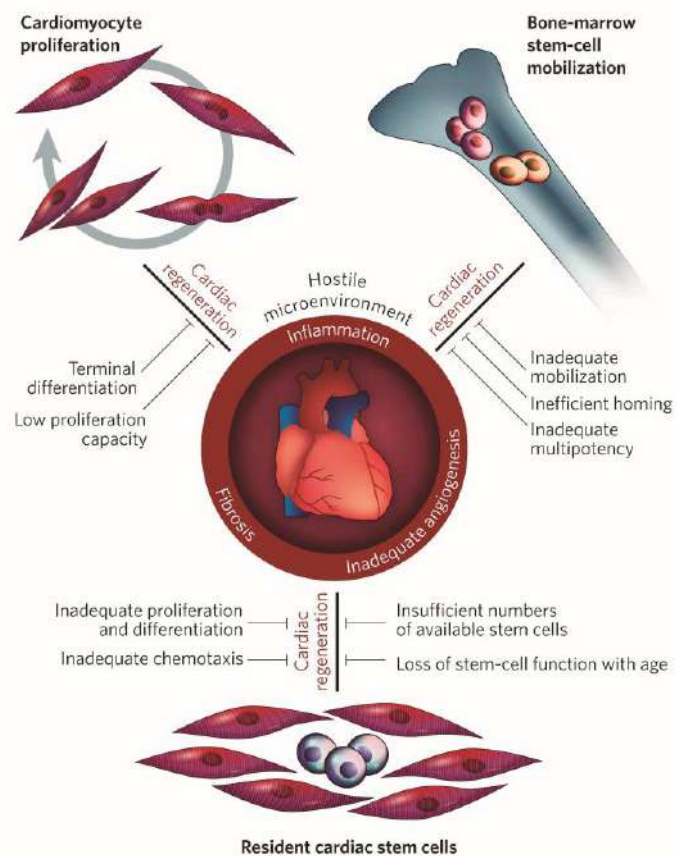


**Figure 13.** Cell populations contributing to endogenous heart regeneration. The three main actors are the cardiomyocytes themselves, through proliferation; the resident cardiac stem cells within the heart niche; and the mobilized extracardiac stem cells. Also, the most important barriers hampering the activation of cardiac regeneration have been indicated. This image was reproduced from Segers and Lee, 2008.

The resident cardiac stem cells, or cardiac progenitor cells (CPCs), are a heterogeneous group of cells distributed throughout the heart. These cells are typically associated with a pattern of overlapping stem cell markers. Among the CPC populations, it can be found the stem cell antigen-1 (Sca-1<sup>+</sup>)-CPCs; c-kit<sup>+</sup>-CPCs; Islet-1<sup>+</sup>-CPCs; cardiosphere-derived cells; side population cells (expressing ATP-binding cassette transporter marker); or epicardium-derived cells (Le and Chong, 2016). First evidences of a putative CPC population were presented by Hierlihy and collaborators, when they showed a group of cells with stem cell-like activity and capable of differentiating to cardiomyocytes in the postnatal mouse heart (Hierlihy *et al.*, 2002). The Sca-1<sup>+</sup>-CPCs discovery was reported by Oh and collaborators, as a cell reservoir that differentiated towards cardiomyocytes in response to 5'-azacytidine chemical treatment (Oh *et al.*, 2003). Later on, new CPCs were properly discovered and isolated in human hearts: the Islet-1<sup>+</sup>-CPCs (Laugwitz *et al.*, 2005) and the c-kit<sup>+</sup>-CPCs (Bearzi *et al.*, 2007). However, latest comprehensive studies reported that both Islet-1 and c-kit are not considered CPC markers, since they can also be indicative of cells with cardiac neural crest embryonic origin (Engleka *et al.*, 2012; Weinberger *et al.*, 2012) and endothelial cells, respectively (van Berlo *et al.*, 2014; Sultana *et al.*, 2015). Therefore, for these two specific populations, their biological role remains unknown, and their classification as CPCs, controversial. Interestingly, the regenerative contribution of CPCs was addressed when they were injected locally in the infarcted myocardium of immunodeficient animals, driving necrotic tissue repair and improving ventricular function (Messina *et al.*, 2004).

Lastly, cardiac chimerism helped to identify the mobilization of extracardiac cells to the injury site for damaged tissue repair. First insights were given taking advantage of human male-to-female cardiac transplants and the consequent gender-mismatch of the Y chromosome (Hruban *et al.*, 1993). An estimated percentage of 0.04% were cardiomyocytes with a detectable fraction of Y chromosome, identified through fluorescence *in situ* hybridization (FISH), thus indicating that these cardiomyocytes arose from the male recipient, rather than the female donor. Besides, the presence of these cells was gathered in the injury focus (Laflamme *et al.*, 2002). Similar results supporting the previous findings were obtained from different

studies collecting heart biopsies of male patients who underwent sex-mismatched cardiac transplantation, with 0.16% of Y chromosome positive cardiomyocytes (Müller *et al.*, 2002), or even higher numbers one year posttransplantation, with around 1-2% (Bayes-Genis *et al.*, 2002) (Figure 14). Fetal microchimerism was also confirmed in pregnant women hearts with male progeny (Bayes-Genis *et al.*, 2005a). Once confirmed the existence of extracardiac cells recruitment into the heart, their origin was in-depth studied. In patients who received peripheral-blood and stem cell transplantation, cardiac chimerism was again reported using FISH Y chromosome labeling, indicating that these cells were derived from the transplanted ones (Bayes-Genis *et al.*, 2004). Therefore, the extracardiac cell recruitment and homing also play an important role in maintaining heart homeostasis.

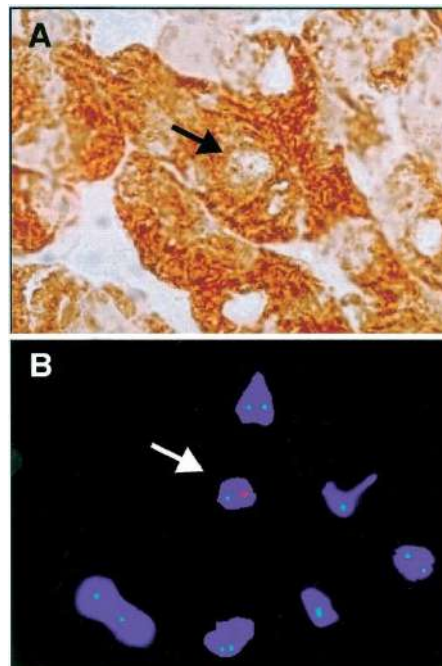


**Figure 14.** Identification of chimeric cells in male heart receptors from female donors. (A) Light microscopy showing cardiac muscle  $\alpha$ -actin immunostaining. (B) Fluorescence microscopy of the same section labeling a chimeric recipient cell identified with both X chromosome (green nuclear signal) and Y chromosome (red nuclear signal). Nuclei were counterstained with DAPI. Arrows highlight the chimeric cell of the male receptor. Images taken from Bayes-Genis *et al.*, 2002.

Despite the intrinsic regenerative ability of the heart and its plasticity, it results to be insufficient to repair myocardial damage when MI occurs. Therefore, the

current therapeutic options under investigation are focused on boosting the regenerative capacity, either enhancing the endogenous heart potential, or providing new exogenous biological elements with cardioregenerative activity, such as stem cell administration or implantation of biomimetic materials. Thus far, the therapies proved to have a greater chance of success and fulfill the clinical translation to their use in humans are cardiac gene therapy, cardiac cell therapy and cardiac tissue engineering.

## ***6.1. Cardiac gene therapy***

Gene therapy refers to the use of gene-carriers, the vectors, to deliver genes of interest for MI treatment, either by expressing new beneficial proteins or modulating the expression of endogenous ones. The main advantage of gene therapy is the possibility to locally administrate the gene product with a long-lasting effect and without systemic side effects, targeting specific cells including smooth muscle cells, endothelial cells or cardiomyocytes. The induction of angiogenesis in the ischemic myocardium and the restoration and regeneration of the injured area are primary objectives that cardiac gene therapy pretends to cover after MI.

### **6.1.1. Strategies for gene delivery**

To accomplish the individual cell targeting for gene delivery, it is necessary to choose the appropriate gene delivery method for individual applications, along with the optimal gene transfer vector systems discussed in the next section. For this purpose, there are four different delivery procedures to administrate the vector containing the gene:

- ***Ex vivo gene therapy***: the preferred method for vascular tissue injuries, since vessels can be removed during surgery, genetically modified with the

administration of the desired vectors, and then implanted again into the receptor.

- **Cell-based genetic modification:** it involves patient cell harvesting, transduction with the chosen vectors *ex vivo* and subsequent reengraftment of the genetically-modified cells. However, the high biological complexity in coping with living cells limits the feasibility and applicability of this option.
- **Local gene delivery:** the most widely used strategy, since it enables to specifically administer the gene within the designed zone at local level. It includes intramyocardial, intracoronary, intravenous and pericardial delivery routes. While the intramyocardial injection allows selecting with higher precision the region of interest and is the preferred method for lentiviral transduction, as they do not cross the endothelial barrier if delivered through circulatory system (Fleury *et al.*, 2003); the intracoronary delivery is less invasive and appears to induce a lower level of inflammation in the heart (French *et al.*, 1994). The third possibility, the intravenous route, seems to be more efficient when adeno-associated viruses (AAV) are used (Inagaki *et al.*, 2006). Finally, another approach is the pericardial delivery, but this administration route exclusively transfects the epicardial cells (Ladage *et al.*, 2011). Nevertheless, these strategies require high doses of virus, which may restrict their future applicability to humans.
- **Systemic route:** vector administration through either the portal or the tail vein (Jaffe *et al.*, 1992). However, usually the vector uptake by the liver is too efficient, leaving low vector concentration to reach the target organ, in this case, the heart.

### 6.1.2. Gene transfer vectors

Most likely, the election of the adequate vector system is the key point to ensure an efficient and accurate delivery of the introduced transgene and its subsequent

expression into the target cell. The criteria that the optimal vector should accomplish are: non-pathogenicity, high efficiency of gene transduction and minimal immune response elicited by the vector (Dishart *et al.*, 2003). The gene transfer vectors can be classified into two primary categories: the viral and the non-viral vectors. Despite the advantages provided by each vector system, they do not fulfill all the requirements for the ideal vector; so, the search for the optimal carrier is still ongoing.

- **Viral vectors:** The viral vehicle is used to infect the target cells, which receive the gene of interest in the form of a transgene incorporated into the cell genome, encoding the desired protein. Their enhanced transduction efficiency makes them the preferable gene carrier system. Englobed inside this group, the following subdivisions can be distinguished:
  - **Lentiviral vectors:** the use of these vectors has been very popular due to their ability to stably integrate within the cell genome, which translates into a permanent expression of the transgene. These viruses can infect both dividing and non-dividing cells, but safety concerns such as random integration, that can trigger insertional oncogenesis, and a relatively low transduction efficiency have undermined their use. Despite these limitations, two studies successfully transduced both *in vitro* and *in vivo* cardiomyocytes (Bonci *et al.*, 2003) and reported efficient SERCA2 transduction in rats after MI, with a cardioprotective role, using lentiviral vectors (Niwano *et al.*, 2008)
  - **Retroviral vectors:** unlike lentivirus, the retrovirus only infects mitotically active cells. As it occurs with lentiviral vectors, retroviruses present the advantage of transgene incorporation into the genome, displaying gene of interest persistent, long-term expression. Some negative points for their application are the non-specific integration, tumorigenesis, limited transduction efficiency and inactivation of retroviral particles by complement in serum (Cornetta *et al.*, 1990).



- **Adenoviral vectors:** these vectors are non-enveloped, non-integrating double-stranded DNA vectors that promote a transient transgene expression within the transduced cells, which lasts for at least two weeks ([Wright et al., 2001](#)). Nonetheless, the main drawback associated with adenovirus utilization is the activation of the innate immunological response contributing to toxicity. All the same, it has not compromised adenovirus testing in humans, using it as a carrier for the vascular endothelial growth factor (VEGF) gene for treating reversible ischemia in coronary artery disease. Although the inoculation process was well tolerated, there is some controversy regarding the beneficial outcomes derived from it ([Stewart et al., 2006](#); [Kastrup et al., 2011](#)).
- **AAV vectors:** these single-stranded DNA vectors display the most favorable safety profile, and are able to maintain the transgene expression in a permanent-basis. Among the existent serotypes, AAV9 displays elevated cardiac tropism and apparently shows the strongest efficiency for cardiac delivery ([Pacak et al., 2006](#)). Similarly to what happens with the adenoviral vectors, the AAV vectors still present some immune issues that need to be addressed, for instance, the rapid vector neutralization exerted by the antibodies or the T-cell immune response ([Mingozzi and High, 2013](#)). This fact, however, was not observed in the first clinical trial administering AAV-SERCA2 vectors to heart failure patients ([Jaski et al., 2009](#)).
- **Non-viral vectors:** consist of all the other gene vectors that use a chemical or physical procedure. In contrast to viral vectors, non-viral vectors efficiency is not so high, but they are easily produced, have minimal toxicity and low immunogenicity. The main and most utilized non-viral vectors are listed below:
  - **Naked plasmid DNA:** direct delivery of DNA without any carrier, using electroporation, ultrasounds, photoporation, injection or hydroporation, among others. However, the transfection low

efficiency and the gene limited expression in the local area highly limit its application.

- **Lipid-based vectors:** the plasmid is complexed with lipids (liposomes), forming a lipoplex with a net positive charge. Although applied *in vivo* for myocardial gene transfection, transgene expression was also reported to be present in other tissues aside from the heart (Hofland *et al.*, 1997).
- **Polymer-based vectors:** in this case, the DNA forms a complex with cationic polymers, promoting interaction with cells and DNA uptake.
- **Peptides:** short peptides that electrostatically interact with the DNA, generating a strong complex that crosses the cell membrane, generally by endocytosis.
- **small interfering ribonucleic acid:** the delivery method is also based in the complexation with cationic lipids or polymers that drive the internalization of the nucleic acid.

### 6.1.3. Target genes of interest

Different genes have been considered good targets to modulate their expression for MI treatment using gene therapy.

- **Angiogenic genes:** Enhancing angiogenic gene expression is a valid strategy to increase vascular density and restore vascularization within ischemic zones, recovering the normal blood flux towards the cardiac tissue, by either vasculogenesis or angiogenesis (Zachary and Morgan, 2011). The most broadly studied gene has been VEGF, whose overexpression reported a better left ventricular function and revascularization in sheep and dog preclinical MI models (Furlani *et al.*, 2009; Vera Janavel *et al.*, 2012). Also, both FGF and hepatocyte growth factor (HGF), with pleiotropic and angiogenic properties,

have been administered through gene therapy (Heilmann *et al.*, 2003; Yang *et al.*, 2010).

- **Calcium handling proteins:** due to calcium key role in controlling the cardiac contractile cycle, supplying the defective calcium handling genes by gene therapy could be an interesting strategy to explore. One of the most claimed proteins to be targeted is SERCA2, with decreased expression in failing cardiomyocytes (Lipskaia *et al.*, 2010). Specifically, positive results were obtained in sheep MI model when SERCA2 transgene was introduced with AAV6, limiting ventricular remodeling progression (Beerli *et al.*, 2010). Regarding other promising candidate genes, phospholamban, an inhibitory protein of the contractile apparatus, has been also studied. In dominant-negative phospholamban rats that underwent MI and were rescued with wild-type phospholamban gene transfer delivered through intracoronary injection, there was an improvement in cardiac function, less fibrosis and ameliorated ventricular remodeling, even six months after the initial injection (Iwanaga *et al.*, 2004). Finally, S100A1 protein, involved in calcium handling at several nodal points including SERCA2a, is downregulated in human failing myocardium (Most *et al.*, 2007). AAV9-S100A1 gene delivery through the great coronary vein in a pig model of MI reversed left ventricular remodeling and the associated dysfunction, rescuing from the postischemic heart failure (Pleger *et al.*, 2011).
- **$\beta$ -adrenergic receptor signaling pathway genes:** one of the hallmarks of the MI and the derived end-stage heart failure is the downregulation of the  $\beta$ -adrenergic receptor signaling pathway, characterized by a dysfunction in cardiac contractility (Madamanchi, 2007). The  $\beta$ -adrenergic receptor kinase C terminus ( $\beta$ ARKct), that comprises the last 194 amino acids of the G protein-coupled receptor kinase-2, belongs to this pathway. As demonstrated by recent *in vivo* large animal studies, myocardial AAV6 delivery of  $\beta$ ARKct in infarcted swine reversed ventricular dysfunction and remodeling (Raake *et al.*, 2013). Similar benefits were obtained for a heart failure pig model when the adenylyl cyclase VI was introduced, using in this case adenovirus, to

salvage its downregulation. Upon delivery, the echocardiography data displayed an enhancement in ventricular function and a diminution in the ventricle dilation and wall stress (Lai *et al.*, 2004).

- **Gap junction genes:** the most recurrent gene here is Cx43, which forms the intercellular communications (or gap junctions) that lie in-between the cardiac cells. Uncoupling and disturbances of these connections caused by MI slow down the conduction throughout the heart, eventually ending up in mortal arrhythmias, cause of death in many MI episodes (Poelzing and Rosenbaum, 2004). Cx43 gene transfer by using adenovirus in a porcine MI model reported an increase in the conduction velocity and decreased susceptibility to tachycardia (Igarashi *et al.*, 2012).

## 6.2. Cardiac cell therapy

Cardiac cell therapy or cardiomyoplasty consists in the delivery of heterologous or autologous cardiac or proangiogenic stem cells onto the injured myocardial tissue to repair the damaged heart via active cardiac regeneration. The underlying mechanisms following myocardial repair have been widely described, ranging from the *in situ* effects exerted by the implanted cells, such as transdifferentiation into cardiomyocytes or the neovascularization; to the paracrine activity promoted by the stem cell released signals, which leads to the activation of endogenous progenitors, inhibition of apoptosis, induction of neovascularization, or modulation of ECM remodeling (Sanganalmath and Bolli, 2013) (Figure 15).

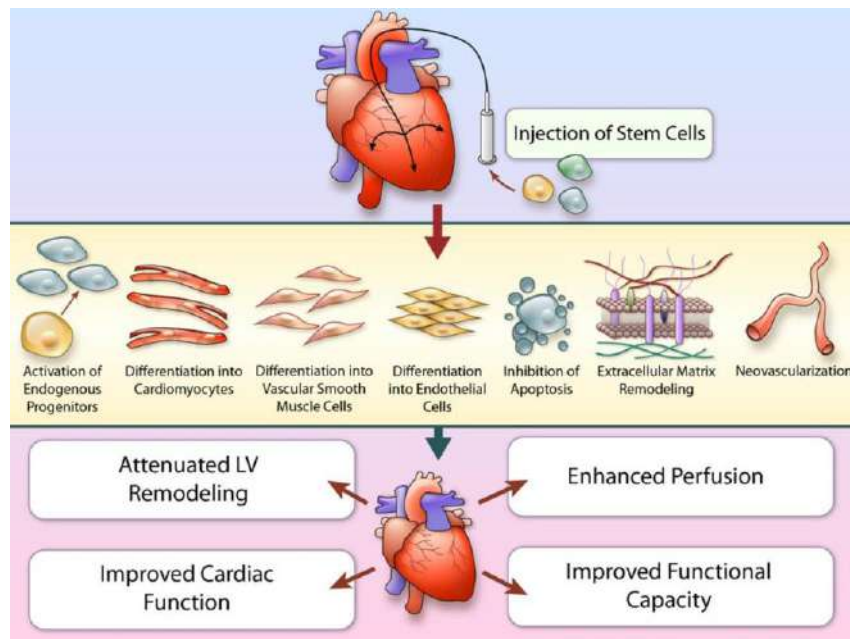


**Figure 15.** Action mechanisms of implanted stem cells in cardiac cell therapy. Scheme extracted from [Sanganalmath and Bolli, 2013](#).

The effectiveness of cellular treatment is determined by two primordial factors: the stem cell source selected for its implantation, and the cell delivery route chosen to direct the cells to the dysfunctional ventricle.

### 6.2.1. Cell sources for cardiac cell therapy

The search for the optimal cell lineage for cardiac cell therapy purposes is still ongoing, with many different cell sources evaluated and tested nowadays. The ideal cell type should fulfill these criteria: be safe; improve heart function; create new and functional cardiac muscle and vasculature, perfectly coupled with the host tissue; be amenable to be introduced through minimally invasive methods; be easily obtained and cultured *in vitro*; if non-autologous, be tolerated by the host immune system; and avoid ethical and social concerns ([Malliaras and Marbán, 2011](#)). Up to date, the most employed cell types include the following:

- **Embryonic stem cells (ESCs):** these pluripotent cells are isolated from the

blastocyst inner mass and can be easily expanded. Their main feature is the ability to differentiate to any cell lineage, including cardiomyocytes, endothelial cells and smooth muscle cells (Vittet *et al.*, 1996; Kehat *et al.*, 2001; Sinha *et al.*, 2006). The ESC-derived cardiomyocytes exhibited typical adult cardiomyocyte morphology, with proper sarcomere organization, expression of cardiac markers GATA4, Nkx2.5 and MEF2, and spontaneous contractility activity (Xu *et al.*, 2002; He *et al.*, 2003; Tomescot *et al.*, 2007). The cardiomyocyte phenotype resemblance has allowed the implantation of ESC-derived cardiomyocytes in MI *in vivo* model, resulting in heart function improvements and attenuation of ventricular remodeling (Ménard *et al.*, 2005; Caspi *et al.*, 2007). Nevertheless, their future applicability has been hindered by many rising issues, such as ethical concerns regarding their extraction from early human embryo, the formation of teratomas upon implantation, and the risk of immune rejection due to their non-autologous origin (Cai *et al.*, 2007; Nussbaum *et al.*, 2007).

- **Umbilical cord blood stem cells (UCBSCs):** UCBSCs are pluripotent cells that can be easily isolated from the umbilical cord blood with no risk for the donor. Their popularity has become greater in the latest times as they present low risk of viral infections and somatic mutations transmission, long-term cryopreservation with no cellular properties loss, and easy accessibility for storage and availability in a bank (Roura *et al.*, 2015). Moreover, their low immunogenic properties make them suitable for allogeneic transplantation (Lee *et al.*, 2014). UCBSCs spontaneously exhibited *in vitro* expression of cardiac traits, as corroborated by the identification of cardiac markers GATA4, Tbx5 and Nkx2.5 (Prat-Vidal *et al.*, 2007); but transdifferentiation towards cardiomyocytes using different protocols did not always succeed (Martin-Rendon *et al.*, 2008; Roura *et al.*, 2010). On the other hand, the vascular potential of UCBSCs seems to be clearer, as upon intravenous injection in MI mouse model they promoted angiogenesis (Ma *et al.*, 2005). Promising data in preclinical MI models in terms of infarct size reduction and ventricular function should encourage the beginning of clinical trials with UCBSCs

(Henning *et al.*, 2004; Hirata *et al.*, 2005; Ma *et al.*, 2005; Leor *et al.*, 2006).

- **Induced pluripotent stem cells (iPSCs):** generated for the first time in 2006 by Takahashi and Yamanaka, these pluripotent stem cells derive from somatic cells that are reprogrammed with viral vector transduction with four defined transcription factors (octamer-binding transcription factor 3/4, sex determining region Y-box 2, c-Myc and Kruppel-like factor 4) to dedifferentiate them towards a primitive, pluripotent state (Takahashi and Yamanaka, 2006). The application of precise, specific cardiac differentiation protocols has enabled to obtain a monolayer of iPSC-derived cardiomyocytes (Zhang *et al.*, 2009a; Karakikes *et al.*, 2014), or to differentiate the original iPSCs to other cells of interest for cardiac repair, for instance smooth muscle cells or endothelial cells (Hill *et al.*, 2010); thus circumventing the ethical controversy concerning ESCs isolation. Preclinical studies have been conducted using either undifferentiated iPSCs (Nelson *et al.*, 2009) or cardiac/vascular derived cells (Carpenter *et al.*, 2012; Xiong *et al.*, 2013); however, clinical translation is still far at present time, since issues such as teratoma formation arising from undifferentiated iPSCs, risk of arrhythmias or genetic abnormalities remain unsolved.
  
- **Adult stem cells:** undifferentiated cells that are able to maintain tissue homeostasis, regenerate tissue after damage due to their self-renewal capacity, and give rise to multiple cell types present in the body. These cells can be obtained from many different sources (e.g., adipose tissue, umbilical cord, bone marrow, skeletal muscle), and the most relevant ones employed in cardiac cell therapy are listed below:
  - **Skeletal myoblasts:** derived from satellite cells, a skeletal muscle progenitor cell population residing under myofibers basal membrane. These cells presented a contractile phenotype, availability for autologous uses, easy *in vitro* expansion, and resistance to ischemia. However, upon implantation, these cells have shown unique commitment towards skeletal myotubes, and not to cardiac muscle

fibers (Murry *et al.*, 1996), lacking gap junctions and blocked conduction, resulting in ventricular arrhythmias (Abraham *et al.*, 2005). This limitation did not discourage their use in the first clinical trial using cell therapy in patients with ischemic cardiomyopathy, the MAGIC study (Myoblast Autologous Grafting in Ischemic Cardiomyopathy; NCT not available) (Menasché *et al.*, 2001; Menasché *et al.*, 2003; Menasché *et al.*, 2008). Although injection of 871 million of skeletal myoblasts in phase I clinical trial reported some modest improvements in left ventricular ejection fraction (LVEF) and New York Heart Association functional class, lack of a control group and concomitant effects of revascularization therapy that may mask cell therapy effects suggest interpreting these data with caution (Menasché *et al.*, 2003). Even more, phase II MAGIC trial results did not prove any functional recovery in patients, and malignant arrhythmias were registered in some of them (Menasché *et al.*, 2008). Few years later, a second clinical trial, the SEISMIC trial (Safety and Effects of Implanted (autologous) Skeletal Myoblasts (myocell) using an Injection Catheter; NCT00375817), confirmed the absence of beneficial effects exerted by the autologous skeletal myoblast injection in heart failure patients (Duckers *et al.*, 2011); therefore, clinical application of skeletal myoblast therapy does not seem to be feasible.

- **Bone marrow-derived stem cells (BMSCs):** this heterogeneous population is composed of hematopoietic, endothelial and mesenchymal stem cells (MSCs), located in the red bone marrow, peripheral blood and bone marrow stroma, respectively. BMSCs have an intrinsic migratory capacity and do not elicit an adverse immune response when allotransplanted (Ferrari *et al.*, 1998; Le Blanc *et al.*, 2003). Moreover, they showed differentiation towards the endothelial and smooth muscle cell lineages, and presented typical cardiac traits (Reyes *et al.*, 2002; Bayes-Genis *et al.*, 2005b; Tamama *et al.*, 2008).



Regarding differentiation towards cardiomyocyte, there is still some controversy: despite some groups reported *in vitro* differentiation using 5-azacytidine treatment (Makino *et al.*, 1999; Xu *et al.*, 2004), *in vivo* cardiac fate determination has not been so clear under physiological microenvironment, with opposite results in mouse, sheep and dog cardiomyopathy models (Toma *et al.*, 2002; Silva *et al.*, 2005; Dixon *et al.*, 2009). Furthermore, even though differentiation towards cardiomyocytes has been described for the mesenchymal lineage (Toma *et al.*, 2002), the hematopoietic population does not transdifferentiate to cardiac lineage (Balsam *et al.*, 2004), but instead they form cardiomyocytes following cell fusion with the resident cardiomyocyte population (Nygren *et al.*, 2004). On the other hand, the bone marrow endothelial population *in vitro* differentiates to endothelial cells, but not to cardiac lineage (Shintani *et al.*, 2001). In line with this, preclinical studies have displayed the contribution of BMSCs to new blood vessel formation, by either direct differentiation to endothelial cells (Silva *et al.*, 2005; Jiang *et al.*, 2006), or through BMSC paracrine action (VEGF, HGF and other proangiogenic cytokines). Paracrine mechanisms have a greater impact on neovascularization processes by inducing endothelial progenitor cell recruitment and differentiation, and endothelial cell sprouting from preexisting vessels (Tang *et al.*, 2005; Chen *et al.*, 2013). However, BMSC promotion of vascularization was not always reflected in significant improvements in heart function (Bel *et al.*, 2003; Waksman *et al.*, 2004). Among the completed clinical trials, again, there is not a clear conclusion about BMSC potential. Intramyocardial injection of BMSCs (Perin *et al.*, 2004), or BMSC intracoronary infusion in the TOPCARE-AMI (Transplantation Of Progenitor Cells And REcovery of left ventricular function In patients with Acute Myocardial Infarction; NCT not available) and the BOOST (BOne marrOw transfer to enhance ST-elevation infarct regeneration; NCT00224536) clinical trials exerted left ventricular function improvement after five-year and six-month

follow-up, respectively (Wollert *et al.*, 2004; Leistner *et al.*, 2011). Conversely, other clinical trials following intramyocardial injection (Ang *et al.*, 2008; Yao *et al.*, 2008; Rodrigo *et al.*, 2013) or intracoronary administration (Janssens *et al.*, 2006; Ang *et al.*, 2008) failed to report substantial benefits regarding global cardiac function.

- **ATDPCs:** this multipotent population was originally isolated from rat fat pads using collagenase solution to detach them, and a centrifugation step to separate the floating adipocytes from the stromal vascular fraction, which contains the ATDPCs that are completely isolated taking advantage of their adherence to plastic once in culture (Rodbell, 1966). Since then, they have been mainly isolated from subcutaneous adipose tissue (subcutaneous ATDPCs) (Gimble *et al.*, 2007) and epicardial fat (cardiac ATDPCs), this latter with higher cardiomyogenic potential (Bayes-Genis *et al.*, 2010). Immunophenotyping of ATDPCs revealed a marker expression profile typical of MSCs (Mitchell *et al.*, 2006), while their potential to differentiate towards multiple cell lineages has been comprehensively evaluated during last years, showing capacity to generate adipocytes (Halvorsen *et al.*, 2001a), cardiomyocytes (Planat-Bénard *et al.*, 2004a), chondrocytes (Estes *et al.*, 2006), endothelial cells (Planat-Bénard *et al.*, 2004b), hepatocytes (Xu *et al.*, 2014), myocytes (Mizuno *et al.*, 2002), neurons (Safford *et al.*, 2002), osteoblasts (Halvorsen *et al.*, 2001b) and pancreatic cells (Lee *et al.*, 2008). Specifically, their cardiomyogenic potential was further demonstrated when implanted ATDPCs in mouse MI model expressed cardiac markers cTnI, Nkx2.5 and myosin heavy chain (Strem *et al.*, 2005). Furthermore, their immunosuppressive properties permit their utilization for allogeneic purposes (Puissant *et al.*, 2005). Cardioregenerative and angiogenic capacity of ATDPCs was successfully proven in preclinical studies, with notable improvements regarding vascularization, function preservation and infarct progression in mouse (Leobon *et al.*, 2009;

Bayes-Genis *et al.*, 2010), rat (Cai *et al.*, 2009; Bayes-Genis *et al.*, 2010) and pig MI models (Valina *et al.*, 2007; Rigol *et al.*, 2010). So far, the unique clinical trial concerning MI with published data is the APOLLO trial (AdiPOse-derived stem ceLLs in the treatment of patients with ST-elevation myOcardial infarction; NCT00442806), a double-blind, randomized, and placebo-controlled study. It revealed that, six months following intracoronary administration of ATDPCs, patients displayed a 4% improvement in LVEF, a 50% reduction in infarct size and amelioration of perfusion defects (Houtgraaf *et al.*, 2012).

- **Resident cardiac stem cells or CPCs:** found in the adult heart, represent approximately the 40% of the mature heart cellular content, generated postnatally (Bergmann *et al.*, 2009). Depending on their surface marker pattern, their origin, ability to form spheroids in culture and to efflux fluorescent dye, they can be classified into: c-kit<sup>+</sup>-cells (Bearzi *et al.*, 2007), cardiospheres and cardiosphere-derived cells (Messina *et al.*, 2004; Smith *et al.*, 2007), Sca-1<sup>+</sup>-cells (Oh *et al.*, 2003), Islet-1<sup>+</sup>-cells (Laugwitz *et al.*, 2005), side population cells expressing ATP-binding cassette transporter marker (Martin *et al.*, 2004) and epicardial-derived cells (Zhou *et al.*, 2008). These cells were able to differentiate into cardiomyocyte lineage, both *in vitro* under specific conditions, and when implanted *in vivo*, showing spontaneous beating; in addition to differentiation to endothelial cells and cardiac fibroblasts (Oh *et al.*, 2003; Martin *et al.*, 2004; Matsuura *et al.*, 2004). The identification of a resident cardiac population within the adult heart led to different strategies to trigger heart repopulation following injury, ranging from activation of CPCs with the introduction of thymosin beta 4 (Bock-Marquette *et al.*, 2004; Smart *et al.*, 2007), or the *ex vivo* propagation of the isolated CPCs and subsequent implantation into the damaged tissue (Smith *et al.*, 2007; Oskouei *et al.*, 2012). Despite the exciting results reported by the CADUCEUS (CArdiosphere-Derived aUtologous stem CElls to reverse ventricUlar

dysfunction; NCT00893360) clinical trial using cardiosphere-derived cells after one-year follow-up (Malliaras *et al.*, 2014), further characterization of these cells is required before moving forward to next trials. Some recent works claim that c-kit<sup>+</sup> cells did not differentiate to cardiomyocytes (Tallini *et al.*, 2009; Zaruba *et al.*, 2010), but they fuse with resident cardiomyocytes (Oh *et al.*, 2003); while others indicate that Islet-1 and c-kit cannot be considered exclusive CPC markers, as they have been also found in cardiac neural crest cells (Weinberger *et al.*, 2012) and endothelial cells, respectively (van Berlo *et al.*, 2014; Sultana *et al.*, 2015). Also, their role in development, homeostasis, aging and reaction to injury must be elucidated to understand the underlying mechanisms of CPC function (Laflamme and Murry, 2011).

### **6.2.2. Cell delivery routes**

Several strategies have been followed to administer cells to the injured heart in the latest years (**Figure 16**). The most used methods have been the intracoronary route (Llano *et al.*, 2009), the endomyocardial route (Hashemi *et al.*, 2008), the intramyocardial injection, administered directly (Hamano *et al.*, 2001) or using either an epicardial approach via sternotomy (Mathiasen *et al.*, 2012) or transendocardial minimally invasive procedure (Fuchs *et al.*, 2006) via catheter, and finally, the intravenous route (Halkos *et al.*, 2008).

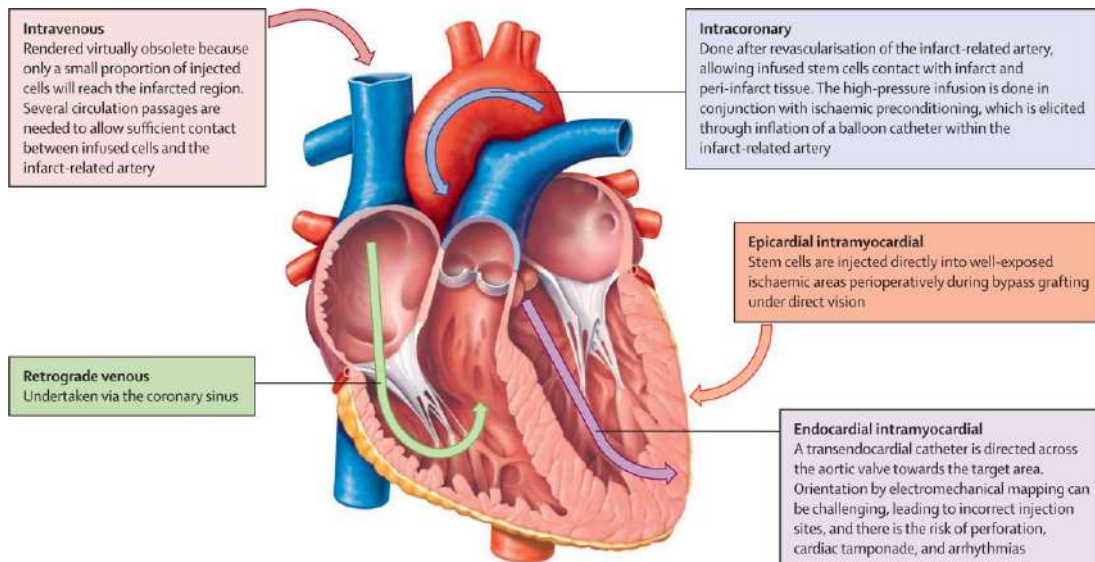


**Figure 16. Cell delivery routes.** Image reproduced from Windecker *et al.*, 2013.

To elucidate the optimal way to deliver cells in terms of safety, feasibility and cell retention in the target organ or tissue, different studies have been conducted evaluating their corresponding effectiveness. Comparative examinations between the different routes suggested better cell retention and increased neovascularization for the intracoronary delivery compared to intravenous and endocardial routes (Freyman *et al.*, 2006; Rigol *et al.*, 2010). However, intracoronary administration was also associated with a higher incidence of decreased coronary blood flow (Freyman *et al.*, 2006). On the other hand, opposite results were obtained in a third comparative study, where initial cell retention was lower than 3% after intracoronary delivery, whereas it reached an 11% following intramyocardial route (Hou *et al.*, 2005). Moreover, both the intracoronary and intravenous routes showed almost half of the delivered cells localized in the lungs, representing a considerable off-target number of cells compared to the 26% for the intramyocardial delivery (Hou *et al.*, 2005). Nevertheless, most cells died 48 hours after administration with the intramyocardial route, indicating poor survival rate (Li *et al.*, 2009), and presence of cells was also detected in other organs, such as liver, spleen or kidney (Hou *et al.*, 2005).

In line with cell retention, a recently published meta-analysis analyzed the effects in heart function based on the cell delivery route (transendocardial,

intramyocardial, intracoronary and intravenous) for preclinical MI swine model and 6 clinical trials (334 patients in total). In swine, the transendocardial administration was the only strategy that promoted infarct size reduction and improvements in LVEF (for this latter, intravenous and intramyocardial methods also registered better LVEF parameter). For humans, both transendocardial and intravenous routes reported LVEF; thus, evoking that, in global terms, transendocardial delivery route is superior to the rest of administration routes (Kanelidis *et al.*, 2017).

### **6.3. Cardiac tissue engineering**

Despite recent advances in cardiomyoplasty, there are some limitations that remain unsolved. Firstly, regardless of the delivery route employed, cell adhesion and survival have resulted to be very low, with less than 10% of cell engraftment and an elevated death rate (Hou *et al.*, 2005), most likely due to the adverse microenvironment conditions (hypoxia, loss of mechanical properties and inflammation) created within the necrotic scar (Boudoulas and Hatzopoulos, 2009). Secondly, the use of specific cell types still has some concerns. For instance, skeletal myoblasts produced arrhythmias upon administration due to the lack of electromechanical coupling (Siminiak *et al.*, 2004), or the formation of teratomas directly related to the undifferentiated state of ESCs (Cao *et al.*, 2007). Finally, results derived from cell therapy clinical trials should be taken with caution. A meta-analysis comprising 12 randomized clinical trials in the context of MI treatment using cell therapy administered via intracoronary, revealed a lack of improvement regarding clinical events or LVEF (Gyöngyösi *et al.*, 2015). For all these reasons exposed, new therapeutic strategies to overcome these hurdles are being developed, such as cardiac tissue engineering.

Tissue engineering was originally defined by Langer and Vacanti as “an interdisciplinary field that applies the principles of engineering and the life sciences toward the development of biological substitutes that restore, maintain, or improve tissue function” (Langer and Vacanti, 1993). In the context of cardiac tissue

engineering, its actions are specifically focused on the regeneration of damaged myocardial tissue, combining different cell populations with intrinsic regenerative capacity along with a cellular supportive material (biological and/or synthetic materials), and growth factors, cytokines, proangiogenic factors or other peptides. For the cellular supportive platform, it is mandatory that accomplishes the following requirements: to mimic the physiological myocardial microenvironment favoring cell nesting and differentiation; to resemble the three-dimensional structural organization and micro/macroscale stiffness; to vascularize upon engrafted ensuring enough nutrient and oxygen flow to the cells; to match electromechanical requirements enabling proper host tissue coupling; to be biocompatible and biodegradable; and to boost cell survival and adhesion (Vunjak-Novakovic *et al.*, 2011). The rationale of these criteria is based on the role of the cardiac ECM, the non-cellular, physiological dynamic architectural network consisting of structural and nonstructural proteins that confers biochemical and mechanical support to the cells within the myocardium. The cardiac ECM regulates, through different released signals, cell behavior, interconnection, alignment for a proper contraction, and facilitates electrical conduction and force transduction (Li *et al.*, 2014; Valiente-Alandi *et al.*, 2016). So, recreating the physiological ECM should provide the embedded cells with the necessary cues for their proper adhesion, survival and differentiation, and ease the electromechanical connection of the whole construct.

### 6.3.1. Cardiac tissue engineering strategies

Cardiac tissue engineering does not always require of an exogenous natural or synthetic matrix, either a hydrogel or a scaffold. This alternative option, the scaffold-free approximation, seeks to create a monolayer cell sheet or patch sustained over their own synthesized ECM (Shimizu *et al.*, 2002). Next, current approaches tested lately are described (**Figure 17**):

- **Monolayer cell sheets:** this scaffold-free option was initially developed by Okano and collaborators, detaching cell cultures of both endothelial cells and

hepatocytes from culture dishes, whose surface was coated with the thermosensitive polymer Poly(N-isopropylacrylamide), lowering temperature and obtaining a cell monolayer (Okano *et al.*, 1995). Later improvements allowed the generation of a cell sheet showing a three-dimensional architecture based on individual cell monolayers alignment and stacking, ready to be engrafted within the damaged tissue. With this methodology, layered or three-dimensional cell sheets were obtained with rat cardiomyocytes, generating a contractile construct whose survival was maintained for up to twelve weeks (Shimizu *et al.*, 2002), with conserved Cx43 to establish cell intercommunication and facilitate electrical signal propagation (Haraguchi *et al.*, 2006), and vascularized in two days once subcutaneously engrafted in nude rats (Shimizu *et al.*, 2006). In comparison with single intramyocardial cell injection, cardiac cell sheet transplantation promoted a higher cell retention and survival (Matsuura *et al.*, 2009; Sekine *et al.*, 2011), as well as triggered higher levels of vascularization and cardiac recovery after MI (Sekine *et al.*, 2011). In this context of cardiac regeneration post-MI, not only cardiomyocyte-based cell sheets have been built up, but many other cellular lineages have been used in preclinical models: myoblasts (Sekiya *et al.*, 2009), ATDPCs (Miyahara *et al.*, 2006), adipocytes (Imanishi *et al.*, 2011), Sca-1<sup>+</sup>-CPCs (Matsuura *et al.*, 2009), cardiomyocytes derived from iPSCs (Kawamura *et al.*, 2012), and cardiomyocytes, endothelial cells and mural cells differentiated from ESCs (Masumoto *et al.*, 2012). All of them resulted in cardiac function improvements and vasculogenesis promotion, most likely due to the reported upregulation of angiogenic factors HGF and VEGF. Nowadays, the main challenge to overcome for clinical translation is the 80  $\mu\text{m}$ -thickness limitation for layered cell sheet generation (Shimizu *et al.*, 2006), that would limit oxygen diffusion and nutrient supply. In this regard, new methods are being investigated to develop thicker layered cell sheets based on intercalated vascular beds (Sakaguchi *et al.*, 2015).

- **Hydrogels:** the hydrogels, the first scaffold-based approach, are defined as water-swollen polymer networks whose water high content, porosity and



diffusivity, possibility of creating biocompatible material based-hydrogel, and tunable chemical and physical properties convert them into an optimal cell platform for cardiac regeneration (Shapira *et al.*, 2008). Hydrogels were first used to maintain avian skeletal myotubes attachment, seeding them over a collagen gel to avoid premature detaching (Vandenburgh *et al.*, 1988), and since then, they have been employed for cell (Birla *et al.*, 2005) or growth factor delivery (Ruvinov *et al.*, 2011), and prepared themselves as cardiac patches (Dvir *et al.*, 2011). Initially, the main inconvenient for hydrogels was the administration through direct injection, which drastically diminished cell survival because of the elevated pressure exerted (Hasan *et al.*, 2015). To overcome this hurdle, cells were embedded within a hydrogel *ex vivo*, which allowed delivery of the created construct in a safer, minimally invasive catheter system (Singelyn *et al.*, 2012).

The election of the hydrogel biomaterial is essential, as they drive many cellular processes such as differentiation, growth, maturation and organization, apart from determining their biodegradability and toxicity of their derived products (Leor *et al.*, 2005). Biomaterial choice options include natural materials (collagen, fibrin, alginate, hyaluronic acid or gelatin, among others) and synthetic materials, for instance, polyacrylic acid, polyethylene oxide, polyurethane, polyacrylamide and polyvinyl alcohol (Hasan *et al.*, 2015), each of them with their own advantages and drawbacks. Natural materials are usually more biodegradable and biocompatible, with no generation of toxic side products, and can provide unique biological cues due to its specific composition, but the lack of malleability of their inherent physicochemical properties limits their applicability. On the other hand, synthetic materials mechanical, biological and chemical properties can be easily modulated and controlled throughout the hydrogel synthesis process, tailoring a hydrogel with predesigned parameters that can match native environment (Shoichet, 2010). Therefore, it seems more appropriate and suitable to combine the properties of both types of materials, thus generating a hybrid natural/synthetic hydrogel that displays the advantages of both

components (Li and Guan, 2011).

- **Natural or synthetic matrices:** matrices, the second scaffold-based strategy, are prefabricated porous and solid materials that aim to mimic the natural and native cardiac ECM. Thus, cells are provided with the initial biological and mechanical support, and eventually it is degraded and replaced by the new cell-synthesized ECM. Matrices can also be distinguished between natural and synthetic depending on the biomaterial source (Sarig and Machluf, 2011; Hirt *et al.*, 2014). On the one hand, natural matrices made of collagen (Chachques *et al.*, 2008), fibrin (Xiong *et al.*, 2011), alginate (Leor *et al.*, 2000), gelatin (Li *et al.*, 1999), chitosan (Pok *et al.*, 2014) and Matrigel (Laflamme *et al.*, 2007) have been tested for treating MI. Inside the natural matrices class, we can also find the decellularized matrices, with special interest in pericardium- (Gálvez-Montón *et al.*, 2015) and myocardium-derived decellularized matrices (Wassenaar *et al.*, 2016), obtained after eliminating all the tissue cellular population while preserving the ECM (Sarig and Machluf, 2011). On the other hand, several synthetic polymers have been already used: polyglycolic acid, polylactic acid (PLA) (Kellar *et al.*, 2005), polyurethane (Siepe *et al.*, 2006) or poly(lactide-co- $\epsilon$ -caprolactone) (Jin *et al.*, 2009), among others. To take advantage of material properties, a new technique, the bioprinting, is emerging to create multilayered matrices with total control of micro- and macrostructure, as well as the porosity, employing different materials and cells as bioink to print the three-dimensional scaffold (Duan, 2017). This technology has enabled the synthesis of both alginate (Gaetani *et al.*, 2012) and polyester urethane (Gaebel *et al.*, 2011) bioprinted matrices, patterned as previously computer-designed, with a defined framework and microenvironment. A recent study in mouse MI model using bioprinted, native-like scaffolds, refilled with cells, demonstrated function improvement and promotion of vascularization (Gao *et al.*, 2017). Hence, acquisition of myocardial ECM properties and composition knowledge may speed up the generation of matrices through bioprinting, accurately selecting the materials and precisely reproducing mechanical and structural parameters.

- **Whole decellularized heart:** as mentioned before and tightly related to natural scaffold approach, decellularization procedures allow the removal of the cellular content, leaving only the cardiac ECM that can support cell perfusion. First decellularized heart was generated by Ott and collaborators, through coronary perfusion of the rat cardiac organ with detergents. The acellular heart was then reperfused with either cardiac or endothelial cells and maintained within a bioreactor that recapitulated physiological cardiac conditions. By day 4, macroscopical contractions were evident, and by day 8, the reseeded heart could generate a weak contractile pump force (Ott *et al.*, 2008). Since then, whole porcine (Weymann *et al.*, 2011) and human hearts (Johnson *et al.*, 2016) were also successfully decellularized; and in-depth ECM characterization showed preservation of microvasculature, structure and protein profile, conserving the physiological cardiac microenvironment (Guyette *et al.*, 2016; Johnson *et al.*, 2016). Moreover, different cell administration perfusion routes have been tested with endothelial cells to find out the optimal delivery path for heart recellularization: through brachiocephalic artery, retrograde artery, or inferior vena cava combined with brachiocephalic artery infusion; and was this latter the one which showed the best results in terms of lower thrombogenicity and enhanced contractility (Robertson *et al.*, 2014). The use of other cell sources for repopulation also reported promising results. Indeed, whole decellularized human hearts recolonized with human iPSC-derived cardiomyocytes resulted in contractile organs, with electrical conductivity, left ventricular pressure development and metabolic function (Guyette *et al.*, 2016). Similar results were obtained using not only iPSC-derived cardiomyocytes, but also iPSC-derived endothelial cells and smooth muscle cells (Lu *et al.*, 2013). Interestingly, the generated recellularized cardiac organ was responsive to drugs, emerging as a novel *in vitro* model for specific drug testing with accurate physiological conditions recreation (Lu *et al.*, 2013).

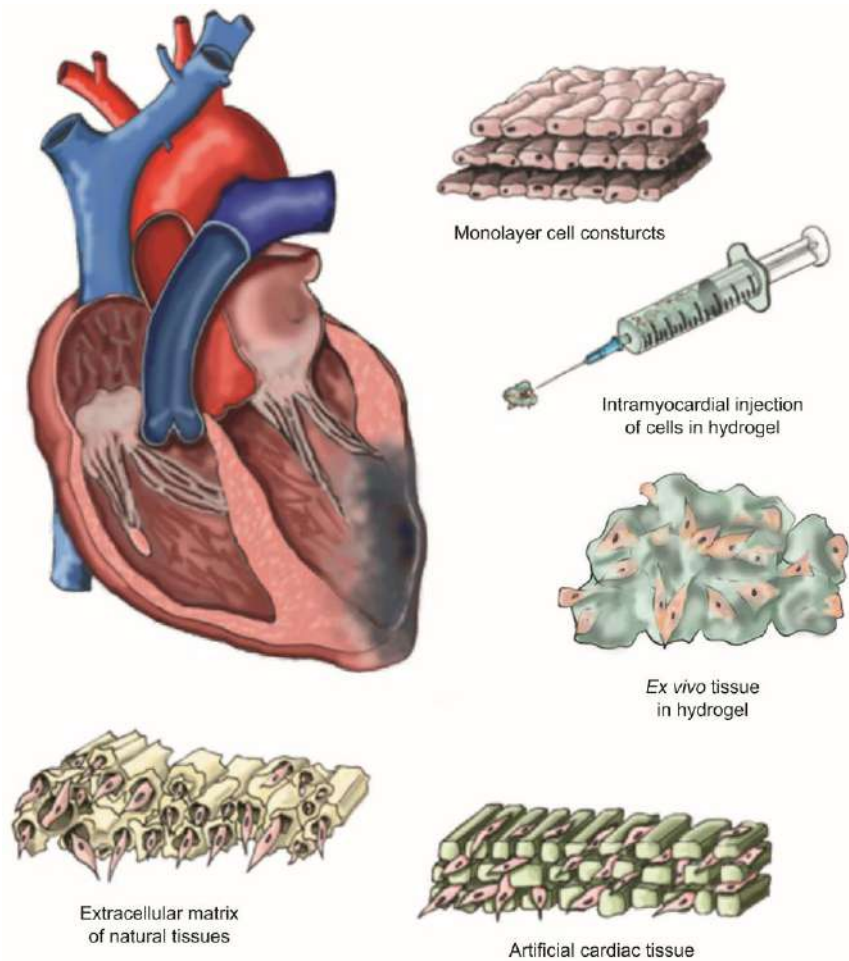


**Figure 17.** Cardiac tissue engineering approaches. Drawing summarizing the main current cardiac tissue engineering strategies for treating MI. Image obtained from [Gálvez-Montón et al., 2013](#).

### 6.3.2. Scaffold materials

For the scaffold-based approximations, namely hydrogels and matrices, it is primordial to choose wisely the scaffold material in order to reproduce the cardiac ECM and match its physiological properties. Based on their origin, they can be classified as natural or synthetic materials. Generally, the biomaterials are used alone, forming a uniform scaffold, but they can be generated as a combination of both natural and synthetic materials, forming a hybrid scaffold which gathers the advantages of both components ([Rane and Christman, 2011](#)). Below, a description of the most employed materials in cardiac tissue engineering for MI repair is provided.

### 6.3.2.1. Natural materials

As it has been briefly exposed in the previous section, using scaffolds composed of natural materials displays a series of advantages. First, they tend to be more biodegradable and biocompatible with the host organism, ensuring reabsorption and elimination of the matrix via the excretory system with no harmful derived products. Second, the high biodegradability enables quick scaffold turnover, substituting the initial implanted scaffold for the ECM excreted by the introduced cells. Finally, the unique protein composition better resembles that present in the native cardiac ECM, simulating and recreating the environment necessary for the cellular-ECM crosstalk (Chen *et al.*, 2008b; Shoichet, 2010; Vunjak-Novakovic *et al.*, 2010; Vunjak-Novakovic *et al.*, 2014). On the contrary, inability to control or modulate inherent properties and high variability among samples appear as the main drawbacks to overcome (Sarig and Machluf, 2011). Nowadays, natural materials to build up cardiac scaffolds have been extensively used, highlighting the following ones with better outcomes and/or widespread application:

- **Collagen:** is the predominant component of the mammalian cardiac ECM, and provides structural and mechanical support for tissue integrity sustainability, as well as specifically contributes to the individuality and uniqueness of the ECM (Gelse *et al.*, 2003). The main advantages of collagen-based scaffolds are their high biocompatibility, easy degradation by endogenous collagenases, involvement in many cellular activities (i.e. attachment, proliferation and migration) and thermal reversibility (Hasan *et al.*, 2015). On the other hand, the major limitation is their low inherent stiffness, but it can be increased with chemical modification through glutaraldehyde crosslinking (Chandran *et al.*, 2012). First use of collagen scaffolds was reported in 1988, when Vandeburgh and collaborators seeded avian skeletal myotubes over a collagen hydrogel, and as a result, contractility was prolonged and structural characteristics maintained (Vandeburgh *et al.*, 1988). Next steps were headed to generate contractile collagen matrices repopulated with cardiomyocytes to *in vitro* recreate cardiac physiological conditions (Souren

*et al.*, 1992; Eschenhagen *et al.*, 1997). From this point, the use and applications of collagen scaffolds took off. The first engineered heart tissues were designed based on collagen ring-shaped scaffolds mixed with Matrigel and combined with cardiomyocytes. These constructs recreated some of the native cardiac tissue traits: contractility at a physiological electrical pace of 1 Hz, organized sarcomeres, gap junctions, a basement membrane surrounding cells and sensitivity to calcium (Zimmermann *et al.*, 2000; Zimmermann *et al.*, 2002b). *In vivo* engraftment of engineered heart tissues in rat MI model showed vascularization of the scaffold within the host tissue, an organized heart muscle structure, preserved contractility, electrical coupling and cardiac function enhancement (Zimmermann *et al.*, 2002a; Zimmermann *et al.*, 2006). Since then, several advances have been done using different combinations of collagen scaffolds with cells and growth factors to treat MI, for instance, ATDPCs (Araña *et al.*, 2014), BMSCs (Maureira *et al.*, 2012), CPCs (Shi *et al.*, 2011) or VEGF (Gao *et al.*, 2011). The previous results opened the door for the first clinical trial in humans, the MAGNUM (Myocardial Assistance by Grafting a New bioartificial Upgraded Myocardium; NCT not available) study. Here, 10 patients suffering from myocardial ischemia were treated with a type-I collagen scaffold embedded with autologous BMSCs, and compared to control patients who only received BMSCs. Ten months later, no death events were recorded, and the scaffold-treated patients experienced an enhancement in left ventricular end-diastolic volume and deceleration time, and showed an increased scar area thickness; apart from a better LVEF, common to both study groups (Chachques *et al.*, 2007; Chachques *et al.*, 2008).

- **Fibrin:** this fibrous, non-globular protein, derived from fibrinogen truncation, is involved in many different blood clotting and wound healing processes, by macrophage recruitment to the injury site. Also, it plays an important role in cell-matrix interactions and inflammatory responses (Mosesson *et al.*, 2001). Aside from its high biodegradability and biocompatibility, fibrin displays two main advantages that recommend its use as scaffold: it can be isolated from

each own patient blood, which enables autologous administration, preventing an adverse immunological host response; and its matrix density, rheological properties, mechanical strength and structure can be easily modulated by proper adjustment of fibrinogen starting concentration and/or polymerization rate (Ye *et al.*, 2000; Linnes *et al.*, 2007; Rowe *et al.*, 2007). The favorable features of fibrin led to the use of fibrin scaffolds to treat MI. Cell retention, increase of angiogenesis and improvement of heart function were achieved when fibrin scaffolds were implanted in preclinical MI models repopulated with different types of cells, such as UCBCs (Roura *et al.*, 2012), ATDPCs (Bagó *et al.*, 2013), BMSCs (Nakamuta *et al.*, 2009) or ESCs (Xiong *et al.*, 2011). Moreover, these scaffolds did not only support cell embedding, but also they were satisfactorily supplemented with chemokines (Zhang *et al.*, 2007), electromechanically-trained cells (Llucà-Valldeperas *et al.*, 2017), or even mixed with either other natural compounds (Godier-Furnémont *et al.*, 2011) or synthetic polymers (Zhang *et al.*, 2007), with promising outcomes regarding cell behavior and heart function recovery. Currently, a phase I clinical trial, the ESCORT (transplantation of Embryonic Stem Cell-derived prOgenitors in severe heart failure; NCT02057900) study, has been approved to test the safety, feasibility and effectiveness of human ESCs embedded within a fibrin scaffold (Menasché *et al.*, 2015). This clinical trial is currently recruiting patients, and to date, no results have been published.

- **Chitosan:** a natural polymer obtained by chitin deacetylation, widely employed for tissue replacement purposes (Guzmán *et al.*, 2014; Revi *et al.*, 2014). Chitosan displays a high biodegradability and biocompatibility, and its capacity to combine with conductive materials helps to improve electrical conductivity, especially important for electrical coupling with the cardiac host tissue (Martins *et al.*, 2014). Also, chitosan hydrophilicity facilitates growth factor retention, resulting in an enhanced, synergistic actuation of scaffold, cells and growth factors (Tsuchiya *et al.*, 2014). Chitosan scaffold specific role in MI has been assessed in two different scenarios. First, in an *in vitro* MI-simulating milieu with reactive oxygen species, a chitosan scaffold embedded

with ATDPCs improved cell attachment and survival. Second, translating these findings into an *in vivo* rat MI environment, the injection of the chitosan-ATDPC construct also reported endogenous cell homing, neovascularization, infarct size diminution and cardiac function improvement (Liu *et al.*, 2012). In line with this study, another work conducted by Wang and collaborators demonstrated the potential of chitosan to direct cardiac differentiation of ATDPCs, as indicated by the increased cardiac marker profile of the ATDPCs seeded in the chitosan scaffold, suggesting chitosan capacity to namely modulate cell fate towards cardiac lineage (Wang *et al.*, 2014). Moreover, preclinical studies carried out in MI animal models demonstrated chitosan beneficial effects in terms of heart recovery and infarcted zone vascularization (Lu *et al.*, 2009; Wang *et al.*, 2010b; Wang *et al.*, 2014).

- **Alginate:** the anionic linear polysaccharide alginate has been extensively used to create scaffolds through an ionic crosslinking process with divalent cations (Bidarra *et al.*, 2014). This fabrication system allows modifying the intrinsic alginate stiffness by simply changing the crosslinking agent (Augst *et al.*, 2006). Moreover, the alginate by itself is not capable of eliciting an immune response in the host system (Ménard *et al.*, 2010), and it is able to retain the incorporated cells and proteins within its matrix structure (Wang *et al.*, 2012b). Prior works performed in rat (Landa *et al.*, 2008), dog (Sabbah *et al.*, 2013) and swine MI models (Leor *et al.*, 2009) revealed significant improvements in heart recovery; however, a discordant study showed that the administration of combined alginate scaffolds with ESCs did not report so beneficial effects, in terms of cell retention within the scarred region and ventricular function (Leor *et al.*, 2007). These negative results have not discouraged the initiation of the first clinical trial with alginate in patients with dilated cardiomyopathy, the AUGMENT-HF study (A randomized, controlled study to evaluate ALGisyl-LVR™ as a Method of Left ventricular augmentation for Heart Failure; NCT01311791). Results from the primary endpoints after six-month follow-up showed an increase in exercise capacity and clinical status, and a tendency to improve clinical symptoms (Anker *et al.*, 2015).



These positive effects were confirmed by the one-year follow-up outcomes, as well as the safety and feasibility of alginate administration (Mann *et al.*, 2016).

- **Hyaluronic acid:** hyaluronic acid is an unbranched, non-sulfated glycosaminoglycan of the ECM that plays an important role in wound healing, regulation of cell behavior and attachment, matrix organization, angiogenesis promotion, suppression of fibrosis and inflammatory responses (Prestwich, 2011). It presents a high biodegradability, biocompatibility, capability of retaining water and adequate rheological properties (Yoon *et al.*, 2009); and its main inconvenient, the poor mechanical properties of hyaluronic acid native form, can be solved with the use of different crosslinkers to induce chemical modifications (Bonafè *et al.*, 2014). Altogether, hyaluronic acid gathers the necessary characteristics that enables its utilization for MI treatment. Accordingly, the implantation of a hyaluronic acid scaffold, with no cells or proteins added, led to significant improvements in vascularization, infarct size, cellular apoptosis and heart function in a rat MI model (Yoon *et al.*, 2014). When engrafted along with cells, it also resulted in similar improvements, regardless of the cell source or the MI animal model tested (Chen *et al.*, 2013; Muscari *et al.*, 2013; Chen *et al.*, 2014). So far, no clinical trials have started yet, but the positive results obtained should pave hyaluronic acid scaffold road to the clinics.
- **Matrigel:** this biomaterial is derived from the ECM secreted by Engelbreth-Holm-Swarm mouse sarcoma cells (Li and Guan, 2011). Even though its exact molecular composition has not been fully scrutinized, it is known that it includes laminin, type-IV collagen, entactin, heparan sulfate proteoglycan and growth factors, which resembles and mimics the myocardial native ECM. This heterogeneous composition regulates cell attachment, differentiation and proliferation (Ou *et al.*, 2011). Besides, both *in vitro* and *in vivo*, it has been demonstrated the Matrigel angiogenic potential (Huang *et al.*, 2005). *In vivo*, Matrigel scaffold administration with no cell refilling was enough to promote vascularization of the injured myocardium, as well as improvements in heart

function and contractility and endogenous cell recruitment increase (Ou *et al.*, 2011). Similarly, Matrigel scaffold filled with either ESC-derived cardiomyocytes or undifferentiated ESCs also triggered heart recovery (Kofidis *et al.*, 2004; Laflamme *et al.*, 2007). However, no positive effects were observed when BMSCs were used (Wall *et al.*, 2010), and, in comparison with collagen and fibrin, Matrigel did not elicit any additional benefit, apart from increased vascularization that fibrin and collagen also did (Huang *et al.*, 2005). Therefore, further studies may be required to completely elucidate the functional impact of Matrigel in MI recovery.

- **Decellularized ECM:** the ECM, the non-cellular component of tissues, is a dynamic mixture of structural and functional molecules synthesized by the tissular cells, which acts as a cellular supportive microenvironment, releasing the necessary signals to guide cell proliferation, attachment, differentiation, migration and viability (Badylak *et al.*, 2011). In this context, the extraction of an intact ECM matching the myocardial ECM properties, or the myocardium ECM itself, would provide an appropriate milieu of great utility as a cellular scaffold (Sarig and Machluf, 2011). For ECM isolation, it is necessary a process known as decellularization, a combination of enzymatic, chemical and/or physical procedures, to remove all the nuclear and cellular content while preserving the physiological ECM. Selection of the decellularization agents is primordial, as each of them has negative and/or disruptive effects over the architecture, composition and mechanics of the ECM; thus, the sequential or combinatorial use of them should pursue the maximal preservation of ECM properties (Crapo *et al.*, 2011). Among them, the most important characteristic to maintain is the three-dimensional framework, as its correct organization influences cell adhesion, differentiation and survival (Badylak *et al.*, 2011; Crapo *et al.*, 2011). Since the first organ decellularization was conducted by Ott and collaborators to generate an acellular heart that was subsequently recellularized with cardiac and endothelial cell populations (Ott *et al.*, 2008), many other tissues and organs have been decellularized: heart valves, myocardium, pericardium, lung, pancreas, kidney, liver, mammary

gland, nerves, urinary bladder and small intestinal submucosa (Crapo *et al.*, 2011; Song and Ott, 2011). From these options, the last two non-cardiac ECMs, urinary bladder and small intestinal submucosa matrices, have been successfully administered *in vivo* for MI repair, reporting benefits concerning heart contractility and function (Potapova *et al.*, 2008; Okada *et al.*, 2010). On the other hand, the cardiac-related pericardial ECM, a porous material easily obtained after cardiac surgery that favors cell retention and vascularization, also showed better cardiac function, smaller infarct size, a limited fibrosis progression limitation and vessel density increase (Wei *et al.*, 2008; Gálvez-Montón *et al.*, 2015). Moreover, the use of decellularized pericardium has been approved by the Food and Drug Administration for stent covers, dural grafts, prosthetic valve materials and soft tissue defects repair (Seif-Naraghi *et al.*, 2010). Finally, local administration of myocardial ECM, the best match for native cardiac ECM, led to significant improvements in terms of ventricular function, fibrosis regression, infarct size reduction and promotion of angiogenesis (Dai *et al.*, 2013; Wassenaar *et al.*, 2016). These results set the starting point for a clinical trial using small intestinal submucosa (CorMatrix) (Restore Myocardial Function With CorMatrix<sup>®</sup> ECM<sup>®</sup> Particulate; NCT02139189), which has already completed the follow-up, although the final results have not been published yet.

### **6.3.2.2. Synthetic materials**

In contrast with natural materials, synthetic polymers generally present a lower inherent biodegradability capacity and biocompatibility with the host organism, but have a robust manufacturing capacity, which translates into a precise control of biochemical, physical and biological scaffold features. The ability to generate synthetic materials with exactly the same features enables mass production and standardization, reducing intersample variability (Sarig and Machluf, 2011). Moreover, the addition of bioactive molecules can help to improve their poor cellular

adhesion and survival (Vunjak-Novakovic *et al.*, 2010). These advantages encouraged the administration of several synthetic materials for post-MI recovery, such as polyurethane (Siepe *et al.*, 2006; Siepe *et al.*, 2007), poly(N-isopropylacrylamide) (Li *et al.*, 2010b) or polyester urethane urea (Fujimoto *et al.*, 2007). Up to date, the only four synthetic materials approved by the Food and Drug Administration for clinical purposes have been polyethylene glycol (PEG), PLA, poly(lactic-co-glycolic) acid (PLGA), and polycaprolactone (PCL), detailed below (Li and Guan, 2011; Reis *et al.*, 2016):

- **PEG:** this water-soluble polymer is synthesized following a ring-opening polymerization process of the ethylene oxide, but it is its gel phase obtained under UV irradiation photo-polymerization of diacrylate-modified PEG the final product employed as scaffold. Contrary to what happens with most of the synthetic materials, PEG displays a high biocompatibility and an inert surface that contributes to avoid triggering of adverse immune response in most cases (Li and Guan, 2011). The main disadvantage of PEG is its intrinsically low protein adsorption, which negatively affects cellular processes such as adhesion, viability and cell-matrix crosstalk. This issue, however, can be corrected by the conjugation of adhesive peptides or the incorporation of growth factors to reinforce cell retention and prolong cell survival, as it was demonstrated with the conjugation of the RGD-peptide in PEG scaffolds, which highly increased cardiomyocyte viability (Jongpaiboonkit *et al.*, 2008). Besides, when embryonal carcinoma cells were encapsulated *in vitro* within a PEG hydrogel, these were committed towards a cardiac lineage, particularly when the scaffold stiffness was softer (Kraehenbuehl *et al.*, 2008). Nevertheless, the *in vivo* assessment in MI models did not show a clear response about PEG effects. While the injection of PEG scaffold with encapsulated BMSCs promoted angiogenesis, cell retention, prevention of scar expansion, attenuation of left ventricular dilation and improvement of LVEF (Wang *et al.*, 2009a), the administration of the scaffold itself was only able to reduce left ventricular end-diastolic diameter four weeks post-MI. Unfortunately, these short-term benefits were not maintained thirteen weeks

following MI induction, and macrophage-associated inflammation was observed in treated animals (Dobner *et al.*, 2009). Here, the scaffold administration timing seems to be a key parameter, as a later study demonstrated that delivery of PEG scaffold one week following MI elicited a beneficial recovery response (Kadner *et al.*, 2012), contrary to what happened when injected just immediately after MI was induced (Dobner *et al.*, 2009; Kadner *et al.*, 2012).

- **PLA:** it is obtained through the polymerization of lactic acid monomers, following many different methods: polycondensation, lactide ring opening polymerization, azeotropic dehydration or enzymatic polymerization. This synthetic material has some favorable properties that make it suitable to create a scaffold, such as high versatility to tune its properties, thermoplastic processability, an appropriate mechanical profile, and biocompatibility and biodegradability, due to the degradation product lactic acid innocuousness and its aliphatic nature, respectively (Lopes *et al.*, 2012). These advantageous features were valuable not only for cardiac tissue engineering, but also for bone (Kellomäki *et al.*, 2000) and cartilage regeneration (Gong *et al.*, 2014). For MI therapy, PLA scaffolds have been used in combination with cardiac stem cells and VEGF, triggering vascularization of the injured area and an enhancement of global cardiac function (Chung *et al.*, 2015). More often, PLA has been used within a mixture of other materials: with synthetic polyglycolic acid (Kellar *et al.*, 2005) or PCL (Jin *et al.*, 2009), or combined with different synthetic materials and additional natural materials collagen and Matrigel (Krupnick *et al.*, 2002); resulting in cardiac recovery in all cases.
- **PLGA:** synthesized usually by means of lactic and glycolic acids copolymerization, it presents a high biocompatibility as their degradation products are inherently degradable, robust physical properties, and favorable degradation features that have made of it an appropriate drug carrier for controlled and sustained drug delivery (Makadia and Siegel, 2011). It has been used to repair defects in bone (Shuqiang *et al.*, 2008), liver (Li *et al.*, 2010a), nerve (Xiong *et al.*, 2009), skin (Yang *et al.*, 2002), blood vessels (Han *et al.*,

2011) and myocardium (Stout *et al.*, 2011). In this latter context, culture of cardiomyocytes in a PLGA scaffold reinforced with carbon nanofibers increased electrical conductivity, and the final cardiomyocyte density was higher compared to controls (Stout *et al.*, 2011). *In vivo*, administration of PLGA scaffolds loaded with cytokines (Pascual-Gil *et al.*, 2017), dermal fibroblasts (Kellar *et al.*, 2005), or ATDPCs reinforced with growth factors (Madonna *et al.*, 2015; Savi *et al.*, 2015), demonstrated increased angiogenesis and improved ventricular function post-MI, hence confirming the potential of PLGA as a cell/protein carrier and the positive effects that can exert in myocardial recovery.

- **PCL:** this aliphatic polyester displays a high hydrophobicity and biocompatibility, a slow-degradation rate and a semicrystalline nature. Moreover, it has a good stability under ambient conditions and an easy processability (Mondal *et al.*, 2016). To overcome the low cell adhesion associated with its elevated hydrophobicity, its surface can be coated with functional molecules or polymers providing a better cellular retention (Xu *et al.*, 2010). Suitability for cardiac tissue engineering was previously demonstrated, according to the seeded myoblast retention, survival and expression of skeletal muscle proteins, generating functional multinucleated myotubes, over a PCL scaffold (Yeong *et al.*, 2010). When PCL was mixed with an oligomer hydrogel and cardiac cells were embedded inside, these showed increased proliferation and high retention (Wang *et al.*, 2009b). Finally, several studies *in vivo* demonstrated the versatility of PCL to mingle with other natural and synthetic material and provide satisfactory results regarding cardiac function improvement following MI (Wang *et al.*, 2009a; Li *et al.*, 2010b; Soler-Botija *et al.*, 2014; Liu *et al.*, 2016).

### **6.3.3. Final considerations regarding scaffold requirements**

In spite of the material origin and the election of the cardiac tissue engineering

approximation (hydrogel or matrix) detailed previously, the optimal scaffold selected should fulfill a set of other criteria to maximize its efficiency and coupling with the host, and minimize possible harmful side effects (**Figure 18**).

First of all, scaffold surface area should oscillate between 10-50 cm<sup>2</sup>, and a thickness contained within the range of millimeters for proper tissue integration (Vunjak-Novakovic *et al.*, 2010). In fact, a thickness of approximately 1 mm showed the best revascularization and recolonization and no signs of matrix degeneration, compared to thinner and thicker vascular scaffolds (Walles *et al.*, 2003). However, thicker scaffolds have limited oxygen diffusion, phenomenon that only occurs in up to 200 µm; so, it is not sufficient for complete oxygenation and cannot replace blood vessel irrigation. Accordingly, vascularization of the scaffold and connection with the host vasculature network is essential to supply the oxygen quantities required in the whole cellular construct (Vunjak-Novakovic *et al.*, 2010). Latest research has been focused on different approximations to create proangiogenic scaffolds that could enhance vascularization: (i) control of the scaffold structure by modulating porosity (Park *et al.*, 2011), or introducing topographic cues (Madden *et al.*, 2010) headed to facilitate cardiomyocyte organization and pore interconnection; (ii) introduction of proangiogenic factors such as FGF (Wang *et al.*, 2010b), VEGF (Miyagi *et al.*, 2011) or HGF (Wang *et al.*, 2004); (iii) use of bioreactors to homogeneously distribute oxygen flow (Dvir *et al.*, 2006); (iv) addition of preexisting vasculature to the scaffold that further promotes endothelial cell recruitment and spreads vascular connections (Chiu *et al.*, 2012); and (v) culture of cardiac, smooth muscle and endothelial cells over the scaffold to promote angiogenesis directly or through paracrine signaling (Ye *et al.*, 2014).

Another important point to consider is the electromechanical coupling of the scaffold to conduit electrical propagation, eventually leading to synchronous contraction to pump out blood volume with no arrhythmia episodes. Rather than show a spontaneous contractility, the generated scaffold should be able to connect with the electrical syncytium of the host myocardium (Vunjak-Novakovic *et al.*, 2010). Moreover, the scaffold should be able to resist the mechanical demands of the human heart, ranging from 20 kPa (end of diastole) to 500 kPa (end of systole), of

special relevance in natural materials due to their intrinsic low stiffness (range of tens of Pa to tens of kPa) (Reis *et al.*, 2016). Several strategies have been directed to improve electromechanical properties to fit with the physiological requirements:

- Engineered heart tissues subjected to **mechanical stretch** resulted in the development of better mechanical properties and mechanical coupling with the host tissue, as well as normalization of electrical impulse propagation. As a consequence, a synchronous contraction was observed (Zimmermann *et al.*, 2002b; Zimmermann *et al.*, 2006).
- Introduction of **conductive nanomaterials** to enhance electrical signal velocity and spreading. One study reported spontaneous electrical activity of cardiac myocytes when seeded in a carbon nanotube scaffold (Martinelli *et al.*, 2012); and in line with this, a second work used a gelatin hydrogel supplemented with carbon nanotubes that electromechanically integrated with the underlying myocardium, improved electrical conduction, and enhanced global cardiac function when implanted in infarcted rats (Zhou *et al.*, 2014).
- **Electrical cell preconditioning**, applying electrical signal stimuli over a collagen sponge with ventricular myocytes, induced cell alignment, coupling and internal ultrastructural reorganization, as well as highly increased the amplitude of synchronous contractions, after only eight days of *in vitro* culture (Radisic *et al.*, 2004).
- **Pretreatment** of synthetic poly(glycerol sebacate) scaffold **with cardiac fibroblasts**, which contribute to reinforce mechanical properties of myocardium and electrical stimuli conduction, and subsequent reseeding with cardiomyocytes, presents a better cell alignment and paced synchronous contraction, with a lower electrical stimulation threshold and a higher contraction amplitude, compared to non-pretreated scaffolds (Radisic *et al.*, 2008).

To end up with, the last properties to mention are biodegradability and



biocompatibility, this latter tightly related to the immunogenic potential of the scaffold. Regarding biodegradability, the scaffold should stand for at least one week to provide cells with an initial support considering the harsh microenvironment within the infarct bed that the cells would face; and fully degraded after 6-8 weeks, when the ventricular remodeling has taken place (Reis *et al.*, 2016). In relation with biocompatibility, it is essential that the scaffold itself and the degradation-derived products did not trigger a deleterious immunological response. Recent studies have shown, however, that the administration of acellular ECM promoted M1 to M2 macrophages transition, associated with tissue regeneration and graft acceptance (Brown *et al.*, 2012). To reduce material immunogenicity, scaffolds have been modified in different ways: surface modification, with the addition of hydrophilic and anionic substrates that leads to macrophage apoptosis; or the incorporation of bioactive molecules (Franz *et al.*, 2011). Ultimately, these measures are aimed to diminish a potential immune rejection of the scaffold and to induce a Th2-tolerant immune response.

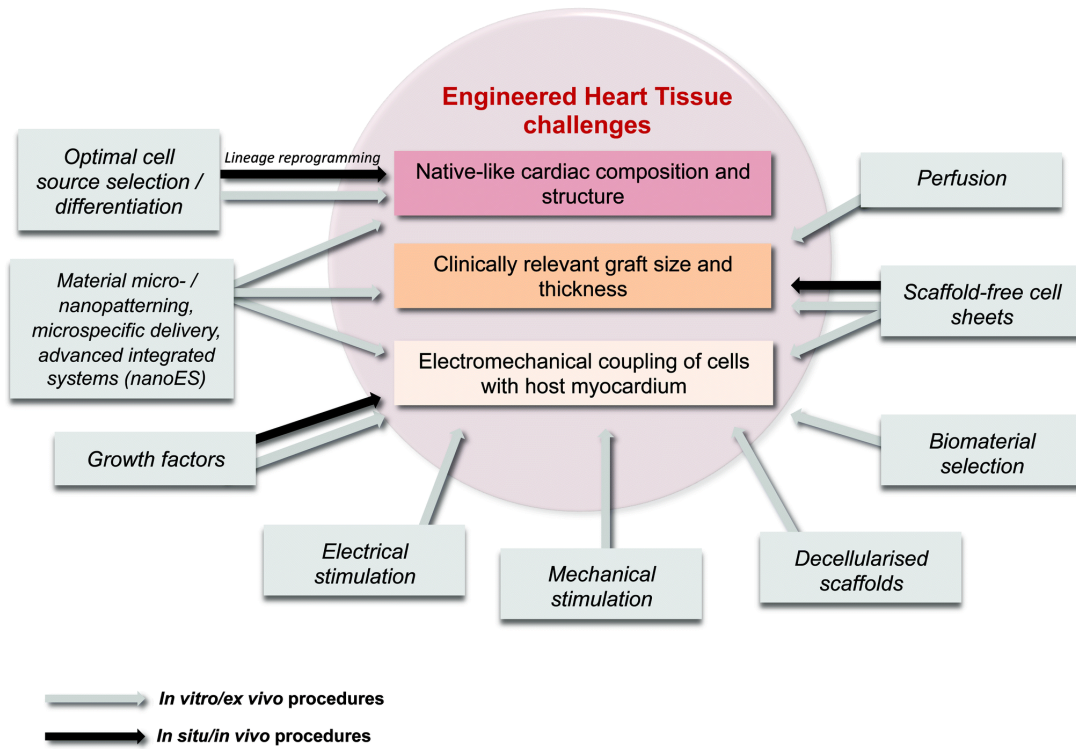


**Figure 18.** Optimal scaffold building up requirements and strategies. This image was reproduced from [Georgiadis et al., 2014](#).

## **Hypothesis and objectives**

---



Despite the latest advances and efforts to find out a definitive treatment against MI, none of them has resulted to be adequate to completely restore cardiac function and reverse ventricular remodeling following MI. The only current therapy that allows a total recovery post-MI is heart transplantation, hampered by low donor availability and immunorejection of the received heart. Thereby, the research of new therapeutic alternatives is still ongoing, with cell therapy and cardiac tissue engineering as novel and valid approaches. However, the optimal cell source to be applied is under scrutiny; and the best cellular platform or scaffold in which embed the cells to overcome the adverse milieu left post-MI has not been completely elucidated.

In line with this, we hypothesized that the implantation of an engineered myocardial graft (EMG) or an engineered pericardial graft (EPG), composed of a decellularized myocardial or pericardial scaffold repopulated with cardiac ATDPCs, generating an EMG-ATDPC or EPG-ATDPC, respectively, could restore the cardiac function and regenerate the ischemic myocardium in a porcine MI model.

Accordingly, the main objectives set up for this thesis have been the following ones:

1. *In vitro* determination of the immunomodulatory capacity of the candidate cells, the cardiac ATDPCs.
2. Obtaining of a decellularized myocardial scaffold from porcine myocardial tissue employing two different decellularization processes; and characterization of the resulting decellularized product at different levels: acellularity grade, protein components, mechanical properties and ultrastructure.
3. Generation of a decellularized pericardial scaffold and comprehensive assessment of its acellularity, protein content, physical properties and three-dimensional structure.
4. Recellularization of both decellularized cardiac scaffolds with the cardiac ATDPCs to generate the engineered cardiac grafts, the EMG-ATDPC or the EPG-ATDPC; and *in vitro* analysis of cell retention and behavior after the

recolonization.

5. Examination of the cardioregenerative capacity of EMG-ATDPC implantation in a porcine MI model.
6. Evaluation of the beneficial effects exerted by the EPG-ATDPC in a porcine MI model.

**Report on the PhD candidate's participation in  
the articles presented in the thesis**

---





The thesis directors of the PhD candidate Isaac Perea Gil, Dr. Antoni Bayés Genís, head of the Cardiology service at Hospital Universitari Germans Trias i Pujol, and chief of the ICREC cardiology research group at Fundació Institut d'Investigació en Ciències de la Salut Germans Trias i Pujol, and Dr. Cristina Prat Vidal, postdoc researcher in charge of cardiac tissue engineering research lines of the ICREC group, expose the PhD candidate publications impact factor, dedication, admission and complete reference.

And to validate and certificate the present information below, we hereby sign the present document.

In Badalona, June 2nd, 2017

Dr. Antoni Bayés Genís, PhD, MD, FESC

Chief at Cardiology Service  
Hospital Universitari Germans Trias i Pujol  
Full Professor, UAB  
Ctra. de Canyet, s/n. 08916 Badalona. Spain  
Tel: +34-93 497 89 15  
E-mail: [abayes.germanstrias@gencat.cat](mailto:abayes.germanstrias@gencat.cat)

Dr. Cristina Prat Vidal, PhD

Fundació Institut d'Investigació en Ciències  
de la Salut Germans Trias i Pujol  
(IGTP)  
Carretera de Can Ruti, Camí de les Escoles, s/n  
08916 Badalona, Spain  
Tel. +34-93 497 86 62  
E-mail: [cpratv@gmail.com](mailto:cpratv@gmail.com)

Carretera de Can Ruti, Camí de les Escoles s/n  
08916 Badalona, Barcelona, Spain

Tel: (+34) 934 978 655 Fax: (+34) 934 978 654 <http://www.germanstrias.org>

*Inscrita amb el número 909 en el Registre de Fundacions Privades de la Generalitat de Catalunya VAT code/CIF G-60805462*



The thesis entitled “Cell-enriched engineered cardiac grafts improve heart function and promote cardiac regeneration: a novel therapy for myocardial infarction” herein presented is composed of a compendium of five published articles (four original research papers and one review) in different peer-reviewed journals, and one more paper in preparation. The participation of the PhD candidate Isaac Perea-Gil, as well as the journal impact factor and quartile and tercile categories, have been detailed below.

Of the five published articles, only one part of the first article entitled “*In vitro* comparative study of two decellularization protocols in search of an optimal myocardial scaffold for recellularization” has been used as part of a thesis by the co-author Juan José Uriarte, member of the Biophysics and Bioengineering Unit at Universitat de Barcelona, responsible for carrying out the mechanical analysis of the myocardial scaffolds. Particularly, Dr. Uriarte presented in his thesis in 2016 the results belonging to the mechanical characterization. Upon requested permission to the Biomedicine PhD program coordinator at the University of Barcelona, Dr. Albert Tauler, no incompatibilities nor issues are considered to include this article as part of the current thesis as original work, accomplishing the necessary requirements and criteria to be recognized as an original article.

***First article: Preclinical evaluation of the immunomodulatory properties of cardiac adipose tissue progenitor cells using umbilical cord blood mesenchymal stem cells: a direct comparative study***

Perea-Gil I, Monguió-Tortajada M, Gálvez-Montón C, Bayes-Genis A, Borràs FE, Roura S. Preclinical evaluation of the immunomodulatory properties of cardiac adipose tissue progenitor cells using umbilical cord blood mesenchymal stem cells: a direct comparative study. *Biomed Res Int* 2015; 2015:439808.

- Impact factor (2015): 2.134
- Quartile and tercile according to JCR impact factor (2015): Q3 and T2 in Biotechnology and Applied Microbiology (82 out of 161); Q3 and T2 in Medicine, Research and Experimental (72 out of 124).

In this paper, the PhD candidate participates as a first author and contributed exhaustively to the work presented. Specifically, Isaac isolated and cultured the human cardiac ATDPCs from the adipose tissue obtained from routine surgery. Also, he isolated the T cell subpopulation from the human blood received from the Banc de Sang i Teixits. He designed and carried out the allostimulatory assay to test the immunomodulatory properties of the cardiac ATDPCs, and he collaborated with the flow cytometer analysis. Finally, Isaac interpreted the results, and he wrote the manuscript and prepared the figures with our supervision.

***Second article: In vitro comparative study of two decellularization protocols in search of an optimal myocardial scaffold for recellularization***

Perea-Gil I\*, Uriarte JJ\*, Prat-Vidal C, Gálvez-Montón C, Roura S, Lluçà-Vallderas A, Soler-Botija C, Farré R, Navajas D, Bayes-Genis A. *In vitro* comparative study of two decellularization protocols in search of an optimal myocardial scaffold for recellularization. *Am J Trans Res* 2015; 7(3):558-73.

- Impact factor (2015): 3.146
- Quartile and tercile according to JCR impact factor (2015): Q2 and T2 in Oncology (92 out of 213); Q2 and T1 in Medicine, Research and Experimental (41 out of 124).

In this publication, the PhD candidate is displayed as a co-author of this work, being responsible for most of it, except for the scaffold mechanical properties analysis. Herein, the PhD candidate collected and completely decellularized all the porcine myocardial samples applying two different decellularization protocols. Once decellularized, Isaac carried out the comprehensive *in vitro* characterization of the generated scaffolds, at distinct levels: levels of DNA, ultrastructure and protein components. Moreover, he also isolated and cultured the porcine cardiac ATDPCs from the porcine adipose tissue; and Isaac also performed the acellular scaffold recellularization and the subsequent study of cell behavior one week postrecellularization. Finally, Isaac contributed to the statistical analysis with our support and the final data interpretation; as well as he wrote the manuscript and designed the figures under our supervision.

### ***Third article: Online monitoring of myocardial bioprosthesis for cardiac repair***

Prat-Vidal C, Gálvez-Montón C, Puig-Sanvicens V, Sanchez B, Díaz-Güemes I, Bogónez-Franco P, Perea-Gil I, Casas-Solà A, Roura S, Lluçà-Valdeperas A, Soler-Botija C, Sánchez-Margallo FM, Semino CE, Bragos R, Bayes-Genis A. Online monitoring of myocardial bioprosthesis for cardiac repair. *Int J Cardiol* 2014; 174(3):654-61.

- Impact factor (2015): 4.638
- Tercile according to JCR impact factor (2015): Q1 and T1 in Cardiac & Cardiovascular Systems (20 out of 124).

In this third publication, the PhD candidate mainly contributed to the pericardium decellularization procedure. Specifically, Isaac carried out the decellularization of some pericardial samples, as well as he helped out with the acellularity determination of the resulting decellularized tissues through DNA analysis. Also, as part of the recellularization process, Isaac isolated, expanded and maintained in culture the cardiac ATDPCs necessary for the scaffold recolonization.

***Fourth article: A cell-enriched engineered myocardial graft limits infarct size and improves cardiac function. Pre-clinical study in the porcine myocardial infarction model***

Perea-Gil I\*, Prat-Vidal C\*, Gálvez-Montón C\*, Roura S, Llucià-Valldeperas A, Soler-Botija C, Iborra-Egea O, Díaz-Güemes I, Crisóstomo V, Sánchez-Margallo FM, Bayes-Genis A. A cell-enriched engineered myocardial graft limits infarct size and improves cardiac function. Pre-clinical study in the porcine myocardial infarction model. *J Am Coll Cardiol Basic Trans Science* 2016; 1(5):360-72.

- Impact factor (2016): Scientific journal not indexed yet.
- Tercile according to JCR impact factor (2016): Scientific journal not indexed yet.

In this fourth publication, the PhD candidate appears as the first author, co-authoring this study with Dr Prat-Vidal and Dr Gálvez-Montón. Herein, Isaac contributed to this work by decellularizing and subsequently repopulating the acellular myocardial scaffolds to generate the EMG, ready to be engrafted in the porcine MI model. Despite not taking part directly in the cardiac surgery nor animal manipulation, he assisted in the engraftment of the EMG, and he collected cardiac pieces after animal sacrifice as well. He developed the different analysis present in the study: histological and immunological stainings, the morphometry to measure infarct size, vessel quantification and the interpretation of the cardiac function data. Also, he tightly helped and contributed to the statistical analysis of the results batch. Finally, the PhD candidate wrote up the article, and he also prepared and edited the different figures and tables shown in the publication.

***Fifth article: Head-to-head comparison of two engineered cardiac grafts for myocardial repair: a pre-clinical myocardial infarction swine model***

Perea-Gil I, Gálvez-Montón C, Prat-Vidal C, Jorba I, Roura S, Soler-Botija C, Iborra-Egea O, Revuelta-López E, Farré R, Navajas D, Bayes-Genis A. Head-to-head comparison of two engineered cardiac grafts for myocardial repair: a pre-clinical myocardial infarction swine model. *In preparation*.

- Impact factor (2016): To be determined
- Tercile according to JCR impact factor (2016): To be determined

In this fifth publication, Isaac actively contributed in decellularizing both cardiac tissues, particularly the porcine myocardium, as well as he took part in the cardiac ATDPCs cell culture and the subsequent recellularization process for the scaffolds. He carried out the matrix protein extraction and preparation for the proteomic analysis, prepared the samples for SEM and mechanic analysis, conducted cell retention and migration analysis postrecellularization, and assisted during the mechanical properties measurements. Besides, he did some of the immunohistochemistries included in the present work, analyzed the *in vivo* data obtained after EMG-ATDPC engraftment, and helped with the remaining *in vivo* results analysis. Finally, he drafted the manuscript and designed some of the figures and tables for the article.



***Sixth article: In vivo experience with natural scaffolds for myocardial infarction: the times they are a-changin'***

Perea-Gil I, Prat-Vidal C, Bayes-Genis A. In vivo experience with natural scaffolds for myocardial infarction: the times they are a-changin'. *Stem Cell Res Ther* 2015; 6:248.

- Impact factor (2015): 4.504
- Quartile and tercile according to JCR impact factor (2014): Q2 and T1 in Cell Biology (52 out of 187); Q1 and T1 in Medicine, Research and Experimental (21 out of 124).

Here, the PhD candidate is listed as the first author of this review. Isaac did an exhaustive search to look for all the published papers that made an *in vivo* study, in small or large animal model, using in either case a natural scaffold to treat MI. He also wrote the manuscript and prepared the figures within the review, as well as the different tables throughout the text.



## Results summary

---



The main aim of this thesis was to develop two different engineered cardiac grafts, based on the combination of either decellularized myocardial or pericardial scaffold recellularized with cardiac ATDPCs (EMG-ATDPC and EPG-ATDPC, respectively), to determine their effectiveness as a novel therapy against MI.

The conducted work performed throughout this thesis was divided into four main sections. First, the previous characterization of the immunological properties of cardiac ATDPCs, the chosen cell lineage to repopulate the scaffolds. Second, the generation of acellular scaffolds starting from native myocardium and pericardium, with intact ECM properties. Third, the repopulation of these comprehensively characterized, decellularized scaffolds with the mentioned cardiac ATDPCs to generate both engineered cardiac grafts. And fourth, the *in vivo* assessment of the exerted effects by the developed constructs in swine MI model.



## 1. Immunomodulatory properties of cardiac ATDPCs

The selected cell lineage for cardiac tissue engineering, the cardiac ATDPCs, were previously characterized by the ICREC research group in terms of stem cell markers profile, capacity of differentiation, and even their potential benefits in attenuating MI symptoms. However, their immunomodulatory features and capacity not to elicit a host immune response upon administration have not been assessed in depth yet. Here, we provide the first insights regarding their immune tolerance, co-culturing cardiac ATDPCs with T-cells, which in turn were either activated or not with dendritic cells, and comparing the results with the well-established, low immunogenic UCBSC line. We observed that cardiac ATDPCs were able not only to avoid immune system stimulation, but also were capable of reducing T-cell proliferation and their proinflammatory cytokine profile once activated in a dose-dependent manner. Particularly, the concentration of secreted interleukin-6, tumor necrosis factor-alpha (TNF- $\alpha$ ) and interferon-gamma (IFN- $\gamma$ ) was significantly reduced after coculturing T-cells with cardiac ATDPCs. Thus, cardiac ATDPCs did not induce a T-cell mediated immune response *in vitro*, indicating a low intrinsic immunogenic capacity, which makes them suitable for allogeneic administration.

The data generated were published in one international peer-reviewed journal (first article):

- Perea-Gil J, Monguió-Tortajada M, Gálvez-Montón C, Bayes-Genis A, Borràs FE, Roura S. Preclinical evaluation of the immunomodulatory properties of cardiac adipose tissue progenitor cells using umbilical cord blood mesenchymal stem cells: a direct comparative study. *Biomed Res Int* 2015; 2015:439808.





## Research Article

# Preclinical Evaluation of the Immunomodulatory Properties of Cardiac Adipose Tissue Progenitor Cells Using Umbilical Cord Blood Mesenchymal Stem Cells: A Direct Comparative Study

Isaac Perea-Gil,<sup>1</sup> Marta Monguió-Tortajada,<sup>2</sup> Carolina Gálvez-Montón,<sup>1</sup>  
Antoni Bayes-Genis,<sup>1,3,4</sup> Francesc E. Borràs,<sup>2,5</sup> and Santiago Roura<sup>1</sup>

<sup>1</sup>ICREC Research Program, Germans Trias i Pujol Health Science Research Institute, Can Ruti Campus, 08916 Badalona, Spain

<sup>2</sup>IVECAT Group, Germans Trias i Pujol Health Science Research Institute, Can Ruti Campus, 08916 Badalona, Spain

<sup>3</sup>Cardiology Service, Germans Trias i Pujol University Hospital, 08916 Badalona, Spain

<sup>4</sup>Department of Medicine, UAB, 08916 Badalona, Spain

<sup>5</sup>Nephrology Service, Germans Trias i Pujol University Hospital, 08916 Badalona, Spain

Correspondence should be addressed to Santiago Roura; [sroure@igtp.cat](mailto:sroure@igtp.cat)

Received 25 November 2014; Revised 20 January 2015; Accepted 16 February 2015

Academic Editor: Betti Giusti

Copyright © 2015 Isaac Perea-Gil et al. This is an open access article distributed under the Creative Commons Attribution License, which permits unrestricted use, distribution, and reproduction in any medium, provided the original work is properly cited.

Cell-based strategies to regenerate injured myocardial tissue have emerged over the past decade, but the optimum cell type is still under scrutiny. In this context, human adult epicardial fat surrounding the heart has been characterized as a reservoir of mesenchymal-like progenitor cells (cardiac ATDPCs) with potential clinical benefits. However, additional data on the possibility that these cells could trigger a deleterious immune response following implantation are needed. Thus, in the presented study, we took advantage of the well-established low immunogenicity of umbilical cord blood-derived mesenchymal stem cells (UCBMSCs) to comparatively assess the immunomodulatory properties of cardiac ATDPCs in an *in vitro* allostimulatory assay using allogeneic mature monocyte-derived dendritic cells (MDDCs). Similar to UCBMSCs, increasing amounts of seeded cardiac ATDPCs suppressed the alloproliferation of T cells in a dose-dependent manner. Secretion of proinflammatory cytokines (IL6, TNF $\alpha$ , and IFN $\gamma$ ) was also specifically modulated by the different numbers of cardiac ATDPCs cocultured. In summary, we show that cardiac ATDPCs abrogate T cell alloproliferation upon stimulation with allogeneic mature MDDCs, suggesting that they could further regulate a possible harmful immune response *in vivo*. Additionally, UCBMSCs can be considered as valuable tools to preclinically predict the immunogenicity of prospective regenerative cells.

## 1. Introduction

The use of multipotent “stem” or progenitor cells in multiple clinical settings is rather encouraging [1–3]. This is, for instance, the case of interest in the regenerative ability of the human heart following acute myocardial infarction, which overloads the functional capacity of the surviving myocardium and ultimately leads to heart failure [4]. To date, the unique treatment that fully restores lost cardiac function after advanced heart failure is heart transplantation. Cell-based strategies to regenerate myocardial tissue have emerged over

the past decade, but the optimum cell type is still under scrutiny. Although the existence of resident cardiac stem cells has been reported [5, 6], their capacity of tissue repair after damage is scarce; thus, one of the main objectives in this field of research is to find the best cell type for repairing injured cardiac tissue [7].

A population of human adult mesenchymal-like progenitor cells derived from cardiac adipose tissue (cardiac ATDPCs), with inherent cardiac and endothelial cell potential, was isolated and characterized for the first time in our laboratory [8]. Taken together, our results showed that cardiac ATDPCs

could play a role in heart homeostasis, perhaps as a cell reservoir for renewing myocardial tissue. Based on these findings, we are planning to investigate the potential clinical benefits of these cells. However, additional data on the possibility that they could elicit a deleterious antidonor immune response are needed.

In this context, recent data have showed that mesenchymal stem cells (MSCs) derived from umbilical cord blood (UCB) have low immunogenicity and are, therefore, immunologically safe for use in allogeneic clinical applications [9]. The lower immunogenicity of UCBMSCs is attributed to its immaturity, in contrast to alternative adult cell sources. Yet, not all adult cell sources have been characterized regarding their immunogenicity.

Thus, in the presented study, we took advantage of the well-established low immunogenicity of UCBMSCs to comparatively assess the immunomodulatory properties of cardiac ATDPCs in an *in vitro* allostimulatory assay.

## 2. Materials and Methods

**2.1. Cardiac ATDPC and UCBMSC Isolation and Culture.** The study protocols were approved by the Clinical Research Ethics Committee of our institution (Comitè Ètic d'Investigació Clínica, HuGTiP, Refs. CEIC: EO-10-13, EO-10-016, and EO-12-022) and conformed to the principles outlined in the Declaration of Helsinki. Written informed consent was obtained from donors.

Cardiac ATDPCs were extracted from adipose tissue surrounding the base of the heart and around the aortic root from patients undergoing cardiothoracic surgery prior to cardiopulmonary bypass initiation, as reported in [8]. Adipose tissue specimens were washed in sterile PBS (Invitrogen, Carlsbad, CA) to remove red blood cell contamination and treated with a 0.05% collagenase type-II solution (Gibco Life Technologies/Invitrogen, Carlsbad, CA) for 30 min at 37°C in gentle agitation. Cell suspension was centrifuged at 1200 ×g for 10 min, resuspended in complete medium corresponding to α-MEM (Sigma Aldrich, St. Louis, MO) supplemented with 10% heat-inactivated FBS, 2 mM L-glutamine (Gibco), 1% penicillin/streptomycin, and 5 μg/mL Plasmocin (InvivoGen, San Diego, CA), and grown under standard culture conditions.

UCBMSCs were isolated and cultured as described previously [10–12]. In brief, UCB samples were collected from the umbilical cord vein and processed within 12 hours after extraction. Blood was clarified by centrifugation, and blood cells were resuspended in magnesium- and calcium-free PBS (Invitrogen). The cell suspension was then layered over 1.077 g/mL Lymphoprep (Axis-Shield, Oslo, Norway), and mononuclear cells (MNCs) were recovered by centrifugation at 400 ×g for 30 min. Red blood cells were eliminated after incubation with Lysis Reagent Pharm-Lyse (BD Biosciences) for 15 min. Adherent cells were cultured in complete α-MEM under standard culture conditions.

**2.2. Monocyte-Derived Dendritic Cell Generation.** Culture media were composed of RPMI 1640 (Gibco Life Technologies/Invitrogen) supplemented with L-glutamine (Sigma

Aldrich, St. Louis, MO), 100 U/mL penicillin (Cepa S.L., Madrid, Spain), 100 μg/mL streptomycin (Normon Laboratories S.A., Madrid, Spain), and 5% (v/v) human serum AB (BioWhittaker/Lonza, Basel, Switzerland).

Peripheral blood MNCs were obtained from leukocyte residues from healthy donors from the Blood and Tissue Bank (Barcelona, Spain) by Ficoll Hypaque Plus density gradient centrifugation (GE Healthcare Biosciences, Uppsala, Sweden) at 1800 rpm for 30 minutes. Monocytes were then isolated using the EasySep Human Anti-CD14 Positive Selection Kit (StemCell Technologies, Grenoble, France), and recovered cells were counted using PerfectCount Microspheres (Cytognos, Salamanca, Spain). The purity obtained was >90% and viability ≥93% FSC/SSC gating. Monocytes were then either differentiated to dendritic cells or kept frozen until use.

In particular, monocyte-derived dendritic cells (MDDCs) were generated by plating  $1 \cdot 10^6$  monocytes/mL in complete medium supplemented with the dendritic cell differentiation cytokines 300 IU/mL IL4 and 450 IU/mL GM-CSF (both from Miltenyi Biotec, Bergisch Gladbach, Germany). Cell feeding was performed every two days and the maturation stimulus LPS (500 ng/mL, Sigma Aldrich) was added at day 5. Mature MDDCs were obtained at day 6 after washing with PBS (Thermo Scientific HyClone, Logan, UT, USA) and detaching cells with accutase (eBioscience, San Diego, CA) for 30 minutes at 37°C. Cells were then counted using Perfect-Count Microspheres (Cytognos) obtaining a >80% viability.

**2.3. Allostimulatory Assays.** For these experiments, peripheral blood MNCs from leukocytes residues from healthy donors (Blood and Tissue Bank) were also obtained by Ficoll Hypaque Plus (GE Healthcare) density centrifugation. T cells were then isolated from peripheral blood MNCs using the EasySep Human T cell Enrichment Kit (StemCell Technologies) following manufacturer's instructions. Briefly, cells were diluted in column buffer at a concentration of  $5 \cdot 10^7$  cells/mL, labeled with the Tetrameric Antibody Complexes (TAC) recognizing human CD14, CD16, CD19, CD20, CD36, CD56, CD66b, CD123, glycophorin A, and dextran-coated magnetic particles, and separated using the EasySep magnet (StemCell Technologies). Enriched T cells were then washed and stained with carboxyfluorescein diacetate succinimidyl ester (CFSE) (Molecular Probes, Leiden, Netherlands) to assess cell proliferation as described previously [13]. Briefly, enriched T cells were resuspended in PBS for staining with an equal volume of 0.8 μM CFSE. After 10 minutes, labeled T cells were washed twice with RPMI (Sigma Aldrich) supplemented with 10% FBS and plated at  $3 \cdot 10^5$  cells/well in flat-bottomed well plates in which allogeneic cardiac ATDPCs or UCBMSCs (20.000, 10.000, 5.000, 2.500, or 1.250 cells/well) had been previously seeded. T cells had a viability of over 94% in all experiments performed.

After an overnight resting period, allogeneic mature MDDCs were added at either 20:1 or 40:1 T cell:MDDC ratios to the indicated wells. Alloproliferation was determined after 4.5 days by measuring the CFSE<sup>low/neg</sup> population by flow cytometry in a LSR Fortessa Analyzer (BD Biosciences). Results were reported as the mean % FSC<sup>high</sup>CFDA-SE<sup>low</sup>

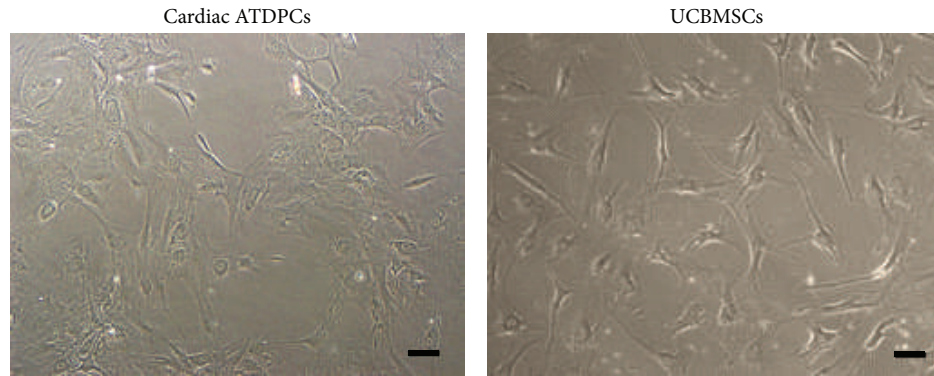


FIGURE 1: Cardiac ATDPC and UCBMSC cultures. Representative phase-contrast images of cardiac ATDPCs and UCBMSCs grown in standard conditions of *in vitro* culture. Scale bars = 100  $\mu$ m.

population  $\pm$  SD in triplicate culture wells relative to the 20 : 1 ratio with 1250 MSCs seeded.

**2.4. Measurement of Cytokine Production.** Cytokines present in supernatants from alloproliferation assays collected at day 4.5 were measured using the CBA human Th1/Th2 Cytokine kit II (BD Biosciences). Concentrations of IL2, IL4, IL6, IL10, and TNF $\alpha$  were assessed following manufacturer's instructions in a LSR Fortessa Analyzer (BD). The minimum detectable concentration (pg/mL) of each protein was 2.6 for IL2 and IL4, 3.0 for IL6, and 2.8 for IL10 and TNF $\alpha$ . All the cytokines measured exceeded the detection limit mentioned before.

**2.5. Statistical Analysis.** Values are expressed as mean  $\pm$  standard deviation (SD). Statistical analysis was performed using two-tailed Student's *t*-tests when two groups were compared, and the Greenhouse-Geisser method for repeated measures was applied to determine significance between two groups with different cell number data. All analyses were performed with SPSS statistic software (19.0.1 version, SPSS Inc., Chicago, IL), and differences were considered significant when  $P < 0.05$ .

### 3. Results

**3.1. Cardiac ATDPCs Reduce the Alloproliferative Response of T Cells.** In these experiments, we sought to compare the immunomodulatory properties of the uncharacterized cardiac ATDPCs (Figure 1(a)) with the well-established nonimmunogenic UCBMSCs (Figure 1(b)). Cardiac ATDPCs had originally been characterized as MSC-like cell progenitors, with over 90% of cells staining strongly positive for CD105, CD44, CD166, CD29, and CD90 and negative for CD106, CD45, and CD14 [8]. Interestingly, their culture in adipogenic differentiation media did not result in intracellular accumulation of lipid droplets [8]. Moreover, primary cultures of elongated fibroblast-like cells established from UCB had strictly been homogeneous and previously recognized as MSCs by our group [10, 12]. These cell cultures were consistently positive for CD105, CD44, CD166, CD29, and CD90 and negative

for CD117, CD106, CD34, CD45, CD14, VEGF-R2, and CD133 as well as differentiated into adipogenic, chondrogenic, and osteogenic cell lineages under specific conditions.

T cell proliferation was induced by allogeneic mature MDDCs at two different T cell : MDDC ratios (20 : 1 and 40 : 1) in the presence of increasing numbers of either cardiac ATDPCs or UCBMSCs, both from a third party donor. As shown in Figure 2(a), increasing amounts of seeded cardiac ATDPCs significantly suppressed the alloproliferation of T cells in a dose-dependent manner ( $P < 0.001$  for both 20 : 1 and 40 : 1 ratios). Similarly, UCBMSCs also significantly suppressed the induced alloproliferation of T cells ( $P < 0.001$  for both 20 : 1 and 40 : 1 ratios) (Figure 2(b)). However, a minimum amount of seeded UCBMSCs (5,000 cells or higher) was able to drastically abrogate T cell alloproliferation, fully reaching the values of the negative control (no MDDC stimulation), while lower numbers did not show a clear immunomodulatory effect. Importantly, this effect was observed at the two T cell : MDDC ratios studied ( $P < 0.001$  comparing 2,500 with higher UCBMSC numbers, for both ratios).

Remarkably, the lower proliferation levels of T cells cocultured with cardiac ATDPCs or UCBMSCs were not related to the induction of cell death, as the viability of cultured T cells was at least maintained in all conditions tested (Figures 2(c) and 2(d)). In fact, T cell viability was actually higher in cells cocultured with increasing numbers of cardiac ATDPCs, although the values did not reach statistical significance ( $P = 0.371$ ,  $P = 0.238$ , and  $P = 0.835$  for 20 : 1 ratio, 40 : 1 ratio, and without MDDCs, resp.) (Figure 2(c)). This would indicate a feeding-like effect of cardiac ATDPCs on allogeneic T cells, promoting cell viability while minimizing immune response to alloantigens.

Figure 3 depicts some images of the cell culture experiments showing the three types of cell partners and the proliferative cell clusters induced by allogeneic mature MDDCs in the presence of low numbers of cardiac ATDPCs and UCBMSCs.

**3.2. Modulation of Cytokine Secretion during Allostimulation in the Presence of Cardiac ATDPCs and UCBMSCs.** To further compare the immunomodulation ability of cardiac ATDPCs, the production of several cytokines was assessed in the

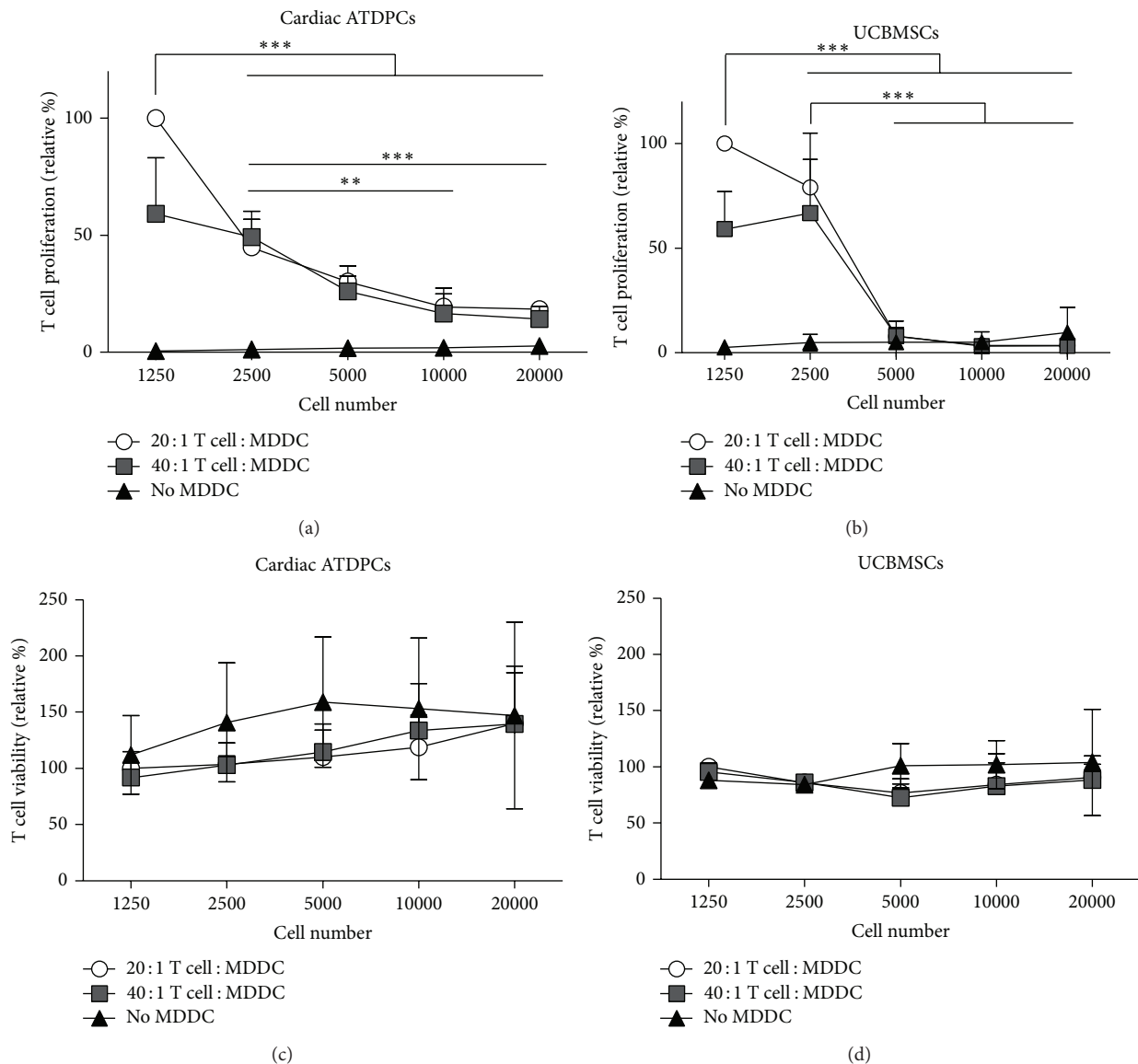


FIGURE 2: T cell alloproliferation induced by MDDCs is abrogated with either cardiac ATDPCs or UCBMSCs. Proliferation was calculated as % of FSC<sup>high</sup>CFSE<sup>low</sup> T cells after a 4.5-day coculture with allogeneic mature MDDCs in 20:1 and 40:1 ratios, together with different numbers (1,250, 2,500, 5,000, 10,000, and 20,000 cells) of either cardiac ATDPCs (a) or UCBMSCs (b). Viability of T cells was assessed according to FSC/SSC gating in coculture with cardiac ATDPCs (c) and UCBMSCs (d). Results are reported as % of proliferation or viability relative to the proliferation or viability level of T cells stimulated with MDDCs in a 20:1 ratio, respectively. Data is depicted as mean  $\pm$  SD of four independent experiments ( $n = 4$  for UCBMSCs, cardiac ATDPCs, and responder T cells), calculated from three experimental replicates. Statistical differences, indicated as \*\*  $P < 0.01$  and \*\*\*  $P < 0.001$ , are only shown for the 20:1 T cell : MDDC ratio.

supernatants from T cell cocultures with allogeneic mature MDDCs (20:1 T cell : MDDC ratio) in the presence of different numbers of cardiac ATDPCs or UCBMSCs (1,250, 5,000, or 20,000). The secretion of proinflammatory cytokines during allostimulation, including IL6, TNF $\alpha$ , and IFN $\gamma$ , was significantly decreased when experiments were performed in the presence of increasing numbers of cardiac ATDPCs (Figure 4(a)). Although the levels of TNF $\alpha$  and IFN $\gamma$  were slightly higher in alloproliferation assays cocultured with low numbers of UCBMSCs compared to cardiac ATDPCs, the results obtained were not significantly different (for 1,250

cells,  $P = 0.195$  and  $P = 0.256$ , for TNF $\alpha$  and IFN $\gamma$ , resp.). Regarding IL6, the levels were almost identical in allostimulatory cocultures with both cardiac ATDPCs and UCBMSCs. In particular, cardiac ATDPCs showed an important reduction of IL6 production (about 50%) when 20,000 cells were seeded compared to 1,250 cells ( $P = 0.001$ ). Other cytokines analyzed were IL2, IL4, and IL10 (Figure 4(b)). A modest increase in IL2 levels was observed when increasing numbers of both tested cell populations had been seeded, but no statistical difference was reached ( $P = 0.157$  and  $P = 0.552$  for cardiac ATDPCs and UCBMSCs, resp.). In contrast, IL4 secretion

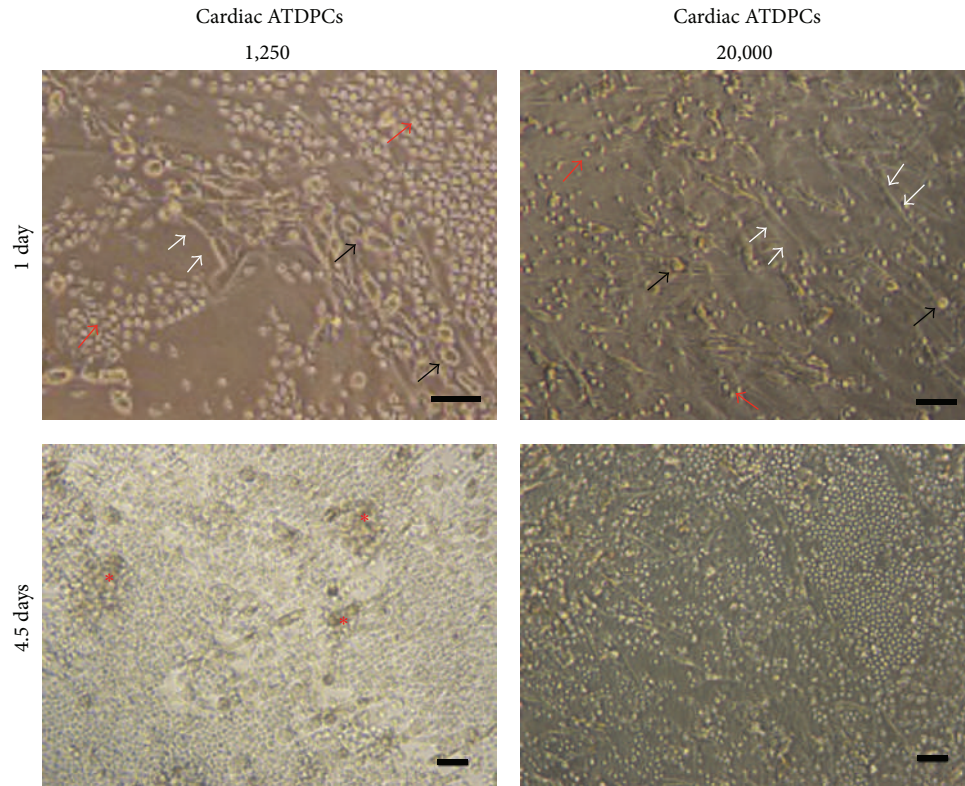


FIGURE 3: Formation of T cell proliferation clusters is affected by increasing numbers of cardiac ATDPCs in the allostimulatory assay. Representative phase-contrast images of 1,250 and 20,000 cardiac ATDPCs (white arrows) cocultured along with T cells (red arrows) and allogeneic mature MDDCs (black arrows) at 1 and 4.5 days. Red asterisks indicate T cell proliferation clusters at 4.5 days. Similar images were taken from UCBMSC cocultures. Scale bars = 100  $\mu\text{m}$ .

was equally reduced with the presence of increasing amounts of both cardiac ATDPCs and UCBMSCs. Regarding IL10, their levels were significantly reduced with increasing numbers of cardiac ATDPCs ( $P = 0.021$ ). Conversely, UCBMSCs cultures did not show a clear reduction of IL10 levels.

#### 4. Discussion

Researchers concur with the idea that the optimal source of cells for cardiac regeneration should (1) be autologous, in order to reduce severe complications of the immune system and disease transmission; (2) exhibit a controlled cell division capacity; (3) differentiate towards both cardiomyogenic and endothelial cell lineages; and (4) integrate efficiently and functionally into injured myocardium after cell implantation. Although considerable efforts have been made, the finding of the cell type with the best regenerative potential remains a challenge [14]. In this context, we focused our attention on cardiac adipose tissue [15], identifying a progenitor cell population resident in the adult human cardiac adipose tissue, which showed potential to differentiate into cardiac and endothelial cell lineages *in vitro* and exhibit beneficial effects upon transplantation in experimental models of myocardial infarction in rodents, promoting angiogenesis in the ischemic

tissue [8]. This cell population also expressed MSC-like surface markers but, unlike bona fide MSCs such as those derived from subcutaneous adipose tissue, showed less plasticity as evaluated by flow cytometry and in adipogenic differentiation assays [8]. Therefore we concluded that, although residing in an adipocytic environment, cardiac ATDPCs show a committed condition to cardiac-like phenotype.

Regarding immunoreactivity, as an exception, allogeneic MSCs are also being considered for tissue regeneration due to their inherent immunoprivileged features. Particularly, MSCs show low expression of major histocompatibility complex (MHC) class I and lack of class II MHC in resting conditions and/or costimulatory molecules, such as CD40, CD80, or CD86 [16, 17]. Moreover, they are characterized to have immunomodulatory effects via the inhibition of both B and T cell proliferation, promoting allograft survival and reducing graft versus host disease [18–25]. However, other studies have suggested that MSCs are immunogenic and promote the immune response, as infusions of allogeneic MSCs were found to foster the rejection of skin allografts and exacerbate T cell proliferation towards the infused MSCs themselves, leading to the generation of functional memory T cells [26–29]. Collectively, these controversial results point out different immunological outcomes of infused MSCs depending on their activated state [24, 30], and reinforce the importance of more

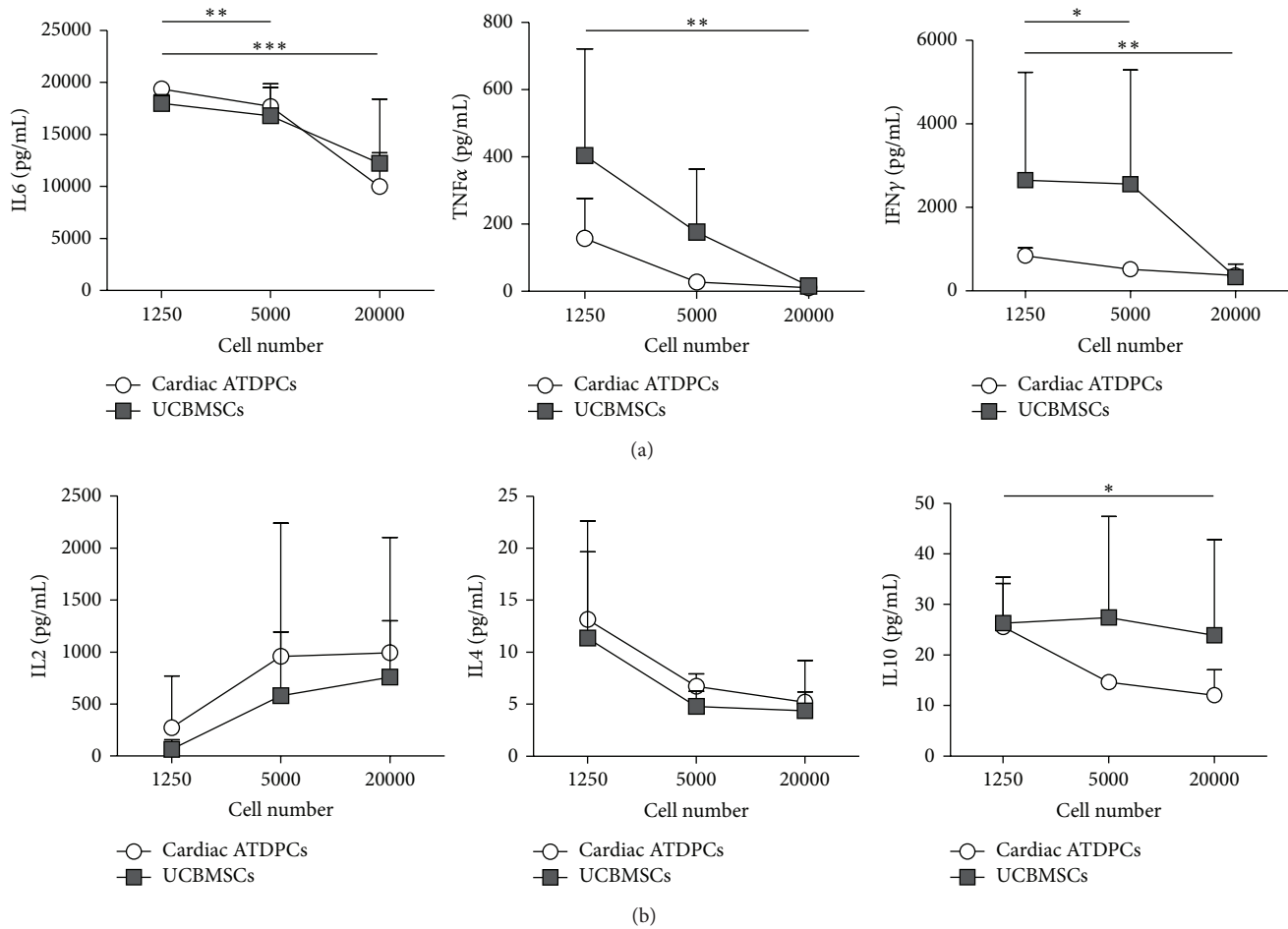


FIGURE 4: Cytokine levels are specifically modulated by the number of cardiac ATDPCs or UCBMSCs seeded in the allostimulatory assay. Histograms represent detected levels of early stage (a) and late stage (b) cytokines in the supernatants from cocultures of increasing numbers of cardiac ATDPCs (white circles) or UCBMSCs (black squares) with T cells and allogeneic mature MDDCs (20 : 1 ratio). Data are expressed as mean  $\pm$  SD from four independent experiments ( $n = 4$  for UCBMSCs, cardiac ATDPCs, and responder T cells). Statistical differences, indicated as \* $P < 0.05$ , \*\* $P < 0.01$ , and \*\*\* $P < 0.001$ , were only found for cardiac ATDPCs.

preclinical studies and screening of MSC immunoreactivity before their clinical use.

With this goal, we focused on the immunophenotyping of the uncharacterized human adult mesenchymal-like progenitor cells derived from cardiac adipose tissue (cardiac ATDPCs). For this purpose, we compared these cells to the already well-studied nonimmunogenic human UCBMSCs [9]. UCB is considered the most plentiful reservoir of regenerative cells for a variety of clinical applications [31, 32]. Although used mainly against blood disorders such as blood malignancies and immune deficiencies, the spectrum of diseases for which UCB provides helpful treatment has been expanded to nonhematopoietic conditions, including cell-based therapy and immunomodulation [33]. Despite MSCs were sought to be present in UCB at a low frequency in contrast to their presence in other tissue sources, such as bone marrow, adipose tissue, or umbilical cord, transplantation of double partially HLA-matched UCB units is a simple approach for overcoming this important limitation [33, 34]. Moreover, procedures for UCBMSCs' isolation have been enhanced along the last

years. Importantly, recent work demonstrates that MSCs can be expanded successfully from 30% to 60% of low-volume UCB units [35]. In terms of advantages, in contrast to other perinatal stem cell sources such as umbilical cord, establishment of primary UCBMSC cultures does not lead to a relatively high-cost and long procedure based in enzymatic digestion or explant methods. UCB can also be safe and painlessly extracted, long-term cryopreserved, and has a lower risk of transmitting viral infections or somatic mutations than adult tissues (i.e., bone marrow). In line, we also recognize UCBMSCs as a useful cellular population to preclinically assess the immunoreactivity of prospective therapeutic cells.

Thus, in the presented study, we demonstrate for the first time that cardiac ATDPCs also exert a great immunosuppression activity because increasing numbers of these cells abrogate T cell proliferation in a coculture setting using third party mature MDDCs [36]. These findings are in line with previous studies indicating that adipose tissue-derived multipotent stromal cells were more active in reducing T cell proliferation at lower cell ratios than their bone marrow-derived

counterparts [18–20, 37–39]. Importantly, this behavior of cardiac ATDPCs is not significantly different from that exhibited by the well-described immunosuppressive UCBMSCs. However, some differences arise from the comparative immunomodulatory analysis of the two cellular populations tested. The antiproliferative effect of cardiac ATDPCs is dose-dependent in comparison with that exerted by UCBMSCs. Apparently, seeding a minimum amount of UCBMSCs is able to drastically abrogate T cell alloproliferation. This result may indicate a stronger immunoregulatory capacity of UCBMSCs, probably attributed to their immature characteristics.

We further show that proinflammatory cytokine secretion in alloproliferation assays is specifically modulated by the different numbers of cardiac ATDPCs cocultured. In particular, the low levels of early stage cytokines (IL6, TNF $\alpha$ , and IFN $\gamma$ ) would correlate with the immunosuppressive effect seen when analyzing the proliferation assays. Remarkably, in an *in vivo* scenario, the induction of low on-site inflammation would diminish the probabilities of effector cell recruitment towards implanted cells. In addition, the analysis of the production of late stage cytokines (IL2, IL4, and IL10) revealed a modest increase in IL2 levels when increasing numbers of both cardiac ATDPCs and UCBMSCs had been seeded. These results may correlate with the sustained viability of T cells cocultured with both cell types, as seen before for other MSC sources [40], and ruling out the possibility of reduced T cell proliferation due to cell death induction [38, 39].

Our results also suggest that cardiac ATDPCs would not be responsible for the proinflammatory state in patients with heart failure and atherosclerosis [41]. Human epicardial fat surrounding the heart, which consists of adipocytes and a stromal fraction, is an active source of multiple bioactive molecules that substantially influence the myocardium and coronary arteries [15]. Moreover, expression levels of the anti-inflammatory molecule adiponectin are shown to be significantly reduced in epicardial fat in comparison with subcutaneous adipose tissue [42]. However, as our findings appear to indicate, the stromal fraction of epicardial fat containing the cardiac ATDPC population may confer some protective effects counteracting its well-described proinflammatory activity.

In summary, the main finding of the present study is that cardiac ATDPCs abrogate the alloproliferation of T cells upon stimulation with allogeneic mature MDDCs, suggesting that they could further regulate a possible harmful antidonor immune response following *in vivo* implantation [43]. Additionally, we suggest that UCBMSCs can be considered as valuable tools to preclinically predict the immunogenicity of prospective regenerative cells.

## Conflict of Interests

The authors declare that the research was conducted in the absence of any commercial or financial relationships that could be construed as a potential conflict of interests.

## Authors' Contribution

Isaac Perea-Gil and Marta Monguió-Tortajada contributed equally to this work.

## Acknowledgments

This work was supported by Grants from Ministerio de Educación y Ciencia (SAF2011-30067-C02-01), Fundació La MARATÓ de TV3 (122232), Red de Terapia Celular (Ter-Cel) (RD12/0019/0029), Red de Investigación Cardiovascular (RIC) (RD12/0042/0047), Societat Catalana de Cardiologia, and Fondo de Investigación Sanitaria, Instituto de Salud Carlos III (FIS PI14/01682) and also from the SGR programme of “Generalitat de Catalunya” (2014SGR804, Grup REMAR) and from REDinREN 2.0 (RD12/0021/0027). In particular, Isaac Perea-Gil is sponsored by a Grant (BES-2012-059761) from the “Ministerio de Economía y Competitividad.” Francesc E. Borràs is sponsored by the “Researchers Stabilization Program” from the Spanish “Sistema Nacional de Salud” (SNS-ISCIII) and “Direcció d'Estratègia i Coordinació,” Catalan Health Department (CES07/015). Marta Monguió-Tortajada is sponsored by a Grant (2014FI.B00649) from the “Agència de Gestió d'Ajuts Universitaris i de Recerca” (AGAUR) from the Catalan Government.

## References

- [1] H. M. Blau, T. R. Brazelton, and J. M. Weimann, “The evolving concept of a stem cell: entity or function?” *Cell*, vol. 105, no. 7, pp. 829–841, 2001.
- [2] G. Q. Daley, “The promise and perils of stem cell therapeutics,” *Cell Stem Cell*, vol. 10, no. 6, pp. 740–749, 2012.
- [3] H. Main, M. Munsie, and M. D. O'Connor, “Managing the potential and pitfalls during clinical translation of emerging stem cell therapies,” *Clinical and Translational Medicine*, vol. 3, article 10, 2014.
- [4] G. Olivetti, J. M. Capasso, L. G. Meggs, E. H. Sonnenblick, and P. Anversa, “Cellular basis of chronic ventricular remodeling after myocardial infarction in rats,” *Circulation Research*, vol. 68, no. 3, pp. 856–869, 1991.
- [5] A. P. Beltrami, L. Barlucchi, D. Torella et al., “Adult cardiac stem cells are multipotent and support myocardial regeneration,” *Cell*, vol. 114, no. 6, pp. 763–776, 2003.
- [6] H. Oh, S. B. Bradfute, T. D. Gallardo et al., “Cardiac progenitor cells from adult myocardium: homing, differentiation, and fusion after infarction,” *Proceedings of the National Academy of Sciences of the United States of America*, vol. 100, no. 21, pp. 12313–12318, 2003.
- [7] C. Soler-Botija, J. R. Bagó, and A. Bayes-Genis, “A bird's-eye view of cell therapy and tissue engineering for cardiac regeneration,” *Annals of the New York Academy of Sciences*, vol. 1254, no. 1, pp. 57–65, 2012.
- [8] A. Bayes-Genis, C. Soler-Botija, J. Farré et al., “Human progenitor cells derived from cardiac adipose tissue ameliorate myocardial infarction in rodents,” *Journal of Molecular and Cellular Cardiology*, vol. 49, no. 5, pp. 771–780, 2010.
- [9] M. Lee, S. Y. Jeong, J. Ha et al., “Low immunogenicity of allogeneic human umbilical cord blood-derived mesenchymal stem

- cells *in vitro* and *in vivo*,” *Biochemical and Biophysical Research Communications*, vol. 446, no. 4, pp. 983–989, 2014.
- [10] C. Prat-Vidal, S. Roura, J. Farré et al., “Umbilical cord blood-derived stem cells spontaneously express cardiomyogenic traits,” *Transplantation Proceedings*, vol. 39, no. 7, pp. 2434–2437, 2007.
- [11] S. Roura, J. Farré, L. Hove-Madsen et al., “Exposure to cardiomyogenic stimuli fails to transdifferentiate human umbilical cord blood-derived mesenchymal stem cells,” *Basic Research in Cardiology*, vol. 105, no. 3, pp. 419–430, 2010.
- [12] S. Roura, J. R. Bagó, C. Soler-Botija et al., “Human umbilical cord blood-derived mesenchymal stem cells promote vascular growth *in vivo*,” *PLoS ONE*, vol. 7, no. 11, Article ID e49447, 2012.
- [13] M. Naranjo-Gómez, N. Climent, J. Cos et al., “Tacrolimus treatment of plasmacytoid dendritic cells inhibits dinucleotide (CpG)-induced tumour necrosis factor- $\alpha$  secretion,” *Immunology*, vol. 119, no. 4, pp. 488–498, 2006.
- [14] L. Badimon and G. Vilahur, “Experimental cell therapy: the search for the best stem cell continues,” *Journal of the American College of Cardiology*, vol. 64, pp. 1695–1697, 2014.
- [15] H. S. Sacks and J. N. Fain, “Human epicardial adipose tissue: a review,” *The American Heart Journal*, vol. 153, no. 6, pp. 907–917, 2007.
- [16] P. Comoli, F. Ginevri, R. Maccario et al., “Human mesenchymal stem cells inhibit antibody production induced *in vitro* by allostimulation,” *Nephrology Dialysis Transplantation*, vol. 23, no. 4, pp. 1196–1202, 2008.
- [17] G. Chamberlain, J. Fox, B. Ashton, and J. Middleton, “Concise review: mesenchymal stem cells: their phenotype, differentiation capacity, immunological features, and potential for homing,” *Stem Cells*, vol. 25, no. 11, pp. 2739–2749, 2007.
- [18] S. Aggarwal and M. F. Pittenger, “Human mesenchymal stem cells modulate allogeneic immune cell responses,” *Blood*, vol. 105, no. 4, pp. 1815–1822, 2005.
- [19] M. D. Nicola, C. Carlo-Stella, M. Magni et al., “Human bone marrow stromal cells suppress T-lymphocyte proliferation induced by cellular or nonspecific mitogenic stimuli,” *Blood*, vol. 99, no. 10, pp. 3838–3843, 2002.
- [20] A. Bartholomew, C. Sturgeon, M. Siatskas et al., “Mesenchymal stem cells suppress lymphocyte proliferation *in vitro* and prolong skin graft survival *in vivo*,” *Experimental Hematology*, vol. 30, no. 1, pp. 42–48, 2002.
- [21] W. T. Tse, J. D. Pendleton, W. M. Beyer, M. C. Egalka, and E. C. Guinan, “Suppression of allogeneic T-cell proliferation by human marrow stromal cells: implications in transplantation,” *Transplantation*, vol. 75, no. 3, pp. 389–397, 2003.
- [22] K. le Blanc, I. Rasmusson, B. Sundberg et al., “Treatment of severe acute graft-versus-host disease with third party haploidentical mesenchymal stem cells,” *The Lancet*, vol. 363, no. 9419, pp. 1439–1441, 2004.
- [23] O. Ringdén, M. Uzunel, I. Rasmusson et al., “Mesenchymal stem cells for treatment of therapy-resistant graft-versus-host disease,” *Transplantation*, vol. 81, no. 10, pp. 1390–1397, 2006.
- [24] M. Krampera, L. Cosmi, R. Angeli et al., “Role for interferon- $\gamma$  in the immunomodulatory activity of human bone marrow mesenchymal stem cells,” *Stem Cells*, vol. 24, no. 2, pp. 386–398, 2006.
- [25] R. Herrmann, M. Sturm, K. Shaw et al., “Mesenchymal stromal cell therapy for steroid-refractory acute and chronic graft versus host disease: a phase 1 study,” *International Journal of Hematology*, vol. 95, no. 2, pp. 182–188, 2012.
- [26] M. J. Hoogduijn, M. Roemeling-Van Rhijn, A. U. Engela et al., “Mesenchymal stem cells induce an inflammatory response after intravenous infusion,” *Stem Cells and Development*, vol. 22, no. 21, pp. 2825–2835, 2013.
- [27] M. J. Crop, C. C. Baan, S. S. Korevaar, J. N. M. Ijzermans, W. Weimar, and M. J. Hoogduijn, “Human adipose tissue-derived mesenchymal stem cells induce explosive T-Cell proliferation,” *Stem Cells and Development*, vol. 19, no. 12, pp. 1843–1853, 2010.
- [28] A. J. Nauta, G. Westerhuis, A. B. Kruisselbrink, E. G. A. Lurvink, R. Willemze, and W. E. Fibbe, “Donor-derived mesenchymal stem cells are immunogenic in an allogeneic host and stimulate donor graft rejection in a nonmyeloablative setting,” *Blood*, vol. 108, no. 6, pp. 2114–2120, 2006.
- [29] P. Sbano, A. Cuccia, B. Mazzanti et al., “Use of donor bone marrow mesenchymal stem cells for treatment of skin allograft rejection in a preclinical rat model,” *Archives of Dermatological Research*, vol. 300, no. 3, pp. 115–124, 2008.
- [30] P. Kebriaei and S. Robinson, “Mesenchymal stem cell therapy in the treatment of acute and chronic graft versus host disease,” *Frontiers in Oncology*, vol. 1, article 16, 2011.
- [31] E. Gluckman, “Milestones in umbilical cord blood transplantation,” *Blood Reviews*, vol. 25, no. 6, pp. 255–259, 2011.
- [32] S. Roura, J.-M. Pujal, and A. Bayes-Genis, “Umbilical cord blood for cardiovascular cell therapy: from promise to fact,” *Annals of the New York Academy of Sciences*, vol. 1254, no. 1, pp. 66–70, 2012.
- [33] A. J. Cutler, V. Limbani, J. Girdlestone, and C. V. Navarrete, “Umbilical cord-derived mesenchymal stromal cells modulate monocyte function to suppress T cell proliferation,” *The Journal of Immunology*, vol. 185, no. 11, pp. 6617–6623, 2010.
- [34] H. Mayani and P. M. Lansdorp, “Biology of human umbilical cord blood-derived hematopoietic stem/progenitor cells,” *Stem Cells*, vol. 16, no. 3, pp. 153–165, 1998.
- [35] H. Mayani, “Umbilical cord blood: lessons learned and lingering challenges after more than 20 years of basic and clinical research,” *Archives of Medical Research*, vol. 42, no. 8, pp. 645–651, 2011.
- [36] K. Le Blanc, L. Tammik, B. Sundberg, S. E. Haynesworth, and O. Ringdén, “Mesenchymal stem cells inhibit and stimulate mixed lymphocyte cultures and mitogenic responses independently of the major histocompatibility complex,” *Scandinavian Journal of Immunology*, vol. 57, no. 1, pp. 11–20, 2003.
- [37] S. M. Melief, J. J. Zwaginga, W. E. Fibbe, and H. Roelofs, “Adipose tissue-derived multipotent stromal cells have a higher immunomodulatory capacity than their bone marrow-derived counterparts,” *Stem Cells Translational Medicine*, vol. 2, no. 6, pp. 455–463, 2013.
- [38] R. Meisel, A. Zibert, M. Laryea, U. Göbel, W. Däubener, and D. Dilloo, “Human bone marrow stromal cells inhibit allogeneic T-cell responses by indoleamine 2,3-dioxygenase-mediated tryptophan degradation,” *Blood*, vol. 103, no. 12, pp. 4619–4621, 2004.
- [39] A. Augello, R. Tasso, S. M. Negrini et al., “Bone marrow mesenchymal progenitor cells inhibit lymphocyte proliferation by activation of the programmed death 1 pathway,” *European Journal of Immunology*, vol. 35, no. 5, pp. 1482–1490, 2005.
- [40] F. Benvenuto, S. Ferrari, E. Gerdoni et al., “Human mesenchymal stem cells promote survival of T cells in a quiescent state,” *Stem Cells*, vol. 25, no. 7, pp. 1753–1760, 2007.



- [41] G. Iacobellis and A. C. Bianco, "Epicardial adipose tissue: emerging physiological, pathophysiological and clinical features," *Trends in Endocrinology and Metabolism*, vol. 22, no. 11, pp. 450–457, 2011.
- [42] R. M. Agra, E. Teijeira-Fernández, D. Pascual-Figal et al., "Adiponectin and p53 mRNA in epicardial and subcutaneous fat from heart failure patients," *European Journal of Clinical Investigation*, vol. 44, no. 1, pp. 29–37, 2014.
- [43] M. Monguió-Tortajada, R. Lauzurica-Valdemoros, and F. E. Borràs, "Tolerance in organ transplantation: from conventional immunosuppression to extracellular vesicles," *Frontiers in Immunology*, vol. 5, article 416, 2014.



## 2. Generation of cardiac acellular scaffolds and recellularization using cardiac ATDPCs

To obtain the acellular cardiac scaffolds, two different tissues were employed: porcine myocardium and human pericardium, designing two decellularization protocols (one for the pericardium) for that purpose. Upon decellularization completion, in all cases, mechanical and structural properties, and protein content were preserved, as well as all of them displayed a high biodegradability. In this regard, detergent-decellularized myocardial scaffolds showed a significantly higher biodegradability compared to trypsin-based decellularized myocardial scaffolds.

Moreover, when the scaffolds were repopulated with cardiac ATDPCs, these remained alive after one week. Moreover, and particularly for the recellularized myocardial scaffolds, the cells maintained their vasculogenic potential, regardless of the decellularization protocol used, and their inherent cardiomyogenic potential when the appropriate decellularization protocol was employed. Specifically, the detergent-based protocol was slightly superior, according to the higher cell retention ( $236 \pm 106$  and  $98 \pm 56$  cells/mm<sup>2</sup>;  $P=0.04$ ) and the better preservation of cardiac ATDPCs differentiation capacity, with expression of cardiac markers cTnT, Cx43 and GATA4. Therefore, apparently both generated cardiac scaffolds are promising candidates to test *in vivo* their cardioregenerative capacity, pursuing MI recovery.

Here, the obtained results were published in two different international, peer-reviewed scientific journals, listed below (second and third articles):

- Perea-Gil I\*, Uriarte JJ\*, Prat-Vidal C, Gálvez-Montón C, Roura S, Lluçia-Valldeperas A, Soler-Botija C, Farré R, Navajas D, Bayes-Genis A. *In vitro* comparative study of two decellularization protocols in search of an optimal myocardial scaffold for recellularization. *Am J Trans Res* 2015; 7(3):558-73.
- Prat-Vidal C, Gálvez-Montón C, Puig-Sanvicens V, Sanchez B, Díaz-Güemes I, Bogónez-Franco P, Perea-Gil I, Casas-Solà A, Roura S, Lluçia-Valldeperas A, Soler-Botija C, Sánchez-Margallo FM, Semino CE, Bragos R, Bayes-Genis A.

Online monitoring of myocardial bioprosthesis for cardiac repair. *Int J Cardiol*  
2014;174(3):654-6

## Original Article

# In vitro comparative study of two decellularization protocols in search of an optimal myocardial scaffold for recellularization

Isaac Perea-Gil<sup>1\*</sup>, Juan J Uriarte<sup>2,3\*</sup>, Cristina Prat-Vidal<sup>1</sup>, Carolina Gálvez-Montón<sup>1</sup>, Santiago Roura<sup>1</sup>, Aida Lucià-Valldeperas<sup>1</sup>, Carolina Soler-Botija<sup>1</sup>, Ramon Farré<sup>2,3,4</sup>, Daniel Navajas<sup>2,3,5</sup>, Antoni Bayes-Genis<sup>1,6</sup>

<sup>1</sup>ICREC (Heart Failure and Cardiac Regeneration) Research Lab, Health Sciences Research Institute Germans Trias i Pujol (IGTP), Cardiology Service, Hospital Universitari Germans Trias i Pujol, Badalona, Barcelona, Spain; <sup>2</sup>Biophysics and Bioengineering Unit, Faculty of Medicine, University of Barcelona, Barcelona, Spain; <sup>3</sup>CIBER Enfermedades Respiratorias, Madrid, Spain; <sup>4</sup>Institut d'Investigacions Biomèdiques August Pi i Sunyer, Barcelona, Spain; <sup>5</sup>Institute for Bioengineering of Catalonia, Barcelona, Spain; <sup>6</sup>Department of Medicine, Autonomous University of Barcelona (UAB), Barcelona, Spain. \*Equal contributors.

Received December 10, 2014; Accepted February 8, 2015; Epub March 15, 2015; Published March 30, 2015

**Abstract:** Introduction. Selection of a biomaterial-based scaffold that mimics native myocardial extracellular matrix (ECM) architecture can facilitate functional cell attachment and differentiation. Although decellularized myocardial ECM accomplishes these premises, decellularization processes may variably distort or degrade ECM structure. Materials and methods. Two decellularization protocols (DP) were tested on porcine heart samples (epicardium, mid myocardium and endocardium). One protocol, DP1, was detergent-based (SDS and Triton X-100), followed by DNase I treatment. The other protocol, DP2, was focused in trypsin and acid with Triton X-100 treatments. Decellularized myocardial scaffolds were reseeded by embedding them in RAD16-I peptidic hydrogel with adipose tissue-derived progenitor cells (ATDPCs). Results. Both protocols yielded acellular myocardial scaffolds (~82% and ~94% DNA reduction for DP1 and DP2, respectively). Ultramicroscopic assessment of scaffolds was similar for both protocols and showed filamentous ECM with preserved fiber disposition and structure. DP1 resulted in more biodegradable scaffolds ( $P = 0.04$ ). Atomic force microscopy revealed no substantial ECM stiffness changes post-decellularization compared to native tissue. The Young's modulus did not differ between heart layers ( $P = 0.69$ ) or decellularization protocols ( $P = 0.15$ ). After one week, recellularized DP1 scaffolds contained higher cell density ( $236 \pm 106$  and  $98 \pm 56$  cells/mm<sup>2</sup> for recellularized DP1 and DP2 scaffolds, respectively;  $P = 0.04$ ). ATDPCs in both DP1 and DP2 scaffolds expressed the endothelial marker isolectin B4, but only in the DP1 scaffold ATDPCs expressed the cardiac markers GATA4, connexin43 and cardiac troponin T. Conclusions. In our hands, DP1 produced myocardial scaffolds with higher cell repopulation and promotes ATDPCs expression of endothelial and cardiomyogenic markers.

**Keywords:** Myocardial infarction, acellular myocardial scaffold, extracellular matrix, decellularization protocols, recellularization, adipose tissue-derived progenitor cells

## Introduction

In 2012, cardiovascular diseases were ranked as the leading cause of death worldwide (3 in every 10 deaths), with coronary heart diseases representing almost half of these deaths [<http://www.who.int/mediacentre/factsheets/fs310/en/>]. After myocardial infarction (MI), effective treatments are needed to reduce scar formation, enhance cardiac regeneration and improve ventricular remodeling. MI manage-

ment has evolved dramatically during the past few decades and now includes both drug administration (aspirin,  $\beta$ -blockers, or angiotensin-converting enzyme inhibitors) and the widespread use of coronary angioplasty and stents. However, cardiac function recovers completely only after heart transplantation, which is hindered by heart donor availability and immunological rejection. Stem cells and tissue engineering are emerging as viable additional therapies for conventional cases [1, 2]. Generation of

## Protocols for myocardial decellularization

bioartificial hearts [3, 4], delivery of stem cells with cardiomyogenic or angiogenic potential to the dysfunctional myocardium [5-8], and engineered tissue grafts and myocardial bioprotheses [9-11] are just a few examples of the proposed therapeutical approaches.

Advances in cardiac tissue engineering have enabled the development of myocardial bioprotheses, based on seeding cells onto natural or synthetic three-dimensional (3D) matrices or scaffolds. In this context, scaffold biomaterial choice is a crucial step, as the scaffold must be able to provide functional cell attachment niches and microenvironments resembling the native structural organization and promoting vascularization to ensure nutrients and oxygen supply into the host tissue [12-15]. Although several synthetic matrices have been tested in small animal models [16-22], natural matrices have appeared as promising myocardial scaffolds due to their greater biocompatibility and biodegradability, as their properties are more similar to those of native cardiac tissue [23]. Compared to other natural matrices, myocardial extracellular matrix (ECM), obtained after decellularization procedures, shows better preservation of the original composition, 3D-architecture and ECM microenvironment [4, 24]. These properties make myocardial ECM a suitable scaffold for cell reseeding and subsequent engraftment into damaged myocardium as a cardiac bioprosthesis.

In this study, we generated decellularized porcine myocardial scaffolds using two distinct decellularization protocols. We then characterized the resulting acellular structures at both mechanical and structural levels and determined their biodegradability. We also compared their properties to those of native myocardium to determine whether the ECM architecture and microenvironment were similar in the decellularized and native tissues. Ultimately, the acellular scaffolds were recellularized with porcine adipose tissue-derived progenitor cells (ATD-PCs), a cellular lineage with demonstrated mesenchymal stem cell pluripotency and cardiomyogenic and endothelial potential [11].

### Materials and methods

#### *Decellularization of porcine myocardial tissue*

Cadaveric hearts were obtained from healthy slaughterhouse pigs and immersed in ice-cold

phosphate buffer saline (PBS) supplemented with 1% penicillin and streptomycin (P/S) (Gibco) overnight (O/N) at 4°C. The atrium was removed, and the ventricle was transversally excised to obtain five ventricular sections. The apical and basal sections were discarded due to their smaller size. In the three remaining sections, transverse abscission of the lateral wall of left ventricle was performed to obtain three differentiated myocardial blocks (25 mm x 25 mm x 3 mm) corresponding to each of the three differentiated heart layers i.e. epicardium, mid myocardium and endocardium (**Figure 1A**). The basal lamina and endothelial lamina were preserved for the epicardium and endocardium myocardial blocks, respectively. Prior to decellularization, native (non-decellularized) tissue from each heart layer was frozen in liquid nitrogen and stored at -80°C until use. Two decellularization protocols were tested (**Figure S1**); both were adapted from methods published previously [3, 9, 11].

The decellularization protocol 1, termed DP1, consisted of detergent treatment using 1% SDS (Sigma) for 72 h, followed by 1% Triton X-100 (Sigma) for 48 h, with solution replacement every 24 h. The myocardial scaffolds were then washed 3 times in 24 h using PBS with 1% P/S [3, 11]. This process was repeated once more with an intermediate sterile distilled water wash between the two cycles. After the second cycle, the scaffolds were treated with 0.1 mg/ml DNase I (Roche) in sterile distilled water for 72 h. Finally, the scaffolds were washed (3 x 2 h) with sterile distilled water [3, 11]. DP1 was performed at room temperature (RT) with constant moderate stirring.

The initial step of the decellularization protocol 2, termed DP2, was a treatment with sterile hypertonic (1.1% NaCl (Sigma)) and hypotonic (0.7% NaCl) solutions. The solutions were alternated every 2 h and repeated twice. This step was followed by an enzymatic incubation with 0.05% trypsin supplemented with 0.02% EDTA (Gibco) for 48 h at 37°C with mild agitation, and then by detergent treatment consisting of PBS supplemented with 1% Triton X-100 plus 1% ammonium hydroxide (Alfa Aesar) for 96 h at RT with moderate stirring; all solutions were replaced every 24 h. The enzymatic and detergent incubations were performed twice with sterile distilled water washes between cycles [9]. Finally, the scaffolds were washed with sterile distilled water O/N.

Protocols for myocardial decellularization

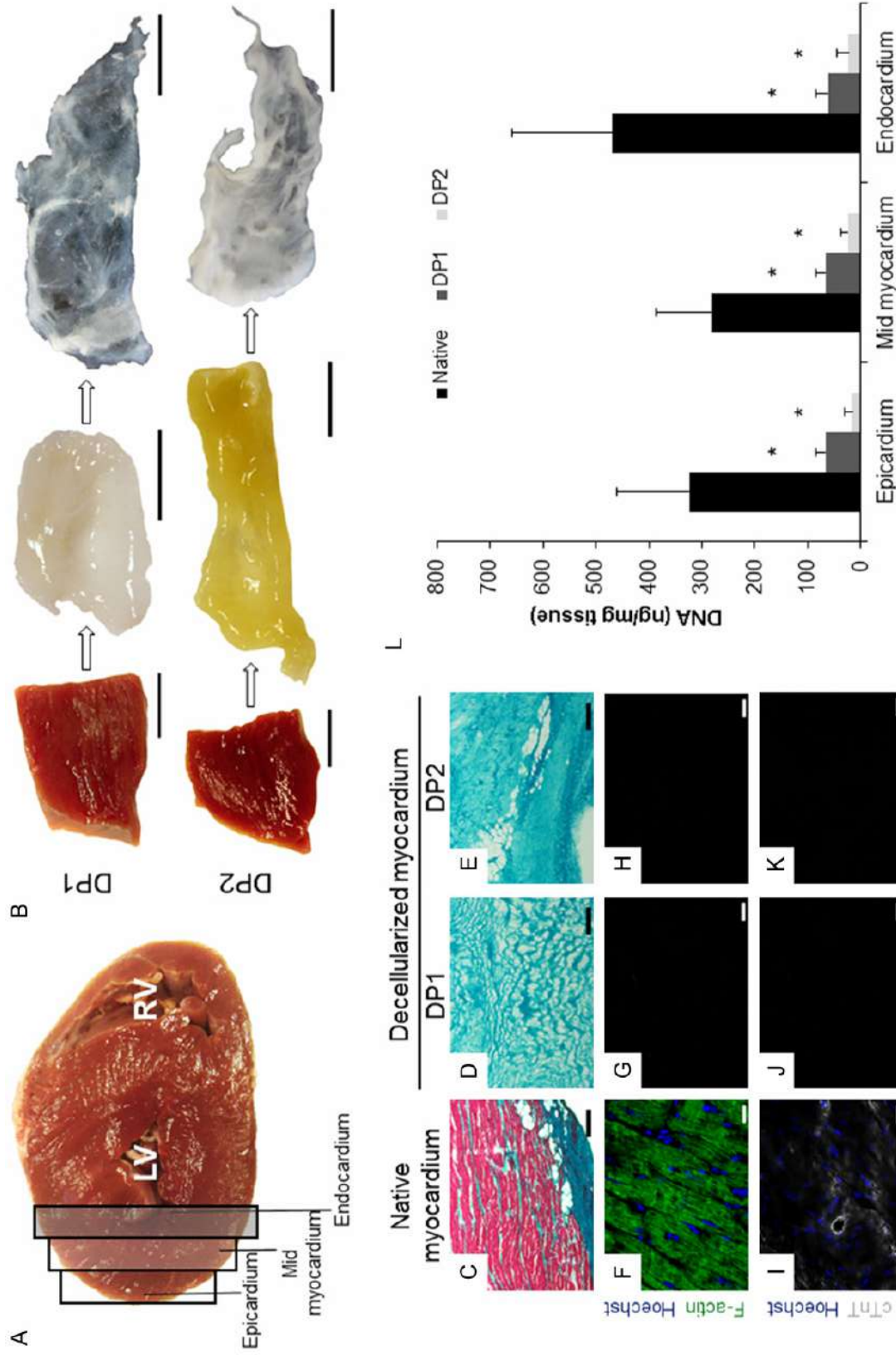


**Figure 1.** Myocardial tissue decellularization. (A) Transversal excision of ventricle (LV: left ventricle; RV: right ventricle) from porcine heart. LV myocardial samples were obtained from the three heart layers (epicardium, mid myocardium and endocardium), as represented in the figure. (B) Photographs showing each step of DP1 and DP2, respectively: native myocardium sample prior to the decellularization; myocardium after one DP1 or DP2 cycle; and after DP1 or DP2 was completed. Scale bars = 1 cm. (C) Masson's trichrome staining of the native, (D) the DP1-decellularized and (E) the DP2-decellularized myocardium. Collagen fibers are stained light green, and the cytoplasm is stained purple. Scale bars = 200  $\mu$ m. (F-H) Representative photographs of F-actin (green) and cTnT (grey) immunostaining in native, DP1 and DP2 decellularized myocardium. (I-K) Representative photographs of F-actin (green) and cTnT (grey) immunostaining in native, DP1 and DP2 decellularized myocardium. Scale bars = 200  $\mu$ m.

## Protocols for myocardial decellularization

munostaining for native myocardium, the DP1-treated and the DP2-treated myocardium, respectively. Nuclei were counterstained with Hoechst 33342 (blue). Scale bars = 20  $\mu\text{m}$ . (L) Genomic DNA quantification of the native tissue and decellularized scaffolds for both DP1 and DP2 decellularization protocols and for each of the three heart layers (n = 7). DNA quantity was normalized to the scaffold weight, and data are shown as mean  $\pm$  SD. \*P < 0.001, native myocardium from each heart layer vs. decellularized scaffold.

After completed decellularization procedures, the samples were frozen in liquid nitrogen and stored at  $-80^{\circ}\text{C}$  for DNA quantification or stored at  $4^{\circ}\text{C}$  in sterile distilled water plus 1% P/S for further applications.

### *Lyophilization and sterilization of decellularized scaffolds*

Decellularized scaffolds were lyophilized at  $-23^{\circ}\text{C}$  for 24 h using a freeze-drier chamber (Christ loc-1 m, B. Braun Biotech International). The lyophilized scaffolds were sterilized under a certified UV dosage of 30 kGy (Aragogamma S.L.) and stored at RT until use.

### *Histological and immunohistochemical analysis*

Native, decellularized myocardial samples and recellularized scaffolds were embedded in TissueTek<sup>®</sup> OCT compound (Sakura). For primary histological examination, Masson's trichrome (Sigma) and Oil Red O (Sigma) staining were performed on 10  $\mu\text{m}$  sections. Images were taken with an optical microscope (CKX41 Olympus, Olympus).

For immunostaining analysis, decellularized and native myocardium samples were incubated with primary antibodies against type-I collagen (1:100, Abcam), type-III collagen (1:100, Abcam), elastin (1:50, Abcam), Alexa Fluor<sup>®</sup> 488-conjugated phalloidin for F-actin filament labeling (1:50, Molecular Probes) and cardiac troponin T (1:100, AbD Serotec) followed by incubation with secondary antibodies conjugated to Alexa Fluor<sup>®</sup> 594 and Alexa Fluor<sup>®</sup> 488 (1:500, Molecular Probes).

For recellularized myocardial scaffolds, primary antibody labeling was carried out for elastin, biotinylated isolectin B4 (1:50, Vector Labs), GATA4 (1:20, R&D Systems), Alexa Fluor<sup>®</sup> 488-conjugated phalloidin for F-actin filament labeling, connexin43 (1:100, BD Transduction), and cardiac troponin T. The secondary antibodies were conjugated to Alexa Fluor<sup>®</sup> 488, Alexa Fluor<sup>®</sup> 594 and Alexa Fluor<sup>®</sup> 647 (1:500, Molecular Probes). Nuclei were counterstained with

Hoechst 33342 (1:10000, Sigma). Images were captured on a laser confocal microscope (Axio Observer Z1, Zeiss).

### *DNA quantification*

Total genomic DNA was isolated using the PureLink<sup>®</sup> Genomic DNA kit (Invitrogen) from native myocardium and decellularized scaffolds (n = 7) following the manufacturer's instructions. The total amount of DNA was quantified using spectrophotometry (NanoDrop ND-1000, NanoDrop Technologies) and normalized to the sample tissue weight (average weight: 8.3-24.7 mg).

### *In vitro assessment of the biodegradability of decellularized scaffolds*

Decellularized lyophilized scaffolds (n = 8) were weighed and incubated with 10 ml of a PBS solution containing 0.1% collagenase I (Gibco) for 24 h at  $37^{\circ}\text{C}$  with gentle stirring [25]. Samples were rinsed with sterile distilled water and lyophilized as described above. After 24 h, lyophilized scaffolds were weighed and the percentage of biodegradability (BD) was calculated as previously reported [25].

### *Scanning electron microscopy (SEM)*

Native myocardium and decellularized myocardial scaffolds were washed extensively in sterile distilled water and fixed in 10% formalin O/N at  $4^{\circ}\text{C}$ . The fixed tissue was washed 3 x 10 min with sterile distilled water followed by dehydration with 15 min incubations in increasing ethanol solutions (50%, 60%, 70%, 80%, 90%, and 100% absolute). The dehydrated samples were transferred to a critical point dryer (Emitech Inc.) and dried with  $\text{CO}_2$ . Samples were sputter-coated with gold using an ion sputter (JFC 1100, JEOL) and visualized at 15 kV with a scanning electron microscopy (JSM-6510, JEOL).

### *Mechanical testing*

Native and decellularized myocardium samples (n = 5) were embedded in TissueTek<sup>®</sup> OCT com-



pound, and 25  $\mu\text{m}$ -thick slices were thawed at RT and rinsed continuously with PBS until the OCT was completely removed. The slides were then immersed in PBS and placed on the atomic force microscopy (AFM) sample holder.

Stiffness measurements were performed using a custom-built AFM mounted on the stage of an inverted optical microscope (TE2000, Nikon) using a previously described method [26, 27]. The samples were probed with a spherical polystyrene bead of radius  $R = 2.25 \mu\text{m}$  attached to a V-shaped gold-coated silicon nitride cantilever with a nominal spring constant  $k = 0.1 \text{ N}\cdot\text{m}^{-1}$  (Novascan Technologies). The 3D-cantilever displacement was controlled with sub-nanometer resolution using piezoactuators coupled to strain gauge sensors (Physik Instrumente) that allow measurement of vertical cantilever displacement ( $z$ ). Cantilever deflection ( $d$ ) was measured with a quadrant photodiode (S4349, Hamamatsu) using the optical lever method. The slope of a deflection-displacement curve ( $d$ - $z$ ) obtained on a bare region of the rigid substrate was used to calibrate the relationship between cantilever deflection and photodiode signal. A linear calibration curve with a sharp contact point was taken to indicate a clean undamaged tip. The spring constant was calibrated using the thermal fluctuation method [28]. The force applied by the tip was computed as  $F = k\cdot d$ .

For each of the three heart layers, local stiffness was measured as follows: for the epicardium, measurements were made 200  $\mu\text{m}$  from the basal lamina edge; for the mid myocardium, measurements were performed in the middle of the sample; and for the endocardium, measurements were made 200  $\mu\text{m}$  from the endothelial lamina edge. In a given region, measurements were performed in 3 locations separated by  $\sim 600 \mu\text{m}$ . At each of the 3 locations, 5 measurements were made separated by  $\sim 7 \mu\text{m}$ ; these 5 measurements were taken in a linear or square pattern for native and decellularized samples, respectively. The Young's modulus ( $E$ ) at each measurement point was computed by recording 5  $d$ - $z$  curves (triangular ramp, peak-to-peak amplitude of 5  $\mu\text{m}$ , and oscillation frequency of 1 Hz) with a maximum indentation of  $\sim 1 \mu\text{m}$ .

Sample indentation ( $\delta$ ) was computed as  $\delta = (z - z_c) - (d - d_o)$ , where  $z_c$  is the displacement of the

cantilever at the tip-sample contact point and  $d_o$  is the offset of cantilever deflection. Force-indentation data were analyzed using the spherical Hertz model (**Equation 1**) [29]:

$$F = \frac{4ER^{\frac{1}{2}}}{3(1-\mu^2)}\delta^{\frac{3}{2}} \quad (1)$$

where  $\mu$  is the Poisson's ratio (assumed to be 0.5). The spherical Hertz model can be expressed in terms of cantilever displacement and deflection as follows:

$$d = d_o \frac{4ER^{1/2}}{3(1-\mu^2)} [z - z_c - (d - d_o)]^{3/2} \quad (2)$$

The Young's modulus, together with  $z_c$  and  $d_o$ , were computed by least squares fitting of **Equation 2** to the loading phase of the  $d$ - $z$  curve using custom-built software (MATLAB, MathWorks). The fitting was performed with a maximum indentation of 0.5  $\mu\text{m}$  to avoid inaccurate  $z_c$  determination for shallow indentations and the effect of a rigid substrate for deep indentations [29]. Moreover, to verify that  $E$  was not affected by the substrate, force curves recorded in both native and decellularized myocardium were fitted using **Equation 2** by progressively increasing the indentation depth up to 1  $\mu\text{m}$ .

For a given measurement point,  $E$  was computed as the average of the values obtained in the 5  $d$ - $z$  curves. The stiffness of each heart region was taken as the average of the  $E$  values computed from the fifteen measured points (3 locations x 5 points/location).

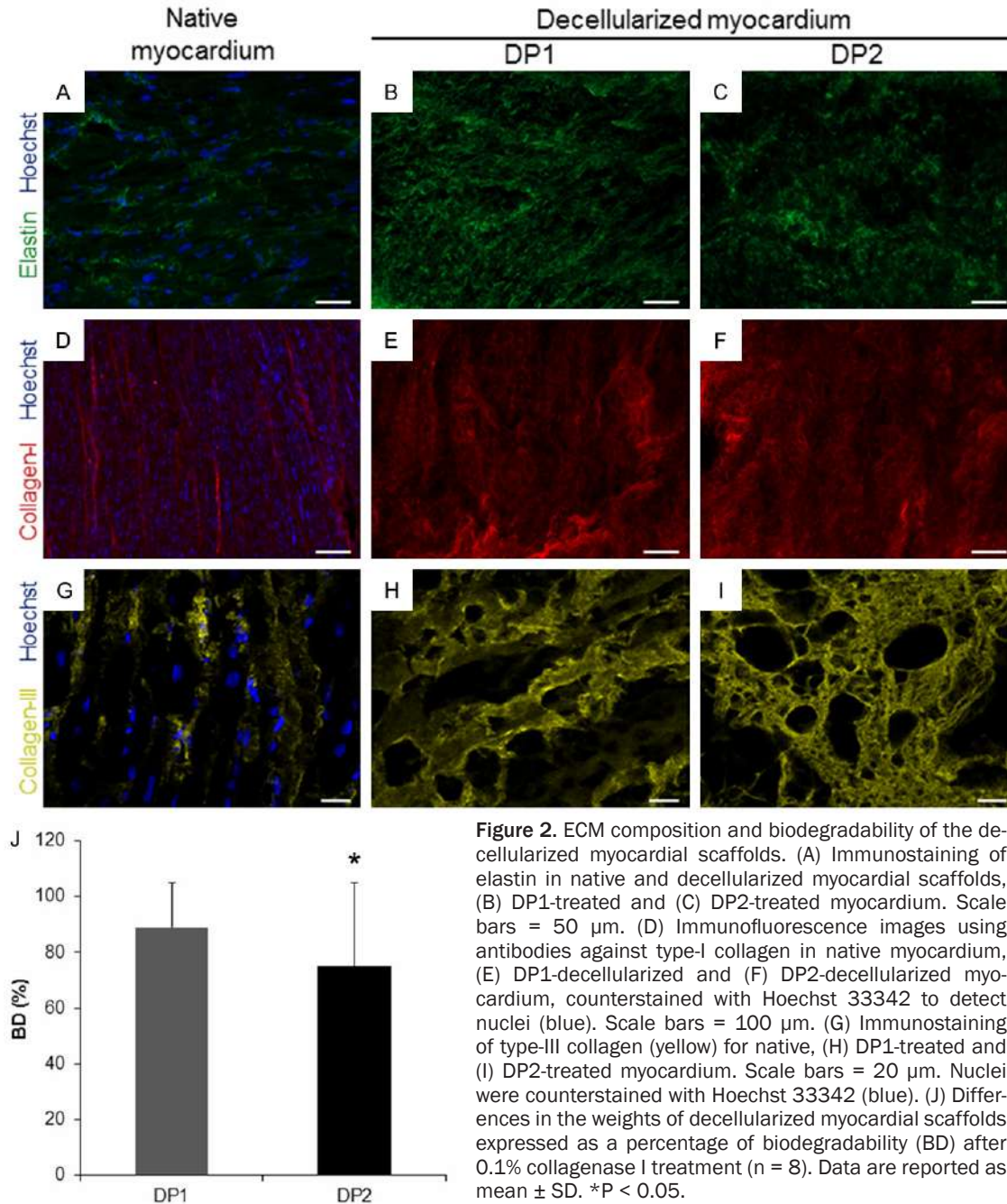
#### Cell culture

Biopsy samples of mediastinal adipose tissue were extracted from juvenile swine and processed to isolate ATDPCs as previously described [30]. ATDPCs were incubated with growth medium:  $\alpha$ -MEM (Sigma) medium supplemented with 10% heat-inactivated fetal bovine serum (FBS), 2 mM L-glutamine (Gibco), 1% P/S, and 5  $\mu\text{g}/\text{ml}$  Plasmocin™ (Invivogen) under standard culture conditions (37°C, 5%  $\text{CO}_2$ ), with medium replacement every three days.

#### Recellularization of decellularized scaffolds

Sterile lyophilized decellularized scaffolds (scaffold surface area, 2-2.5  $\text{cm}^2$ ) were pre-warmed

## Protocols for myocardial decellularization



at 37°C in 10-cm diameter plates. Peptidic hydrogel RAD16-I (BD Biosciences) in 0.3% sucrose (Sigma) was sonicated for 5 minutes, and 175  $\mu$ l of the hydrogel was added to the scaffold. A cellular suspension of  $1.75 \times 10^6$  ATDPCs in 175  $\mu$ l of 0.22- $\mu$ m filtered 10% sucrose solution was added onto the scaffolds surface. After 1 hour of incubation under standard culture conditions, growth medium was added to the plates to facilitate RAD16-I hydro-

gel self-assembly and gel formation. The medium was replaced after 1 h at RT, and the reseeded scaffolds were incubated in standard culture conditions for one week. The medium was replaced every two days.

### *Cell viability analysis on the recellularized scaffolds*

One week post-reseeding, the recellularized scaffolds were washed exhaustively in PBS and

## Protocols for myocardial decellularization

stained using the LIVE/DEAD® Viability/Cytotoxicity Kit (Molecular Probes) following the manufacturer's instructions. Images were acquired using a confocal laser microscope.

### *Determination of cellular density*

Total number of cell nuclei was quantified using ImageJ software (National Institute of Health) in native myocardium and recellularized scaffolds one week post-reseeding ( $n = 3$ ). At least 5 visual fields were counted for each sample.

### *Statistical analyses*

Data are presented as mean  $\pm$  SD, and differences among groups were evaluated using the one-way ANOVA and the Tukey post-hoc pairwise multiple comparison tests (SPSS statistics software v.20, IBM).  $P$  values  $< 0.05$  were considered statistically significant.

## Results

### *Evaluation of myocardial scaffold acellularity*

Decellularized myocardial scaffolds were generated using two decellularization protocols (**Figure 1B**). Macroscopically, a single decellularization cycle was not sufficient to obtain completely pale scaffolds for either protocol. After two decellularization cycles, these scaffolds were almost transparent and appeared to be cell-free. There were no notable differences in scaffolds generated from the two protocols or from the three different heart layers.

Histological analysis by Masson's trichrome staining showed no detectable cells remaining in the myocardial scaffolds and no discernable differences between the two protocols or the different heart layers were found (**Figure 1C-E**). Immunostaining revealed absence of cytoskeletal elements and cellular nuclei once myocardium was decellularized (**Figure 1F-K**). In addition, no adipocytes were detected after Oil Red O staining of the myocardial scaffolds (**Figure S2**).

The DNA content was significantly reduced in the decellularized scaffolds compared to the native myocardium for each of the three heart layers [DNA (ng/mg tissue): epicardium: native =  $324 \pm 136$ , DP1 =  $67 \pm 19$ , DP2 =  $17 \pm 14$ ;  $P < 0.001$ ; mid myocardium: native =  $282 \pm 106$ ,

DP1 =  $67 \pm 18$ , DP2 =  $26 \pm 13$ ;  $P < 0.001$ ; endocardium: native =  $468 \pm 190$ , DP1 =  $62 \pm 24$ , DP2 =  $23 \pm 21$ ;  $P < 0.001$ ]. The DNA removal efficiency was not significantly different in DP1 vs. DP2 samples ( $P = 0.31$ ) or in decellularized scaffolds from different heart layers ( $P = 0.52$ ) (**Figure 1L**). There were thus  $\sim 82\%$  and  $\sim 94\%$  reductions in the DNA content of the scaffold-associated cells after DP1 and DP2, respectively, compared to native myocardium.

### *Identification of ECM components and determination of decellularized scaffold biodegradability*

Immunostaining showed that type-I, type-III collagen and elastin, characteristic ECM components, were detected in the myocardial scaffolds after both decellularization protocols (**Figure 2A-I**).

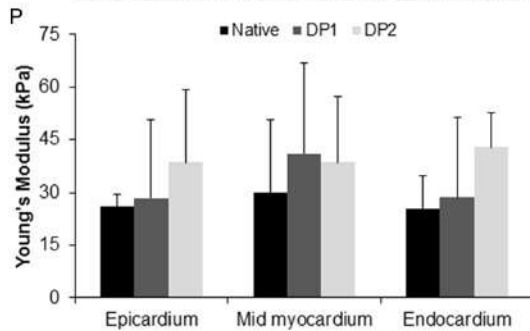
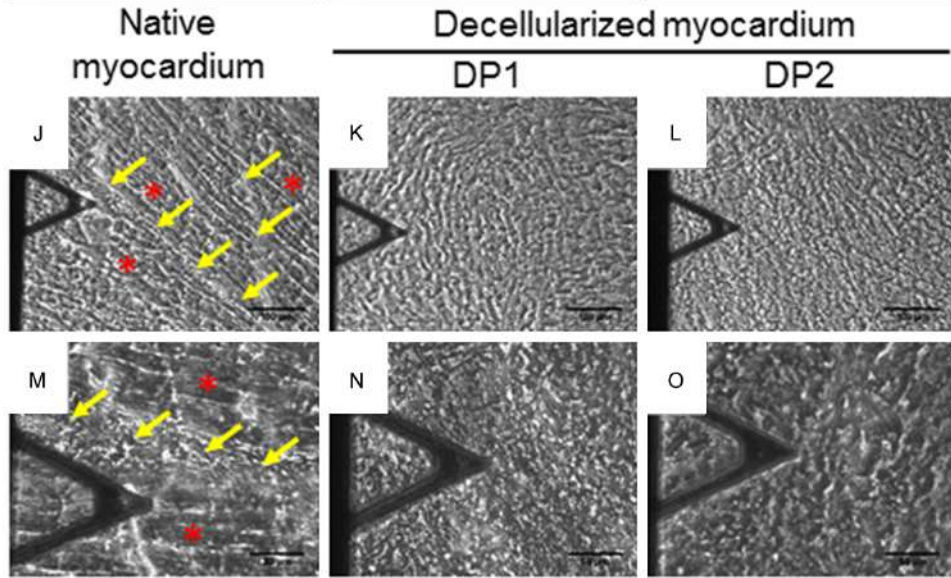
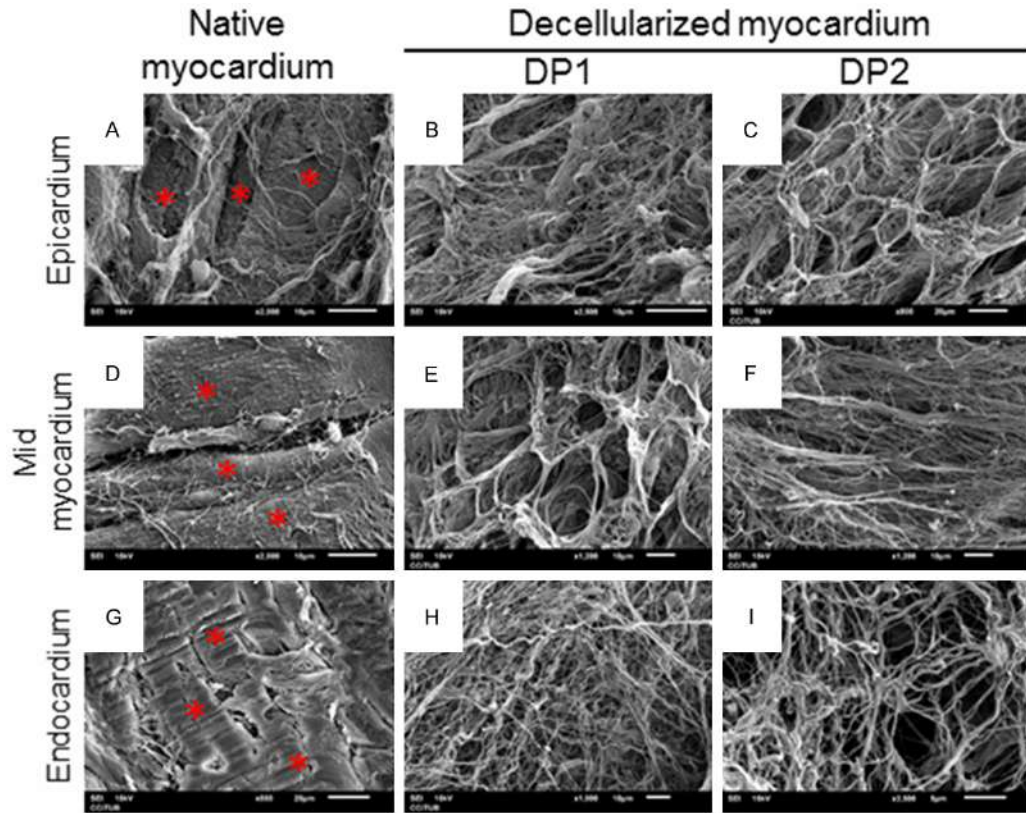
Decellularized scaffolds also exhibited high levels of BD as determined by scaffold weight loss after 24 h of collagenase I treatment [BD (%): epicardium: DP1 =  $85 \pm 17$ , DP2 =  $63 \pm 33$ ; mid myocardium: DP1 =  $94 \pm 13$ , DP2 =  $87 \pm 23$ ; endocardium: DP1 =  $89 \pm 14$ , DP2 =  $75 \pm 32$ ]. Even though no significant differences were found between heart layers ( $P = 0.15$ ), DP1 produced acellular scaffolds that were significantly more biodegradable than those produced after DP2 ( $P = 0.04$ ) (**Figure 2J**).

### *Structural and mechanical properties of the acellular scaffolds*

Ultrastructural assessment showed decellularized myocardium rich in ECM filaments. Notably, the fiber organization and structure were preserved. In contrast, the scaffolds lacked cardiomyocytes (**Figure 3A-I**), as demonstrated above. No differences were found at ultramicroscopical level between scaffolds generated from the two decellularization protocols or from the different heart layers.

The ECM was easily identified in native myocardium and in decellularized myocardial scaffolds using phase contrast microscopy (**Figure 3J-O**). Mechanical characterization of the ECM using AFM revealed no significant changes in ECM stiffness post-decellularization compared to the native tissue [E (kPa): epicardium: native =  $26.1 \pm 3.6$ , DP1 =  $28.4 \pm 22.3$ , DP2 =  $38.6 \pm 20.8$ ;  $P = 0.51$ ; mid myocardium: native =  $30.0$

Protocols for myocardial decellularization



## Protocols for myocardial decellularization

**Figure 3.** Structural and mechanical properties of acellular myocardial scaffolds. (A) Scanning electron microscope images of native epicardium, (B) DP1-treated and (C) DP2-treated epicardium; (D) native mid myocardium, (E) DP1-decellularized and (F) DP2-decellularized mid myocardium; (G) native endocardium, (H) endocardium after DP1 treatment and (I) DP2 treatment. (J) Phase contrast images of 25- $\mu$ m thick slices of myocardium probed with a spherical tip at the end of a V-shaped cantilever by AFM of native myocardium, (K) DP1-decellularized and (L) DP2-decellularized myocardium. Scale bars = 100  $\mu$ m. (M) Zoomed images of native myocardium, (N) DP1-decellularized and (O) DP2-decellularized myocardium. Scale bars = 50  $\mu$ m. Red stars indicate cardiomyocytes. Yellow arrows indicate ECM fibers measured with the AFM. (P) Determination of the Young's modulus ECM, E, for native and decellularized myocardium generated using both decellularization protocols, and for the three heart layers (n = 5). Data are reported as mean  $\pm$  SD.

$\pm 20.6$ , DP1 =  $41.0 \pm 25.7$ , DP2 =  $38.6 \pm 18.8$ ; P = 0.71; endocardium: native =  $25.5 \pm 9.4$ , DP1 =  $28.6 \pm 22.9$ , DP2 =  $42.9 \pm 10$ ; P = 0.21]. Stiffness was not significantly different in scaffolds from different heart layers (P = 0.69) or in scaffolds generated using DP1 vs. DP2 (P = 0.15) (**Figure 3P**). Thus, the native ECM myocardial stiffness was retained after decellularization.

### *Recellularization of the decellularized myocardial scaffolds*

One week after ATDPCs reseeding within RAD16-I hydrogel onto decellularized myocardial scaffolds, cells were detected inside the scaffold (**Figure 4A-C**) and remained viable as analyzed by live/dead assay (**Figure S3**). ATDPCs seeded onto scaffolds generated using DP1 and DP2 expressed the endothelial marker isolectin B4 (**Figure 4D, 4E**). However, only ATDPCs seeded onto scaffolds generated using DP1 expressed the cardiac markers GATA4, connexin43, and cardiac troponin T (**Figure 4D-I**). The capacity of DP1- and DP2-generated scaffolds to retain cells was determined and compared to each other and to the cell density in native myocardium. Cell density was significantly lower in the recellularized scaffolds compared to native myocardium (P < 0.001). Remarkably, recellularized DP1 scaffolds had more cells per surface area than the DP2 ( $236 \pm 106$  and  $98 \pm 56$  cells/mm<sup>2</sup> for recellularized DP1 and DP2 decellularized scaffolds, respectively; P = 0.04) (**Figure 4J**).

### **Discussion**

Cardiac tissue engineering is based on placing a mixture of cells with cardioregenerative potential onto a supportive biomaterial. The main challenge in cardiac tissue engineering is finding an optimal biomaterial to serve as a matrix for recellularization in order to generate a bioprosthesis. Matrix composition, its 3D-

structure and the microenvironment affect the survival and growth of the reseeded cells and the biomaterial integration success into the host tissue [23, 31]. This challenge can be met using natural myocardial ECM, which is more biodegradable. It is not only a better match than synthetic materials, it also matches the composition and structure of native myocardium better than other natural materials [23]. Notably, the structure and composition of the native ECM constantly varies due to cellular metabolic activity, which in turn causes changes in cell responses to the new ECM environment [32]. These initial microenvironmental cues and normal ECM turnover are only provided by the natural myocardial ECM obtained by decellularization, a mixture of functional and structural molecules which guides cellular proliferation, attachment, differentiation, migration, and viability [33, 34].

To obtain only intact ECM, we need decellularization processes that use physical, enzymatic, and/or chemical treatments to remove all cellular content from the tissue while preserving the integrity of the ECM [2, 35]. Up to date, several organs and tissues have been successfully decellularized, such as heart valves, myocardium, pericardium, lung, pancreas, kidney, liver, mammary gland or nerve [24, 36]. In this study, we chose to test two published decellularization protocols that combine different treatments and to adapt them to our specific conditions. Decellularization treatments used can have a variable effect on ECM: detergents employed, SDS and Triton X-100, can effectively remove cell content, but prolonged exposure could alter ECM ultrastructure and eliminate growth factors. On the other hand, trypsin used in DP2 even though reported to be one of the more commonly used decellularization agents as an initial step, tends to be disruptive to elastin and collagen and ECM ultrastructure, whereas acid treatment of DP2, effective in solubiliz-

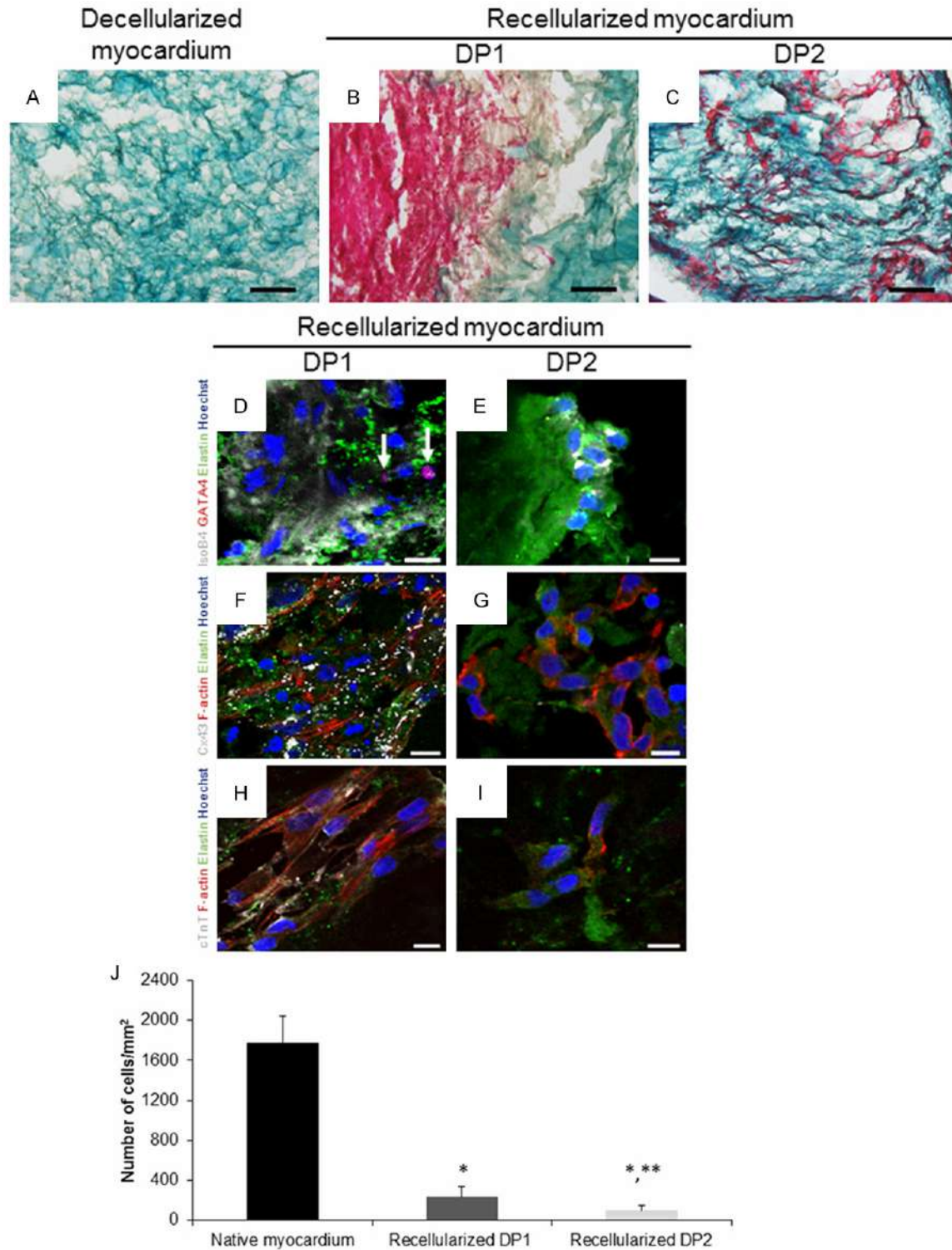


**Figure 4.** Recellularization of previously decellularized myocardial scaffolds. (A) Representative images of Masson's trichrome staining for decellularized (DP2) myocardial scaffold; (B) DP1- and (C) DP2-decellularized scaffolds one week after recellularization. Collagen fibers are stained light green, and the cytoplasm is stained purple. Scale bars = 100  $\mu$ m. (D, E) Immunofluorescence against isolectin B4 (IsoB4, grey), GATA4 (red) and elastin (green), (F, G) connexin43 (Cx43, grey) and F-actin (red) and (H, I) cardiac troponin T (cTnT, grey) of DP1- and DP2-decellularized scaffolds, respectively, one week after recellularization with ATDCs. Nuclei were counterstained with Hoechst 33342 (blue). White arrows indicate cells with positive expression of GATA4. Scale bars = 10  $\mu$ m. (J) Quantification of cells/mm<sup>2</sup> in native myocardium and in recellularized scaffolds (n = 3). Data are reported as mean  $\pm$  SD. \*P < 0.001, native myocardium vs. recellularized scaffolds; \*\*P < 0.05, DP1- vs. DP2-recellularized scaffolds.

ing cytoplasmatic components and eliminating nucleic acids, could damage collagen, GAGs and remove growth factors. DNase I and hyper/hypotonic treatments have no described negative effects on ECM [24, 36]. Then, we performed a detailed analysis of each decellularization setup for two reasons. First, we wanted to specifically assess the variability of the decellularization effects, which depend on tissue cellularity, origin, density, thickness, lipid content, incubation time, and decellularization technique. Second, we wanted to determine the specific requirements of the cells used for recellularization [24, 37].

Removing cells and nuclear material is necessary to eliminate allogeneic or xenogeneic cell antigens to avoid an adverse immunological host response and graft rejection [38, 39]. It is suggested that a DNA concentration of < 50 ng per mg of scaffold plus no detection of nuclei by immunostaining largely prevents an immunological response [24]. In the present study, we obtained cell-free myocardial scaffolds using two protocols, confirming no presence of cell nuclei in our decellularized scaffolds, and DNA levels were close (DP1) or lower (DP2) than the 50 ng/mg ECM limit, with DNA reduction percentage similar to those obtained in previous work [11, 40]. Additionally, absence of cytosolic remnants ensures cellular surface molecule  $\alpha$ -Gal removal, major factor in the hyperacute rejection of porcine organs transplant [41].

Type-I and III collagen, which contribute mainly to heart stiffness, and elastin, which is involved in cell adhesion and the load-bearing capacity of the heart, are two predominant components of the myocardial ECM [42]. Scaffolds produced by decellularization with DP1 and DP2 were immunopositive for both type-I and III collagen and elastin, indicating that the major ECM components that are needed for subsequent cell reseeding were present.

Regarding biodegradability, an *in vitro* estimation with single enzymatical digestion has been carried out, similarly to those made in previous studies for acellular scaffolds [25, 43-45]. High levels of biodegradability facilitate the replacement of the scaffold ECM by newly-synthesized ECM produced by the reseeded cells. Greater biodegradability thus enhances and promotes the integration of the recellularized scaffold

into the engrafted myocardium [35, 42]. Our decellularized scaffolds were highly biodegradable *in vitro*, with the DP1-derived scaffolds being significantly more biodegradable (> 90% for DP1 and > 75% for DP2). Accordingly, our data suggest that it is better to use the DP1 protocol for decellularization. One plausible explanation could be the disruptive effect of trypsin over collagen ultrastructure, which may mask or alter collagenase I cleavage sites, diminishing enzymatic activity on it, as it happens when collagen structure is affected by crosslinking agents [24, 36, 44]. However, these results should be interpreted with caution as an *in vitro* approximation, and degradation kinetics of decellularized scaffolds should be determined *in vivo* once engrafted, according to the high number of metalloproteases involved on ECM degradation [46].

We found that the ECM structure was preserved after decellularization, and microscopic examination showed that the ECM fibers were not only present but that the 3D-organization and ultrastructure were preserved. Conservation of the 3D-ECM ultrastructure post-decellularization facilitates cell adhesion, differentiation, survival, and integration, so ideally the ultrastructure in the scaffold should be similar to that of the native myocardium [23, 24, 33]. The local intrinsic mechanical properties of native and decellularized scaffolds, which are closely related to scaffold structure, were assessed in thin (~25  $\mu$ m) tissue slices by AFM. This technique has the advantage over bulk mechanical measurements that can directly measure myocardial ECM stiffness in a precisely selected region at a local micro-scale, providing further insights into the cell-microenvironment interconnection [26, 27, 47].

The AFM measurements of the Young's modulus revealed that the local stiffness of the decellularized scaffold is very close to the ECM stiffness in the native myocardium. This suggests that the decellularized scaffold may be able to modulate cell behavior (e.g. cell phenotype, morphology, function, and contractibility) in a manner similar to the modulation that occurs in native tissue [48, 49]. The local stiffness of the decellularized scaffold in the pig myocardium is comparable to that we reported recently in mouse (30-75 kPa) using the same technique [27]. Interestingly, although there are

no other published studies that use AFM in micrometer-thin myocardium slices, similar stiffness values (~20 kPa) were obtained with AFM in thick (0.5-1 mm) native samples of rat [50] and mouse [51] ventricles. Nevertheless, it should be noted that the native myocardium is a composite material with cells embedded in an ECM network. Therefore, indentation of the surface of a thick tissue sample deforms both cells and ECM matrix providing a measurement of the bulk stiffness that depends on the cell-ECM stiffness and volume ratios as well as scaffold architecture. Other studies have measured bulk mechanical properties of thick (~0.3 mm) myocardial slabs dissected from native rat ventricles and perfused-decellularized hearts by means of biaxial tensile testing [3, 52]. The results for the tangential modulus in the native rat ventricle compare with our Young's modulus measurements in native pig myocardium. By contrast, the tangential modulus of the decellularized rat heart was ~10-fold stiffer than the native tissue [3]. This marked increase in the bulk stiffness of the decellularized tissue can be attributed to decellularization-induced shrinkage and compression of the 3D-ECM network after cell loss. Mechanical properties of native and acellular thick (2-10 mm) slabs of porcine myocardium were also probed with uniaxial testing [9, 10]. Although these studies reported a very high stiffness (220-370 kPa) of the native tissue they also showed a 5- to 20-fold stiffer acellular tissue providing additional evidence of the effect of scaffold shrinkage in tensile assays. Taken together, these data suggest that although the stiffness of the decellularized heart can be altered by changes in the 3D-structure of the ECM network at the macroscopic levels, it is unaffected on the microscopic scale, which is the level at which cardiomyocytes sense mechanical cues from the microenvironment.

We finally characterized the decellularized myocardial scaffolds from each of the heart layers (epicardium, mid myocardium, and endocardium) by examining and comparing several properties. ECM derived from these layers differs in terms of protein composition and in its specific role in the early stages of embryonic heart development [53-55]. Accordingly, we hypothesized that adult heart epicardium and endocardium might have slightly different ECM composition, structure, and/or function than myocar-

dial ECM and that these differences might affect cell reseeded. We found that myocardium from each of the three heart layers showed similar acellularity, ECM proteins detection, ECM biodegradability, 3D-structure and mechanical properties. Consequently, with the decellularization protocols employed, it is suggested that decellularized scaffolds from any of the three heart layers could be used for subsequent cell reseeded, as no differences in ECM characteristics were found.

To date, several types of porcine-derived mesenchymal stem cells have been used for recellularization, including subcutaneous adipose tissue [56], umbilical cord blood [57] and bone marrow [58]. Mediastinal ATDPCs, the porcine mesenchymal stem cells we used for scaffold reseeded, were characterized previously by our group [11]. ATDPCs are pluripotent and express cardiac markers in basal conditions and when cultured in endothelial growth medium, ATDPCs showed endothelial-like morphology and increased isolectin B4 endothelial marker expression, reflecting differentiation towards an endothelial-like cellular lineage [11]. These properties make ATDPCs appropriate to use for scaffold repopulation.

ATDPCs were introduced into the scaffold along with RAD16-I hydrogel, which self-assembles into the matrix and provides an environment that enhances cell viability and cell differentiation towards a cardiac lineage [11, 22, 59]. RAD16-I hydrogel also promotes endothelial cell adhesion and proliferation as well as capillary formation [60]. One week after recellularization, the ATDPCs we observed in the scaffold remained viable and had adhered to the mixture of scaffold plus RAD16-I. ATDPCs expressed isolectin B4 in both DP1- and DP2-decellularized scaffolds, indicating endothelial differentiation potential. Nevertheless, only ATDPCs in DP1-generated scaffolds expressed GATA4, connexin43, and cardiac troponin T, all of which are markers for cardiac lineage differentiation. By mimicking native cardiac ECM or by using decellularized myocardial ECM itself, reseeded cells can be directed to differentiate into mature cardiomyocytes, and in some cases, towards endothelial lineage [4, 61, 62]. Our results indicated that the acellular DP1-generated scaffolds had properties that were more similar to the properties of native ECM.



DP1-generated scaffolds not only promoted ATDPCs endothelial potential, as did DP2-generated scaffolds, but DP1-generated scaffolds also induced cardiac differentiation potential to seeded ATDPCs. Moreover, ATDPCs density was higher for recellularized DP1 scaffolds than for recellularized DP2 scaffolds. Comparing with published data, a similar study recellularized porcine myocardial slabs with 200,000 mesenchymal stem cells seeded onto 0.5 cm<sup>2</sup> of tissue and reported a cell density of 1,000 cells/mm<sup>2</sup> after 30 days [9]. That study started with fewer cells than we did, but the surface area was also smaller. Thus, although they achieved a slightly higher cell density, their results in recellularized porcine myocardium were fairly similar to ours.

Characterization of the decellularized ECM, as well as the recellularization data, indicates that scaffolds decellularized using DP1 were preferable to scaffolds decellularized using DP2. DP1-derived scaffolds were more biodegradable; importantly, they showed a higher density of ATDPCs, and these cells differentially expressed some cardiac markers. All decellularization agents disrupt the scaffold to some extent, but trypsin is more disruptive than other treatments. Prolonged exposure to trypsin can remove ECM elements such as laminin and fibronectin, as well as collagens and elastin (investigated in this study), and GAGs. Acid treatment may remove ECM-bound growth factors [24]. It is difficult to determine the exact exposure time that should be considered as prolonged exposure, i.e. that removes too much of these important ECM proteins and thus alters the ECM microenvironment. Removal of too many key ECM proteins may decrease the number of ATDPCs that adhere to the scaffold and may reduce their expression of cardiac markers as their physiological microenvironment has been altered. Despite trypsin-mediated alterations to the ECM in porcine aortic valves, endothelial cells can grow and proliferate [63]. This suggests that ECM treated with trypsin may still be suitable for endothelial cell proliferation and explains why ATDPCs in DP2-decellularized scaffolds express isolectin B4 but not cardiac markers.

### Conclusion

In summary, both decellularization protocols generated acellular myocardial scaffolds with

conserved native ECM properties that could be repopulated with ATDPCs. However, decellularized scaffolds obtained with DP1 were more biodegradable and retained more ATDPCs per unit of surface area. Only the ATDPCs reseeded onto DP1-decellularized scaffolds expressed cardiac markers. For these reasons, in our hands, combined use of detergents and DNase, DP1, is an optimal decellularization protocol to obtain acellular scaffolds for recellularization. In the future, these recellularized scaffolds could be enhanced by adding growth factors in order to develop an improved myocardial bioprosthesis.

### Acknowledgements

The authors want to thank the members of the Jesús Usón Minimally Invasive Surgery Centre (Cáceres, Spain) for providing mediastinal adipose tissue samples from pigs that underwent cardiothoracic surgery. This work was supported in part by the Instituto de Salud Carlos III: Redes Temáticas de Investigación Cooperativa en Salud [Red de Investigación Cardiovascular (RIC; RD12/0042/0047) and Red de Investigación en Terapia Celular-TerCel (RD12/0019/0029)] and by Infrastructure Grant (IF09-/3667). The study also received funding from the Ministerio de Ciencia e Innovación (SAF-2011-30067-C02-01/02 to ABG, SAF2011-22576 to RF, FIS-P11/00089 to DN and FIS-PI14/01682); from the Fundació Privada Daniel Bravo Andreu; from La Marató de TV3 (12/2232 to SR); and from the Societat Catalana de Cardiologia and the Sociedad Española de Cardiología.

**Address correspondence to:** Dr. Antoni Bayes-Genis, ICREC Research Lab, Health Sciences Research Institute Germans Trias i Pujol (IGTP), Cardiology Service, Hospital Universitari Germans Trias i Pujol Crta, Canyet, s/n, 08916 Badalona, Barcelona, Spain. Tel: +34-93-4973743; Fax: +34-93-497865; E-mail: abayesgenis@gmail.com

### References

- [1] Soler-Botija C, Bagó JR, Bayes-Genis A. A bird's-eye view of cell therapy and tissue engineering for cardiac regeneration. *Ann N Y Acad Sci* 2012; 1254: 57-65.
- [2] Gálvez-Montón C, Prat-Vidal C, Roura S, Soler-Botija C, Bayes-Genis A. Cardiac tissue engineering and the bioartificial heart. *Rev Esp Cardiol* 2013; 66: 391-399.

## Protocols for myocardial decellularization

- [3] Ott HC, Matthiesen TS, Goh SK, Black LD, Kren SM, Netoff TI, Taylor DA. Perfusion-decellularized matrix: using nature's platform to engineer a bioartificial heart. *Nat Med* 2008; 14: 213-221.
- [4] Lu TY, Lin B, Kim J, Sullivan M, Tobita K, Salama G, Yang L. Repopulation of decellularized mouse heart with human induced pluripotent stem cell-derived cardiovascular progenitor cells. *Nat Commun* 2013; 4: 2307.
- [5] Bayes-Genis A, Soler-Botija C, Farré J, Sepúlveda P, Raya A, Roura S, Prat-Vidal C, Gálvez-Montón C, Montero JA, Büscher D, Izpisua Belmonte JC. Human progenitor cells derived from cardiac adipose tissue ameliorate myocardial infarction in rodents. *J Mol Cell Cardiol* 2010; 49: 771-789.
- [6] Rigol M, Solanes N, Roura S, Roqué M, Novensà L, Dantas AP, Martorell J, Sitges M, Ramírez J, Bayés-Genís A, Heras M. Allogeneic adipose stem cell therapy in acute myocardial infarction. *Eur J Clin Invest* 2014; 44: 83-92.
- [7] Templin C, Zweigerdt R, Schwanke K, Olmer R, Ghadri JR, Emmert MY, Müller E, Küest SM, Cohrs S, Schibli R, Kronen P, Hilbe M, Reinisch A, Strunk D, Haverich A, Hoerstrup S, Lüscher TF, Kaufmann PA, Landmesser U, Martin U. Transplantation and tracking of human-induced pluripotent stem cells in a pig model of myocardium infarction: assessment of cell survival, engraftment, and distribution by hybrid single photon emission computed tomography/computed tomography of sodium iodide symporter transgene expression. *Circulation* 2012; 126: 430-439.
- [8] Kawamoto A, Gwon HC, Iwaguro H, Yamaguchi JI, Uchida S, Masuda H, Silver M, Ma H, Kearney M, Isner JM, Asahara T. Therapeutic potential of ex vivo expanded endothelial progenitor cells for myocardial ischemia. *Circulation* 2001; 103: 634-637.
- [9] Sarig U, Au-Yeung GC, Wang Y, Bronshtein T, Dahan N, Boey FY, Venkatraman SS, Machluf M. Thick acellular heart extracellular matrix with inherent vasculature: Potential platform for myocardial tissue regeneration. *Tissue Eng Part A* 2012; 18: 2125-2137.
- [10] Wang B, Borazjani A, Tahai M, Curry AL, Simionescu DT, Guan J, To F, Elder SH, Liao J. Fabrication of cardiac patch with decellularized porcine myocardial scaffold and bone marrow mononuclear cells. *J Biomed Mater Res A* 2010; 94: 1100-1110.
- [11] Prat-Vidal C, Gálvez-Montón C, Puig-Sanvicens V, Sanchez B, Díaz-Güemes I, Bogóñez-Franco P, Perea-Gil I, Casas-Solà A, Roura S, Llucà-Valldeperas A, Soler-Botija C, Sánchez-Margallo FM, Semino CE, Bragos R, Bayes-Genis A. Online monitoring of myocardial bioprosthesis for cardiac repair. *Int J Cardiol* 2014; 174: 654-661.
- [12] Zhou C, Chen J, Sun H, Qiu X, Mou Y, Liu Z, Zhao Y, Li X, Han Y, Duan C, Tang R, Wang C, Zhong W, Liu J, Luo Y, Mengqiu Xing M, Wang C. Engineering the heart: evaluation of conductive nanomaterials for improving implant integration and cardiac function. *Sci Rep* 2014; 4: 3733.
- [13] Dvir T, Timko BP, Kohane DS, Langer R. Nanotechnological strategies for engineering complex tissues. *Nat Nanotechnol* 2011; 6: 13-22.
- [14] Vunjak-Novakovic G, Lui KO, Tandon N, Chien KR. Bioengineering heart muscle: a paradigm for regenerative medicine. *Annu Rev Biomed Eng* 2011; 13: 245-267.
- [15] Song JJ, Ott HC. Organ engineering based on decellularized matrix scaffolds. *Trends Mol Med* 2014; 17: 424-432.
- [16] Jin J, Jeong SI, Shin YM, Lim KS, Shin HS, Lee YM, Koh HC, Kim KS. Transplantation of mesenchymal stem cells within a poly(lactide-co-ε-caprolactone) scaffold improves cardiac function in a rat myocardial infarction model. *Eur J Heart Fail* 2009; 11: 147-153.
- [17] Miyagi Y, Zeng F, Huang XP, Foltz WD, Wu J, Mihic A, Yau TM, Weisel RD, Li RK. Surgical ventricular restoration with a cell- and cytokine-seeded biodegradable scaffold. *Biomaterials* 2010; 31: 7684-7694.
- [18] Chen QZ, Ishii H, Thouas GA, Lyon AR, Wright JS, Blaker JJ, Chrzanowski W, Boccaccini AR, Ali NN, Knowles JC, Harding SE. An elastomeric patch derived from poly(glycerol sebacate) for delivery of embryonic stem cells to the heart. *Biomaterials* 2010; 31: 3885-3893.
- [19] Siepe M, Giraud MN, Pavlovic M, Recepto C, Beyersdorf F, Menasché P, Carrel T, Tevæearai HT. Myoblast-seeded biodegradable scaffolds to prevent post-myocardial infarction evolution toward heart failure. *J Thorac Cardiovasc Surg* 2006; 132: 124-131.
- [20] Dobner S, Bezuidenhout D, Govender P, Zilla P, Davies N. A synthetic non-degradable polyethylene glycol hydrogel retards adverse post-infarct left ventricular remodeling. *J Card Fail* 2009; 15: 629-636.
- [21] Jiang XJ, Wang T, Li XY, Wu DQ, Zheng ZB, Zhang JF, Chen JL, Peng B, Jiang H, Huang C, Zhang XZ. Injection of a novel synthetic hydrogel preserves left ventricle function after myocardial infarction. *J Biomed Mater Res A* 2009; 90: 472-477.
- [22] Soler-Botija C, Bagó JR, Llucà-Valldeperas A, Vallés-Lluch A, Castells-Sala C, Martínez-Ramos C, Fernández-Muiños T, Chachques JC, Pradas MM, Semino CE, Bayes-Genis A. Engineered 3D bioimplants using elastomeric scaffold

- fold, self-assembling peptide hydrogel, and adipose tissue-derived progenitor cells for cardiac regeneration. *Am J Transl Res* 2014; 6: 291-301.
- [23] Sarig U, Machluf M. Engineering cell platforms for myocardial regeneration. *Expert Opin Biol Ther* 2011; 11: 1055-1077.
- [24] Crapo PM, Gilbert TW, Badylak SF. An overview of tissues and whole organ decellularization processes. *Biomaterials* 2011; 32: 3233-3243.
- [25] Kim BS, Choi JS, Kim JD, Choi YC, Cho YW. Recellularization of decellularized human adipose-tissue-derived extracellular matrix sheets with other human cell types. *Cell Tissue Res* 2012; 348: 559-567.
- [26] Luque T, Melo E, Garreta E, Cortiella J, Nichols J, Farré R, Navajas D. Local micromechanical properties of decellularized lung scaffolds measured with atomic forces microscopy. *Acta Biomater* 2013; 9: 6852-6859.
- [27] Andreu I, Luque T, Sancho A, Pelacho B, Iglesias-García O, Melo E, Farré R, Prósper F, Elizalde MR, Navajas D. Heterogeneous micromechanical properties of the extracellular matrix in healthy and infarcted hearts. *Acta Biomater* 2014; 10: 3235-3242.
- [28] Butt HJ, Jaschke M. Calculation of thermal noise in atomic force microscopy. *Nanotechnology* 1995; 6: 1-7.
- [29] Rico F, Roca-Cusachs P, Gavara N, Farré R, Rotger M, Navajas D. Probing mechanical properties of living cells by atomic force microscopy with blunted pyramidal cantilever tips. *Phys Rev E Stat Nonlin Soft Matter Phys* 2005; 72: 021914.
- [30] Martínez-Estrada OM, Muñoz-Santos Y, Julve J, Reina M, Vilaró S. Human adipose tissue as a source of Flk-1<sup>+</sup> cells: new method of differentiation and expansion. *Cardiovasc Res* 2005; 65: 328-333.
- [31] Grayson WL, Martens TP, Eng GM, Radisic M, Vunjak-Novakovic G. Biomimetic approach to tissue engineering. *Semin Cell Dev Biol* 2009; 20: 665-673.
- [32] Bissell MJ, Aggeler J. Dynamic reciprocity: How do extracellular matrix and hormones direct gene expression? *Prog Clin Biol Res* 1987; 249: 251-262.
- [33] Badylak SF, Taylor D, Uygun K. Whole-organ tissue engineering: decellularization and recellularization of three-dimensional matrix scaffolds. *Annu Rev Biomed Eng* 2011; 13: 27-53.
- [34] Midwood KS, Williams LV, Schwarzbauer TE. Tissue repair and the dynamics of the extracellular matrix. *Int J Biochem Cell Biol* 2004; 36: 1031-1037.
- [35] Robinson KA, Li J, Mathison M, Redkar A, Cui J, Chronos NA, Matheny RG, Badylak S. Extracellular matrix scaffold for cardiac repair. *Circulation* 2005; 112: 135-143.
- [36] Song JJ, Ott HC. Organ engineering based on decellularized matrix scaffolds. *Trends in Molecular Medicine* 2011; 17: 424-432.
- [37] Akhyari P, Aubin H, Gwanmesia P, Barth M, Hoffmann S, Huelsmann J, Preuss K, Lichtenberg A. The quest for an optimized protocol for whole-Heart decellularization: a comparison of three popular and a novel decellularization technique and their diverse effects on crucial extracellular matrix qualities. *Tissue Eng Part C Methods* 2011; 17: 915-926.
- [38] Zheng MH, Chen J, Kirilak Y, Willers C, Xu J, Wood D. Porcine small intestine submucosa (SIS) is not an acellular collagenous matrix and contains porcine DNA: Possible implications in human implantation. *J Biomed Mater Res B Appl Biomater* 2005; 73: 61-67.
- [39] Nagata S, Hanayama R, Kawane K. Autoimmunity and the clearance of dead cells. *Cell* 2010; 140: 619-630.
- [40] Wainwright JM, Czajka CA, Patel UB, Freytes DO, Tobita K, Gilbert TW, Badylak SF. Preparation of cardiac extracellular matrix from an intact porcine heart. *Tissue Eng Part C Methods* 2010; 16: 525-532.
- [41] Badylak SF, Gilbert TW. Immune response to biologic scaffold materials. *Semin Immunol* 2009; 20: 109-116.
- [42] Vunjak Novakovic G, Eschenhagen T, Mummery C. Myocardial tissue engineering: in vitro models. *Cold Spring Harb Perspect Med* 2014; 4: a014076.
- [43] Lu Q, Ganesan K, Simionescu DT, Vyavahare NR. Novel porous aortic elastin and collagen scaffolds for tissue engineering. *Biomaterials* 2004; 25: 5227-5237.
- [44] Liang CH, Chang Y, Hsu CK, Lee MH, Sung HW. Effects of crosslinking degree of an acellular biological tissue on its tissue regeneration pattern. *Biomaterials* 2004; 25: 3541-3552.
- [45] Ma L, Gao C, Mao Z, Zhou J, Shen J. Enhanced biological stability of collagen porous scaffolds by using amino acids as novel cross-linking bridges. *Biomaterials* 2004; 25: 2997-3004.
- [46] Lu P, Takai K, Weaver VM, Werb Z. Extracellular matrix degradation and remodeling in development and disease. *Cold Spring Harb Perspect Biol* 2011; 3: a005058.
- [47] Hersch N, Wolters B, Dreissen G, Springer R, Kirchgeßner N, Merkel R, Hoffmann B. The constant beat: cardiomyocytes adapt their forces by equal contraction upon environmental stiffening. *Biol Open* 2013; 2: 351-361.
- [48] Engler AJ, Carag-Krieger C, Johnson CP, Raab M, Tang HY, Speicher DW, Sanger JW, Sanger JM, Discher DE. Embryonic cardiomyocytes beat best on a matrix with heart-like elasticity:

## Protocols for myocardial decellularization

- scar-like rigidity inhibits beating. *J Cell Sci* 2008; 121: 3794-3802.
- [49] Bhana B, Iyer RK, Chen WL, Zhao R, Sider KL, Likhitpanichkul M, Simmons CA, Radisic M. Influence of substrate stiffness on the phenotype of heart cells. *Biotechnol Bioeng* 2010; 105: 1148-1160.
- [50] Berry MF, Engler AJ, Woo YJ, Pirolli TJ, Bish LT, Jayasankar V, Morine KJ, Gardner TJ, Discher DE, Sweeney HL. Mesenchymal stem cell injection after myocardial infarction improves myocardial compliance. *Am J Physiol Heart Circ Physiol* 2006; 290: H2196-H2203.
- [51] Zhang S, Sun A, Ma H, Yao K, Zhou N, Shen L, Zhang C, Zou Y, Ge J. Infarcted myocardium-like stiffness contributes to endothelial progenitor lineage commitment of bone marrow mononuclear cells. *J Cell Mol Med* 2011; 15: 2245-2261.
- [52] Witzenburg C, Raghupathy R, Kren SM, Taylor DA, Barocas VH. Mechanical changes in the rat right ventricle with decellularization. *J Biomech* 2012; 45: 842-849.
- [53] Lockhart M, Wirrig E, Phelps A, Wessels A. Extracellular matrix and heart development. *Birth Defects Res A Clin Mol Teratol* 2011; 91: 535-550.
- [54] Aleksandrova A, Czirók A, Szabó A, Filla MB, Hossain MJ, Whelan PF, Lansford R, Rongish BJ. Connective tissue movements play a major role in avian endocardial morphogenesis. *Dev Biol* 2012; 362: 348-361.
- [55] Trinh LA, Stainier DY. Fibronectin regulates epithelial organization during myocardial migration in zebrafish. *Dev Cell* 2004; 6: 371-382.
- [56] Rigol M, Solanes N, Farré J, Roura S, Roqué M, Berruezo A, Bellera N, Novensà L, Tamborero D, Prat-Vidal C, Huzman MA, Batlle M, Hoefsloot M, Sitges M, Ramírez J, Dantas AP, Merino A, Sanz G, Brugada J, Bayés-Genís A, Heras M. Effects of adipose tissue derived stem cell therapy after myocardial infarction: impact of the route of administration. *J Card Fail* 2010; 16: 357-366.
- [57] Kumar BM, Yoo JG, Ock SA, Kim JG, Song HJ, Kang EJ, Cho SK, Lee SL, Cho JH, Balasubramanian S, Rho GJ. In vitro differentiation of mesenchymal progenitor cells derived from porcine umbilical cord blood. *Mol Cells* 2007; 24: 343-350.
- [58] Ock SA, Jeon BG, Rho GJ. Comparative characterization of porcine mesenchymal stem cells derived from bone marrow extract and skin tissues. *Tissue Eng Part C Methods* 2010; 16: 1481-1491.
- [59] Cui XJ, Xie H, Wang HJ, Guo HD, Zhang JK, Wang C, Tan YZ. Transplantation of mesenchymal stem cells with self-assembling polypeptide scaffolds is conducive to treating myocardial infarction in rats. *Tohoku J Exp Med* 2010; 222: 281-289.
- [60] Sieminski AL, Semino CE, Gong H, Kamm RD. Primary sequence of ionic self-assembling peptide gel affects endothelial cell adhesion and capillary morphogenesis. *J Biomed Mater Res Part A* 2008; 87: 494-504.
- [61] Xu Y, Patnaik S, Guo X, Li Z, Lo W, Butler R, Claude A, Liu Z, Zhang G, Liao J, Anderson PM, Guan J. Cardiac differentiation of cardiosphere-derived cells in scaffolds mimicking morphology of the cardiac extracellular matrix. *Acta Biomater* 2014; 10: 3449-3662.
- [62] Zhang J, Klos M, Wilson GF, Herman AM, Lian X, Raval KK, Barron MR, Hou L, Soerens AG, Yu J, Palecek SP, Lyons GE, Thomson JA, Herron TJ, Jalife J, Kamp TJ. Extracellular matrix promotes highly efficient cardiac differentiation of human pluripotent stem cells: the matrix sandwich method. *Circ Res* 2013; 111: 1125-1136.
- [63] Grauss RW, Hazekamp MG, Oppenhuizen F, van Munsteren CJ, Gittenberger-de Groot AC, DeRuiter MC. Histological evaluation of decellularised porcine aortic valves: matrix changes due to different decellularisation methods. *Eur J of Cardiothorac Surg* 2005; 27: 566-571.

## Protocols for myocardial decellularization

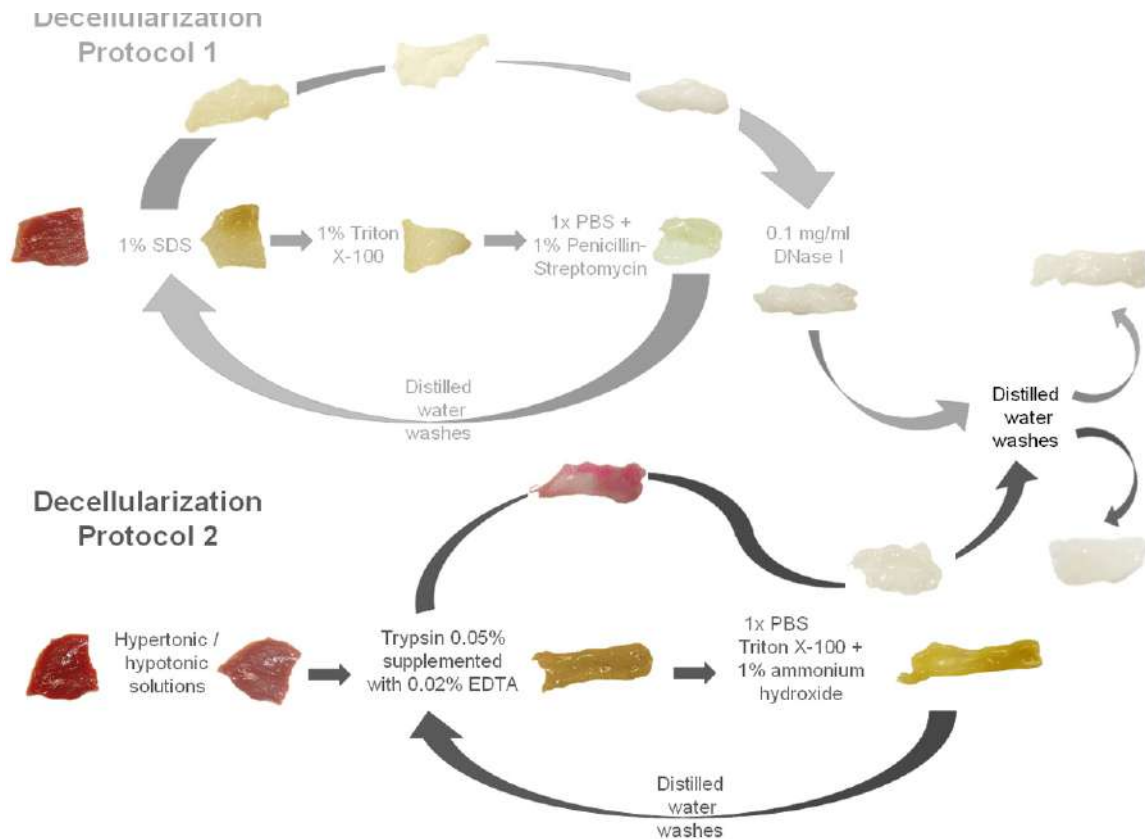


**Figure S1.** Decellularization protocols at a glance. A schematic view of the decellularization protocols plus photographs taken after each step. DP1 started with 1% SDS treatment for 72 h, followed by Triton X-100 treatment for 48 h, and PBS + 1% penicillin/streptomycin washes. This cycle was repeated again with a distilled water wash between cycles. After the second cycle, samples were treated with 0.1 mg/ml DNase I for 72 h at RT. Finally, the scaffolds were washed 3 times with distilled water (2 h/wash). For DP2, tissue was subjected to hypertonic and hypotonic solutions for 2 h each; this cycle was repeated twice, followed by 0.05% trypsin + 0.02% EDTA for 48 h at 37 °C. The solution was replaced after 24 h. Trypsin was replaced by PBS supplemented with 1% Triton X-100 and 1% ammonium hydroxide for 96 h at RT; the solutions were changed every 24 h. Treatment with trypsin and Triton X-100 was repeated with an intermediate wash with distilled water. After the second cycle, the samples were washed with distilled water O/N.

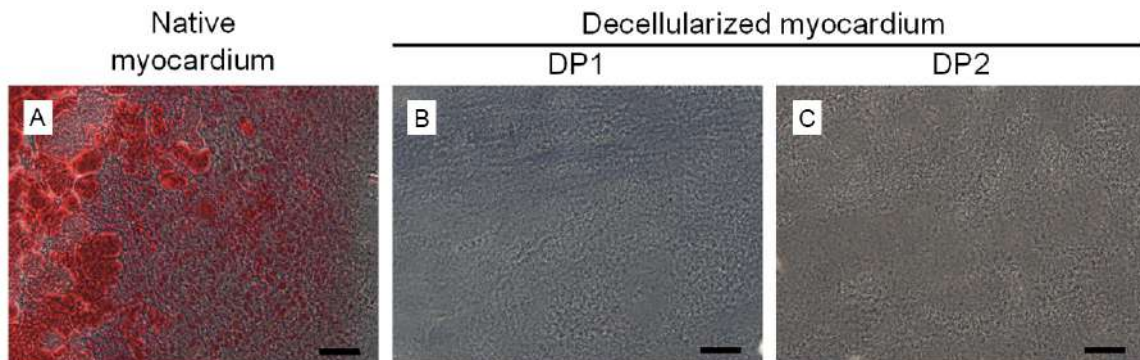


**Figure S2.** Evaluation of adipocyte remnants in decellularized myocardial scaffolds. (A) Oil Red O staining of native myocardium, (B) DP1-decellularized and (C) DP2-decellularized myocardial scaffolds. Lipid and adipocyte remnants are stained red. Scale bars = 50  $\mu$ m.

## Protocols for myocardial decellularization

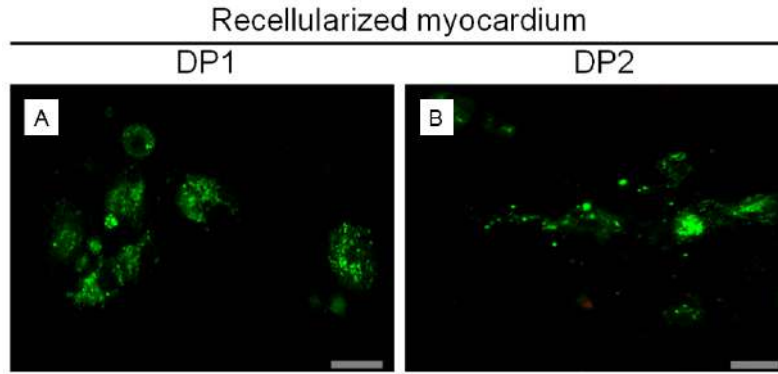
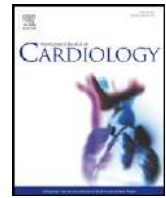


**Figure S3.** ATDPCs viability assessment in the recellularized scaffolds. (A) LIVE/DEAD® assay to test ATDPCs viability in DP1- and (B) DP2-decellularized scaffolds one week after recellularization (n = 3). Green, live cells; red, dead cells. Scale bars = 20  $\mu$ m.



## Online monitoring of myocardial bioprosthesis for cardiac repair



Cristina Prat-Vidal <sup>a,\*</sup>, Carolina Gálvez-Montón <sup>a,1</sup>, Verónica Puig-Sanvicens <sup>b</sup>, Benjamin Sanchez <sup>c</sup>, Idoia Díaz-Güemes <sup>d</sup>, Paco Bogónez-Franco <sup>c</sup>, Isaac Perea-Gil <sup>a</sup>, Anna Casas-Solà <sup>a</sup>, Santiago Roura <sup>a</sup>, Aida Llucià-Valldeperas <sup>a</sup>, Carolina Soler-Botija <sup>a</sup>, Francisco M. Sánchez-Margallo <sup>d</sup>, Carlos E. Semino <sup>b</sup>, Ramon Bragos <sup>c</sup>, Antoni Bayes-Genis <sup>a,e,\*\*</sup>

<sup>a</sup> ICREC (Heart Failure and Cardiac Regeneration) Research Lab, Health Sciences Research Institute Germans Trias i Pujol (IGTP), Cardiology Service, Hospital Universitari Germans Trias i Pujol, Badalona, Barcelona, Spain

<sup>b</sup> Department of Bioengineering, Institut Químic de Sarrià (IQS), Universitat Ramon Llull, Barcelona, Spain

<sup>c</sup> Electronic and Biomedical Instrumentation Group, Departament d'Enginyeria Electrònica, Universitat Politècnica de Catalunya (UPC), Barcelona, Spain

<sup>d</sup> Jesús Usón Minimally Invasive Surgery Centre, JUMISC, Cáceres, Spain

<sup>e</sup> Department of Medicine, University Autonomous of Barcelona (UAB), Barcelona, Spain

### ARTICLE INFO

#### Article history:

Received 14 November 2013

Received in revised form 7 March 2014

Accepted 17 April 2014

Available online 26 April 2014

#### Keywords:

Myocardial infarction

Decellularized pericardium

Adipose tissue derived progenitor cells

Myocardial bioprosthesis

Swine model

### ABSTRACT

**Background/objectives:** The aim of this study was to develop a myocardial bioprosthesis for cardiac repair with an integrated online monitoring system.

Myocardial infarction (MI) causes irreversible myocyte loss and scar formation. Tissue engineering to reduce myocardial scar size has been tested with variable success, yet scar formation and modulation by an engineered graft is incompletely characterized.

**Methods:** Decellularized human pericardium was embedded using self-assembling peptide RAD16-I with or without GFP-labeled mediastinal adipose tissue-derived progenitor cells (MATPCs). Resulting bioprostheses were implanted over the ischemic myocardium in the swine model of MI ( $n = 8$  treated and  $n = 5$  control animals). For *in vivo* electrical impedance spectroscopy (EIS) monitoring, two electrodes were anchored to construct edges, covered by NanoGold particles and connected to an impedance-based implantable device. Histological evaluation was performed to identify and characterize GFP cells on *post mortem* myocardial sections. **Results:** Pluripotency, cardiomyogenic and endothelial potential and migratory capacity of porcine-derived MATPCs were demonstrated *in vitro*. Decellularization protocol efficiency, biodegradability, as well as *in vitro* biocompatibility after recellularization were also verified. One month after myocardial bioprosthesis implantation, morphometry revealed a 36% reduction in infarct area, Ki67<sup>+</sup>-GFP<sup>+</sup>-MATPCs were found at infarct core and border zones, and bioprosthesis vascularization was confirmed by presence of *Griffonia simplicifolia* lectin I (GSLI) B4 isolectin<sup>+</sup>-GFP<sup>+</sup>-MATPCs. Electrical impedance measurement at low and high frequencies (10 kHz–100 kHz) allowed online monitoring of scar maturation.

**Conclusions:** With clinical translation as ultimate goal, this myocardial bioprosthesis holds promise to be a viable candidate for human cardiac repair.

© 2014 Elsevier Ireland Ltd. All rights reserved.

\* Correspondence to: C. Prat-Vidal, ICREC (Heart Failure and Cardiac Regeneration) Research Lab, Health Sciences Research Institute Germans Trias i Pujol (IGTP), Ctra. De Can Ruti, Camí de les Escoles s/n, 08916 Badalona (Barcelona), Spain. Tel.: +34 93 4978662; fax: +34 93 4978654.

\*\* Correspondence to: A. Bayes-Genis, ICREC (Heart Failure and Cardiac Regeneration) Research Lab, Head of Cardiology Service, Hospital Universitari Germans Trias i Pujol, Crta. Canyet, s/n, 08916 Badalona (Barcelona), Spain. Tel.: +34 93 4978915; fax: +34 93 4978939.

E-mail addresses: [cprat@igtp.cat](mailto:cprat@igtp.cat) (C. Prat-Vidal), [abayesgenis@gmail.com](mailto:abayesgenis@gmail.com)

(A. Bayes-Genis).

<sup>1</sup> Both authors contributed equally to this work.

### 1. Introduction

Myocardial infarction (MI) management has dramatically evolved in the past 50 years with the incorporation of evidence-based medicine (aspirin,  $\beta$ -blockers and ACE-I), and the widespread use of coronary stents for occluded coronary arteries. Although the residual scar has become smaller as innovations emerged, there is still a portion of the heart that becomes hypo- or akinetic following MI. Progenitor cells and tissue engineering are being proposed as an addition to conventional therapies of damaged myocardium [1]. Engineered tissue grafts and myocardial bioprostheses aim to improve cellular engraftment and viability, combining cellular components with supporting materials. A myocardial bioprosthesis should be able to mimic structural cardiac muscle architecture, be deformable to support cardiac contraction, and encourage

cell coupling with host tissue as well as promote the vascularization of the newly formed tissue [2].

Online monitoring of biological parameters is evolving quickly. New generation implantable cardioverter defibrillators already wear monitoring algorithms for online testing of ventricular arrhythmias [3]. Tele-health systems are also under development and validation for a closer monitoring of post-infarction patients [4,5]. In that way, electrical impedance spectroscopy (EIS) has been proven to be a valid technique to properly identify healthy from necrotic myocardium both *in vivo* and *ex vivo post mortem* studies [6–9]. Accordingly, we developed and tested a new 3D cell-based myocardial bioprosthesis, composed by human decellularized pericardium refilled with a mixture of RAD16-I hydrogel and porcine mediastinal adipose tissue-derived progenitor cells (MATPCs), together with an implantable EIS measurement system for *in vivo* online monitoring of scar formation in the swine model of MI.

## 2. Methods

### 2.1. Mediastinal adipose tissue-derived progenitor cells (MATPCs)

Mediastinal adipose tissue biopsy samples (average 0.4–5.9 g) were obtained from pigs undergoing cardiac surgery ( $n = 5$ ) and processed as previously described [10].

#### 2.1.1. Flow cytometry

Isolated MATPCs (passages 4–8) were collected and immunostained with specific monoclonal antibodies against CD105 (Abcam), CD44, CD45, CD14 (AbD Serotec), CD29, CD34, CD90 and CD106 (BD Pharmingen). Intensity levels of each antigen were defined by the ratio between specific antibody and IgG isotype control or secondary antibody (1 = no difference). A FACSCanto II flow cytometer (BD Biosciences) was used for all data acquisitions, and analyses were carried out using the BD FACSDiva™ software (BD Biosciences).

#### 2.1.2. Quantitative real-time PCR

Total RNA was isolated from MATPCs using the AllPrep RNA/Protein Kit (Qiagen). cDNA was synthesized from 2 µg of total RNA using random hexamers (Qiagen) and the iScript™ One-Step RT-PCR Kit (BioRad Laboratories) according to the manufacturer's protocol. Each sample was run in duplicate and experiments were repeated three times to confirm the results. Quantitative real-time PCR protocol is detailed in the Supplementary Methods.

#### 2.1.3. Immunocytofluorescence staining

MATPCs were labeled with anti-GATA4 (2 µg/mL; R&D Systems), anti-cTnI, anti-Ki67 (2 µg/mL; Santa Cruz Biotechnology), anti-Cx43 (2.5 µg/mL; BD Transduction) or with biotinylated *Griffonia simplicifolia* lectin I (GSLI) B4 isolectin (0.5 µg/mL; Vectors labs). Detailed protocol is provided in the Supplementary Methods.

### 2.2. Pericardial scaffold and RAD16-I hydrogel

#### 2.2.1. Preparation of decellularized pericardial scaffold

Surgical samples of human pericardium were obtained from 39 patients (27 males, 12 females; mean age = 68 ± 11 years; range = 50 to 84 years) undergoing cardiothoracic surgery, with apparently healthy pericardia. This study was approved by local ethics committee, and written informed consent was obtained from all individuals. The study protocols conformed to the principles outlined in the Declaration of Helsinki.

Superficial adhered adipose tissue was removed mechanically from pericardia by scrapping in PBS. For decellularization, detergent washes with 1% sodium dodecyl sulfate (Sigma) for 72 h followed by 1% Triton X-100 for 48 h were performed at room temperature with stirring to facilitate cell removal [11,12], and solutions were replaced every 24 h. Decellularized pericardial scaffolds were rinsed 3 times during 24 h using PBS with 1% penicillin-streptomycin and then treated with 0.1 mg/mL DNase (Roche) in sterile distilled water for 3 additional days. Finally, scaffolds were washed in PBS and stored at 4 °C until further use.

#### 2.2.2. DNA detection and quantification

Decellularized pericardial scaffolds were embedded in Tissue-Tek® OCT compound (Sakura) and sectioned at a thickness of 10 µm. Slices were stained 10 min with Hoechst 33342 (Sigma) for cell nuclei detection. PureLink® Genomic DNA kit (Invitrogen) was used to isolate total genomic DNA from both native pericardium ( $n = 5$ ) and decellularized scaffolds ( $n = 5$ ) following the manufacturer's instructions, and later quantified by spectrophotometry (NanoDrop ND-1000, NanoDrop Technologies). Total amount of DNA was normalized according to the weight in mg for each sample (average 16.5–22.8 mg), and results were presented as mean ± SD. Differences between groups were evaluated using Student *t*-test, and a *P* value < 0.05 was considered significant.

#### 2.2.3. In vitro degradation of decellularized scaffolds

Lyophilized pericardial scaffolds ( $n = 12$ ) were weighed and incubated with 0.1% collagenase I (Gibco) under shaking at 37 °C. After 24 h, samples were removed, rinsed with

distilled water, lyophilized and weighed again. Percentage of biodegradability was calculated as previously detailed [13]. Results were showed as mean ± SD, and statistical significance was evaluated using paired Student *t*-test. Statistical test was considered significant when  $p < 0.05$ .

### 2.2.4. Pericardial scaffold assembling and recellularization

When indicated, sterilized platinum electrodes were anchored to the lyophilized scaffold (20 mm × 10 mm) before hydrogel loading. Then, NanoGold solution (20 µL) was applied to the anchoring area of electrodes to favor the flow electrical current within the scaffold to the hydrogel. Parallel GFP<sup>+</sup>-MATPCs were trypsinized, counted and resuspended in 10% sucrose at a final concentration of  $1 \times 10^7$  cells/mL, and hydrogel was diluted with sucrose to obtain a solution of 0.3% (w/v) RAD16-I in sucrose 10%. Next, equal volume (175 µL) of cell suspension and RAD16-I 0.3% solution were mixed to render a final cell suspension of  $1.75 \times 10^6$  cells/mL in 0.15% RAD16-I, 10% sucrose. This suspension was mixed carefully, loaded into the scaffold and covered with 350 µL of α-MEM to increase the ionic strength, inducing RAD16-I peptide self-assembling and gel formation. When indicated, pericardial scaffolds were loaded with 350 µL of RAD16-I 0.15% (w/v) sucrose 10% without GFP<sup>+</sup>-MATPCs.

### 2.3. EIS monitoring system and in vivo experiments

The bioimpedance measurement system consisted of a custom-implantable bioimpedance device for tissue impedance measurement with a wireless Zigbee link to transmit impedance records and a computer to log, process and display data [14]. The healthy myocardium should present an impedance relaxation (magnitude fall) in the upper part of the measurement frequency range, while the healed scar displays a flat frequency spectrum, as a result of the absence of viable cell membranes [15]. The impedance at 10 kHz is below the relaxation while the impedance at 100 kHz is close to the relaxation. The bioimpedance devices were encapsulated with a biocompatible polydimethylsiloxane silicone (Sylgard 184, Dow Corning Corp.) and sterilized by prior to the implantation using chemical agents, as previously described [16].

The study protocol was approved by the local Animal Experimentation Unit Ethical Committee and complies with all guidelines concerning the use of animals in research and teaching as defined by the *Guide for the Care and Use of Laboratory Animals* (NIH Publication No. 80-23, revised 1996). A total of 13 female crossbreed Landrace × Large White pigs (20–30 kg) were used for the study. After left lateral thoracotomy through the fourth intercostal space, acute MI was induced by a permanent double ligation of the first marginal branch of the circumflex artery, as previously described [1]. Thirty minutes after MI induction, myocardial bioprosthesis implantation over the ischemic myocardium was performed with surgical glue (Glubran®2, Cardioliink) (treated group;  $n = 8$ ). Prostheses without GFP<sup>+</sup>-MATPCs were implanted in a control group of animals ( $n = 5$ ). Additionally, 10 animals with MI (without any prosthesis) and 3 sham animals (healthy myocardium with GFP<sup>+</sup>-MATPCs bioprosthesis) were included. In the five controls and in two of treated animals myocardial bioprosthesis were connected to the EIS monitoring system. Reliable EIS results were only obtained from one control and one treated animal. After 1 month, animals were sacrificed with an intravenous injection of potassium chloride solution to obtain samples for histological analysis. In all animals, left ventricular (LV) infarct size was double blindly measured in digitally photographed transverse heart sections from 1 cm distally to coronary ligation. Quantitative morphometric measurements were completed with Image-Pro Plus software (6.2.1 version; Media Cybernetics, Inc.). Data are presented as mean ± SD. All analyses were performed with SPSS (15.0.1 version, SPSS, Inc.). Differences between groups were compared using Student's *t*-test, and values of  $p < 0.05$  were considered significant.

## 3. Results

### 3.1. Isolation and characterization of porcine MATPCs

Primary cell cultures from porcine mediastinal adipose tissue were successfully established and characterized. A few elongated fibroblast-like cells appeared attached after 3–4 days and could be maintained in culture (~15 passages) with a duplication time of  $3.7 \pm 0.9$  days. Immunophenotypical characterization revealed an MSC-like pattern, with over 80% of cells positive for CD29, CD44, CD90 and CD105 and negative for CD14, CD34, CD45 and CD106 (Fig. 1A). Porcine MATPCs pluripotency was demonstrated by cell differentiation into osteogenic, adipogenic and chondrogenic lineages (Supplementary Fig. 1A). Basal expression of cardiac markers was analyzed using both quantitative real-time PCR and immunofluorescence. MATPC gene expression analysis revealed high expression of Cx43 and traces of GATA4 (Fig. 1B). At protein level, MATPCs expressed Cx43 and GATA4 and were negative for cTnI (Fig. 1C). As observed in 2D cultures, 3D-MATPCs constructs showed positive expression for Cx43 and GATA4 and were negative for cTnI (Supplementary Fig. 1B). To determine endothelial potential, MATPCs were cultured in EGM-2 medium for 15 days. The majority of



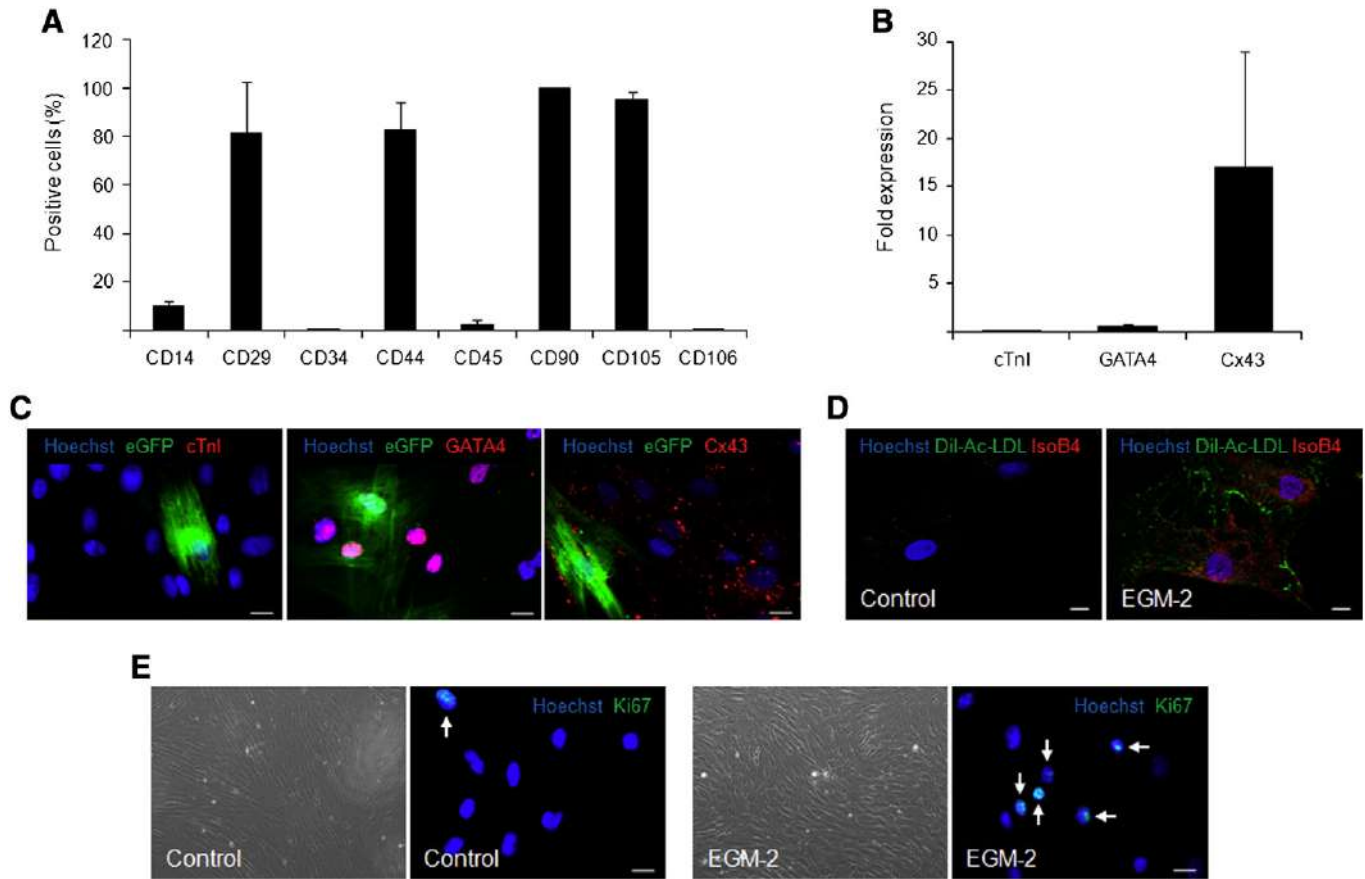


**Fig. 1.** Isolation and characterization of porcine MATPCs. (A) Flow cytometry analysis of MATPCs immunophenotyping ( $n = 5$ ). (B) Quantitative real-time PCR of cardiomyogenic genes in MATPCs ( $n = 5$ ). Values were normalized to GUSB housekeeping gene expression and shown as mean  $\pm$  SEM. Each sample was run in duplicate and experiments were repeated three times. (C) Basal expression of cardiac markers in GFP<sup>+</sup>-MATPCs assessed by immunocytofluorescence ( $n = 3$ ). Specific immunodetection of GFP (green) and cardiac proteins cTnI, GATA4 and Cx43 (red) is shown. Nuclei were counterstained with Hoechst 33342 (blue). Scale bars, 20  $\mu$ m. (D) Representative images showing differences in Dil-Ac-LDL uptake by MATPCs and GSLI B4 isolectin-staining in both control and EGM-2 conditions. A minimum of 5 visual fields per condition and experiment ( $n = 3$ ) were analyzed. Scale bars, 50  $\mu$ m. (E) Representative phase-contrast images of MATPCs cultured in control and EGM-2 conditions exhibiting endothelial cell-like morphology in treated cells;  $\times 100$  magnification. Specific detection of Ki67 as cell proliferation marker by indirect immunofluorescence is also shown (arrows indicate positive cells).  $n = 3$ ; scale bars, 20  $\mu$ m.

cells cultured in EGM-2 exhibited a small, endothelial cell-like morphology, a faster proliferation rate, incorporation Dil-Ac-LDL and expression of GSLI B4 isolectin (Fig. 1D, E). Cell migration assays using culture-inserts showed a high capacity to colonize cell-free tissue by swine MATPCs (surface recovery index) (Supplementary Fig. 1C, D).

### 3.2. Pericardial scaffold preparation and recellularization

After detergent treatment, human pericardia were pale collagen scaffolds free of cellular debris and rich in filaments (Fig. 2A–H). Total DNA content within the acellular scaffold ( $66 \pm 24$  ng DNA/mg scaffold) was significantly lower ( $p = 0.012$ ) than that obtained for native pericardium ( $214 \pm 79$  ng DNA/mg pericardium), serving as positive control (Fig. 2I). Furthermore, the biodegradability of decellularized pericardial scaffolds was determined (Fig. 2J). Pericardial scaffolds lost ~70% of their original weight after 24 h of incubation in PBS containing 0.1% collagenase I at 37 °C ( $p < 0.001$ ). Xenotransplantation of human pericardial constructs to swine myocardium did not elicit an inflammatory response.

The RAD16-I peptide nanofibers spontaneously self-assemble by contact with salt-containing buffers or media [17]. Thus, after washing in PBS solution, pericardia were lyophilized (Fig. 2K–N) and rehydrated with distilled water or with a solution of RAD16-I at 0.15% (Fig. 2L, N). We observed positive Congo red staining exclusively in pericardia embedded with RAD16-I, confirming the presence of  $\beta$ -sheet structures spontaneously generated in the self-assembling phenomenon promoted

by PBS salts (Fig. 2N). Combining MATPCs with the hydrogel we generated an optimal 3D network inside the scaffold. To evaluate the ability of pericardial scaffold to support cell adhesion and proliferation, *in vitro* experiments were performed with RAD16-I and porcine MATPCs. Recellularization was verified by Masson's trichrome 1-week after cell reseeding *in vitro* (Fig. 2O, P) and live/dead staining was used to visualize cell viability within the scaffolds (Fig. 2Q, R).

### 3.3. Myocardial bioprosthesis implantation in a swine model of acute MI

Steps for electrode assembling, NanoGold loading and hydrogel RAD16-I refilling of pericardial scaffold are shown in Fig. 3. Culture medium was applied to induce hydrogel self-assembling and gel formation (Fig. 3A–E), and 30 min after coronary artery ligation, myocardial bioprosthesis were implanted over ischemic myocardium (Fig. 3F–L). None of the studied animals died during experimentation or follow-up and cardiac examination upon sacrifices showed myocardial bioprostheses remaining covering the infarct area in all pigs (Fig. 3K). No statistically significant differences in the circulating levels of cTnI, creatine kinase-MB and myoglobin were found between treated (bioprosthesis filled with GFP<sup>+</sup>-MATPCs) and control (matrix without cells) groups. There were no significant differences in infarct size between infarct animals without bioprosthesis and infarct animals with matrix alone ( $7.7 \pm 3.9\%$  vs.  $10.3 \pm 5.2\%$ , respectively;  $p = 0.31$ ) (Supplementary Fig. 2). Moreover, sham animals did not show myocardial injury caused by bioprosthesis implantation (data not shown).

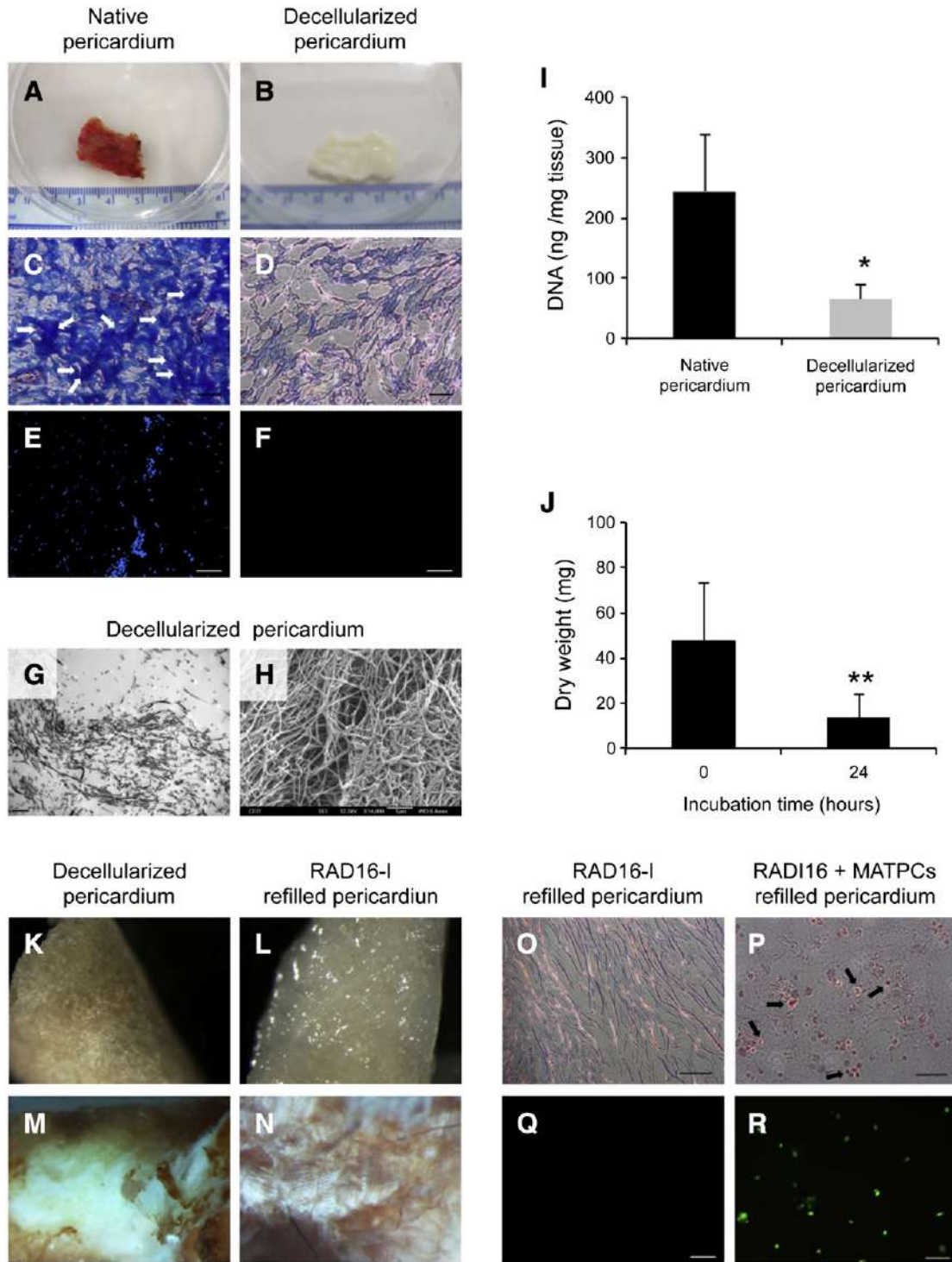


**Fig. 2.** Obtaining of decellularized pericardial scaffolds. (A) Photograph of a native pericardial sample obtained from a patient undergoing cardiac surgery. (B) Resulting decellularized pericardial scaffold after detergent treatment. (C) Masson's trichrome staining of the native pericardium (D) and the acellular pericardial scaffold. Collagen fibers stain as dark blue and cytoplasm in light red. (E) Hoechst 33324 nuclei staining (blue) before (F) and after decellularization protocol shows no residual nucleic acids in decellularized pericardial scaffold. (G) Transmission (H) and scanning electron microscope images of a decellularized pericardium showing filaments structure;  $\times 15000$  and  $\times 14000$  magnification, respectively. (I) DNA quantification before and after decellularization treatment in pericardial pieces ( $n = 5$ ). Samples were normalized to the scaffold weight and data are shown as mean  $\pm$  SD ( $*p = 0.012$ ). (J) Weight loss of decellularized pericardial scaffolds ( $n = 12$ ) after incubation with 0.1% collagenase I at 37 °C for 24 h. Data are represented as mean  $\pm$  SD ( $**p < 0.001$ ). (K) Macroscopic morphology of human lyophilized pericardium under stereoscope observation (L) and after being rehydrated with RAD16-I 0.15%. (M) Congo red staining of a pericardium embedded with water, rich in  $\alpha$ -helix structures, (N) and embedded with RAD16-I 0.15%, rich in  $\beta$ -sheet nanofibers. (O) Masson's trichrome staining of decellularized pericardial scaffold (P) and after 1 week of recellularization with porcine MATPCs. (Q–R) Scaffold biocompatibility was confirmed by Live/Dead assay after 1 week of culture ( $n = 3$ ) (green, live cells; red, dead cells). Scale bars, 100  $\mu$ m.

However, morphometry revealed that LV infarct area was 36% smaller in pigs implanted with cell-rich myocardial bioprostheses compared to controls ( $6.5 \pm 3.6\%$  vs.  $10.2 \pm 4\%$ ). In treated animals, GFP<sup>+</sup>-MATPCs

were detected at both infarct core (Fig. 3M, N) and border zones (Fig. 3Q, R) 1 month after implantation as well as within the myocardial bioprosthesis (Fig. 3U, V), not at remote myocardium (data not shown).

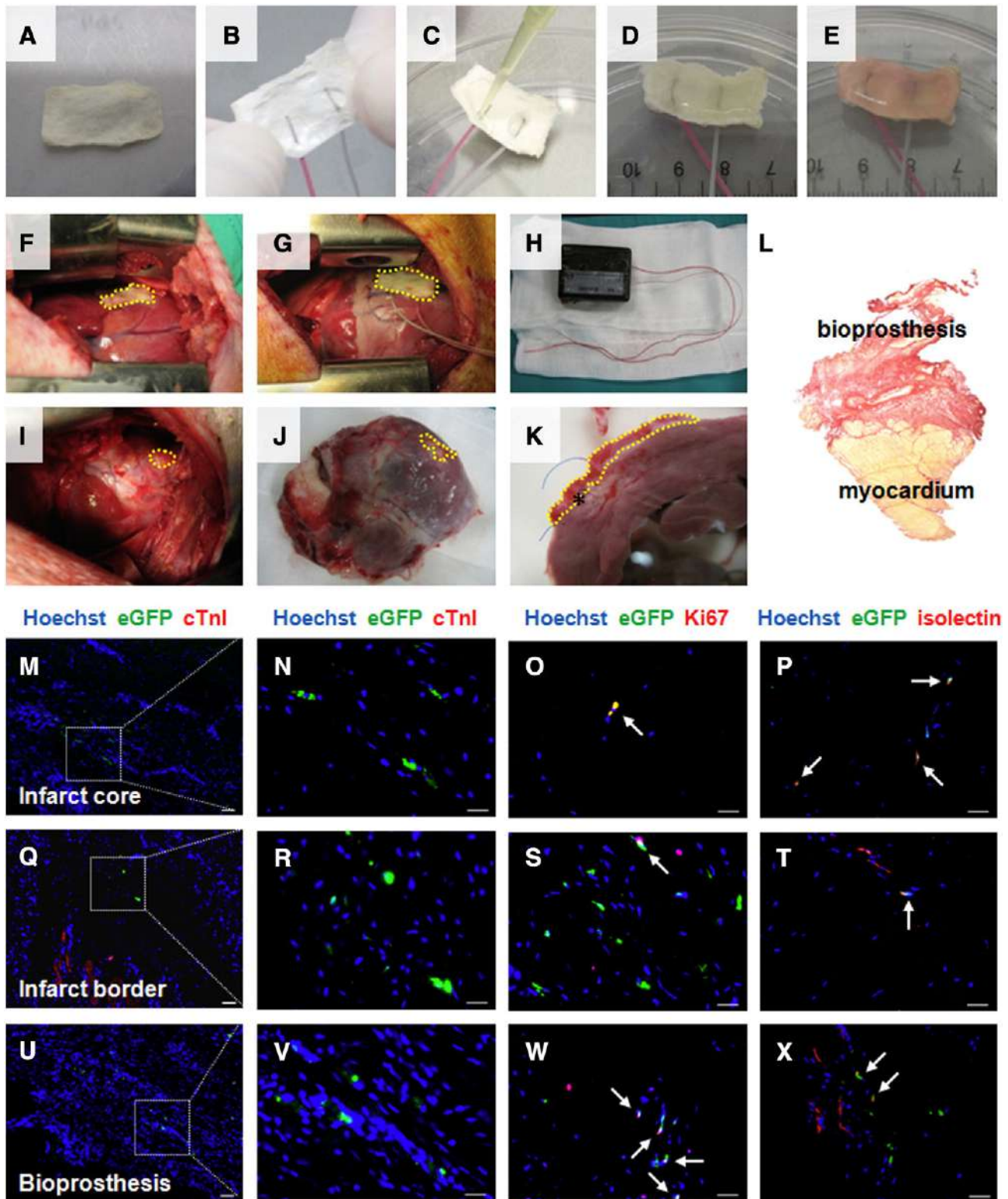


**Fig. 3.** Myocardial bioprosthesis assembling, implantation and histological examination of MATPCs engraftment in porcine infarcted hearts. (A) Pericardial scaffold after being decellularized, lyophilized and sterilized. (B) After metallic electrodes anchoring, (C) NanoGold solution, (D) hydrogel (E) and culture medium are loaded in the decellularized pericardial scaffold. (F) A myocardial bioprosthesis implanted over the ischemic myocardium (G) and another bioprosthesis with anchored platinum electrodes implanted in an infarcted heart. (H) Implantable system sealed with biocompatible polydimethylsiloxane silicone. (I) Bioprosthesis placed over the infarcted myocardium in a control pig at sacrifice. (J) Myocardial bioprosthesis residues remained 1 month post-implantation over the explanted heart surface. (K) Transversal heart section of a treated pig with the attached bioprosthesis indicated (dotted yellow line). (L) Photomontage of Sirius red-stained histological images obtained from a section of myocardium with the attached myocardial bioprosthesis distinguishing cardiac muscle (yellow) and collagen content in the bioprosthesis (red). (M) Immunofluorescence against cTnI (red) and GFP (green) shows GFP<sup>+</sup>-MATPCs at the infarct core, (Q) infarct border and (U) myocardial bioprosthesis after 1 month of implantation. Nuclei are counterstained with Hoechst 33342 (blue). (N, R, V) Zoomed images from M, Q and U, respectively. Scale bars, 20  $\mu$ m. (O, S, W) Fluorescence images showing some GFP<sup>+</sup>-MATPCs expressing Ki67 (P, T, X) and GS LI B4 isolectin (indicated by arrows) together with Hoechst nuclei staining. Scale bars, 20  $\mu$ m.

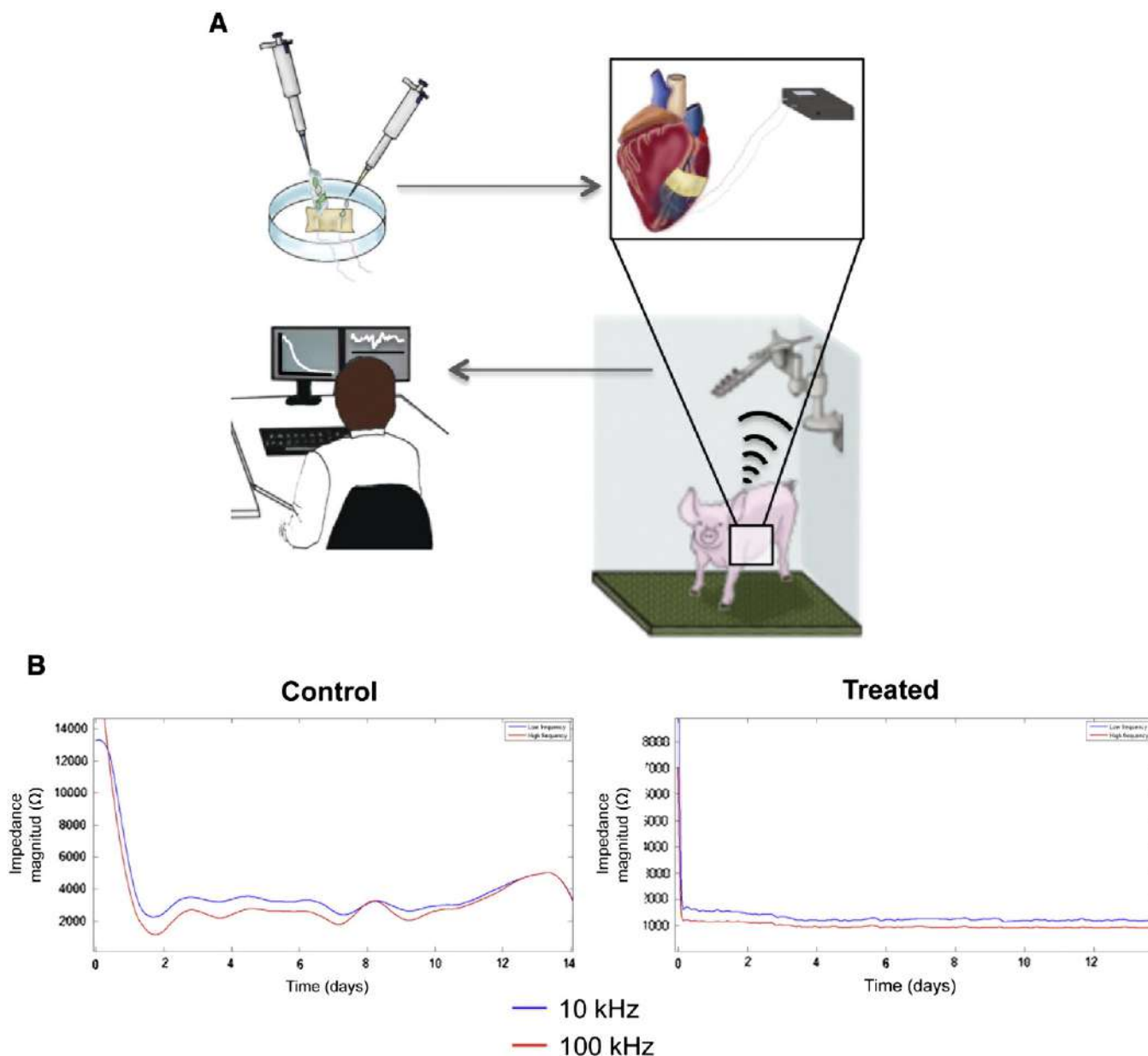


**Fig. 4.** Schematic illustration for the *in vivo* bioprosthesis implantation process in the swine heart. (A) The recording electrodes of the impedance monitoring system are connected to the myocardial bioprosthesis to measure its electrical properties. After implantation, a wireless link between the implantable system and a PC is established to transmit data for processing and displaying purposes. (B) Graph showing temporal evolution of the myocardial bioprosthesis impedance magnitude at 10 kHz (blue) and 100 kHz (green) during 10 days. Data correspond to a control and a treated pig.

Proliferation capacity was demonstrated with nuclear expression of Ki67 by GFP<sup>+</sup> cells (Fig. 3O, S, W). In addition, we found GSL1 B4 isolectin<sup>+</sup>-GFP<sup>+</sup>-MATPCs in infarct and border regions and frank vascularization inside the myocardial bioprosthesis (Fig. 3P, T, X). The wireless electrical impedance measurement system and the impedance magnitude records during 10 days after myocardial bioprosthesis implantation from a control and a treated animal are shown in Fig. 4. Low-frequency measurements present a higher impedance value than high frequency measurements the first days and both converge to similar values over time, which is coherent with which could be expected along the gradual scar formation.

#### 4. Discussion

In the present study, we developed a new myocardial bioprosthesis, composed by decellularized human pericardium embedded with a mixture of the hydrogel RAD16-I and GFP-labeled MATPCs isolated from

porcine mediastinal fat. First, we characterized MATPCs phenotypically and demonstrated standard MSC pluripotency, cardiomyogenic and endothelial potential and migratory capacity of these cell populations *in vitro*. Next, we evaluated decellularization protocol efficiency and biodegradability of pericardial scaffolds before hydrogel refilling as well as *in vitro* biocompatibility after recellularization. Afterwards, we implanted the myocardial bioprosthesis in the porcine model of MI for cardiac repair and monitored the scar evolution *in vivo* during 10 days using an implantable EIS measurement system. One month after implantation, we found GFP-labeled MATPCs in the myocardial tissue and an apparent vascularization inside the myocardial bioprosthesis. Finally, we registered bioimpedance at low and high frequencies by an implanted EIS system, allowing online monitoring of scar evolution.

Up to now, porcine-derived mesenchymal stem cells (MSCs) have been reported from bone marrow [18], subcutaneous adipose tissue [19], umbilical cord blood [20] and peripheral blood [21]. Our data show that porcine MATPCs can be easily isolated from mediastinal fat

and expanded in culture forming a homogenous cell population with MSC-like phenotype, denoting standard pluripotency as well as expression of some cardiac markers and endothelial potential. Taken together, these results suggest that porcine MATPCs may be promising candidates for cardiac regeneration pre-clinical studies.

To mimic a native healthy tissue the best option is the native extracellular matrix itself, which guides cellular attachment, survival, migration, proliferation and differentiation [22]. Although pericardial matrix is not an exact match for ventricular myocardial matrix, the pericardium is thought to influence myocardial contraction and epicardial vessel properties [23]. Furthermore, while the pericardium provides some structural support for the heart, it is routinely left unsutured, cut or even removed when cardiothoracic surgery is complete, without adverse consequences. Thus, in this work, we used decellularized human pericardium (thicker and more resistant than swine pericardium), obtained from patients undergoing cardiothoracic surgery who would be the likely targets of this therapy. Considering its ready availability, a piece of pericardium could be obtained by thoracoscopic pericardiectomy, a minimally invasive procedure, and processed with low cost to be an autologous/allogeneic treatment, as has been done for valve replacement and LV reconstruction [24,25].

Self-assembling peptides, which are able to form nanofibrous gels at physiologic pH, are ideal candidate as cell culture matrix in tissue engineering since its biomechanical properties are similar to natural ECM [26]. Specifically, RAD16-I peptide provides a suitable mechanism for self-assembly into highly organized nanostructures associated with 3D network formation, a favorable milieu for cell adhesion, spreading, migration, growth and differentiation. Extensive studies have already indicated their good biocompatibility and biodegradability [27]. A bioresorbable scaffold should be able to support cell growth and have a relatively fast rate of degradation [28]. In general, ECM-based scaffolds show relatively fast degradation *in vivo* and are generally replaced by the ECM proteins secreted by the ingrowing cells [29]. Here, we used a complex ECM-based bioprosthesis, composed by decellularized human pericardium refilled with a combination of porcine MATPCs and the self-assembling peptide RAD16-I. Combining these progenitor cells with the hydrogel, we generated an optimal 3D network inside the scaffold, promoting MATPCs proliferation and differentiation toward endothelial lineage and favouring cell migration from the myocardial bioprosthesis to the injured myocardium. In addition, evidences of biocompatibility and biodegradation of the resulting bioprosthesis were further provided both *in vitro* and *in vivo*.

Nanoparticles have been increasingly used in the design of hybrid nanomaterials for diverse fields. Combination of nanosized inorganic particles, such as NanoGold, with materials or biomolecules optimizes the properties of the tailored product [30,31]. In this study, we combined NanoGold particles with the self-assembling peptide RAD16-I to permit electrical current flow within the myocardial bioprosthesis to the peptide hydrogel. Attaching conductive metal nanocrystals to a peptide is one of the greatest challenges in electronics industry [32]. Indeed, we used pre-synthesized RAD16-I cross-linked to biotin motifs. Taking advantage of the high affinity of biotin to streptavidin, we mixed biotin-RAD16-I to a suspension of streptavidin-NanoGold and, after self-assembling at high ionic strength, the scaffold enclosed particles of gold in its tertiary structure. Tailored scaffold with NanoGold particles around the electrode area should result in a reduction of the electrode contact impedance and, thus, in a more sensitive record of the myocardial bioprosthesis passive electrical properties.

The wireless electrical impedance measurement system recorded impedance values during 10 days after myocardial bioprosthesis implantation. In all animals, the initial transient with high impedance values is coherent with impedance behavior during acute myocardial infarction [33], although it may be also caused by the electrode-implant or implant-tissue stabilization. The phase with low-frequency impedance higher than high frequency impedance is consistent with the formation of the scar [15]. Ultimately, the resistive behavior of

healed scar is revealed from days 9 to 21, when the impedance magnitude remains stable. A prolonged bioimpedance measurement should be considered for quantifying *in situ* related changes to cardiac regeneration by the myocardial bioprosthesis in the infarcted tissue.

In summary, proof of concept has been established for the use of a new myocardial bioprosthesis for cardiac repair. In a next step, this pericardium-based bioprosthesis could be deliverable via currently used, minimally invasive methods, to promote neovascularization and progenitor cell homing into damaged myocardium *in vivo*, with the EIS-based system serving as a non-invasive online audit of scar evolution. Novel myocardial bioprosthesis with online monitoring of cardiac repair may accelerate clinical translation.

Supplementary data to this article can be found online at <http://dx.doi.org/10.1016/j.ijcard.2014.04.181>.

## Acknowledgments

The authors wish to thank the consenting patients who made this study possible. We also thank Department of Cardiac Surgery members for their collaboration in obtaining human samples; Dr. J. Blanco for the kind donation of the CMV-PLuc-GFP lentiviral vector and Dr. Juli R. Bagó for his support on transduction experiments; Laura Hernández from the JUMISC for her support on animal surgery; and Anatomical Pathology Service and Dr. Maite Fernández-Figueras from the Electron Microscopy Unit of our institution for the kind assistance with transmission electron microscopy.

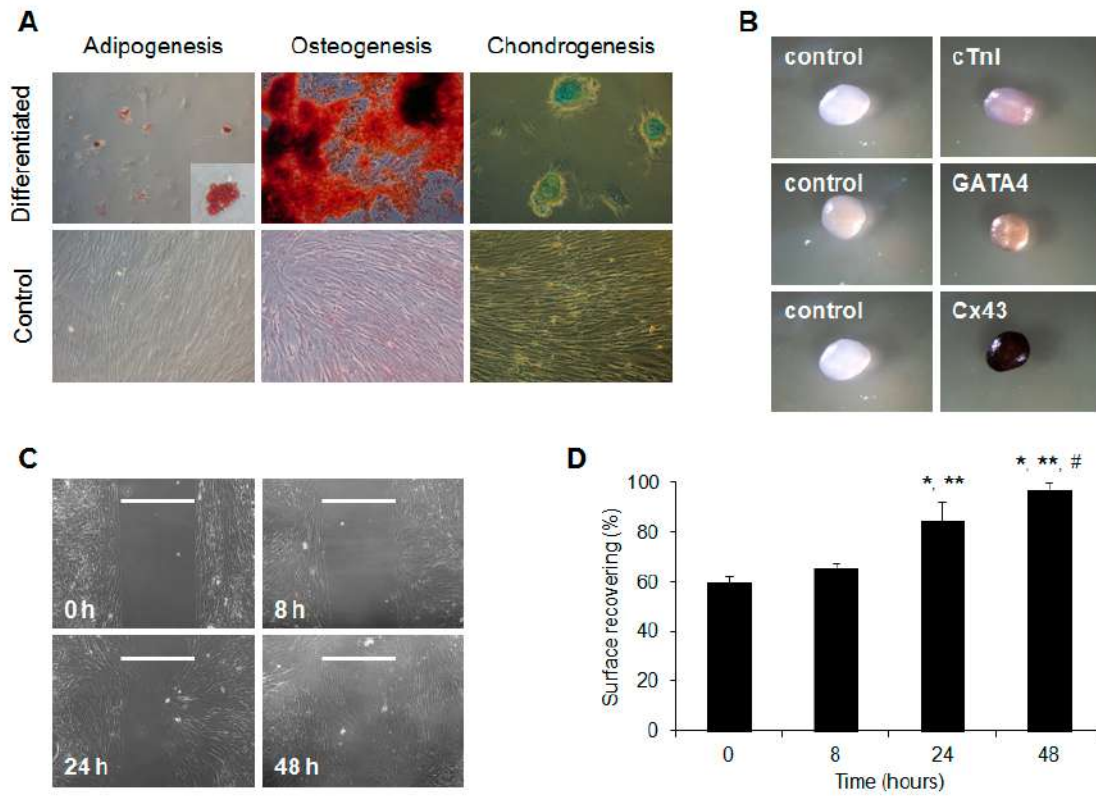
**Grant support:** This work was supported in part by the Instituto de Salud Carlos III: Redes Temáticas de Investigación Cooperativa en Salud (Red de Investigación Cardiovascular [RIC, RD12/0042/0047 and Red de Investigación en Terapia Celular–TerCel, RD12/0019/0029] and Infrastructure Grant [IF09/3667]; by the Ministerio de Ciencia e Innovación [SAF2011-30067-C02-01/02 to A.B.G.]; and from Fundació Privada Daniel Bravo Andreu, and La Marató de TV3 [080330 to A.B.G. and 12/2232 to S.R.].

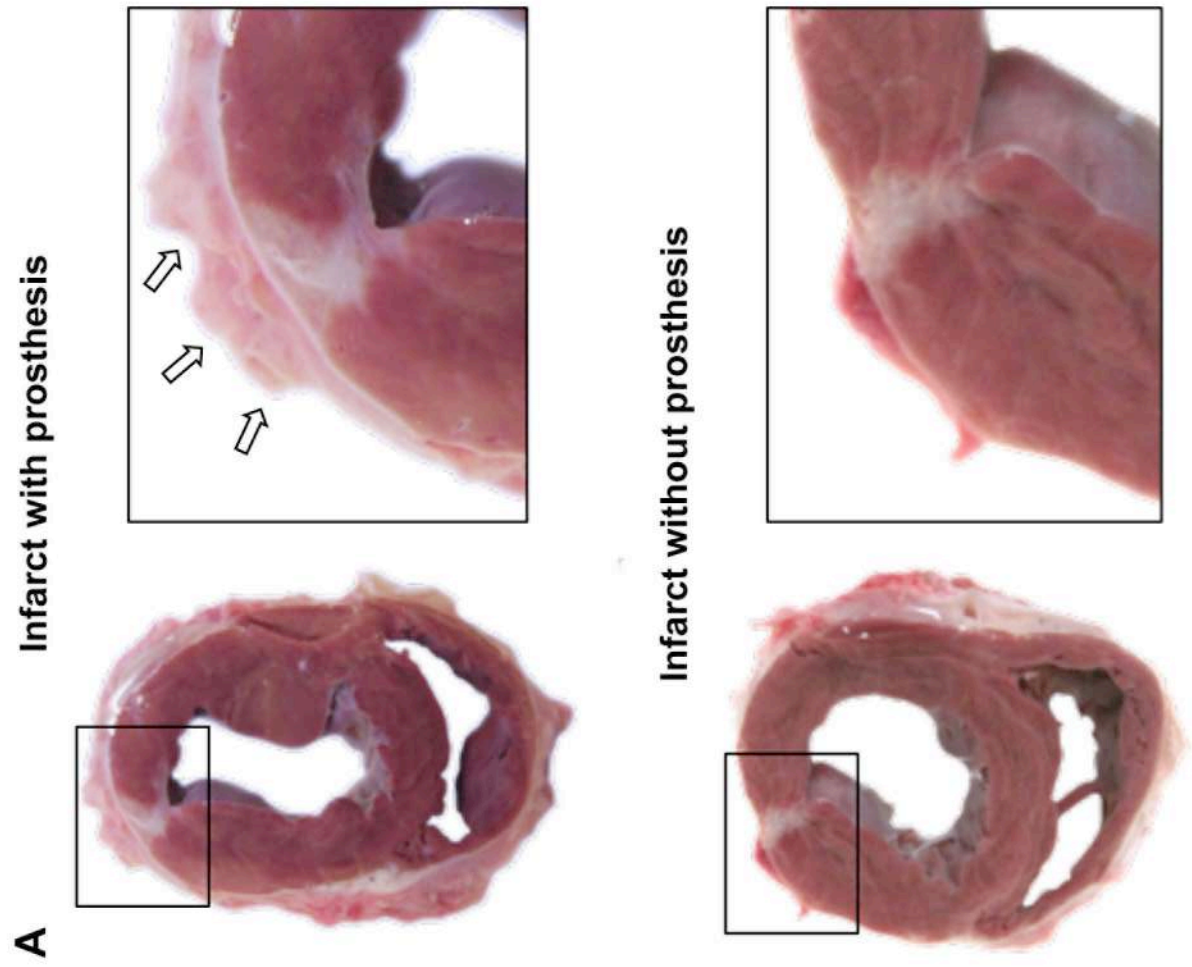
## References

- Gálvez-Montón C, Prat-Vidal C, Roura S, et al. Transposition of a pericardial-derived vascular adipose flap for myocardial salvage after infarct. *Cardiovasc Res* 2011;91:659–67.
- Vunjak-Novakovic G, Lui KO, Tandon N, Chien KR. Bioengineering heart muscle: a paradigm for regenerative medicine. *Annu Rev Biomed Eng* 2011;13:245–67.
- Gunderson BD, Gillberg JM, Wood MA, Vijayaraman P, Shepard RK, Ellenbogen KA. Development and testing of an algorithm to detect implantable cardioverter-defibrillator lead failure. *Heart Rhythm* 2006;3:155–62.
- Shah BR, Adams M, Peterson ED, et al. Secondary prevention risk interventions via telemedicine and tailored patient education (SPRITE): a randomized trial to improve postmyocardial infarction management. *Circ Cardiovasc Qual Outcomes* 2011;4:235–42.
- de Waure C, Cadeddu C, Gualano MR, Ricciardi W. Telemedicine for the reduction of myocardial infarction mortality: a systematic review and a meta-analysis of published studies. *Telem J E Health* 2012;18:323–8.
- Cinca J, Warren M, Carreno A, et al. Changes in myocardial electrical impedance induced by coronary artery occlusion in pigs with and without preconditioning: correlation with local ST-segment potential and ventricular arrhythmias. *Circulation* 1997;96:3079–86.
- Warren M, Bragos R, Casas O, et al. Percutaneous electrocatheter technique for on-line detection of healed transmural myocardial infarction. *Pacing Clin Electrophysiol* 2000;23:1283–7.
- Sanchez B, Schoukens J, Bragos R, Vandersteen G. Novel estimation of the electrical bioimpedance using the local polynomial method. Application to *in vivo* real-time myocardium tissue impedance characterization during the cardiac cycle. *IEEE Trans Biomed Eng* 2011;58:3376–85.
- Sanchez B, Louarroudi E, Jorge E, Cinca J, Bragos R, Pintelon R. A new measuring and identification approach for time-varying bioimpedance using multisine electrical impedance spectroscopy. *Physiol Meas* 2013;34:339–57.
- Martinez-Estrada OM, Munoz-Santos Y, Julve J, Reina M, Vilario S. Human adipose tissue as a source of Flk-1+ cells: new method of differentiation and expansion. *Cardiovasc Res* 2005;65:328–33.
- Pasquino E, Pascale S, Andreon M, Rinaldi S, Laborde F, Galloni M. Bovine pericardium for heart valve bioprosthesis: *in vitro* and *in vivo* characterization of new chemical treatments. *J Mater Sci Mater Med* 1994;5:850–4.
- Ott HC, Matthiesen TS, Goh SK, et al. Perfusion-decellularized matrix: using nature's platform to engineer a bioartificial heart. *Nat Med* 2008;14:213–21.

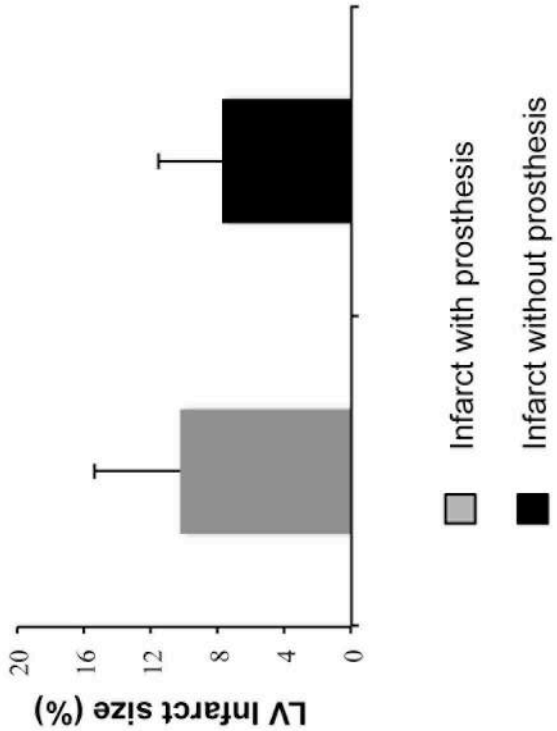
- [13] Kim BS, Choi JS, Kim JD, Choi YC, Cho YW. Recellularization of decellularized human adipose-tissue-derived extracellular matrix sheets with other human cell types. *Cell Tissue Res* 2012;348:559–67.
- [14] Bogonez-Franco P, Nescolarde L, Galvez-Monton C, Bragos R, Rosell-Ferrer J. An implantable bioimpedance monitor using 2.45 GHz band for telemetry. *Physiol Meas* 2013;34:1–16.
- [15] Salazar Y, Bragos R, Casas O, Cinca J, Rosell J. Transmural versus nontransmural in situ electrical impedance spectrum for healthy, ischemic, and healed myocardium. *IEEE Trans Biomed Eng* 2004;51:1421–7.
- [16] Sanchez B, Guasch A, Bogonez P, et al. Towards on line monitoring the evolution of the myocardium infarction scar with an implantable electrical impedance spectrum monitoring system. *Conf Proc IEEE Eng Med Biol Soc* 2012;2012:3223–6.
- [17] Zhang S, Holmes T, Lockshin C, Rich A. Spontaneous assembly of a self-complementary oligopeptide to form a stable macroscopic membrane. *Proc Natl Acad Sci U S A* 1993;90:3334–8.
- [18] Ock SA, Jeon BG, Rho GJ. Comparative characterization of porcine mesenchymal stem cells derived from bone marrow extract and skin tissues. *Tissue Eng C Methods* 2010;16:1481–91.
- [19] Rigol M, Solanes N, Farre J, et al. Effects of adipose tissue-derived stem cell therapy after myocardial infarction: impact of the route of administration. *J Card Fail* 2010;16:357–66.
- [20] Kumar BM, Yoo JG, Ock SA, et al. In vitro differentiation of mesenchymal progenitor cells derived from porcine umbilical cord blood. *Mol Cells* 2007;24:343–50.
- [21] Wang X, Moutsoglou D. Osteogenic and adipogenic differentiation potential of an immortalized fibroblast-like cell line derived from porcine peripheral blood. *In Vitro Cell Dev Biol Anim* 2009;45:584–91.
- [22] Midwood KS, Williams LV, Schwarzbauer JE. Tissue repair and the dynamics of the extracellular matrix. *Int J Biochem Cell Biol* 2004;36:1031–7.
- [23] Singelyn JM, Christman KL. Injectable materials for the treatment of myocardial infarction and heart failure: the promise of decellularized matrices. *J Cardiovasc Transl Res* 2010;3:478–86.
- [24] David TE, Feindel CM, Ropchan GV. Reconstruction of the left ventricle with autologous pericardium. *J Thorac Cardiovasc Surg* 1987;94:710–4.
- [25] Duran CM, Gometza B, Kumar N, Gallo R, Martin-Duran R. Aortic valve replacement with freehand autologous pericardium. *J Thorac Cardiovasc Surg* 1995;110:511–6.
- [26] Semino CE. Can we build artificial stem cell compartments? *J Biomed Biotechnol* 2003;2003:164–9.
- [27] Semino CE. Self-assembling peptides: from bio-inspired materials to bone regeneration. *J Dent Res* 2008;87:606–16.
- [28] Huttmacher DW, Schantz T, Zein I, Ng KW, Teoh SH, Tan KC. Mechanical properties and cell cultural response of polycaprolactone scaffolds designed and fabricated via fused deposition modeling. *J Biomed Mater Res* 2001;55:203–16.
- [29] Place ES, Evans ND, Stevens MM. Complexity in biomaterials for tissue engineering. *Nat Mater* 2009;8:457–70.
- [30] Su B, Tang D, Li Q, Tang J, Chen G. Gold-silver-graphene hybrid nanosheets-based sensors for sensitive amperometric immunoassay of alpha-fetoprotein using nanogold-enclosed titania nanoparticles as labels. *Anal Chim Acta* 2011;692:116–24.
- [31] Liang KZ, Qi JS, Mu WJ, Liu ZX. Conductometric immunoassay for interleukin-6 in human serum based on organic/inorganic hybrid membrane-functionalized interface. *Bioprocess Biosyst Eng* 2009;32:353–9.
- [32] Zhang S. Fabrication of novel biomaterials through molecular self-assembly. *Nat Biotechnol* 2003;21:1171–8.
- [33] Cinca J, Warren M, Rodriguez-Sinovas A, et al. Passive transmission of ischemic ST segment changes in low electrical resistance myocardial infarct scar in the pig. *Cardiovasc Res* 1998;40:103–12.

**Supplementary Fig. 1**





**B**





## SUPPLEMENTARY METHODS

**Cell culture.** Isolated MATPCs were grown to subconfluence in  $\alpha$ -MEM (Sigma) supplemented with 10% heat-inactivated fetal bovine serum (FBS), 2 mM L-glutamine, 1% penicillin-streptomycin (P/S) (Gibco), 5  $\mu$ g/ml Plasmocin<sup>TM</sup> (InvivoGen) and cultured under standard conditions, with media replacement every three days. Endothelial growth medium (EGM)-2 comprised endothelial basal medium (EBM)-2 supplemented with SingleQuots Bullet-Kit [0.5 ng/ml VEGF, 5 ng/ml EGF, 10 ng/ml bFGF, 20 ng/ml long R3-IGF-1, 22.5  $\mu$ g/ml heparin, 1  $\mu$ g/ml ascorbic acid, 0.2  $\mu$ g/ml hydrocortisone, gentamicin (1/1000 dilution) and 2% FBS], all purchased from Lonza.

**Cell proliferation.** MATPCs were seeded into 6-well plates in duplicate at 1,000 cells/cm<sup>2</sup> density. At indicated time points, cells were serially washed with PBS, collected by standard trypsinization, and viable cells counted by trypan blue exclusion method using a hemocytometer. Cell population doubling time (Td) was calculated during the log phase of culture growth curves as previously reported [1]. Proliferation data were plotted on a common log scale and fit by linear regression. Td values were determined using the formula:  $Td = \text{Log}(2)/K$  (days), where K is the slope of the regression line.

**Differentiation assays.** StemPro<sup>®</sup> osteogenesis differentiation kit (Gibco) was used for *in vitro* MATPCs osteogenic differentiation for 14 days, as previously reported [2]. Deposition of calcium matrix by differentiated cells was examined by Alizarin red S (Sigma) staining [3]. For *in vitro* adipogenic and chondrogenic induction, cells were

grown with StemPro<sup>®</sup> adipogenesis or chondrogenesis differentiation kits (Gibco) following the manufacturer's instruction. Oil red O and Alcian blue (Sigma) staining were performed to confirm the presence of intracellular lipid vacuoles and to visualize glycosaminoglycan biosynthesis by differentiated cells, respectively [4].

MATPCs were expanded in complete EGM-2 medium for 15 days and endothelial differentiation was assayed as previously described [5]. To assess endothelial differentiation degree, control and EGM-2-induced MATPCs were labeled with Dil-Ac-LDL (10 µg/mL, Biomedical Technologies) in complete medium for 4 h at 37 °C, fixed and examined under confocal laser scanning microscope (TCS SP5, Leica).

**Quantitative real-time PCR.** Real-time PCR amplifications were carried out with as previously described in detail [6], using 2 µL of porcine FAM-labelled TaqMan<sup>®</sup> Gene Expression assays (Applied Biosystems): GATA4 (Ss03383805\_u1), cardiac troponin I (cTnI) (Ss03385977\_u1), connexin-43 (Cx43) Ss03374839\_u1, GAPDH (Ss03375435\_u1) and GUSB (Ss03387751\_u1). Each sample was run in duplicate, and amplification data collected and analyzed on the ABI Prism<sup>®</sup> 7000 Sequence Detection System (Applied Biosystems). Relative quantification was determined by normalizing each gene expression to GUSB housekeeping gene following the  $2^{-\Delta\Delta Ct}$  method [7].

**Lentiviral particle production and MATPCs transduction.** Viral particles were produced using human embryonic kidney cells 293T, according to a previously described method [8]. Briefly, lentiviral transfer vector DNA (pCMV-PLuc-IRES-eGFP, 6 µg) was mixed with viral envelope plasmid (pMD-G-VSV-G, 2 µg) and packaging construct (pCMV-ΔR8.2, 4 µg) in 250 µL of 150 mM NaCl and then mixed

with 48  $\mu\text{L}$  of polyethylenimine (PEI, Polyscience) in 250  $\mu\text{L}$  of 150 mM NaCl, and incubated at room temperature (RT) for 20 min. This DNA solution was added dropwise to the seeded 293T cells, swirled gently and incubated for 16 h at 37 °C with 5% CO<sub>2</sub>. The following day, the transfection solution was removed, cells were rinsed with PBS and medium without FBS was added to the cells. After 48 h incubation the supernatant was collected, centrifuged at 400 g to remove cell debris, and filtered through a 0.45- $\mu\text{m}$  low-protein-binding filter (Corning). Expanded MATPCs (70% confluence) were transfected with pCMV-PLuc-IRES-eGFP lentiviral vector stocks (MOI = 20), using 10  $\mu\text{g}/\text{mL}$  polybrene (Sigma) and incubated for 24 to 48 h.

**Immunocytofluorescence staining.** Lentivirally transduced MATPCs (passages 5-6) were formalin-fixed, permeabilized with 0.25% Triton-X-100 in PBS (PBST), blocked with 1% BSA-PBST for 30 min and incubated with primary antibodies against GATA4 (2  $\mu\text{g}/\text{mL}$ ; R&D Systems), cTnI (2  $\mu\text{g}/\text{mL}$ ; Santa Cruz Biotechnology), or Cx43 (2.5  $\mu\text{g}/\text{mL}$ ; BD Transduction) for 1 h at RT. A secondary antibody conjugated with Cy3 (1:200; Jackson ImmunoResearch) was applied and nuclei counterstained with Hoechst 33342 (1  $\mu\text{g}/\text{mL}$ ; Sigma). Images were acquired with an Axio Observer Z1 inverted microscope (Zeiss).

Control and EGM-2-induced ATDPCs were incubated with a specific antibody against Ki67 (2  $\mu\text{g}/\text{mL}$ , Santa Cruz Biotechnology) or with biotinylated *Griffonia simplicifolia* Lectin I (GSLI) B4 isolectin (0.5  $\mu\text{g}/\text{mL}$ ; Vectors labs). Secondary antibodies conjugated to Alexa Fluor 488 and Streptavidin-Alexa Fluor 568 (1  $\mu\text{g}/\text{mL}$ ; Molecular Probes) were used to detect labelled cells and nuclei stained blue with Hoechst.

**3D culture of MATPCs.** MATPCs expanded in culture flasks were trypsinized, washed with PBS and resuspended in sucrose 10% at a final concentration of  $8 \cdot 10^6$  cells/mL. Next, cells were embedded in the peptide 3D scaffold RAD16-I [9] (PuraMatrix™ Peptide Hydrogel, BD Bioscience). Specifically, cell suspension was mixed with an equal volume of RAD16-I 0.3% (w/v) in sucrose 10%. As a result, we obtained a final concentration of  $4 \cdot 10^6$  cells/mL in RAD16-I 0.15%, sucrose 10%. We loaded 40  $\mu$ L of the mixture into cell culture inserts (Millicell Cell Culture Insert, Millipore) placed in 6-well plates and added progressively supplemented  $\alpha$ -MEM medium. The slow addition of medium washes out the sucrose from the cells, which is crucial for the cell survival. Finally, we removed the medium from the wells and added 0.5 mL into the cell culture inserts containing the gelled constructs and 2.5 mL into the well. Every day, 0.5 mL of medium from the well was removed and 0.5 mL of fresh medium was added into the cell culture insert [10].

**Enzyme-tag 3D immunocytochemistry.** After 10 days of 3D-MATPCs cultures, constructs were washed with PBS, fixed with 1% paraformaldehyde (Sigma) for 30 min at 4 °C and washed three times with PBS for 10 min with stirring (all the steps of this protocol are carried out with stirring). Next, constructs were incubated with 0.1% H<sub>2</sub>O<sub>2</sub> in methanol for 45 min in order to block endogenous peroxidases, and air bubbles inside the constructs generated by peroxidases were removed by gently pipetting with PBS. Cells were then blocked in filtered-blocking buffer (BB) (PBS + 20% FBS) + 1% dimethyl sulfoxide (DMSO, Sigma) + 0.1% Triton-X-100 for 2 h RT. Constructs were incubated with primary antibodies against GATA4, cTnI or Cx43 (1  $\mu$ g/mL, Santa Cruz Biotechnologies) for 1.5 h at RT. After washing twice with BB, cells were

kept in BB overnight (ON) at 4 °C. The following day, constructs were washed with BB and incubated with anti-rabbit or anti-mouse secondary antibodies (1:400, Santa Cruz Biotechnologies) conjugated to horseradish peroxidase (HRP) for 1.5 h at RT. Again, cells were washed with BB and kept in BB ON. The third day, cells were washed with PBS and revealed with 3,3-diaminobenzidine (DAB Substrate, Roche) diluted to 1X with DAB buffer until a brown precipitation was observed. Pictures were taken with a stereoscope.

***In vitro* migration assay.** Migration capacity was assayed using Culture-Inserts (Ibidi). Briefly, MATPCs ( $3.5 \cdot 10^4$ /well) were seeded and grown to confluence. When the two wells were filled with adherent cells, a cell-free gap of 500  $\mu$ m was created by culture-insert removal. Migratory cells were tracked by phase-contrast microscopy and the percentage of surface recovering index was quantified using the Image J software (NIH). Data are the mean  $\pm$  s.d. from two independent experiments performed in duplicate and statistical significance was evaluated using one-way ANOVA with Tukey's test for the *post hoc* analysis. *P* values < 0.05 were considered significant.

**Lyophilization and sterilization procedures.** Decellularized scaffolds were lyophilized by drying under vacuum at  $-25$  °C for 24 h in a freeze-dry system (Christ loc-1m, B. Braun Biotech International), individually-sealed, sterilized by gamma irradiation and stored under sterile conditions at RT prior to evaluation. The standard dose for medical devices sterilization by gamma irradiation is 25 kGy (ISO 11137-2:2012). However, in practice, this dose is usually exceeded to ensure thorough sterilization. Thus, a certified dosage of 31 kGy was used in these experiments at a commercial facility (Aragogamma S.L.).

**Self-assembling peptide scaffold RAD16-I combined to NanoGold.** We prepared a mixture of peptide hydrogel with nanoparticles of NanoGold to make the scaffold more electrically conductive. Pre-synthesized lyophilized Biotin-RAD16-I was solubilized in distilled water at a final concentration of 0.15%. Therefore, 9  $\mu\text{L}$  Biotin-RAD16-I 0.15% were mixed with 1  $\mu\text{L}$  Streptavidin-NanoGold ( $5.5 \cdot 10^5$  particles). After 20 min allowing specific binding, 90  $\mu\text{L}$  of RAD16-I 0.15% in distilled water were added and the mixture gently pipetted. The final working solution contained 1% NanoGold (at a final concentration of  $5.5 \cdot 10^7$  particles/ $\mu\text{L}$ ) and 99% RAD16-I in distilled water at 0.15% (9% of it was Biotin-RAD16-I).

**Congo red staining.** Congo red binds to amyloid-like peptides having a  $\beta$ -sheet conformation [11]. Gelated RAD16-I is rich in  $\beta$ -sheet structures and appears highly positive when stained with this dye. Conversely, pericardial matrix is mostly constituted of collagens enclosing  $\alpha$ -helix structures [12]. Human pericardia were wet with distilled water (control) or RAD16-I 0.15% and stained with Congo red (Sigma) overnight at RT with stirring. In the following two days, the pericardia were washed exhaustively with PBS (several washes with stirring), transversally cut with a scalpel and observed under the stereoscope.

***In vitro* biocompatibility assay.** Hydrogel (with or without GFP<sup>+</sup>-MATPCs) were loaded in the pericardial scaffolds as described above and cultured *in vitro* under standard conditions with supplemented  $\alpha$ -MEM. After 1-week, scaffolds were formalin-fixed 1 h at 4 °C, rinsed twice with PBS, embedded in Tissue-Tek<sup>®</sup> OCT compound (Sakura) and cryopreserved. Masson's trichrome staining was performed

to verify recellularization. For cell viability analysis reseeded pericardial scaffolds were stained with the commercially available Live/Dead<sup>®</sup> Viability/Cytotoxicity Kit (Molecular Probes) following manufacturer's protocol and observed under an Axio Observer Z1 inverted microscope.

**Electron microscopy.** For transmission electron microscopy (TEM) imaging, pericardial samples were fixed in 2.5% glutaraldehyde in 0.1 M phosphate buffer, post fixed in 1.5% osmium tetroxide and processed using the tEPON 812 embedding Kit (Tousimis<sup>®</sup>). The ultrathin sections, stained with uranyl acetate and lead citrate, were examined at 80 kV with a JEM-1011 (JEOL) transmission electron microscope. For field emission gun-scanning electron microscopy (FEG-SEM) imaging, pericardial samples were fixed using 5% (w/v) glutaraldehyde. After fixation, 3D cultures were washed twice in PBS and subsequently dehydrated. Dehydration process included several immersions for 10 min in ethanolic solutions: once in 30% (v/v) ethanol, twice in 50% (v/v) ethanol, three times in 70% (v/v) ethanol, three times in 90% (v/v) ethanol, three times in 96% (v/v) ethanol, and three more times in 100% (v/v) ethanol. Once dehydrated, the cultures were dried using a CO<sub>2</sub> critical point dryer (Polaron, CPD Jumbo E-3100). Then, the samples were sputter-coated with gold and platinum alloy using the equipment Emitech SC7620 (60 s, 18 mA, and chamber pressure 0.2 mbar). Samples were examined with a JSM-7100F (JEOL) at a 13 kV.

**Myocardial infarction model.** Thirteen female crossbreed Landrace x Large White pigs (20 - 30 kg) were premedicated with an intramuscularly (IM) mixture of ketamine (20 mg/kg), diazepam (0.25 mg/kg), and atropine (0.25 mg/kg). Anesthetic induction was done with an intravenously (IV) propofol bolus (4 mg/kg). Animals

underwent endotracheal intubation, and anesthesia was maintained by 2% sevoflurane inhalation. A continued IV infusion of ketorolac (0.15 mg/kg/h) and tramadol (0.5 mg/kg/h) was used as an intraoperative analgesic. At the beginning of the intervention, an IV lidocaine bolus (1 mg/kg) was administered, followed by a continuous infusion (1 mg/kg/h) maintained for 1 h after MI induction. At the end of the surgery, tulatromicin (2.5 mg/kg, IM) was administered as antibiotic therapy.

All surgical procedures were done under monitoring conditions with ECG registration and measures of capnography, pulse oximetry, non-invasive arterial blood pressure, and temperature. After left lateral thoracotomy through the fourth intercostal space, acute MI was induced by a permanent double-ligation of the first marginal branch of the circumflex artery, as previously described [13]. Thirty minutes after MI induction, myocardial bioprosthesis implantation over the ischemic myocardium was performed with surgical glue (Glubran®2, Cardioliink) (treated group: n = 8). Prostheses without GFP+-MATPCs were implanted in a control group of animals (n = 5). In the five control and in two of treated animals myocardial bioprostheses were connected to the EIS monitoring system. Reliable EIS results were only obtained from the control group. After 1 month, animals were sacrificed with an intravenous injection of potassium chloride solution to obtain samples for histological analysis.

**Biochemical analysis.** To determine circulating cTnI, creatine kinase-MB (CK-MB), and myoglobin levels, blood samples were collected by direct jugular venipuncture into serum gel tubes at baseline and 2 h after MI induction. After centrifugation, serum cTnI, CK-MB and myoglobin were measured with commercially available immunometric assays in a fluorometric immunoassay analyzer (AQT90 FLEX, Radiometer Medical ApS).



**Tissue collection, histological and immunohistochemical analysis.** After sternotomy, hearts were immediately excised and washed in ice-cold saline buffered solution to remove any residual blood. Left ventricular (LV) infarct size and quantitative morphometric measurements were completed as previously reported [13]. Biopsies from infarct core, infarct border and remote myocardium were taken, embedded in Tissue-Tek® OCT compound and cryopreserved. Masson's trichrome and Sirius red staining were performed for the primary histological examination.

Immunostaining was carried out on 10 µm-thick heart cryosections. Briefly, tissues were fixed with 10% formalin and blocked for 1 h at RT with 20% horse serum, followed by primary antibody incubation (ON at 4 °C) against GFP (1:1000), cTnI, and Ki67 (2 µg/mL). Antibodies were visualized by incubating the sections with Alexa Fluor 488 and Alexa Fluor 568-conjugated secondary antibodies (5 µg/mL), and nuclei counterstained with Hoechst. Isolectin staining was performed using biotinylated GSLI B4 isolectin (1:25) and Alexa Fluor 568-conjugated Streptavidin (1:500; Molecular Probes). Immunofluorescence images were captured with an Axio Observer Z1 inverted microscope.

## SUPPLEMENTARY FIGURES

**Supplementary Fig. 1. Analysis of cardiac markers in 3D cultures, baseline pluripotency and migration capacity of MATPCs.** (A) Standard MSC pluripotency was demonstrated by specifically cell differentiation into adipogenic, osteogenic and chondrogenic lineages. Images show differentiated (upper row) and control (bottom row) MATPCs cultures following staining with, from left to right, Oil red O, Alizarin red S, and Alcian blue (x200 magnification). (B) Immunostaining against cardiac-specific markers cTnI, GATA4 and Cx43 in 3D-cultured MATPCs at day 10. Stereoscopic images from constructs incubated only with secondary antibodies are shown at left (control). (C) Representative images of the *in vitro* tracking of migratory MATPCs in Culture-Inserts. Bars, 500  $\mu\text{m}$ . (D) Histogram represents quantitative differences in the surface recovery index exhibited by tested cells.  $n = 4$ ;  $*p < 0.001$  vs. 0 h,  $**p \leq 0.001$  vs. 8 h,  $\#p < 0.01$  vs. 24 h.

**Supplementary Fig. 2. Effect of prosthesis without GFP<sup>+</sup>-MATPCs on infarct size.** (A) Representative images of heart sections from MI with and without prosthesis after 35 days of follow-up. Enlarged images showing infarct area are presented. Arrows indicate implanted prosthesis. (B) Histogram represents percentage of LV infarct size in both groups.

## SUPPLEMENTARY REFERENCES

1. Zhuang SH, Burnstein KL. Antiproliferative effect of 1alpha,25-dihydroxyvitamin D3 in human prostate cancer cell line LNCaP involves reduction of cyclin-dependent kinase 2 activity and persistent G1 accumulation. *Endocrinology*. 1998; 139:1197-207.
2. Bago JR, Aguilar E, Alieva M, Soler-Botija C, Vila OF, Claros S, et al. *In vivo* bioluminescence imaging of cell differentiation in biomaterials: a platform for scaffold development. *Tissue Eng Part A*. 2013; 19:593-603.
3. Wang YH, Ho ML, Chang JK, Chu HC, Lai SC, Wang GJ. Microporation is a valuable transfection method for gene expression in human adipose tissue-derived stem cells. *Mol Ther*. 2009; 17:302-8.
4. Roura S, Bago JR, Soler-Botija C, Pujal JM, Galvez-Monton C, Prat-Vidal C, et al. Human umbilical cord blood-derived mesenchymal stem cells promote vascular growth *in vivo*. *PloS One*. 2012; 7:e49447.
5. Heydarkhan-Hagvall S, Schenke-Layland K, Yang JQ, Heydarkhan S, Xu Y, Zuk PA, et al. Human adipose stem cells: a potential cell source for cardiovascular tissue engineering. *Cells, tissues, organs*. 2008; 187:263-74.
6. Prat-Vidal C, Galvez-Monton C, Nonell L, Puigdecenet E, Astier L, Sole F, et al. Identification of temporal and region-specific myocardial gene expression patterns in response to infarction in swine. *PloS One*. 2013; 8:e54785.
7. Livak KJ, Schmittgen TD. Analysis of relative gene expression data using real-time quantitative PCR and the 2(-Delta Delta C(T)) Method. *Methods*. 2001; 25: 402-8.

8. Alieva M, Bago JR, Aguilar E, Soler-Botija C, Vila OF, Molet J, et al. Glioblastoma therapy with cytotoxic mesenchymal stromal cells optimized by bioluminescence imaging of tumor and therapeutic cell response. *PloS One*. 2012; 7:e35148.
9. Zhang S, Gelain F, Zhao X. Designer self-assembling peptide nanofiber scaffolds for 3D tissue cell cultures. *Semin Cancer Biol*. 2005; 15:413-20.
10. Quintana L, Muinos TF, Genove E, Del Mar Olmos M, Borros S, Semino CE. Early tissue patterning recreated by mouse embryonic fibroblasts in a three-dimensional environment. *Tissue Eng Part A*. 2009; 15:45-54.
11. Klunk WE, Pettegrew JW, Abraham DJ. Quantitative evaluation of congo red binding to amyloid-like proteins with a beta-pleated sheet conformation. *J Histochem Cytochem*. 1989; 37:1273-81.
12. Mirsadraee S, Wilcox HE, Korossis SA, Kearney JN, Watterson KG, Fisher J, et al. Development and characterization of an acellular human pericardial matrix for tissue engineering. *Tissue Eng*. 2006; 12:763-73.
13. Gálvez-Montón C, Prat-Vidal C, Roura S, Farre J, Soler-Botija C, Lluçà-Valldeperas A, et al. Transposition of a pericardial-derived vascular adipose flap for myocardial salvage after infarct. *Cardiovasc Res*. 2011; 91:659-67.

### 3. *In vivo* effects promoted by the engineered cardiac grafts for cardiac regeneration post-MI

In the next two manuscripts, we wanted to explore in detail the protein content, and the mechanical and structural properties of both myocardial and pericardial scaffolds; and eventually assess the triggered benefits after engraftment of both engineered cardiac grafts, the EMG-ATDPC and EPG-ATDPC, in a porcine MI model. First of all, following proteomic study, we detected the main ECM components, such as collagens, fibronectin, laminin, nidogen and different proteoglycans, in both decellularized myocardial and pericardial scaffolds, but the number of matrisome-related proteins was significantly higher in the decellularized pericardial scaffolds (40 versus 51). Additionally, the comparison between detergent- and trypsin-decellularized myocardial scaffolds revealed a higher number of matrisome proteins (40 versus 29) and less non-ECM proteins (119 versus 162) in the myocardial scaffolds obtained with the detergent protocol (**Figure 19**, *unpublished data*), endorsing previous data reported in this thesis in regard to detergent decellularization protocol as the optimal procedure for myocardial scaffolds. Moreover, the macro- and micromechanical, and structural analysis revealed preservation of the intrinsic tissue stiffness and framework postdecellularization, and a pore size significantly bigger for the pericardial scaffolds ( $10.2 \pm 0.5 \mu\text{m}$  vs.  $22.2 \pm 1.5 \mu\text{m}$ ;  $P=0.002$ ). Furthermore, cell penetrance and retention was significantly higher for recellularized pericardial scaffolds ( $226.4 \pm 13.9 \text{ cells/mm}^2$  vs.  $338.8 \pm 36.0 \text{ cells/mm}^2$  for recellularized myocardial and pericardial scaffolds, respectively;  $P=0.027$ ), and cardiac ATDPC differentiation potential towards endothelial and cardiac phenotype was retained when cells were seeded over myocardial or pericardial scaffolds (**Figure 20**, *unpublished data*). Regarding *in vivo* effects promoted by the engineered cardiac grafts, we observed an ~11% improvement in cardiac function, a smaller infarct size, a 2-fold higher infarct core vascularization, and a notable fibrosis progression attenuation for the EMG-ATDPC, compared to non-recellularized myocardial scaffolds. Moreover, the scaffold was innervated, vascularized and integrated within

the host vasculature system. On the other hand, the EPG-ATDPC also reported benefits in terms of cardiac function recovery and enhanced vascularization. Similarly to what occurred to EMG-ATDPC, the EPG-ATDPC also showed *de novo* nerve sprouting and blood vessel formation. The multiple group comparison displayed, in general, superior positive outcomes for the engineered cardiac grafts in relation to their cell-free scaffolds counterparts and the control animals regarding heart functionality. Besides, even though EMG-ATDPC significantly reduced infarct size compared to the other groups, no remarkable differences were encountered among EMG-ATDPC and EPG-ATDPC in terms of functional recovery improvement. Therefore, both cardiac constructs seem appropriate and promising candidates as a valid and effective therapy for MI, with EPG-ATDPCs a step ahead due to higher cell retention and penetrance and pericardial human origin. In the end, this should enable autologous engraftment with no associated drawbacks, facilitating the road to the clinics.

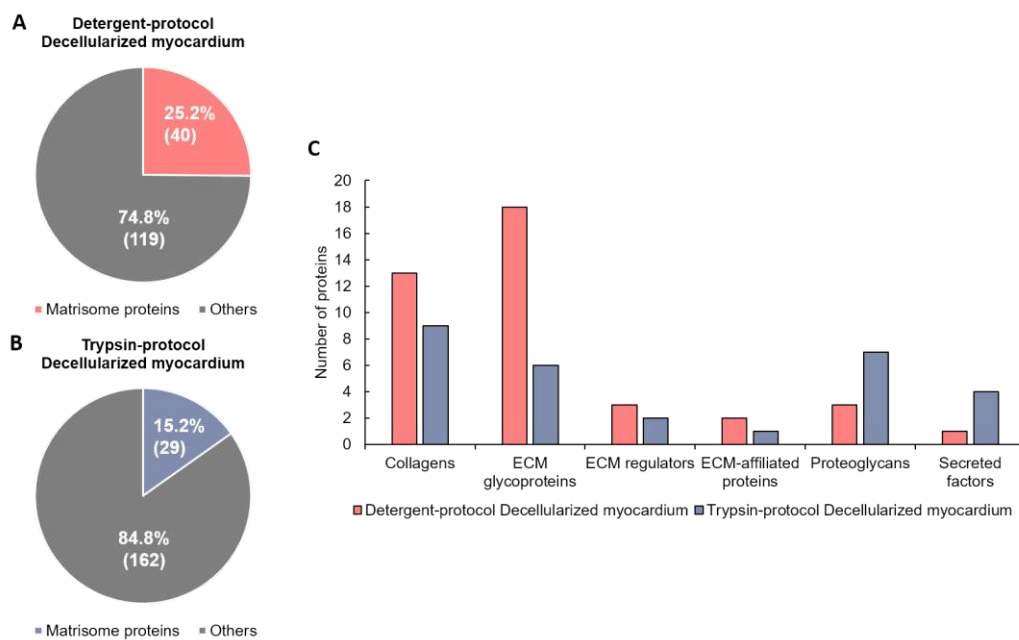


**Figure 19.** Proteomic analysis of detergent- and trypsin-based decellularized myocardial scaffolds. **(A)** Unique proteins of matrisome and cellular remnants identified for detergent-based protocol and **(B)** trypsin-based protocol decellularized myocardium. **(C)** Classification of the matrisome proteins for myocardium decellularized using both decellularization protocols. *Unpublished data.*

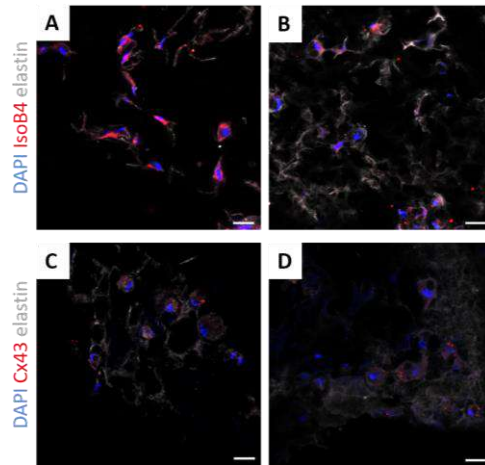


**Figure 20.** *In vitro* assessment of endothelial and cardiac differentiation potential for cardiac ATDPCs seeded over decellularized pericardial scaffolds. (A,B) Immunofluorescence against IsoB4 (red) and (C,D) Cx43 (red). ECM was stained with elastin (grey), and nuclei were counterstained with DAPI (blue). Scale bars=20 μm. *Unpublished data.*

The results generated have been published in part in one international journals (fourth article), and also compiled in a draft manuscript (attached below) to be published in another peer-reviewed international journal:

- Perea-Gil I\*, Prat-Vidal C\*, Gálvez-Montón C\*, Roura S, Llucà-Valldeperas A, Soler-Botija C, Iborra-Egea O, Díaz-Güemes I, Crisóstomo V, Sánchez-Margallo FM, Bayes-Genis A. A cell-enriched engineered myocardial graft limits infarct size and improves cardiac function. Pre-clinical study in the porcine myocardial infarction model. *J Am Coll Cardiol Basic Trans Science* 2016; 1(5):360-72.
- Perea-Gil I, Gálvez-Montón C, Prat-Vidal C, Jorba I, Roura S, Soler-Botija C, Iborra-Egea O, Revuelta-López E, Farré R, Navajas D, Bayes-Genis A. Head-to-head comparison of two engineered cardiac grafts for myocardial repair: a pre-clinical myocardial infarction swine model. *In preparation.*





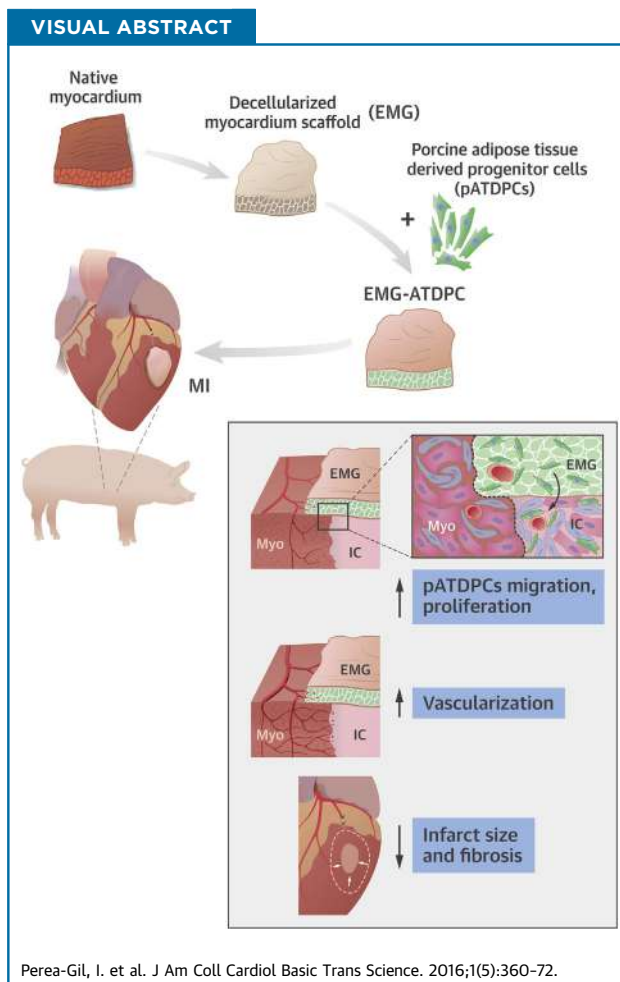
## PRE-CLINICAL RESEARCH

# A Cell-Enriched Engineered Myocardial Graft Limits Infarct Size and Improves Cardiac Function



## Pre-Clinical Study in the Porcine Myocardial Infarction Model

Isaac Perea-Gil, MS,<sup>a</sup> Cristina Prat-Vidal, PhD,<sup>a</sup> Carolina Gálvez-Montón, DVM, PhD,<sup>a</sup> Santiago Roura, PhD,<sup>a,b</sup> Aida Lluçà-Valldeperas, PhD,<sup>a</sup> Carolina Soler-Botija, PhD,<sup>a</sup> Oriol Iborra-Egea, MS,<sup>a</sup> Idoia Díaz-Güemes, DVM, PhD,<sup>c</sup> Verónica Crisóstomo, DVM, PhD,<sup>c</sup> Francisco M. Sánchez-Margallo, DVM, PhD,<sup>c</sup> Antoni Bayes-Genis, MD, PhD<sup>a,d,e</sup>



## HIGHLIGHTS

- MI remains a major cause of morbidity and mortality despite major treatment advances achieved during the past decades.
- Administration of an engineered myocardial graft, composed of decellularized myocardial matrix refilled with ATDPCs (EMG-ATDPC), in a porcine pre-clinical MI model, may support cardiac recovery following MI.
- Thirty days post-EMG-ATDPC implantation, cardiac magnetic resonance imaging and comprehensive histological analysis were performed to evaluate its impact on myocardial restoration.
- EMG-ATDPC resulted in better left ventricular ejection fraction, higher vessel density and neovascularization, and reduced infarct size by 68%, as well as limited fibrosis.
- Accordingly, EMG-ATDPC is ready to start the translational avenue toward phase I first-in-man clinical trials.

From the <sup>a</sup>ICREC (Heart Failure and Cardiac Regeneration) Research Program, Health Science Research Institute Germans Trias i Pujol (IGTP), Badalona, Spain; <sup>b</sup>Center of Regenerative Medicine in Barcelona, Barcelona, Spain; <sup>c</sup>Jesús Usón Minimally Invasive Surgery Centre, JUMISC, Cáceres, Spain; <sup>d</sup>Cardiology Service, Germans Trias i Pujol University Hospital, Badalona, Spain; and the <sup>e</sup>Department of Medicine, Autonomous University of Barcelona (UAB) Barcelona, Spain. This work was supported by grants from

## SUMMARY

Myocardial infarction (MI) remains a dreadful disease around the world, causing irreversible sequelae that shorten life expectancy and reduce quality of life despite current treatment. Here, the authors engineered a cell-enriched myocardial graft, composed of a decellularized myocardial matrix refilled with adipose tissue-derived progenitor cells (EMG-ATDPC). Once applied over the infarcted area in the swine MI model, the EMG-ATDPC improved cardiac function, reduced infarct size, attenuated fibrosis progression, and promoted neovascularization of the ischemic myocardium. The beneficial effects exerted by the EMG-ATDPC and the absence of identified adverse side effects should facilitate its clinical translation as a novel MI therapy in humans. (J Am Coll Cardiol Basic Trans Science 2016;1:360-72) © 2016 The Authors. Published by Elsevier on behalf of the American College of Cardiology Foundation. This is an open access article under the CC BY-NC-ND license (<http://creativecommons.org/licenses/by-nc-nd/4.0/>).

## ABBREVIATIONS AND ACRONYMS

**ATDPC** = adipose tissue-derived progenitor cells

**CMR** = cardiac magnetic resonance imaging

**cTnl** = cardiac troponin I

**EMG** = engineered myocardial graft

**GFP** = green fluorescent protein

**IsoB4** = isolectin B4

**LV** = left ventricle/ventricular

**LVEF** = left ventricular ejection fraction

**MI** = myocardial infarction

**pATDPC** = porcine adipose tissue-derived progenitor cell

**SMA** = smooth muscle actin

Cardiovascular disease is the foremost cause of death worldwide, accounting for almost 30% of all deaths and exceeding other growing pandemics, such as diabetes mellitus, cancer, and respiratory infections (1). Myocardial infarction (MI) leads to massive cardiomyocyte loss, collagen scar formation, and ultimately, maladaptive adverse ventricular remodeling (2). Cardiac homeostasis self-regeneration is insufficient following MI injury (3,4). Hence, alternative therapies—including cell and gene therapy and tissue engineering—are being investigated as a means of overcoming current therapeutic limitations and challenges.

### SEE PAGE 373

Cardiac tissue engineering uses natural or synthetic support platforms generating functional grafts that can be tightly implanted over injured myocardium (5,6). For optimal cell seeding, the supporting material or scaffold should provide a biomimetic niche resembling the physiological microenvironment, supplying the necessary cues to direct cell differentiation and proliferation, and favoring electromechanical coupling with host tissue (7,8). Decellularized myocardial extracellular matrix meets these requirements because it preserves the native myocardium ultrastructure, mechanical properties, and local matrix milieu (9-12). A recent study reports a refined protocol for obtaining an optimal myocardial scaffold for

recellularization (9). Despite the favorable qualities of decellularized myocardial scaffolds, few studies have investigated their use in pre-clinical MI animal models. To date, only 1 report describes administration of a decellularized myocardial scaffold in swine, and it was a cell-free scaffold (13).

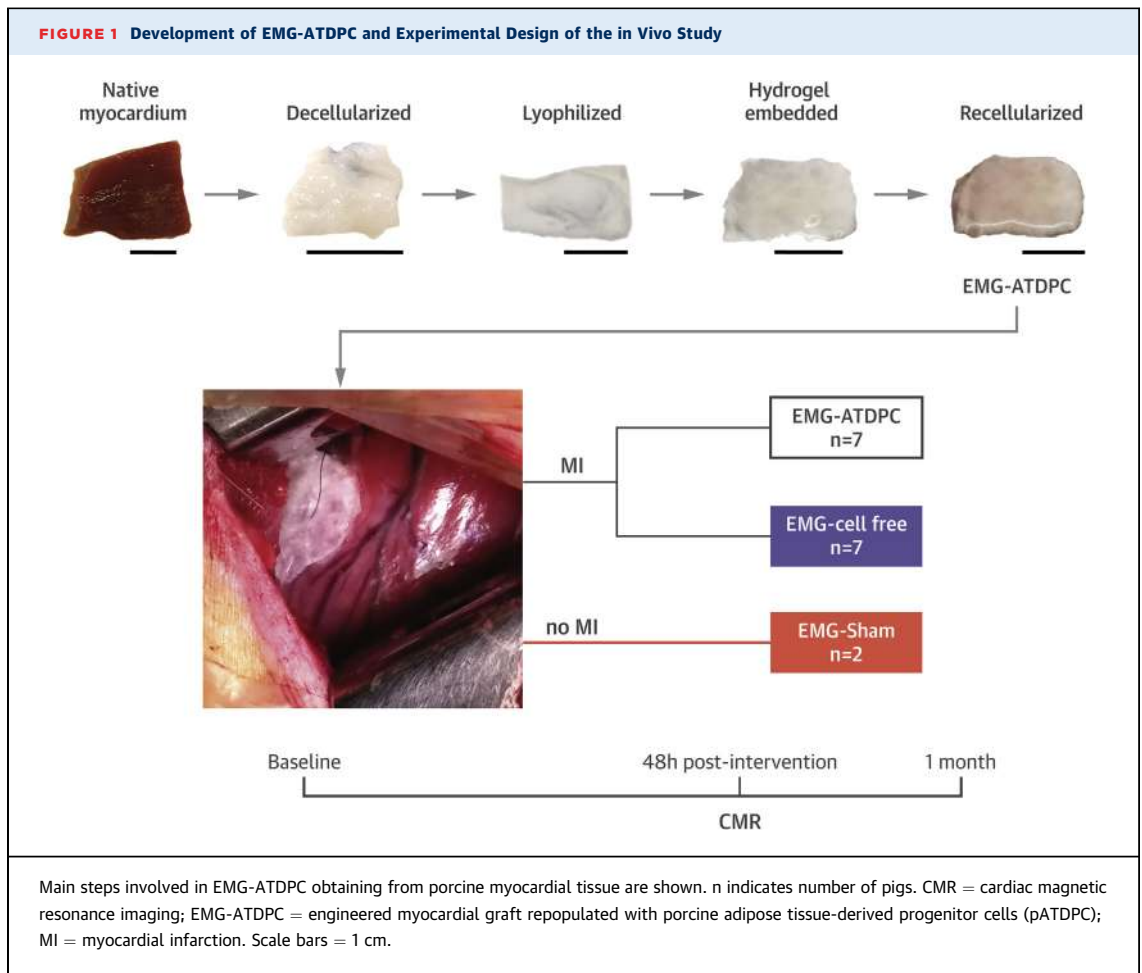
In our present study, we applied in a swine acute MI model a novel engineered myocardial graft (EMG) obtained by decellularization of porcine myocardial tissue. Decellularized myocardial scaffolds were left acellular (EMG-cell free) or were repopulated with green fluorescent protein (GFP)-labeled porcine adipose tissue-derived progenitor cells (GFP<sup>+</sup> pATDPCs) to generate cell-enriched grafts (EMG-ATDPC). Both engineered grafts (EMG-cell free and EMG-ATDPC) were applied over infarcted myocardium in allogeneic wild-type swine to assess cardiac function and modulation of scar healing.

## METHODS

**GENERATION OF EMGs.** Myocardial decellularization was performed as previously described (Figure 1) (9). Briefly, porcine myocardial tissue slices of ~25 × 25 × 3 mm were initially treated for 72 h with 1% sodium dodecyl sulfate (Sigma-Aldrich, St. Louis, Missouri), followed by a 48-h treatment with Triton X-100 (Sigma-Aldrich). Both solutions were replaced every

the Ministerio de Ciencia e Innovación [SAF2014-59892-R]; Red de Terapia Celular-TerCel (RD12/0019/0029), Red de Investigación Cardiovascular-RIC (RD12/0042/0047) and Fondo de Investigación Sanitaria, Instituto de Salud Carlos III (FIS PI14/01682) projects as part of the Plan Nacional de I+D+I and cofunded by ISCIII-Sudirección General de Evaluación y el Fondo Europeo de Desarrollo Regional (FEDER); Fundació La Marató de TV3 [201502; 201516]; Beca de Recerca Bàsica de l'Acadèmia de Ciències Mèdiques i de la Salut de Catalunya i de Balears 2015; Beca d'Investigació Bàsica de la Societat Catalana de Cardiologia 2015; Generalitat de Catalunya (SGR 2014); and Sociedad Española de Cardiología. The authors also appreciate support from the Fundació Privada Daniel Bravo Andreu. The authors have reported that they have no relationships relevant to the contents of this paper to disclose. Drs. Perea-Gil, Prat-Vidal, and Gálvez-Montón contributed equally to this work.

Manuscript received April 11, 2016; revised manuscript received June 16, 2016, accepted June 16, 2016.



24 h. Next, the myocardial tissue was exhaustively washed with phosphate-buffered saline containing 1% penicillin/streptomycin (Gibco, Grand Island, New York), 3 times for 24 h each. All of these steps were repeated twice, and the tissue was washed with sterile distilled water between cycles. Following completion of the second cycle, a 72-h DNase I (Roche, Basel, Switzerland) digestion was performed. The obtained decellularized myocardial scaffolds were next lyophilized in a freeze-drier chamber (Christ loc-1 m, B. Braun Biotech International, Melsungen, Germany), sterilized with a certified gamma irradiation dosage of 30 kGy (Aragogamma, Barcelona, Spain), and stored at room temperature until use.

The EMG-ATDPC was generated by rehydrating the decellularized myocardial scaffold using a mixture of 175  $\mu$ l of peptide hydrogel RAD16-I (Corning, Corning, New York) and 175  $\mu$ l of  $1.75 \times 10^6$  GFP<sup>+</sup> pATDPCs in 10% sucrose (Sigma-Aldrich) (Figure 2A). pATDPCs used were isolated and cultured from pericardial adipose tissue as previously described (14). To obtain

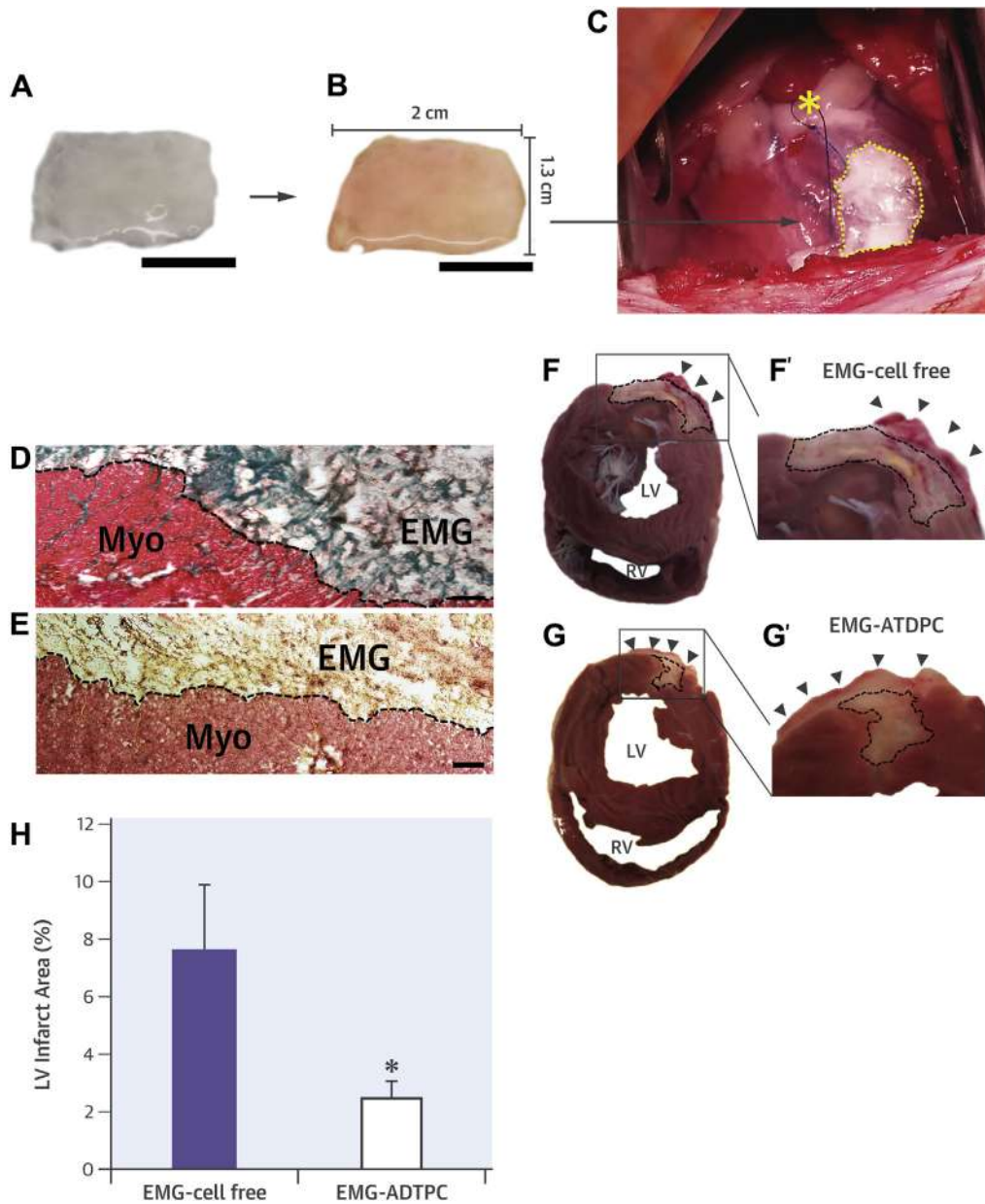
the EMG-cell free, the decellularized myocardial scaffold was only rehydrated with 350  $\mu$ l of RAD16-I hydrogel. Fifteen minutes later, 350  $\mu$ l of  $\alpha$ -MEM (Sigma-Aldrich) was added to the EMG (Figure 2B), and constructs (EMG-ATDPC or EMG-cell free) were implanted in the infarcted area.

**EXPERIMENTAL DESIGN.** All study procedures followed the guidelines regarding the use of animals in research as established in the Guide for the Care and Use of Laboratory Animals (NIH Publication No. 80-23, revised 1996), and conformed to the principles outlined in the Declaration of Helsinki. The study was approved by the local Animal Experimentation Unit Ethical Committee (Number: ES 100370001499).

A total of 16 crossbred Landrace  $\times$  Large White pigs (39.0  $\pm$  3.7 kg) were randomly distributed in the following 3 groups:

1. EMG-cell free (n = 8), with MI induction and EMG-cell free implantation;
2. EMG-ATDPC (n = 10), with MI induction and EMG-ATDPC treatment; and

**FIGURE 2** EMG-ATDPC Preparation and Implantation, and Post-MI Morphometric Analysis



(A) The myocardial scaffold was embedded with the mixture of hydrogel and GFP<sup>+</sup> pATDPCs. (B) Then culture medium was added, to facilitate hydrogel gelification and to generate the definitive EMG-ATDPC. Scale bars = 1 cm. (C) EMG-ATDPC (surrounded by a dotted yellow line) engrafted in the porcine heart over the MI performed by a coronary artery ligation (indicated with a yellow asterisk). (D) Panoramic microphotograph of the implanted EMG-ATDPC over the myocardium, with histological assessment under Masson's trichrome and (E) Movat's pentachrome stains. Scale bars = 100 μm. (F) Representative images showing the intact EMG (black arrowheads) retained over the infarcted myocardium (discontinuous black line) after animal sacrifice in EMG-cell free and (G) EMG-ATDPC pigs. (F') Magnification of the infarcted area and EMG in the EMG-cell free and (G') EMG-ATDPC groups, respectively. (H) Percentage of LV infarct area measured in the EMG-ATDPC and EMG-cell free groups. Data are expressed as mean ± SEM. \*p = 0.048. GFP = green fluorescent protein; LV = left ventricle; Myo = host myocardium; RV = right ventricle; other abbreviations as in Figure 1.

- EMG-sham (n = 2), with no MI and EMG-ATDPC over healthy myocardium.

Acute MI was induced by performing a left lateral thoracotomy, followed by permanent double ligation of the first marginal branch of the circumflex artery, as previously described (15). Thirty minutes later, the EMG-ATDPC or EMG-cell free was attached over the infarcted area using surgical glue (Glubran2, Cardiolink, Barcelona, Spain) (Figure 2C). To ensure induction of similar MI, blood samples were collected from all animals through jugular venipuncture at baseline and 2 h post-MI. The circulating cardiac biomarkers cardiac troponin I (cTnI) and creatinine kinase were measured using a fluorometric immunoassay analyzer (AQT90 FLEX, Radiometer Medical, Brønshøj, Denmark). Following completion of these procedures, the animals were housed for 1 month before sacrifice.

**CARDIAC FUNCTION EVALUATION.** Investigators blinded to treatment groups assessed the animals' cardiac function using cardiac magnetic resonance imaging (CMR) at 1.5-T (Intera, Philips, Amsterdam, the Netherlands) with a 4-channel, phased array surface coil (SENSE Body Coil). Acquired images were taken in apnea with electrocardiogram gating. At 3 time points—baseline, 48 h post-MI, and 1 month after treatment—we analyzed the following cardiac parameters: cardiac output, end-diastolic wall mass, left ventricular end-diastolic volume, left ventricular ejection fraction (LVEF), left ventricular end-systolic volume, and stroke volume.

**HISTOPATHOLOGICAL EXAMINATION.** Animals were sacrificed by administering an anesthesia overdose at  $33.4 \pm 4.2$  days after the initial MI induction. Porcine hearts were then excised and sectioned. Extracted biopsies were embedded in Tissue O.C.T. compound (VWR Chemicals, Radnor, Pennsylvania), snap-frozen in liquid nitrogen, and then properly stored until analysis.

For morphometric quantitation of infarct size, the left ventricular (LV) infarct area was measured in photographed heart sections, 1.5 cm distally to the coronary ligation. Quantification was performed using Image J software (version 1.48, National Institutes of Health, Bethesda, Maryland). Infarct size was double-blindly measured by 2 independent investigators and calculated as the percentage of the LV infarct area relative to the LV total area.

Histological analyses of 10- $\mu$ m frozen sections were performed with hematoxylin/eosin, Masson's trichrome, and Movat's pentachrome stains. We also used picrosirius red staining for scar fibrosis analysis to examine collagen deposition and changes in the

amounts of type I and III collagens. Total collagen and specific I and III types were quantified for 6 random fields using Image-Pro Plus software (version 6.2.1, Media Cybernetics, Rockville, Maryland).

For detailed information about immunohistochemical analysis, see the [Supplemental Appendix](#).

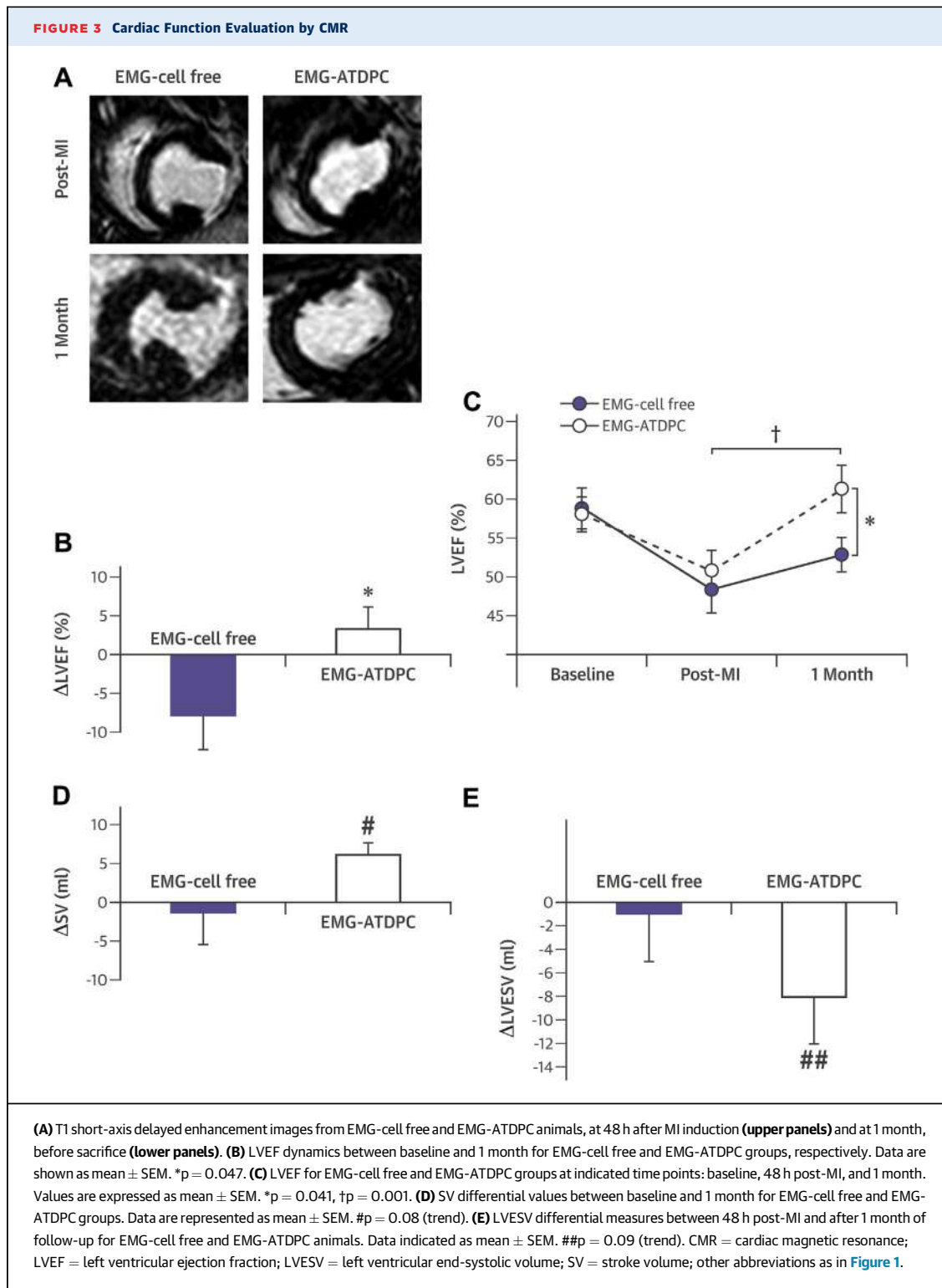
**STATISTICAL ANALYSIS.** Statistical analyses were performed using the statistics program SPSS (version 20, IBM, Armonk, New York). Both cardiac function differences and quantitative histopathological evaluation between groups were compared using the Student *t* test for paired and independent samples. Baseline CMR parameters differences were assessed with an analysis of variance test. Data are represented as mean  $\pm$  SEM, and a *p* value  $<0.05$  was considered statistically significant.

## RESULTS

Following MI induction, 1 animal died due to ventricular fibrillation, 1 exhibited no evidence of MI and was thus not considered in the final analysis, and 2 animals were excluded due to post-surgical infection associated with inappropriate EMG handling during the preparation process before implantation. Thus, a total of 16 animals were finally included in the analysis (cardiac function and histopathology), distributed as follows: 7 in the EMG-cell free group, 7 in the EMG-ATDPC, and 2 in the EMG-sham group (Figure 1). The EMG-cell free and EMG-ATDPC groups showed similar levels of the circulating cardiac markers cTnI ( $0.06 \pm 0.02$   $\mu$ g/l vs.  $0.03 \pm 0.05$   $\mu$ g/l; *p* = 0.55) and creatinine kinase MB ( $0.66 \pm 0.29$   $\mu$ g/l vs.  $0.43 \pm 0.19$   $\mu$ g/l; *p* = 0.52), indicating similar MI induction in both groups. After macroscopic and microscopic examination, in 10 animals of 16 (n = 6 and n = 4 for EMG-cell free and EMG-ATDPC groups, respectively), the EMG remained properly attached to the underlying myocardium and was identifiable at both levels after 1 month (Figures 2D to 2G). In the remaining animals, the EMG was reabsorbed and could not be distinguished following sacrifice.

**EMG-ATDPC IMPLANTATION REDUCED INFARCT SIZE AND IMPROVED CARDIAC FUNCTION.** LV infarct size was 68% smaller in the EMG-ATDPC compared with the EMG-cell free group ( $2.5 \pm 0.6\%$  vs.  $7.6 \pm 2.3\%$ , respectively; *p* = 0.048) (Figure 2H).

Baseline CMR data analysis showed no differences between the studied groups (Supplemental Table 1). Cardiac function assessed by LVEF at 1 month follow-up after infarction significantly improved in the EMG-ATDPC group ( $50.8 \pm 2.6\%$  vs.  $61.3 \pm 3.4\%$ ; *p* = 0.001) and remained nonsignificant in the EMG-cell free group ( $48.4 \pm 3.0\%$  vs.  $52.9 \pm 2.2\%$ ;



$p = 0.30$ ) (**Figures 3A to 3C, Table 1**). Similar trends were observed for stroke volume ( $6.1 \pm 1.6$  ml vs.  $-1.5 \pm 4.0$  ml,  $p = 0.08$ , for EMG-ATDPC vs. EMG-cell free, respectively) and LV end-systolic volume

( $-8.1 \pm 1.4$  ml vs.  $-1.0 \pm 3.5$  ml,  $p = 0.09$ , for EMG-ATDPC vs. EMG-cell free, respectively), indicating limited ventricular remodeling in treated animals (**Figures 3D and 3E**).

**TABLE 1 CMR-Derived Cardiac Function Parameters**

	EMG-Sham (n = 2)			EMG-Cell Free (n = 7)			EMG-ATDPC (n = 7)		
	48 h Post-Intervention	1 Month	p Value	48 h Post-MI	1 Month	p Value	48 h Post-MI	1 Month	p Value
CO (l/min)	2.9 ± 0.5	3.1 ± 0.5	0.76	3.1 ± 0.4	2.9 ± 0.1	0.41	2.9 ± 0.1	2.9 ± 0.2	0.95
EDWM (g)	66.9 ± 9.7	68.2 ± 5.6	0.81	69.9 ± 5.5	68.4 ± 4.7	0.60	69.0 ± 3.2	71.1 ± 3.5	0.42
LVEDV (ml)	61.5 ± 6.3	60.5 ± 10.0	0.83	64.7 ± 5.5	67.0 ± 5.1	0.63	66.2 ± 2.7	62.9 ± 2.6	0.21
LVEF (%)	54.4 ± 5.0	60.2 ± 0.3	0.44	48.4 ± 3.0	52.9 ± 2.2	0.30	50.8 ± 2.6	61.3 ± 3.1	<b>0.001</b>
LVESV (ml)	27.7 ± 0.2	24.1 ± 3.8	0.53	33.3 ± 3.3	32.3 ± 3.6	0.77	32.8 ± 2.5	24.7 ± 2.8	<b>0.001</b>
SV (ml)	33.8 ± 6.6	36.4 ± 6.2	0.08	31.4 ± 3.3	34.7 ± 1.9	0.34	33.5 ± 1.7	38.2 ± 1.1	<b>0.03</b>

Values are mean ± SEM. Cardiac function parameters in the EMG-sham, EMG-cell free, and EMG-ATDPC groups are at 48 h after MI induction (or post-intervention for EMG-sham) and at the time of sacrifice (1 month). The p values in **bold** are statistically significant.

ATDPC = adipose tissue-derived progenitor cells; CMR = cardiac magnetic resonance; CO = cardiac output; EDWM = end-diastolic wall mass; EMG = engineered myocardial graft; LVEDV = left ventricular end-diastolic volume; LVEF = left ventricular ejection fraction; LVESV = left ventricular end-systolic volume; MI = myocardial infarction; SV = stroke volume.

**EMG-ATDPC PROMOTED NEOVASCULARIZATION OF SUBJACENT MYOCARDIUM AND INCREASED VESSEL DENSITY.** EMG-ATDPC displayed notable vascularization, including formation of new vessels inside the construct (Figures 4A and 4B), with presence of erythrocytes and polymorphonuclear cells within, confirming functional conduits with blood flow (Figure 4C). These vessels showed positive staining for smooth muscle actin (SMA) in the tunica media (Figure 4D) and for CD31 and isolectin B4 (IsoB4) in the endothelial layer comprising the tunica intima (Figures 4E and 4F). Interestingly, some of the newly formed vessels connected the EMG-ATDPC with the underlying myocardium (Figures 4G to 4I), confirming its integration with the vascular network of the host myocardium. Moreover, vessel quantification revealed 2-fold higher vessel area in the EMG-ATDPC animals than in the EMG-cell free animals, both in the infarct core ( $3.6 \pm 0.5\%$  vs.  $1.7 \pm 0.1\%$ ;  $p = 0.011$ ) and within the EMG ( $3.3 \pm 0.3\%$  vs.  $1.5 \pm 0.2\%$ ;  $p < 0.001$ ) (Figure 4J).

**GFP<sup>+</sup> pATDPCs MIGRATED TO THE HOST MYOCARDIUM AND EXPRESSED ENDOTHELIAL MARKERS.** Histological analysis of the EMG-ATDPC explanted hearts revealed GFP<sup>+</sup> pATDPCs within the EMG (Figure 5A), as well as cell migration to the underlying infarct core (Figure 5B). Implanted cells were positive for SMA, maintaining its baseline expression, and remarkably, de novo expressed CD31 and IsoB4 (Figures 5C to 5E, Supplemental Figure 1). Altogether, this suggests that the introduced cell lineage contributed to the generation of new vessels and increased vascularization. These results also provided evidence of the commitment of pATDPCs toward an endothelial differentiation phenotype.

Evaluation of cell proliferative status in the infarct core revealed that GFP<sup>+</sup> pATDPCs exhibited nuclear co-staining with phospho-histone H3, a marker of

active proliferation (data not shown). The total phospho-histone H3-positive cell count in the infarct core was almost 2-fold higher in the EMG-ATDPC group compared with the EMG-cell free group ( $1.5 \pm 0.2\%$  vs.  $0.8 \pm 0.2\%$ , respectively;  $p = 0.019$ ) (Supplemental Figure 2).

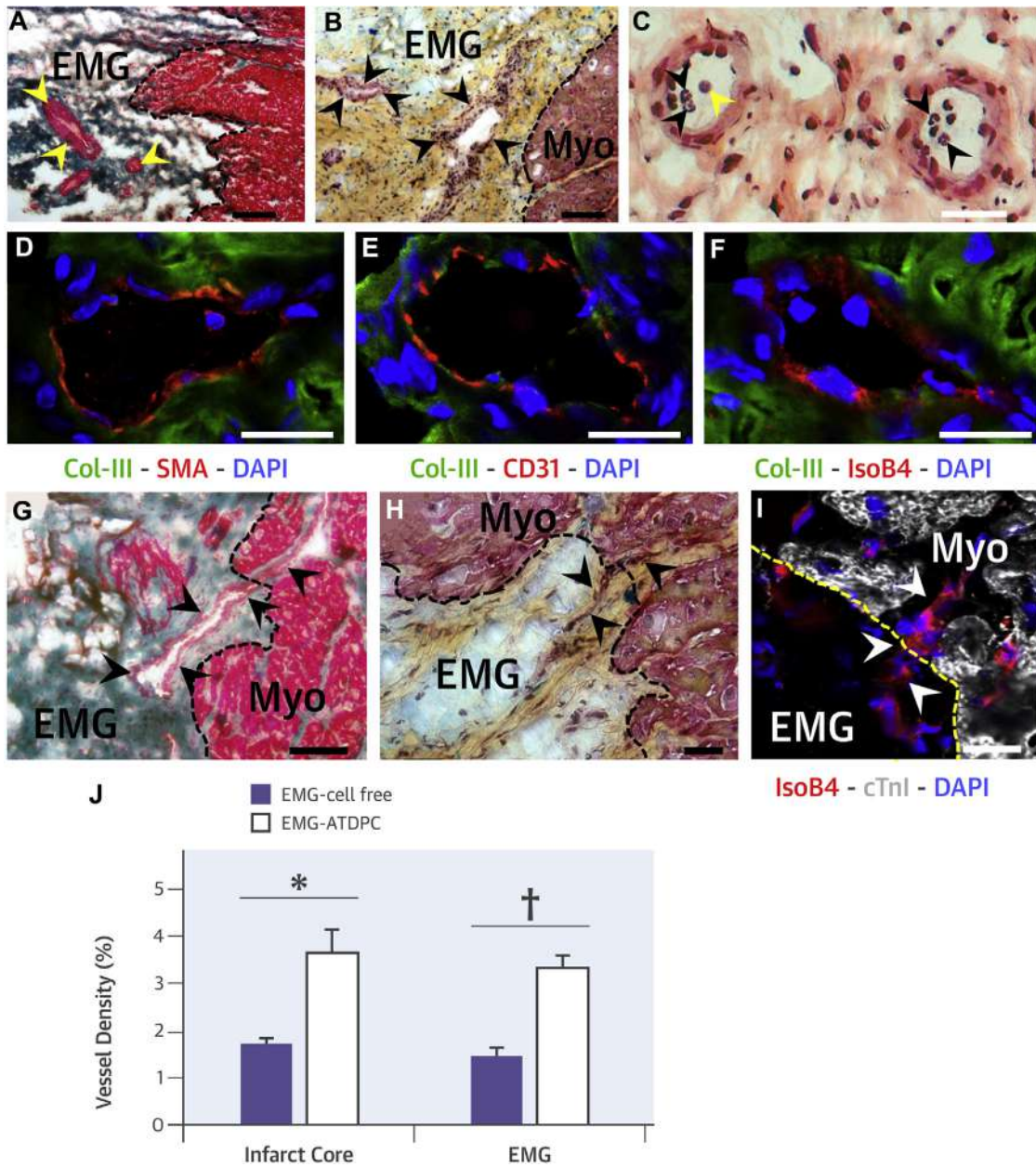
**TREATMENT WITH EMG-ATDPC ATTENUATED MYOCARDIAL FIBROSIS FOLLOWING MI.** We further examined the collagen content in the myocardial scar following MI induction to assess how the EMG engraftment affected fibrosis progression (Figures 6A to 6D). Focusing on the infarct area, total collagen content was significantly reduced in the EMG-ATDPC group compared to the EMG-cell free group ( $28.6 \pm 6.1\%$  vs.  $49.9 \pm 4.1\%$ , respectively;  $p = 0.016$ ). Collagen fibril subtype analysis revealed reduced type I collagen ( $19.8 \pm 4.6\%$  vs.  $46.3 \pm 4.4\%$ ;  $p = 0.002$ ) and increased type III collagen ( $8.8 \pm 2.0\%$  vs.  $3.6 \pm 1.1\%$ ;  $p = 0.042$ ) in EMG-ATDPC-treated animals. Hence, the ratio of type I to III was also significantly lower in EMG-ATDPC animals ( $2.3 \pm 0.7$  vs.  $13.0 \pm 6.9$ ;  $p = 0.032$ ) (Figure 6E).

## DISCUSSION

The present study is the first, to our knowledge, to test an EMG comprising a decellularized myocardial scaffold plus adipose-derived progenitors (EMG-ATDPC) in a pre-clinical MI model. Herein, we investigated the functional benefits derived from EMG-ATDPC engraftment in terms of cardiac function, neovascularization, and scar healing. EMG-ATDPC treatment led to improved contractility (assessed by surrogate LVEF), 2-fold higher vascular density in the infarct area, 3-fold smaller infarct size, and modulation of scar healing with attenuated ventricular remodeling.

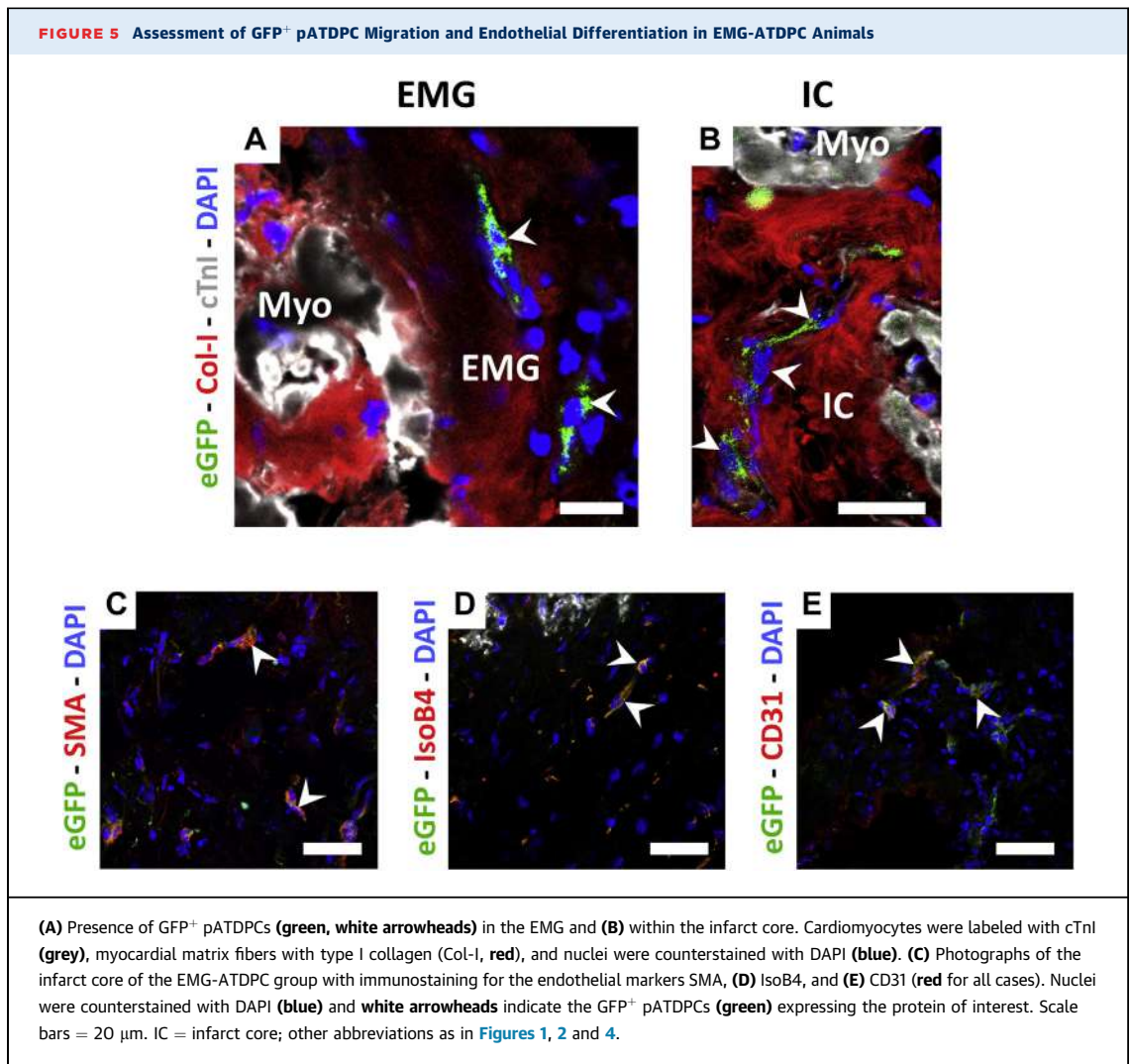
The pATDPC lineage chosen to repopulate the scaffold has previously exhibited cardiomyogenic

**FIGURE 4 Analysis of Post-MI Vascularization After EMG-ATDPC Engraftment**



(A) Masson's trichrome and (B) Movat's pentachrome stains reveal presence of blood vessels in the EMG-ATDPC (yellow and black arrowheads, respectively). Scale bars = 100 and 50  $\mu$ m, in that order. (C) Hematoxylin/eosin staining showing functional blood vessels in EMG-ATDPC with presence of polymorphonuclear cells (black arrowheads) and erythrocytes (yellow arrowheads) in the lumen. Scale bar = 20  $\mu$ m. (D) Images of the EMG-ATDPC with immunohistochemistry revealing neovessels positive for SMA, (E) CD31, and (F) IsoB4 (red for all cases). Type III collagen (Col-III) was stained in green, and nuclei were counterstained with DAPI (blue). Scale bars = 20  $\mu$ m. (G) Neovessels connecting the engrafted EMG-ATDPC with the host myocardium (arrowheads) revealed with Masson's trichrome, (H) Movat's pentachrome, and (I) immunohistochemical staining (red indicates IsoB4; grey, cTnI; blue, nuclei). Scale bars = 50  $\mu$ m (G and H) and 20  $\mu$ m (I). All images shown belong to the EMG-ATDPC animal group. (J) Percentage of vascular density in the infarct core and inside the EMG in the EMG-cell free and EMG-ATDPC groups. Final data are shown as mean  $\pm$  SEM. \* $p$  = 0.011, † $p$  < 0.001. cTnI = cardiac troponin I; IsoB4 = isolectin B4; SMA = smooth muscle actin; other abbreviations as in Figures 1 and 2.



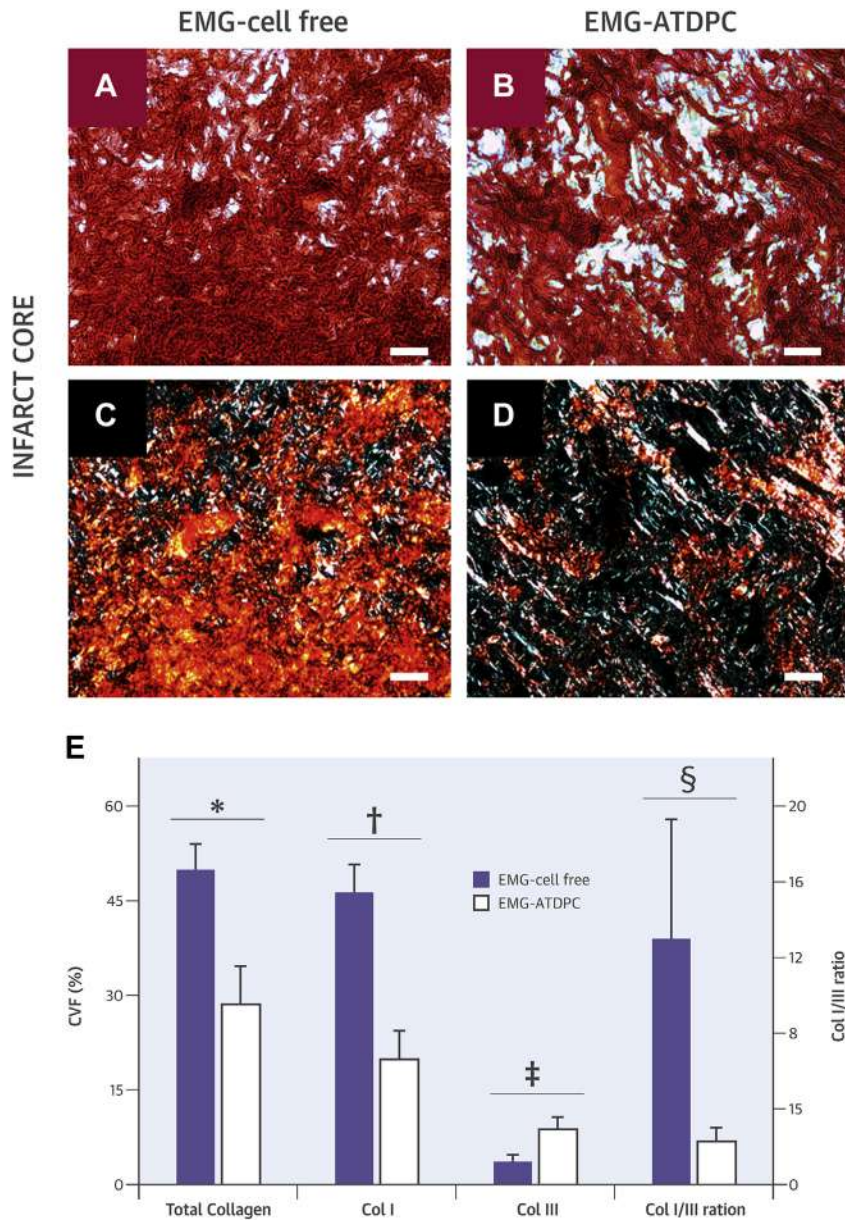


commitment and regenerative potential appropriate for cardiac tissue engineering (9,14,16). Moreover, their inherent immunomodulatory capacity facilitates delivery, eliminating the need for immunosuppressive treatments in the context of allogeneic transplantation (17,18). In vivo studies have also demonstrated that ATDPC delivery within scaffolds of diverse origin promotes remarkable cardiac function improvement in mice (19), rat (20,21), and porcine (14,22) MI models, supporting their suitability for in vivo application.

To better understand the beneficial effects exerted by the EMG-ATDPC, we must examine the synergistic contributions from the decellularized myocardial scaffold and the pATDPCs. The decellularized myocardial scaffold must preserve the native myocardial matrix integrity and organization, such that it can provide adequate cues to drive cell

differentiation and to ensure cell attachment, survival, and migration (23,24). We must also acknowledge the role of the decellularized scaffolds themselves, in terms of neovascularization and cell recruitment. Engraftment of an acellular pericardial scaffold over porcine infarcted myocardium can reportedly prompt scaffold neoinnervation and neovascularization (25). Decellularized myocardial scaffolds apparently attract endogenous endothelial and smooth muscle cells, increasing vascular sprouting (26), and enabling scaffold-host tissue connections with vascular networks and irrigation of injured tissue. Thus, the decellularized myocardial scaffold both provides cellular supportive function and participates in direct vascularization of ischemic myocardium. Likewise, its porcine origin is advantageous for 2 main reasons: first, decellularized scaffolds can be easily obtained from pig hearts, with high

**FIGURE 6** Determination of Collagen Content and Composition in the Infarct Core



(A and B) Representative bright light microscopy images with sirius red staining distinguishing collagen fibers (red) and healthy myocardium (yellow/orange) from EMG-cell free and EMG-ATDPC animals, respectively. (C and D) Polarized light microscopy images with sirius red staining showing type I collagen (red/yellow) and type-III collagen (green) in the EMG-cell free and EMG-ATDPC groups, respectively. Scale bars = 50  $\mu$ m. (E) Collagen percentage—expressed as collagen volume fraction (CVF [%], left y-axis)—for total collagen, type I collagen (Col I), and type III collagen (Col III); as well as the ratio between type I and III collagens (Col I/III ratio, right y-axis), for both the EMG-cell free and EMG-ATDPC groups. Results are displayed as mean  $\pm$  SEM. \* $p = 0.016$ , † $p = 0.002$ , ‡ $p = 0.042$ , § $p = 0.032$ . Abbreviations as in Figure 1.

availability, and generated in large quantities; and second, some studies demonstrated feasible and viable administration in clinical practice of decellularized non-glutaraldehyde fixed xenograft with no associated side effects, immunological response, or rejection (27), overcoming fixation of porcine heart valves before implantation in humans to reduce immunogenicity and strengthen the tissue, but which in turn would impede cell repopulation and in some cases has led to calcification (28). Hence, clinical translation of this xenograft should not be hampered by regulatory issues.

On the other hand, the contribution of pATDPCs to infarct repair is likely even more important, and may be the key to understand post-MI recovery. The GFP<sup>+</sup> pATDPCs that migrated to the infarct core were positive for the endothelial markers SMA, IsoB4, and CD31. Thus, cell delivery within the EMG contributed to new blood vessel synthesis, as was previously reported (14). This explains the higher vascular density observed in EMG-ATDPC animals—which increases the supplies of nutrients, oxygen, and endogenous stem cells to the hypoxic area, probably preventing infarct expansion due to EMG-ATDPC implantation effect.

Most likely, paracrine effects would be the most plausible mechanism by which pATDPCs exerted their beneficial effects, which has been broadly described as one of the putative mechanisms for implanted cells to regenerate the scarred area (29,30). Once placed on top of the infarcted myocardium, the pATDPCs can also exert autocrine and paracrine effects. They secrete growth factors—such as vascular endothelial, fibroblast, hepatocyte and insulin growth factors, and transforming growth factor- $\beta$ —which increase the vasculogenic, antiapoptotic/cardioprotective, and proliferative activities, as well as the recruitment of endogenous stem cells (31,32). It is also reported pATDPCs secrete interleukin-6, -7, -8, and -11, which act as phagocyte chemoattractants to eliminate cell debris and encourage cellular turnover and regeneration (31). Such actions are consistent with the reduced infarct size and enhanced vascular density observed after EMG-ATDPC treatment, as well as the higher cell proliferation displayed in the EMG-ATDPC group. Moreover, collagen content reduction may be correlated with the secretion of metalloproteinases by pATDPCs, which inhibits collagen synthesis, as it has been described for mesenchymal stem cells (33). However, there is no clear explanation for the increase in type III collagen. One possibility is that synthesis of type III collagen increases when pATDPCs are under mechanical stress or inside a 3-dimensional scaffold (34). The mechanical stimuli

in the myocardium and the scaffold environment could have up-regulated pATDPCs type III collagen production, compensating for its degradation.

Along with the altered collagen content, we observed a decrease in the ratio of type I to type III collagen, indicating a reduction of collagen I deposition. Type III collagen is typically present during wound healing, and organizes to form an elastic fibrillar network, providing a framework to ensure correct alignment of type I collagen fibers and maintenance of normal heart shape and myocardium stiffness. On the other hand, type I collagen exhibits high stiffness, thus permitting chamber remodeling (35,36). Overall, the observed histopathological changes—including neovascularization, infarct area regeneration, and attenuation of fibrosis—globally enhanced cardiac function in terms of better LVEF, which is the most clinically relevant parameter for assessing heart function. Our results reflect an ~11% improvement in LVEF after MI in EMG-ATDPC group, which is higher than the 3% to 4% enhancement obtained with percutaneous coronary intervention (37), the 4% registered with bone marrow cell therapies (38), or the improvements obtained with other scaffolds in the swine MI model (13,39,40).

The reported feasibility and functional potential of catheter delivery of a decellularized myocardial scaffold *in vivo* (26) encouraged previous studies to use such scaffolds in pre-clinical models, although earlier studies showed little or modest benefits. Initial studies in the rat MI model produced controversial results regarding LVEF. Although Singelyn *et al.* (41) did not observe LVEF changes following decellularized myocardial scaffold administration, Dai *et al.* (42) reported a 4.3% increase in LVEF with scaffold treatment compared with controls. Neither study described higher neovascularization or altered final infarct size after scaffold treatment, nor examined collagen content modifications (41,42). Another study in rats investigated the addition of mesenchymal progenitor cells into a decellularized myocardial-fibrin composite scaffold, and reported increased angiogenesis, but did not assess LVEF, infarct size, or collagen variations (43). Finally, a prior work conducted in swine reported that administration of cell-free decellularized myocardial scaffold did not significantly affect LVEF when comparing post-MI and final LVEF values (13), in contrast to our presently remarkable LVEF increase in EMG-ATDPC-treated swine.

**STUDY LIMITATIONS.** One of the limitations in the present study is the lack of a MI-only control group, with no EMG-cell free or EMG-ATDPC implantation.

Although the data provided here by themselves indicate a meaningful improvement in cardiac function and myocardial restoration in EMG-ATDPC-treated animals, further studies including a MI-only group may help in elucidating the role of the decellularized myocardial scaffold and its beneficial effects over infarcted myocardium by itself.

Thus, the promising data reported here support proceeding to clinical translation. Our group has already started EMG-ATDPC production under good manufacturing practice conditions and has initiated the road to obtain approval by local regulators as first steps for a phase I clinical trial.

## CONCLUSIONS

To summarize, we generated an EMG-ATDPC comprising a decellularized myocardial scaffold that was repopulated with pATDPCs. This EMG-ATDPC was implanted in a swine MI model, and cardiac recovery was assessed by CMR. The engrafted EMG-ATDPC promoted revascularization of the damaged tissue, reduced infarct size, attenuated ventricular remodeling and fibrosis progression, and improved cardiac function. This EMG-ATDPC is ready for clinical translation.

**ACKNOWLEDGMENTS** The authors thank L. Hernández, B. Fernández, and J. Maestre for technical assistance

with animal surgeries and magnetic resonance imaging analysis.

**REPRINT REQUESTS AND CORRESPONDENCE:** Dr. Antoni Bayes-Genis, Head of Cardiology Service, Germans Trias i Pujol University Hospital, Crta. Canyet, s/n, 08916 Badalona, Barcelona, Spain. E-mail: [abayesgenis@gmail.com](mailto:abayesgenis@gmail.com).

## PERSPECTIVES

**COMPETENCY IN MEDICAL KNOWLEDGE:** MI remains a top-ranked cause of death worldwide. Local delivery of natural scaffolds repopulated with cardiac progenitor cells (EMG-ATDPC) is a feasible approach with beneficial impact in cardiac function recovery. In our hands, the engraftment of a cell-enriched engineered myocardial graft in the pre-clinical MI model in swine resulted in better left ventricular ejection fraction, higher vessel density and neovascularization, reduced infarct size by 68%, and limited fibrosis.

**TRANSLATIONAL OUTLOOK:** EMG-ATDPC implantation in the infarcted myocardium improves cardiac recovery in the porcine pre-clinical MI model. The design of a phase I to II clinical trial in humans is mandatory to confirm and validate safety and efficacy. Thus, the EMG-ATDPC is ready to start the translational avenue toward first-in-man clinical trials.

## REFERENCES

1. World Health Organization. The Top 10 Causes of Death. Fact sheet N°310. Updated May 2014. Available at: <http://www.who.int/mediacentre/factsheets/fs310/en/>. Accessed December 16, 2015.
2. Pfeffer MA, Braunwald E. Ventricular remodeling after myocardial infarction. Experimental observations and clinical implications. *Circulation* 1990;81:1161-72.
3. Bergmann O, Bhardwaj RD, Bernard S, et al. Evidence for cardiomyocyte renewal in humans. *Science* 2009;324:98-102.
4. Mollova M, Bersell K, Walsh S, et al. Cardiomyocyte proliferation contributes to heart growth in young humans. *Proc Natl Acad Sci U S A* 2013;110:1446-51.
5. Langer R, Vacanti JP. Tissue engineering. *Science* 1993;260:920-6.
6. Hirt MN, Hansen A, Eschenhagen T. Cardiac tissue engineering: state of the art. *Circ Res* 2014;114:354-67.
7. Vunjak-Novakovic G, Lui KO, Tandon N, et al. Bioengineering heart muscle: a paradigm for regenerative medicine. *Annu Rev Biomed Eng* 2011;13:245-67.
8. Radisic M, Park H, Gerecht S, et al. Biomimetic approach to cardiac tissue engineering. *Philos Trans R Soc Lond B Biol Sci* 2007;362:1357-68.
9. Perea-Gil I, Uriarte JJ, Prat-Vidal C, et al. In vitro comparative study of two decellularization protocols in search of an optimal myocardial scaffold for recellularization. *Am J Transl Res* 2015;7:558-73.
10. Ott HC, Matthiesen TS, Goh SK, et al. Perfusion-decellularized matrix: using nature's platform to engineer a bioartificial heart. *Nat Med* 2008;14:213-21.
11. Crapo PM, Gilbert TW, Badyal SF. An overview of tissue and whole organ decellularization processes. *Biomaterials* 2011;32:3233-43.
12. Guyette JP, Charest J, Mills RW, et al. Bioengineering human myocardium on native extracellular matrix. *Circ Res* 2016;118:56-72.
13. Seif-Naraghi SB, Singelyn JM, Salvatore MA, et al. Safety and efficacy of an injectable extracellular matrix hydrogel for treating myocardial infarction. *Sci Transl Med* 2013;5:173ra25.
14. Prat-Vidal C, Gálvez-Montón C, Puig-Sanvicens V, et al. Online monitoring of myocardial bioprosthesis for cardiac repair. *Int J Cardiol* 2014;174:654-61.
15. Gálvez-Montón C, Prat-Vidal C, Roura S, et al. Adipose flap for myocardial salvage after infarct. *Cardiovasc Res* 2011;91:659-67.
16. Bayes-Genis A, Gálvez-Montón C, Prat-Vidal C, et al. Cardiac adipose tissue: a new frontier for cardiac regeneration? *Int J Cardiol* 2013;167:22-5.
17. Perea-Gil I, Monguió-Tortajada M, Gálvez-Montón C, et al. Preclinical evaluation of the immunomodulatory properties of cardiac adipose tissue progenitor cells using umbilical cord blood mesenchymal stem cells: a direct comparative study. *Biomed Res Int* 2015;2015:439808.
18. Cho KS, Park HK, Park HY, et al. IFATS collection: immunomodulatory effects of adipose tissue-derived stem cells in an allergic rhinitis mouse model. *Stem Cells* 2009;27:259-65.
19. Bagó JR, Soler-Botija C, Casani L, et al. Bioluminescence imaging of cardiomyogenic and vascular differentiation of cardiac and subcutaneous adipose tissue-derived progenitor cells in fibrin patches in a myocardial infarct model. *Int J Cardiol* 2013;169:288-95.
20. Wang H, Shi J, Wang Y, et al. Promotion of cardiac differentiation of brown adipose derived stem cells by chitosan hydrogel for repair after myocardial infarction. *Biomaterials* 2014;35:3986-98.

21. Sun CK, Zhen YY, Leu S, et al. Direct implantation versus platelet-rich fibrin-embedded adipose-derived mesenchymal stem cells in treating rat acute myocardial infarction. *Int J Cardiol* 2014;173:410-23.
22. Araña M, Gavira JJ, Peña E, et al. Epicardial delivery of collagen patches with adipose-derived stem cells in rat and minipig models of chronic myocardial infarction. *Biomaterials* 2014;35:143-51.
23. Badyalak SF, Taylor D, Uygun K. Whole-organ tissue engineering: decellularization and recellularization of three-dimensional matrix scaffolds. *Annu Rev Biomed Eng* 2011;13:27-53.
24. French KM, Boopathy AV, DeQuach JA, et al. A naturally derived cardiac extracellular matrix enhances cardiac progenitor cell behavior in vitro. *Acta Biomater* 2012;8:4357-64.
25. Gálvez-Montón C, Fernandez-Figueras MT, Martí M, et al. Neoinnervation and neovascularization of acellular pericardial-derived scaffolds in myocardial infarcts. *Stem Cell Res Ther* 2015;6:108.
26. Singelyn JM, DeQuach JA, Seif-Naraghi SB, et al. Naturally derived myocardial matrix as an injectable scaffold for cardiac tissue engineering. *Biomaterials* 2009;30:5409-16.
27. Konertz W, Angeli E, Tarusinov G, et al. Right ventricular outflow tract reconstruction with decellularized porcine xenografts in patients with congenital heart disease. *J Heart Valve Dis* 2011;20:341-7.
28. Erdbrügger W, Konertz W, Dohmen P, et al. Decellularized xenogenic heart valves reveal remodeling and growth potential in vivo. *Tissue Eng* 2006;12:2059-68.
29. Doppler SA, Deutsch MA, Lange R, et al. Cardiac regeneration: current therapies-future concepts. *J Thorac Dis* 2013;5:683-97.
30. Hoke NN, Salloum FN, Loesser-Casey KE, et al. Cardiac regenerative potential of adipose tissue-derived stem cells. *Acta Physiol Hung* 2009;96:251-65.
31. Gimble JM, Katz AJ, Bunnell BA. Adipose-derived stem cells for regenerative medicine. *Circ Res* 2007;100:1249-60.
32. Kokai LE, Marra K, Rubin JP. Adipose stem cells: biology and clinical applications for tissue repair and regeneration. *Transl Res* 2014;163:399-408.
33. Mias C, Lairez O, Trouche E, et al. Mesenchymal stem cells promote matrix metalloproteinase secretion by cardiac fibroblasts and reduce cardiac ventricular fibrosis after myocardial infarction. *Stem Cells* 2009;27:2734-43.
34. Colazzo F, Sarathchandra P, Smolenski RT, et al. Extracellular matrix production by adipose-derived stem cells: implications for heart valve tissue engineering. *Biomaterials* 2011;32:119-27.
35. Pauschinger M, Knopf D, Petschauer S, et al. Dilated cardiomyopathy is associated with significant changes in collagen type I/III ratio. *Circulation* 1999;99:2750-6.
36. Weber KT. Cardiac interstitium in health and disease: the fibrillar collagen network. *J Am Coll Cardiol* 1989;13:1637-52.
37. Strauer BE, Steinhoff G. 10 years of intracoronary and intramyocardial bone marrow stem cell therapy of the heart: from the methodological origin to clinical practice. *J Am Coll Cardiol* 2011;58:1095-104.
38. Jeevanantham V, Butler M, Saad A, et al. Adult bone marrow cell therapy improves survival and induces long-term improvement in cardiac parameters: a systematic review and meta-analysis. *Circulation* 2012;126:551-68.
39. Mukherjee R, Zavadzka JA, Saunders SM, et al. Targeted myocardial microinjections of a biocomposite material reduces infarct expansion in pigs. *Ann Thorac Surg* 2008;86:1268-76.
40. Ye L, Chang YH, Xiong Q, et al. Cardiac repair in a porcine model of acute myocardial infarction with human induced pluripotent stem cell-derived cardiovascular cells. *Cell Stem Cell* 2014;15:750-61.
41. Singelyn JM, Sundaramurthy P, Johnson TD, et al. Catheter-deliverable hydrogel derived from decellularized ventricular extracellular matrix increases endogenous cardiomyocytes and preserves cardiac function post-myocardial infarction. *J Am Coll Cardiol* 2012;59:751-63.
42. Dai W, Gerczuk P, Zhang Y, et al. Intramyocardial injection of heart tissue-derived extracellular matrix improves postinfarction cardiac function in rats. *J Cardiovasc Pharmacol Ther* 2013;18:270-9.
43. Godier-Furnémont AFG, Martens TP, Koeckert MS, et al. Composite scaffold provides a cell delivery platform for cardiovascular repair. *Proc Natl Acad Sci U S A* 2011;108:7974-9.

---

**KEY WORDS** adipose tissue-derived progenitor cells, cardiac tissue engineering, decellularized myocardial scaffold, myocardial infarction, pre-clinical model

---

**APPENDIX** For an expanded Methods section as well as a supplemental table and figures, please see the online version of this article.

## **Immunohistological analysis**

To analyze blood vessel and endothelial differentiation, 10- $\mu$ m frozen tissue sections were immunostained with biotinylated *Griffonia simplicifolia* lectin I B4 (IsoB4; 1:50; Vector Labs, Burlingame, California), smooth muscle actin (SMA; 1:50; Sigma-Aldrich), von Willebrand factor (vWF) (1:200, Abcam), CD34 (1:100, Abcam), and CD31 (1:50; Abcam, Cambridge, England) primary antibodies. Cardiac differentiation was assessed using primary antibodies against GATA4 (1:20; R&D Systems, Minneapolis, Minnesota), SERCA2 (1:50; Santa Cruz, Santa Cruz, California), connexin43 (1:100; BD Transduction, San Jose, California), and cardiac troponin I (cTnI; 1:100; Abcam). Cell proliferation was evaluated using phospho-histone H3 antibody (1:100; Cell Signaling, Danvers, Massachusetts). GFP+ pATDPCs were detected using anti-GFP antibody (1:500; Abcam). EMG was detected using either type I or type III collagen (1:100, Abcam). Secondary antibodies included Alexa Fluor 488, 568, 594, and 647 (1:500; Molecular Probes, Eugene, Oregon), and Cy2, Cy3, and Cy5 (1:500; Jackson ImmunoResearch Laboratories, West Grove, Pennsylvania). Nuclei were counterstained with DAPI (1:10000; Sigma-Aldrich). Images were captured under a laser confocal microscope (Axio-Observer Z1; Zeiss, Oberkochen, Germany). Quantitative measurements of blood vessel area (IsoB4 staining) in both infarct core and myocardial scaffold, and of cell proliferation (phospho-histone H3 expression) in the infarct core were performed using Image-Pro Plus software in six different random fields.

Additionally, basal expression of the cardiac and endothelial markers described previously were also analyzed for pATDPCs cultured *in vitro*.

**Supplementary Table 1. MRI-derived data at baseline time point**

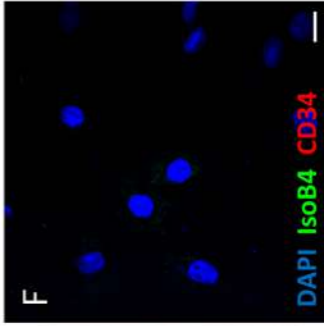
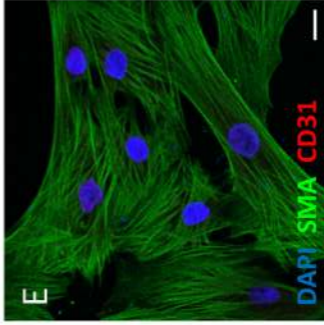
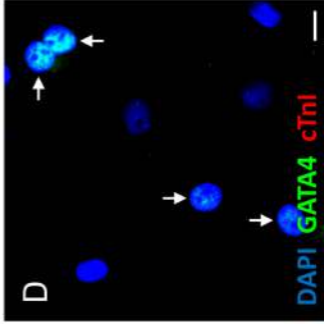
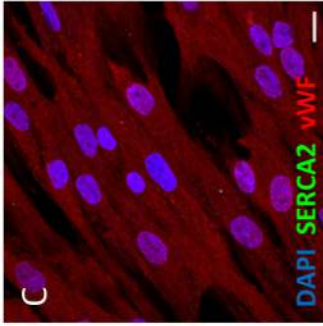
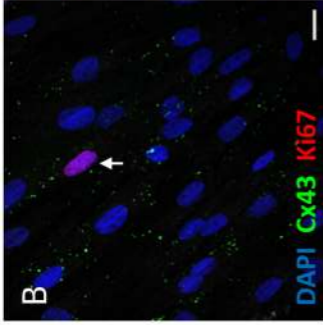
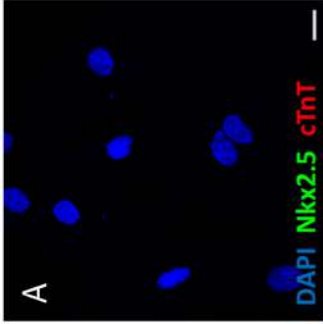
	<b>EMG-cell free (n=7)</b>	<b>EMG-ATDPC (n=7)</b>	<b>P value</b>
<b>CO (L/min)</b>	3.05 ± 0.28	2.53 ± 0.13	0.13
<b>EDWM (g)</b>	63.63 ± 4.30	57.71 ± 3.11	0.28
<b>LVEDV (mL)</b>	63.71 ± 6.31	55.78 ± 3.11	0.26
<b>LVEF (%)</b>	58.78 ± 2.60	58.04 ± 2.22	0.83
<b>LVESV (mL)</b>	26.45 ± 3.37	23.71 ± 2.40	0.51
<b>SV (mL)</b>	37.27 ± 3.71	32.07 ± 1.22	0.23

Cardiac function parameters in the EMG-cell free and EMG-ATDPC groups at baseline. Data are displayed as mean±SEM. CO indicates cardiac output; EDWM, end-diastolic wall mass; LVEDV, left ventricular end-diastolic volume; LVEF, left ventricular ejection fraction; LVESV, left ventricular end-systolic volume; SV, stroke volume.

**Supplementary Figure 1. pATDPCs baseline expression of cardiac and endothelial markers *in vitro*.**

Representative images of *in vitro* cultured pATDPCs showing baseline expression of cardiac proteins (A) Nkx2.5, cTnT, (B) Cx43, (C) SERCA2, (D) GATA4 and cTnI, as well as endothelial markers (E) vWF, (F) SMA, CD31, (G) IsoB4 and CD34. Specific detection of Ki67 as cell proliferation marker by indirect immunofluorescence is also shown. Nuclei were counterstained with DAPI (blue). Arrows indicate positive cells. Scale bars=20  $\mu\text{m}$ .

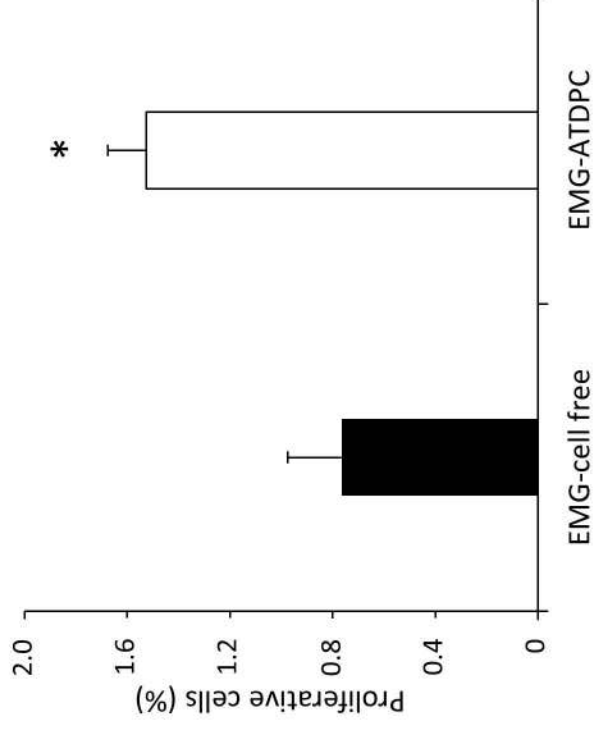




**Supplementary Figure 2. Cell proliferation in the infarcted myocardium.**

(A) Quantification of actively proliferating cells in the infarct core of EMG-cell free and EMG-ATDPC animals. Results are shown as mean $\pm$ SEM. \* $P=0.01$ .

# Supplementary Figure 2





# **Head-to-head comparison of two engineered cardiac grafts for myocardial repair: a pre-clinical myocardial infarction swine model**

Isaac Perea-Gil<sup>1</sup>, Carolina Gálvez-Montón<sup>1</sup>, Cristina Prat-Vidal<sup>1</sup>, Ignasi Jorba<sup>2,3,4</sup>, Santiago Roura<sup>1,5</sup>, Carolina Soler-Botija<sup>1</sup>, Oriol Iborra-Egea<sup>1</sup>, Elena Revuelta-López<sup>1</sup>, Ramon Farré<sup>2,4,6</sup>, Daniel Navajas<sup>2,3,4</sup>, Antoni Bayes-Genis<sup>1,7,8</sup>.

<sup>1</sup>ICREC Research Program, Health Science Research Institute Germans Trias i Pujol, Badalona, Spain.

<sup>2</sup>Biophysics and Bioengineering Unit, Faculty of Medicine, University of Barcelona, Barcelona, Spain.

<sup>3</sup>Institut de Bioenginyeria de Catalunya, Barcelona, Spain.

<sup>4</sup>CIBER de Enfermedades Respiratorias, Madrid, Spain.

<sup>5</sup>Centre of Regenerative Medicine in Barcelona, Barcelona, Spain.

<sup>6</sup>Institut d'Investigacions Biomèdiques August Pi i Sunyer, Barcelona, Spain.

<sup>7</sup>Cardiology Service, Germans Trias i Pujol University Hospital, Badalona, Spain.

<sup>8</sup>Department of Medicine, Universitat Autònoma de Barcelona, Bellaterra, Spain.

**Running head:** Cell-Enriched Engineered Cardiac Grafts for Myocardial Regeneration

**Word count:** 4984

**Address for correspondence:**

**Dr. Antoni Bayes-Genis, MD, PhD, FESC, FHFA**

Heart Institute Director ([www.icor.cat](http://www.icor.cat)). Head of Cardiology Service, Germans Trias i Pujol University Hospital, Crta. Canyet, s/n, 08916 Badalona, Barcelona, Spain.

E-mail: [abayes.germanstrias@gencat.cat](mailto:abayes.germanstrias@gencat.cat).

Phone: +34 93 4973743. Fax: +34 93 4978654.

## **Abstract**

Cardiac tissue engineering, which combines cells and supportive scaffolds, has been proved to be an effective treatment for myocardial infarction (MI), but the optimal combination still remains a challenge. We developed two engineered cardiac grafts, based on decellularized scaffolds from myocardial and pericardial tissue, repopulated with adipose tissue mesenchymal stem cells (ATMSCs). Structure, macro and micromechanical scaffold properties were preserved upon decellularization and recellularization processes, except for the recellularized myocardium micromechanics; and presence of ATMSCs was confirmed after scaffold recellularization. Moreover, the generated matrices, no matter the origin, were enriched in matrisome proteins, maintaining major cardiac extracellular matrix components, whereas cell penetrance and retention was higher for the recellularized pericardial scaffold. The effects of both engineered cardiac grafts were evaluated in a swine MI model. Forty days after graft implantation, both engineered cardiac grafts exerted ventricular function recovery. Irrespective of scaffold origin or cell recolonization, all scaffolds matched and integrated with the underlying myocardium, as well as showed signs of neovascularization and nerve sprouting. These data demonstrate the potential of engineered cardiac grafts as an effective MI therapy, which could ultimately pave the road towards the clinics and the application in humans.

**Keywords:** cardiac tissue engineering – decellularized scaffolds – myocardial infarction – proteomics – adipose tissue mesenchymal stem cells – swine model

## **Introduction**

Cardiac tissue engineering, which combines the use of cells and biomaterials, has been proposed as an alternative therapy for myocardial infarction (MI) [1], with the goal of repairing the damaged myocardium and recover heart function, preventing ventricular remodeling and end-stage heart failure. In this therapeutic approximation, cells are embedded within a natural or synthetic scaffold, avoiding the harsh infarcted milieu, and improving the low cell retention and survival reported for direct cell injection [2,3]. For this reason, the election of the scaffold biomaterial is crucial, and ideally it should resemble as much as possible the physiological myocardial extracellular matrix (ECM) properties. For instance, internal scaffold conformation, rheology, and composition, modulate cellular differentiation, migration, and adhesion [4-8].

In this context, decellularized cardiac tissues provide a close match to the native, physiological microenvironment, as they preserve the inherent stiffness, composition, vasculature network, and three-dimensional framework [9], and enable electromechanical coupling with the host myocardium upon implantation [10,11]. Herein, we tested two decellularized scaffolds generated from cardiac tissues, myocardium and pericardium, as previously published [12,13], either repopulated with porcine adipose tissue mesenchymal stem cells (pATMSCs) or without cells, tested as cell-free scaffolds. Mechanical and structural characteristics, and protein content of the decellularized scaffolds were evaluated prior to recellularization. The functional benefits associated to both acellular and recellularized scaffolds implantation were assessed in a preclinical MI swine model. Accordingly, cardiac function was analyzed through magnetic resonance imaging (MRI), and impact over infarct size was also properly determined.



## **Methods**

### **Generation of decellularized myocardial and pericardial scaffolds.**

Myocardial tissue samples were isolated from 5 different cadaveric hearts from healthy slaughterhouse pigs; and for pericardial tissue, human pericardium samples were obtained from routine surgery from 5 patients undergoing cardiac intervention at Germans Trias i Pujol University Hospital after signed written consent. This study was revised and approved by the local ethics committee, and all the protocols conformed the principles outlined in the Declaration of Helsinki. Prior to decellularization, 5 native cardiac tissue samples were stored in Krebs-Henseleit solution (Sigma-Aldrich, Madrid, Spain) at room temperature for less than 4 hours following heart collection, and immediately used for the mechanical characterization; while other 5 native samples were either immersed and frozen within optimal cutting temperature compound (VWR, Radnor, PA) or frozen in liquid nitrogen; and properly stored at -80 °C for further analysis. Regarding decellularized cardiac scaffolds obtaining, both cardiac tissues were decellularized, lyophilized and sterilized as described elsewhere [12,13].

### **Recellularization of sterilized cardiac scaffolds**

The sterilized acellular cardiac scaffolds were repopulated with pATMSCs obtained from porcine pericardial adipose tissue as reported in the literature [13], to generate both the engineered myocardial graft (EMG-ATMSC) and the engineered pericardial graft (EPG-ATMSC), respectively. Initially, the decellularized scaffolds were rehydrated with a mixture of 175  $\mu$ L of peptide hydrogel RAD16-I (Corning, Corning, NY) and 175  $\mu$ L containing  $1.75 \times 10^6$  GFP<sup>+</sup>-pATMSCs in 10% sucrose (Sigma-Aldrich), added dropwise on top of the scaffold. To promote hydrogel gelification,  $\alpha$ -

minimum essential medium eagle ( $\alpha$ -MEM) (Sigma-Aldrich) was disposed over the scaffold. The produced cell-enriched grafts were maintained during one week under standard culture conditions (37 °C, 95% air, 5% CO<sub>2</sub>), changing medium every 2 days.

### **Measurement of micromechanical properties (atomic force microscopy (AFM))**

From native heart blocks (n=5), 50  $\mu$ m thick slices were obtained using a vibratome (0.01 mm/s blade velocity; 2 mm amplitude) without freezing the tissue. The slices were attached to glutaraldehyde pre-treated glass slides and directly measured. For the rest of samples (n=5), frozen 50- $\mu$ m slices cut using a cryostat (HM 560 CryoStar, Thermo Fisher, Madrid, Spain), were placed on top a positively charged glass slides and stored at -20 °C.

Before measurements, slices with OCT were rinsed several times with PBS until OCT was completely removed. The perimeter of glass slides was outlined with a water repellent marker (Super PAP PEN, Invitrogen, Carlsbad, CA), keeping 1 ml of PBS pooled over the samples. Then, slides were placed on the sample holder of a custom-built atomic force microscopy (AFM) attached to an inverted optical microscope (TE 2000, Nikon, Tokyo, Japan), and Young's modulus (E) was measured as previously described [12]. For all samples, two slices were measured and in every slice, measurements were performed in two locations separated by ~500  $\mu$ m. At each of the two locations, 5 measurements were made separated by ~10  $\mu$ m following a linear pattern. Each measurement point was the average of five force curves, with a maximum indentation of 1  $\mu$ m.

### **Measurement of macromechanical properties (tensile test)**

For macromechanical measurements, the samples were placed at room temperature in Krebs-Henseleit solution (Sigma-Aldrich). A strip of ~8x1x1 mm was cut with a scalpel along the long-axis direction and its mass (M) was measured. The resting length ( $L_0$ ) of the strip was measured and its cross-sectional area (A) was computed as

$$A = \frac{M}{\rho \cdot L_0} \quad (1)$$

where  $\rho$  is tissue density (assumed to be 1 g/cm<sup>3</sup>). One end of the strip was glued with cyanoacrylate to a hook attached to the lever of a servocontrolled displacement actuator which permitted to stretch the strip and measure the stretched length (L) and the applied force (F) (300C-LR, Aurora Scientific, Ontario, Canada). The other end of the strip was glued to a fixed hook. Measurements were performed inside a bath with Krebs-Henseleit solution at 37 °C to maintain physiological conditions. The stress ( $\sigma$ ) applied to the strip was defined as,

$$\sigma = \frac{F}{A} \quad (2)$$

Tissue stretch ( $\lambda$ ) was defined as,

$$\lambda = \frac{L}{L_0} \quad (3)$$

strips were initially preconditioned by applying cyclical stretch at a frequency of 0.2 Hz and maximum stretch of 50% for 10 cycles.  $L_0$  was measured again and 10 more cycles were acquired. Tissue stiffness was characterized by the Young's modulus (E) defined as  $d\sigma/d\lambda$ . Stress-stretch ( $\sigma$ - $\lambda$ ) curves were analyzed with Fung's model which assumes that E increases linearly with stress as

$$E = \alpha \cdot \sigma + \beta \quad (4)$$

Then, the stress increases exponentially with stretch

$$\sigma = (\sigma_r + \beta)e^{\alpha(\lambda - \lambda_r)} - \beta \quad (5)$$

where  $\sigma_r$  and  $\lambda_r$  define an arbitrary point of the  $\sigma$ - $\lambda$  curve. The parameters of Eq. 5

were computed for each curve by non-linear least-squares fitting using custom built code (MATLAB, The MathWorks, Natick, MA). The Young's modulus was computed at 20% stretch ( $\lambda=1.2$ ).

### **Proteomic analysis**

Protein content from decellularized tissues were initially extracted and digested as detailed in the *Supplementary methods*. Peptides were analyzed in an Impact II Q-TOF mass spectrometer (Bruker, Billerica, MA) using the nano-LC dedicated CaptiveSpray source, coupled to a nanoRSLC ultimate 3000 system (Thermo Fisher). For peptide separation details, see *Supplementary methods*.

The mass spectrometer was operated in the Instant Expertise mode, consisting in a cycle of: (i) One MS spectrum in 250 msec, mass range 150-2200 Da; (ii) as many as possible MS/MS spectra in 1.75 sec, at 32-250 msec, depending on precursor intensity, mass range 150-2200 Da; and (iii) precursor exclusion after one selection. Searches against Swissprot (2015-08) library of mammal protein sequences were performed using the Mascot 2.5 search engine (MatrixScience, Boston, MA), with 7 ppm tolerance at MS level and 0.01 Da tolerance at MS/MS level, false discovery rate fixed to a maximum value of 1%, carbamidomethyl, Gln->pyro-Glu, acetyl, oxidation, and deamidation as variable modifications.

### **Animal experimental design**

All animal studies were approved by the local Animal Experimentation Unit Ethical Committee (Number: ES 100370001499) and complied with all the guidelines concerning the use of animals in research and teaching, as defined by the Guide for

the Care and Use of Laboratory Animals (NIH Publication No. 80–23, revised 1996).

Seventy-four crossbred Landrace × Large White pigs (30.6±5.5 kg) were subjected to MI and randomly distributed into 5 groups of study as follows:

1. Control MI (n=17), without any scaffold implantation;
2. Per-MI (n=17), human cell-free pericardial scaffold implantation;
3. Myo-MI (n=8), porcine cell-free myocardial scaffold implantation;
4. Per-ATMSCs (n=22), human ATMSC-enriched pericardial scaffold implantation;
5. Myo-ATMSCs (n=10), porcine ATMSC-enriched myocardial scaffold implantation;

After a left lateral thoracotomy, a MI was induced by double ligation of the first marginal branch of the circumflex artery, as previously described [14]. After 30 minutes, the scaffolds were attached over the infarcted area with 0.1–0.2 mL of surgical glue (Glubran®2, Cardiolinek, Barcelona, Spain). Finally, the animals were recovered and housed for forty days before sacrifice.

### **Cardiac Function Assessment**

Cardiac MRI was performed at 1.5 T (Intera, Philips, Amsterdam, the Netherlands) in all animals using a four-channel phased array surface coil (SENSE Body Coil, Philips). Breath-held, ECG-gated cine steady-state precession MRI was acquired (TR/TE 4.1/2.1 ms; flip angle 60°; field of view 320×320 mm; matrix 160×160 pixels, slice thickness 7 mm; bandwidth 1249.7 Hz/pixel). Delayed enhancement images were acquired after intravenous gadolinium (Gd-DTPA, 0.2 mL/kg) using a phase-sensitive inversion recovery sequence (TR/TE 4.9/1.6 ms; flip angle 15°; inversion time 157

ms; field of view  $330 \times 330$  mm; matrix  $224 \times 200$  pixels; slice thickness 10 mm, bandwidth 282.3 Hz/pixel). Left ventricular ejection fraction (LVEF), cardiac output (CO), stroke volume (SV), left ventricular end-systolic volume (LVESV), and left ventricular end-diastolic volume (LVEDV) were measured at baseline, 48 h after MI, and before sacrifice. Independent blinded investigators carried out MRI data acquisition and analysis.

### **Morphometric analysis**

Sacrifices were performed an average of  $39.3 \pm 7.5$  days after MI with an overdose of anesthesia. Following lateral thoracotomy, porcine hearts were excised. Left ventricular (LV) infarct area was measured in photographed heart sections obtained 1.5 cm distally to the artery ligation as previously described [14]. Quantification was double-blindly performed by two independent investigators using Image J software (version 1.48, National Institutes of Health, Bethesda, MD).

### **Histopathological and immunohistological analysis**

On 4- $\mu$ m paraffin slices, hematoxylin/eosin (H/E), Movat's pentachrome (pentachrome for simultaneous collagen and mucopolysaccharide acid staining [15]), and Gallego's modified trichrome staining were performed to analyze histological changes and scaffold recellularization, under a computer-associated Olympus CKX41 microscope (Olympus, Tokyo, Japan) with ProgRes® CF Cool camera (Jenoptik, Jena, Germany).

Frozen 10- $\mu$ m sections were immunostained with biotinylated *Griffonia simplicifolia* lectin I B4 (IsoB4; 1:25; Griffonia simplicifolia lectin I B4, Vector Labs, Burlingame, CA), phalloidin-Atto 565 (1:50; Sigma-Aldrich), smooth muscle actin (SMA; 1:50;

Sigma-Aldrich), type-I collagen (col-I) and type-III collagen (col-III) (1:100; Abcam, Cambridge, UK), cardiac troponin I (cTnI) (1:100; Abcam), cardiac troponin T (cTnT) (1:100; AbD Serotec), and elastin (1:100; Abcam) primary antibodies to characterize the scaffolds before and after their implantation. Secondary antibodies included Alexa Fluor 488-conjugated streptavidin (1:500; Molecular Probes, Eugene, OR), Cy2, Cy3, and Cy5 (1:500; Jackson ImmunoResearch Laboratories, West Grove, PA) secondary antibodies were also used. All sections were counterstained with 4',6-diamidino-2-phenylindole (DAPI) (1:10000; Sigma-Aldrich) and analyzed by confocal microscopy (Axio-Observer Z1, Zeiss, Oberkochen, Germany).

### **Scanning electron microscopy (SEM)**

Native tissues, decellularized and recellularized scaffolds were first washed with sterile distilled water and fixed in 10% formalin (Sigma-Aldrich) O/N at 4 °C. Then, samples were then washed with sterile distilled water, subsequently dehydrated in increasing concentrations of ethanol solutions and preserved in absolute ethanol at 4 °C, until transference to a CO<sub>2</sub> critical point dryer (EmiTech K850; Quorum Technologies, Lewes, UK). Finally, the scaffolds were sputter-coated with gold using an ion sputter (JFC 1100, JEOL, Tokyo, Japan) and examined with a JSM-6510 (JEOL) scanning electron microscope at 15 kV.

### **Pore size measurements**

The pore size of both decellularized myocardial and pericardial scaffolds (n=3 of each) was evaluated manually at 10 randomly selected SEM images with a magnification range from 500 to 1500, and at least 10 different pores from each image were randomly chosen and measured to generate an average value. For each pore, long and short axis

length was determined by using the ImageJ software, and pore sphericity was calculated as a ratio between short and long axis.

### **Statistical analysis**

Data are represented as the mean $\pm$ SEM. Statistical analyses were performed using paired Student *t* test, 1-way analysis of variance (ANOVA) with the Tukey's correction for multiple comparisons using the SPSS 21.0.0.0 (SPSS, Inc, Chicago, IL). Values of  $P<0.05$  were considered significant.

## **Results**

### **Structural and mechanical characterization**

Decellularized scaffolds maintained native matrix fibrils intrinsic organization and spatial three-dimensional distribution (**Figure 1A-B; 1G-H**). These data were confirmed through immunohistochemistry, where no nuclei or cellular proteins were identified after decellularization. Moreover, two major representative matrix proteins, type-I and type-III collagens, were also properly marked, thus indicating preservation of matrix protein components (**Figure 1D-E; J-K**). On the other hand, upon scaffold recellularization, presence of cells was detected using both SEM (**Figure 1C,I**) and immunohistochemistry (**Figure 1F,L**), confirming cell retention inside the scaffolds one week after repopulation. Two-hours post-recellularization, visual examination of scaffolds suggested a more regular retention of the cell-hydrogel mixture for the pericardial scaffold, with no liquid leakage observed (**Figure 2A-B**). However, cell quantification did not reveal significant differences between both scaffolds ( $361\pm 105$  arbitrary fluorescence units vs.  $647\pm 242$  arbitrary fluorescence units;  $P=0.340$ ) (**Figure 2C-E**). On another note, cell retention one week post-recellularization was



significantly higher on pericardial scaffolds ( $226.4 \pm 13.9$  cells/mm<sup>2</sup> vs.  $338.8 \pm 36.0$  cells/mm<sup>2</sup>;  $P=0.027$ ) (**Supplementary Figure 1**). Cell distribution, penetrance and retention through the scaffold thickness was different between myocardial and pericardial origin. A superficial cellular distribution, limited cell migration and concentration of few cell islets was observed in myocardial scaffolds; whereas a uniform distribution with complete migration of porcine ATMSCs throughout the scaffold thickness, from top to bottom, was present in pericardial scaffolds (**Figure 2F-M**), resulting in a higher cell retention at the bottom for pericardial decellularized scaffolds (Surface:  $112.9 \pm 21.0$  cells/mm<sup>2</sup> vs.  $52.3 \pm 15.8$  cells/mm<sup>2</sup>;  $P=0.082$ ; upper-middle:  $77.1 \pm 27.5$  cells/mm<sup>2</sup> vs.  $126.2 \pm 51.6$  cells/mm<sup>2</sup>;  $P=0.449$ ; inferior-middle:  $21.8 \pm 4.5$  cells/mm<sup>2</sup> vs.  $158.7 \pm 32.1$  cells/mm<sup>2</sup>;  $P=0.048$ ; bottom:  $28.0 \pm 9.6$  cells/mm<sup>2</sup> vs.  $133.9 \pm 36.2$  cells/mm<sup>2</sup>;  $P=0.047$ , for recellularized myocardial and pericardial scaffolds, respectively) (**Figure 2N**). Decellularized scaffolds pore size was significantly higher in pericardial scaffolds ( $10.2 \pm 0.5$   $\mu$ m vs.  $22.2 \pm 1.5$   $\mu$ m;  $P=0.002$ ; **Figure 3A**), although no differences in pore sphericity were observed between decellularized myocardial and pericardial scaffolds ( $0.53 \pm 0.01$  vs.  $0.55 \pm 0.03$ , respectively;  $P=0.469$ ; **Figure 3B**).

Regarding determination of cardiac tissue mechanical properties, these were evaluated at 2 different levels: macroscopically by tensile tests; and microscopically under AFM. For the myocardial tissue, tensile analysis did not reveal significant differences between native, decellularized or recellularized states ( $14.0 \pm 2.3$  kPa vs.  $18.7 \pm 5.4$  kPa vs.  $19.2 \pm 6.2$  kPa, respectively;  $P=0.614$ ; **Figure 3C**). Of interest, these stiffness values did not display any significant change when the acellular myocardial scaffold was submitted to lyophilization, sterilization, or RAD16-I hydrogel embedding ( $18.7 \pm 5.4$

kPa vs.  $22.1 \pm 10.1$  kPa vs.  $25.9 \pm 13.5$  kPa vs.  $15.7 \pm 1.6$  kPa, respectively;  $P=0.904$ ; **Supplementary Figure 2A**). Additionally, decellularized myocardial scaffolds after one freezing/thawing cycle showed the same macroscopical stiffness compared to the native or the decellularized tissues ( $14.4 \pm 2.1$  kPa vs.  $14.0 \pm 2.3$  kPa vs.  $14.0 \pm 2.5$  kPa vs. respectively;  $P=0.992$ ; **Supplementary Figure 2C**).

In terms of microscopical mechanical properties, significant differences were observed between native and decellularized myocardium compared to recellularized myocardium ( $13.4 \pm 0.9$  kPa vs.  $11.6 \pm 2.4$  kPa vs.  $22.0 \pm 2.2$  kPa, respectively;  $P=0.004$ ; **Figure 3D**). Similar to macroscopical examination, no variations were observed between decellularized, lyophilized, sterilized, or hydrogel-added samples ( $11.6 \pm 2.4$  kPa vs.  $8.5 \pm 2.4$  kPa vs.  $8.9 \pm 1.4$  kPa vs.  $9.4 \pm 1.8$  kPa, respectively;  $P=0.943$ ; **Supplementary Figure 2B**). Moreover, freezing/thawing cycle did not alter decellularized myocardium micromechanics ( $13.4 \pm 0.9$  kPa vs.  $15.2 \pm 0.6$  kPa vs.  $16.1 \pm 1.1$  kPa, for native, decellularized, and frozen/thawed myocardium, respectively;  $P=0.127$ ; **Supplementary Figure 2D**).

No differences between decellularized and recellularized pericardium were revealed following macroscopic ( $60.9 \pm 27.4$  kPa vs.  $82.9 \pm 22.4$  kPa, respectively;  $P=0.551$ ; **Figure 3C**), and microscopic ( $15.0 \pm 4.3$  kPa vs.  $24.1 \pm 4.6$  kPa, respectively;  $P=0.185$ ; **Figure 3D**) mechanic analysis; but recellularized pericardium micromechanical stiffness was significantly higher when compared with recellularized myocardium counterpart ( $P=0.044$ ) (**Figure 3D**). Interestingly, decellularized pericardium mechanical properties did not differ from that measured for decellularized myocardium, at both macro- and micromechanical levels ( $P=0.201$  and  $P=0.508$ ,

respectively; **Figure 3C-D**). Also, macro and micro-mechanical similarities were reported among decellularized, lyophilized, sterilized, and hydrogel-added pericardial scaffolds ( $60.9\pm 27.4$  kPa vs.  $78.2\pm 29.4$  kPa vs.  $51.3\pm 32.1$  kPa vs.  $53.6\pm 12$  kPa;  $P=0.485$ ; and  $15.0\pm 4.3$  kPa vs.  $16.3\pm 7.3$  kPa vs.  $20.4\pm 6.7$  kPa vs.  $19.7\pm 3.4$  kPa;  $P=0.885$ ; for macro and micromechanical characterization, respectively; **Supplementary Figure 2A-B**)

### **Proteomic characterization**

The decellularization of both cardiac tissues supposed an enrichment in matrisome/ECM-related proteins, starting from the 7.7% and 9.8% in native myocardium and pericardium, respectively, to the final 25.2% and 41.1% for the decellularized myocardial and pericardial scaffolds, respectively (**Figure 4A-D**). Of these decellularized myocardium detected matrisome proteins, 24 out of 40 protein components were common with the native tissue, and 16 new proteins were detected exclusively within the decellularized myocardium. Regarding pericardium, the matrisome enrichment was more pronounced: only 3 proteins were common between both decellularized and native pericardium; while 48 proteins were detected for the first time in decellularized pericardium, and just one differentially identified in the native pericardium (**Figure 4E-F**).

Comparative analysis of both generated acellular cardiac tissues revealed a 40% of common matrisome proteins between them. Among them, the most remarkable proteins were the different collagen subtypes, responsible for maintaining ECM framework and modulating cell differentiation; the laminin family and heparan sulfate; mainly involved in cell adhesion; and fibronectin, involved in different cellular

processes such as adhesion, survival and differentiation. Besides, the number of unique proteins identified was notably higher for the pericardium, with up to 25 matrix proteins non-detected for the myocardial tissue, and with just 14 unique myocardium proteins (**Figure 5A and Tables 1-3**). Finally, the subdivision of ECM-proteins showed a major number of proteins within each ECM protein subtype for the decellularized pericardium, with the only exception of collagen subclass (**Figure 5B**).

### **Animal Experimentation**

Four animals died during MI induction due to ventricular fibrillation and 4 were excluded from the study after post-operative infections. Finally, 66 animals were included in the experimental protocol in the Per-MI (n=15), Myo-MI (n=7), Per-ATMSCs (n=20), Myo-ATMSCs (n=7), and Control-MI (n=17) groups.

### **Cardiac Function Assessment**

Differentials between final and baseline between Per-MI (n=15), Myo-MI (n=7), Per-ATMSCs (n=19), Myo-ATMSCs (n=7), and Control-MI (n=7) groups showed significant differences in LVEF ( $5.8 \pm 1.7\%$  vs.  $-8.0 \pm 4.3\%$  vs.  $9.1 \pm 2.2\%$  vs.  $3.3 \pm 2.9\%$  vs.  $-4.8 \pm 2.71$ , respectively;  $P < 0.001$ ), and a tendency in LVESV ( $0.39 \pm 1.36$  mL vs.  $8.89 \pm 4.95$  mL vs.  $1.14 \pm 1.89$  mL vs.  $1.02 \pm 2.08$  mL vs.  $7.79 \pm 2.76$  mL, respectively;  $P = 0.063$ ) (**Figure 6A**). Differentials between final and post-MI were also significant in terms of LVEF ( $8.2 \pm 1.7\%$  vs.  $4.5 \pm 4.0\%$  vs.  $8.5 \pm 1.8\%$  vs.  $10.5 \pm 1.7\%$  vs.  $-4.2 \pm 3.1\%$ , respectively;  $P = 0.004$ ), and LVESV ( $-1.49 \pm 1.39$  mL vs.  $-1.04 \pm 3.46$  mL vs.  $-0.38 \pm 1.78$  mL vs.  $-8.05 \pm 1.36$  mL vs.  $4.58 \pm 2.61$  mL, respectively;  $P = 0.031$ ) (**Figure 6B**). At 40 days, ANOVA test also displayed significant differences between above-mentioned groups in LVEF ( $60.7 \pm 1.5\%$  vs.  $52.9 \pm 2.2\%$  vs.  $60.5 \pm 2.4\%$  vs.  $61.3 \pm 3.0\%$  vs.

50.6±2.3%, respectively;  $P=0.017$ ), and LVESV (21.59±1.21 mL vs. 32.25±3.59 mL vs. 24.63±2.56 mL vs. 24.73±2.82 mL vs. 32.26±1.18 mL, respectively;  $P=0.020$ ).

### **Infarct size**

After digital morphometric analysis, LV infarct size was statistically different between Per-MI (n=15), Myo-MI (n=7), Per-ATMSCs (n=18), Myo-ATMSCs (n=7), and Control-MI (n=10) animals (5.9±0.9 vs. 7.6±2.3 vs. 4.8±0.6% vs. 2.5±0.6% vs. 7.7±1.2%, respectively;  $P=0.021$ ) (**Figure 6C-D**).

### **Immunohistological analysis**

Correct adhesion of the implanted graft with subjacent myocardium was observed in all animals after sacrifice. Moreover, scaffolds of all experimental groups showed the existence of functional blood vessels connected to the host vascularization confirmed by the presence of erythrocytes in the lumen (**Figure 7A-B**) after H/E and Movat's pentachrome stainings. Furthermore, there were also new-formed nerves within the scaffolds (**Figure 7A**). After simultaneous collagen and mucopolysaccharide acid staining, decellularized pericardium of Per-MI animals showed high levels of mucopolysaccharides (purple), despite collagen (red) presence was similar in all scaffolds (**Figure 7A**). In addition, lymphocytes and plasma cells were also present in ATMSCs treated animals confirmed by modified Movat's pentachrome staining (green) and modified Gallego's staining confirmed the presence of collagen in all scaffolds (green) and the existence of elastic fibers (fuchsin red) in the vessels of the scaffolds (**Figure 7A**).

After immunohistochemical analysis, upon sacrifice, scaffolds from all animals showed neovessel incorporation, some of which showed vascular media layer presence

positive for SMA (**Figure 7C**).

## **Discussion**

Cardiac tissue engineering is mainly based on the combination of a biomimetic scaffold with a cell lineage of interest. Specifically for the scaffold design when using an acellular framework, it is primordial to maintain intact the ECM inherent properties, such as structure, mechanics, and protein composition, avoiding matrix disruption due to decellularization agents to recreate the native physiological milieu. For instance, structure preservation has been related to cell differentiation, migration, and alignment processes [7,8]; while mechanical stiffness is involved in cell adhesion, differentiation, proliferation, and migration [4,6,18], as well as contractility [19], which, in our hands, were well-maintained following decellularization process for both cardiac scaffolds. To note, matrix pore size was significantly larger in pericardial scaffolds, and is well-correlated with cardiomyocyte transversal section reported in previous studies [20]; and the addition of ATMSCs only significantly increased myocardial micromechanical parameters. Nevertheless, the resulting stiffness for both recellularized myocardial and pericardial scaffolds was included within the optimal stiffness range (10-20 kPa) to drive cardiomyocyte maturation and contraction, and cardiodifferentiation [21,22]. Therefore, presence of seeded ATMSCs on top of the decellularized myocardium does not have a critical impact over the matrix micromechanics, resulting in an overall preservation of scaffold structure and mechanics following recellularization process.

Regarding protein content, a clear native matrix protein preservation was achieved in both cardiac tissues upon decellularization completion, similarly to prior reported

studies [16], with the identification of some of the main cardiac ECM components: type-I, -III, -IV, -V, -VI collagens, laminin, Emilin-1, fibronectin, lumican, heparan sulfate proteoglycan, nidogen, or periostin. These key proteins act as mediators or effectors of many cellular processes, thus resulting in favored ATMSCs adhesion and survival. Indeed, laminins, fibronectin, and type-I and IV collagens have been described to enhance cellular survival [23,24]; whereas fibronectin [25], lumican [26], or type-IV and -VI collagens [27,28] are associated with cell attachment through specific interaction with integrin cell receptors. In this regard, galectin-1, vitronectin, decorin, and tenascin-X, reported to be involved in cell adhesion [25,29,30] and identified in our pericardial scaffolds; along with the optimal pore diameter suitable for cell infiltration, similar to previous studies [20,31], may explain the increased cell retention observed in these particular acellular scaffolds. Also, the cell penetrance within the scaffold was by far greater in the recellularized pericardial scaffolds, with cell migration throughout the scaffold thickness, confirming the previously described chemoattractant potential of decellularized pericardium [32]. Based on our proteomic analysis, the exclusive identification in pericardial scaffolds of proteins involved in cell migration and cytoskeletal changes, i.e. biglycan, decorin, vitronectin [33,34], may provide migratory cues that drive ATMSC migration across the pericardial scaffold.

According to the principles of the 3Rs (Replacement, Reduction and Refinement), in the present work we have included previous animal experimentation models [12,13,35] performed by the same surgical team under identical conditions in order to compare them. Thus, we demonstrated that the implantation of the obtained engineered cardiac grafts led to an improvement in LVEF and/or LVESV, limiting infarct size

expansion, and coupling with the underlying myocardium, as indicated by the vascularization and innervation of the grafts. The benefits exhibited here by both recellularized scaffolds have been greater than those reported for direct intracoronary or intramyocardial injection of ATMSCs [36], or administration of either an acellular myocardial [37] or pericardial scaffold [38]. The combination of the cardiac scaffold with ATMSCs showed higher improvements compared to non-recellularized scaffolds, indicating a synergistic effect, as reported previously [39]. On the one hand, the role of scaffolds has been reported to be beneficial for triggering MI salvage, providing a favorable microenvironment for the seeded ATMSCs, and recruiting endogenous stem cells towards the infarct bed [40], boosting both the vascularization and cardiomyogenesis processes. On the other hand, the contribution of ATMSCs to MI recovery has also been previously described. Latest evidences point out that the more probable mechanism of action of these cells is through a paracrine signaling, rather than ATMSC direct effects [41]. Paracrine action would be in consonance with a low number of retained or seeded cells, as it happens in our study, being able of promoting these effects even at low cell concentrations [42], inducing vessel formation, protecting the resident cardiomyocytes from apoptosis, and mobilizing resident stem cells to potentiate vascularization and cardiomyogenesis [43]. Remarkably, in the present work, both cell-free and ATMSC recellularized cardiac scaffolds, regardless of their origin, were successfully well integrated, being neovascularized and neoinnervated by host cells as previously reported [10]. However, further studies are required to discern which are the mechanisms responsible for these processes, studying ECM signaling and/or host cell recruitment pathways.



## **Conclusions**

Two engineered cardiac grafts were successfully generated by combining ATMSCs with either myocardial or pericardial acellular scaffolds, which preserved structural and mechanical intrinsic properties, and displayed major cardiac ECM proteins. *In vitro*, the recellularized pericardial scaffold showed higher cell retention and penetrance. In the context of a preclinical MI model, the engineered grafts integrated with the underlying myocardium, with signs of neoinnervation and neovascularization, irrespective of scaffold origin or presence of cells; and improved cardiac function post-MI. Collectively, these data indicate the suitability and effectiveness of ATMSC-recellularized pericardial scaffold after MI, ready for the clinical translation.

## **Acknowledgements**

The authors thank I. Díaz-Güemes for technical assistance in the animal surgeries, and J. Maestre and V. Crisóstomo for MRI execution and analysis. We also thank the IGTP Proteomic Core Facility staff J.M. Hernández, L. Fluvià, and E. Aragall for their support in proteomic analysis.

## **Funding**

This work was supported by grants from the Spanish Ministry of Economy and Competitiveness-MINECO (SAF2014-59892), Instituto de Salud Carlos III (FISPI14/01682), Red de Terapia Celular - TerCel (RD16/0011/0006), the CIBER Cardiovascular - (CB16/11/00403) projects, as part of the Plan Nacional de I+D+I, and it was cofunded by ISCIII-Sudirección General de Evaluación y el Fondo Europeo de Desarrollo Regional (FEDER). This work was also funded by the Fundació La MARATÓ de TV3 (201516-10, 201502-20), Generalitat de Catalunya-AGAUR

(2014-SGR-699), CERCA Programme/Generalitat de Catalunya and by “la Caixa” Banking Foundation. This work has been developed in the context of AdvanceCat with the support of ACCIÓ (Catalonia Trade & Investment; Generalitat de Catalunya) under the Catalonian ERDF operational program (European Regional Development Fund) 2014-2020.

## References

- [1] M.W. Curtis, B. Russell, Cardiac tissue engineering, *J. Cardiovasc. Nurs.* 24 (2009) 87-92.
- [2] D. Hou, E.A. Youssef, T.J. Brinton, P. Zhang, P. Rogers, E.T. Price, *et al.*, Radiolabeled cell distribution after intramyocardial, intracoronary, and interstitial retrograde coronary venous delivery: implications for current clinical trials, *Circulation.* 112 (2005) I150-I156.
- [3] C.J. Teng, J. Luo, R.C. Chiu, D. Shum-Tim, Massive mechanical loss of microspheres with direct intramyocardial injection in the beating heart: implications for cellular cardiomyoplasty, *J. Thorac. Cardiovasc. Surg.* 132 (2007) 628-632.
- [4] A.J. Engler, S. Sen, H.L. Sweeney, D.E. Discher, Matrix elasticity directs stem cell lineage specification, *Cell.* 126 (2006) 677-689.
- [5] T. Yeung, P.C. Georges, L.A. Flanagan, B. Marg, M. Ortiz, M. Funaki, *et al.*, Effects of substrate stiffness on cell morphology, cytoskeletal structure, and adhesion, *Cell Motil. Cytoskeleton.* 60 (2005) 24-34.
- [6] M. Murrell, R. Kamm, P. Matsudaira, Substrate viscosity enhances correlation in epithelial sheet movement, *Biophys. J.* 101 (2011) 297-306.
- [7] F. Guilak, D.M. Cohen, B.T. Estes, J.M. Gimble, W. Liedtke, C.S. Chen, Control

of stem cell fate by physical interactions with the extracellular matrix, *Cell Stem Cell*. 5 (2009) 17-26.

[8] B. Brown, K. Lindberg, J. Reing, D.B. Stolz, S.F. Badylak, The basement membrane component of biologic scaffolds derived from extracellular matrix, *Tissue Eng.* 12 (2006) 519-526.

[9] H.C. Ott, T.S. Matthiesen, S.K. Goh, L.D. Black, S.M. Kren, T.I. Netoff, *et al.*, Perfusion-decellularized matrix: using nature's platform to engineer a bioartificial heart, *Nat. Med.* 14 (2008) 213-221.

[10] C. Gálvez-Montón, M.T. Fernandez-Figueras, M. Martí, C. Soler-Botija, S. Roura, I. Perea-Gil, *et al.*, Neoinnervation and neovascularization of acellular pericardial-derived scaffolds in myocardial infarcts, *Stem Cell Res. Ther.* 6 (2015) 208.

[11] S.B. Seif-Naraghi, J.M. Singelyn, M.A. Salvatore, K.G. Osborn, J.J. Wang, U. Sampat, *et al.*, Safety and efficacy of an injectable extracellular matrix hydrogel for treating myocardial infarction, *Sci. Transl. Med.* 5 (2013) 173ra25.

[12] I. Perea-Gil, J.J. Uriarte, C. Prat-Vidal, C. Gálvez-Montón, S. Roura, A. Llucià-Valldeperas, *et al.*, In vitro comparative study of two decellularization protocols in search of an optimal myocardial scaffold for recellularization, *Am. J. Transl. Res.* 7 (2015) 558-573.

[13] C. Prat-Vidal, C. Gálvez-Montón, V. Puig-Sanvicens, B. Sanchez, I. Díaz-Güemes, P. Bogónez-Franco, *et al.*, Online monitoring of myocardial bioprosthesis for cardiac repair. *Int. J. Cardiol.* 174 (2014) 654-661.

[14] C. Gálvez-Montón, C. Prat-Vidal, S. Roura, J. Farré, C. Soler-Botija, A. Llucià-

Valdeperas, *et al.*, Transposition of a pericardial-derived vascular adipose flap for myocardial salvage after infarct, *Cardiovasc. Res.* 91 (2011) 659-667.

[15] K. Doello, A new pentachrome method for the simultaneous staining of collagen and sulphated mucopolysaccharides, *Yale J. Biol. Med.* 87 (2014) 341-347.

[16] J.P. Guyette, J.M. Charest, R.W. Mills, B.J. Jank, P.T. Moser, S.E. Gilpin, *et al.*, Bioengineering human myocardium on native extracellular matrix, *Circ. Res.* 118 (2016) 56-72.

[17] L.G. Griffiths, L. Choe, K.H. Lee, K.F. Reardon, E.C. Orton, Protein extraction and 2-DE of water- and lipid-soluble proteins in bovine pericardium, a low-cellularity tissue, *Electrophoresis.* 29 (2008) 4508-4515.

[18] M. Levy-Mishali, J. Zoldan, S. Levenberg. Effect of scaffold stiffness on myoblast differentiation, *Tissue Eng. Part A.* 15 (2009) 935-944.

[19] A. Marsano, R. Maidhof, L.Q. Wan, Y. Wang, J. Gao, N. Tandon, *et al.*, Scaffold stiffness affects the contractile function of three-dimensional engineered cardiac constructs, *Biotechnol. Prog.* 26 (2010) 1382-1390.

[20] B. Wang, A. Borazjani, M. Tahai, A.L. Curry, D.T. Simionescu, J. Guan, *et al.*, Fabrication of cardiac patch with decellularized porcine myocardial scaffold and bone marrow mononuclear cells, *J. Biomed. Mater. Res. A.* 94 (2010) 1100-1110.

[21] A.J. Engler, C. Carag-Krieger, C.P. Johnson, M. Raab, H.Y. Tang, D.W. Speicher, *et al.*, Embryonic cardiomyocytes beat best on a matrix with heart-like elasticity: scar-like rigidity inhibits beating, *J. Cell. Sci.* 121 (2008) 3794-3802.

[22] J.G. Jacot, A.D. McCulloch, J.H. Omens, Substrate stiffness affects the functional maturation of neonatal rat ventricular myocytes, *Biophys. J.* 95 (2008) 3479-3487.

- [23] E. Vecino, J.P. Heller, P. Veiga-Crespo, K.R. Martin, J.W. Fawcett, Influence of extracellular matrix components on the expression of integrins and regeneration of adult retinal ganglion cells, *PLoS One*. 10 (2015) e0125250.
- [24] J. Daoud, M. Petropavlovskaja, L. Rosenberg, M. Tabrizian, The effect of extracellular matrix components on the preservation of human islet function in vitro, *Biomaterials*. 31 (2010) 1676-1682.
- [25] H. Wang, X. Luo, J. Leighton, Extracellular matrix and integrins in embryonic stem cell differentiation, *Biochem. Insights*. 8 (2015) 15-21.
- [26] D. Nikitovic, P. Katonis, A. Tsatsakis, N.K. Karamanos, G.N. Tzanakakis, Lumican, a small leucine-rich proteoglycan, *IUBMB Life*. 60 (2008) 818-823.
- [27] T. Kaido, M. Yebra, V. Cirulli, A.M. Montgomery, Regulation of human beta-cell adhesion, motility, and insulin secretion by collagen IV and its receptor alpha1beta1, *J. Biol. Chem*. 279 (2004) 53762-53769.
- [28] M. Cescon, F. Gattazzo, P. Chen, P. Bonaldo, Collagen VI at a glance, *J. Cell. Sci*. 128 (2015) 3525-3531.
- [29] I. Camby, M. Le Mercier, F. Lefranc, R. Kiss, Galectin-1: a small protein with major functions, *Glycobiology*. 16 (2006) 137R-157R.
- [30] M. Rienks, A.P. Papageorgiou, N.G. Frangogiannis, S. Heymans, Myocardial extracellular matrix, *Circ. Res*. 114 (2014) 872-888.
- [31] J.M. Singelyn, J.A. DeQuach, S.B. Seif-Naraghi, R.B. Littlefield, P.J. Schup-Magoffin, K.L. Christman, Naturally derived myocardial matrix as an injectable scaffold for cardiac tissue engineering, *Biomaterials*. 30 (2009) 5409-5416.
- [32] S.B. Seif-Naraghi, M.A. Salvatore, P.J. Schup-Magoffin, D.P. Hu, K.L.

Christman, Design and characterization of an injectable pericardial matrix gel: a potentially autologous scaffold for cardiac tissue engineering, *Tissue Eng. Part A*. 16 (2010) 2017-2027.

[33] E. Tufvesson, G. Westergren-Thorsson, Biglycan and decorin induce morphological and cytoskeletal changes involving signalling by the small GTPases RhoA and Rac1 resulting in lung fibroblast migration, *J. Cell Sci.* 116 (2003) 4857-4864.

[34] Y. Fukushima, M. Tamura, H. Nakagawa, K. Itoh, Induction of glioma cell migration by vitronectin in human serum and cerebrospinal fluid, *J. Neurosurg.* 107 (2007) 578-585.

[35] C. Gálvez-Montón, R. Bragós, C. Soler-Botija, I. Díaz-Güemes, C. Prat-Vidal, V. Crisóstomo, *et al.* Noninvasive assessment of an engineered bioactive graft in myocardial infarction: impact on cardiac function and scar healing, *Stem Cells Transl. Med.* 6 (2017) 647-655.

[36] J. Bobi, N. Solanes, R. Fernández-Jiménez, C. Galán-Arriola, A.P. Dantas, L. Fernández-Friera, *et al.*, Intracoronary administration of allogeneic adipose tissue-derived mesenchymal stem cells improves myocardial perfusion but not left ventricle function, in a translational model of acute myocardial infarction, *J. Am. Heart. Assoc.* 6 (2017). doi: 10.1161/JAHA.117.005771.

[37] J.M. Singelyn, P. Sundaramurthy, T.D. Johnson, P.J. Schup-Magoffin, D.P. Hu, D.M. Faulk, *et al.*, Catheter-deliverable hydrogel derived from decellularized ventricular extracellular matrix increases endogenous cardiomyocytes and preserves cardiac function post-myocardial infarction, *J. Am. Coll. Cardiol.* 59 (2012) 751-763.

[38] S.B. Sonnenberg, A.A. Rane, C.J. Liu, N. Rao, G. Agmon, S. Suarez, *et al.*,

Delivery of an engineered HGF fragment in an extracellular matrix-derived hydrogel prevents negative LV remodeling post-myocardial infarction, *Biomaterials*. 45 (2015) 56-63.

[39] M. Araña, J.J. Gavira, E. Peña, A. González, G. Abizanda, M. Cilla, *et al.*, Epicardial delivery of collagen patches with adipose-derived stem cells in rat and minipig models of chronic myocardial infarction, *Biomaterials*. 35 (2014) 143-151.

[40] J.W. Wassenaar, R. Gaetani, J.J. Garcia, R.L. Braden, C.G. Luo, D. Huang, *et al.*, Evidence for mechanisms underlying the functional benefits of a myocardial matrix hydrogel for post-MI treatment, *J. Am. Coll. Cardiol.* 67 (2016) 1074-1086.

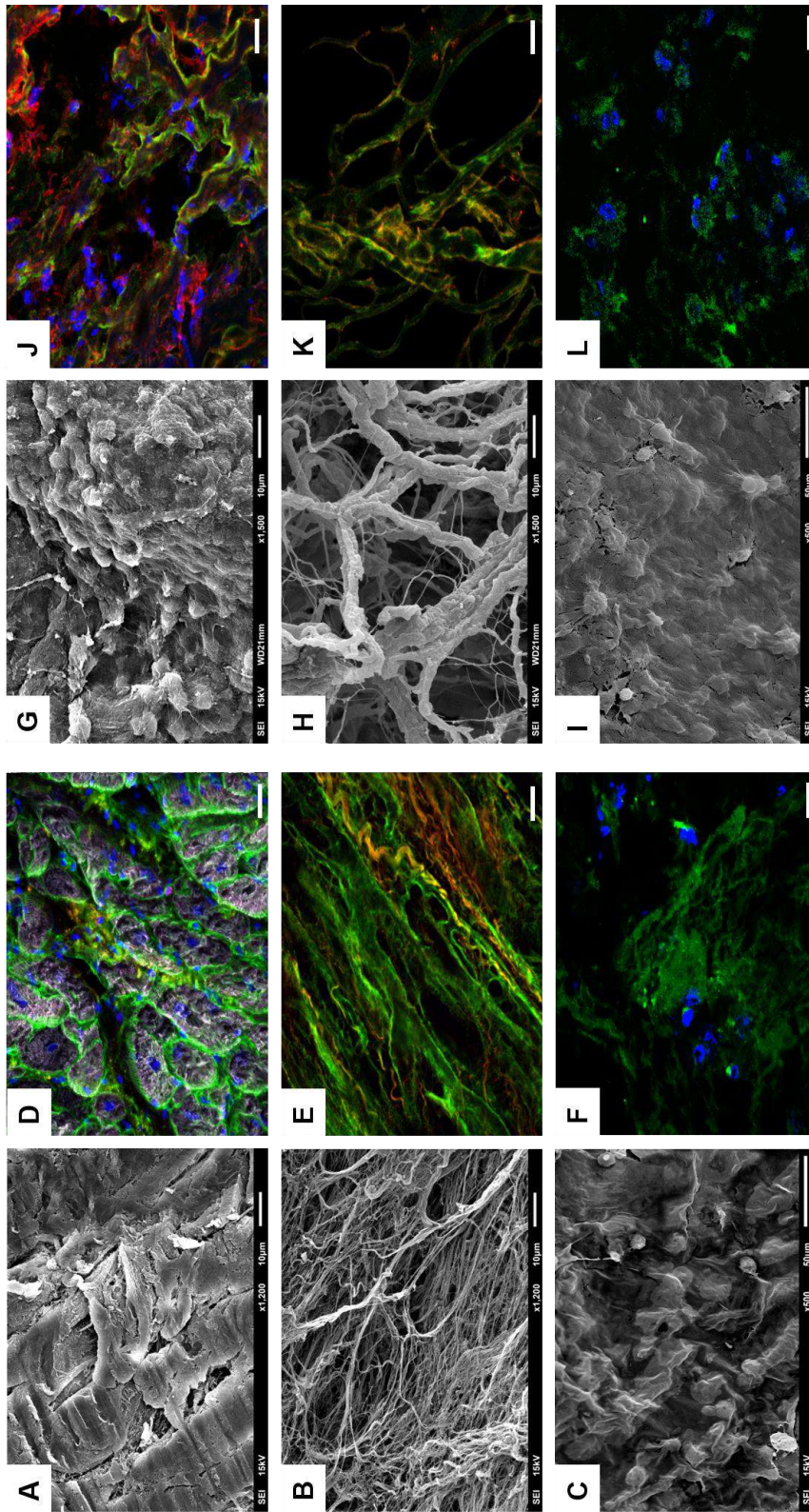
[41] M. Mazo, J.J. Gavira, B. Pelacho, F. Prosper, Adipose-derived stem cells for myocardial infarction, *J. Cardiovasc. Transl. Res.* 4 (2011) 145-153.

[42] L.H. Yu, M.H. Kim, T.H. Park, K.S. Cha, Y.D. Kim, M.L. Quan, *et al.*, Improvement of cardiac function and remodeling by transplanting adipose tissue-derived stromal cells into a mouse model of acute myocardial infarction, *Int. J. Cardiol.* 139 (2010) 166-172.

[43] N.N. Hoke, F.N. Salloum, K.E. Loesser-Casey, R.C. Kukreja, Cardiac regenerative potential of adipose tissue-derived stem cells, *Acta Physiol. Hung.* 96 (2009) 251-265.

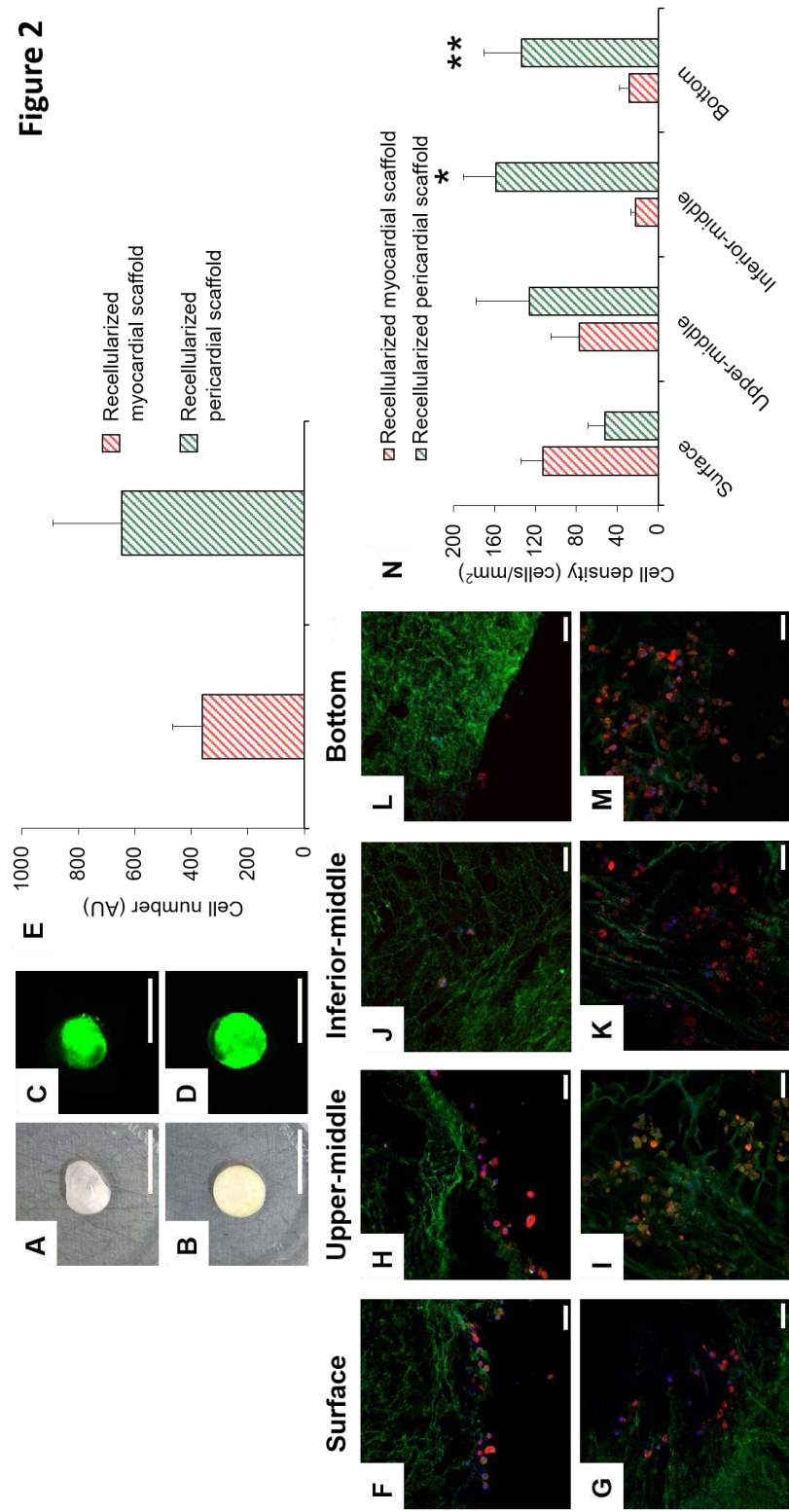
# Figures

Figure 1





**Figure 2**



**Figure 3**

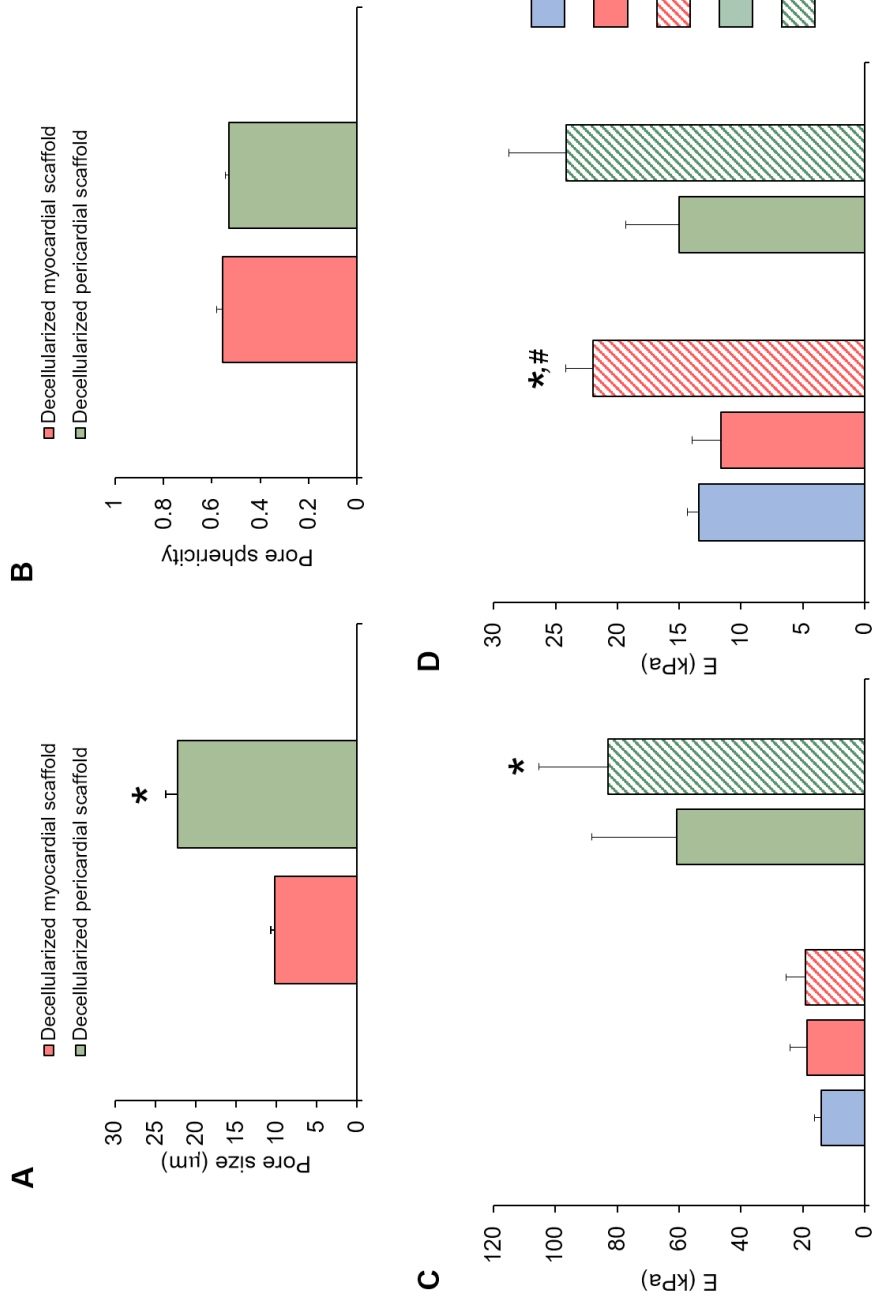


**Figure 4**

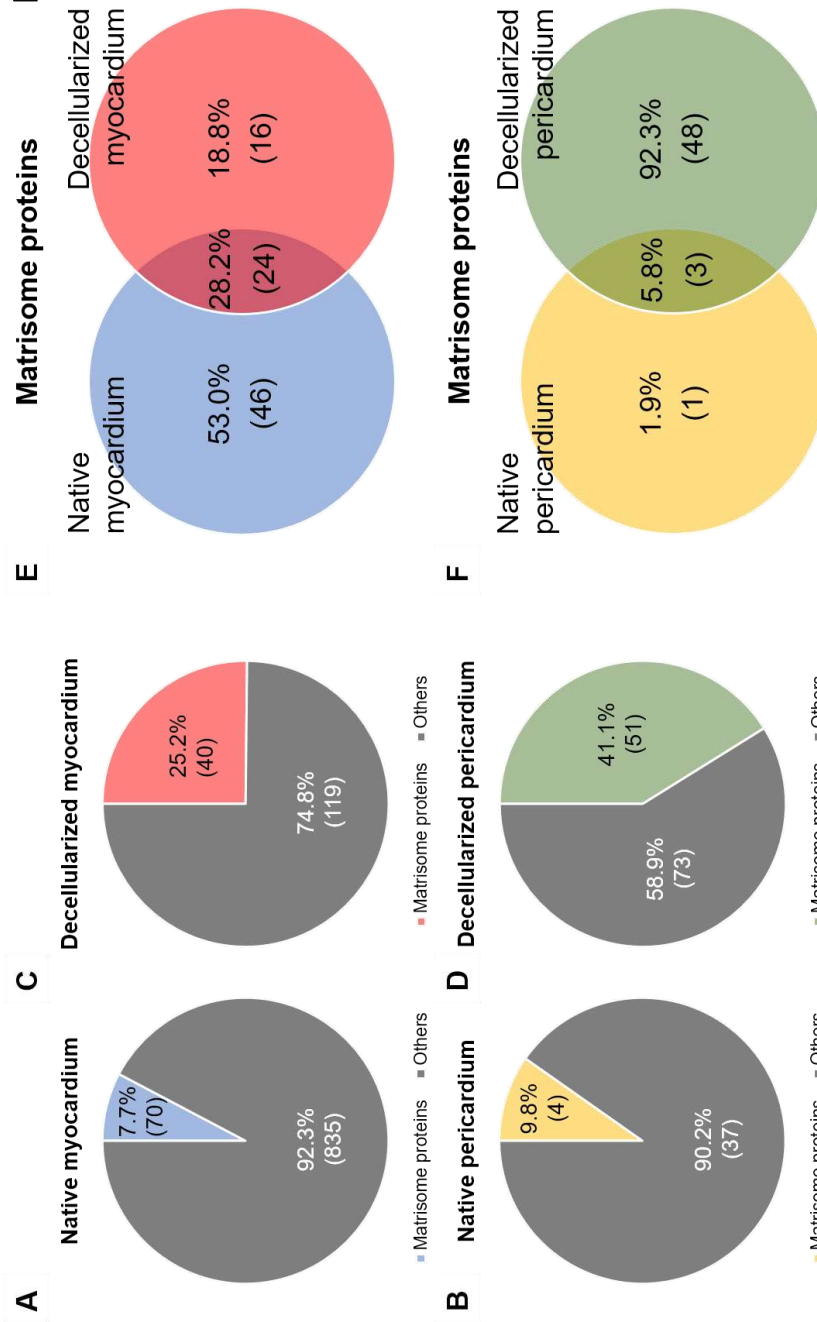


**Figure 5**

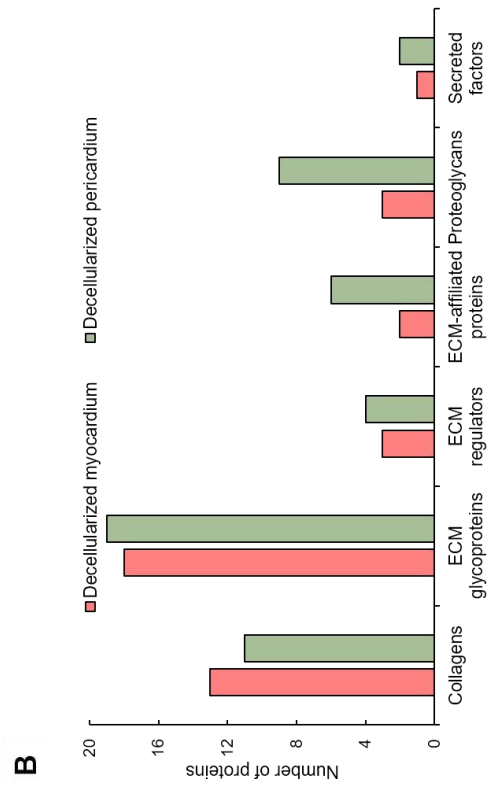
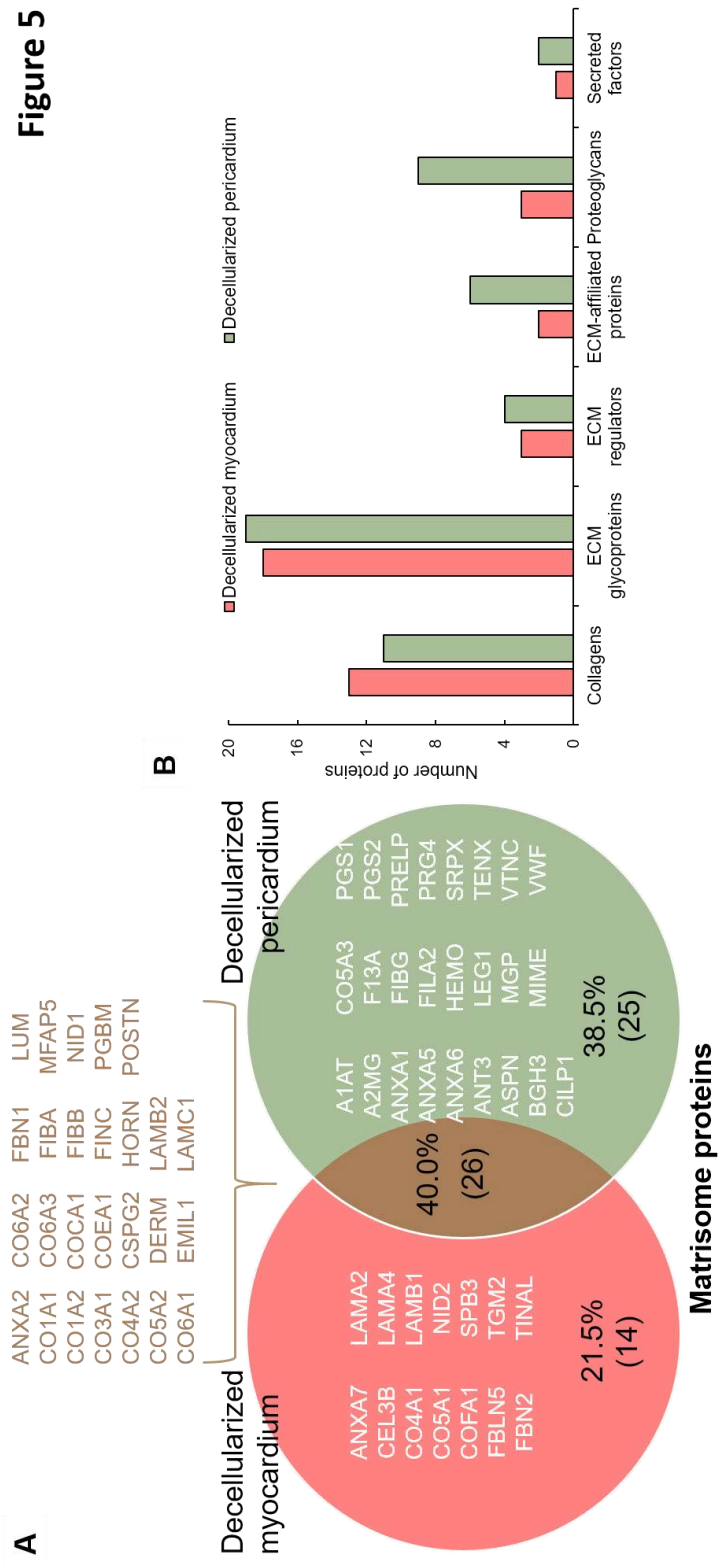


**Figure 6**

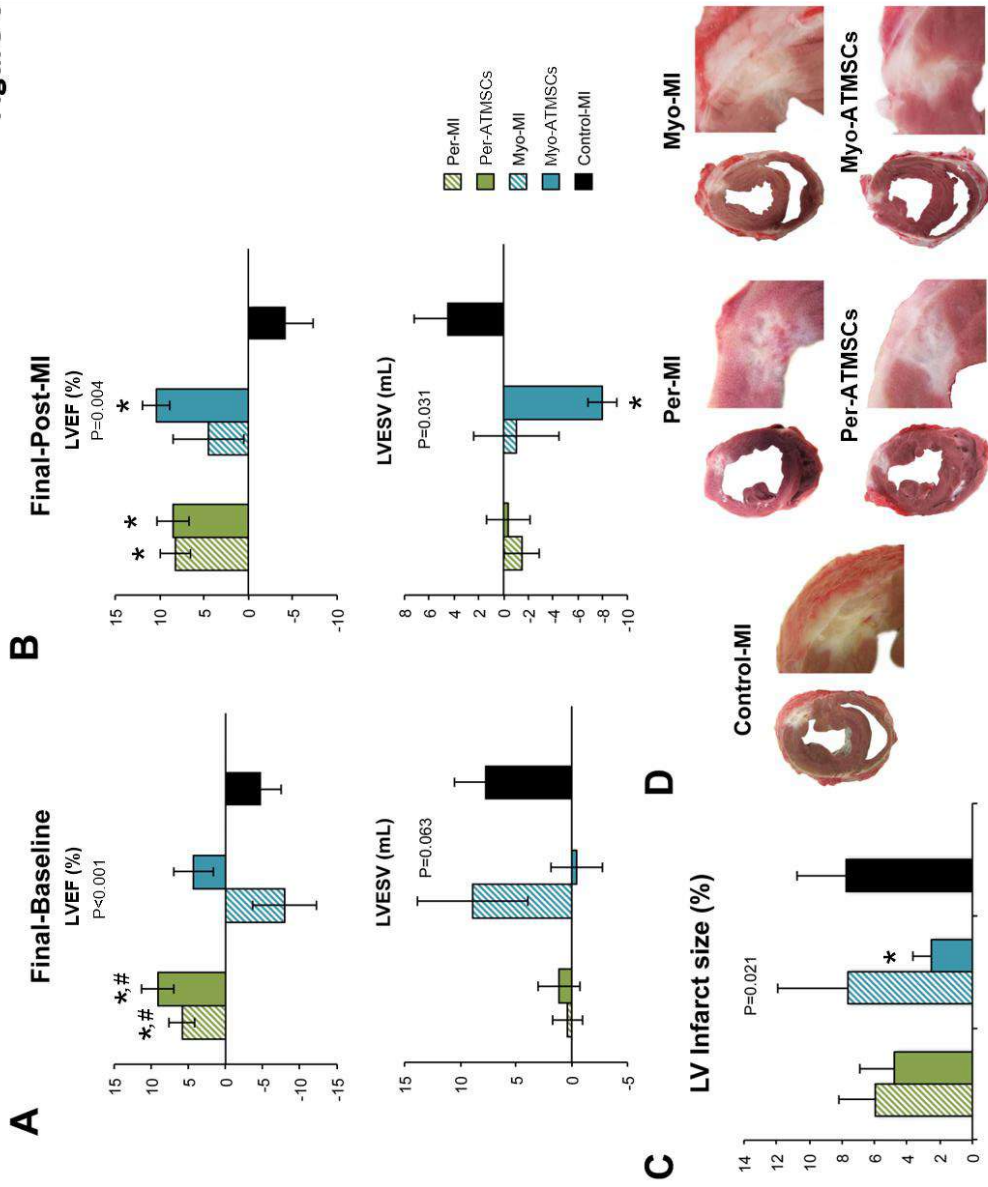
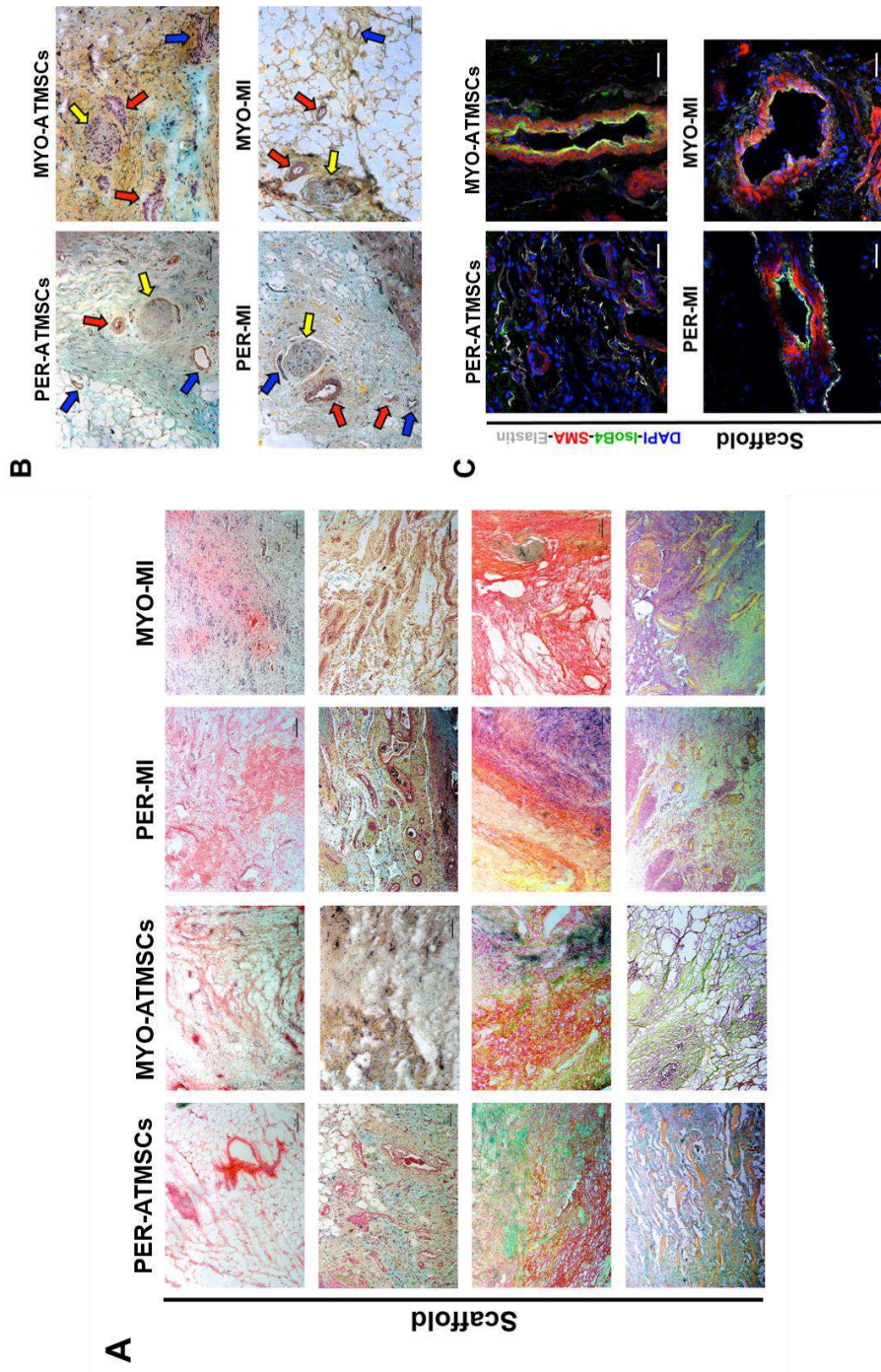


Figure 7



**Table 1**

<b>Accession</b>	<b>Protein</b>	<b>Score</b>	<b>Category</b>
ANXA2	Annexin A2	59	ECM-affiliated Proteins
CO1A1	Collagen alpha-1(I) chain	89.6	Collagens
CO1A2	Collagen alpha-2(I) chain	46.6	Collagens
CO3A1	Collagen alpha-1(III) chain	89.3	Collagens
CO4A2	Collagen alpha-2(IV) chain	74.8	Collagens
CO5A2	Collagen alpha-2(V) chain	49.7	Collagens
CO6A1	Collagen alpha-1(VI) chain	471	Collagens
CO6A2	Collagen alpha-2(VI) chain	401.7	Collagens
CO6A3	Collagen alpha-3(VI) chain	765.2	Collagens
COCA1	Collagen alpha-1(XII) chain	41.6	Collagens
COEA1	Collagen alpha-1(XIV) chain	149.1	Collagens
CSPG2	Versican core protein	62.5	Proteoglycans
DERM	Dermatopontin	72.5	ECM Glycoproteins
EMIL1	EMILIN-1	159.7	ECM Glycoproteins
FBN1	Fibrillin-1	1734	ECM Glycoproteins
FIBA	Fibrinogen alpha chain	42.1	ECM Glycoproteins
FIBB	Fibrinogen beta chain	75.1	ECM Glycoproteins
FINC	Fibronectin	485.2	ECM Glycoproteins
HORN	Hornerin	58.4	Secreted Factors
LAMB2	Laminin subunit beta-2	307.8	ECM Glycoproteins
LAMC1	Laminin subunit gamma-1	674.8	ECM Glycoproteins
LUM	Lumican	146.2	Proteoglycans
MFAP5	Microfibrillar-associated protein 5	69.2	ECM Glycoproteins
NID1	Nidogen-1	107.4	ECM Glycoproteins
PGBM	Basement membrane-specific heparan sulfate proteoglycan core protein	696.8	Proteoglycans
POSTN	Periostin	68.5	ECM Glycoproteins

**Table 2**

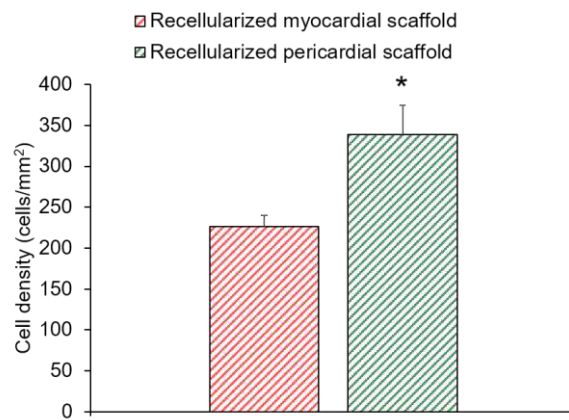
<i>Accession</i>	<i>Protein</i>	<i>Score</i>	<i>Category</i>
ANXA7	Annexin A7	68.7	ECM-affiliated Proteins
CEL3B	Chymotrypsin-like elastase family member 3B	51.7	ECM Regulators
CO4A1	Collagen alpha-1(IV) chain	60.9	Collagens
CO5A1	Collagen alpha-1(V) chain	46.4	Collagens
COFA1	Collagen alpha-1(XV) chain	98.6	Collagens
FBLN5	Fibulin-5	58.1	ECM Glycoproteins
FBN2	Fibrillin-2	170.7	ECM Glycoproteins
LAMA2	Laminin subunit alpha-2	145.3	ECM Glycoproteins
LAMA4	Laminin subunit alpha-4	186	ECM Glycoproteins
LAMB1	Laminin subunit beta-1	86.8	ECM Glycoproteins
NID2	Nidogen-2	98.6	ECM Glycoproteins
SPB3	Serpin B3	40	ECM Regulators
TGM2	Protein-glutamine gamma-glutamyltransferase 2	173.2	ECM Regulators
TINAL	Tubulointerstitial nephritis antigen-like	131.1	ECM Glycoproteins



**Table 3**

<i>Accession</i>	<i>Protein</i>	<i>Score</i>	<i>Category</i>
A1AT	Alpha-1-antitrypsin	64.3	ECM Regulators
A2MG	Alpha-2-macroglobulin	208.8	ECM Regulators
ANT3	Antithrombin-III	46.6	ECM Regulators
ANXA1	Annexin A1	244.4	ECM-affiliated Proteins
ANXA5	Annexin A5	301.9	ECM-affiliated Proteins
ANXA6	Annexin A6	101.1	ECM-affiliated Proteins
ASPN	Asporin	48.2	Proteoglycans
BGH3	Transforming growth factor-beta-induced protein ig-h3	233.6	ECM Glycoproteins
CILP1	Cartilage intermediate layer protein 1	49.5	ECM Glycoproteins
CO5A3	Collagen alpha-3(V) chain	49.3	Collagens
F13A	Coagulation factor XIII A chain	86.2	ECM Regulators
FIBG	Fibrinogen gamma chain	1172.9	ECM Glycoproteins
FILA2	Filaggrin-2	49.8	Secreted Factors
HEMO	Hemopexin	54.7	ECM-affiliated Proteins
LEG1	Galectin-1	143.1	ECM-affiliated Proteins
MGP	Matrix Gla protein	60.8	ECM Glycoproteins
MIME	Mimecan	125.8	Proteoglycans
PGS1	Biglycan	193.4	Proteoglycans
PGS2	Decorin	212.3	Proteoglycans
PRELP	Prolargin	151.2	Proteoglycans
PRG4	Proteoglycan 4	83.7	Proteoglycans
SRPX	Sushi repeat-containing protein SRPX	72.5	ECM Glycoproteins
TENX	Tenascin-X	56.2	ECM Glycoproteins
VTNC	Vitronectin	229.2	ECM Glycoproteins
VWF	von Willebrand factor	135.5	ECM Glycoproteins

**SFigure 1**



**SFigure 2**

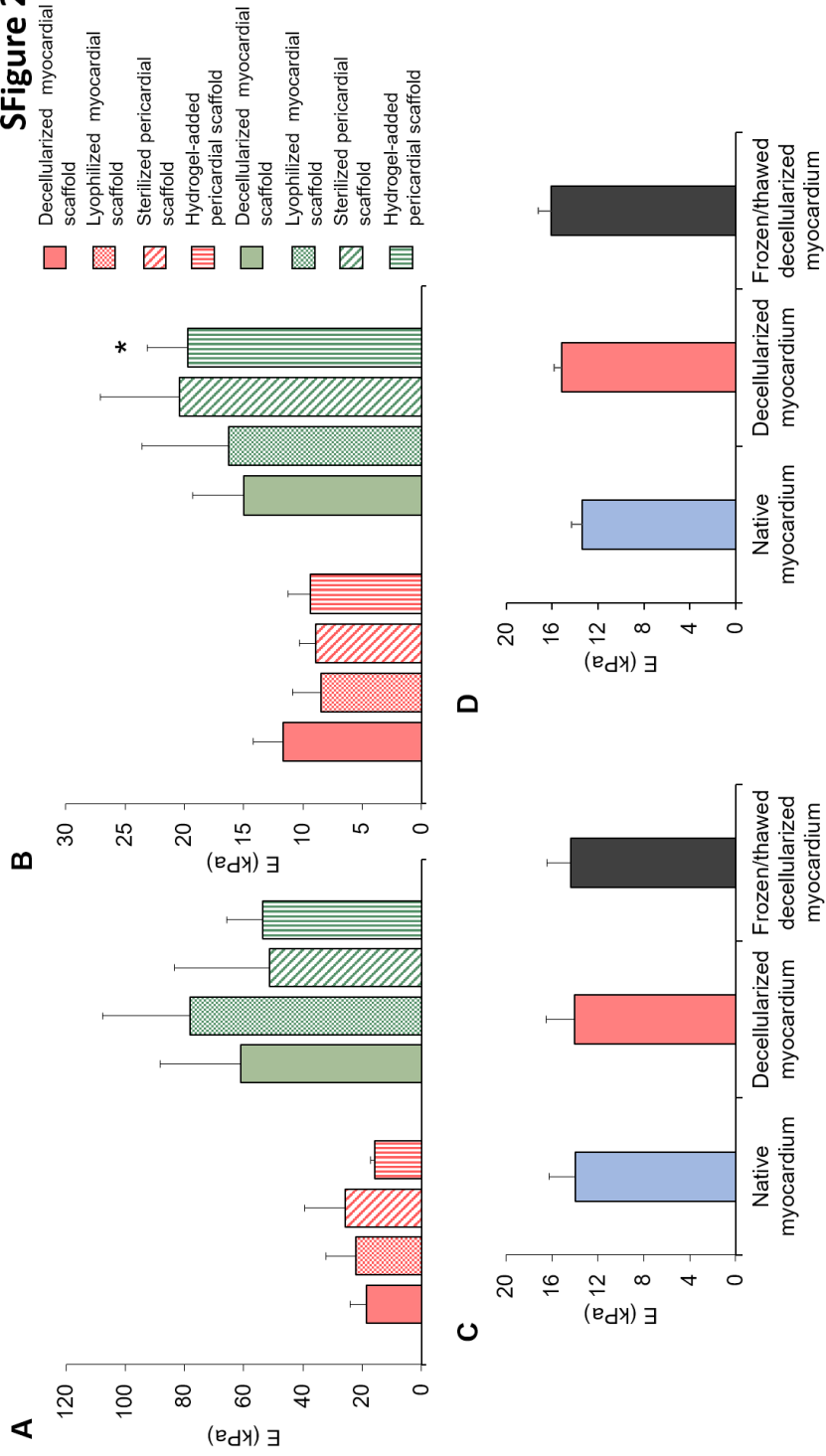


## Figure legends

**Figure 1. Internal structure and protein composition of the cardiac scaffolds.** (A) Ultrastructure determined by SEM of the native myocardium and (G) pericardium; (B) acellular myocardial and (H) pericardial scaffolds; and (C) recellularized myocardial and (I) pericardial scaffolds. (D,J) Representative images for the native and (E,K) acellular myocardium and pericardium showing immunostaining for col-I (green), col-III (red), and cTnI (white). (F,L) Photographs displaying immunostaining for col-I (green). Nuclei were counterstained with DAPI (blue). Scale bars=50  $\mu$ m.

**Figure 2. Cardiac ATMSCs retention and scaffold penetrance after recellularization.** (A) Photograph of the decellularized myocardial and (B) pericardial scaffolds 2h after cell repopulation. (C) Representative caption for recellularized myocardial and (D) pericardial scaffolds 2h-post recellularization showing labeled cardiac ATMSCs with NIR815 fluorescent dye (green). Scale bars=1 cm. (E) Quantification of NIR815 fluorescence (arbitrary units, AU) for both recellularized cardiac scaffolds. (F-G) Immunohistochemistry images for recellularized myocardial and pericardial scaffolds at different thickness levels: scaffold surface, (H-I) upper-middle, (J-K) inferior-middle, (L-M) and bottom, respectively. ECM was stained with col-I (green), and cardiac ATDPCs with F-actin (red). Nuclei were counterstained with DAPI (blue). Scale bars=50  $\mu$ m. (N) Quantification of cell density for each scaffold depth (surface, upper-middle, inferior-middle, and bottom). \* $P=0.048$ ; \*\* $P=0.047$ .

**Figure 3. Ultrastructure, macroscopic and microscopic mechanical characterization.** (A) Pore size and (B) pore sphericity measurements in both myocardial and pericardial scaffolds. \* $P=0.002$ . (C) Measurements of the Young's

modulus (E) using the tensile test for the native myocardium, and both decellularized, and recellularized myocardial and pericardial scaffolds. \* $P=0.04$  between recellularized pericardium and recellularized myocardium. (D) Determination of the microscopical stiffness by means of the E measured through AFM, for the same tissue conditions: native myocardium, and decellularized, and recellularized myocardial and pericardial scaffolds. \* $P=0.013$  and # $P=0.005$  between recellularized myocardium vs. native and decellularized myocardium, respectively.

**Figure 4. Decellularized cardiac scaffolds protein content.** (A) Number of matrisome and other proteins identified in the native myocardium reported by Guyette *et al.* [16]; and (B) for the native pericardium collected in Griffiths *et al.* [17]. (C) Total protein content, classified in matrisome and other proteins, for the decellularized myocardial and (D) decellularized pericardial scaffolds. (E) Venn's diagram displaying the unique proteins identified for either native or decellularized myocardium, and their common proteins. (F) Venn's diagram indicating the number of unique and shared proteins between native and decellularized pericardium. Results are represented as the percentage of the total protein number, and in brackets, as the number of proteins for each classification.

**Figure 5. Decellularized myocardial and pericardial scaffolds matrisome proteins comparison.** (A) Individual and common proteins between decellularized myocardial and pericardial scaffolds. Data are represented as a relative percentage to the total number of proteins and, within brackets, the number of proteins for each classification. UniProt accession name for the detected proteins is provided for each case. (B) Number of proteins for decellularized myocardial and pericardial scaffolds in each of

the following matrisome protein subdivisions: collagens, ECM glycoproteins, ECM regulators, ECM-affiliated proteins, proteoglycans, and secreted factors.

**Figure 6. Cardiac function and infarct morphometric analysis.** (A) Histograms of the differentials between 40 days of follow up and baseline or (B) post-MI among Per-MI, Per-ATMSCs, Myo-MI, Myo-ATMSCs, and Control-MI of LVEF and LVESV. \*P<0,05 vs. control-MI; #P<0,05 vs. Myo-MI. (C) Percentage of the LV infarct area measured in all heart sections for all study groups after 40 days of follow-up (Myo-MI vs Myo-ATMSCs; \*P<0,05 vs. control-MI); and (D) representative heart sections for each study group showing the infarcted area of the LV.

**Figure 7. Histological and immunohistochemical analysis after scaffold in vivo implantation.** (A) Representative images of H/E, Movat's pentachrome, pentachrome for simultaneous collagen and mucopolysaccharide acid staining, and Gallego's modified trichrome. Scale bar=100  $\mu$ m. (B) Movat's pentachrome of the scaffolds from Per-ATMSCs, Myo-ATMSCs, Per-MI, and Myo-MI groups displaying the presence of arterial blood vessels (red arrows), veins (blue arrows), and nerve fibers (yellow arrows). Scale bar=50  $\mu$ m. (C) Immunohistochemical images of the scaffolds against IsoB4 (green), SMA (red), and elastin (white) antibodies confirming the presence of arteriolar blood vessels positive for SMA. Nuclei appear counterstained in blue. Scale bars=50  $\mu$ m.

**Table 1. Common proteins shared by decellularized myocardial and pericardial scaffolds.** List of the common proteins (26) between both decellularized cardiac tissues, indicating their UniProt accession name, protein name, identification score,

and matrixome category classification.

**Table 2. Unique proteins identified for the decellularized myocardial scaffolds.**

List of the unique proteins (14) detected for the acellular myocardial scaffolds, including their UniProt accession name, protein whole name, identification score, and matrixome category.

**Table 3. Unique proteins detected in the decellularized pericardial scaffolds.**

Table containing the unique identified proteins (25) for the decellularized pericardial scaffold, with the following information detailed: UniProt accession name, complete protein name, identification score, and matrixome category inclusion.

**Supplementary Figure 1. Cell density for recellularized myocardial and pericardial scaffolds.** Quantification of cells/mm<sup>2</sup> in recellularized myocardial and pericardial scaffolds. \* $P=0.027$ .

**Supplementary Figure 2. Macro- and micromechanics of different stages between decellularized and recellularized cardiac scaffolds and after freeze/thaw cycle.**

(A) Measurement of the macromechanical and (B) micromechanical properties, indicated by the Young's modulus (E), for either myocardium or pericardium, for each of the following conditions: decellularized, lyophilized, sterilized with gamma irradiation, and embedded with hydrogel. \* $P=0.021$  when compared hydrogel-refilled pericardial scaffold vs. hydrogel-added myocardial scaffold. (C) Characterization of macroscopic and (D) microscopic mechanical properties for the native myocardium, decellularized myocardial scaffold, and decellularized myocardium submitted to a

freeze/thaw cycle.

## **Supplementary methods**

### **Protein extraction and digestion**

From a starting amount of 100 mg of decellularized cardiac samples minced in a cold mortar, proteins were extracted using three different extraction buffers prepared in homogenizer tubes (Miltenyi Biotec, Madrid, Spain). In the first and second procedures, an urea/thiourea buffer (5M urea (Sigma-Aldrich, Madrid, Spain), 2M thiourea (Amersham Biosciences, Little Chalfont, UK), 50mM DTT (Sigma-Aldrich), 0.1% SDS), or an SDS buffer (1% SDS, 50mM TRIS HCl adjusted to pH = 6.8 (Sigma-Aldrich), 12.5% glycerol (Sigma-Aldrich), in a buffer volume ( $\mu$ L):sample weight (mg) relation 10:1, was added to the mashed samples and mechanically homogenized using a gentleMACS<sup>TM</sup> Dissociator (Miltenyi Biotec) at 4 °C. Samples were centrifuged at 2,000xg for 10 min at 4 °C, both supernatant and pellet recovered and transferred to a new tube, and sonicated on ice with 3 consecutive cycles of 2 sec sonication pulses, followed by 3 sec sonication stand by, each 15 min for a total time of 1 h. The sonicated samples were centrifuged at 16,000xg for 30 minutes at RT, and the supernatant was collected and properly stored until use. For the third process, Reagent 4 buffer (R4) (Sigma-Aldrich) was put in following a buffer volume ( $\mu$ L):sample weight (mg) relation 1:3.3. After 4 °C mechanical dissociation with the gentleMACS<sup>TM</sup> Dissociator, samples were spun down at 2,000xg for 10 min at 4 °C, and the total content vortexed briefly each 5 min for 45 min at RT and centrifuged at 16,000xg for 1 min at 4 °C. The resulting supernatant was stored at -80 °C, and the insoluble pellet was incubated with guanidine buffer (4M guanidine hydrochloride and 50mM sodium acetate (Sigma-Aldrich)) for 48 h at RT with moderate stirring at 1,000



rpm during 5 sec every 30 sec. Centrifugation at 1,500xg for 25 min at 4 °C was performed, and supernatant stored at -80 °C. The pellet was washed with 90% ethanol, resuspended in deglycosylation buffer (150mM sodium chloride (Sigma-Aldrich), 50mM sodium acetate, and 0.05U/mL buffer of the enzymes Chondroitinase ABC from *Proteus vulgaris*, Endo- $\beta$ -galactosidase from *Bacteroides fragilis*, and Heparinase II from *Flavobacterium heparinum* (Sigma-Aldrich), and incubated 16 h at 37 °C. Upon incubation completion, a centrifugation at 16,000xg for 10 min at 4 °C was done, and the supernatant recovered. Finally, the stored fraction from R4 buffer, and the combined fraction from guanidine and deglycosylation buffers, were precipitated O/N at 4 °C with ice-cold acetone in an acetone volume:buffer volume 5:1 ratio and subsequently dried. All buffers were supplemented with cOmplete™, Mini, EDTA-free protease inhibitor cocktail (1 tablet for 10 ml of buffer) (Roche, Basel, Switzerland) and 25mM EDTA (Sigma-Aldrich) or 10mM EDTA for the deglycosylation buffer.

The extracted proteins were denatured and reduced in lithium dodecyl sulfate sample buffer (NuPAGE, Thermo Fisher) with reducing sample agent (NuPAGE, Thermo Fisher, Madrid, Spain), boiled for 10 min at 70 °C, and a known quantity of protein was loaded on Bis-Tris discontinuous 4%-12% polyacrylamide gradient gels (NuPAGE, Thermo Fisher). After electrophoresis, gels were stained using SimplyBlue™ SafeStain Coomassie Blue (NuPAGE, Thermo Fisher), and gel bands were excised in parallel positions across lanes and subjected to in-gel digestion by utilizing Trypsin Gold (Promega, Madison, WI). Digestion was stopped by adding trifluoroacetic acid (Sigma-Aldrich), and desalted and concentrated through a C18 SpinTips columns (Protea Biosciences, Morgantown, WV) prior to LC-MS/MS

analysis.

### **Peptide separation**

Peptide separation was performed on a Thermo PepMap 15-cm column with an inner diameter of 75  $\mu\text{m}$ , packed with 2  $\mu\text{m}$  C18 particles (Thermo Fisher) and a Thermo PepMap 2-cm pre-column with an inner diameter of 100  $\mu\text{m}$ , coated with 5  $\mu\text{m}$  C18 particles (Thermo Fisher). Loading solvent was H<sub>2</sub>O 0.1% trifluoroacetic acid at loading flow of 7  $\mu\text{l}/\text{minute}$ . The chromatographic gradient increased from 1% B to 5% B during 5 min; from 5 to 61 min B phase raised to 99 %; and after that, at 62 min, % B phase was 1%, until minute 72 to equilibrate the column; where solvent A was H<sub>2</sub>O 0.1% formic acid; and solvent B was acetonitrile with 0.1% formic acid, and the flow rate was 0.5  $\mu\text{l}/\text{min}$ . The column oven operated at 35 °C.

### **Cardiac ATMSCs labeling for *in vitro* scaffold cell tracking**

Before cell seeding over decellularized scaffolds, cardiac ATMSCs were labeled with the CellVue® NIR815 cell labeling kit (LI-COR Biosciences, Inc., Lincoln, NE) following manufacturer instructions. The near-infrared fluorescent dye NIR815 was detected and quantified at a wave length of 800 nm by using the Odyssey® CLx Imaging system (LI-COR).

### **Cell migration and density quantification**

For cellular penetrance and migration, total number of cell nuclei was quantified using ZenBlue software (Zeiss) in recellularized scaffolds two-hours post-reseeding (n=3), at different scaffold depth thickness: surface (from 0 to 25% of total thickness); upper-middle (from 0% to 25% of total thickness); inferior-middle (from 25% to 50% of total

thickness); and bottom (from 75% to 100% of total thickness). Cell retention 1 week after recellularization was also quantified using nuclei recount for both cardiac recellularized scaffolds (n=4) using ZenBlue software (Zeiss). At least 5 visual fields were counted for each sample.



## 4. Collection of *in vivo* conducted work using natural scaffolds for treating MI: a current review

Even though the last publication did not contain direct results derived from the thesis project, the breaking and more remarkable studies employing natural scaffolds as a MI therapy, in preclinical models and clinical trials, were collected and discussed in a review. This work helped us to contextualize and update the state of the art for cardiac tissue engineering, analyzing the more recent studies in order to incorporate innovative methodologies and novel designs to our engineered grafts, not only for the current work, but also for future projects.

The resulting manuscript was published in a peer-reviewed international journal (sixth article):

- Perea-Gil J, Prat-Vidal C, Bayes-Genis A. In vivo experience with natural scaffolds for myocardial infarction: the times they are a-changin'. *Stem Cell Res Ther* 2015; 6:248.



REVIEW

Open Access



# In vivo experience with natural scaffolds for myocardial infarction: the times they are a-changin'

Isaac Perea-Gil<sup>1</sup>, Cristina Prat-Vidal<sup>1\*</sup> and Antoni Bayes-Genis<sup>1,2</sup>

## Abstract

Treating a myocardial infarction (MI), the most frequent cause of death worldwide, remains one of the most exciting medical challenges in the 21st century. Cardiac tissue engineering, a novel emerging treatment, involves the use of therapeutic cells supported by a scaffold for regenerating the infarcted area. It is essential to select the appropriate scaffold material; the ideal one should provide a suitable cellular microenvironment, mimic the native myocardium, and allow mechanical and electrical coupling with host tissues. Among available scaffold materials, natural scaffolds are preferable for achieving these purposes because they possess myocardial extracellular matrix properties and structures. Here, we review several natural scaffolds for applications in MI management, with a focus on pre-clinical studies and clinical trials performed to date. We also evaluate scaffolds combined with different cell types and proteins for their ability to promote improved heart function, contractility and neovascularization, and attenuate adverse ventricular remodeling. Although further refinement is necessary in the coming years, promising results indicate that natural scaffolds may be a valuable translational therapeutic option with clinical impact in MI repair.

## Introduction

Myocardial infarction (MI) occurs when coronary artery blood flow is blocked. Currently, MI remains the most frequent cause of death worldwide [1]. In the United States alone, approximately 8 million people per year have a MI episode [2]. For effective MI treatment, it is necessary to limit adverse ventricular remodeling,

attenuate myocardial scar expansion, enhance cardiac function and regeneration, and preserve synchronous contractility. Among the current therapies, only heart transplantation can fully achieve all these outcomes. Nonetheless, transplantation is highly limited by heart donor availability and host immunological response against the donated organ [3].

An alternative, novel therapeutic option is to deliver cells into the injured myocardium; this approach was demonstrated to be safe and feasible [4, 5]. To date, several cell types have been used for cardiac regeneration, including embryonic stem cells (ESCs) [6], cardiomyocytes (CMs) derived from induced pluripotent stem cells (iPSCs) [7], mesenchymal stem cells (MSCs) [8], bone marrow MSCs [9], cardiac stem cells [10], cardiac progenitor cells [11], skeletal myoblasts [12], endothelial cells (ECs) [13], adipose tissue-derived stem cells (ATDSCs) [14], and CMs [15]. However, modest results have been obtained due to massive cell loss after administration, low cellular survival or lack of cellular effect triggered by hypoxic conditions in the host tissue, failure to establish electrical or mechanical heart coupling, which results in arrhythmias, and low rates of cell differentiation into a cardiac lineage [3]. To overcome these limitations, new methods for enhancing the final outcome have been proposed.

Cardiac tissue engineering offers a plausible solution to the drawbacks encountered previously. This alternative consists of seeding cells onto a structural, supportive platform, known as a scaffold, and may also be supplemented with cytokines, growth factors, or peptides. The scaffold provides a biomimetic environment which resembles the physiological cardiac environment; thus, it favors cell attachment and differentiation, and it avoids direct administration of cells into an adverse environmental niche (that is, infarcted myocardium) [16, 17]. Therefore, an optimal scaffold for cardiac repair should recreate the myocardial microenvironment, structure,

\* Correspondence: cprat@igtp.cat

<sup>1</sup>ICREC (Heart Failure and Cardiac Regeneration) Research Lab, Health Sciences Research Institute Germans Trias i Pujol (IGTP). Cardiology Service, Hospital Universitari Germans Trias i Pujol, 08916 Badalona, Barcelona, Spain  
Full list of author information is available at the end of the article

and three-dimensional organization, permit vascularization to ensure oxygen and nutrient flow to the cells, match electrical and mechanical requirements for proper host tissue coupling, be easily replaceable, and enhance cell survival and engraftment [3, 16, 17].

Depending on the origin of scaffold material, scaffolds are divided into two groups: natural and synthetic. Although synthetic materials offer the ability to directly control and adjust scaffold properties, natural materials appear to be more biodegradable and biocompatible. In addition, natural materials can better recreate the native myocardial microenvironment [18], which is necessary for generating the optimal, most suitable scaffold.

Here, we review natural scaffolds and hydrogel applications developed to repair injured myocardium after a MI. We describe constructs of natural materials combined with different cell types and other elements, and we analyze the main outcomes of heart function recovery in pre-clinical MI models and in clinical trials currently available (Tables 1, 2, 3, 4, 5 and 6). This summary provides an in-depth view of the current state of natural scaffold use in cardiac tissue engineering. Finally, we discuss the positive and negative aspects of the latest investigations in the field of myocardial regeneration.

### **Natural scaffold materials for myocardial regeneration**

In recent years, *in vitro* studies have consolidated our understanding of natural scaffold generation and their application in cardiac tissue engineering. This progress has enabled further investigation and improvements in this field, leading ultimately to *in vivo* progressive implantation of the developed scaffolds, supported by the positive results obtained *in vitro* (Fig. 1). In the following sections we review the most notable and latest improvements for *in vivo* MI treatment using different natural scaffold implantation methods (Fig. 2).

#### **Collagen**

Collagen, the predominant protein in mammalian extracellular matrix (ECM), provides structural support for maintaining tissue integrity and contributes to the specificity of ECM microenvironments [19]. Several optimal properties, such as being biocompatible, adhesive, suturable, porous and readily combined with other materials, have made collagen appropriate for use as a natural scaffold in tissue engineering applications [20–25].

In cardiac tissue engineering, collagen scaffolds promote cardiac commitment, vascularization, and electrical coupling, thus representing a good candidate platform for MI repair. Collagen scaffold-associated benefits have been observed in different MI models (Table 1). Specifically, collagen type I delivery 3 hours after induction of a MI, without cells or added growth factors, can prevent

adverse ventricular remodeling and long-term deterioration of heart function [26]. Furthermore, collagen can increase angiogenesis, reduce cell death, and limit the area of fibrosis, although these therapeutic effects were lost when the collagen scaffold was administered 1 or 2 weeks post-MI [26]. Another study revealed similar results when they inserted a collagen type I patch into rats subjected to MI [27]. After 4 weeks, compared with infarcted rats without the collagen patch, those with the patch had reduced adverse ventricular remodeling, limited fibrosis propagation, and significantly greater blood vessel formation. Remarkably, cardiac function was significantly increased, with an improvement of approximately 25 % in ejection fraction (EF) compared with non-treated infarcted animals [27]. These results were also confirmed in a rat MI model where the collagen type I-treated group showed attenuated left ventricular (LV) remodeling and increased angiogenesis, which promoted the formation of new connective vasculature between the scaffold and the host myocardium, pointing out the importance of the collagen scaffold itself [28].

In addition, constructs combining different growth factors, proteins, cells or other natural or biological materials onto collagen scaffolds have been placed over infarcted myocardium (Table 1). One study in rats delivered a collagen type I scaffold combined with MSCs and interleukin-10 to the infarcted area of the heart [29]. When analyzed 28 days after treatment, the group that received the scaffold combination exhibited higher EF (mean recovery of 7 %), a 40 % increase in infarcted wall thickness, a higher collagen III/I ratio, and less apoptosis inside the implant compared with the group that received the scaffold alone. Of interest, lower CD80+ macrophage and higher regulatory CD163+ macrophage infiltration was detected in the ischemic zone when the scaffold was applied, suggesting less associated inflammatory response. Nonetheless, these parameters were not significantly different when rats were treated with MSCs combined with the collagen scaffold but without interleukin-10, lacking the expected combinatory positive effect of cells plus interleukin-10 [29]. Another study compared a non-crosslinked collagen scaffold and crosslinked collagen scaffolds (both collagen type I) with variable degrees of crosslinking to modulate the material stiffness [30]. All were seeded with ATDSCs and sutured into rats with cardiac infarction. Only the non-crosslinked scaffold presented high biocompatibility and complete adhesion to the heart; a mild inflammatory reaction was observed 7 and 30 days after implantation. Moreover, this scaffold retained approximately 25 % of the seeded cells. However, heart contractility, cardiac function, and cell growth and survival were not assessed for all the scaffolds [30]. These gaps in assessment were partially covered in a later study which showed that, at 1 week and 1 month after



**Table 1** The principal in vivo studies using a collagen-based scaffold and the outcomes obtained

Scaffold material	Cell lines and/or other components	MI model	Main results	References
Collagen	–	Mouse	Negative ventricular remodeling prevented, deterioration of heart function prevented, lack of inflammatory response, angiogenesis↑, fibrosis↓, cell death↓	[26]
	–	Mouse	Patch attached, colonization of patch by native cells, EF↑, FS↑, LV internal diameter↓, LV posterior wall dimension↑, fibrosis↓, dilatation of LV chamber↓, angiogenesis↑, no immunological response	[27]
	–	Rat	LV dilatation↓, LV inner and outer diameters↓, LV pressure-volume curve shift (to the left towards control), angiogenesis↑	[28]
	Rat MSCs+interleukin-10	Rat	LV EF↑, apoptosis↓, infarcted wall average thickness↑, ratio collagen III/I↑, regulatory macrophage markers↑	[29]
	Rat ATDSCs	Rat	Evaluation of inflammatory response to diverse collagen scaffolds (non-crosslinked or crosslinked), presence of cells in the non-crosslinked scaffold	[30]
	Rat ATDSCs	Rat and pig	Rat: cell engraftment↑, LV EF↑, stiffer mechanical behavior, fibrosis↓, revascularization↑. Pig: LV EF↑, fibrosis↓, vascularization↑	[31]
	Sheep adipose tissue MSCs	Sheep	LV end-diastolic dimension improvement, diastolic function↑, angiogenesis↑, fibrosis extension↓	[32]
	Rat bone marrow MSCs	Rat	LV wall thickness↑, EF preservation, FS↑, fractional area change↑	[33]
	Rat bone marrow MSCs	Rat	Infarcted segment perfusion↑, infarct area↓, contractility↑, low inflammation, angiogenesis↑, ventricular wall thickness↑, LV dilatation↓	[34]
	Rat bone marrow MSCs +glycosaminoglycans	Rat	No inflammation, neovascularization↑, presence of cells	[35]
Collagen+chitosan	Mouse Sca-1 <sup>+</sup> cells (collagen conjugated with anti-Sca-1 antibody)	Mouse	Number of infiltrated cells↑, capillary density↑, cell density↑, myocardium regeneration↑	[36]
	Human mononuclear bone marrow stem cells	Human	No mortality or related adverse effects, New York Heart Association functional class↑, LV end-diastolic volume↓, LV filling deceleration time improvement, scar area thickness↑, EF↑	[37, 38]
	Encapsulated thymosin β4	Rat	Cardiac tissue loss↓, vascularization↑	[25]
Collagen+oligo (acryloyl carbonate)-poly(ethylene glycol)-oligo(acryloyl carbonate)	Integrin-binding, angiopoietin-1-derived peptide QHREDGS	Rat	Cardiac function↑, scar thickness and scar area fraction improved, presence of CMs↑, no inflammation	[39]
	Rat bone marrow MSCs	Rat	Preserved EF, infarct size↓, LV wall thickness↑, vessel density↑	[41]

ATDSC adipose tissue-derived stem cell, CM cardiomyocyte, EF ejection fraction, FS fractional shortening, LV left ventricle/left ventricular, MI myocardial infarction, MSC mesenchymal stem cell, Sca stem cell antigen

implantation, the non-crosslinked collagen scaffold seeded with ATDSCs displayed more cell engraftment than ATDSC administration alone [31]. In addition, in both rat and pig chronic MI models, the groups that received both collagen and cells had significant increases in heart function (approximately 16 %) and revascularization, and a significant decrease in fibrotic area 4 months post-treatment compared with untreated animals and animals treated with either scaffold alone or cells alone. The reduction in collagen content of treated animals could be explained by the lower detected levels of procollagen C-proteinase and lysyl oxidase, reducing collagen crosslinking [31]. Similar

results were obtained in a sheep MI model, in terms of cardiac function recovery and revascularization [32], thus indicating the suitability and promise of combined administration of collagen scaffold and ATDSCs. In addition, bone marrow MSCs combined with a collagen type I platform also preserved heart function after up to 6 weeks of treatment, in contrast to infarcted groups that were not treated or treated with cells only [33]. Further experiments demonstrated that bone marrow MSCs in a collagen type I scaffold had beneficial effects on contractility, wall thickness, angiogenesis, and infarcted area perfusion, and curbed ventricular dilatation and infarct zone expansion [34].

**Table 2** Main achievements in myocardial infarction recovery after the administration of a fibrin scaffold

Scaffold material	Cell lines and/or other components	MI model	Main results	References
Fibrin	Rat skeletal myoblasts	Rat	FS and infarct wall thickness preservation	[52]
	Rat skeletal myoblasts	Rat	Infarct scar size↓, arteriole density↑	[53]
	Human cardiac and subcutaneous ATDPCs	Mouse	CM and EC differentiation, vessel density↑, LV EF↑, infarct size↓	[55]
	Rat bone marrow cells	Rat	Cell retention↑, LV perimeter↓, stroke volume and contractility preservation, cardiac function↑	[56]
	hESCs	Mouse and pig	Cardiac function↑, cell engraftment↑, angiogenesis↑, EF↑, infarct size↓, LV hypertrophy↓, systolic LV wall stress↓, LV systolic thickening fraction↓	[57]
	Rat adipose-derived MSCs	Rat	Preserved wall thickness, LV end-diastolic and systolic dimensions↓, LV end-diastolic volume↓, LV end-systolic volume↓, LV remodeling suppressed	[58]
	hESC-derived cardiac progenitors	Rat	LV end-systolic volume↓, EF↑, angiogenesis↑, absence of teratomas	[59]
	Human iPSC-derived CMs, ECs, and smooth muscle cells	Pig	Cell survival↑, LV EF↑, contractility↑, infarct size↓, regional wall stress↓, energetic efficiency↑, lack of arrhythmias, apoptosis↓, cellular expression of Nkx2.5↑, angiogenesis↑, immune response delayed, protective paracrine effects	[54]
	Rat heart cells; native population or CM-depleted population	Rat	EF and FS↑ (only for patch with native cell population), wall thickness↑, infarct size↓, cell migration, vascularization↑, electrical coupling and alignment not achieved	[60]
	Human umbilical cord blood MSCs	Mouse	Infarct size↓, vessel density↑	[61]
	Human umbilical cord blood MSCs	Mouse	Microvasculature formation↑, FS↑, EF↑	[62]
	Swine MSCs	Pig	LV thickness fraction↑, neovascularization↑, differentiation into myocyte-like cell lineage	[63]
	Swine MSCs+thymosin β4	Rat	Proliferation↑, protection against hypoxia, LV EF↑, LV FS↑, wall thickening↑, vasculogenesis↑, cell survival↑	[64]
Fibrin+PEG	SDF-1α	Mouse	c-kit <sup>+</sup> cell recruitment↑, LV function↑	[68]
Fibrin+decellularized myocardial ECM	Human mesenchymal progenitor cells (TGF-β-conditioned or not)	Rat	Angiogenesis↑, cell migration↑, LV diameter and area preservation, contractility↑	[70]

ATDPC adipose tissue-derived progenitor cell, CM cardiomyocyte, EC endothelial cell, ECM extracellular matrix, EF ejection fraction, FS fractional shortening, hESC human embryonic stem cell, iPSC induced pluripotent stem cell, LV left ventricle/left ventricular, MI myocardial infarction, MSC mesenchymal stem cell, PEG polyethylene glycol, SDF stromal cell-derived factor, TGF transforming growth factor

Moreover, when the collagen type I and bone marrow MSC combination was supplemented with glycosaminoglycans, the results demonstrated reduced inflammation, increased neovascularization, and improved retention of cells, but no LV function parameters were evaluated [35]. In another study, collagen type I was conjugated with antibodies that specifically recognized stem cell antigen-1 (Sca-1), a surface marker for hematopoietic, cardiac, and muscle stem cells. These antibodies enriched the scaffold by capturing Sca-1<sup>+</sup> cells. When this scaffold combination was applied to the infarcted myocardium, it retained a high number of cells, increased cardiac tissue regeneration, and expanded capillary density compared with infarcted hearts that did not receive the enriched scaffold. It is important to emphasize that scaffolds with Sca-1 showed faster degradation of the collagen scaffold, and fiber arrangement was better organized [36].

In the Myocardial Assistance by Grafting a New bioartificial Upgraded Myocardium (MAGNUM) clinical trial,

the delivery, safety, and effectiveness of a collagen type I scaffold loaded with autologous bone marrow MSCs was tested in humans (Tables 1 and 6) [37]. In this study, a total of 20 patients with myocardial ischemia that displayed indications for bypass surgery were included and divided into two treatment groups: one group (n = 10) was treated with cells only, and the other group (n = 10) received the collagen scaffold with cells. After completing a 10-month follow-up, no adverse events or death occurred. With both treatments, patients experienced improvements in EF and the New York Heart Association functional class. Compared with the group treated with cells alone, the scaffold-plus-cells treatment group showed enhanced LV end-diastolic volume, LV filling deceleration time, and scar area thickness, which indicated LV function improvement and limited adverse remodeling. Therefore, the collagen scaffold with cells was demonstrated to be both safe and effective for treating ischemia in humans compared with administration of cells alone [38]. These

**Table 3** In vivo improvements achieved with scaffolds composed of the polysaccharides chitosan, alginate or hyaluronic acid

Scaffold material	Cell lines and/or other components	MI model	Main results	References
Chitosan	Rat brown ATDSCs	Rat	Cell survival and retention↑, EF↑, FS↑, LV end-diastolic pressure↓, LV pressure change↑, infarct size↓, fibrosis↓, ATDSC to cardiac lineage differentiation↑, vessel density↑, endothelial and smooth muscle cell differentiation	[81]
	Mouse ESCs	Rat	Infarct zone cell retention↑, ESC to cardiac differentiation, heart function↑, LV end-diastolic and end-systolic diameters↓, EF↑, FS↑, infarct size↓, wall thickness↑, complete chitosan degradation, microvessel density↑	[82]
	Mouse nuclear-transferred ESCs or fertilization-derived mouse ESC	Rat	For both cell types: infarcted area covered↑, possible differentiation into CMs, smooth muscle cells and ECs, heart function↑, LV end-diastolic and end-systolic diameters↓, EF↑, FS↑, infarct size↓, wall thickness↑, complete chitosan degradation, neovascularization↑	[83]
	bFGF	Rat	LV EF↑, LV FS↑, arteriole density↑, infarct size↓, fibrosis area↓	[84]
	RoY peptide	Rat	Angiogenesis↑, ventricular wall thickness↑, fibrosis↓, infarct size↓, LV FS↑, LV EF↑	[85]
Chitosan+alginate	Rat MSCs	Rat	EF↑, LV function↑, angiogenesis↑	[77]
	–	Rat	Angiogenesis↑, no inflammation exacerbation, apoptosis↓, presence of c-kit <sup>+</sup> cells↑, proliferation↑, wall thickness↑, LV expansion↓, LV EF↑	[87]
Alginate	–	Rat	Absence of arrhythmias or thrombus formation, scaffold degraded, scar thickness↑, diastolic and systolic anterior wall thicknesses↑, LV end-diastolic and systolic dimensions↓, LV end-diastolic and systolic areas↓, cardiac dysfunction↓	[98]
	–	Dog	End-systolic and end-diastolic wall thicknesses↑, LV end-diastolic and systolic volumes↓, end-systolic sphericity index↑, LV EF↑, functional mitral regurgitation↓, LV function↑	[99]
	–	Pig	No arrhythmias or conduction blocks, no remote infarcts in other organs, LV enlargement↓, LV function↑, coronary blood flow not affected, scar thickness↑, anterior wall thickness↑	[100]
	Rat fetal cardiac cells	Rat	Vascularization↑, formation of myofibers and gap junctions, preservation of LV dimensions and FS	[102]
	Human ESCs or human embryonic bodies	Rat	FS↑, LV dilation, absence of inflammation, no cardiomyogenic differentiation, no cell retention	[103]
	RGD peptide	Rat	FS↑, LV dimension↓, LV wall thickness↑, angiogenesis↑	[105]
	RGD peptide+encapsulated MSCs (microbeads)	Rat	LV function↑, wall thickness preservation, LV internal dimensions preserved, infarct size↓, angiogenesis↑, high cell retention	[106]
	Unmodified alginate; RGD or YIGSR peptide-modified alginate; or RGE peptide-modified alginate	Rat	Unmodified-alginate: scar thickness↑, attenuated LV systolic and diastolic dilatations, LV FS↑, fractional area change↑, LV expansion index↓ (compared with all peptide-modified alginates)	[107]
	IGF/HGF (microbeads)	Rat	Scar thickness preservation, infarct expansion index↓, scar collagen accumulation↓, vascularization↑, apoptosis↓	[110]
–	Human	New York Heart Association functional class↑, Kansas City Cardiomyopathy Questionnaire score↑	[111]	
Alginate+fibrin	–	Pig	LV posterior wall thickness↑, infarct expansion↓, extractable collagen↓	[115]
Alginate+Matrigel +omentum	Neonatal rat cardiac cells with SDF-1, IGF-1 and VEGF	Rat	Mechanical and electrical coupling, relative scar thickness↑, angiogenesis↑, infarct expansion index↓, FS and fractional area change preserved, LV end-diastolic and systolic dimensions↓	[117]
Alginate+polypyrrole	–	Rat	No inflammation, angiogenesis↑, myofibroblast population↑	[118]

**Table 3** In vivo improvements achieved with scaffolds composed of the polysaccharides chitosan, alginate or hyaluronic acid (Continued)

Hyaluronic acid	Alone or with VEGF	Rat	Ventricle thickness↑, infarct size↓, apoptosis↓, vascularization↑, heart function↑	[121]
	Rat BMMNCs	Rat	Apoptosis↓, inflammatory response↓, EF↑, ventricular dilatation↓, scar size↓, collagen content↓, angiogenesis↑, cell differentiation into ECs	[124]
	Pig BMMNCs	Pig	LV EF↑, interventricular septum thickness↑, LV end-diastolic pressure and volume↓, contractility↑, scar size and length↓, fibrosis↓, high cell retention, neovascularization↑	[125]
	Rat bone marrow MSCs (esterified hyaluronic acid)	Rat	Construct integration, vascularization↑, fibrosis↓	[126]
	Pig bone marrow MSCs (esterified hyaluronic acid)	Pig	Inflammation↓, fibrosis↓, degeneration of cardiac cells↓	[127]
	Hydroxyethyl methacrylate, SDF-1 $\alpha$ , mouse bone marrow cells	Mouse	Cell homing in the myocardium↑	[128]
	rTIMP-3	Pig	LV end-diastolic dimension↓, LV EF↑, wall stress↓, infarct expansion↓, wall thickness↑, LV end-diastolic volume preserved, myofibroblast number↑, collagen content↑	[130]
	Gelin-S	Rat	LV EF↑, LV FS↑, neovascularization↑, collagen deposition↓	[131]
	Methacrylic anhydride	Sheep	Regional wall thickness↑, infarcted area↓ (only for highly stiff scaffold)	[132]
	Methacrylic anhydride or/and hydroxyethylmethacrylate	Sheep	Wall thickness↑, vascularization↑, inflammation↑, LV end-systolic volume↓ (only for highly stiff, stable scaffold)	[133]
Hyaluronic acid+gelatin	Human cardiosphere-derived cells	Mouse	Cardiac function↑, LV remodeling and abnormal heart morphology↓, viable tissue↑, wall thickness↑, cardiac and endothelial cellular differentiation, cellular engraftment↑, neovascularization↑, apoptosis↓	[134]
Hyaluronic acid+silk fibroin	Rat bone marrow MSCs	Rat	LV inner diameter↓, wall thickness↑, FS↑, inflammation↓, apoptosis↓, vascularization↑, $\alpha$ -MHC expression↑, paracrine factor secretion↑	[135]
Hyaluronic acid+chitosan +silk fibroin		Rat	LV inner diameter↓, wall thickness↑, LV FS↑, angiogenesis↑, paracrine factor expression↑	[136]
Hyaluronic acid+butyric and retinoic acids	Human placenta-derived MSCs	Pig	Scar size↓, infarct core zone↓, angiogenesis↑, fibrosis↓, end-systolic wall thickening and circumferential shortening↑, high homology with healthy myocardium	[137]

ATDSC adipose tissue-derived stem cell, bFGF basic fibroblast growth factor, BMMNC bone marrow mononuclear cell, CM cardiomyocyte, EC endothelial cell, EF ejection fraction, ESC embryonic stem cell, FS fractional shortening, HGF hepatocyte growth factor, IGF insulin growth factor, LV left ventricle/left ventricular, MHC myosin heavy chain, MI myocardial infarction, MSC mesenchymal stem cell, rTIMP recombinant tissue inhibitor of matrix metalloproteinases, SDF stromal cell-derived factor, VEGF vascular endothelial growth factor

positive results should encourage further investigation following administration of combined collagen scaffold and MSCs, recruiting more patients and extending the clinical trial follow-up.

With regard to combinations of natural or biological materials, a mixture of chitosan, collagen type I, and encapsulated thymosin  $\beta$ 4 was used to treat a rat MI model, with diverse results (Table 1). At 3 weeks after MI induction, treated rats showed reduced tissue loss (only 13 % compared with 58 % and 30 % for non-treated and thymosin  $\beta$ 4-free hydrogel-treated animals, respectively) and enhanced vascularization compared with untreated animals or thymosin  $\beta$ 4-treated animals, but no functional benefits were achieved [25]. When the integrin-binding, angiopoietin-1-derived peptide QHREDGS was attached to the same collagen and chitosan scaffold, infarcted animals displayed

abundant CMs, no inflammatory response, and, more importantly, improved cardiac function [39].

Finally, collagen combined with synthetic materials would retain the properties of collagen (that is, degradability and compatibility) and could provide a means to recreate a natural, appropriate microenvironment, which could enhance proliferation, survival, and cardiac differentiation [40]. An injectable, hybrid hydrogel was created by combining collagen type I with the copolymer oligo(acryloyl carbonate)-poly(ethylene glycol)-oligo(acryloyl carbonate); cultured bone marrow MSCs were then added and the refilled scaffold was tested in a rat MI model (Table 1). Infarcted rats injected with this hybrid hydrogel plus MSCs exhibited an approximately 26 % reduction of the infarct area, a sixfold ventricular wall thickness enhancement, and increased vessel density compared with untreated infarcted rats.

**Table 4** Outcomes in function recovery after myocardial infarction following gelatin and Matrigel scaffold delivery

Scaffold material	Cell lines and/or other components	MI model	Main results	References
Gelatin	Fetal rat ventricular cells	Rat	Scaffold adhered to tissue, presence of blood vessels, cell to cell linking and spontaneous contraction, no cardiac function improvements	[140]
	Erythropoietin	Rabbit	LV end-systolic and end-diastolic dimensions↓, LV EF↑, FS↑, $\pm dP/dt$ ↑, erythrocyte number↑, hematocrit↑, infarct size↓, fibrosis↓, infarct border zone capillary density↑	[142]
	bFGF	Rat	FS↑, infarct size↓, infarcted/non-infarcted wall thickness ratio↑, LV expansion index↓, capillary and arteriolar density↑, CM apoptosis↓	[143]
	bFGF alone or with human bone marrow-derived MSCs or human cardiosphere-derived cells	Pig	bFGF alone: arterial vessels↑, myocardial perfusion↑, LV EF↑. With human cardiosphere-derived cells: LV EF↑, infarct volume↓, wall motion↑, differentiation to CM↑. With human bone marrow-derived MSCs: LV EF↑, infarct volume↓	[144]
	Human cardiac-derived stem cells+bFGF	Human	No adverse side effects↑, LV EF↑, infarct size↓, maximal aerobic exercise capacity↑	[145], NCT00981006
Matrigel	–	Rat	Capillary density↑	[147]
	–	Rat	LV EF↑, contractility↑, infarct wall thickness↑, angiogenesis↑, c-kit+and CD43+ stem cell myocardial homing↑	[148]
	Rat adipose-derived stromal cells	Rat	LV EF↑, LV akinesis↓, contractility↑, infarcted area size↓	[149]
	Mouse ESCs	Mouse	Connexin 43 expression, graft/infarct area↑, FS↑, LV wall thickness preservation	[150]
	Mouse ESCs	Rat	FS↑, myocardial wall thickness↑, LV dilatation prevention, connexin 43 and $\alpha$ -sarcomeric actin expression	[151]
	Human ESC-derived CMs with prosurvival cocktail	Rat	Cell engraftment↑, LV end-diastolic and systolic dimensions↓, FS↑, EF↑, infarcted area wall thickening↑	[152]
Matrigel+collagen	Mouse bone marrow-derived MSCs	Mouse	No improvements in FS, EF, or LV diastolic end volume	[153]
	Rat H9c2 cardiomyoblasts alone, with VEGF, or with bFGF	Rat	Three groups: cell survival↑, LV wall thickness↑, LV EF↑, FS↑. No significant additional improvements were observed with VEGF or bFGF	[154]
	Rat myoblasts	Rat	Inflammatory response↑, FS↑, LV end-systolic diameter↓, scaffold vascularized	[155]
	Rat cardiac myocytes	Rat	No improvements in cardiac function or LV wall thickness, sarcomere integrity, vascularized and innervated graft, contraction preserved, electrical and mechanical coupling requires further evaluation	[156]
	Rat neonatal ventricular CMs	Rat	CM sarcomeric structural integrity, FS↑, anterior wall thickness↑, LV end-systolic diameter↓	[157]
	Rat neonatal heart cells	Rat	Non-delayed electrical coupling, dilatation↓, systolic wall thickening↑, FS area↑	[158]

*bFGF* basic fibroblast growth factor, *CM* cardiomyocyte; *dP/dt* change in pressure over time, *EF* ejection fraction, *ESC* embryonic stem cell, *FS* fractional shortening, *LV* left ventricle/left ventricular, *MI* myocardial infarction, *MSC* mesenchymal stem cell, *VEGF* vascular endothelial growth factor

Notably, EF values reached those measured prior to MI induction, showing excellent heart function recovery for treated rats [41].

It is important to point out that all the *in vivo* studies which used collagen scaffolds were performed with type I collagen; thus, the observed differences between the different parameters can not be attributed to the collagen type. It would be interesting to carry out future animal experimentation using other collagen types (that is, collagen type III), evaluating the final outcomes and comparing them with the extensive work done with type I collagen scaffolds.

### Fibrin

Fibrin, a truncated form of fibrinogen, attracts and recruits leukocytes, principally macrophages, to participate in blood clot formation and wound healing processes [42–44], and also plays important roles in cell matrix interactions, inflammatory responses, and neoplasia [42].

Fibrin can be obtained from patient blood, which avoids the risk of adverse immunological responses, and can be easily manipulated by readjusting fibrinogen concentrations and/or polymerization rates to modulate matrix density, mechanical strength, and microstructure [45–49]. Moreover, fibrin scaffolds are good candidates for

**Table 5** Myocardial infarction animal models and the progress in infarction regeneration for decellularized extracellular matrix-based scaffolds

Scaffold material	Cell lines and/or other components	MI model	Main results	References
Decellularized myocardial ECM	–	Rat	LV EF↑, LV bulging↓, infarct LV wall thickness↑, infarct expansion index↓	[166]
	–	Rat	Viable myocardium islands inside infarcted zone↑, no arrhythmia induction, proliferative cell density (mainly lymphocytes)↑, EF preservation	[167]
	–	Rat and pig	Rat: ECM biodegradable and biocompatible with host myocardium, absence of embolization or ischemia. Pig: LV EF↑, LV end diastolic and systolic volumes↓, contractility↑, global wall motion score↑, proportion of endocardial muscle↑, fibrosis↓, presence of neovascularization, unaltered cardiac rhythm or blood chemistry	[168]
Decellularized pericardium ECM	Rat bone marrow MSCs	Rat	LV cavity enlargement prevented, LV FS↑, LV end diastolic and systolic pressures improved, no apoptosis, microvessel density↑, differentiation to smooth muscle cells or myofibroblasts, growth factor expression and cytokine release↑	[176]
	Rat bone marrow MSCs	Rat	LV FS↑, LV end diastolic and systolic pressure improvements, LV dilatation↓, absence of apoptosis, blood vessel density↑, differentiation into smooth muscle cells or myofibroblasts	[177]
	bFGF	Rat	bFGF retention↑, arteriole density↑, confirmation of vessel functionality	[178]
	HGF fragment	Rat	LV remodeling prevention, fractional area change↑, arteriole density↑	[179]
Decellularized pericardium ECM+ RAD16-I peptidic hydrogel	Porcine mediastinal ATDPCs	Pig	Infarct size↓, vascularization↑	[174]
SIS	–	Mouse	LV end systolic area↓, contractility↑, infarct size↓, capillary formation↑	[180]
	Rabbit MSCs	Rabbit	LV dimensions improved, anterior wall thickness↑, contractility↑, LV relaxation↑, vascular density↑, no immunological response, cardiac troponin T and $\alpha$ -smooth muscle actin expression	[181]
	bFGF	Rat	EF↑, LV end systolic and diastolic volumes↓, contractility↑	[182]
UBM	–	Pig	Smooth muscle cells↑, myofibroblast recruitment, inflammation↓, thrombus extension↓	[162]
	–	Dog	Myocyte recruitment with normal morphology and organization, myocyte proliferation↑, regional stroke work↑, systolic contraction↑	[185]
	Human MSCs (spheroid or non-manipulated)	Dog	Regional stroke work↑, systolic area contraction↑, organized sarcomeric structure	[186]

ATDPC adipose tissue-derived progenitor cell, bFGF basic fibroblast growth factor, ECM extracellular matrix, EF ejection fraction, FS fractional shortening, HGF hepatocyte growth factor, LV left ventricle/left ventricular, MI myocardial infarction, MSC mesenchymal stem cell, SIS small intestine submucosa, UBM urinary bladder matrix

treating MIs due to their high biocompatibility, biodegradability, and capacity for incorporating different cell types. In addition, fibrin scaffolds can be assembled with either growth factors or other scaffold materials [49–51].

Due to its intrinsic properties, application of a fibrin patch alone (without cells) over the infarcted myocardium exerts beneficial effects (Table 2). In a rat MI model, application of a fibrin glue, which formed a scaffold, reduced the infarct size and increased microvessel formation. Similar results were observed when rat

neonatal skeletal myoblasts were mixed with the fibrin glue. However, vessel density was greatest in the fibrin-alone group [52, 53]. Fibrin scaffolds have been most frequently used as a cell platform to test delivery of adipose-derived MSCs, bone marrow cells, ESC-derived cardiac progenitors, human iPSC-derived ECs, smooth muscle cells and CMs, a native cardiac cell population, umbilical cord blood MSCs, ESCs, and MSCs in different in vivo MI models (Table 2). Results have shown improved preservation of cardiac function post-MI, increased cell retention

**Table 6** Detailed data of clinical trials in progress or completed using different natural scaffolds

Scaffold material	Study name	Cell lines and/or other components	State	Follow-up	Main results/objectives	References/clinical trial identifier
Collagen	MAGNUM	Human mononuclear bone marrow stem cells	Completed with 20 patients	10 months	No adverse related events, 1 point reduction of New York Heart Association functional class, 26 % reduction of LV end-diastolic volume, 22 % improvement of LV filling deceleration time, 50 % increase of scar thickness, 26 % enhancement of EF	[37, 38]
Fibrin	ESCORT	hESC	Recruiting patients	-	Study the number and nature of adverse events (clinical/biological abnormalities, arrhythmias and cardiac or extracardiac tumors). Test feasibility and efficacy of the scaffold in cardiac function recovery	NCT02057900
Alginate	AUGMENT-HF	-	Completed with 6 patients	3 months	Increase of Kansas City Cardiomyopathy Questionnaire from 39.4 to 74, number of patients with New York Heart Association class III/IV reduced from 6 to 1. No improves in EF and LV end-diastolic and end-systolic volumes	[111]
Gelatin	ALCADIA	Human cardiac-derived stem cells+bFGF	Completed with 6 patients	6 months	12 % increase in LV EF, 3.3 % decrease of infarct size, maximal aerobic exercise capacity enhanced by 4.5 ml/kg/min	[145], NCT00981006
SIS	-	-	Enrolling participants (by invitation only)	-	Evaluate scaffold safety and beneficial effects in heart function	NCT02139189

bFGF basic fibroblast growth factor, EF ejection fraction, hESC human embryonic stem cell, LV left ventricle/left ventricular, SIS small intestine submucosa

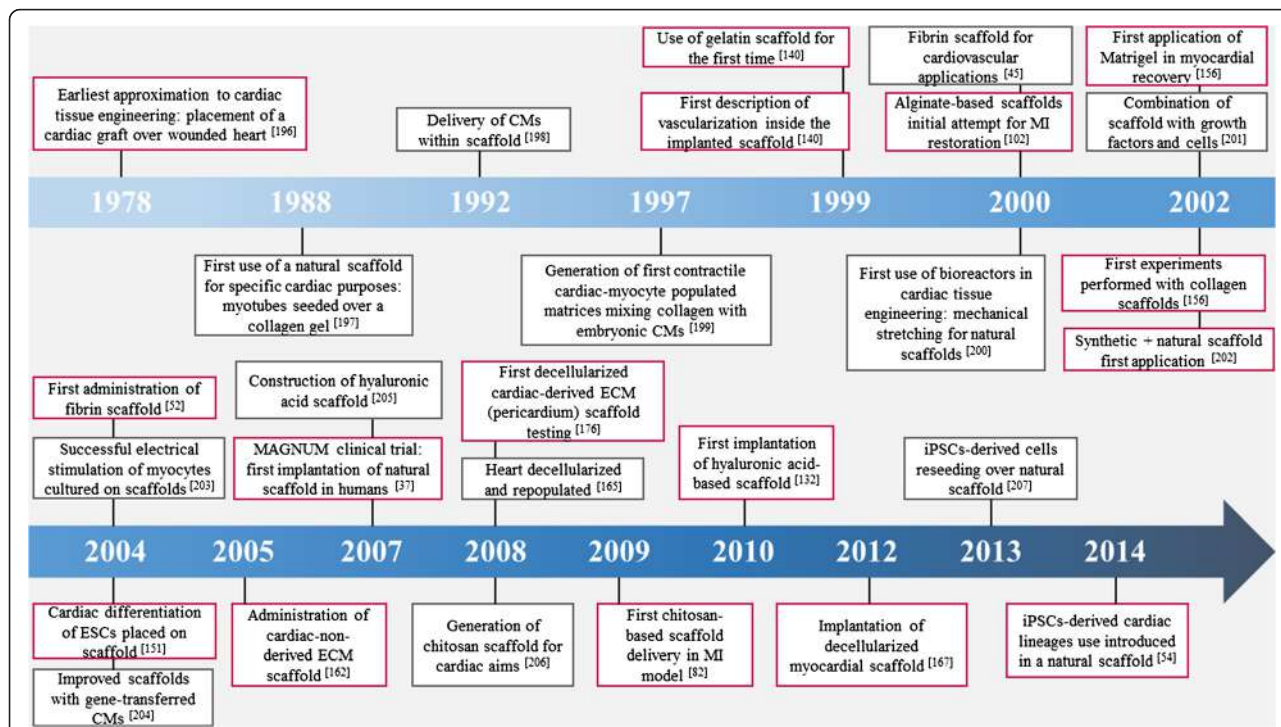


**Fig. 1** Milestones in the history of natural scaffolds in cardiac tissue engineering for myocardial infarction treatment. Boxes with a grey outline refer to natural scaffolds used in vitro. Boxes with a red outline indicate in vivo highlights related to natural scaffold application. CM cardiomyocyte, ECM extracellular matrix, ESC embryonic stem cell, iPSC induced pluripotent stem cell, MI myocardial infarction

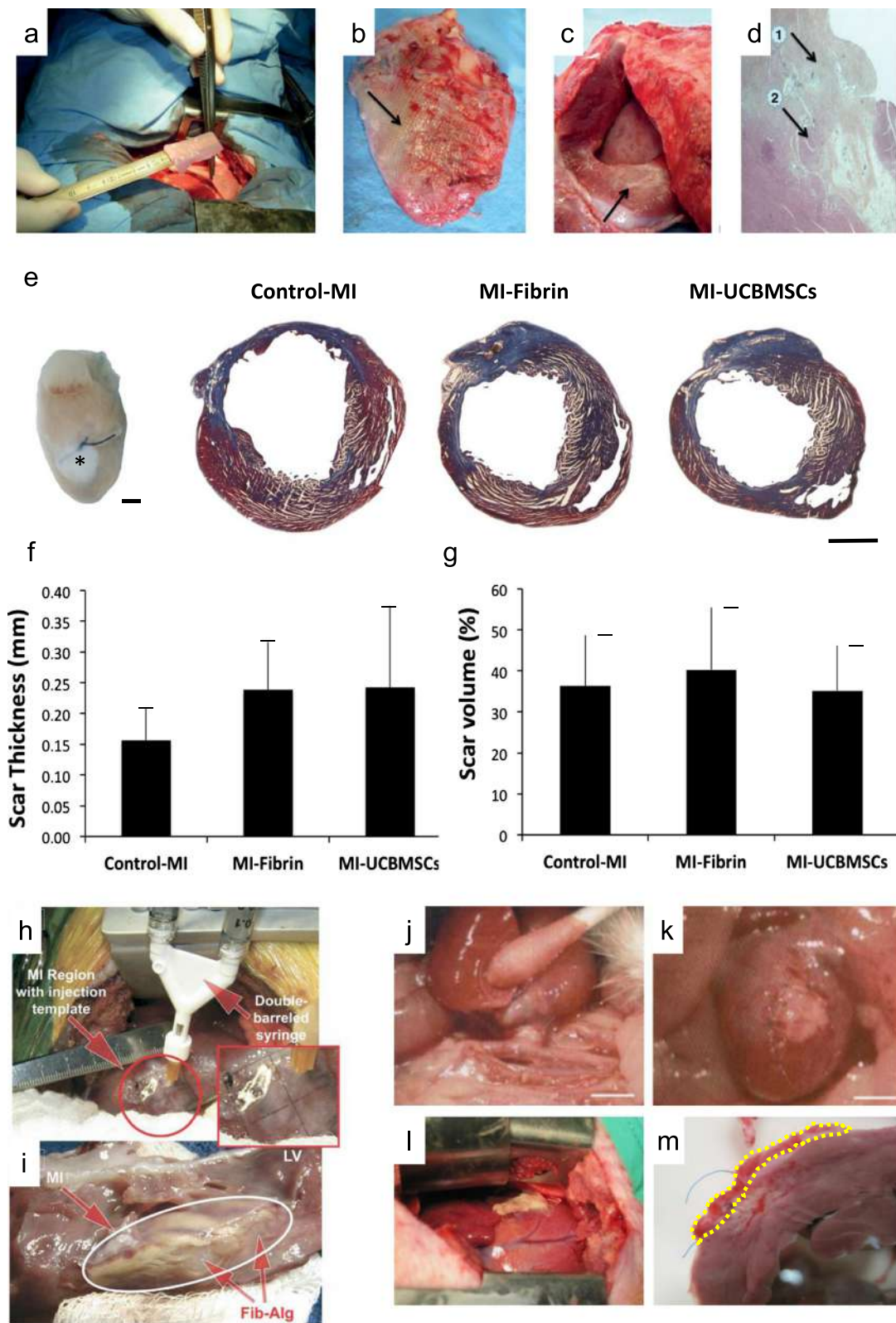


**Fig. 2** (See legend on next page.)



(See figure on previous page.)

**Fig. 2** Natural scaffolds for cardiac tissue engineering. Combined surgical procedure using CorCap ventricular constraint device and collagen scaffold implantation in a sheep ischemic model for myocardial repair and ventricular chamber remodeling. **a** Introduction of the cell-seeded collagen matrix between the heart and the CorCap polyester device (Shafy et al. [32]). **b** Autopsy at 3 months showing the CorCap mesh covering both ventricles (arrow) (Shafy et al. [32]). **c** Left ventricular infarct scar (arrow) (Shafy et al. [32]). **d** Histology at 3 months of the ischemic/reperfused myocardium. Arrows show the mixed configuration: patchy fibrosis (1) and subnormal myocardium (2) (Shafy et al. [32]). **a–c** Reproduced, with permission, from [32]. **e–g** Three-dimensional engineered fibrin-cell patches implanted over infarcted myocardium wounds in mice. **e** Representative photograph of a mouse heart excised from a post-myocardial infarction (MI) animal at 4 weeks post-implantation of an adhesive fibrin-based patch composed of human umbilical cord blood mesenchymal stem cells (UCBMSCs) (asterisk). Images of Masson's trichrome staining of cross-sections from the three groups of post-infarcted animals. Scale bar = 1 mm (Roura et al. [62]). Histograms represent the percentage of LV scar thickness (**f**) and volume (**g**) (Roura et al. [62]). **e–g** Reproduced, with permission, from [62]. **h** Intraoperative injection of the fibrin–alginate composite was performed using a 2 × 2 cm template with injection sites arrayed at 0.5 cm intervals within the region of MI. **i** At necropsy, the fibrin–alginate (Fib–Alg) could be visualized as amorphous densities within the MI region (LV left ventricle) (Mukherjee et al. [115]); reproduced, with permission, from [115]. **j, k** Heterotopic heart transplant surgery and hyaluronan-based scaffold (HYAFF<sup>®</sup>11) implantation in the rat MI model. The heart–lung block was carefully excised, the left lung removed, and the cardiac infarction induced by left descending coronary artery ligation on the bench (Fiumana et al. [126]); reproduced, with permission from [126]. **j** The allograft was transplanted by end-to-side anastomosis of the aorta to the abdominal aorta of the recipient. Scale bar = 5 mm (Fiumana et al. [126]). **k** The bioengineered HYAFF<sup>®</sup>11 was introduced into a pouch made in the thickness of the ventricular wall of the heterotopic heart at the level of the post-infarction scar. Scale bar = 5 mm (Fiumana et al. [126]). **l, m** Myocardial bioprosthesis implantation in porcine infarcted hearts; reproduced, with permission, from [174]. **l** A myocardial bioprosthesis, composed by decellularized human pericardium embedded with RAD16-I and mediastinal adipose tissue-derived progenitor cells, was implanted over the ischemic myocardium (Prat-Vidal et al. [174]). **m** Transversal heart section of a treated pig with the attached bioprosthesis indicated (dotted yellow line) (Prat-Vidal et al. [174])

and, in some cases, reduced infarct size and enhanced angiogenesis [54–63]. The study by Ye and colleagues [54] used ECs, smooth muscle cells and CMs derived from iPSCs—the first in vivo use of iPSC-derived cells—and reported highly improved cardiac function (EF approximately 52 %) and contractility (thickening fractions of approximately 20 % and approximately 7 % at the border and infarct zone, respectively) compared with infarcted animals without treatment after 4 weeks [54]. Alternatively, fibrin scaffolds were enhanced by thymosin  $\beta$ 4 encapsulation, which increased cell survival almost threefold, protected against hypoxic conditions, and improved cardiac function and wall thickness measured 28 days after MI [64].

Experiments in rat and non-human primate MI models, where a fibrin patch was applied with human ESC-derived cardiac progenitor cells, have produced convincing data that have led to approval of a first-in-human clinical trial (Tables 2 and 6) [65]. The study, entitled ‘Transplantation of human embryonic stem-cell derived progenitors in severe heart failure (ESCORT)’ (NCT02057900), is currently in phase 1 and recruiting participants. Its objective is to investigate the feasibility and safety of fibrin scaffolds combined with cells for treating patients with MI.

In order to increase the intrinsic low fibrin stiffness, fibrin scaffolds can be used in combination with other materials (Table 2) [47]. For example, when fibrin was mixed with the synthetic material poly(ether)urethane-polydimethylsiloxane or with poly(lactide-co-glycolide), in vitro experiments showed that it formed a suitable microenvironment which mimicked native myocardium, enhanced cell proliferation, and contributed to proper cell differentiation towards a cardiac lineage [66, 67].

Also, a hybrid polyethylene glycol/fibrin scaffold was combined with stromal cell-derived factor (SDF)-1 $\alpha$ , a key factor in injured myocardium cell mobilization, and administered (without cells) into a mouse MI model [68]. This treatment promoted c-kit<sup>+</sup> cell homing and increased EF and fractional shortening (FS), measured at 28 days post-MI. Nevertheless, no angiogenic activity was assessed and no significative reduction of infarct area was observed [68].

In another approach, fibrin scaffold combined with cardiac ECM provided acceptable cell viability, and its administration was feasible [69]. This scaffold was tested in vivo with mesenchymal progenitor cells injected into a nude rat MI model (Table 2). At 28 days after scaffold implantation in the infarcted myocardium, treated rats showed increased angiogenesis and cell migration, and preserved cardiac function compared with untreated animals. Next, the same scaffold was enhanced by preconditioning the MSCs with transforming growth factor (TGF)- $\beta$  [70]. This treatment induced greater cell migration and vasculogenesis compared with MSCs not preconditioned with TGF- $\beta$ , but no additional improvements in LV functionality were observed [70]. Therefore, combining fibrin with other materials could adjust the properties of fibrin itself and, to some extent, recreate the local stiffness, composition and fiber network present in the native myocardium, representing a good and plausible possibility for regenerating infarcted myocardium.

#### Chitosan

Chitosan, a natural linear polymer obtained by chitin deacetylation, has been widely used for tissue replacement [71–76]. This natural material displays high biocompatibility and biodegradability and has the capacity

to combine with conductive materials to improve electrical signal transmission and/or with other biomaterials [77, 78]. Additionally, chitosan was shown to be capable of high growth factor retention and strong cellular receptor adhesion due to its hydrophilicity [79, 80]; these properties make chitosan a suitable scaffold material for injured myocardial repair.

An *in vivo* study in a rat MI model also demonstrated that brown ATDSCs differentiated into cardiac lineage cells when applied into the infarcted area inside a chitosan scaffold, as they increased cardiac troponin I and T and connexin 43 expression (Table 3) [81]. This treatment resulted in improved cardiac function and contractility (better EF, FS and LV end-diastolic pressure), reduced infarct size and fibrotic area, and a remarkable increase in vessel density, measured 28 days after scaffold implantation [81]. Interestingly, ATDSCs partially contributed to this new vessel formation, showing von Willebrand factor- and  $\alpha$ -smooth muscle actin-positive labeling. Altogether, chitosan plus ATDSCs appears to be a valuable approach for myocardial restoration.

Thermo-sensitive chitosan hydrogel (which polymerizes at body temperature) has been widely used with positive effects (Table 3). A rat MI model was treated with a thermo-sensitive chitosan hydrogel, combined with ESCs, nuclear transferred ESCs, or fertilization-derived ESCs, and exhibited enhanced heart function, increased vascularization in the damaged myocardium, and reduced infarct areas, measured 4 weeks after hydrogel transplantation. Importantly, implanted cells seemed to slightly differentiate towards CMs, smooth muscle cells and ECs [82, 83]. Temperature-sensitive chitosan was also applied, enriched with basic fibroblast growth factor (bFGF), in a rat MI model for 28 days [84]. The results included improved cardiac function, significant reductions in infarct size and fibrotic area (9.27 % and 22.91 %, respectively), and 2.7-fold more blood vessels in treated animals compared with controls. Another option is to modify the temperature-responsive chitosan scaffold by adding RoY peptide, a factor involved in cell proliferation, survival, and angiogenesis under hypoxic conditions. This construct exhibited satisfactory post-MI results, including infarct size reduction, angiogenesis promotion, ventricular wall thickness and cardiac function improvement [85].

When mixed with natural materials, chitosan scaffolds acquire other properties that favor cell maturation, adhesion, and scaffold coupling with the host myocardium (Table 3). Several natural materials have been tested with chitosan in cardiac tissue engineering, including myocardial ECM [86], alginate [77, 87], gelatin [88], collagen [89], and silk fibroin [90]. Chitosan mixed with alginate with MSCs was tested *in vivo* in a rat MI model, where it promoted improved cardiac function, new blood vessel

formation, cellular survival, and cell proliferation [77]. Remarkably, the chitosan–alginate scaffold applied alone, without cell incorporation, provided the same beneficial effects in the damaged area after implantation. Of interest, the analysis of biodegradability displayed a low scaffold degradation rate, determined 8 weeks post-administration. However, an alginate-only scaffold provided better results in terms of wall thickness, LV expansion, and cardiac function than the chitosan–alginate scaffold, reducing the beneficial impact of the chitosan–alginate combination [87]. Moreover, despite the variety of possibilities and good results obtained with chitosan scaffolds, it is necessary to evaluate their effects in a large animal MI model to ensure that the described effects can be realized in a large cardiovascular system, similar to human. Therefore, further experimentation is mandatory to obtain satisfactory results combining chitosan with other materials.

### Alginate

Alginate is an anionic linear polysaccharide which can form a hydrogel through ionic crosslinking with divalent cations (mainly  $\text{Ca}^{2+}$ ) [91, 92]. This property also enables incorporation and retention of cells and proteins inside the hydrogel; thus, it can be used as a scaffold for tissue regeneration [93, 94]. Interestingly, the implantation of highly purified alginate, free of protein contaminants, resulted in a complete absence of adverse host immune response [95, 96]. Moreover, alginate mechanical behavior is easily modifiable by different crosslinking or by changing the molecular weight distribution to match the intrinsic stiffness of host myocardium [97].

Administration of alginate scaffolds alone resulted in significant improvements in cardiac function and increased scar thickness in various MI models, including rat [98], dog [99], and swine [100] (Table 3). Remarkably, alginate application was followed by the total absence of arrhythmias or thrombus formation [98, 100] and the replacement of the applied scaffold by connective tissue and myofibroblasts [98]. Pig models have enabled cell-filled scaffolds to be generated and tested *in vivo* with promising outcomes, including significant decreases in LV dilatation and LV mass, and a 53 % and 34 % increase in scar thickness and wall thickness, respectively [100]. Alginate scaffold hydrophilicity and porosity facilitate the incorporation and retention of cultured CMs on the scaffold (>90 % retention). These retained cells exhibited spontaneous contraction, which indicated that alginate platforms are suitable for cell seeding [101]. In a rat MI model, an alginate scaffold seeded with rat fetal cardiac cells enhanced neovascularization, preserved FS and end diastolic and systolic internal diameters, and promoted the formation of myofibers and cardiac gap junctions, measured 65 days after scaffold implantation [102]. On the other hand, not-so-positive results were obtained *in vivo* with human ESCs

or embryonic bodies; neither new myocardium formation nor cardiomyogenic differentiation was observed in the implanted scaffold [103]. Additionally, treated animals developed LV dilatation and no ESCs were retained in the scarred area 3 weeks after injection. Nonetheless, the alginate composite did not trigger a deleterious immune response and FS increased by 4 % [103]. So far, fetal cardiac cells appear to be the most suitable cell source to continue investigation with alginate scaffolds.

Alginate scaffolds are typically modified, through integrin-mediated binding, with the addition of an arginine-glycine-aspartate sequence (the RGD peptide) derived from ECM proteins involved in cell adhesion, proliferation, migration, survival, and differentiation [104]. Promising results have been obtained in vivo (Table 3). A rat MI model showed remarkable enhancement of FS, LV dimension, angiogenesis, and LV wall thickness measured 5 weeks post-administration of modified scaffolds [105]. The RGD–alginate scaffold also promoted angiogenesis more effectively than the unmodified alginate scaffold in the animal MI model ( $12.6 \pm 2.7$  versus  $9.3 \pm 4.2$  arteriole/ $\text{mm}^2$ , respectively). Although not considered a scaffold, similar effects were described for RGD–alginate microbeads with encapsulated MSCs, evaluated 10 weeks after MI [106]. Nevertheless, in a comparative study, the unmodified scaffolds promoted better LV FS, greater fractional area changes, more attenuation of LV dilatation, a lower LV expansion index, and greater scar thickness increases compared with RGD-modified alginate scaffolds [107]. Thus, further experiments should be performed in vivo to elucidate under what conditions RGD has beneficial effects over unmodified alginate scaffolds and its effectiveness in improving cardiac function in order to determine the added value of RGD introduction.

For cardiac regeneration, alginate scaffolds have also been supplemented with two growth factors, insulin growth factor (IGF)-1, with cytoprotective effects, and hepatocyte growth factor (HGF), which is related to mainly anti-fibrotic and pro-angiogenic processes [108, 109]. When evaluated 4 weeks after MI, IGF/HGF plus alginate microbeads injected into the infarcted myocardium preserved scar thickness, reduced infarct expansion and fibrosis, enhanced angiogenesis and reduced cell apoptosis (Table 3) [110]. It would be interesting to test different combinations of growth factors with alginate scaffolds to determine whether they improve cardiac recovery post-infarction, and to explore the possibility of synergistic effects.

The ongoing AUGMENT-HF clinical trial (Tables 3 and 6), a first-in-human study, aims to evaluate the effects of alginate injection (Algisyl-LVR) in patients with dilated cardiomyopathy. An early follow-up at 3 months demonstrated the feasibility and safety of the scaffold injection. Cardiac evaluations demonstrated that patients who

received treatment tended to show enhanced cardiac function and LV size, but no statistical differences were achieved compared with controls; in addition, treated patients showed significant improvements in quality of life and clinical status [111]. Future measurements at longer post-treatment times are expected to show significant beneficial effects on LV function parameters.

Alginate has been mixed with other biomaterials, including hyaluronic acid [112], gelatin [113], elastin [114], chitosan [77], fibrin [115], synthetic polymers [116], and omentum [117]. However, the effects of these combinations in pre-clinical MI models have not been fully defined in most cases (Table 3). One exception is the alginate plus Matrigel patch, assembled with neonatal rat cardiac cells and a growth factor supplement (IGF-1, vascular endothelial growth factor (VEGF), and SDF-1) [117]. This patch was pre-cultured in rat omentum for 1 week to induce pre-vascularization inside the patch prior to its engraftment into the infarcted area of a MI rat model. Then, 28 days after treatment with the pre-vascularized alginate–Matrigel scaffold, rats showed reduced LV dilatation, enhanced local angiogenesis, mechanical and electrical coupling with the host myocardium, limited LV dilatation, and improved cardiac function, preserving FS and diminishing LV dimensions [117]. In another study, a rat MI model was treated with polypyrrole added to alginate, then evaluated 5 weeks after the MI [118]. These rats exhibited increased angiogenesis and enhanced myofibroblast population recruitment compared with a control group treated with phosphate-buffered saline, and the presence of polymer was confirmed in the infarcted area with a non-associated inflammatory response. However, no functional benefits were assessed, and infarct size remained invariable after treatment, thus limiting its clinical application [118].

#### **Hyaluronic acid**

Hyaluronic acid, a glycosaminoglycan component of the ECM, plays key roles in cell behavior and attachment, wound healing, inflammatory responses, tumor development, and connective tissue joining [119]. In addition to applications in damaged myocardium, hyaluronic acid-based scaffolds have been successfully used for space filling and wound repair, bone and cartilage restoration, nerve and brain regeneration, cell and protein delivery, and soft tissue and smooth muscle repair [120].

The molecular weight of the hyaluronic acid construct highly impacts infarcted myocardium recovery and its beneficial effects on cardiac function because the unit size affects mechanical properties, angiogenic processes, and other effects of the biomaterial itself [121, 122] (Table 3). A comparative study of scaffolds that comprised 50 kDa, 130 kDa, and 170 kDa hyaluronic acid

units demonstrated that scaffolds composed of 50 kDa units showed the best effects, reducing apoptosis and infarct size from 29.4 % to 3.72 % and increasing ventricular wall thickness fourfold and heart function (LV end-diastolic pressure and Tau-weiss parameter), as analyzed 28 days after therapy [121]. These results were consistent with previous studies that described lower apoptotic rates and higher angiogenic activities with scaffolds composed of low molecular weight hyaluronic acid [122, 123]. Additionally, this study also evaluated the effects of the 50 kDa hyaluronic acid scaffold, alone or loaded with VEGF, on cardiac regeneration in both sub-acute and chronic MI animal models [121]. The effects on myocardial recovery and angiogenesis were similar between groups; therefore, VEGF addition did not act synergistically to achieve a significantly different outcome and hyaluronic acid is responsible for the described cardiac benefits [121].

In some cases, hyaluronic acid scaffolds have been seeded with cells of different lineages, mainly pluripotent stem cells, committed to differentiating into endothelial or cardiomyogenic phenotypes, which would reinforce the proangiogenic and regenerative impact of the scaffold. Taking advantage of hyaluronic acid scaffolds, which promoted high adhesion and proliferation, low apoptosis, paracrine factor gene expression, and regulated cell differentiation [124], experiments were conducted to assess the effectiveness of bone marrow mononuclear cells (BMMNCs) [124, 125] and bone marrow MSCs [126] for treating MI (Table 3). The combined action of the scaffold seeded with rat BMMNCs was tested in a rat MI model [124]. After 28 days, rats that received the scaffold plus BMMNCs exhibited less apoptosis, improved EF and LV internal dimensions, indicators of cardiac function, reduced macrophage and neutrophil infiltration and scar size, and enhanced angiogenesis compared with untreated rats. Interestingly, the BMMNC-seeded hyaluronic acid scaffold also induced better CM survival and cardiac output and smaller scars than an injection of BMMNCs alone or the hyaluronic acid scaffold alone. Furthermore, the hyaluronic acid scaffold promoted BMMNC differentiation towards ECs [124]. These outcomes were confirmed with porcine BMMNCs seeded in hyaluronic acid scaffolds and implanted into infarcted pigs; wall thickness, EF (increased 3.3 %), LV pressures and volumes and angiogenesis were improved while fibrotic area was reduced compared with untreated animals and animals treated with BMMNCs alone or hyaluronic acid scaffolds alone [125]. Alternatively, when harvested in an esterified hyaluronic acid scaffold, rat bone marrow MSCs promoted an increase in angiogenesis and a reduction in fibrosis in a rat MI model [126]. MSCs of porcine origin were also tested in swine [127]. In that study, the scaffold plus cell

treatment induced a lower CD3 inflammatory response, less fibrosis by reducing the total amount of collagen I and III, and less cardiac cell degeneration compared with no treatment or treatment with a similar level of scaffold alone (except for inflammation attenuation) [127]. When bone marrow cells and SDF-1 $\alpha$  were used to fill a methacrylated hyaluronic acid scaffold, bone marrow cell homing into the myocardium was increased approximately 8.5-fold, a higher value than that exhibited with administration of cells alone [128]. Nevertheless, despite all the data collected for bone marrow MSCs with hyaluronic acid scaffolds, function and other cardiac function parameters were not evaluated. Hence, the favorable results obtained with bone marrow MSC in hyaluronic acid scaffolds need to be corroborated in other studies to confirm these promising outcomes.

Other factors and compounds have been combined with hyaluronic acid scaffolds (Table 3). In one study, a recombinant tissue inhibitor of matrix metalloproteinases (rTIMP), which leads to adverse cardiac remodeling and fibrosis when deleted [129], was attached to the acid hyaluronic scaffold [130]. In infarcted pigs, the rTIMP plus scaffold treatment resulted in higher EF and wall thickness, less ventricular dilatation, reduced remodeling due to metalloproteinase activity, and a 50 % smaller infarcted area compared with untreated animals and compared with animals treated with the scaffold alone [130]. Thus, the addition of rTIMP seems to have had a positive and extra effect on cardiac regeneration post-MI. In another study, Gelin-S, a compound that enhances cell adhesion, was attached to the hyaluronic acid scaffold [131]. When applied to infarcted rats, this construct increased EF by 18.2 %, FS by 12.3 %, and neovascularization and decreased collagen deposition by approximately 50 %; however, this treatment was not compared with hyaluronic acid scaffold alone [131]. Finally, methacrylated hyaluronic acid scaffolds with different biomaterial stiffness (7.7 and 43 kPa) were injected into the infarcted myocardium to evaluate the impact of different mechanical properties on cardiac function and myocardial regeneration. Compared with controls, only the 43 kPa scaffold increased ventricular wall thickness and significantly decreased the infarct area (by approximately 20 %), although cardiac output and EF remained unchanged [132]. A similar study investigated the same hyaluronic acid scaffolds (approximately 7 kPa and 35 to 40 kPa) but in the context of low or high scaffold sensitivity to hydrolytic degradation [133]. Eight weeks after treatment, all scaffolds increased vascularization and inflammatory responses, but the ventricular wall thickened with more stable scaffolds, while LV systolic volume decreased with higher stiffness scaffolds. Thus, the results suggested that prolonged

material stabilization provided the best benefits for myocardial restoration. The finding that optimal results were achieved with stiff scaffolds emphasized the notion that the mechanical properties of scaffolds play an important role in cardiac regeneration [133].

For cardiac repair, several supplementary materials have been combined with hyaluronic acid to improve scaffold properties, including gelatin [134], silk fibroin [135], chitosan plus silk fibroin [136], and butyric acid plus retinoic acid [137] (Table 3). A gelatin plus hyaluronic acid scaffold seeded with cardiosphere-derived cells was evaluated at 3 weeks after MI induction [134]. This construct induced increases in EF (approximately 17 %), viable tissue, wall thickness, and angiogenesis, enhanced cell survival, and promoted the uncompromised differentiation of cardiosphere-derived cells into endothelial and cardiac lineages compared with untreated animals and animals treated with cardiosphere-derived cells or scaffold alone [134]. Similarly, when silk fibroin plus hyaluronic acid scaffolds populated with bone marrow MSCs were injected into animal MI models, they reduced the LV inner diameter and inflammatory responses, and enhanced FS compared with animals with MI and without treatment [135]. Compared with untreated animals or animals treated with bone marrow MSCs alone, animals receiving the scaffold plus cells also exhibited increases in LV wall thickness, cell survival, alpha myosin heavy chain expression (a cardiac contractility protein), and release of VEGF, bFGF, and HGF paracrine factors. These results indicated that combining scaffold and cells produced synergistic effects [135]. In another study, a rat MI model was treated with chitosan plus silk fibroin plus hyaluronic acid scaffolds without cells [136]. At 8 weeks post-treatment, rats showed improved heart function parameters, increased angiogenesis, and upregulated expression of VEGF, bFGF, and HGF paracrine factors. These results suggested that the scaffold without cell seeding had positive effects on cardiac function, being a suitable scaffold for different cell harvesting and for determining scaffold effects independently of cellular ones [136]. Finally, infarcted pigs were treated with a combination of human placenta-derived MSCs placed in a hyaluronic acid scaffold that had been modified with butyric and retinoic acids [137]. This treatment resulted in increased FS, wall thickness, and blood vessel density compared with phosphate-buffered saline or cell-only treatment. Importantly, the collagen content was reduced after treatment, and scar size and fibrotic area core were reduced by 64 % and 44.6 %, respectively. Of interest, this study performed a proteomic analysis of the LV border zone; the group with the implanted scaffold displayed higher proteomic homology (45 %) to the healthy myocardium compared with the other groups, which corroborated the regenerative effects and functional recovery provided by scaffold delivery [137].

## Gelatin

Gelatin is a natural polymer that can be produced from bone, skin, or tendon collagen by partial hydrolysis with acid or alkaline solutions. Gelatin is highly biocompatible and biodegradable, has low antigenicity and can be produced and prepared at relatively low cost [138, 139]. These properties make gelatin ideal for use as a natural scaffold in cardiac tissue engineering.

Despite the small number of *in vivo* studies that used gelatin scaffolds alone or combined with other materials, some promising results are likely to encourage their future application (Table 4). For example, a gelatin mesh seeded with fetal rat ventricular cells was evaluated 5 weeks after implantation into infarcted rat hearts [140]. This construct showed good engraftment to the host myocardium, and the presence of blood vessels indicated vascularization of the cardiac graft. Furthermore, the cells rearranged to form connections between them, and exhibited spontaneous contractions. However, lack of functional or structural cardiac improvements dissuades further application of this particular combination [140]. The scaffold effects could be enhanced by adding erythropoietin, a glycoprotein hormone used in the treatment of anemia in patients with heart failure, which reduces ventricular hypertrophy and increases EF [141]. In a rabbit MI model, gelatin plus erythropoietin scaffolds were applied 20 minutes after inducing the MI [142]. At 14 days and 2 months after treatment, the treated rabbits displayed reduced LV diastolic and systolic dimensions, infarct size, and fibrosis, and enhanced EF, FS, and capillary density in the infarct border zone. In another study, bFGF was added to gelatin scaffolds for treating a rat MI model [143]. After 2 and 4 weeks of treatment, these animals showed lower CM apoptotic rates, higher arteriole densities, higher expansion indexes, greater infarcted/non-infarcted wall thickness ratios, and smaller infarct sizes in comparison with untreated animals (except for infarct size, which was only reduced after 2 weeks). Compared with scaffold alone, the scaffold plus bFGF treatment induced, at 2 weeks post-treatment, smaller infarct areas, lower expansion indexes, lower apoptotic rates, and higher arteriole numbers; at 4 weeks, more arterioles and capillaries and less apoptosis were observed [143]. In a pig MI model, bFGF was combined with the gelatin scaffold, with or without either human bone marrow-derived MSCs or human cardiosphere-derived cells [144]. When the three groups were compared (scaffold plus bFGF, scaffold plus bFGF plus human bone marrow-derived MSCs, and scaffold plus bFGF plus human cardiosphere-derived cells), optimal results were achieved with the combination of scaffold plus bFGF plus human cardiosphere-derived cells, which displayed the highest EF increase (approximately 9 %) and infarct volume reduction (approximately 3.7 %), the greatest wall

motion index variation (approximately 13 %), and the most differentiation into CMs. Thus, the results confirmed that bFGF and the cells had additive effects [144].

Collectively, the outstanding results obtained with bFGF and MSCs in a gelatin scaffold have led to its implementation in humans. In a phase I clinical trial, ALCADIA (AutoLogous human CArdiac-Derived stem cell to treat Ischemic cArDiomyopathy, NCT00981006), patients with MI were treated with a combination of gelatin hydrogel embedded with human cardiac-derived stem cells and bFGF (Tables 4 and 6). Of six treated patients, one was excluded due to graft occlusion. Of the five remaining patients, only one experienced heart failure worsening. Evaluation after 6 months revealed a 12 % increase in the LV EF, an improvement in maximum aerobic exercise capacity, and a 3.3 % decrease in infarct size [145]. Nevertheless, a larger number of patients and a longer follow-up are required to evaluate treatment effectiveness.

### Matrigel

Matrigel is a biomaterial derived from ECM secreted by Engelbreth-Holm-Swarm mouse sarcoma cells [146]—whose composition has not been fully defined—which resembles and mimics myocardial ECM. Matrigel promoted angiogenesis both *in vitro* with ECs and *in vivo* [147]; thus, it appears to be a good candidate biomaterial for constructing a scaffold for cellular support.

Matrigel (without cells) was administered to infarcted myocardium to evaluate its effects on cardiac function and tissue regeneration (Table 4). In a comparative study, fibrin, collagen, or Matrigel was injected into a rat MI model [147]. Matrigel enhanced capillary density but did not improve cardiac function. On top of that, only collagen significantly increased myofibroblast infiltration compared with untreated animals [147]. Conversely, another study injected Matrigel alone into infarcted rats [148]. At 4 weeks after treatment, increases were observed in LV EF (improvement of 22.7 %), contractility (a 24.5 % enhancement of LV pressure decline), infarct wall thickness, angiogenesis, and recruitment of c-kit<sup>+</sup> and CD43<sup>+</sup> stem cells to the myocardium.

Taking advantage of the described regenerative effects of Matrigel, several studies have mixed Matrigel with different cell types (Table 4). In one study, Matrigel was combined with adipose-derived stromal cells and injected into a rat MI model [149]. At 4 weeks after the MI, treated rats showed increased normalized EF, less LV akinesis, increased heart contractility, and a smaller infarct area. ESCs have also been used extensively. In one study, a mixture of mouse ESC plus Matrigel scaffold improved FS, preserved LV wall thickness, and increased expression of the cardiac gap junction marker connexin 43 in comparison with untreated animals and animals treated with Matrigel alone [150]. Consistent

with this study, a Matrigel plus mouse ESC combination was administered to infarcted rats and evaluated 2 weeks post-treatment [151]. Treated rats exhibited increased FS and LV wall thickness and reduced LV dilatation compared with untreated rats. In addition, introduced cells expressed the cardiac markers connexin 43 and  $\alpha$ -sarcomeric actin. In spite of these results, a comparison between Matrigel alone and Matrigel with cells showed non-significant differences in terms of FS, LV wall thickness, and prevention of LV dilatation, outlining the role of Matrigel in myocardial restoration [151]. Human ESC-derived CMs seeded onto a Matrigel scaffold and supplemented with a pro-survival cocktail were evaluated in a rat MI model [152]. Treated rats showed significantly enhanced cell engraftment in the scarred area compared with Matrigel plus cells alone. Additionally, at 4 weeks after treatment, the pro-survival cocktail complementation also revealed better results with regard to ventricular dilatation, FS, EF, and infarct zone wall thickness [152]. Conversely, when bone marrow-derived MSCs were mixed with Matrigel, only modest results were observed; there was no improvement in FS, EF, or other cardiac function parameters, hampering future research with these cells [153]. To sum up, extensive good results obtained with ESCs could lead next to *in vivo* testing in a porcine MI model, prior to clinical trials.

In most cases, Matrigel was combined with collagen, the primary structural protein of the ECM (Table 4). When these two compounds were combined with rat cardiomyoblasts, significant improvements were observed regarding cell survival, cardiac function, and LV wall thickness compared with controls and collagen-matrix treated animals [154]. When a growth factor, either VEGF or bFGF, was added to the Matrigel plus collagen scaffold, no other positive cardiac effects were obtained compared with Matrigel plus collagen alone [154]. Nevertheless, modest results were obtained in a similar study that also employed a Matrigel plus collagen cellular scaffold, but filled with myoblasts [155]. In this study, only a significant FS improvement was detected in infarcted rats after 4 weeks of treatment compared with pre-treatment (42 % versus 33 %); no significant effects were observed in other cardiac parameters. Moreover, the group that received the Matrigel plus collagen scaffold displayed a larger adverse immunological response than untreated rats or rats treated with fibrin [155]. In another study, cardiac myocytes were harvested and incorporated into a Matrigel plus collagen scaffold for treating a rat MI model [156]. This treatment did not provide any benefit in terms of heart function or LV wall thickness. Nonetheless, the generated scaffold was able to couple with the host myocardium, preserved contraction and sarcomere integrity, and presented high levels of neovascularization and innervation after

engraftment. It is important to point out that although connexin 43 and cadherin expression were demonstrated, further investigation is necessary to show complete electrical and mechanical coupling [156]. The addition of CMs to a Matrigel plus collagen scaffold promoted FS and increased anterior wall thickness [157]. Also, at 4 weeks after MI induction, rats that received this treatment maintained sarcomere integrity and structure and exhibited decreased LV end-systolic volume in comparison with untreated infarcted rats or animals treated with either cells or scaffold alone [157]. Administration of neonatal rat heart cells supported by the Matrigel plus collagen scaffold also led to electrical assembly with the myocardium, diminished ventricular dilatation, enhanced ventricular wall thickening, and increased FS area [158]. Data collected suggest that a Matrigel–collagen scaffold combined with cardiomyoblasts or CMs should have a high impact in future investigations.

#### **Decellularized extracellular matrix**

ECM consists of a dynamic blend of structural and functional molecules that are secreted by cells, with a slightly different composition depending on tissue source [159]. This physiological cellular support platform gives cells a suitable microenvironment; it guides cellular proliferation, attachment, differentiation, migration, and viability by providing different signals or cues [160, 161]. Hence, the isolation of an intact ECM would supply cellular support that best matched the native or physiological extracellular environment [18]. For ECM extraction, it is necessary to remove all cellular and nuclear content, in a process called decellularization, and the acellular ECM must maintain its integrity and architecture [3, 162]. Successful tissue decellularization requires the careful selection of physical, chemical, and enzymatic agents that can remove cellular material without disrupting the ECM. Decellularizing agents have variable effects on ECM structure and composition; any negative distortion of the matrix organization or integrity may affect its ability to support cells [163, 164]. Therefore, maximal cell removal and ECM property retention are mandatory for obtaining optimal ECM for use as a cellular scaffold. Among the essential properties to maintain, correct three-dimensional organization of the ECM helps in proper cell adhesion, differentiation, survival, and integration [18, 160, 164]. Closely related to this, mechanical properties are tightly associated with fiber arrangement and three-dimensional architecture, which in turn affects ECM scaffold coupling with the host myocardium and its synchronous contraction.

To date, many organs and tissues have been completely decellularized, including heart valves, myocardium, pericardium, lung, pancreas, kidney, liver, mammary gland,

and nerve [163, 164]. For cardiac tissue engineering, myocardial ECM possesses the best properties; it can exactly recreate the microenvironment of the native myocardium. Thus, it favors coupling with host cardiac tissue when engrafted in the infarcted zone. The first heart decellularization was performed in 2008 by antegrade coronary perfusion with sodium dodecyl sulfate. The generated acellular organ preserved the primary matrix proteins, vascular architecture, valves, and chambers; when it was seeded with CMs and ECs, the recellularized heart exhibited contraction [165].

Several studies have been performed *in vivo* using decellularized myocardium ECM scaffolds (Table 5). Local administration of decellularized myocardial ECM was used to treat the infarcted area in a rat MI model [166]. Six weeks after ECM injection, heart function was enhanced through an 8 % elevation in LV EF, a 1.2-fold increase in LV wall thickness, and a 1.3-fold reduction in the infarct expansion index [166]. In another study, similar improvements were achieved with decellularized myocardial ECM application in a rat MI model; the EF was preserved, a higher proportion of viable myocardium was achieved (1.7-fold higher compared with controls), and arrhythmias were completely absent [167]. These results were corroborated when the decellularized myocardial matrix was administered to a porcine MI model [168]. In that case, EF and contractility were enhanced, LV volumes and fibrotic areas were reduced, and the proportion of endothelial muscle was increased. In addition, adverse side effects (ischemia, embolization, and altered heartbeat) were not detected in either pig or rat infarct models. These results ensured that scaffold delivery was a safe procedure; they also demonstrated that the ECM was highly degradable and biocompatible [168]. These promising results may open the door to repopulate decellularized myocardium with cells. A first attempt showed encouraging outcomes for future pre-clinical applications, even though they used a combination of decellularized myocardial ECM plus fibrin embedded with mesenchymal progenitor cells, and not the matrix alone plus cells [70]. Recently, our group has implanted a combination of decellularized porcine myocardial ECM (previously characterized and successfully recellularized *in vitro*) refilled with hydrogel and adipose tissue-derived progenitor cells (ATDPCs) in an infarcted porcine MI model [169] (Fig. 3). The scaffold remained in the damaged area 28 days after animals were sacrificed (Fig. 3f). Thus, this alternative scaffold is feasible and may provide new promising results using an acellular myocardial scaffold.

ECM derived from decellularized pericardium has also been widely used as a supportive scaffold for MI regeneration (Table 5). Pericardium ECM is a porous material that facilitates cellular retention and vascularization. It is

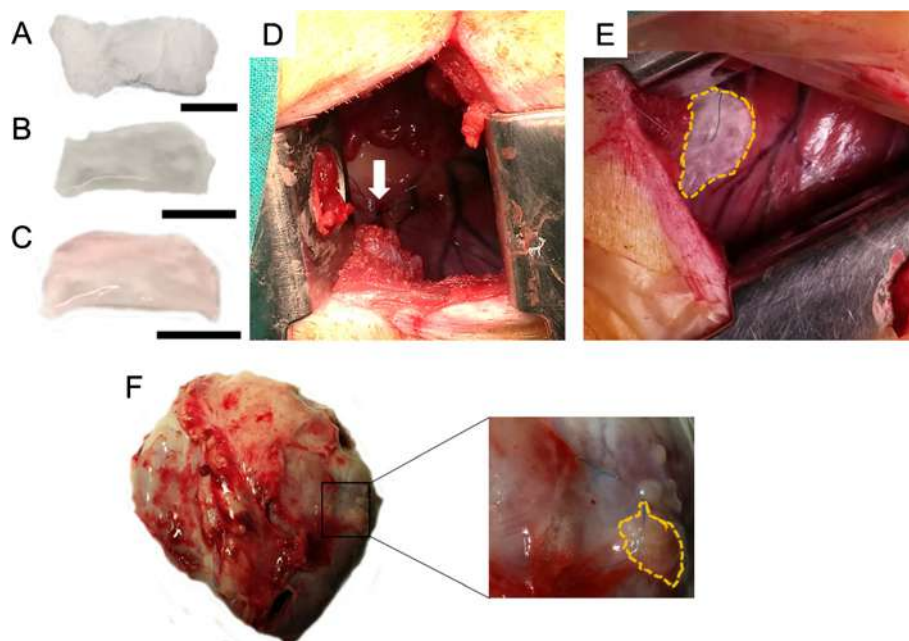


**Fig. 3** Engraftment of a decellularized myocardial ECM scaffold embedded with cells in a swine myocardial infarction model. **a** Lyophilized and gamma ultraviolet sterilized decellularized myocardial ECM scaffold. **b, c** Decellularized scaffold after the addition of peptide hydrogel (**b**) and porcine adipose tissue-derived progenitor cells (**c**). Scale bars = 1 cm. **d** Image of the myocardial infarction site, induced by double ligation in the first marginal branch of the circumflex artery (indicated with *white arrow*). **e** Reseeded decellularized scaffold placed over the injured myocardium. Scaffold is indicated with *yellow dotted lines*. **f** Presence of the implanted scaffold on the infarcted area in explanted hearts 28 days after sacrifice. The remaining scaffold is highlighted with *yellow dotted lines*

easy to perform pericardium resection during surgery and subsequently extract the ECM; moreover, there are no negative consequences [170, 171]. Pericardium properties are comparable among human individuals, and these similar characteristics permit low variability among samples [172]. In vitro results have demonstrated that pericardial ECM seems to resemble myocardial ECM in structure and microenvironment, retain infiltrated cells, and support cardiac differentiation [170, 173–175].

In one in vivo study, rat infarcted myocardium was patched with decellularized pericardium and bone marrow MSCs and evaluated 12 weeks after treatment. The results revealed improvements in LV FS and LV pressures, infarct area vasculogenesis, cardioprotective growth factor and cytokine secretion, and cell differentiation into smooth muscle cells or myofibroblasts [176]. Nearly the same improvements were described when a decellularized pericardium sandwiched between multilayered sheets of bone marrow MSCs was applied to a rat MI model, highlighting functional enhancements in FS and LV pressures [177]. The three-dimensional organization apparently showed correct porosity and pore size, facilitating interconnectivity. Both studies confirm the suitability of MSCs with decellularized pericardial ECM, enabling us to move forward to large animal model experiments. Another study evaluated

the synergistic effects of bFGF combined with decellularized pericardium, which displayed well-organized matrix fibers, for treating a rat MI model [178]. After injection, this combination resulted in higher bFGF retention and a 112 % higher number of functional blood vessels in treated rats compared with animals that did not receive bFGF and rats that received collagen alone, decellularized pericardium alone, bFGF alone, or bFGF combined with collagen. An increase in inflammation was observed, but this was attributed to bFGF, not to the decellularized pericardium, because injection of the latter alone did not show significant inflammation compared with saline-injected control groups [178]. When HGF was mixed with decellularized pericardium, treated rats showed significant prevention of LV remodeling, enhanced cardiac function (only fractional area change), and increased arteriole density [179]. Thus, it is imperative to continue investigating the use of growth factors to determine their effectiveness in heart function and structure recovery. Finally, when decellularized pericardium was assembled with RAD-16 peptidic hydrogel and ATDPCs in a swine MI model, infarct size was 36 % reduced and vascularization inside the scaffold was increased. Of note, the scaffold displayed non-disrupted fiber organization and a high in vitro biodegradability, losing about 70 % of the initial weight after 24 hours [174].



Other, unrelated cardiac ECMs have been used for cardiac restoration (Table 5). One of these is the acellular ECM derived from porcine small intestinal submucosa (SIS), which is highly biocompatible and mechanically modifiable. Injection of SIS alone in a mouse MI model provided good results: it maintained better LV geometry, reduced the infarcted area, and enhanced contractility and blood vessel density after treatment [180]. In a mouse MI model, treatment with SIS seeded with MSCs improved heart function (EF and LV diastolic and systolic dimensions), contractility, and angiogenesis, and attenuated wall thinning, LV enlargement and adverse immunological responses [181]. Notably, the SIS patch was partially degraded and the cells seeded on it seemed to differentiate into cardiac lineages because they expressed cardiac troponin T and  $\alpha$ -smooth muscle actin; however, no connexin 43 expression was detected. This combination was more effective than SIS administration without cells [181]. When SIS was enhanced with bFGF, treated rats displayed higher EF (55.3 % versus 35.1 %), greater prevention of LV remodeling by reducing LV end-diastolic volumes, and improved heart contraction compared with the untreated group. Of interest, non-enhanced SIS only improved cardiac contractility compared with controls [182]. Currently, a clinical trial (NCT02139189) has begun to recruit participants to test the feasibility and safety of an SIS matrix (also called CorMatrix) for treating damaged myocardium (Tables 5 and 6).

Another non-cardiac-derived ECM widely used is the acellular urinary bladder matrix (UBM; Table 5). Extracted from urinary bladder, it is basically composed of type IV collagen, laminin, and entactin [183]. As a scaffold for cardiac repair, a UBM patch was used to repair an excised portion of the myocardium in a dog model [184]. This treatment enhanced ventricular function compared with a synthetic matrix patch composed of Dacron; additionally, CMs were detected in the UBM patch area, which was not observed with Dacron. In another study in a pig MI model, administration of a UBM patch without cells increased myofibroblast recruitment and the presence of smooth muscle cells, reduced the inflammatory response, and limited thrombus expansion compared with treatment with an expanded polytetrafluoroethylene synthetic biomaterial [162]. Moreover, UBM scaffold was not distinguished from the myocardium. Nevertheless, no improvements in cardiac function, LV dilatation, or contractility were achieved [162]. In a similar study performed in dogs, UBM enhanced regional stroke work and systolic contraction by 3.7 % and 4.4 %, respectively [185]. Myocyte recruitment and proliferation, measured 8 weeks after treatment, were also increased. Interestingly, myocyte arrangement in the UBM scaffold was similar to that in the neighboring myocardium [185]. Finally, a comparative study was conducted on UBM patches embedded with

either spheroid-derived MSCs or unmanipulated MSCs in a dog MI model [186]. The results revealed that spheroid-derived cells provided better heart function and improved contractility, as assessed by regional stroke work, in comparison with unmanipulated MSCs. Myocytes present in the scaffold were correctly rearranged and showed an organized sarcomeric structure [186].

### Considerations and future perspectives

With all the collected data provided by the different studies, it is clear that engrafted scaffolds in the injured heart exert a beneficial effect over myocardium. In spite of not being the main point of this review, it is not fully understood how scaffolds promote the described regenerative effects and which mechanisms follow them. It has been described that a scaffold itself is capable of inducing new blood vessel and nerve fiber formation in swine myocardium, thus facilitating revascularization and reoxygenation of the hypoxic area and electrical coupling [187]. Probably, the local hypoxic environment in the infarcted area induces expression of vascular endothelial and platelet-derived growth factors, SDF-1 $\alpha$ , and macrophage chemotactic protein, promoting recruitment of circulating cells to vascularize the affected myocardium in a more favorable microenvironment provided by the scaffold [187, 188]. The addition of cells helps to reinforce this effect by secreting paracrine factors and synthesizing new endogenous ECM, which in turns mobilizes more cells, favoring myocardial regeneration.

Hence, scaffold biodegradability is a key parameter, as scaffolds should not be degraded quickly after engraftment so they can continue to supply a suitable platform for initial cell administration. However, scaffolds should be easily degradable to allow them to be replaced by the new endogenous matrix synthesized by the administered cells. Moreover, components and molecules derived from degradation have to be non-toxic and absorbable by the body. In the specific case of the natural scaffolds reviewed here, elements derived from degradation are biocompatible and naturally absorbable. In most studies, however, the biodegradability parameter has not been determined. In the work reviewed here, only a few have shown detailed information about scaffold degradation rates, with non-exact quantifications and without clear criteria for determining the degradation rate of the scaffolds [36, 87, 168, 174, 181]. Therefore, further investigation seems to be necessary for discerning the optimal scaffold degradability to accomplish a balance between enough time for enabling initial cell nesting and complete scaffold degradation to allow its proper substitution by newly synthesized cell matrix.

Tightly related to degradability, it is also of particular importance to assess changes in the preserved scaffold

matrix (if not degraded), or in the new endogenous matrix secreted by implanted cells, which replaces the scaffold. None of the reviewed studies performed an analysis of scaffold elements post-implantation, which is hard to do as the lack of scaffold or its total integration into the host tissue makes its isolation difficult. Scaffold composition analysis should help us to understand how these changes can affect myocardial regeneration, and how variations in scaffolds can regulate and direct the mechanisms behind these, which could also explain the mechanism by which scaffolds promote cardiac recovery.

Despite the promising results obtained in most pre-clinical studies, some issues and questions remain unresolved regarding cardiac tissue engineering and the use of natural scaffolds. First, few clinical trials have tested scaffolds with or without cells [37, 38, 111, 145] (NCT00981006, NCT02139189, and NCT02057900; Table 6), which limits the ability to translate procedures from pre-clinical studies to humans. In addition, few studies have been performed in large animal MI models. These animal models could provide more realistic expectations of possible effects in humans, because their cardiovascular systems are more closely related to the human system. It is very important to determine influences on LV function, adverse remodeling, and contractility in a similar cardiovascular system. It is also crucial to investigate inflammatory responses after scaffold injection or implantation. Because scaffold materials are typically xenogeneic or allogeneic, they might trigger inflammation and macrophage infiltration and this effect must be assessed prior to testing in humans. It is not meaningful to assess inflammatory responses in small animals because they lack human-like inflammatory responses [16]. Additionally, the absence of experimentation in large animal MI models becomes more relevant in applications where the scaffold incorporates cells, because the effects caused by cells may vary among different species. Special caution should be taken with ESCs or iPSCs because they tend to form teratomas; therefore, detailed follow-up should be conducted in large animal MI models before these treatments can be translated to clinical applications [189].

Second, long-term effects must also be evaluated to ensure maintenance of the positive effects provided by the scaffold. A study performed with synthetic scaffolds and myoblasts indicated that heart failure progression could be prevented and high numbers of cells were present after 9 months, but both effects were lost after 12 months [190]. The transitory nature of these effects, albeit using synthetic materials, should motivate new, longer studies to include several time points for evaluating scaffold properties, cell states, and cardiac function.

Finally, although several types of scaffolds and combinations of scaffolds with different cell types have been studied—and in most cases shown promising results—it

remains unclear what combination of materials, cells, and growth factors or other supplements might be optimal. Ideally, a scaffold should exactly match the cardiac matrix microenvironment and three-dimensional architecture, which would favor cell attachment, proliferation, and differentiation into cardiomyogenic lineages [17]. Nevertheless, it is highly difficult to achieve this because native cardiac ECM is composed of a mixture of different proteins, glycosaminoglycans, proteoglycans, and growth factors in discrete proportions, which are dispersed in a well-organized structure with a unique three-dimensional architecture [191, 192]. Moreover, the scaffold must mechanically couple with the host myocardium and beat synchronously [17]. Decellularized myocardial ECM could probably best accomplish these conditions, but procuring it requires a decellularization process that might alter its intrinsic properties [164]. The newly emerging technology of bioprinting may facilitate the resolution of these problems. This technique employs a three-dimensional bioprinter to generate a scaffold with a predefined pattern and a well-organized, specified structure. It mixes the selected materials in the chosen proportions and provides control over many parameters, such as porosity [193, 194]. For instance, a three-dimensional bioprinter was used to create small blood vessels from a pre-determined ratio of human adult aortic smooth cells, ECs, and dermal fibroblasts. These vessels were functional and sustained mechanical integrity for up to 28 days [195]. New insights gained over the next few years about ECM structure and composition will inform improvements in bioprinting technology to enable precise selections of elements and distributions based on the native myocardial pattern. This emergent technique may provide a means to achieve the goal of re-creating the myocardial ECM.

## Conclusion

Collectively, most recent advances in cardiac tissue engineering using natural scaffolds have shown promising results in myocardial regeneration after MI. These findings should facilitate the development of next-generation scaffolds with enhanced properties, either by adjusting scaffold microenvironments or by delimiting cell choices, thus enabling clinical translation of these newly developed scaffolds. Therefore, natural scaffolds are on the way to be finally implemented as a feasible and alternative MI therapy.

## Abbreviations

ATDPC: Adipose tissue-derived progenitor cells; ATDSC: Adipose tissue-derived stem cells; bFGF: Basic fibroblast growth factor; BMMNC: Bone marrow mononuclear cell; CM: Cardiomyocyte; EC: Endothelial cell; ECM: Extracellular matrix; EF: Ejection fraction; ESC: Embryonic stem cell; FS: Fractional shortening; HGF: Hepatocyte growth factor; IGF: Insulin growth factor; iPSC: Induced pluripotent stem cell; LV: Left ventricle/left ventricular; MI: Myocardial infarction; MSC: Mesenchymal stem cell; rTIMP: Recombinant tissue inhibitor of matrix metalloproteinases; Sca-1: Stem cell antigen-1; SDF: Stromal cell-derived factor;

SIS: Small intestine submucosa; TGF: Transforming growth factor; UBM: Urinary bladder matrix; VEGF: Vascular endothelial growth factor;  $\alpha$ -MHC: Alpha myosin heavy chain.

#### Competing interests

The authors declare that they have no competing interests.

#### Authors' contributions

IP-G performed the literature search, designed the manuscript and wrote the first draft of the manuscript. CP-V and AB-G designed the manuscript and participated in the manuscript redaction and correction. All authors read, revised and approved the final manuscript.

#### Acknowledgements

This work was supported by the Instituto de Salud Carlos III (Red de Investigación Cardiovascular (RIC; RD12/0042/0047), Red de Investigación en Terapia Celular-TerCel (RD12/0019/0029) and FIS-PI14/01682), Ministerio de Ciencia e Innovación (SAF-2011-30067-C02-01/02 and SAF-2014-59892), Fundació Privada Daniel Bravo Andreu, La Marató de TV3 (12/2232), Medical Sciences and Health Academy of Catalonia and Balearics, the Catalan Society of Cardiology and the Spanish Society of Cardiology.

#### Author details

<sup>1</sup>ICREC (Heart Failure and Cardiac Regeneration) Research Lab, Health Sciences Research Institute Germans Trias i Pujol (IGTP). Cardiology Service, Hospital Universitari Germans Trias i Pujol, 08916 Badalona, Barcelona, Spain. <sup>2</sup>Department of Medicine, Autonomous University of Barcelona (UAB), Barcelona, Spain.

Published online: 06 December 2015

#### References

- World Health Organization. The top ten causes of death. 2014. <http://www.who.int/mediacentre/factsheets/fs310/en/>. Accessed 16 Apr 2015.
- Mozaffarian D, Benjamin EJ, Go AS, Arnett DK, Blaha MJ, Cushman M, et al. Heart disease and stroke statistics—2015 update: a report from the American Heart Association. *Circulation*. 2015;131:e29–322.
- Gálvez-Montón C, Prat-Vidal C, Roura S, Soler-Botija C, Bayes-Genis A. Update: Innovation in cardiology (IV). Cardiac tissue engineering and the bioartificial heart. *Rev Esp Cardiol*. 2013;66:391–9.
- Segers VFM, Lee RT. Stem-cell therapy for cardiac disease. *Nature*. 2008;451:937–42.
- Schächinger V, Erbs S, Elsässer C, Haberbosch W, Hambrecht R, Hölschermann H, et al. Intracoronary bone marrow-derived progenitor cells in acute myocardial infarction. *N Engl J Med*. 2006;355:1210–21.
- Yamada S, Nelson TJ, Crespo-Diaz RJ, Perez-Terzic C, Liu XK, Miki T, et al. Embryonic stem cell therapy of heart failure in genetic cardiomyopathy. *Stem Cells*. 2008;26:2644–53.
- Higuchi T, Miyagawa S, Pearson JT, Fukushima S, Saito A, Tsuchimochi H, et al. Functional and electrical integration of induced pluripotent stem cell-derived cardiomyocytes in a myocardial infarction rat heart. *Cell Transplant*. 2015 [Epub ahead of print].
- Amado LC, Saliaris AP, Schuleri KH, St John M, Xie JS, Cattaneo S, et al. Cardiac repair with intramyocardial injection of allogeneic mesenchymal stem cells after myocardial infarction. *Proc Natl Acad Sci USA*. 2005;102:11474–9.
- Chen SL, Fang WW, Ye F, Liu YH, Qian J, Shan SJ, et al. Effect on left ventricular function of intracoronary transplantation of autologous bone marrow mesenchymal stem cell in patients with acute myocardial infarction. *Am J Cardiol*. 2004;94:92–5.
- Beltrami AP, Barlucchi L, Torella D, Baker M, Limana F, Chimenti S, et al. Adult cardiac stem cells are multipotent and support myocardial regeneration. *Cell*. 2003;114:763–76.
- Matsuura K, Honda A, Nagai T, Fukushima N, Iwanaga K, Tokunaga M, et al. Transplantation of cardiac progenitor cells ameliorates cardiac dysfunction after myocardial infarction in mice. *J Clin Invest*. 2009;119:2204–17.
- Ye L, Haider HK, Jiang S, Ling LH, Ge R, Law PK, et al. Reversal of myocardial injury using genetically modulated human skeletal myoblasts in a rodent cryoinjured heart model. *Eur J Heart Fail*. 2005;7:945–52.
- Yoshioka T, Ageyama N, Shibata H, Yasu T, Misawa Y, Takeuchi K, et al. Repair of infarcted myocardium mediated by transplanted bone marrow-derived CD34+ stem cells in a nonhuman primate model. *Stem Cells*. 2005;23:355–64.
- Cai L, Johnstone BH, Cook TG, Tan J, Fishbein MC, Chen PS, et al. IFATS collection: Human adipose tissue-derived stem cells induce angiogenesis and nerve sprouting following myocardial infarction, in conjunction with potent preservation of cardiac function. *Stem Cells*. 2009;27:230–7.
- Li TS, Takahashi M, Ohshima M, Qin SL, Kubo M, Muramatsu K, et al. Myocardial repair achieved by the intramyocardial implantation of adult cardiomyocytes in combination with bone marrow cells. *Cell Transplant*. 2008;17:695–703.
- Vunjak-Novakovic G, Lui KO, Tandon N, Chien KR. Bioengineering heart muscle: a paradigm for regenerative medicine. *Annu Rev Biomed Eng*. 2011;13:245–67.
- Vunjak-Novakovic G, Tandon N, Godier A, Maidhof R, Marsano A, Martens TP, et al. Challenges in cardiac tissue engineering. *Tissue Eng Part B Rev*. 2010;16:169–87.
- Sarig U, Machluf M. Engineering cell platforms for myocardial regeneration. *Expert Opin Biol Ther*. 2011;11:1055–77.
- Gelse K, Pöschl E, Aigner T. Collagens—structure, function, and biosynthesis. *Adv Drug Deliv Rev*. 2003;55:1531–46.
- Xu Y, Dong S, Zhou Q, Mo X, Song L, Hou T, et al. The effect of mechanical stimulation on the maturation of TDSCs-poly(L-lactide-co-ε-caprolactone)/collagen scaffold constructs for tendon tissue engineering. *Biomaterials*. 2014;35:2760–72.
- Gautam S, Chou CF, Dinda AK, Potdar PD, Mishra NC. Surface modification of nanofibrous polycaprolactone/gelatin composite scaffold by collagen type I grafting for skin tissue engineering. *Mater Sci Eng C Mater Biol Appl*. 2014;34:402–9.
- Tedder ME, Simionescu A, Chen J, Liao J, Simionescu DT. Assembly and testing of stem cell-seeded layered collagen constructs for heart valve tissue engineering. *Tissue Eng Part A*. 2011;17:25–36.
- Zhao Y, Xu Y, Zhang B, Wu X, Xu F, Liang W, et al. In vivo generation of thick, vascularized hepatic tissue from collagen hydrogel-based hepatic units. *Tissue Eng Part C Methods*. 2010;16:653–9.
- Kijeńska E, Prabhakaran MP, Swieszkowski W, Kurzydowski KJ, Ramakrishna S. Electrospun bio-composite P(LLA-CL)/collagen I/collagen III scaffolds for nerve tissue engineering. *J Biomed Mater Res B Appl Biomater*. 2012;100:1093–102.
- Chiu LL, Reis LA, Momen A, Radisic M. Controlled release of thymosin  $\beta$ 4 from injected collagen-chitosan hydrogels promotes angiogenesis and prevents tissue loss after myocardial infarction. *Regen Med*. 2012;7:523–33.
- Blackburn NJ, Sofrenovic T, Kuraitis D, Ahmadi A, McNeill B, Deng C, et al. Timing underpins the benefits associated with injectable collagen biomaterial therapy for the treatment of myocardial infarction. *Biomaterials*. 2015;39:182–92.
- Serpooshan V, Zhao M, Metzler SA, Wei K, Shah PB, Wang A, et al. The effect of bioengineered acellular collagen patch on cardiac remodeling and ventricular function post myocardial infarction. *Biomaterials*. 2013;34:9048–55.
- Gaballa MA, Sunkomat JN, Thai H, Morkin E, Ewy G, Goldman S. Grafting an acellular 3-dimensional collagen scaffold onto a non-transmural infarcted myocardium induces neo-angiogenesis and reduces cardiac remodeling. *J Heart Lung Transplant*. 2006;25:946–54.
- Holladay CA, Duffy AM, Chen X, Sefton MV, O'Brien TD, Pandit AS. Recovery of cardiac function mediated by MSC and interleukin-10 plasmid functionalised scaffold. *Biomaterials*. 2012;33:1303–14.
- Araña M, Peña E, Abizanda G, Cilla M, Ochoa I, Gavira JJ, et al. Preparation and characterization of collagen-based ADSC-carrier sheets for cardiovascular application. *Acta Biomater*. 2013;9:6075–83.
- Araña M, Gavira JJ, Peña E, González A, Abizanda G, Cilla M, et al. Epicardial delivery of collagen patches with adipose-derived stem cells in rat and minipig models of chronic myocardial infarction. *Biomaterials*. 2014;35:143–51.
- Shafy A, Fink T, Zachar V, Lila N, Carpentier A, Chachques JC. Development of cardiac support bioprostheses for ventricular restoration and myocardial regeneration. *Eur J Cardiothorac Surg*. 2013;43:1211–9.
- Mokashi SA, Guan J, Wang D, Tchanchaleishvili V, Brigham M, Lipsitz S, et al. Preventing cardiac remodeling: the combination of cell-based therapy and cardiac support therapy preserves left ventricular function in rodent model of myocardial ischemia. *J Thorac Cardiovasc Surg*. 2010;140:1374–80.
- Maureira P, Marie PY, Yu F, Poussier S, Liu Y, Groubatch F, et al. Repairing chronic myocardial infarction with autologous mesenchymal stem cells engineered tissue in rat promotes angiogenesis and limits ventricular remodeling. *J Biomed Sci*. 2012;19:93.
- Xiang Z, Liao R, Kelly MS, Spector M. Collagen-GAG scaffolds grafted onto myocardial infarcts in a rat model: a delivery vehicle for mesenchymal stem cells. *Tissue Eng*. 2006;12:2467–78.

36. Shi C, Li Q, Zhao Y, Chen W, Chen B, Xiao Z, et al. Stem-cell-capturing collagen scaffold promotes cardiac tissue regeneration. *Biomaterials*. 2011;32:2508–15.
37. Chachques JC, Trainini JC, Lago N, Masoli OH, Barisani JL, Cortes-Morichetti M, et al. Myocardial assistance by grafting a new bioartificial upgraded myocardium (MAGNUM clinical trial): one year follow-up. *Cell Transplant*. 2007;16:927–34.
38. Chachques JC, Trainini JC, Lago N, Cortes-Morichetti M, Schussler O, Carpentier A. Myocardial Assistance by Grafting a New Bioartificial Upgraded Myocardium (MAGNUM trial): clinical feasibility study. *Ann Thorac Surg*. 2008;85:901–8.
39. Reis LA, Chiu LL, Wu J, Feric N, Laschinger C, Momen A, et al. Hydrogels with integrin-binding angiopoietin-1-derived peptide, QHREDGS, for treatment of acute myocardial infarction. *Circ Heart Fail*. 2015;8:333–41.
40. Ravichandran R, Venugopal JR, Sundarajan S, Mukherjee S, Ramakrishna S. Cardiogenic differentiation of mesenchymal stem cells on elastomeric poly (glycerol sebacate)/collagen core/shell fibers. *World J Cardiol*. 2013;26:28–41.
41. Xu G, Wang X, Deng C, Teng X, Suuronen EJ, Shen Z, et al. Injectable biodegradable hybrid hydrogels based on thiolated collagen and oligo(acryloyl carbonate)-poly(ethylene glycol)-oligo(acryloyl carbonate) copolymer for functional cardiac regeneration. *Acta Biomater*. 2015;15:55–64.
42. Mosesson MW, Siebenlist KR, Meh DA. The structure and biological features of fibrinogen and fibrin. *Ann N Y Acad Sci*. 2001;936:11–30.
43. Ye L, Zimmermann WH, Garry DJ, Zhang J. Patching the heart: cardiac repair from within and outside. *Circ Res*. 2013;113:922–32.
44. Barsotti MC, Felice F, Balbarini A, Di Stefano R. Fibrin as a scaffold for cardiac tissue engineering. *Biotechnol Appl Biochem*. 2011;58:301–10.
45. Ye Q, Zünd G, Benedikt P, Jockenhoevel S, Hoerstrup SP, Sakyama S, et al. Fibrin gel as a three dimensional matrix in cardiovascular tissue engineering. *Eur J Cardiothorac Surg*. 2000;17:587–91.
46. Jockenhoevel S, Zünd G, Hoerstrup SP, Chalabi K, Sachweh JS, Demircan L, et al. Fibrin gel—advantages of a new scaffold in cardiovascular tissue engineering. *Eur J Cardiothorac Surg*. 2001;19:424–30.
47. Linnes M, Ratner BD, Giachelli CM. A fibrinogen based precision microporous scaffold for tissue engineering. *Biomaterials*. 2007;28:5298–306.
48. Rowe SL, Lee S, Stegemann JP. Influence of thrombin concentration on the mechanical and morphological properties of cell-seeded fibrin hydrogels. *Acta Biomater*. 2007;3:59–67.
49. Wiesel JW. Structure of fibrin: impact on clot stability. *J Thromb Haemost*. 2007;5:116–24.
50. Ahmed TAE, Dare EV, Hincke M. Fibrin: a versatile scaffold for tissue engineering applications. *Tissue Eng Part B Rev*. 2008;14:199–215.
51. Bensaïd W, Triffitt JT, Blanchat C, Oudina K, Sedel L, Petite H. A biodegradable fibrin scaffold for mesenchymal stem cell transplantation. *Biomaterials*. 2003;24:2497–502.
52. Christman KL, Fok HH, Sievers RE, Fang Q, Lee RJ. Fibrin glue alone and skeletal myoblasts in a fibrin scaffold preserve cardiac function after myocardial infarction. *Tissue Eng*. 2004;10:403–9.
53. Christman KL, Vardanian AJ, Fang Q, Sievers RE, Fok HH, Lee RJ. Injectable fibrin scaffold improves cell transplant survival, reduces infarct expansion, and induces neovascularization in ischemic formation. *JACC*. 2004;44:654–60.
54. Ye L, Chang YH, Xiong Q, Zhang P, Zhang L, Somasundaram P, et al. Cardiac repair in a porcine model of acute myocardial infarction with human induced pluripotent stem cell-derived cardiovascular cells. *Cell Stem Cell*. 2014;15:750–61.
55. Bagó JR, Soler-Botija C, Casani L, Aguilar E, Alieva M, Rubio N, et al. Bioluminescence imaging of cardiomyogenic and vascular differentiation of cardiac and subcutaneous adipose tissue-derived progenitor cells in fibrin patches in a myocardium infarct model. *Int J Cardiol*. 2013;169:288–95.
56. Nakamuta JS, Danoviz ME, Marques FLN, dos Santos L, Becker C, Gonçalves GA, et al. Cell therapy attenuates cardiac dysfunction post myocardial infarction: effect of timing, routes of injection and a fibrin scaffold. *PLoS One*. 2009;4:e6005.
57. Xiong Q, Hill KL, Li Q, Suntharalingam P, Mansoor A, Wang X, et al. A fibrin patch-based enhanced delivery of human embryonic stem cell-derived vascular cell transplantation in a porcine model of postinfarction LV remodeling. *Stem Cells*. 2011;29:367–75.
58. Sun CK, Zhen YY, Leu S, Tsai TH, Chang LT, Sheu JJ, et al. Direct implantation versus platelet-rich fibrin-embedded adipose-derived mesenchymal stem cells in treating rat acute myocardial infarction. *Int J Cardiol*. 2014;173:410–23.
59. Bellamy V, Vanneau V, Bel A, Nemetalla H, Emmanuelle Boitard S, Farouz Y, et al. Long-term functional benefits of human embryonic stem cell-derived cardiac progenitors embedded into a fibrin scaffold. *J Heart Lung Transplant*. 2014. doi:10.1016/j.healun.2014.10.008.
60. Wendel JS, Ye L, Zhang P, Tranquillo RT, Zhang JJ. Functional consequences of a tissue-engineered myocardial patch for cardiac repair in a rat infarct model. *Tissue Eng Part A*. 2014;20:1325–35.
61. Roura S, Bagó JR, Soler-Botija C, Pujal JM, Gálvez-Montón C, Prat-Vidal C, et al. Human umbilical cord blood-derived mesenchymal stem cells promote vascular growth in vivo. *PLoS One*. 2012;7:e49447.
62. Roura S, Soler-Botija C, Bagó JR, Lluçà-Vallderas A, Fernández M, Gálvez-Montón C, et al. Post-infarction functional recovery driven by a three-dimensional engineered fibrin patch comprised of human umbilical cord blood-derived mesenchymal stem cells. *Stem Cells Transl Med*. 2015. In press.
63. Liu J, Hu Q, Wang Z, Xu C, Wang X, Gong G, et al. Autologous stem cell transplantation for myocardial repair. *Am J Physiol Heart Circ Physiol*. 2004;287:H501–11.
64. Ye L, Zhang P, Duval S, Su L, Xiong Q, Zhang J. Thymosin  $\beta$ 4 increases the potency of transplanted mesenchymal cells for myocardial repair. *Circulation*. 2013;128:532–41.
65. Menasché P, Vanneau V, Fabreguettes JR, Bel A, Tosca L, Garcia S, et al. Towards a clinical use of human embryonic stem cell-derived cardiac progenitors: a translational experience. *Eur Heart J*. 2015;36:743–50.
66. Lisi A, Briganti E, Ledda M, Losi P, Grimaldi S, Marchese R, et al. A combined synthetic-fibrin scaffold supports growth and cardiomyogenic commitment of human placental derived stem cells. *PLoS One*. 2012;7:e34284.
67. Sreerekha PR, Menon D, Nair SV, Chennazhi KP. Fabrication of electrospun poly (lactide-co-glycolide)-fibrin multiscale scaffold for myocardial regeneration in vitro. *Tissue Eng Part A*. 2013;19:849–59.
68. Zhang G, Nakamura Y, Wang X, Hu Q, Suggs LJ, Zhang J. Controlled release of stromal cell-derived factor-1 $\alpha$  in situ increases c-kit + cell homing to the infarcted heart. *Tissue Eng*. 2007;13:2063–71.
69. Williams C, Budina E, Stoppel WL, Sullivan KE, Emani SM, et al. Cardiac extracellular matrix-fibrin hybrid scaffolds with tuneable properties for cardiovascular tissue engineering. *Acta Biomaterialia*. 2015;14:84–95.
70. Godier-Furnémont AFG, Martens TP, Koeckert MS, Wan L, Parks J, Arai K, et al. Composite scaffold provides a cell delivery platform for cardiovascular repair. *Proc Natl Acad Sci U S A*. 2011;108:7974–9.
71. Revi D, Paul W, Anilkumar TV, Sharma CP. Chitosan scaffold co-cultured with keratinocyte and fibroblast heals full thickness skin wounds in rabbit. *J Biomed Mater Res A*. 2014;102:3273–81.
72. Guzmán R, Nardecchia S, Gutiérrez MC, Ferrer ML, Ramos V, del Monte F, et al. Chitosan scaffolds containing calcium phosphate salts and rhBMP-2: in vitro and in vivo testing for bone tissue regeneration. *PLoS One*. 2014. doi:10.1371/journal.pone.0087149.
73. Gao J, Liu R, Wu J, Liu Z, Li J, Zhou J, et al. The use of chitosan based hydrogel for enhancing the therapeutic benefits of adipose-derived MSCs for acute kidney injury. *Biomaterials*. 2012;33:3673–81.
74. Feng ZQ, Chu X, Huang NP, Wang T, Wang Y, Shi X, et al. The effect of nanofibrous galactosylated chitosan scaffolds on the formation of rat primary hepatocyte aggregates and the maintenance of liver function. *Biomaterials*. 2009;30:2753–63.
75. Xiao W, Hu XY, Zeng W, Huang JH, Luo ZZ. Rapid sciatic nerve regeneration of rats by a surface modified collagen-chitosan scaffold. *Injury*. 2013;44:941–6.
76. Liu Z, Wang H, Wang Y, Lin Q, Yao A, Cao F, et al. The influence of chitosan hydrogel on stem cell engraftment, survival and homing in the ischemic myocardial microenvironment. *Biomaterials*. 2012;33:3093–106.
77. Ceccaldi C, Bushkalova R, Alfarano C, Lairez O, Calise D, Bourin P, et al. Evaluation of polyelectrolyte complex-based scaffolds for mesenchymal stem cell therapy in cardiac ischemia treatment. *Acta Biomater*. 2014;10:901–11.
78. Martins AM, Eng G, Caridade SG, Mano JF, Reis RL, Vunjak-Novakovic G. Electrically conductive chitosan/carbon scaffolds for cardiac tissue engineering. *Biomacromolecules*. 2014;15:635–43.
79. Tsuchiya N, Sato S, Kigami R, Kawano E, Takane M, Arai Y, et al. Effect of a chitosan sponge impregnated with platelet-derived growth factor on bone augmentation beyond the skeletal envelope in rat calvaria. *J Oral Sci*. 2014;56:23–8.
80. Hussain A, Collins G, Yip D, Cho CH. Functional 3-D cardiac co-culture model using bioactive chitosan nanofiber scaffolds. *Biotechnol Bioeng*. 2013;110:637–47.
81. Wang H, Shi J, Wang Y, Yin Y, Wang L, Liu J, et al. Promotion of cardiac differentiation of brown adipose derived stem cells by chitosan hydrogel for repair after myocardial infarction. *Biomaterials*. 2014;35:3986–98.
82. Lu WN, Lü SH, Wang HB, Li DX, Duan CM, Liu ZQ, et al. Functional improvement of infarcted heart by co-injection of embryonic stem cells

- with temperature-responsive chitosan hydrogel. *Tissue Eng Part A*. 2009;15:1437–47.
83. Lu S, Wang H, Lu W, Liu S, Lin Q, Li D, et al. Both the transplantation of somatic cell nuclear transfer- and fertilization-derived mouse embryonic stem cells with temperature-responsive chitosan hydrogel improve myocardial performance in infarcted rat hearts. *Tissue Eng Part A*. 2010;16:1303–15.
  84. Wang H, Zhang X, Li Y, Ma Y, Zhang Y, Liu Z, et al. Improved myocardial performance in infarcted rat heart by co-injection of basic fibroblast growth factor with temperature-responsive chitosan hydrogel. *J Heart Lung Transplant*. 2010;29:881–7.
  85. Shu Y, Hao T, Yao F, Qian Y, Wang Y, Yang B, et al. RoY peptide-modified chitosan-based hydrogel to improve angiogenesis and cardiac repair under hypoxia. *ACS Appl Mater Interfaces*. 2015;7:6505–17.
  86. Pok S, Benavides OM, Hallal P, Jacot JG. Use of myocardial matrix in a chitosan-based full-thickness heart patch. *Tissue Eng Part A*. 2014;20:1877–87.
  87. Deng B, Shen L, Wu Y, Shen Y, Ding X, Lu S, et al. Delivery of alginate-chitosan hydrogel promotes endogenous repair and preserves cardiac function in rats with myocardial infarction. *J Biomed Mater Res A*. 2015;103:907–18.
  88. Pok S, Myers JD, Madhally SV, Jacot JG. A multi-layered scaffold of a chitosan and gelatin hydrogel supported by a PCL core for cardiac tissue engineering. *Acta Biomater*. 2013;9:5630–42.
  89. Chiu LL, Janic K, Radisic M. Engineering of oriented myocardium on three-dimensional micropatterned collagen-chitosan hydrogel. *Int J Artif Organs*. 2012;35:237–50.
  90. Yang MC, Wang SS, Chou NK, Chi NH, Huang YY, Chang YL, et al. The cardiomyogenic differentiation of rat mesenchymal stem cells on silk fibroin-polysaccharide cardiac patches in vitro. *Biomaterials*. 2009;30:3757–65.
  91. Bidarra SJ, Barrias CC, Granja PL. Injectable alginate hydrogels for cell delivery in tissue engineering. *Acta Biomater*. 2014;10:1646–62.
  92. Wee S, Gombotz WR. Protein release from alginate matrices. *Adv Drug Deliv Rev*. 1998;4:267–85.
  93. Moshaverinia A, Xu X, Chen C, Akiyama K, Snead ML, Shi S. Dental mesenchymal stem cells encapsulated in an alginate hydrogel co-delivery microencapsulation system for cartilage regeneration. *Acta Biomater*. 2013;9:9343–50.
  94. Wang L, Shansky J, Borselli C, Mooney D, Vandenburgh D. Design and fabrication of a biodegradable, covalently crosslinked shape-memory alginate scaffold for cell and growth factor delivery. *Tissue Eng Part A*. 2012;18:2000–7.
  95. Ménard M, Dusseault J, Langlois G, Baille WE, Tam SK, Yahia L'H, et al. Role of protein contaminants in the immunogenicity of alginates. *J Biomed Mater Res B Appl Biomater*. 2010;93:333–40.
  96. Orive G, Ponce S, Hernández RM, Gascón AR, Igartua M, Pedraz JL. Biocompatibility of microcapsules for cell immobilization elaborated with different type of alginates. *Biomaterials*. 2002;23:3825–31.
  97. Augst AD, Kong HJ, Mooney DJ. Alginate hydrogels as biomaterials. *Macromol Biosci*. 2006;7:623–33.
  98. Landa N, Miller L, Feinberg MS, Holbova R, Shachar M, Freeman I, et al. Effect of injectable alginate implant on cardiac remodeling and function after recent and old infarcts in rat. *Circulation*. 2008;117:1388–96.
  99. Sabbah HN, Wang M, Gupta RC, Rastogi S, Ilisar I, Sabbah MS, et al. Augmentation of left ventricular wall thickness with alginate hydrogel implants improves left ventricular function and prevents progressive remodeling in dogs with chronic heart failure. *JACC Heart Fail*. 2013;1:252–8.
  100. Leor J, Tuvia S, Guetta V, Manczur F, Castel D, Willenz U, et al. Intracoronary injection of in situ forming alginate hydrogel reverses left ventricular remodeling after myocardial infarction in swine. *J Am Coll Cardiol*. 2009;8:1014–23.
  101. Dar A, Shachar M, Leor J, Cohen S. Optimization of cardiac cell seeding and distribution in 3D porous alginate scaffolds. *Biotechnol Bioeng*. 2002;80:305–12.
  102. Leor J, Aboulaia-Etzion S, Dar A, Shapiro L, Barbash IM, Battler A, et al. Bioengineered cardiac grafts: a new approach to repair the infarcted myocardium? *Circulation*. 2000;102:1156–61.
  103. Leor J, Gerecht S, Cohen S, Miller L, Holbova R, Ziskind A, et al. Human embryonic stem cell transplantation to repair the infarcted myocardium. *Heart*. 2007;93:1278–84.
  104. Ruoslahti E. RGD and other recognition sequences for integrins. *Annu Rev Cell Dev Biol*. 1996;12:697–715.
  105. Yu J, Gu Y, Du KT, Mihardja S, Sievers RE, Lee RJ. The effect of injected RGD modified alginate on angiogenesis and left ventricular function in chronic rat infarct model. *Biomaterials*. 2009;30:751–6.
  106. Yu J, Du KT, Fang Q, Gu Y, Mihardja SS, Sievers RE, et al. The use of human mesenchymal stem cells encapsulated in RGD modified alginate microspheres in the repair of myocardial infarction in the rat. *Biomaterials*. 2010;31:7012–20.
  107. Tsur-Gang O, Ruvinov E, Landa N, Holbova R, Feinberg MS, Leor J, et al. The effects of peptide-based modification of alginate on left ventricular remodeling and function after acute myocardial infarction. *Biomaterials*. 2009;30:189–95.
  108. Li Q, Li B, Wang X, Leri A, Jana KP, Liu Y, et al. Overexpression of insulin-like growth factor-1 in mice protects from myocyte death after infarction, attenuating ventricular dilatation, wall stress, and cardiac hypertrophy. *J Clin Invest*. 1999;100:1991–9.
  109. Wang Y, Ahmad N, Wani MA, Ashraf M. Hepatocyte growth factor prevents ventricular remodeling and dysfunction in mice via Akt pathway and angiogenesis. *J Mol Cell Cardiol*. 2004;37:1041–52.
  110. Ruvinov E, Leor J, Cohen S. The promotion of myocardial repair by the sequential delivery of IGF-1 and HGF from an injectable alginate biomaterial in a model of acute myocardial infarction. *Biomaterials*. 2011;32:565–78.
  111. Lee RJ, Hinson A, Helgerson A, Bauernschmitt R, Sabbah HN. Polymer-based restoration of left ventricular mechanics. *Cell Transplant*. 2013;22:529–33.
  112. Dahlmann J, Krause A, Möller L, Kensah G, Möwes M, Diekmann A, et al. Fully defined in situ cross-linkable alginate and hyaluronidic hydrogels for myocardial tissue engineering. *Biomaterials*. 2013;34:940–51.
  113. Rosellini E, Cristallini C, Barbani N, Vozzi G, Giusti P. Preparation and characterization of alginate/gelatin blend films for cardiac tissue engineering. *J Biomed Mater Res A*. 2009;91:447–53.
  114. Chandy T, Rao GH, Wilson RF, Das GS. The development of porous alginate/elastin/PEG composite matrix for cardiovascular engineering. *J Biomater Appl*. 2003;17:287–301.
  115. Mukherjee R, Zavadzka JA, Saunders SM, McLean JE, Jeffords LB, Beck C, et al. Targeted myocardial microinjections of a biocomposite material reduces infarct expansion in pigs. *Ann Thorac Surg*. 2008;86:1268–76.
  116. Gnanaprakasam Thankam F, Muthu J, Sankar V, Kozhiparambil GR. Growth and survival of cells in biosynthetic poly vinyl alcohol-alginate IPN hydrogels for cardiac applications. *Colloids Surf B Biointerfaces*. 2013;107:137–45.
  117. Dvir T, Kedem A, Ruvinov E, Levy O, Freeman I, Landa N, et al. Prevascularization of cardiac patch on the omentum improves its therapeutic outcome. *Prot Natl Acad Sci U S A*. 2009;106:14990–5.
  118. Mihardja SS, Sievers RE, Lee RJ. The effect of polypyrrole on arteriogenesis in an acute rat infarct model. *Biomaterials*. 2008;29:4205–10.
  119. Toole BP. Hyaluronan: from extracellular glue to pericellular cue. *Nat Rev Cancer*. 2004;4:528–39.
  120. Collins MN, Birkinshaw C. Hyaluronic acid based scaffolds for tissue engineering—a review. *Carbohydr Polym*. 2013;92:1262–79.
  121. Yoon SJ, Hong S, Fang YH, Song M, Son KH, Son HS, et al. Differential regeneration of myocardial infarction depending on the progression of disease and the composition of biomimetic hydrogel. *J Biosci Bioeng*. 2014; 118:461–8.
  122. Slevin M, Kumar S, Gaffney J. Angiogenic oligosaccharides of hyaluronan induce multiple signaling pathways affecting vascular endothelial cell mitogenic and wound healing responses. *J Biol Chem*. 2002;277:41046–59.
  123. Wolf D, Schümann J, Koerber K, Kierner AK, Vollmar AM, Sass G, et al. Low-molecular-weight hyaluronic acid induces nuclear factor-kappaB-dependent resistance against tumor necrosis factor alpha-mediated liver injury in mice. *Hepatology*. 2001;34:535–47.
  124. Chen CH, Wang SS, Wei EI, Chu TY, Hsieh PC. Hyaluronan enhances bone marrow cell therapy for myocardial repair after infarction. *Mol Ther*. 2013;21:670–9.
  125. Chen CH, Chang MY, Wang SS, Hsieh PC. Injection of autologous bone marrow cells in hyaluronan hydrogel improves cardiac performance after infarction in pigs. *Am J Physiol Heart Circ Physiol*. 2014;306:H1078–86.
  126. Fiumana E, Pasquinelli G, Foroni L, Carboni M, Bonafè F, Orrico C, et al. Localization of mesenchymal stem cells grafted with a hyaluronan-based scaffold in the infarcted heart. *J Surg Res*. 2013;179:e21–9.
  127. Muscari C, Bonafè F, Martin-Suarez S, Valgimigli S, Valente S, Fiumana E, et al. Restored perfusion and reduced inflammation in the infarcted heart after grafting stem cells with a hyaluronan-based scaffold. *J Cell Mol Med*. 2013;17:518–30.
  128. Purcell BP, Elser JA, Mu A, Margulies KB, Burdick JA. Synergistic effects of SDF-1 $\alpha$  chemokine and hyaluronan acid release from degradable hydrogels on directing bone marrow derived cell homing to the myocardium. *Biomaterials*. 2012;33:7849–57.

129. Kassiri Z, Defamie V, Hariri M, Oudit GY, Anthwal S, Dawood F, et al. Simultaneous transforming growth factor-tumor necrosis factor activation and cross-talk cause aberrant remodeling response and myocardial fibrosis in Timp3-deficient heart. *J Biol Chem*. 2009;284:29893–904.
130. Eckhouse SR, Purcell BP, McGarvey JR, Lobb D, Logdon CB, Doviak H, et al. Local hydrogel release of recombinant TIMP-3 attenuates adverse left ventricular remodeling after experimental myocardial infarction. *Sci Transl Med*. 2014. doi:10.1126/scitranslmed.3007244.
131. Abdalla S, Makhoul G, Duong M, Chiu RC, Cecere R. Hyaluronic acid-based hydrogel induces neovascularization and improves cardiac function in a rat model of myocardial infarction. *Interact Cardiovasc Thorac Surg*. 2013;17:767–72.
132. Ifkovits JL, Tous E, Minakawa M, Morita M, Robb JD, Koomalsingh KJ, et al. Injectable hydrogel properties influence infarct expansion and extent of postinfarction left ventricular remodeling in an ovine model. *Proc Natl Acad Sci U S A*. 2010;107:11507–12.
133. Tous E, Ifkovits JL, Koomalsingh KJ, Shuto T, Soeda T, Kondo N, et al. Influence of injectable hyaluronic acid hydrogel degradation behavior on infarction-induced ventricular remodeling. *Biomacromolecules*. 2011;12:4127–35.
134. Cheng K, Blusztajn A, Shen D, Li TS, Sun B, Galang G, et al. Functional performance of human cardiosphere-derived cells delivered in an in situ polymerizable hyaluronan-gelatin hydrogel. *Biomaterials*. 2012;33:5317–24.
135. Chi NH, Yang MC, Chung TW, Chen JY, Chou NK, Wang SS. Cardiac repair achieved by bone marrow mesenchymal stem cells/silk fibroin/hyaluronic acid patches in a rat of myocardial infarction model. *Biomaterials*. 2012;33:5541–51.
136. Chi NH, Yang MC, Chung TW, Chou NK, Wang SS. Cardiac repair using chitosan-hyaluronan/silk fibroin patches in a rat heart model with myocardial infarction. *Carbohydr Polym*. 2013;92:591–7.
137. Simioniuc A, Campan M, Lionetti V, Marinelli M, Aquaro GD, Cavallini C, et al. Placental stem cells pre-treated with a hyaluronan mixed ester of butyric and retinoic acid to cure infarcted pig hearts: a multimodal study. *Cardiovasc Res*. 2011;90:546–56.
138. Elzoghby AO. Gelatin-based nanoparticles as drug and gene delivery systems: reviewing three decades of research. *J Control Release*. 2013;172:1075–91.
139. Van Vlierberghe S, Dubrue P, Schacht E. Biopolymer-based hydrogels as scaffolds for tissue engineering applications: a review. *Biomacromolecules*. 2011;9:1387–408.
140. Li RK, Jia ZQ, Weisel RD, Mickle DA, Choi A, Yau TM. Survival and function of bioengineered cardiac grafts. *Circulation*. 1999;100:1163–9.
141. van der Meer P, Voors AA, Lipsic E, van Gilst WH, van Veldhuisen DJ. Erythropoietin in cardiovascular diseases. *Eur Heart J*. 2004;25:285–91.
142. Kobayashi H, Minatoguchi S, Yasuda S, Bao N, Kawamura I, Iwasa M, et al. Post-infarct treatment with an erythropoietin-gelatin hydrogel drug delivery system for cardiac repair. *Cardiovasc Res*. 2008;79:611–20.
143. Shao ZQ, Takaji K, Katayama Y, Kunitomo R, Sakaguchi H, Lai ZF, et al. Effects of intramyocardial administration of slow-release basic fibroblast growth factor on angiogenesis and ventricular remodeling in a rat infarct model. *Circ J*. 2006;70:471–7.
144. Takehara N, Tsutsumi Y, Tateishi K, Ogata T, Tanaka H, Ueyama T, et al. Controlled delivery of basic fibroblast growth factor promotes human cardiosphere-derived cell engraftment to enhance cardiac repair for chronic myocardial infarction. *J Am Coll Cardiol*. 2008;52:1858–65.
145. Yacoub MH, Terrovitis J, CADUCEUS, SCPIO, ALCADIA: Cell therapy trials using cardiac-derived cells for patients with post myocardial infarction LV dysfunction, still evolving. *Glob Cardiol Sci Pract*. 2013;2013:5–8.
146. Li Z, Guan J. Hydrogels for cardiac tissue engineering. *Polymers*. 2011;3:740–61.
147. Huang NF, Yu J, Sievers R, Li S, Lee RJ. Injectable biopolymers enhance angiogenesis after myocardial infarction. *Tissue Eng*. 2005;11:1860–6.
148. Ou L, Li W, Zhang Y, Wang W, Liu J, Sorg H, et al. Intracardiac injection of matrigel induces stem cell recruitment and improves cardiac functions in a rat myocardial infarction model. *J Cell Mol Med*. 2011;15:1310–8.
149. Bagno LL, Werneck-de-Castro JP, Oliveira PF, Cunha-Abreu MS, Rocha NN, Kasai-Brunswick TH, et al. Adipose-derived stromal cell therapy improves cardiac function after coronary occlusion in rats. *Cell Transplant*. 2012;21:1985–96.
150. Kofidis T, Lebl DR, Martinez EC, Hoyt G, Tanaka M, Robbins RC. Novel injectable bioartificial tissue facilitates targeted, less invasive, large-scale tissue restoration on the beating heart after myocardial injury. *Circulation*. 2005;112:1173–7.
151. Kofidis T, de Bruin JL, Hoyt G, Lebl DR, Tanaka M, Yamane T, et al. Injectable bioartificial myocardial tissue for large-scale intramural cell transfer and functional recovery of injured heart muscle. *J Thorac Cardiovasc Surg*. 2004;128:571–8.
152. Laflamme MA, Chen KY, Naumova AV, Muskheli V, Fugate JA, Dupras SK, et al. Cardiomyocytes derived from human embryonic stem cells in pro-survival factors enhance function of infarcted rat hearts. *Nat Biotechnol*. 2007;25:1015–24.
153. Wall ST, Yeh CC, Tu RY, Mann MJ, Healy KE. Biomimetic matrices for myocardial stabilization and stem cell transplantation. *J Biomed Mater Res A*. 2010;95:1055–66.
154. Kutschka I, Chen IY, Kofidis T, Arai T, von Degenfeld G, Sheikh AY, et al. Collagen matrices enhance survival of transplanted cardiomyoblasts and contribute to functional improvement of ischemic rat hearts. *Circulation*. 2006;114:1167–73.
155. Giraud MN, Ayuni E, Cook S, Siepe M, Carrel TP, Tevæarai HT. Hydrogel-based engineered skeletal muscle grafts normalize heart function early after myocardial infarction. *Artif Organs*. 2008;32:692–700.
156. Zimmermann WH, Didié M, Wasmeier GH, Nixdorff U, Hess A, Melnychenko I, et al. Cardiac grafting of engineered heart tissue in syngenic rats. *Circulation*. 2002;106:1151–7.
157. Zhang P, Zhang H, Wang H, Wei Y, Hu S. Artificial matrix helps neonatal cardiomyocytes restore injured myocardium in rats. *Artif Organs*. 2006;30:86–93.
158. Zimmermann WH, Melnychenko I, Wasmeier G, Didié M, Naito H, Nixdorff U, et al. Engineered heart tissue grafts improve systolic and diastolic function in infarcted rat hearts. *Nat Med*. 2006;12:452–8.
159. Bonnans C, Chou J, Werb Z. Remodelling the extracellular matrix in development and disease. *Nat Rev Mol Cell Biol*. 2014;15:786–801.
160. Badyal SF, Taylor D, Uygun K. Whole-organ tissue engineering: decellularization and recellularization of three-dimensional matrix scaffolds. *Annu Rev Biomed Eng*. 2011;13:27–53.
161. Midwood KS, Williams LV, Schwarzbauer TE. Tissue repair and the dynamics of the extracellular matrix. *Int J Biochem Cell Biol*. 2004;36:1031–7.
162. Robinson KA, Li J, Mathison M, Redkar A, Cui J, Chronos NA, et al. Extracellular matrix scaffold for cardiac repair. *Circulation*. 2005;112:135–43.
163. Song JJ, Ott HC. Organ engineering based on decellularized matrix scaffolds. *Trends Mol Med*. 2011;17:424–32.
164. Crapo PM, Gilbert TW, Badyal SF. An overview of tissues and whole organ decellularization processes. *Biomaterials*. 2011;32:3233–43.
165. Ott HC, Matthies TS, Goh SK, Black LD, Kren SM, Netoff TI, et al. Perfusion-decellularized matrix: using nature's platform to engineer a bioartificial heart. *Nat Med*. 2008;14:213–21.
166. Dai W, Gerczuk P, Zhang Y, Smith L, Kopyov O, Kay GL, et al. Intramyocardial injection of heart tissue-derived extracellular matrix improves postinfarction cardiac function in rats. *J Cardiovasc Pharmacol Ther*. 2013;18:270–9.
167. Singelyn JM, Sundaramurthy P, Johnson TD, Schup-Magoffin PJ, Hu DP, Faulk DM, et al. Catheter-deliverable hydrogel derived from decellularized ventricular extracellular matrix increases endogenous cardiomyocytes and preserves cardiac function post-myocardial infarction. *J Am Coll Cardiol*. 2012;59:751–63.
168. Seif-Naraghi SB, Singelyn JM, Salvatore MA, Osborn KG, Wang JJ, Sampat U, et al. Safety and efficacy of an injectable extracellular matrix hydrogel for treating myocardial infarction. *Sci Transl Med*. 2013;5:173ra25.
169. Perea-Gil I, Uriarte JJ, Prat-Vidal C, Gálvez-Montón C, Roura S, Lluçà-Valldeperas A, et al. In vitro comparative study of two decellularization protocols in search of an optimal myocardial scaffold for recellularization. *Am J Transl Res*. 2015;7:558–73.
170. Seif-Naraghi SB, Salvatore MA, Schup-Magoffin PJ, Hu DP, Christman KL. Design and characterization of an injectable pericardial matrix gel: a potentially autologous scaffold for cardiac tissue engineering. *Tissue Eng Part A*. 2010;16:2017–27.
171. Fuster V. *Hurst's the heart*. 13th ed. New York: McGraw-Hill Medical Publishing Division; 2011.
172. Seif-Naraghi SB, Horn D, Schup-Magoffin PA, Madani MM, Christman KL. Patient-to-patient variability in autologous pericardial matrix scaffolds for cardiac repair. *J Cardiovasc Transl Res*. 2011;4:545–56.
173. Oberwallner B, Brodarac A, Choi YH, Saric T, Anić P, Morawietz L, et al. Preparation of cardiac extracellular matrix scaffolds by decellularization of human myocardium. *J Biomed Mater Res A*. 2014;102:3263–72.
174. Prat-Vidal C, Gálvez-Montón C, Puig-Sanvicens V, Sanchez B, Diaz-Güemes I, Bogóñez-Franco P, et al. Online monitoring of myocardial bioprosthesis for cardiac repair. *Int J Cardiol*. 2014;174:654–61.

175. Rajabi-Zeleti S, Jalili-Firoozinezhad S, Azarnia M, Khayyatan F, Vahdat S, Nikeghbalian S, et al. The behavior of cardiac progenitor cells on macroporous pericardium-derived scaffolds. *Biomaterials*. 2014;35:970–82.
176. Wei HJ, Chen CH, Lee WY, Chiu I, Hwang SM, Lin WW, et al. Bioengineered cardiac patch constructed from multilayered mesenchymal stem cells for myocardial repair. *Biomaterials*. 2008;29:3547–56.
177. Chen CH, Wei HJ, Lin WW, Chiu I, Hwang SM, Wang CC, et al. Porous tissue grafts sandwiched with multilayered mesenchymal stromal cell sheets induce tissue regeneration for cardiac repair. *Cardiovasc Res*. 2008;80:88–95.
178. Seif-Naraghi SB, Horn D, Schup-Magoffin PJ, Christman KL. Injectable extracellular matrix derived hydrogel provides a platform for enhanced retention and delivery of a heparin-binding growth factor. *Acta Biomater*. 2012;8:3695–703.
179. Sonnenberg SB, Rane AA, Liu CJ, Rao N, Agmon G, Suarez S, et al. Delivery of an engineered HGF fragment in an extracellular matrix-derived hydrogel prevents negative LV remodeling post-myocardial infarction. *Biomaterials*. 2015;45:56–63.
180. Okada M, Payne TR, Oshima H, Momoi N, Tobita K, Huard J. Differential efficacy of gels derived from small intestinal submucosa as an injectable biomaterial for myocardial infarct repair. *Biomaterials*. 2010;31:7678–83.
181. Tan MY, Zhi W, Wei RQ, Huang YC, Zhou KP, Tan B, et al. Repair of infarcted myocardium using mesenchymal stem cell seeded small intestinal submucosa in rabbits. *Biomaterials*. 2009;30:3234–40.
182. Mewhort HE, Turnbull JD, Meijndert HC, Ngu JM, Fedak PW. Epicardial infarct repair with basic fibroblast growth factor-enhanced CorMatrix-ECM biomaterial attenuates postischemic cardiac remodeling. *J Thorac Cardiovasc Surg*. 2014;147:1650–9.
183. Badylak SF. The extracellular matrix as a scaffold for tissue reconstruction. *Semin Cell Dev Biol*. 2002;13:377–83.
184. Kochupura PV, Azeloglu EU, Kelly DJ, Doronin SV, Badylak SF, Krukenkamp IB, et al. Tissue-engineered myocardial patch derived from extracellular matrix provides regional mechanical function. *Circulation*. 2005;112:1144–9.
185. Kelly DJ, Rosen AB, Schuldt AJ, Kochupura PV, Doronin SV, Potapova IA, et al. Increased myocyte content and mechanical function within a tissue-engineered myocardial patch following implantation. *Tissue Eng Part A*. 2009;15:2189–201.
186. Potapova IA, Doronin SV, Kelly DJ, Rosen AB, Schuldt AJ, Lu Z, et al. Enhanced recovery of mechanical function in the canine heart by seeding an extracellular matrix patch with mesenchymal stem cells committed to a cardiac lineage. *Am J Physiol Heart Circ Physiol*. 2008;295:H2257–63.
187. Gálvez-Montón C, Fernandez-Figueras MT, Martí M, Soler-Botija C, Roura S, Perea-Gil I, et al. Neoinnervation and neovascularization of acellular pericardial-derived scaffolds in myocardial infarcts. *Stem Cell Res Ther*. 2015;6:108.
188. Muylaert DE, Fledderus JO, Bouten CV, Dankers PY, Verhaar MC. Combining tissue repair and tissue engineering; bioactivating implantable cell-free vascular scaffolds. *Heart*. 2014;100:1825–30.
189. Puri MC, Nagy A. Concise review: Embryonic stem cells versus induced pluripotent stem cells: the game is on. *Stem Cells*. 2012;30:10–4.
190. Giraud MN, Flueckiger R, Cook S, Ayuni E, Siepe M, Carrel T, et al. Long-term evaluation of myoblast seeded patches implanted on infarcted rat hearts. *Artif Organs*. 2010;43:E184–92.
191. Barallobre-Barreiro J, Didangelos A, Schoendube FA, Drozdov I, Yin X, Fernández-Caggiano M, et al. Proteomics analysis of cardiac extracellular matrix remodeling in a porcine model of ischemia/reperfusion injury. *Circulation*. 2012;125:789–802.
192. Rienks M, Papageorgiou AP, Frangogiannis NG, Heymans S. Myocardial extracellular matrix. An ever-changing and diverse entity. *Circ Res*. 2014;114:872–88.
193. Gaetani R, Doevendans PA, Metz CH, Alblas J, Messina E, Giacomello A, et al. Cardiac tissue engineering using tissue printing technology and human cardiac progenitor cells. *Biomaterials*. 2012;33:1782–90.
194. Jakab J, Marga F, Norotte C, Murphy K, Vunjak-Novakovic G, Forgacs G. Tissue engineering by self-assembly and bio-printing of living cells. *Biofabrication*. 2010;2:022001.
195. Khatiwala C, Law R, Shepherd B, Dorfman S, Csete M. 3D cell bioprinting for regenerative medicine research and therapies. *Gene Ther Reg*. 2012;7:1–19.
196. Bader D, Oberpriller JO. Repair and reorganization of minced cardiac muscle in the adult newt (*Notophthalmus viridescens*). *J Morphol*. 1977;155:349–57.
197. Vandenberg HH, Karlisch P, Farr L. Maintenance of highly contractile tissue-cultured avian skeletal myotubes in collagen gel. *In Vitro Cell Dev Biol*. 1988;24:166–74.
198. Souren JE, Schneijdenberg C, Verkleij AJ, Van Wijk R. Factors controlling the rhythmic contraction of collagen gels by neonatal heart cells. *In Vitro Cell Dev Biol*. 1992;28:199–204.
199. Eschenhagen T, Fink C, Remmers U, Scholz H, Wattchow J, Weil J, et al. Three-dimensional reconstitution of embryonic cardiomyocytes in a collagen matrix: a new heart muscle model system. *Faseb J*. 1997;11:683–94.
200. Fink C, Ergün S, Kralisch D, Remmers U, Weil J, Eschenhagen T. Chronic stretch of engineered heart tissue induces hypertrophy and functional improvement. *Faseb J*. 2000;14:669–79.
201. Zimmermann WH, Schneiderbanger K, Schubert P, Didié M, Münzel F, Heubach JF, et al. Tissue engineering of a differentiated cardiac muscle construct. *Circ Res*. 2002;90:223–30.
202. Krupnick AS, Kreisel D, Engels FH, Szeto WY, Plappert T, Popma SH. A novel small animal model of left ventricular tissue engineering. *J Heart Lung Transplant*. 2002;21:233–43.
203. Radisic M, Park H, Shing H, Consi T, Schoen FJ, Langer R, et al. Functional assembly of engineered myocardium by electrical stimulation of cardiac myocytes cultured on scaffolds. *Proc Natl Acad Sci U S A*. 2004;101:18129–34.
204. Remppis A, Pleger ST, Most P, Lindenkamp J, Ehlermann P, Schweda C, et al. S100A1 gene transfer: a strategy to strengthen engineered cardiac grafts. *J Gene Med*. 2004;6:387–94.
205. Khademhosseini A, Eng G, Yeh J, Kucharczyk PA, Langer R, Vunjak-Novakovic G, et al. Microfluidic patterning for fabrication of contractile cardiac organoids. *Biomed Microdevices*. 2007;9:149–57.
206. Blan NR, Birla RK. Design and fabrication of heart muscle using scaffold-based tissue engineering. *J Biomed Mater Res A*. 2008;86:195–208.
207. Lu TY, Lin B, Kim J, Sullivan M, Tobita K, Salama G, et al. Repopulation of decellularized mouse heart with human induced pluripotent stem cell-derived cardiovascular progenitor cells. *Nat Commun*. 2013;4:2307.





## Discussion

---



## 1. Immunomodulatory properties of the cardiac ATDPCs

Researchers concur with the requirements that the cell lineage chosen to repopulate the scaffolds should accomplish. Among them, the main points to cover are: non-tumorigenic, non-arrhythmogenic, non-immunogenic, integration with the host cardiac tissue, easily accessible to obtain and expand *in vitro*, capacity to differentiate towards cardiomyocytes or cardiac-like cells and promote vasculogenesis, improve overall heart function and avoid social and ethical concerns (Malliaras and Marbán, 2011; Gálvez-Montón *et al.*, 2013). Nevertheless, a consensus regarding the best or optimal cell population has not been reached yet, as in one-way or another, these candidate cells have shown some drawbacks that need to be faced. For instance, ESC potential is highly limited by its teratogenic potential (Leor *et al.*, 2007; Kroon *et al.*, 2008), its immunological mismatch with the receptor (Murata *et al.*, 2010) and the ethical problems concerning their isolation (Sun *et al.*, 2014); whereas iPSCs reported genomic instability (Laurent *et al.*, 2011) and can induce tumor formation (Gutierrez-Aranda *et al.*, 2010). Other sources, such as skeletal myoblasts, have also reported arrhythmias upon implantation (Menasché *et al.*, 2008), while the use of cardiomyocytes, the native cardiac cell type, is not viable due to the poor viability and low availability, and associated ethical matters (Gálvez-Montón *et al.*, 2013).

Latest investigations have been directed towards other sources of adult stem cells, a multipotent cell lineage isolated from diverse organs and tissues in the adult body, such as bone marrow, heart, blood, nerves, amniotic fluid or adipose tissue (Vunjak-Novakovic *et al.*, 2010), that overcome most of the disadvantages exposed before. In particular, the progenitor cells obtained from adipose tissue, the ATDPCs, have been of great interest because of their cardiomyogenic and endothelial potential (Planat-Bénard *et al.*, 2004a; Miranville *et al.*, 2004), their facility to be obtained from dense cellular reservoir and expanded *in vitro* (Bunnell *et al.*, 2008), and their immune tolerance for allograft/xenograft (Yañez *et al.*, 2006; Jeong *et al.*, 2014). In 2010, our group isolated and characterized for the first time a novel ATDPC population, the cardiac ATDPCs, derived from the cardiac adipose tissue located in

the aortic root and the base of the heart from patients undergoing cardiac surgery. These cells displayed a typical MSC pattern, with positive expression of CD29, CD44, CD90, CD105 and CD166, and negative for CD14, CD45 and CD106. Besides, cardiac ATDPCs showed both cardiomyogenic and vasculogenic potential, and upon delivery *in vivo*, reduced infarct size, promoted neoangiogenesis and improved heart function after MI induction (Bayes-Genis *et al.*, 2010). These features were confirmed in a recent study, as well as the *in vivo* potential of these cells to promote cardiac regeneration following MI was also clearly demonstrated (Nagata *et al.*, 2016). To end up with, and similarly to a cardiac tissue engineering approach using recellularized scaffolds, the transposition of the cardiac fat containing the cardiac ATDPC population also led to significant benefits in heart function, infarct size and apoptosis reduction, and up-regulation of genes involved in proliferation and cell cycle progression in infarcted pigs (Gálvez-Montón *et al.*, 2011), further ascertaining the cardioregenerative potential of cardiac ATDPCs.

The suitable and committed cardiac-like phenotype, together with the promising results reported, should not prevent from fully characterizing the immunological properties of cardiac ATDPCs and their potential to awake the immune system. Herein, we conducted a complete *in vitro* allostimulatory assay to study and determine the immunomodulatory capacity of cardiac ATDPCs, comparing them with an already well-established low immunogenic cell line, the UCBSCs. Particularly, UCBSCs present a dull, low expression of major histocompatibility complex I, and lack the major histocompatibility complex II, both indicative of a low immune activity inductor (Cho *et al.*, 2008). In an allostimulatory assay, coculture of UCBSCs and T-lymphocytes or T-cells from different donors, human leukocyte antigen mismatched, highly suppressed proliferative activity of T-cells, through fine modulation of monocytes function (Cutler *et al.*, 2010). Furthermore, UCBSCs abrogated *in vivo* T-cell proliferation and did not trigger an increase in proinflammatory cytokines TNF- $\alpha$  and IFN- $\gamma$  release (Lee *et al.*, 2014). So, the low immunogenicity of UCBSCs turns them into a valid, suitable model to comparatively assess the immunoregulatory properties of our cardiac ATDPCs.

Following the same guidelines to set up the allostimulatory assay as found in

the literature (Cutler *et al.*, 2010), we coseeded cardiac ATDPCs with T-cells derived from peripheral blood mononuclear cells from a different donor. These T-cells were either activated or not with third-party member, allogeneic monocyte-derived dendritic cells, an antigen-presenting cell that strongly stimulates and activates them (Ni and O'Neill, 1997). Analysis of T-cell proliferation revealed that increasing numbers of seeded cardiac ATDPCs did not induce a higher percentage of active, proliferating cells, but they suppressed and drastically reduced this number in a dose-dependent manner, reaching equal levels to that found for UCBSs. These results are in concordance with previous studies that reported MSC hypoimmunogenicity according to intermediate amounts of major histocompatibility complex I, and lack of major histocompatibility complex II expression (Le Blanc *et al.*, 2003); and T-cell proliferation abrogation with different types of MSCs with known immunosuppressive potential (Jarvinen *et al.*, 2008; Quaedackers *et al.*, 2009; Tipnis *et al.*, 2010). The T-cell mediated response plays a central role as initiators, regulators and effectors of allogeneic cell rejection, as they are involved in T-cell driven lysis executed mainly by macrophages, production of antibodies, activation of accessory cells and complement system activation (Ingulli, 2010); thus, the repression of T-cell activation could aid to avoid the adverse immune response associated with allogeneic rejection. Moreover, the cardiac ATDPC cytokine profile indicated a marked decrease in the proinflammatory cytokines interleukin-6, TNF- $\alpha$  and IFN- $\gamma$ , showing an inverse correlation between cardiac ATDPC number and released cytokine concentration; ascertaining the T-cell inactivating capacity of our studied cells. These mentioned early stage cytokines act synergistically to feedback T-cell proliferation, impair regulatory T-cell ability to inhibit effector T-cell immunity and activate macrophages, all processes also related to inhibition of cell acceptance (Shen and Goldstein, 2009; Monguió-Tortajada *et al.*, 2014). Although it was not the scope of the present work, there are some plausible mechanisms that, alone or combined, could explain the observed effects:

- The first possibility is a straightforward **inhibition of T-cells by direct cell contact**, a stronger T-cell proliferation repressor mechanism in comparison with paracrine, cytokine-mediated suppression (Di Nicola *et al.*, 2002). Several

molecules have been reported to mediate T-cell-MSC adhesion, such as CXCR3, intercellular and vascular adhesion molecules, or programmed cell death protein 1, promoting inhibition of T-cell proliferation (Ren *et al.*, 2008; Ren *et al.*, 2010; Yan *et al.*, 2014).

- The second probable mechanism is **the secretion of soluble factors** that can regulate immune response (Di Nicola *et al.*, 2002). The MSC supernatant itself containing the released factors is not sufficient to abrogate T-cell proliferation, but it is necessary a coculture and direct contact between both cell types (Augello *et al.*, 2005), as it happened in our study. Some of these factors with immunosuppressive activity and known to be secreted by ATDPCs are TGF- $\beta$ , galectin-1, galectin-3 or HGF, among others (Di Nicola *et al.*, 2002; Kokai *et al.*, 2014).
- The last inhibitory pathway could be directed to **act over T-cell activators**, thus indirectly repressing final T-cell stimulation. This third-member repression has been observed for MSCs versus dendritic cells by reducing their maturation from monocytes (Maccario *et al.*, 2005), or directly inhibiting their potential to activate CD4<sup>+</sup> T-cells (Jiang *et al.*, 2005); abrogating natural killer cell proliferation (Sotiropoulou *et al.*, 2006); or suppressing B-cell proliferation and activation (Deng *et al.*, 2005). In our case, the abolition of dendritic cells potential to switch on T-cells could explain the considerable drop seen in T-cell proliferation.

## 2. Generation of cardiac acellular scaffolds

The myocardial ECM consists of a dynamic and changeable mesh of structural and functional proteins that, under physiological conditions, constitutes the cardiac specific microenvironment, maintaining heart structural integrity and acting as a reservoir, supplying cells with mechanical and biological cues which guide their proliferation, attachment, migration, survival and differentiation (Badylak *et al.*, 2011). The onset of pathophysiological conditions, such as MI, turns the initial milieu into a harsh extracellular microenvironment. Following MI, and owing to the limited self-regenerative heart activity, collagen deposition occurs in an ultimate attempt to replace massive cardiomyocyte loss and provide mechanical support to the infarcted heart, leading to the infarct scar formation. Here, the dynamic balance of ECM turnover is really unstable, and the infiltration of immune cells is constant, being both factors determinant of the later MI sequelae (Dobaczewski *et al.*, 2010; Ma *et al.*, 2014). This resulting altered, proinflammatory, hostile milieu negatively affects the regenerative potential of cell therapy, as assessed by low cell retention and survival following direct delivery into the infarct bed (Hofmann *et al.*, 2005; Kang *et al.*, 2006).

Cardiac tissue engineering provides a solution to surpass the adverse microenvironment present in the infarcted myocardium that encounters cell therapy. In this context, the utilization of scaffolds gives cells a physiological, favorable milieu preventing them to face straightaway the hostile MI conditions, thus enhancing their therapeutic effectiveness. It has been reported that the use of scaffolds led to better post-MI recovery outcomes compared to single, direct cell intramyocardial injection (Siepe *et al.*, 2006). Not only to initially support cells, but also the scaffold itself is capable of triggering a beneficial, regenerative process after MI onset (Gálvez-Montón *et al.*, 2015). Therefore, an appropriate scaffold that recapitulates physiological cardiac signaling cascades, and mechanical stiffness and framework, directs MI recovery, not only through direct action and paracrine mechanisms exerted by the introduced cells, but also by the recovery of ECM-cell interactions and correct signaling cues that drive endogenous tissue repair (Blackburn *et al.*, 2015).

Scaffold biomaterial is crucial to ensure a complete coupling with the host cardiac tissue and reproduce the physiological niche and signals present within the myocardial ECM, as specificity for the relationship ECM-cell has been demonstrated to improve adhesion and cellular growth in many other tissues (Zhang *et al.*, 2009b). Despite the several available options, decellularized ECM from cardiac tissues seems the most reliable and suitable option, as it contains identical inherent mechanical strength, biological composition, and preserved vasculature tree and architecture shown in the target tissue, i.e. the myocardium (Sarig and Machluf, 2011). Specifically, in our study, we have chosen two different cardiac related acellular ECMs: decellularized porcine myocardial ECM and decellularized human pericardial ECM. The first option, decellularized myocardial ECM, perfectly mimics the structure and biological cues, and recreates the physiological milieu of the native myocardium; and can be readily obtained from healthy slaughterhouse pigs. Regarding the decellularized pericardial ECM, even though is not an exact match with the myocardial one, it is thought to influence ventricular contraction and epicardial vessel properties. Additionally, the pericardium, which provides structural and mechanical support to the heart, is routinely left unsutured, cut or even removed when cardiothoracic surgery is complete, without adverse consequences. Thus, surgical samples from patients undergoing cardiac surgery and submitted to decellularization can be used for autologous/allogeneic purposes (Seif-Naraghi *et al.*, 2010; Singelyn and Christman, 2010). In both cases, their natural origin ensures a high biodegradability and non-toxicity of the derived products, easily processed and eliminated by the recipient body.

During the decellularization procedure, cardiac ECM properties and internal organization should be retained and preserved as much as it is possible. The decellularization agents employed, no matter whether they are chemical, enzymatic or mechanical, present variable, aggressive effects over the cellular content that is desirable to be eliminated, but also disruptive on the ECM that is expected to maintain intact (Crapo *et al.*, 2011). Thus, the combination, timing, time exposure and conditions to carry out the decellularization process are paramount for succeeding in generating an acellular ECM with retained characteristics. In the



present study, we initially used, for both myocardial and pericardial tissues, a previous published decellularization protocol based on detergents (Ott *et al.*, 2008), introducing slight modifications to properly adapt the procedure to respective specific tissue characteristics, such as cell density, thickness or lipid content (Crapo *et al.*, 2011). Additionally, in myocardial samples, a second decellularization protocol was also tested incorporating two different treatments. On the one hand, an acid incubation to further solubilize cells and disrupt nucleic acids, and, on the other hand, a trypsin incubation to aggressively remove cell debris, at the expense of negative impact on the ECM if exposure is too long (Crapo *et al.*, 2011). In all cases, a comprehensive characterization of the resulting biological product was conducted, as parameters such as acellularity and ECM biological, mechanical and structural features need to be determined (Akhyari *et al.*, 2011).

The first requisite that the generated decellularized scaffold should fulfill is a complete removal of cellular and nuclear remnants. Specifically, DNA material leftovers and cell surface oligosaccharide molecule  $\alpha$ -Gal (or Gal epitope) presence have been described as the two main factors to elicit an adverse host immune response (Badylak and Gilbert, 2008). According to the criteria to avoid immunogenicity, a maximum double stranded DNA concentration threshold of 50 ng per mg ECM dry weight, and lack of visible nuclear staining with DAPI should be accomplished (Crapo *et al.*, 2011). As determined in our work, for both decellularized myocardial and pericardial scaffolds, and regardless of the protocol performed, DNA content was below the established limit, as well as no nuclei or cytosolic proteins were identified. Despite DNA removal was not absolute, this so low DNA concentration is not sufficient to trigger a deleterious immunogenic response, as it also happens with many commercially available ECM devices such as Oasis<sup>TM</sup> or Restore<sup>TM</sup> (Gilbert *et al.*, 2009).

Concerning internal scaffold structure, geometry and conformation, it has been determined their role in guiding cell differentiation (Forte *et al.*, 2008; Guilak *et al.*, 2009) and migration (Brown *et al.*, 2006). In our hands, decellularized myocardium and pericardium ultrastructure was retained, maintaining the native tissue fiber architecture, alignment and porosity. Tightly linked to structure, tissue

stiffness has been reported to be determined by matrix architecture and its fibrillar organization (Hule *et al.*, 2008). Furthermore, to have an accurate and complete point of view, mechanical stiffness has to be evaluated in two different scales: macroscopic and microscopic. The microscopic scale comprises the local niche where cells reside and receive stiffness-dependent mechanical cues, transducing them into biological signals that direct cell differentiation (Engler *et al.*, 2006), morphology, adhesion (Yeung *et al.*, 2005), proliferation (Yeh *et al.*, 2012) and migration capacity (Murrell *et al.*, 2011); while preservation of macroscopic stiffness would be associated with a better mechanical coupling with host cardiac tissue, capable of bearing the tensile strength exerted during heart cycle, transducing the forces generated by myocytes and providing passive stiffness during diastole (Fomovsky *et al.*, 2010). Our data indicate that, at microscopic scale, decellularized myocardial scaffolds displayed similar levels of Young's modulus (a stiffness index) compared to native tissue, and these values were in the same range that others reported for mouse decellularized cardiac ECM (Andreu *et al.*, 2014) and native tissue (Berry *et al.*, 2006; Zhang *et al.*, 2011). Moreover, a low stiffness similar to what we obtained has been associated with reduced cell ageing and preservation of cardiomyogenic differentiation capacity of CPCs (Qiu *et al.*, 2015). On the other hand, macroscopic mechanical properties were also preserved, as assessed by native versus decellularized myocardium comparison. Our findings were in contrast with other previous studies, where increased bulk stiffness in decellularized ventricles was reported, as a probable result of fiber shrinkage and structure compression caused by perfusion-based whole organ decellularization (Ott *et al.*, 2008; Wang *et al.*, 2010a). Therefore, not only the microscale stiffness was preserved after decellularization, ensuring correct mechanotransduction; but also the three-dimensional architecture was well maintained, suggesting no disruption caused during decellularization, which, in turn, correlated with global ECM geometry conservation and retention of macroscopical mechanics determined by tensile tests. Likewise, pretty similar results were observed for the decellularized pericardial scaffolds. These decellularized scaffolds showed comparable Young's modulus to that measured for native myocardium, and its final value is included within the optimal stiffness range for cardiomyocyte maturation and contraction (Engler *et al.*, 2008; Jacot *et al.*, 2008; Rodriguez *et al.*, 2011). Regarding

macromechanics, lower stiffness was determined for the decellularized pericardial scaffolds related to other published works (Mirsadraee *et al.*, 2006; Vinci *et al.*, 2013); thus suggesting lack of fiber compression and structure disruption promoted by decellularization agents that alter macroscopical stiffness and matrix organization. Therefore, even though pericardium is not the exact physiological niche where cardiomyocytes reside, it displays similar mechanical properties compared to myocardium, recreating the mechanical cues indispensable for cell behavior modulation and global mechanical coupling. Finally, it is important to point out that in our study, mechanical stiffness for both decellularized cardiac scaffolds was also conserved after lyophilization and sterilization with gamma irradiation, steps that have been reported to cause some mechanical alterations in non-cardiac decellularized matrices (Gouk *et al.*, 2008; Sheridan *et al.*, 2013).

Scaffold biodegradability assessed *in vitro* with collagenase I revealed a dry weight reduction above 70% after 24 hours for both tissues and regardless of the decellularization protocol applied. However, for the decellularized myocardial scaffolds, the weight reduction was significantly higher (around 90%) when decellularized using the detergent-based protocol. This high degradability represents an advantageous point, as it is desirable that the cardiac acellular matrices are preserved for at least 24 hours, while the degraded portion of matrix is at once replaced by the cell-secreted ECM (Vunjak-Novakovic *et al.*, 2014). Favorably, degradation side products of ECM have been demonstrated to possess chemotactic and mitogenic activities (Reing *et al.*, 2009), which could further increase endogenous stem cell attraction. Nonetheless, it would be desirable to preserve the matrix for a minimum of one week, to maintain the initial, favorable supportive platform prior to complete substitution by the own cellular ECM (Reis *et al.*, 2016). Besides, as a simplified *in vitro* recreation of what occurs physiologically, the data generated should be interpreted with caution. ECM dynamics and turnover are more complex *in vivo*, with many other players taking part in the matrix degradation, with more than 23 members of metalloproteinases and 19 members of a disintegrin and metalloproteinase with thrombospondin motifs enzymes. Thus, the interplay of these factors, their kinetics, concentrations and accessibility to the matrix, may result

in a different degree of degradation *in vivo* (Lu *et al.*, 2011).

The uprising of decellularization processes has contributed to provide new insights into the ECM protein composition. Prior to the use of decellularized tissues, the identification of unique ECM proteins in native tissues was hampered by the presence of cellular proteins that exceeded and masked ECM proteins. From the acellular ECM, with most of the cellular content removed, it is easier to extract and identify the ECM proteins. Thus, the proteomic analysis appeared as a valid tool in our study to find out the protein content remaining after the decellularization protocols carried out in both myocardium and pericardium. In the case of myocardium, the detergent-based decellularization protocol left 40 matrisome proteins and 119 other, non-related ECM proteins; while the trypsin decellularization protocol reduced the amount of matrisome proteins to 29, and increased the number of other, residual proteins to 162. Overall, this indicates that the use of detergents is more efficient in both preserving the protein ECM content and removing the cellular remnants, agreeing with the more disruptive effects over ECM proteins described for acid and trypsin (Crapo *et al.*, 2011), both agents included in our trypsin-based protocol. Comparatively to previous published work in murine (de Castro Brás *et al.*, 2013), porcine (Johnson *et al.*, 2014) and human hearts (Guyette *et al.*, 2016), our results displayed a slightly higher number of matrisome proteins for the detergent-decellularized myocardial scaffolds. Furthermore, major ECM elements reported to be primordial for cardiac matrix structure and function, such as type-I, -III, -IV, -V, -VI collagens, laminin alpha, beta and gamma, periostin, heparan sulfate, lumican or fibrillin-1 (Guyette *et al.*, 2016; Johnson *et al.*, 2016) were identified in detergent-decellularized myocardial scaffolds, while not all of them were preserved following trypsin protocol; thus indicating better ECM composition conservation for the detergent-based decellularization protocol. On the other hand, the decellularized pericardium resulted in a more-enriched ECM in matrisome proteins and less cellular proteins (51 and 73, respectively), compared to decellularized myocardium, while preserving the main myocardial ECM proteins. This represents an important step forward in relation to the only proteomic characterization in native bovine pericardium that only identified 4 matrisome-related proteins and 36 cellular

proteins (Griffiths *et al.*, 2008), or to the 18 and 10 ECM-proteins described for porcine and human decellularized pericardium, respectively (Seif-Naraghi *et al.*, 2010). The decellularized pericardium shares up to 26 and 19 matrisome proteins with the detergent and trypsin-based decellularized myocardium, respectively. Therefore, the pericardium recapitulates the myocardial molecular environment in a very precise way, resulting suitable as an alternative cardiac scaffold to myocardial ECM. The specific role for the most important proteins to modulate cell behavior will be discussed in detail in the next section.

### 3. Repopulation of the decellularized cardiac scaffolds

Once the phenotype, differentiation potential, and immunomodulatory characteristics of cardiac ATDPCs were determined, and the decellularized scaffolds generated, the next step was to repopulate the decellularized cardiac scaffolds with these cells and evaluate cell adhesion, survival and cardiomyogenic/endothelial differentiation within these three-dimensional supports. In recellularized myocardial scaffolds, the number of retained cardiac ATDPCs one week after repopulation was 2.4 times higher in detergent-based decellularized scaffolds than the amount quantified for the trypsin protocol. This number was far from the cellular density residing within the native myocardium, but it should be considered the mince number of cells used to recolonize the scaffolds, less than two million. For the recellularized pericardial scaffolds, cell retention was even higher, 1.5-fold, compared to detergent-decellularized myocardial scaffolds. In line with this, the proteomic evaluation revealed common and tissue-specific proteins involved in cell adhesion. Lumican (Nikitovic *et al.*, 2008), different collagen subtypes (Kaido *et al.*, 2004; Jokinen *et al.*, 2004; Cescon *et al.*, 2015), emilin-1 (Spessotto *et al.*, 2003), heparan sulfate proteoglycan (Moon *et al.*, 2005), fibronectin (Wang *et al.*, 2015), laminin (LaNasa and Bryant, 2009) or nidogen (Konrad *et al.*, 2000), identified by our proteomic study in both cardiac scaffolds; and the differentially detected in pericardial scaffolds galectin-1 (Camby *et al.*, 2006), vitronectin (Wang *et al.*, 2015), decorin and tenascin-X (Rienks *et al.*, 2014), have been described to particularly mediate in cell adhesion, mainly through specific integrin cell receptors-ECM interaction. In this regard, the higher number of proteins apparently mediating in adhesion, along with the larger pore diameter for pericardial scaffolds, may explain the greater cell retention observed upon recellularization within the pericardial scaffold when compared with the myocardial one. In contrast with the pore size of ~10  $\mu\text{m}$  for myocardial scaffolds, the ~22  $\mu\text{m}$  for pericardial scaffolds, in concordance with previous work for other acellular cardiac matrices (Singelyn *et al.*, 2009; Seif-Naraghi *et al.*, 2011; Wang *et al.*, 2012a), is considered optimal to facilitate cellular and vascular infiltration as well as nutrient diffusion. Moreover, cardiac ATDPC

penetrance and migration through the scaffold was greater for the pericardial scaffolds, with a regular cell distribution along the scaffold thickness and a significant number of cells reaching the other scaffold side. Chemoattractant capacity of decellularized pericardium has been demonstrated for epicardial, endothelial and smooth muscle cells (Seif-Naraghi *et al.*, 2010). Furthermore, and according to our proteomic analysis results, decellularized pericardial scaffolds contain unique proteins, such as biglycan, decorin and vitronectin. These proteins have been suggested to specifically drive cell migration and cytoskeletal changes (Tufvesson and Westergren-Thorsson, 2003; Fukushima *et al.*, 2007), and could provide the biological cues for cardiac ATDPC mobility.

On another note, the majority of cells were alive one week postrecellularization in both the myocardial and the pericardial scaffolds. The ECM has been described to provide the necessary regulatory factors to avoid cell anoikis, the apoptosis phenomenon occurring after cell detachment from ECM substrate; thus, ECM mediates and modulates cell survival in an integrin-mediated cell adhesion process (Meredith *et al.*, 1993). Laminins and fibronectin have been described to participate in cell adhesion and survival of cardiomyocytes (Lundgren *et al.*, 1985), while type-I and -IV collagens plus the aforementioned laminins and fibronectin, all of them identified in our proteome analysis for both decellularized cardiac scaffolds, have been shown to favor retinal ganglion cells and human islet survival (Daoud *et al.*, 2010; Vecino *et al.*, 2015). Finally, the identified heparan sulfate proteoglycan has been associated with improved cardiomyocyte survival when increased its presence (Yamauchi *et al.*, 2000; Ma *et al.*, 2015); whereas decorin, exclusively detected in pericardial scaffold, has been described to promote endothelial cell survival (Schönherr *et al.*, 2001) and reduced cell apoptosis (Seidler *et al.*, 2005). Hence, the favorable microenvironment preserved in both decellularized cardiac tissues allowed cells to adhere to the substrate and maintain them alive.

The introduced cells within the scaffold exerted some effect over the myocardial ECM mechanical stiffness, at least at microscopical level. One week following recellularization with cardiac ATDPCs, there was a slight, though significant, increase in the micromechanical stiffness of the recellularized myocardial scaffold, as

assessed by atomic force microscopy (AFM); while for the recellularized pericardial scaffold the stiffness remained unaltered. On the contrary, no differences were observed at macroscopical levels for neither of the two recellularized scaffolds. First of all, it is important to note that, despite the stiffer ECM, the determined Young's modulus for recellularized myocardium, around 22 kPa, is considered favorable for optimal cardiomyocyte contraction and maturation (Engler *et al.*, 2008; Jacot *et al.*, 2008; Rodriguez *et al.*, 2011), thus, this increased ECM stiffness modification does not seem to be critical for cell behavior. A plausible explanation for this stiffness increase in recellularized myocardial scaffolds might be the role of cardiac ATDPCs in the ECM turnover, as these cells seeded over collagen scaffolds synthesized new ECM to remodel original collagen scaffold composition (Colazzo *et al.*, 2011). Specifically, a quantitative assay displayed that ATDPCs secreted a significantly higher amount of collagen (Amable *et al.*, 2014), main contributor to harden the ECM stiffness at microscopic levels (Wegner *et al.*, 2007). So, while the cells were seeded for one week in the scaffold, most likely the initial ECM was gradually replaced by the cardiac ATDPC synthesized ECM, leading to a new, cell-specific niche with slightly different local mechanical properties. Importantly, these data also indicated a high plasticity and capacity to respond by the cardiac ATDPCs to the dynamic incoming signals, and accordingly, modulate their behavior and ECM secretion. Finally, the macroscopic stiffness did not result affected by the microscopic scale mechanical variation, suggesting an accurate distribution and organization of the cellular newly-synthesized ECM, and resembling the native ECM network, that globally did not alter mechanical features.

Decellularized myocardial scaffolds, seeded with cardiac ATDPCs, not only helped to maintain their basal cardiac-like cellular phenotype, but even enhanced their cardiomyogenic commitment and vasculogenic potential. In particular, for the detergent-based protocol, it was preserved the basal expression of cardiac calcium handling protein Cx43, necessary for intercellular junctions and electrical coupling, and cardiac transcription factor GATA4, whose role is to activate downstream signaling pathways directing cardiac differentiation. Besides, *de novo* expression of cTnI, protein of the cardiomyocyte contractile machinery, was identified. These



results agree with previous studies that support the role of myocardial ECM in cardiac differentiation (Higuchi *et al.*, 2013). Two combined factors could provide some insights into the cardiac marker expression pattern observed. On the one hand, and as exposed previously, the micromechanical stiffness plays a key role in cell fate determination. A 10 kPa-substrate stiffness has been demonstrated to optimally guide cardiomyocyte maturation (Jacot *et al.*, 2010) and CPC differentiation to cardiac lineage (Mosqueira *et al.*, 2014), in concordance with our local stiffness determination. On the other hand, the protein mixture remaining in the decellularized scaffold could also provide cardiac ATDPCs with the cardiac differentiation cues, as it does directing ESC cardiogenesis (Higuchi *et al.*, 2013). Accordingly, the individual influence of some ECM components on cardiac commitment has been studied. For instance, type-V collagen, but not types-I and -III, promoted differentiation of MSCs into cardiac phenotype (Tan *et al.*, 2010); fibronectin has been also implicated in meso-endodermal differentiation during embryo development (Pimton *et al.*, 2011); and the interaction of some laminin subtypes with integrins activates the regulatory pathways of cardiac differentiation (van Dijk *et al.*, 2008). Altogether, these proteins, identified in our proteomic study, could explain the cardiac commitment observed. However, we consider that this is not a single-player situation, where just one or two differing proteins can direct differentiation. Instead, the variety of ECM proteins, the precise proportion of them, and the integration of the exerted signals from the whole ECM play a more important role in cell lineage specification, as previously suggested (Higuchi *et al.*, 2013). Indeed, type-V collagen and two laminin subunits were also present in the trypsin-based decellularized myocardial scaffolds (*unpublished data*), but fibronectin and the other three laminin subunits were not properly detected, thus indicating a necessary interplay between all these proteins. Moreover, the total number of proteins was also lower after trypsin decellularization (29 versus 40), indicating a minor variety and a less enriched ECM in collagens and GPs, but higher in proteoglycans. Under these conditions, no trace of cardiac commitment was observed in trypsin-decellularized myocardial scaffolds, highlighting the global, synergistic role of the matrix components and the imperial necessity to achieve a minimum, essential ECM composition, despite conserving ultrastructure and mechanical properties. As

previously exposed, the utilization of more aggressive agents in the trypsin-based decellularization protocol, such as acids and trypsin, which have been described to be disruptive with collagen, laminins, fibronectin, but less destructive with proteoglycans than detergents do, may explain the protein content differences (Crapo *et al.*, 2011). Finally, some of the introduced cardiac ATDPCs in the decellularized myocardial scaffolds, regardless of the decellularization procedure employed, *de novo* expressed the endothelial marker IsolectinB4 (IsoB4). The observed endothelial-committed cells, however, did not reorganize to form new blood vessels and no signs of newly-emerging vasculature or typical endothelial lamina was seen. Myocardial ECM seems to supply the required signaling to induce endothelial commitment (Krug *et al.*, 1987), and even after introducing ECM alterations derived from trypsin decellularization, the endothelial cells can grow and proliferate (Grauss *et al.*, 2005), thus supporting the presence of endothelial-like cells within the decellularized scaffold generated by trypsin decellularization. Also, a stiffness-dependent endothelial differentiation has been described for cardiac stem cells in softer substrates (< 1 kPa), based on nuclear or cytoplasmic cellular location of the Yes-associated protein/ transcriptional coactivator with PDZ-binding motif (YAP/TAZ) complex depending on mechanical cues received (Mosqueira *et al.*, 2014). According to the micromechanics internal fluctuation within the scaffold, due to local composition variation, it is plausible to find softer areas that could modify and switch the cardiac differentiation to the endothelial.

In our hands, the recellularized pericardial scaffolds preserved cardiac ATDPC cardioidifferentiation. These results are in accordance with decellularized pericardium capacity to guide *in vitro* Sca-1-<sup>+</sup>CPC cardioidifferentiation previously reported (Rajabi-Zeleti *et al.*, 2014). Probably, our decellularized pericardial scaffold, displaying the highest number of matrisome proteins of all evaluated scaffolds (51 proteins) and preserving reported cardioidifferentiation key proteins, such as fibronectin, type-V collagen and some laminins (van Dijk *et al.*, 2008; Tan *et al.*, 2010; Pimton *et al.*, 2011), match the proportion of ECM-elements necessary for cardioidifferentiation. Interestingly, the *in vivo* implantation of decellularized pericardial scaffold refilled with cardiac ATDPCs reported cell expression of both

cardiac and endothelial markers (Gálvez-Montón *et al.*, 2017). Therefore, the signals exerted by the pericardial scaffold, combined with the infarcted myocardial microenvironment, further promote cardiac ATDPC differentiation. On another note, the endothelial differentiation capacity of cardiac ATDPCs was also maintained according to IsoB4 endothelial marker expression, similarly to what we described for myocardium, and in line with a prior study describing vascular cells endothelial differentiation over decellularized pericardial scaffolds (Yang *et al.*, 2012).

Overall, the essential microenvironment, combining structure, mechanics and protein composition, has been achieved in a decellularized myocardium, to recreate the biophysical cues to direct the numerous physiological processes, permit cell repopulation, and preserve cardiac ATDPC differentiation capacity, using a detergent-based decellularization protocol. Decellularized pericardial scaffold matched myocardial ECM architecture, stiffness and protein content, and once recellularized, displayed the highest cell retention and maintained cardiac ATDPC differentiation potential. Thus, pericardial scaffold becomes a valid option that recapitulates the native cardiac milieu and supports cardiac ATDPC recolonization.

#### 4. *In vivo* effects exerted by the engineered cardiac grafts for cardiac recovery

Up to date, some *in vivo* approximations have been conducted to assess the effects of decellularized myocardium and pericardium, respectively, and in few cases refilled with stem/progenitor cells. On the one hand, decellularized myocardium administration was initially encouraged by its safe and feasible delivery through catheter (Singelyn *et al.*, 2009), but, as yet, no studies have combined decellularized myocardial scaffolds with cells, losing the possible synergistic effect of administering both components (Singelyn *et al.*, 2012; Dai *et al.*, 2013; Seif-Naraghi *et al.*, 2013; Wassenaar *et al.*, 2016). Another work performed in rat utilized MSCs, but the myocardial scaffold was mixed with fibrin (Godier-Furnémont *et al.*, 2011). Globally, the resulting outcomes were modest, with no changes or minor variations after treatment in the most important clinical index to measure cardiac function improvements, the LVEF; and no concordance between the studies performed regarding infarct size reduction, fibrosis blockage and neovascularization. Moreover, just one was carried out in porcine MI model, using decellularized myocardial-derived hydrogel alone (Seif-Naraghi *et al.*, 2013). Therefore, there is an important gap of research done in swine, the preclinical animal model with a closer cardiovascular system to humans, to be filled with new data examining the potential of myocardial matrix combined with cardiac ATDPCs.

On the other hand, for decellularized pericardial scaffolds, the panorama is slightly different. So far, two studies collected in the literature were made in swine MI preclinical model, by either administering the decellularized pericardial scaffold directly (Gálvez-Montón *et al.*, 2015) or repopulated with cardiac ATDPCs (Gálvez-Montón *et al.*, 2017), reporting improvements in LVEF, reduction of infarct size and fibrosis, as well as neoinnervation and neovascularization. Other studies also tested the benefits exerted by the implantation of decellularized pericardial scaffolds (with and without cells) and corroborated neovascularization and ventricular function recovery, but were conducted in small animal models, limiting the extrapolation of

these benefits to humans (Chen *et al.*, 2008a; Wei *et al.*, 2008; Seif-Naraghi *et al.*, 2012; Sonnenberg *et al.*, 2015). Finally, it is important to note that decellularized pericardial scaffolds were also successfully recellularized with cardiac ATDPCs (Gálvez-Montón *et al.*, 2017) and BMSCs (Chen *et al.*, 2008a; Wei *et al.*, 2008) and tested *in vivo*; so, decellularized pericardial scaffolds seem an appropriate supportive platform for many different cell types.

The use of the specific cardiac ATDPC subpopulation has been widely employed for treating MI, due to its cardiac-like phenotype and vasculogenic potential, low immunogenicity and ease of obtaining and expansion, as mentioned previously. These suitable features encouraged their administration *in vivo*, which resulted in improvements in heart function recovery, vascularization and scarred area reduction (Bayes-Genis *et al.*, 2010; Bagó *et al.*, 2013). With all these premises, we hypothesized that the combination of these cells with cardiac scaffolds could further enhance the beneficial effects exerted by the cardiac ATDPCs, taking advantage of the cardiac environment the cells encounter within the scaffold that provides the physiological cues for their appropriate modulation. Accordingly, in our present work, we evaluated the effects of decellularized myocardial and pericardial scaffolds repopulated with cardiac ATDPCs, generating the EMG-ATDPC and EPG-ATDPC, respectively, upon implantation in a swine MI model. Additionally, we comparatively assessed the effects of both engineered cardiac grafts with the corresponding cell-free decellularized scaffold administration, to ascertain the optimal setting regarding post-MI recovery. For both engineered cardiac grafts, the cardiac function parameters (LVEF and/or left ventricular end-systolic volume (LVESV)) improved, either sacrifice versus baseline or versus post-MI, compared to the controls; and for EMG-ATDPC, infarct expansion was limited according to a reduced infarct size. These notable improvements represented a superior heart function outcome, in relation with low-magnitude results obtained in other *in vivo* studies administering ATDPCs (Rigol *et al.*, 2010; Bagó *et al.*, 2013; Gautam *et al.*, 2015; Bobi *et al.*, 2017), and similar, even better for EMG-ATDPC, reduction of infarcted area (Bayes-Genis *et al.*, 2010; Bagó *et al.*, 2013; Gautam *et al.*, 2015). Indeed, EPG-ATDPC showed similar benefits compared to a previous publication

(Gálvez-Montón *et al.*, 2017), confirming the potential of decellularized pericardial scaffolds.

All the matrices tested, regardless the presence of cardiac ATDPCs, showed neovascularization within the engineered graft and promoted a higher vascular density in the infarct bed. Moreover, the new blood vessels were functional and connected with the underlying myocardium and integrated in the host vasculature network, in concordance with previous publications (Gálvez-Montón *et al.*, 2015; Gálvez-Montón *et al.*, 2017). Connection with receptor blood vessels is critical to supply oxygen and nutrients to both the infarct core and the scaffold, while avoiding reoxygenation through the limited diffusion phenomenon that would cause massive cell death (Lovett *et al.*, 2009). These neovascularization effects for the decellularized myocardial and pericardial scaffolds confirm the vasculogenic capacity of the cardiac matrices that was previously described, with no need of cell seeding to induce vascularization (Seif-Naraghi *et al.*, 2013; Gálvez-Montón *et al.*, 2015). Moreover, and similarly to what happened with vascularization, nerve sprouting was observed in any of the four combinations including decellularized myocardial or pericardial scaffold. Although already reported after the acellular pericardial scaffold implantation (Gálvez-Montón *et al.*, 2015), and following ATDPC delivery (Cai *et al.*, 2009), this is the first time that nerve formation is observed for decellularized myocardium once engrafted, which should permit electrical coupling and action potential conduction. Also, mucopolysaccharides or glycosaminoglycans (long unbranched polysaccharides bound to ECM proteoglycans) were preserved as well, in line with our proteome analysis performed for decellularized scaffolds. These ECM components have been related to cell growth and attachment (Gandhi and Mancera, 2008), enhancing cardiac ATDPC adhesion and proliferation. The last MI sequelae evaluated, only for EMG-ATDPC during this thesis project, was fibrosis, revealing a marked decrease in type-I collagen and total collagen content, and an augment for type-III collagen. Type III collagen is present during wound healing, and self-structures to form an elastic fibrillar network, providing a framework to ensure correct alignment of type I collagen fibers and conservation of normal heart shape and stiffness; while type I collagen shows higher stiffness, enabling deleterious chamber remodeling process.

Therefore, these variations in the infarct ECM composition indicate a fibrosis spreading attenuation and reversion of, to some extent, the adverse ventricular remodeling (Weber, 1989; Pauschinger *et al.*, 1999). In line with this, and despite we did not comparatively evaluated the potential of EPG-ATDPC to revert fibrosis along this thesis project, a parallel study headed by our group concluded that the administration of the same EPG-ATDPCs, equipped with an electrical impedance spectroscopy monitoring system, also shifted the type I/III collagen ratio and increased type-III collagen, limiting fibrosis phenomenon occurring after MI (Gálvez-Montón *et al.*, 2017).

It is important to note that the combined administration of cardiac ATDPCs plus the decellularized scaffold, especially for the EMG-ATDPC, exhibited better outcomes than its non-recellularized scaffold counterpart, as endorsed by previous published works (Kofidis *et al.*, 2005; Chen *et al.*, 2013; Araña *et al.*, 2014; Chen *et al.*, 2014). Synergistic action of cardiac ATDPCs, supported by a favorable platform, along with the effects triggered by the scaffold itself, derived in enhanced cardiac regeneration and infarction salvage. Here, what seems odder is the lack of infarct size reduction or global cardiac improvement for the decellularized myocardial scaffold compared to the non-treated, infarcted control group. Generally, acellular matrices have been able to promote modest, but significant improvements in these two indices when engrafted, even with non-cardiac matrices (Kelly *et al.*, 2009; Okada *et al.*, 2010). Also, as it has been issued earlier (Gálvez-Montón *et al.*, 2015), we observed some improvements conducted following decellularized pericardial scaffold implantation in comparison with MI control animals. Negative decellularized myocardial scaffold results are contained in a controversial field regarding its beneficial effects, where positive (Dai *et al.*, 2013; Wassenaar *et al.*, 2016) and negative outcomes for infarct size and/or LVEF were reported (Singelyn *et al.*, 2012).

To explain the observed benefits, there are two main key players that, through diverse mechanisms, contribute to the cardiac regeneration: the cardiac ATDPCs and the supportive scaffold. For the cell component, three different mechanisms of action have been described: cardiomyocyte regeneration, vascularization and paracrine effects (Hoke *et al.*, 2009). These three mechanisms act

cooperatively, fostering the effects of each process individually and resulting in a higher cardiac recovery. Most likely, paracrine action exerted by the cardiac ATDPCs has a bigger contribution to the final impact in post-MI recovery, more than their cardiac and endothelial differentiation, and the direct, limited *in situ* effects promoted, as previously suggested (Mazo *et al.*, 2011). These paracrine effects have a great impact even if the mass of implanted cells is low (Fedak, 2008), agreeing with the relatively small cell number we transplanted and reinforcing the role of paracrine effects rather than direct action. By releasing diverse growth factors and cytokines, which act in a far distance from the initial place where they were secreted to recruit other cells, several regenerative, beneficial processes take place in the infarcted area:

- **Neovascularization promotion:** ATDPCs secrete several proangiogenic factors, such as VEGF, HGF or TGF- $\beta$ , with VEGF expression further boosted under hypoxia (Rehman *et al.*, 2004), that promote vascularization and endothelial cell mobilization. The effects of these paracrine angiogenic factors, along with the endothelial differentiation of cardiac ATDPCs, assessed by the expression of smooth muscle actin (SMA), IsoB4 and/or CD31, could explain the neovascularization observed not only in the engrafted scaffolds, but also within the infarcted bed. The vascular network sprouting should facilitate the reoxygenation of the injured tissue, as well as the recruitment of endogenous cells.
- **Apoptosis protection:** release of paracrine factors VEGF, FGF, HGF and insulin growth factor (IGF) has been shown to upregulate the antiapoptotic protein B-cell lymphoma-2, protecting the myocytes against cell death (Hoke *et al.*, 2009). Through this cardioprotective mechanism, it is possible to stop cardiomyocyte apoptosis, thus preventing infarct progression. This would correlate with the limitation of the infarct size expansion we have reported here.
- **Endogenous cardiac regeneration:** endogenous cell homing to the infarcted tissue has been pointed out as a putative reparative process. The administration of ATDPCs has reported recruitment of circulating endothelial progenitor cells (Kondo *et al.*, 2009) and mobilization of extracardiac BMSCs



(*li et al., 2011*). These effects are primarily mediated by stromal-derived factor 1 alpha (*Zhang et al., 2007*), secreted by the ATDPCs, which has been implicated in endothelial progenitor cell mobilization (*Moore et al., 2001*), but VEGF has been also associated with endogenous cell homing (*Tang et al., 2011*). The massive cell mobilization to the damaged myocardium influences cardioregeneration, vascularization and prevention of infarct expansion due to the exerted effects, namely, upregulating the formation of new cardiomyocytes (*Malliaras et al., 2013*), recruiting new endothelial progenitor cells to vascularize the myocardium (*Moore et al., 2001*), and through the differentiation of the BMSCs and some CPC subpopulations (the controversial c-kit<sup>+</sup>) to endothelial cells (*Finan and Richard, 2015*).

- **Microenvironment remodeling:** ATDPCs also have a key role in fine tuning of the matrix, modulating its composition. As it has been reported, ATDPC secretion of interleukin-1 $\beta$  has a direct effect over cardiac fibroblast activity (*Palmer et al., 1995*), main responsible for ECM synthesis modulation and collagen deposition during remodeling. Also, the metalloproteinases release, such as number 2, breakdowns the infarcted myocardial ECM and could drive the turnover and replacement by the new, physiological ECM (*Kokai et al., 2014*); whereas other ATDPC released factors, such as stromal-derived factor 1 alpha and HGF, have also antifibrotic function, reducing collagen synthesis (*Tang et al., 2010*). The precise crosstalking between these processes could explain the variations in collagen content after EMG-ATDPC engraftment that correlate with fibrosis halt, that were also observed for EPG-ATDPC (*Gálvez-Montón et al., 2017*).

In addition, the function of the decellularized scaffold to explain the positive outcomes observed should be considered. The preserved favorable cardiac ECM microenvironment, and the conservation of ECM-cell adhesion proteins support cardiac ATDPCs and foster their biological actions. Not only this, but also the decellularized scaffolds themselves can alter several pathways related to cardiac healing after MI. Indeed, a transcriptomic study for decellularized myocardial scaffold

administered in the infarcted area, reported upregulation of angiogenic and cardiac development genes, and downregulation of fibrotic, hypertrophic and apoptotic genes (Wassenaar *et al.*, 2016). Moreover, the recruitment of endogenous stem cells triggered by scaffolds, described elsewhere (Ou *et al.*, 2011; Wassenaar *et al.*, 2016), plays a key role in cardiac recovery through generation of new cardiomyocytes and neovascularization. Most likely, the hypoxic milieu triggers the secretion by local residing cells of proangiogenic factors VEGF, platelet-derived growth factor or stromal-derived factor 1 alpha, which remain retained within the matrix, stimulating host-circulating cell recruitment and attachment to the decellularized ECM, promoting cardiomyogenesis and vascularizing the damaged tissue (Muylaert *et al.*, 2014). These vascularizing events can be further potentiated by the addition of cardiac ATDPCs through their vasculogenic inherent potential and endogenous cell homing paracrine effects (Hoke *et al.*, 2009). Also, ECM protein fibronectin, identified in both decellularized cardiac tissues, seems to be essential for CPC mobilization, as its genetic ablation diminished CPC presence and conducted to a lower vasculogenesis and cardiogenesis after MI (Konstandin *et al.*, 2013). Post-MI neoinnervation is known to occur induced by the MI milieu, with elevated levels of nerve growth factor and growth associated protein 43, both involved in nerve proliferation and survival that lead to *de novo* formation of Schwann cells and axons following injury (Vracko *et al.*, 1990; Zhou *et al.*, 2004), similarly to what we reported here. Along with the demonstrated ATDPC synthesis of nerve growth factor (Cai *et al.*, 2009), it may cause the scaffold innervation.

Last but not least, degradation fragments derived from the ECM after *in vivo* proteolysis, the matrikines, can also exert beneficial effects and regulate cell behavior by cell receptor binding. Among the determined proteins through our proteomic analysis, it has been demonstrated that C-terminus of decorin inhibits connective tissue growth factor activity, blocking fibrosis progression (Vial *et al.*, 2011); while the first Fasciclin-1 domain of periostin has been associated with cell migration and angiogenesis processes (Kim *et al.*, 2014). Finally, the C-1158/59 fragment resulting from type-I collagen cleavage, has been related to scar healing, angiogenesis and reduction of left ventricular dilation post-MI (Lindsey *et al.*, 2015).

To summarize, both engineered cardiac grafts were able to promote cardiac regeneration and limit infarct expansion, as corroborated by the improvement in LVEF, reduction in infarct size and vascularization of the injured myocardium. The range of the benefits observed was comparable for both EMG-ATDPC and EPG-ATDPC, altogether with the similar individual ECM properties for the decellularized matrices, recreating with high fidelity the cardiac microenvironment. Thus, due to its higher cellular retention and its human origin that enables autologous implantation, of high importance for bench to bedside translation, the decellularized pericardium as the cellular scaffold should be the optimal to initiate clinical trials.



## Conclusions

---



In the present project, we reported the successful generation of two decellularized scaffolds from two different cardiac tissues: porcine myocardium and human pericardium. In both cases, the intrinsic tissue ECM properties after decellularization were well-preserved, maintaining the physiological cardiac microenvironment. This conserved cardiac milieu, *in vitro*, enabled the recellularization of the decellularized cardiac scaffolds with the cardiac ATDPCs, a cellular lineage with vasculogenic and cardiomyogenic potential. Moreover, this cell population displayed an immunosuppressive phenotype, suitable for their administration with allogeneic purposes.

*In vivo* engraftment of the recellularized myocardial and pericardial scaffolds, the EMG-ATDPC and EPG-ATDPC, respectively, resulted in beneficial effects regarding cardiac recovery following MI onset. Particularly, the implantation of both engineered cardiac grafts improved cardiac function. Furthermore, the scaffold showed *de novo* formation of nerves and blood vessels, which were coupled with the underlying myocardium vasculature network, and incremented vascularization within the injured tissue. Finally, for the EMG-ATDPC, the infarct core ECM composition was modulated, with a clear diminution in the present collagen content, indicative of fibrosis limitation and ventricular remodeling attenuation.

Therefore, the employment of two different recolonized cardiac scaffolds has been demonstrated to be safe, feasible and effective to promote cardioregenerative effects to treat MI in the swine preclinical model. As both scaffolds displayed similar positive functional outcomes, the human origin of the pericardium, which permits its autologous use to avoid a possible harmful immune response upon implantation, and its higher cell retention, should facilitate its translation to the first clinical trial in humans. Thus, the decellularized pericardium is ready to start the transition towards the clinics as a viable MI therapy.

The conclusions derived from this thesis project are:

**1. Cardiac ATDPCs display an immunosuppressive behavior.**

- Use of cardiac ATDPCs does not trigger T-cell proliferation.
- Cardiac ATDPCs abrogate activated T-cells alloproliferation.
- Cardiac ATDPCs reduce the secretion of proinflammatory cytokines.
- The immunomodulatory properties of cardiac ATDPCs are similar to the well-established low immunogenic characteristics of UCBSCs.

**2. The generated decellularized myocardial scaffolds preserve their cardiac ECM intrinsic properties and recreate the physiological cardiac microenvironment, strongly dependent on the decellularization protocol employed.**

- The resulting decellularized scaffolds are completely acellular, with no presence of nuclear and/or cytosolic debris.
- The structural and mechanical properties are well-preserved after decellularization, but biodegradability is higher when detergent-based protocol is used.
- The ECM protein components are also maintained, and typical myocardial matrix proteins important for ECM function and structure are identified. A higher number of matrisome proteins and less cellular proteins are detected for detergent-decellularized myocardial scaffolds.
- The decellularization protocol alters myocardial ECM biodegradability and protein content: the use of a trypsin-based procedure leaves a lower biodegradability and a reduced number of unique ECM proteins.

**3. The obtained decellularized pericardial scaffolds maintain their inherent ECM**



**characteristics (structure, stiffness and protein content), comparable to myocardial ECM.**

- The generated decellularized pericardial scaffolds are completely free of cellular remnants.
- Ultrastructure and mechanical properties are conserved following decellularization, similar to decellularized myocardial scaffolds.
- Decellularized pericardial scaffolds maintain the typical myocardial ECM components, and display a higher number of identified matrix proteins compared to decellularized myocardial scaffolds.
- Biodegradability of decellularized pericardial scaffolds is elevated and comparable to decellularized myocardial ones.

**4. The repopulated acellular cardiac scaffolds support cell recolonization and modulate cell behavior in a tissue- and decellularization protocol-dependent manner.**

- Cardiac ATDPC cell density after recellularization is more elevated in detergent-decellularized myocardial scaffolds compared to trypsin decellularization protocol (236 versus 98 cells/mm<sup>2</sup>), and recellularized pericardial scaffolds display the highest cell density (339 cells/mm<sup>2</sup>).
- Recellularized pericardial scaffolds present a more elevated cell penetration and a uniform distribution of cardiac ATDPCs throughout the scaffold thickness.
- Retention of cardiac ATDPC vasculogenic potential is maintained in all decellularized cardiac scaffolds, regardless of their origin and/or decellularization protocol employed.
- The preservation of cardiac ATDPC cardiomyogenic potential depends on the decellularization protocol used, and it is maintained in both myocardium or pericardium only when decellularized with the detergent-based method.

**5. The engraftment of an EMG-ATDPC in a swine MI model potentiates the vasculogenic potential of cardiac ATDPCs, and enhances injured myocardium vascularization and cardiac recovery following MI.**

- The cardiac ATDPCs refilled in the scaffold are retained, maintain endothelial marker expression and contribute to neovascularization.
- The EMG-ATDPC forms new blood vessels, which are functional and connect with the host vasculature network.
- The implantation of the EMG-ATDPC increases the vascular density within the infarct core.
- The EMG-ATDPC shows *de novo* nerve sprouting upon implantation.
- The engraftment of EMG-ATDPC improves the LVEF and the LVESV, parameters of cardiac function.
- The EMG-ATDPC reduces the infarct size, limits fibrosis progression, modulates collagen content and attenuates ventricular remodeling.
- The cell-free EMG revascularizes and innerves once administered, but it does not elicit any benefit in terms of cardiac function recovery or infarct expansion prevention.
- The implantation of EMG-ATDPC is safe, feasible and effective as a novel and promising therapeutic approach for MI treatment.

**6. The administration of an EPG-ATDPC improves neovascularization and promotes heart function enhancement in a porcine MI model.**

- The EPG-ATDPC promotes vascularization in both the infarct core and the decellularized scaffold, which integrates with the receptor vascular system.
- The EPG-ATDPC shows nerve sprouting within the decellularized scaffold.
- The implantation of EPG-ATDPC enhances cardiac function postimplantation.

- The introduction of a cell-free EPG promotes neovascularization and nerve spreading, and enhances cardiac function, but to a lesser extent compared to EPG-ATDPC.
- EPG-ATDPC engraftment is a safe and plausible approximation that exerts beneficial effects regarding cardiac recovery, and can be used as a therapeutic strategy to restore MI.

**7. EMG-ATDPC and EPG-ATDPC promote similar positive outcomes in terms of cardiac function improvement and infarction rescue, and are suitable candidates for clinical translation as MI therapeutic approaches. The human origin of decellularized pericardium scaffolds along with their higher cellular retention and penetrance after recellularization, makes EPG-ATDPC more readily committed to allogeneic use and may ease its road to the clinics.**



## **Bibliography**

---



**A**braham MR, Henrikson CA, Tung L, *et al.* Antiarrhythmic engineering of skeletal myoblasts for cardiac transplantation. *Circ Res* 2005; 97:159-67.

Abu-Issa R, Kirby ML. Heart field: from mesoderm to heart tube. *Annu Rev Cell Dev Biol* 2007; 23:45-68.

Acquapendente HF. *De Venarum Ostiolis*. 1603.

Aird WC. Discovery of the cardiovascular system: from Galen to William Harvey. *J Thromb Haemost* 2011; 9:118-29.

Akhyari P, Aubin H, Gwanmesia P, *et al.* The quest for an optimized protocol for whole-heart decellularization: a comparison of three popular and a novel decellularization technique and their diverse effects on crucial extracellular matrix qualities. *Tissue Eng Part C Methods* 2011; 17:915-26.

Amable PR, Teixeira MV, Carias RB, *et al.* Protein synthesis and secretion in human mesenchymal cells derived from bone marrow, adipose tissue and Wharton's jelly. *Stem Cell Res Ther* 2014; 5:53.

Andreu I, Luque T, Sancho A, *et al.* Heterogeneous micromechanical properties of the extracellular matrix in healthy and infarcted hearts. *Acta Biomater* 2014; 10:3235-42.

Ang KL, Chin D, Leyva F, *et al.* Randomized, controlled trial of intramuscular or intracoronary injection of autologous bone marrow cells into scarred myocardium during CABG versus CABG alone. *Nat Clin Pract Cardiovasc Med* 2008; 5:663-70.

Anker SD, Coats AJ, Cristian G, *et al.* A prospective comparison of alginate-hydrogel with standard medical therapy to determine impact on functional capacity and clinical outcomes in patients with advanced heart failure (AUGMENT-HF trial). *Eur Heart J* 2015; 36:2297-309.

Araña M, Gavira JJ, Peña E, *et al.* Epicardial delivery of collagen patches with adipose-derived stem cells in rat and minipig models of chronic myocardial infarction. *Biomaterials* 2014; 35:143-51.

Armstrong PW, Westerhout CM, Welsh RC. Duration of symptoms is the key

modulator of the choice of reperfusion for ST-elevation myocardial infarction. *Circulation* 2009; 119:1293-303.

Augello A, Tasso R, Negrini SM, *et al.* Bone marrow mesenchymal progenitor cells inhibit lymphocyte proliferation by activation of the programmed death 1 pathway. *Eur J Immunol* 2005; 35:1482-90.

Augst AD, Kong HJ, Mooney DJ. Alginate hydrogels as biomaterials. *Macromol Biosci* 2006; 6:623-33.

**B**adylak SF, Gilbert TW. Immune response to biologic scaffold materials. *Semin Immunol* 2008; 20:109-16.

Badylak SF, Taylor D, Uygun K. Whole-organ tissue engineering: decellularization and recellularization of three-dimensional matrix scaffolds. *Annu Rev Biomed Eng* 2011; 13:27-53.

Bagó JR, Soler-Botija C, Casani L, *et al.* Bioluminescence imaging of cardiomyogenic and vascular differentiation of cardiac and subcutaneous adipose tissue-derived progenitor cells in fibrin patches in a myocardium infarct model. *Int J Cardiol* 2013; 169:288-95.

Balsam LB, Wagers AJ, Christensen JL, *et al.* Haematopoietic stem cells adopt mature haematopoietic fates in ischaemic myocardium. *Nature* 2004; 428:668-73.

Bayes-Genis A, Salido M, Solé Ristol F, *et al.* Host cell-derived cardiomyocytes in sex-mismatch cardiac allografts. *Cardiovasc Res* 2002; 56:404-10.

Bayes-Genis A, Muñiz-Diaz E, Catusus L, *et al.* Cardiac chimerism in recipients of peripheral-blood and bone marrow stem cells. *Eur J Heart Fail* 2004; 6:399-402.

Bayes-Genis A, Belosillo B, de la Calle O, *et al.* Identification of male cardiomyocytes of extracardiac origin in the hearts of women with male progeny: male fetal cell microchimerism of the heart. *J Heart Lung Transplant* 2005a; 24:2179-83.

Bayes-Genis A, Roura S, Soler-Botija C, *et al.* Identification of cardiomyocyte lineage markers in untreated human bone marrow-derived mesenchymal stem cells.



*Transplant Proc* 2005b; 37:4077-9.

Bayes-Genis A, Soler-Botija C, Farré J, *et al.* Human progenitor cells derived from cardiac adipose tissue ameliorate myocardial infarction in rodents. *J Mol Cell Cardiol* 2010; 49:771-80.

Bearzi C, Rota M, Hosoda T, *et al.* Human cardiac stem cells. *Proc Natl Acad Sci U S A* 2007; 104:14068-73.

Beeri R, Chaput M, Guerrero JL, *et al.* Gene delivery of sarcoplasmic reticulum calcium ATPase inhibits ventricular remodeling in ischemic mitral regurgitation. *Circ Heart Fail* 2010; 3:627-34.

Bel A, Messas E, Agbulut O, *et al.* Transplantation of autologous fresh bone marrow into infarcted myocardium: a word of caution. *Circulation* 2003; 108:11247-52.

Berger PB, Ellis SG, Holmes DR Jr, *et al.* Relationship between delay in performing direct coronary angioplasty and early clinical outcome in patients with acute myocardial infarction: results from the Global Use of Strategies to Open Occluded Arteries in Acute Coronary Syndromes (GUSTO-IIb) trial. *Circulation* 1999; 100:14-20.

Bergmann O, Bhardwaj RD, Bernard S, *et al.* Evidence for cardiomyocyte renewal in humans. *Science* 2009; 324:98-102.

Berry MF, Engler AJ, Woo YJ, *et al.* Mesenchymal stem cell injection after myocardial infarction improves myocardial compliance. *Am J Physiol Heart Circ Physiol* 2006; 290:H2196-203.

Bidarra SJ, Barrias CC, Granja PL. Injectable alginate hydrogels for cell delivery in tissue engineering. *Acta Biomater* 2014; 10:1646-62.

Birla RK, Borschel GH, Dennis RG, *et al.* Myocardial engineering in vivo: formation and characterization of contractile, vascularized three-dimensional cardiac tissue. *Tissue Eng* 2005; 11:803-13.

Blackburn NJ, Sofrenovic T, Kuraitis D, *et al.* Timing underpins the benefits associated with injectable collagen biomaterial therapy for the treatment of myocardial infarction. *Biomaterials* 2015; 39:182-92.

Bobi J, Solanes N, Fernández-Jiménez R, *et al.* Intracoronary administration of allogeneic adipose tissue-derived mesenchymal stem cells improves myocardial perfusion but not left ventricle function, in a translational model of acute myocardial infarction. *J Am Heart Assoc* 2017; 6. doi: 10.1161/JAHA.117.005771.

Bock-Marquette I, Saxena A, White MD, *et al.* Thymosin beta4 activates integrin-linked kinase and promotes cardiac cell migration, survival and cardiac repair. *Nature* 2004; 432:466-72.

Bonafè F, Govoni M, Giordano E, *et al.* Hyaluronan and cardiac regeneration. *J Biomed Sci* 2014; 21:100.

Bonci D, Cittadini A, Latronico MV, *et al.* 'Advanced' generation lentiviruses as efficient vectors for cardiomyocyte gene transduction in vitro and in vivo. *Gene Ther* 2003; 10:630-6.


Boudoulas KD, Hatzopoulos AK. Cardiac repair and regeneration: the Rubik's cube of cell therapy for heart disease. *Dis Model Mech* 2009; 2:344-58.

Brown B, Lindberg K, Reing J, *et al.* The basement membrane component of biologic scaffolds derived from extracellular matrix. *Tissue Eng* 2006; 12:519-26.

Brown BN, Londono R, Tottey S, *et al.* Macrophage phenotype as a predictor of constructive remodeling following the implantation of biologically derived surgical mesh materials. *Acta Biomater* 2012; 8:978-87.

Buckingham M, Meilhac S, Zaffran S. Building the mammalian heart from two sources of myocardial cells. *Nat Rev Genet* 2005; 6:826-35.

Bunnell BA, Flaat M, Gagliardi C, *et al.* Adipose-derived stem cells: isolation, expansion and differentiation. *Methods* 2008; 45:115-20.

aesalpinus A. *Quaestionum peripateticarum libri quinque*. 1571.

Cai J, Yi FF, Yang XC, *et al.* Transplantation of embryonic stem cell-derived cardiomyocytes improves cardiac function in infarcted rat hearts. *Cytotherapy* 2007; 9:283-91.

Cai L, Johnstone BH, Cook TG, *et al.* IFATS Collection: human adipose tissue-derived stem cells induce angiogenesis and nerve sprouting following myocardial infarction, in conjunction with potent preservation of cardiac function. *Stem Cells* 2009; 27:230-7.

Camby I, Le Mercier M, Lefranc F, *et al.* Galectin-1: a small protein with major functions. *Glycobiology* 2006; 16:137R-57R.

Cao F, van der Bogt KE, Sadrzadeh A, *et al.* Spatial and temporal kinetics of teratoma formation from murine embryonic stem cell transplantation. *Stem Cells Dev* 2007; 16:883-91.

Carden DL, Granger DN. Pathophysiology of ischaemia-reperfusion injury. *J Pathol* 2000; 190:255-66.

Carpenter L, Carr C, Yang CT, *et al.* Efficient differentiation of human induced pluripotent stem cells generates cardiac cells that provide protection following myocardial infarction in the rat. *Stem Cells Dev* 2012; 21:977-86.

Caspi O, Huber I, Kehat I, *et al.* Transplantation of human embryonic stem cell-derived cardiomyocytes improves myocardial performance in infarcted rat hearts. *J Am Coll Cardiol* 2007; 50:1884-93.

Cescon M, Gattazzo F, Chen P, *et al.* Collagen VI at a glance. *J Cell Sci* 2015; 128:3525-31.

Chachques JC, Trainini JC, Lago N, *et al.* Myocardial assistance by grafting a new bioartificial upgraded myocardium (MAGNUM clinical trial): one year follow-up. *Cell Transplant* 2007; 16:927-34.

Chachques JC, Trainini JC, Lago N, *et al.* Myocardial Assistance by Grafting a New Bioartificial Upgraded Myocardium (MAGNUM trial): clinical feasibility study. *Ann Thorac Surg* 2008; 85:901-8.

Chandran PL, Paik DC, Holmes JW. Structural mechanism for alteration of collagen gel mechanics by glutaraldehyde crosslinking. *Connect Tissue Res* 2012; 53:285-97.

Chen CH, Wei HJ, Lin WW, *et al.* Porous tissue grafts sandwiched with multilayered

mesenchymal stromal cell sheets induce tissue regeneration for cardiac repair. *Cardiovasc Res* 2008a; 80:88-95.

Chen CH, Wang SS, Wei EI, *et al.* Hyaluronan enhances bone marrow cell therapy for myocardial repair after infarction. *Mol Ther* 2013; 21:670-9.

Chen CH, Chang MY, Wang SS, *et al.* Injection of autologous bone marrow cells in hyaluronan hydrogel improves cardiac performance after infarction in pigs. *Am J Physiol Heart Circ Physiol* 2014; 306:H1078-86.

Chen QZ, Harding SE, Ali NN, *et al.* Biomaterials in cardiac tissue engineering: ten years of research survey. *Mat Sci Eng R-Rep* 2008b; 59:1-37.

Chiu LL, Montgomery M, Liang Y, *et al.* Perfusable branching microvessel bed for vascularization of engineered tissues. *Proc Natl Acad Sci U S A* 2012; 109:E3414-23.

Cho PS, Messina DJ, Hirsh EL, *et al.* Immunogenicity of umbilical cord tissue-derived cells. *Blood* 2008; 111:430-8.

Chung HJ, Kim JT, Kim HJ. Epicardial delivery of VEGF and cardiac stem cells guided by 3-dimensional PLLA mat enhancing cardiac regeneration and angiogenesis in acute myocardial infarction. *J Control Release* 2015; 205:218-30.

Colazzo F, Sarathchandra P, Smolenski RT, *et al.* Extracellular matrix production by adipose-derived stem cells: implications for heart valve tissue engineering. *Biomaterials* 2011; 32:119-27.

Columbus MR. *De Re Anatomica*. 1559.

Colvin M, Smith JM, Skeans MA, *et al.* OPTN/SRTR 2015 annual data report: heart. *Am J Transplant* 2017; 17:286-356.

Cornetta K, Moen RC, Culver K, *et al.* Amphotropic murine leukemia retrovirus is not an acute pathogen for primates. *Hum Gene Ther* 1990; 1:15-30.

Crapo PM, Gilbert TW, Badylak SF. An overview of tissues and whole organ decellularization processes. *Biomaterials* 2011; 32:3233-43.

Cutler AJ, Limbani V, Girdlestone J, *et al.* Umbilical cord-derived mesenchymal

stromal cells modulate monocyte function to suppress T cell proliferation. *J Immunol* 2010; 185:617-23.

**D**ai W, Ger czuk P, Zhang Y, *et al.* Intramyocardial injection of heart tissue-derived extracellular matrix improves postinfarction cardiac function in rats. *J Cardiovasc Pharmacol Ther* 2013; 18:270-9.

Dale HH, Richards AN. The vasodilator action of histamine and of some other substances. *J Physiol* 1918; 52:110-65.

Daoud J, Petropavlovskaja M, Rosenberg L, *et al.* The effect of extracellular matrix components on the preservation of human islet function in vitro. *Biomaterials* 2010; 31:1676-82.

De Castro Brás LE, Ramirez TA, DeLeon-Pennell KY, *et al.* Texas 3-step decellularization protocol: looking at the cardiac extracellular matrix. *J Proteomics* 2013; 86:43-52.

Deng W, Han Q, Liao L, *et al.* Effects of allogeneic bone marrow-derived mesenchymal stem cells on T and B lymphocytes from BXSB mice. *DNA Cell Biol* 2005; 24:458-63.

Di Nicola M, Carlo-Stella C, Magni M, *et al.* Human bone marrow stromal cells suppress T-lymphocyte proliferation induced by cellular or nonspecific mitogenic stimuli. *Blood* 2002; 99:3838-43.

Dishart KL, Work LM, Denby L, *et al.* Gene therapy for cardiovascular disease. *J Biomed Biotechnol* 2003; 2003:138-48.

Dixon JA, Gorman RC, Stroud RE, *et al.* Mesenchymal cell transplantation and myocardial remodeling following myocardial infarction. *Circulation* 2009; 120:S220-9.

Dobaczewski M, Gonzalez-Quesada, Frangogiannis NG. The extracellular matrix as a modulator of the inflammatory and reparative response following myocardial infarction. *J Mol Cell Cardiol* 2010; 48:504-11.

Dobner S, Bezuidenhout D, Govender P, *et al.* A synthetic non-degradable

polyethylene glycol hydrogel retards adverse post-infarct left ventricular remodeling. *J Card Fail* 2009; 15:629-36.

Drawnel FM, Archer CR, Roderick HL. The role of the paracrine/autocrine mediator endothelin-1 in regulation of cardiac contractility and growth. *Br J Pharmacol* 2013; 168:296-317.

Duan B. State-of-the-art review of 3D bioprinting for cardiovascular tissue engineering. *Ann Biomed Eng* 2017; 45:195-209.

Duckers HJ, Houtgraaf J, Hehrlein C, *et al.* Final results of a phase IIa, randomised, open-label trial to evaluate the percutaneous intramyocardial transplantation of autologous skeletal myoblasts in congestive heart failure patients: the SEISMIC trial. *EuroIntervention* 2011; 6:805-12.

Dvir T, Benishti N, Shachar M, *et al.* A novel perfusion bioreactor providing a homogenous milieu for tissue regeneration. *Tissue Eng* 2006; 12:2843-52.

Dvir T, Timko BP, Brigham MD, *et al.* Nanowired three dimensional cardiac patches. *Nat Nanotechnol* 2011; 6:720-5.

Dyer LA, Kirby ML. The role of secondary heart field in cardiac development. *Dev Biol* 2009; 336:137-44.

**E**ngelmann TW. Ueber die Leitung der Erregung im Herzmuskel. *Pflüg Arch ges Physiol* 1875; 11:465-80.

Engleka KA, Manderfield LJ, Brust RD, *et al.* Islet1 derivatives in the heart are of both neural crest and second heart field origin. *Circ Res* 2012; 110:922-6.

Engler AJ, Sen S, Sweeney HL, *et al.* Matrix elasticity directs stem cell lineage specification. *Cell* 2006; 126:677-89.

Engler AJ, Carag-Krieger C, Johnson CP, *et al.* Embryonic cardiomyocytes beat best on a matrix with heart-like elasticity: scar-like rigidity inhibits beating. *J Cell Sci* 2008; 121:3794-802.

Eschenhagen T, Fink C, Remmers U, *et al.* Three-dimensional reconstitution of embryonic cardiomyocytes in a collagen matrix: a new heart muscle model system. *FASEB J* 1997; 11:683-94.

Estes BT, Wu AW, Guilak F. Potent induction of chondrocytic differentiation of human adipose-derived adult stem cells by bone morphogenetic protein 6. *Arthritis Rheum* 2006; 54:1222-32.

**F**edak PW. Paracrine effects of cell transplantation: modifying ventricular remodeling in the failing heart. *Semin Thorac Cardiovasc Surg* 2008; 20:87-93.

Ferrari G, Cusella-De Angelis G, Coletta M, *et al.* Muscle regeneration by marrow-derived myogenic precursors. *Science* 1998; 279:1528-30.

Finan A, Richard S. Stimulating endogenous cardiac repair. *Front Cell Dev Biol* 2015; 3:57.

Fleury S, Simeoni E, Zuppinger C, *et al.* Multiply attenuated, self-inactivating lentiviral vectors efficiently deliver and express genes for extended periods of time in adult rat cardiomyocytes in vivo. *Circulation* 2003; 107:2375-82.

Fomovsky GM, Thomopoulos S, Holmes JW. Contribution of extracellular matrix to the mechanical properties of the heart. *J Mol Cell Cardiol* 2010; 48:490-6.

Forte G, Carotenuto F, Pagliari F, *et al.* Criticality of the biological and physical stimuli array inducing resident cardiac stem cell determination. *Stem Cells* 2008; 26:2093-103.

Franz S, Rammelt S, Scharnweber D, *et al.* Immune responses to implants - a review of the implications for the design of immunomodulatory biomaterials. *Biomaterials* 2011; 32:6692-709.

French BA, Mazur W, Geske RS, *et al.* Direct in vivo gene transfer into porcine myocardium using replication-deficient adenoviral vectors. *Circulation* 1994; 90:2414-24.

Freyman T, Polin G, Osman H, *et al.* A quantitative, randomized study evaluating three

methods of mesenchymal stem cell delivery following myocardial infarction. *Eur Heart J* 2006; 27:1114-22.

Fuchs S, Kornowski R, Weisz G, *et al.* Safety and feasibility of transendocardial autologous bone marrow cell transplantation in patients with advanced heart disease. *Am J Cardiol* 2006; 97:823-9.

Fujimoto KL, Tobita K, Merryman WD, *et al.* An elastic, biodegradable cardiac patch induces contractile smooth muscle and improves cardiac remodeling and function in subacute myocardial infarction. *J Am Coll Cardiol* 2007; 49:2292-300.

Fukushima Y, Tamura M, Nakagawa H, *et al.* Induction of glioma cell migration by vitronectin in human serum and cerebrospinal fluid. *J Neurosurg* 2007; 107:578-85.

Furlani AP, Kalil RA, Castro I, *et al.* Effects of therapeutic angiogenesis with plasmid VEGF165 on ventricular function in a canine model of chronic myocardial infarction. *Rev Bras Cir Cardiovasc* 2009; 24:143-9.

**G**

aebel R, Ma N, Liu J, *et al.* Patterning human stem cells and endothelial cells with laser printing for cardiac regeneration. *Biomaterials* 2011; 32:9218-30.

Gaetani R, Doevendans PA, Metz CH, *et al.* Cardiac tissue engineering using tissue printing technology and human cardiac progenitor cells. *Biomaterials* 2012; 33:1782-90.

Gálvez-Montón C, Prat-Vidal C, Roura S, *et al.* Transposition of a pericardial-derived vascular adipose flap for myocardial salvage after infarct. *Cardiovasc Res* 2011; 91:659-67.

Gálvez-Montón C, Prat-Vidal C, Roura S, *et al.* Update: innovation in cardiology (IV). Cardiac tissue engineering and the bioartificial heart. *Rev Esp Cardiol (Engl Ed)* 2013; 66:391-9.

Gálvez-Montón C, Fernandez-Figueras MT, Martí M, *et al.* Neoinnervation and neovascularization of acellular pericardial-derived scaffolds in myocardial infarcts. *Stem Cell Res Ther* 2015; 6:108.



Gálvez-Montón C, Bragós R, Soler-Botija C, *et al.*, Noninvasive assessment of an engineered bioactive graft in myocardial infarction: impact on cardiac function and scar healing. *Stem Cells Transl Med* 2017; 6:647-55.

Gandhi NS, Mancera RL. The structure of glycosaminoglycans and their interaction with proteins. *Chem Biol Drug Des* 2008; 72:455-82.

Gao J, Liu J, Gao Y, *et al.* A myocardial patch made of collagen membranes loaded with collagen-binding human vascular endothelial growth factor accelerates healing of the injured rabbit heart. *Tissue Eng Part A* 2011; 17:2739-47.

Gao L, Kupfer ME, Jung JP, *et al.* Myocardial tissue engineering with cells derived from human-induced pluripotent stem cells and a native-like, high-Resolution, 3-dimensionally printed scaffold. *Circ Res* 2017; 120:1318-25.

Garber A, Livingston M. History of the circulatory system: discovery of the basis. *UWOMJ* 2008; 77:22-4.

Garrison FH. An outline of the history of the circulatory system. *Bull N Y Acad Med* 1931; 7:781-806.

Gaskell WH. Observations on the innervation of the heart. On the sequence of the contractions of the different portions of the heart. *Brit Med J* 1882; 2:572-3.

Gaskell WH. On the innervation of the heart, with especial reference to the heart of the tortoise. *J Physiol* 1883; 4:43-230.14.

Gautam M, Fujita D, Kimura K, *et al.* Transplantation of adipose tissue-derived stem cells improves cardiac contractile function and electrical stability in a rat myocardial infarction model. *J Mol Cell Cardiol* 2015; 81:139-49.

Gavaghan M. Cardiac anatomy and physiology. A review. *AORN Journal* 1998; 67:802-22.

Gelse K, Pöschl E, Aigner T. Collagens—structure, function, and biosynthesis. *Adv Drug Deliv Rev* 2003; 55:1531-46.

Georgiadis V, Knight RA, Jayasinghe SN, *et al.* Cardiac tissue engineering: renewing the arsenal for the battle against heart disease. *Integr Biol (Camb)* 2014; 6:111-26.

Gilbert TW, Freund JM, Badylak SF. Quantification of DNA in biologic scaffold materials. *J Surg Res* 2009; 152:135-9.

Gimble JM, Katz AJ, Bunnell BA. Adipose derived stem cells for regenerative medicine. *Circ Res* 2007; 100:1249-60.

Godier-Furnémont AF, Martens TP, Koeckert MS, *et al.* Composite scaffold provides a cell delivery platform for cardiovascular repair. *Proc Natl Acad Sci U S A* 2011; 108:7974-9.

Gong L, Zhou X, Wu Y, *et al.* Proteomic analysis profile of engineered articular cartilage with chondrogenic differentiated adipose tissue-derived stem cells loaded polyglycolic acid mesh for weight-bearing area defect repair. *Tissue Eng A* 2014; 20:575-87.

Gouk SS, Lim TM, Teoh SH, *et al.* Alterations of human acellular tissue matrix by gamma irradiation: histology, biomechanical property, stability, in vitro cell repopulation, and remodeling. *J Biomed Mater Res B Appl Biomater* 2008; 84:205-17.

Grauss RW, Hazekamp MG, Oppenhuizen F, *et al.* Histological evaluation of decellularised porcine aortic valves: matrix changes due to different decellularisation methods. *Eur J Cardiothorac Surg* 2005; 27:566-71.

Griffiths LG, Choe L, Lee KH, *et al.* Protein extraction and 2-DE of water- and lipid-soluble proteins in bovine pericardium, a low-cellularity tissue. *Electrophoresis* 2008; 29:4508-15.

Guilak F, Cohen DM, Estes BT, *et al.* Control of stem cell fate by physical interactions with the extracellular matrix. *Cell Stem Cell* 2009; 5:17-26.

Gutierrez-Aranda I, Ramos-Mejia V, Bueno C, *et al.* Human induced pluripotent stem cells develop teratoma more efficiently and faster than human embryonic stem cells regardless the site of injection. *Stem Cells* 2010; 28:1568-70.

Guyette JP, Charest JM, Mills RW, *et al.* Bioengineering human myocardium on native extracellular matrix. *Circ Res* 2016; 118:56-72.

Guzmán R, Nardecchia S, Gutiérrez MC, *et al.* Chitosan scaffolds containing calcium

phosphate salts and rhBMP-2: in vitro and in vivo testing for bone tissue regeneration. *PLoS One* 2014; 9:e87149.

Gyöngyösi M, Wojakowski W, Lemarchand P, *et al.* Meta-Analysis of Cell-based CaRdiac stUdiEs (ACCRUE) in patients with acute myocardial infarction based on individual patient data. *Circ Res* 2015; 116:1346-60.

**H**alkos ME, Zhao ZQ, Kerendi F, *et al.* Intravenous infusion of mesenchymal stem cells enhances regional perfusion and improves ventricular function in a porcine model of myocardial infarction. *Basic Res Cardiol* 2008; 103:525-36.

Halvorsen YD, Bond A, Sen A, *et al.* Thiazolidinediones and glucocorticoids synergistically induce differentiation of human adipose tissue stromal cells: biochemical, cellular, and molecular analysis. *Metabolism* 2001a; 50:407-13.

Halvorsen YD, Franklin D, Bond AL, *et al.* Extracellular matrix mineralization and osteoblast gene expression by human adipose tissue-derived stromal cells. *Tissue Eng* 2001b; 7:729-41.

Hamano K, Nishida M, Hirata K, *et al.* Local implantation of autologous bone marrow cells for therapeutic angiogenesis in patients with ischemic heart disease: clinical trial and preliminary results. *Jpn Circ J* 2001; 65:845-7.

Han J, Lazarovici P, Pomerantz C, *et al.* Co-electrospun blends of PLGA, gelatin, and elastin as potential nonthrombogenic scaffolds for vascular tissue engineering. *Biomacromolecules* 2011; 12:399-408.

Haraguchi Y, Shimizu T, Yamato M, *et al.* Electrical coupling of cardiomyocyte sheets occurs rapidly via functional gap junction formation. *Biomaterials* 2006; 27:4765-74.

Harvey W. *Exercitatio Anatomica de Motu Cordis et Sanguinis in Animalibus*. 1628.

Hasan A, Khattab A, Islam MA, *et al.* Injectable hydrogels for cardiac tissue repair after myocardial infarction. *Adv Sci (Weinh)* 2015; 2:1500122.

Hashemi SM, Ghods S, Kolodgie FD, *et al.* A placebo controlled, dose-ranging, safety study of allogenic mesenchymal stem cells injected by endomyocardial delivery after

an acute myocardial infarction. *Eur Heart J* 2008; 29:251-9.

He JQ, Ma Y, Lee Y, *et al.* Human embryonic stem cells develop into multiple types of cardiac myocytes: action potential characterization. *Circ Res* 2003; 93:32-9

Heilmann CA, Attmann T, Thiem A, *et al.* Gene therapy in cardiac surgery: intramyocardial injection of naked plasmid DNA for chronic myocardial ischemia. *Eur J Cardiothorac Surg* 2003; 24:785-93.

Henle J. Allgemeine Anatomie: Lehre von den Mischungs- und Formbestandtheilen des menschlichen Körpers. 1841.

Henning RJ, Abu-Ali H, Balis JU, *et al.* Human umbilical cord blood mononuclear cells for the treatment of acute myocardial infarction. *Cell Transplant* 2004; 13:729-39.

Hierlihy AM, Seale P, Lobe CG, *et al.* The post-natal heart contains a myocardial stem cell population. *FEBS Lett* 2002; 530:239-43.

Higuchi S, Lin Q, Wang J, *et al.* Heart extracellular matrix supports cardiomyocyte differentiation of mouse embryonic stem cells. *J Biosci Bioeng* 2013; 115:320-5.

Hill KL, Obrtlíkova P, Alvarez DF, *et al.* Human embryonic stem cell-derived vascular progenitor cells capable of endothelial and smooth muscle cell function. *Exp Hematol* 2010; 38:246-57.

Hirata Y, Sata M, Motomura N, *et al.* Human umbilical cord blood cells improve cardiac function after myocardial infarction. *Biochem Biophys Res Commun* 2005; 327:609-14.

Hirt MN, Hansen A, Eschenhagen T. Cardiac tissue engineering. State of the art. *Circ Res* 2014; 114:354-67.

His W. Die Thätigkeit des embryonalen Herzens und deren Bedeutung für die Lehre von der Herzbewegung beim Erwachsenen. *Arb Med Klin Leipzig* 1893; 1:14-50.

Hofland HE, Nagy D, Liu JJ, *et al.* In vivo gene transfer by intravenous administration of stable cationic lipid/DNA complex. *Pharm Res* 1997; 14:742-9.

Hofmann M, Wollert KC, Meyer GP, *et al.* Monitoring of bone marrow cell homing

into the infarcted human myocardium. *Circulation* 2005; 111:2198-202.

Hoke NN, Salloum FN, Loesser-Casey KE, *et al.* Cardiac regenerative potential of adipose tissue-derived stem cells. *Acta Physiol Hung* 2009; 96:251-65.

Hou D, Youssef EA, Brinton TJ, *et al.* Radiolabeled cell distribution after intramyocardial, intracoronary, and interstitial retrograde coronary venous delivery: implications for current clinical trials. *Circulation* 2005; 112:1150-6.

Houtgraaf JH, den Dekker WK, van Dalen BM, *et al.* First experience in humans using adipose tissue-derived regenerative cells in the treatment of patients with ST-segment elevation myocardial infarction. *J Am Coll Cardiol* 2012; 59:539-40.

Hruban RH, Long PP, Perlman EJ, *et al.* Fluorescence in situ hybridization for the Y-chromosome can be used to detect cells of recipient origin in allografted hearts following cardiac transplantation. *Am J Pathol* 1993; 142:975-80.

Hsieh PC, Segers VF, Davis ME, *et al.* Evidence from a genetic fate-mapping study that stem cells refresh adult mammalian cardiomyocytes after injury. *Nat Med* 2007; 13:970-4.

Huang NF, Yu J, Sievers R, *et al.* Injectable biopolymers enhance angiogenesis after myocardial infarction. *Tissue Eng* 2005; 11:1860-6.

Hule RA, Nagarkar RP, Altunbas A, *et al.* Correlations between structure, material properties and bioproperties in self-assembled  $\beta$ -hairpin peptide hydrogels. *Faraday Discuss* 2008; 139:251-64.

laizzo PA. General Features of the Cardiovascular System. In: laizzo PA. Handbook of cardiac anatomy, physiology, and devices. 2nd Edition. Minneapolis, MN: *Springer Science*, 2009:7-8.

Igarashi T, Finet JE, Takeuchi A, *et al.* Connexin gene transfer preserves conduction velocity and prevents atrial fibrillation. *Circulation* 2012; 125:216-25.

li M, Horii M, Yokoyama A, *et al.* Synergistic effect of adipose-derived stem cell therapy and bone marrow progenitor recruitment in ischemic heart. *Lab Invest* 2011;

91:539-52.

Imanishi Y, Miyagawa S, Maeda N, *et al.* Induced adipocyte cell-sheet ameliorates cardiac dysfunction in a mouse myocardial infarction model: a novel drug delivery system for heart failure. *Circulation* 2011; 124:S10-7.

Inagaki K, Fuess S, Storm TA, *et al.* Robust systemic transduction with AAV9 vectors in mice: efficient global cardiac gene transfer superior to that of AAV8. *Mol Ther* 2006; 14:45-53.

Ingulli E. Mechanism of cellular rejection in transplantation. *Pediatr Nephrol* 2010; 25:61-74.

Ito H, Okamura A, Iwakura K, *et al.* Myocardial perfusion patterns related to thrombolysis in myocardial infarction perfusion grades after coronary angioplasty in patients with acute anterior wall myocardial infarction. *Circulation* 1996; 93:1993-9.

Iwanaga Y, Hoshijima M, Gu Y, *et al.* Chronic phospholamban inhibition prevents progressive cardiac dysfunction and pathological remodeling after infarction in rats. *J Clin Invest* 2004; 113:727-36.

**J**acot JG, McCulloch AD, Omens JH. Substrate stiffness affects the functional maturation of neonatal rat ventricular myocytes. *Biophys J* 2008; 95:3479-87.

Jacot JG, Kita-Matsuo H, Wei KA, *et al.* Cardiac myocyte force development during differentiation and maturation. *Ann N Y Acad Sci* 2010; 1188:121-7.

Jaffe HA, Danel C, Longenecker G, *et al.* Adenovirus-mediated in vivo gene transfer and expression in normal rat liver. *Nat Genet* 1992; 1:372-8.

Janssens S, Dubois C, Bogaert J, *et al.* Autologous bone marrow-derived stem-cell transfer in patients with ST-segment elevation myocardial infarction: double-blind, randomised controlled trial. *Lancet* 2006; 367:113-21.

Jarvinen L, Badri L, Wettlaufer S, *et al.* Lung resistant mesenchymal stem cells isolated from human lung allografts inhibit T proliferation via a soluble mediator. *J Immunol* 2008; 181:4389-96.

Jaski BE, Jessup ML, Mancini DM, *et al.* Calcium upregulation by percutaneous administration of gene therapy in cardiac disease (CUPID trial), a first-in-human phase 1/2 clinical trial. *J Card Fail* 2009; 15:171-81.

Jeong SH, Ji YH, Yoon ES. Immunosuppressive activity of adipose tissue-derived mesenchymal stem cells in a rat model of hind limb allotransplantation. *Transplant Proc* 2014; 46:1606-14.

Jessup M, Brozena S. Medical progress. Heart failure. *N Engl J Med* 2003; 348:2007-18.

Jiang W, Ma A, Wang T, *et al.* Homing and differentiation of mesenchymal stem cells delivered intravenously to ischemic myocardium in vivo: a time-series study. *Pflugers Arch* 2006; 453:43-52.

Jiang XX, Zhang Y, Liu B, *et al.* Human mesenchymal stem cells inhibit differentiation and function of monocyte-derived dendritic cells. *Blood* 2005; 105:4120-6.

Jin J, Jeong SI, Shin YM, *et al.* Transplantation of mesenchymal stem cells within a poly(lactide-co-epsilon-caprolactone) scaffold improves cardiac function in a rat myocardial infarction model. *Eur J Heart Fail* 2009; 11:147-53.

Johnson TD, Dequach JA, Gaetani R, *et al.* Human versus porcine tissue sourcing for an injectable myocardial matrix hydrogel. *Biomater Sci* 2014; 2014:60283D.

Johnson TD, Hill RC, Dzieciatkowska M, *et al.* Quantification of decellularized human myocardial matrix: a comparison of six patients. *Proteomics Clin Appl* 2016; 10:75-83.

Jokinen J, Dadu E, Nykvist P, *et al.* Integrin-mediated cell adhesion to type I collagen fibrils. *J Biol Chem* 2004; 279:31956-63.

Jongpaiboonkit L, King WJ, Lyons GE, *et al.* An adaptable hydrogel array format for 3-dimensional cell culture and analysis. *Biomaterials* 2008; 29:3346-56.

Jopling C, Sleep E, Raya M, *et al.* Zebrafish heart regeneration occurs by cardiomyocyte dedifferentiation and proliferation. *Nature* 2010; 464:606-9.

**K**adner K, Dobner S, Franz T, *et al.* The beneficial effects of deferred delivery on the efficiency of hydrogel therapy post myocardial infarction. *Biomaterials* 2012; 33:2060-6.

Kaido T, Yebra M, Cirulli V, *et al.* Regulation of human beta-cell adhesion, motility, and insulin secretion by collagen IV and its receptor alpha1beta1. *J Biol Chem* 2004; 279:53762-9.

Kanelidis AJ, Premer C, Lopez J, *et al.* Route of delivery modulates the efficacy of mesenchymal stem cell therapy for myocardial infarction: A meta-analysis of preclinical studies and clinical trials. *Circ Res* 2017; 120:1139-50.

Kang WJ, Kang HJ, Kim HS, *et al.* Tissue distribution of 18F-FDG-labeled peripheral hematopoietic stem cells after intracoronary administration in patients with myocardial infarction. *J Nucl Med* 2006; 47:1295-301.

Karakikes I, Senyei GD, Hansen J, *et al.* Small molecule-mediated directed differentiation of human embryonic stem cells toward ventricular cardiomyocytes. *Stem Cells Transl Med* 2014; 3:18-31.

Kastrup J, Jørgensen E, Fuchs S, *et al.* A randomised, double-blind, placebo-controlled, multicentre study of the safety and efficacy of BIOBYPASS (AdGVVEGF121.10NH) gene therapy in patients with refractory advanced coronary artery disease: the NOVA trial. *EuroIntervention* 2011; 6:813-8.

Katz AM. Structure of the heart and cardiac muscle. In: Katz AM. Physiology of the heart. 5th Edition. Philadelphia, PA: *Lippincott Williams & Williams - Wolters Kluwer*, 2011:8-9.

Kawamura M, Miyagawa S, Miki K, *et al.* Feasibility, safety, and therapeutic efficacy of human induced pluripotent stem cell-derived cardiomyocyte sheets in a porcine ischemic cardiomyopathy model. *Circulation* 2012; 126:S29-37.

Keeley EC, Boura JA, Grines CL. Primary angioplasty versus intravenous thrombolytic therapy for acute myocardial infarction: a quantitative review of 23 randomised trials. *Lancet* 2003; 361:13-20.



Kehat I, Kenyagin-Karsenti D, Snir M, *et al.* Human embryonic stem cells can differentiate into myocytes with structural and functional properties of cardiomyocytes. *J Clin Invest* 2001; 108:407-14.

Keith A, Flack M. The form and nature of the muscular connections between the primary divisions of the vertebrate heart. *J Anat Physiol* 1907; 41:172-89.

Kellar RS, Shepherd BR, Larson DF, *et al.* Cardiac patch constructed from human fibroblasts attenuates reduction in cardiac function after acute infarct. *Tissue Eng* 2005; 11:1678-87.

Kellomäki M, Niiranen H, Puumanen K, *et al.* Bioabsorbable scaffolds for guided bone regeneration and degeneration. *Biomaterials* 2000; 21:2495-505.

Kelly DJ, Rosen AB, Schuldt AJ, *et al.* Increased myocyte content and mechanical function within a tissue-engineered myocardial patch following implantation. *Tissue Eng Part A* 2009; 15:2189-201.

Kent AF. Researches on the structure and function of the mammalian heart. *J Physiol* 1893; 14:i2-254.

Kim BR, Jang IH, Shin SH, *et al.* Therapeutic angiogenesis in a murine model of limb ischemia by recombinant periostin and its fasciclin I domain. *Biochim Biophys Acta* 2014; 1842:1324-32.

Kofidis T, de Bruin JL, Hoyt G, *et al.* Injectable bioartificial myocardial tissue for large-scale intramural cell transfer and functional recovery of injured heart muscle. *J Thorac Cardiovasc Surg* 2004; 128:571-8.

Kofidis T, Lebl DR, Martinez EC, *et al.* Novel injectable bioartificial tissue facilitates targeted, less invasive, large-scale tissue restoration on the beating heart after myocardial injury. *Circulation* 2005; 112:l173-7.

Kokai LE, Marra K, Rubin JP. Adipose stem cells: biology and clinical applications for tissue repair and regeneration. *Transl Res* 2014; 163:399-408.

Kondo K, Shintani S, Shibata R, *et al.* Implantation of adipose-derived regenerative cells enhances ischemia-induced angiogenesis. *Arterioscler Thromb Vasc Biol* 2009;

29:61-6.

Konrad L, Albrecht M, Renneberg H, *et al.* Mesenchymal entactin-1 (nidogen-1) is required for adhesion of peritubular cells of the rat testis in vitro. *Eur J Cell Biol* 2000; 79:112-20.

Konstandin MH, Toko H, Gastelum GM, *et al.* Fibronectin is essential for reparative cardiac progenitor cell response following myocardial infarction. *Circ Res* 2013; 113:115-25.

Kraehenbuehl TP, Zammaretti P, Van der Vlies AJ, *et al.* Three-dimensional extracellular matrix-directed cardioprogenitor differentiation: systematic modulation of a synthetic cell-responsive PEG-hydrogel. *Biomaterials* 2008; 29:2757-66.

Krogh A. The number and distribution of capillaries in muscles with calculations of the oxygen pressure head necessary for supplying the tissue. *J Physiol* 1919; 52:409-15.

Kroon E, Martinson LA, Kadoya K, *et al.* Pancreatic endoderm derived from human embryonic stem cells generates glucose-responsive insulin-secreting cells in vivo. *Nat Biotechnol* 2008; 26:443-52.

Krug EL, Mjaatvedt CH, Markwald RR. Extracellular matrix from embryonic myocardium elicits an early morphogenetic event in cardiac endothelial differentiation. *Dev Biol* 1987; 120:348-55.

Krupnick AS, Kreisel D, Engels FH, *et al.* A novel small animal model of left ventricular tissue engineering. *J Heart Lung Transplant* 2002; 21:233-43.

**L**adage D, Turnbull IC, Ishikawa K, *et al.* Delivery of gelfoam-enabled cells and vectors into the pericardial space using a percutaneous approach in a porcine model. *Gene Ther* 2011; 18:979-85.

Laflamme MA, Myerson D, Saffitz JE, *et al.* Evidence for cardiomyocyte repopulation by extracardiac progenitors in transplanted human hearts. *Circ Res* 2002; 90:634-40.

Laflamme MA, Chen KY, Naumova AV, *et al.* Cardiomyocytes derived from human embryonic stem cells in pro-survival factors enhance function of infarcted rat hearts. *Nat Biotechnol* 2007; 25:1015-24.

Laflamme MA, Murry CE. Heart regeneration. *Nature* 2011; 473:326-35.

Lai NC, Roth DM, Gao MH, *et al.* Intracoronary adenovirus encoding adenylyl cyclase VI increases left ventricular function in heart failure. *Circulation* 2004; 110:330-6.

LaNasa SM, Bryant SJ. Influence of ECM proteins and their analogs on cells cultured on 2-D hydrogels for cardiac muscle tissue engineering. *Acta Biomater* 2009; 5:2929-38.

Landa N, Miller L, Feinberg MS, *et al.* Effect of injectable alginate implant on cardiac remodeling and function after recent and old infarcts in rat. *Circulation* 2008; 117:1388-96.

Langer R, Vacanti JP. Tissue engineering. *Science* 1993; 260:920-6.

Laugwitz KL, Moretti A, Lam J, *et al.* Postnatal isl1+ cardioblasts enter fully differentiated cardiomyocyte lineages. *Nature* 2005; 433:647-53.

Laurent LC, Ulitsky I, Slavin I, *et al.* Dynamic changes in the copy number of pluripotency and cell proliferation genes in human ESCs and iPSCs during reprogramming and time in culture. *Cell Stem Cell* 2011; 8:106-18.

Le Blanc K, Tammik C, Rosendahl K, *et al.* HLA expression and immunologic properties of differentiated and undifferentiated mesenchymal stem cells. *Exp Hematol* 2003; 31:890-6.

Le T, Chong J. Cardiac progenitor cells for heart repair. *Cell Death Discov* 2016; 2:16052.

Lee J, Han DJ, Kim SC. In vitro differentiation of human adipose tissue-derived stem cells into cells with pancreatic phenotype by regenerating pancreas extract. *Biochem Biophys Res Commun* 2008; 375:547-51.

Lee M, Jeong SY, Ha J, *et al.* Low immunogenicity of allogeneic human umbilical cord blood-derived mesenchymal stem cells in vitro and in vivo. *Biochem Biophys Res*

*Commun* 2014; 446:983-9.

Leistner DM, Fischer-Rasokat U, Honold J, *et al.* Transplantation of progenitor cells and regeneration enhancement in acute myocardial infarction (TOPCARE-AMI): final 5-year results suggest long-term safety and efficacy. *Clin Res Cardiol* 2011; 100:925-34.

Leobon B, Roncalli J, Joffre C, *et al.* Adipose-derived cardiomyogenic cells: in vitro expansion and functional improvement in a mouse model of myocardial infarction. *Cardiovasc Res* 2009; 83:757-67.

Leor J, Aboulafia-Etzion S, Dar A, *et al.* Bioengineered cardiac grafts: a new approach to repair the infarcted myocardium? *Circulation* 2000; 102:III56-61.

Leor J, Amsalem Y, Cohen S. Cells, scaffolds, and molecules for myocardial tissue engineering. *Pharmacol Ther* 2005; 105:151-63.

Leor J, Guetta E, Feinberg MS, *et al.* Human umbilical cord blood-derived CD133+ cells enhance function and repair of the infarcted myocardium. *Stem Cells* 2006; 24:772-80.

Leor J, Gerecht S, Cohen S, *et al.* Human embryonic stem cell transplantation to repair the infarcted myocardium. *Heart* 2007; 93:1278-84.

Leor J, Tuvia S, Guetta V, *et al.* Intracoronary injection of in situ forming alginate hydrogel reverses left ventricular remodeling after myocardial infarction in swine. *J Am Coll Cardiol* 2009; 54:1014-23.

LeWinter MM, Samer K. Pericardial diseases. In: Zipes DP, Libby P, Bonow RO, *et al.* Braunwald's Heart Disease: a textbook of cardiovascular medicine 2. 7th Edition. Philadelphia, PA: Elsevier, 2005:1757-8.

Lewis T. The blood vessels of the human skin. *Br Med J* 1926; 2:61-2.

Li AH, Liu PP, Villarreal FJ, *et al.* Dynamic changes in myocardial matrix and relevance to disease: translational perspectives. *Circ Res* 2014; 114:916-27.

Li J, Tao R, Wu W, *et al.* 3D PLGA scaffolds improve differentiation and function of bone marrow mesenchymal stem cell-derived hepatocytes. *Stem Cells Dev* 2010a;

19:1427-36.

Li RK, Jia ZQ, Weisel RD, *et al.* Survival and function of bioengineered cardiac grafts. *Circulation* 1999; 100:II63-9.

Li SH, Lai TYY, Sun Z, *et al.* Tracking cardiac engraftment and distribution of implanted bone marrow cells: comparing intra-aortic, intravenous, and intramyocardial delivery. *J Thorac Cardiovasc Surg* 2009; 137:1225-33.

Li XY, Wang T, Jiang XJ, *et al.* Injectable hydrogel helps bone marrow-derived mononuclear cells restore infarcted myocardium. *Cardiology* 2010b; 115:194-9.

Li Z, Guan J. Hydrogels for cardiac tissue engineering. *Polymers* 2011; 3:740-61.

Lindsey ML, Iyer RP, Zamilpa R, *et al.* A novel collagen matricryptin reduces left ventricular dilation post-myocardial infarction by promoting scar formation and angiogenesis. *J Am Coll Cardiol* 2015; 66:1364-74.

Linnes M, Ratner BD, Giachelli CM. A fibrinogen based precision microporous scaffold for tissue engineering. *Biomaterials* 2007; 28:5298-306.

Lipskaia L, Chemaly ER, Hadri L, *et al.* Sarcoplasmic reticulum Ca<sup>(2+)</sup> ATPase as a therapeutic target for heart failure. *Expert Opin Biol Ther* 2010; 10:29-41.

Liu Y, Xu Y, Wang Z, *et al.* Electrospun nanofibrous sheets of collagen /elastin/polycaprolactone improve cardiac repair after myocardial infarction. *Am J Transl Res* 2016; 8:1678-94.

Liu Z, Wang H, Wang Y, *et al.* The influence of chitosan hydrogel on stem cell engraftment, survival and homing in the ischemic myocardial microenvironment. *Biomaterials* 2012; 33:3093-106.

Llano R, Epstein S, Zhou R, *et al.* Intracoronary delivery of mesenchymal stem cells at high flow rates after myocardial infarction improves distal coronary blood flow and decreases mortality in pigs. *Catheter Cardiovasc Interv* 2009; 73:251-7.

Llucià-Valldeperas A, Soler-Botija C, Gálvez-Montón C, *et al.* Electromechanical conditioning of adult progenitor cells improves recovery of cardiac function after myocardial infarction. *Stem Cells Transl Med* 2017; 6:970-81.

Lopes MS, Jardini AL, Maciel Filho R. Poly (lactic acid) production for tissue engineering applications. *Procedia Eng* 2012; 42:1402-13.

Lovett M, Lee K, Edwards A, *et al.* Vascularization strategies for tissue engineering. *Tissue Eng Part B Rev* 2009; 15:353-70.

Lu P, Takai K, Weaver VM, *et al.* Extracellular matrix degradation and remodeling in development and disease. *Cold Spring Harb Perspect Biol* 2011; 3:a005058.

Lu TY, Lin B, Kim J, *et al.* Repopulation of decellularized mouse heart with human induced pluripotent stem cell-derived cardiovascular progenitor cells. *Nat Commun* 2013; 4:2307.

Lu WN, Lü SH, Wang HB, *et al.* Functional improvement of infarcted heart by co-injection of embryonic stem cells with temperature-responsive chitosan hydrogel. *Tissue Eng Part A* 2009; 15:1437-47.

Lundgren E, Terracio L, Mårdh S, *et al.* Extracellular matrix components influence the survival of adult cardiac myocytes in vitro. *Exp Cell Res* 1985; 158:371-81.

**M**

a N, Stamm C, Kaminski A, *et al.* Human cord blood cells induce angiogenesis following myocardial infarction in NOD/scid-mice. *Cardiovasc Res* 2005; 66:45-54.

Ma Y, de Castro Brás LE, Toba H, *et al.* Myofibroblasts and the extracellular matrix network in post-myocardial infarction cardiac remodeling. *Pflugers Arch* 2014; 466:1113-27.

Ma Y, Wang J, Gao J, *et al.* Antithrombin up-regulates AMP-activated protein kinase signalling during myocardial ischaemia/reperfusion injury. *Thromb Haemost* 2015; 113:338-49.

Maccario R, Podestà M, Moretta A, *et al.* Interaction of human mesenchymal stem cells with cells involved in alloantigen-specific immune response favors the differentiation of CD4<sup>+</sup> T-cell subsets expressing a regulatory/suppressive phenotype. *Haematologica* 2005; 90:516-25.

Madamanchi A.  $\beta$ -Adrenergic receptor signaling in cardiac function and heart failure.

*Mcgill J Med* 2007; 10:99-104.

Madden LR, Mortisen DJ, Sussman EM, *et al.* Proangiogenic scaffolds as functional templates for cardiac tissue engineering. *Proc Natl Acad Sci U S A* 2010; 107:15211-6.

Madonna R, Petrov L, Teberino MA, *et al.* Transplantation of adipose tissue mesenchymal cells conjugated with VEGF-releasing microcarriers promotes repair in murine myocardial infarction. *Cardiovasc Res* 2015; 108:39-49.

Makadia HK, Siegel SJ. Poly lactic-co-glycolic acid (PLGA) as biodegradable controlled drug delivery carrier. *Polymers (Basel)* 2011; 3:1377-97.

Makino S, Fukuda K, Miyoshi S, *et al.* Cardiomyocytes can be generated from marrow stromal cells in vitro. *J Clin Invest* 1999; 103:697-705.

Malliaras K, Marbán E. Cardiac cell therapy: where we've been, where we are, and where we should be headed. *Br Med Bull* 2011; 98:161-85.

Malliaras K, Zhang Y, Seinfeld J, *et al.* Cardiomyocyte proliferation and progenitor cell recruitment underlie therapeutic regeneration after myocardial infarction in the adult mouse heart. *EMBO Mol Med* 2013; 5:191-209.

Malliaras K, Makkar RR, Smith RR, *et al.* Intracoronary cardiosphere-derived cells after myocardial infarction: evidence of therapeutic regeneration in the final 1-year results of the CADUCEUS trial (CARDiosphere-Derived aUtologous stem CELls to reverse ventricULar dySfunction). *J Am Coll Cardiol* 2014; 63:110-22.

Malpighi M. *De Pulmonibus*. 1661.

Mann DL, Lee RJ, Coats AJ, *et al.* One-year follow-up results from AUGMENT-HF: a multicentre randomized controlled clinical trial of the efficacy of left ventricular augmentation with Algisyl in the treatment of heart failure. *Eur J Heart Fail* 2016; 18:314-25.

Marieb EN, Hoehn K. The cardiovascular system: the heart. In: Marieb EN, Hoehn K. Human anatomy & physiology. 7th Edition. San Francisco, CA: *Pearson Education*, 2006:680.

Martin CM, Meeson AP, Robertson SM, *et al.* Persistent expression of the ATP-binding cassette transporter, *Abcg2*, identifies cardiac SP cells in the developing and adult heart. *Dev Biol* 2004; 265:262-75.

Martinelli V, Cellot G, Toma FM, *et al.* Carbon nanotubes promote growth and spontaneous electrical activity in cultured cardiac myocytes. *Nano Lett* 2012; 12:1831-8.

Martini FH, Nath JL, Bartholomew EF. The Heart. In: Martini FH, Nath JL, Bartholomew EF. *Fundamentals of anatomy & physiology*. 10th Edition. San Francisco, CA: *Pearson Education*, 2014:689-93; 697-702.

Martin-Rendon E, Sweeney D, Lu F, *et al.* 5-Azacytidine-treated human mesenchymal stem/progenitor cells derived from umbilical cord, cord blood and bone marrow do not generate cardiomyocytes in vitro at high frequencies. *Vox Sang* 2008; 95:137-48.

Martins AM, Eng G, Caridade SG, *et al.* Electrically conductive chitosan/carbon scaffolds for cardiac tissue engineering. *Biomacromolecules* 2014; 15:635-43.

Masumoto H, Matsuo T, Yamamizu K, *et al.* Pluripotent stem cell-engineered cell sheets reassembled with defined cardiovascular populations ameliorate reduction in infarct heart function through cardiomyocyte-mediated neovascularization. *Stem Cells* 2012; 30:1196-205.

Mathiasen AB, Jørgensen E, Qayyum AA, *et al.* Rationale and design of the first randomized, double-blind, placebo-controlled trial of intramyocardial injection of autologous bone-marrow derived Mesenchymal Stromal Cells in chronic ischemic Heart Failure (MSC-HF Trial). *Am Heart J* 2012; 164:285-91.

Matsuura K, Nagai T, Nishigaki N, *et al.* Adult cardiac Sca-1-positive cells differentiate into beating cardiomyocytes. *J Biol Chem* 2004; 279:11384-91.

Matsuura K, Honda A, Nagai T, *et al.* Transplantation of cardiac progenitor cells ameliorates cardiac dysfunction after myocardial infarction in mice. *J Clin Invest* 2009; 119:2204-17.

Matteucci C. Sur un phenomene physiologique produit par les muscles en



contraction. *Ann Chim Phys* 1842; 6:339-41.

Maureira P, Marie PY, Yu F, *et al.* Repairing chronic myocardial infarction with autologous mesenchymal stem cells engineered tissue in rat promotes angiogenesis and limits ventricular remodeling. *J Biomed Sci* 2012; 19:93.

Mayow J. *Tractatus Duo. Quorum prior agit de respiratione: alter de rachitide.* 1668.

Mazo M, Gavira JJ, Pelacho B, *et al.* Adipose-derived stem cells for myocardial infarction. *J Cardiovasc Transl Res* 2011; 4:145-53.

Ménard C, Hagège AA, Agbulut O, *et al.* Transplantation of cardiac-committed mouse embryonic stem cells to infarcted sheep myocardium: a preclinical study. *Lancet* 2005; 366:1005-12.

Ménard M, Dusseault J, Langlois G, *et al.* Role of protein contaminants in the immunogenicity of alginates. *J Biomed Mater Res B Appl Biomater* 2010; 93:333-40.

Menasché P, Hagège AA, Scorsin M, *et al.* Myoblast transplantation for heart failure. *Lancet* 2001; 357:279-80.

Menasché P, Hagège AA, Vilquin JT, *et al.* Autologous skeletal myoblast transplantation for severe postinfarction left ventricular dysfunction. *J Am Coll Cardiol* 2003; 41:1078-83.

Menasché P, Alfieri O, Janssens S, *et al.* The Myoblast Autologous Grafting in Ischemic Cardiomyopathy (MAGIC) trial: first randomized placebo-controlled study of myoblast transplantation. *Circulation* 2008; 117:1189-200.

Menasché P, Vanneaux V, Fabreguettes JR, *et al.* Towards a clinical use of human embryonic stem cell-derived cardiac progenitors: a translational experience. *Eur Heart J* 2015; 36:743-50.

Meredith JE Jr, Fazeli B, Schwartz MA. The extracellular matrix as a cell survival factor. *Mol Biol Cell* 1993; 4:953-61.

Messina E, De Angelis L, Frati G, *et al.* Isolation and expansion of adult cardiac stem cells from human and murine heart. *Circ Res* 2004; 95:911-21.

Milnor WR. The heart as a pump. In: Milnor WR. Cardiovascular Physiology. New York, NY: Oxford University Press, 1990:114.

Mingozzi F, High KA. Immune responses to AAV vectors: overcoming barriers to successful gene therapy. *Blood* 2013; 122:23-36.

Miranville A, Heeschen C, Sengenès C, *et al.* Improvement of postnatal neovascularization by human adipose tissue-derived stem cells. *Circulation* 2004; 110:349-55.

Mirsadraee S, Wilcox HE, Korossis SA, *et al.* Development and characterization of an acellular human pericardial matrix for tissue engineering. *Tissue Eng* 2006; 12:763-73.

Mitchell JB, McIntosh K, Zvonic S, *et al.* Immunophenotype of human adipose-derived cells: temporal changes in stromal-associated and stem cell-associated markers. *Stem Cells* 2006; 24:376-85.

Miyagi Y, Chiu LL, Cimini M, *et al.* Biodegradable collagen patch with covalently immobilized VEGF for myocardial repair. *Biomaterials* 2011; 32:1280-90.

Miyahara Y, Nagaya N, Kataoka M, *et al.* Monolayered mesenchymal stem cells repair scarred myocardium after myocardial infarction. *Nat Med* 2006; 12:459-65.

Mizuno H, Zuk PA, Zhu M, *et al.* Myogenic differentiation by human processed lipoaspirate cells. *Plast Reconstr Surg* 2002; 109:199-209.

Mollova M, Bersell K, Walsh S, *et al.* Cardiomyocyte proliferation contributes to heart growth in young humans. *Proc Natl Acad Sci U S A* 2013; 110:1446-51.

Mondal D, Griffith M, Venkatraman SS. Polycaprolactone-based biomaterials for tissue engineering and drug delivery: current scenario and challenges. *Int J Polym Mater* 2016; 65:255-65.

Monguió-Tortajada M, Lauzurica-Valdemoros R, Borràs FE. Tolerance in organ transplantation: from conventional immunosuppression to extracellular vesicles. *Front Immunol* 2014; 5:416.

Moon JJ, Matsumoto M, Patel S, *et al.* Role of cell surface heparan sulfate

proteoglycans in endothelial cell migration and mechanotransduction. *J Cell Physiol* 2005; 203:166-76.

Moore MA, Hattori K, Heissig B, *et al.* Mobilization of endothelial and hematopoietic stem and progenitor cells by adenovector-mediated elevation of serum levels of SDF-1, VEGF, and angiopoietin-1. *Ann N Y Acad Sci* 2001; 938:36-45.

Moorman AF, Christoffels VM. Cardiac chamber formation: development, genes, and evolution. *Physiol Rev* 2003; 83:1223-67.

Mosesson MW, Siebenlist KR, Meh DA. The structure and biological features of fibrinogen and fibrin. *Ann N Y Acad Sci* 2001; 936:11-30.

Mosqueira D, Pagliari S, Uto K, *et al.* Hippo pathway effectors control cardiac progenitor cell fate by acting as dynamic sensors of substrate mechanics and nanostructure. *ACS Nano* 2014; 8:2033-47.

Most P, Remppis A, Pleger ST, *et al.* S100A1: a novel inotropic regulator of cardiac performance. Transition from molecular physiology to pathophysiological relevance. *Am J Physiol Regul Integr Comp Physiol* 2007; 293:R568-77.

Mozaffarian D, Benjamin EJ, Go AS, *et al.* Heart disease and stroke statistics - 2016 update. A report from the American Heart Association. *Circulation* 2016; 133:e38-360.

Müller P, Pfeiffer P, Koglin J, *et al.* Cardiomyocytes of noncardiac origin in myocardial biopsies of human transplanted hearts. *Circulation* 2002; 106:31-5.

Murata M, Tohyama S, Fukuda K. Impacts of recent advances in cardiovascular regenerative medicine on clinical therapies and drug discovery. *Pharmacol Ther* 2010; 126:109-18.

Murrell M, Kamm R, Matsudaira P. Substrate viscosity enhances correlation in epithelial sheet movement. *Biophys J* 2011; 101:297-306.

Murry CE, Wiseman RW, Schwartz SM, *et al.* Skeletal myoblasts transplantation for repair of myocardial necrosis. *J Clin Invest* 1996; 98:2512-23.

Muscari C, Bonafè F, Martin-Suarez S, *et al.* Restored perfusion and reduced

inflammation in the infarcted heart after grafting stem cells with a hyaluronian-based scaffold. *J Cell Mol Med* 2013; 17:518-30.

Muylaert DE, Fledderus JO, Bouten CV, *et al.* Combining tissue repair and tissue engineering; bioactivating implantable cell-free vascular scaffolds. *Heart* 2014; 100:1825-30.

**N**agata H, li M, Kohbayashi E, *et al.* Cardiac adipose-derived stem cells exhibit high differentiation potential to cardiovascular cells in C57BL/6 mice. *Stem Cells Transl Med* 2016; 5:141-51.

Nakamuta JS, Danoviz ME, Marques FL, *et al.* Cell therapy attenuates cardiac dysfunction post myocardial infarction: effect of timing, routes of injection and a fibrin scaffold. *PLoS One* 2009; 4:e6005.

Nakazawa G, Otsuka F, Nakano M, *et al.* The pathology of neoatherosclerosis in human coronary implants bare-metal and drug-eluting stents. *J Am Coll Cardiol* 2011; 57:1314-22.

National Heart, Lung, and Blood Institute (NHLBI). What is a heart attack? 2015. Available at: <https://www.nhlbi.nih.gov/health/health-topics/topics/heartattack>. Accessed November 21, 2016.

Nelson TJ, Martinez-Fernandez A, Yamada S, *et al.* Repair of acute myocardial infarction by human stemness factors induced pluripotent stem cells. *Circulation* 2009; 120:408-16.

Ni K, O'Neill HC. The role of dendritic cells in T cell activation. *Immunol Cell Biol* 1997; 75:223-30.

Nichols M, Townsend N, Scarborough P, *et al.* Cardiovascular disease in Europe 2014: epidemiological update. *Eur Heart J* 2014; 35:2950-9.

Nikitovic D, Katonis P, Tsatsakis A, *et al.* Lumican, a small leucine-rich proteoglycan. *IUBMB Life* 2008; 60:818-23.

Niwano K, Arai M, Koitabashi N, *et al.* Lentiviral vector-mediated SERCA2 gene

transfer protects against heart failure and left ventricular remodeling after myocardial infarction in rats. *Mol Ther* 2008; 16:1026-32.

Nosedá M, Peterkin T, Simões FC, *et al.* Cardiopoietic factors. Extracellular signals for cardiac lineage commitment. *Circ Res* 2011; 108:129-52.

Nussbaum J, Minami E, Laflamme MA, *et al.* Transplantation of undifferentiated murine embryonic stem cells in the heart: teratoma formation and immune response. *FASEB J* 2007; 21:1345-57.

Nygren JM, Jovinge S, Breitbach M, *et al.* Bone marrow-derived hematopoietic cells generate cardiomyocytes at a low frequency through cell fusion, but not transdifferentiation. *Nat Med* 2004; 10:494-501.

**O**berpriller JO, Oberpriller JC. Response of the adult newt ventricle to injury. *J Exp Zool* 1974; 187:249-53.

Oh H, Bradfute SB, Gallardo TD, *et al.* Cardiac progenitor cells from adult myocardium: homing, differentiation, and fusion after infarction. *Proc Natl Acad Sci U S A* 2003; 100:12313-8.

Okada M, Payne TR, Oshima H, *et al.* Differential efficacy of gels derived from small intestinal submucosa as an injectable biomaterial for myocardial infarct repair. *Biomaterials* 2010; 31:7678-83.

Okano T, Yamada N, Okuhara M, *et al.* Mechanism of cell detachment from temperature-modulated, hydrophilic-hydrophobic polymer surfaces. *Biomaterials* 1995; 16:297-303.

Orozco-Beltrán D, Cooper RS, Gil-Guillén V, *et al.* Trends in mortality from myocardial infarction. A comparative study between Spain and the United States: 1990-2006. *Rev Esp Cardiol (Engl Ed)* 2012; 65:1079-85.

Oskoueí BN, Lamirault G, Joseph C, *et al.* Increased potency of cardiac stem cells compared with bone marrow mesenchymal stem cells in cardiac repair. *Stem Cells Transl Med* 2012; 1:116-24.

Ott HC, Matthiesen TS, Goh SK, *et al.* Perfusion-decellularized matrix: using nature's platform to engineer a bioartificial heart. *Nat Med* 2008; 14:213-21.

Ou L, Li W, Zhang Y, *et al.* Intracardiac injection of matrigel induces stem cell recruitment and improves cardiac functions in a rat myocardial infarction model. *J Cell Mol Med* 2011; 15:1310-8.

**P**acak CA, Mah CS, Thattaliyath BD, *et al.* Recombinant adeno-associated virus serotype 9 leads to preferential cardiac transduction in vivo. *Circ Res* 2006; 99:e3-9.

Palmer JN, Hartogensis WE, Patten M, *et al.* Interleukin-1 beta induces cardiac myocyte growth but inhibits cardiac fibroblast proliferation in culture. *J Clin Invest* 1995; 95:2555-64.

Park H, Larson BL, Guillemette MD, *et al.* The significance of pore microarchitecture in a multi-layered elastomeric scaffold for contractile cardiac muscle constructs. *Biomaterials* 2011; 32:1856-64.

Pascual-Gil S, Simón-Yarza T, Garbayo E, *et al.* Cytokine-loaded PLGA and PEG-PLGA microparticles showed similar heart regeneration in a rat myocardial infarction model. *Int J Pharm* 2017; 523:531-33.

Pauschinger M, Knopf D, Petschauer S, *et al.* Dilated cardiomyopathy is associated with significant changes in collagen type I/III ratio. *Circulation* 1999; 99:2750-6.

Perin EC, Dohmann HF, Borojevic R, *et al.* Improved exercise capacity and ischemia 6 and 12 months after transendocardial injection of autologous bone marrow mononuclear cells for ischemic cardiomyopathy. *Circulation* 2004; 110:II213-8.

Pfeffer MA, Braunwald E. Ventricular remodeling after myocardial infarction. Experimental observations and clinical implications. *Circulation* 1990; 81:1161-72.

Pimton P, Sarkar S, Sheth N, *et al.* Fibronectin-mediated upregulation of  $\alpha 5\beta 1$  integrin and cell adhesion during differentiation of mouse embryonic stem cells. *Cell Adh Migr* 2011; 5:73-82.

Planat-Bénard V, Menard C, André M, *et al.* Spontaneous cardiomyocyte

differentiation from adipose tissue stroma cells. *Circ Res* 2004a; 94:223-9.

Planat-Bénard V, Silvestre JS, Cousin B, *et al.* Plasticity of human adipose lineage cells toward endothelial cells: physiological and therapeutic perspectives. *Circulation* 2004b; 109:656-63.

Pleger ST, Shan C, Ksienzyk J, *et al.* Cardiac AAV9-S100A1 gene therapy rescues post-ischemic heart failure in a preclinical large animal model. *Sci Transl Med* 2011; 3:92ra64.

Pocock G, Richards CD, Richards DA. The cardiovascular system. In: Pocock G, Richards CD, Richards DA. *Human Physiology*. 4th Edition. Oxford, United Kingdom: *Oxford University Press*, 2013:361-2.

Poelzing S, Rosenbaum DS. Altered connexin43 expression produces arrhythmia substrate in heart failure. *Am J Physiol Heart Circ Physiol* 2004; 287:H1762-70.

Pok S, Benavides OM, Hallal P, *et al.* Use of myocardial matrix in a chitosan-based full-thickness heart patch. *Tissue Eng Part A* 2014; 20:1877-87.

Porrello ER, Mahmoud AI, Simpson E, *et al.* Transient regenerative potential of the neonatal mouse heart. *Science* 2011; 331:1078-80.

Poss KD, Wilson LG, Keating MT. Heart regeneration in zebrafish. *Science* 2002; 298:2188-90.

Potapova IA, Doronin SV, Kelly DJ, *et al.* Enhanced recovery of mechanical function in the canine heart by seeding an extracellular matrix patch with mesenchymal stem cells committed to a cardiac lineage. *Am J Physiol Heart Circ Physiol* 2008; 295:H2257-63.

Prat-Vidal C, Roura S, Farré J, *et al.* Umbilical cord blood-derived stem cells spontaneously express cardiomyogenic traits. *Transplant Proc* 2007; 39:2434-7.

Prestwich GD. Hyaluronic acid-based clinical biomaterials derived for cell and molecule delivery in regenerative medicine. *J Control Release* 2011; 155:193-9.

Puissant B, Barreau C, Bourin P, *et al.* Immunomodulatory effect of human adipose tissue-derived adult stem cells: comparison with bone marrow mesenchymal stem

cells. *Br J Haematol* 2005; 129:118-29.

Purkinje JE. Mikroskopisch-neurologische Beobachtungen. *Arch Anat Physiol Wiss Med* 1845; 12:281-96.

**Q**iu Y, Bayomy AF, Gomez MV, *et al.* A role for matrix stiffness in the regulation of cardiac side population cell function. *Am J Physiol Heart Circ Physiol* 2015; 308(9):H990-7.

Quaedackers ME, Baan CC, Weimar W, *et al.* Cell contact interaction between adipose-derived stromal cells and allo-activated T lymphocytes. *Eur J Immunol* 2009; 39:3436-46.

**R**aake PW, Schlegel P, Ksienzyk J, *et al.* AAV6.βARKct cardiac gene therapy ameliorates cardiac function and normalizes the catecholaminergic axis in a clinically relevant large animal heart failure model. *Eur Heart J* 2013; 34:1437-47.

Radisic M, Park H, Shing H, *et al.* Functional assembly of engineered myocardium by electrical stimulation of cardiac myocytes cultured on scaffolds. *Proc Natl Acad Sci U S A* 2004; 101:18129-34.

Radisic M, Park H, Martens TP, *et al.* Pre-treatment of synthetic elastomeric scaffolds by cardiac fibroblasts improves engineered heart tissue. *J Biomed Mater Res A* 2008; 86:713-24.

Raja SG, Haider Z, Ahmad M, *et al.* Saphenous vein grafts: to use or not to use? *Heart Lung Circ* 2004; 13:403-9.

Rajabi-Zeleti S, Jalili-Firoozinezhad S, Azarnia M, *et al.* The behavior of cardiac progenitor cells on macroporous pericardium-derived scaffolds. *Biomaterials* 2014; 35:970-82.

Rane AA, Christman KL. Biomaterials for the treatment of myocardial infarction: a 5-year update. *J Am Coll Cardiol* 2011; 58:2615-29.



Raya A, Koth CM, Büscher D, *et al.* Activation of Notch signaling pathway precedes heart regeneration in zebrafish. *Proc Natl Acad Sci U S A* 2003; 100:11889-95.

Rehman J, Traktuev D, Li J, *et al.* Secretion of angiogenic and antiapoptotic factors by human adipose stromal cells. *Circulation* 2004; 109:1292-8.

Reikvam A, Hagen TP. Changes in myocardial infarction mortality. *Tidsskr Nor Laegeforen* 2011; 131:468-70.

Reing JE, Zhang L, Myers-Irvin J, *et al.* Degradation products of extracellular matrix affect cell migration and proliferation. *Tissue Eng Part A* 2009; 15:605-14.

Reis LA, Chiu LL, Feric N, *et al.* Biomaterials in myocardial tissue engineering. *J Tissue Eng Regen Med* 2016; 10:11-28.

Ren G, Zhang L, Zhao X, *et al.* Mesenchymal stem cell-mediated immunosuppression occurs via concerted action of chemokines and nitric oxide. *Cell Stem Cell* 2008; 2:141-50.

Ren G, Zhao X, Zhang L, *et al.* Inflammatory cytokine-induced intercellular adhesion molecule-1 and vascular cell adhesion molecule-1 in mesenchymal stem cells are critical for immunosuppression. *J Immunol* 2010; 184:2321-8.

Revi D, Paul W, Anilkumar TV, *et al.* Chitosan scaffold co-cultured with keratinocyte and fibroblast heals full thickness skin wounds in rabbit. *J Biomed Mater Res A* 2014; 102:3273-81.

Reyes M, Dudek A, Jahagirdar B, *et al.* Origin of endothelial progenitors in human postnatal bone marrow. *J Clin Invest* 2002; 109:337-46.

Rezkalla SH, Kloner RA. No-reflow phenomenon. *Circulation* 2002; 105:656-62.

Rienks M, Papageorgiou AP, Frangogiannis NG, *et al.* Myocardial extracellular matrix. An ever-changing and diverse entity. *Circ Res* 2014; 114:872-88.

Rigol M, Solanes N, Farré J, *et al.* Effects of adipose tissue-derived stem cell therapy after myocardial infarction: impact on the route of administration. *J Card Fail* 2010; 16:357-66.

Robertson MJ, Dries-Devlin JL, Kren SM, *et al.* Optimizing recellularization of whole decellularized heart extracellular matrix. *PLoS One* 2014; 9:e90406.

Rodbell M. Metabolism of isolated fat cells. II. The similar effects of phospholipase C (*Clostridium perfringens* alpha toxin) and of insulin on glucose and amino acid metabolism. *J Biol Chem* 1966; 241:130-9.

Rodrigo SF, van Ramshorst J, Hoogslag GE, *et al.* Intramyocardial injection of autologous bone marrow-derived ex vivo expanded mesenchymal stem cells in acute myocardial infarction patients is feasible and safe up to 5 years of follow-up. *J Cardiovasc Transl Res* 2013; 6:816-25.

Rodriguez AG, Han SJ, Regnier M, *et al.* Substrate stiffness increases twitch power of neonatal cardiomyocytes in correlation with changes in myofibril structure and intracellular calcium. *Biophys J* 2011; 101:2455-64.

Rodriguez ER, Tan CD. Structure and anatomy of the human pericardium. *Prog Cardiovasc Dis* 2017; 59:327-40.

Roffi M, Patrono C, Collet JP, *et al.* 2015 ESC Guidelines for the management of acute coronary syndromes in patients presenting without persistent ST-segment elevation: task force for the management of acute coronary syndromes in patients presenting without persistent ST-segment elevation of the European Society of Cardiology (ESC). *Eur Heart J* 2016; 37:267-315.

Roura S, Farré J, Hove-Madsen L, *et al.* Exposure to cardiomyogenic stimuli fails to transdifferentiate human umbilical cord blood-derived mesenchymal stem cells. *Basic Res Cardiol* 2010; 105:419-30.

Roura S, Bagó JR, Soler-Botija C, *et al.* Human umbilical cord blood-derived mesenchymal stem cells promote vascular growth in vivo. *PLoS One* 2012; 7:e49447.

Roura S, Pujal JM, Gálvez-Montón C, *et al.* The role and potential of umbilical cord blood in an era of new therapies: a review. *Stem Cell Res Ther* 2015; 6:123.

Rowe SL, Lee S, Stegemann JP. Influence of thrombin concentration on the mechanical and morphological properties of cell-seeded fibrin hydrogels. *Acta*

*Biomater* 2007; 3:59-67.

Royal College of Physicians. Myocardial ischaemia national audit project. 2013. Available at: [https://www.ucl.ac.uk/nicor/audits/minap/documents/annual\\_reports/minap-report-2013](https://www.ucl.ac.uk/nicor/audits/minap/documents/annual_reports/minap-report-2013). Accessed December 27, 2016.

Rumyantsev PP. Ultrastructural reorganization, DNA synthesis and mitotic division of myocytes in atria of rats with left ventricle infarction. An electron microscopic and autoradiographic study. *Virchows Arch B Cell Pathol* 1974; 15:357-78.

Ruvinov E, Leor J, Cohen S. The promotion of myocardial repair by the sequential delivery of IGF-1 and HGF from an injectable alginate biomaterial in a model of acute myocardial infarction. *Biomaterials* 2011; 32:565-78.

**S**abbah HN, Wang M, Gupta RC, *et al.* Augmentation of left ventricular wall thickness with alginate hydrogel implants improves left ventricular function and prevents progressive remodeling in dogs with chronic heart failure. *JACC Heart Fail* 2013; 1:252-8.

Safford KM, Hicok KC, Safford SD, *et al.* Neurogenic differentiation of murine and human adipose-derived stromal cells. *Biochem Biophys Res Commun* 2002; 294:371-9.

Sahara M, Santoro F, Chien KR. Programming and reprogramming a human heart cell. *EMBO J* 2015; 34:710-38.

Sakaguchi K, Shimizu T, Okano T. Construction of three-dimensional vascularized cardiac tissue with cell sheet engineering. *J Control Release* 2015; 205:83-8.

Sanganalmath SK, Bolli R. Cell therapy for heart failure: a comprehensive overview of experimental and clinical studies, current challenges, and future directions. *Circ Res* 2013; 113:810-34.

Sarig U, Machluf M. Engineering cell platforms for myocardial regeneration. *Expert Opin Biol Ther* 2011; 11:1055-77.

Savi M, Bocchi L, Fiumana E, *et al.* Enhanced engraftment and repairing ability of human adipose-derived stem cells, conveyed by pharmacologically active microcarriers continuously releasing HGF and IGF-1, in healing myocardial infarction in rats. *J Biomed Mater Res A* 2015; 103:3012-25.

Schleich JM. Images in cardiology. Development of the human heart: days 15-21. *Heart* 2002; 87:487.

Schoenwolf GC, Bleyl SB, Brauer PR, *et al.* Development of the heart. In: Schoenwolf GC, Bleyl SB, Brauer PR, *et al.* Larsen's human embryology. 4th Edition. Philadelphia, PA: Elsevier, 2009:341-84.

Schönherr E, Levkau B, Schaefer L, *et al.* Decorin-mediated signal transduction in endothelial cells. Involvement of Akt/protein kinase B in up-regulation of p21<sup>WAF1/CIP1</sup> but not p27<sup>KIP1</sup>. *J Biol Chem* 2001; 276:40687-92.

Segers VF, Lee RT. Stem-cell therapy for cardiac disease. *Nature* 2008; 451:937-42.

Seidler DG, Schaefer L, Robenek H, *et al.* A physiologic three-dimensional cell culture system to investigate the role of decorin in matrix organisation and cell survival. *Biochem Biophys Res Commun* 2005; 332:1162-70.

Seif-Naraghi SB, Salvatore MA, Schup-Magoffin PJ, *et al.* Design and characterization of an injectable pericardial matrix gel: a potentially autologous scaffold for cardiac tissue engineering. *Tissue Eng Part A* 2010; 16:2017-27.

Seif-Naraghi SB, Horn D, Schup-Magoffin PA, *et al.* Patient-to-patient variability in autologous pericardial matrix scaffolds for cardiac repair. *J Cardiovasc Transl Res* 2011; 4:545-56.

Seif-Naraghi SB, Horn D, Schup-Magoffin PJ, *et al.* Injectable extracellular matrix derived hydrogel provides a platform for enhanced retention and delivery of a heparin-binding growth factor. *Acta Biomater* 2012; 8:3695-703.

Seif-Naraghi SB, Singelyn JM, Salvatore MA, *et al.* Safety and efficacy of an injectable extracellular matrix hydrogel for treating myocardial infarction. *Sci Transl Med* 2013; 5:173ra25.

Sekine H, Shimizu T, Dobashi I, *et al.* Cardiac cell sheet transplantation improves damaged heart function via superior cell survival in comparison with dissociated cell injection. *Tissue Eng Part A* 2011; 17:2973-80.

Sekiya N, Matsumiya G, Miyagawa S, *et al.* Layered implantation of myoblast sheets attenuates adverse cardiac remodeling of the infarcted heart. *J Thorac Cardiovasc Surg* 2009; 138:985-93.

Senyo SE, Steinhauser ML, Pizzimenti CL, *et al.* Mammalian heart renewal by preexisting cardiomyocytes. *Nature* 2013; 493:433-6.

Servetus M. *Christianismi Restitutio*. 1553.

Shapira K, Dikovsky D, Habib M, *et al.* Hydrogels for cardiac tissue regeneration. *Biomed Mater Eng* 2008; 18:309-14.

Shen H, Goldstein DR. IL-6 and TNF-alpha synergistically inhibit allograft acceptance. *J Am Soc Nephrol* 2009; 20:1032-40.

Sheridan WS, Duffy GP, Murphy BP. Optimum parameters for freeze-drying decellularized arterial scaffolds. *Tissue Eng Part C Methods* 2013; 19:981-90.

Shi C, Li Q, Zhao Y, *et al.* Stem-cell-capturing collagen scaffold promotes cardiac tissue regeneration. *Biomaterials* 2011; 32:2508-15.

Shimizu T, Yamato M, Isoi Y, *et al.* Fabrication of pulsatile cardiac tissue grafts using a novel 3-dimensional cell sheet manipulation technique and temperature-responsive cell culture surfaces. *Circ Res* 2002; 90:e40.

Shimizu T, Sekine H, Yang J, *et al.* Polysurgery of cell sheet grafts overcomes diffusion limits to produce thick, vascularized myocardial tissues. *FASEB J* 2006; 20:708-10.

Shin SR, Jung SM, Zalabany M, *et al.* Carbon-nanotube-embedded hydrogel sheets for engineering cardiac constructs and bioactuators. *ACS Nano* 2013; 7:2369-80.

Shintani S, Murohara T, Ikeda H, *et al.* Mobilization of endothelial progenitor cells in patients with acute myocardial infarction. *Circulation* 2001; 103:2776-9.

Shoichet MS. Polymer scaffolds for biomaterial applications. *Macromolecules* 2010;

43:581-91.

Shuqiang M, Kunzheng W, Xiaoqiang D, *et al.* Osteogenic growth peptide incorporated into PLGA scaffolds accelerates healing of segmental long bone defects in rabbits. *J Plast Reconstr Aesthet Surg* 2008; 61:1558-60.

Siepe M, Giraud MN, Pavlovic M, *et al.* Myoblast-seeded biodegradable scaffolds to prevent post-myocardial infarction evolution toward heart failure. *J Thorac Cardiovasc Surg* 2006; 132:124-31.

Siepe M, Giraud M, Liljensten E, *et al.* Construction of skeletal myoblast-based polyurethane scaffolds for myocardial repair. *Artif Organs* 2007; 31:425-33.

Silva GV, Litovsky S, Assad JA, *et al.* Mesenchymal stem cells differentiate into an endothelial phenotype, enhance vascular density, and improve heart function in a canine chronic ischemia model. *Circulation* 2005; 111:150-6.

Siminiak T, Kalawski R, Fiszer D, *et al.* Autologous skeletal myoblast transplantation for the treatment of postinfarction myocardial injury: phase I clinical study with 12 months of follow-up. *Am Heart J* 2004; 148:531-7.

Singelyn JM, DeQuach JA, Seif-Naraghi SB, *et al.* Naturally derived myocardial matrix as an injectable scaffold for cardiac tissue engineering. *Biomaterials* 2009; 30:5409-16.

Singelyn JM, Christman KL. Injectable materials for the treatment of myocardial infarction and heart failure: the promise of decellularized matrices. *J Cardiovasc Transl Res* 2010; 3:478-86.

Singelyn JM, Sundaramurthy P, Johnson TD, *et al.* Catheter-deliverable hydrogel derived from decellularized ventricular extracellular matrix increases endogenous cardiomyocytes and preserves cardiac function post-myocardial infarction. *J Am Coll Cardiol* 2012; 59:751-63.

Sinha S, Wamhoff BR, Hoofnagle MH, *et al.* Assessment of contractility of purified smooth muscle cells derived from embryonic stem cells. *Stem Cells* 2006; 24:1678-88.

Smart N, Risebro CA, Melville AA, *et al.* Thymosin beta-4 is essential for coronary vessel development and promotes neovascularization via adult epicardium. *Ann N Y Acad Sci* 2007; 1112:171-88.

Smith RR, Barile L, Cho HC, *et al.* Regenerative potential of cardiosphere-derived cells expanded from percutaneous endomyocardial biopsy specimens. *Circulation* 2007; 115:896-908.

Smolina K, Wright FL, Rayner M, *et al.* Determinants of the decline in mortality from acute myocardial infarction in England between 2002 and 2010: linked national database study. *BMJ* 2012; 344:d8059.

Soler-Botija C, Bagó JR, Llucà-Valldeperas A, *et al.* Engineered 3D bioimplants using elastomeric scaffold, self-assembling peptide hydrogel, and adipose tissue-derived progenitor cells for cardiac regeneration. *Am J Transl Res* 2014; 6:291-301.

Song JJ, Ott HC. Organ engineering based on decellularized matrix scaffolds. *Trends Mol Med* 2011; 17:424-32.

Sonnenberg SB, Rane AA, Liu CJ, *et al.* Delivery of an engineered HGF fragment in an extracellular matrix-derived hydrogel prevents negative LV remodeling post-myocardial infarction. *Biomaterials* 2015; 45:56-63.

Soonpaa MH, Field LJ. Assessment of cardiomyocyte DNA synthesis in normal and injured adult mouse hearts. *Am J Physiol* 1997; 272:H220-6.

Sotiropoulou PA, Perez SA, Gritzapis AD, *et al.* Interactions between human mesenchymal stem cells and natural killer cells. *Stem Cells* 2006; 24:74-85.

Souren JE, Schneijdenberg C, Verkleij AJ, *et al.* Factors controlling the rhythmic contraction of collagen gels by neonatal heart cells. *In Vitro Cell Dev Biol* 1992; 28A:199-204.

Später D, Hansson EM, Zangi L, *et al.* How to make a cardiomyocyte. *Development* 2014; 141:4418-31.

Spessotto P, Cervi M, Mucignat MT, *et al.* Beta 1 Integrin-dependent cell adhesion to EMILIN-1 is mediated by the gC1q domain. *J Biol Chem* 2003; 278:6160-7.

Srivastava D. Making or breaking the heart: from lineage determination to morphogenesis. *Cell* 2006; 126:1037-48.

Stannius HF. Zwei Reihen physiologischer Versuche. *Arch Anat Physiol Wiss Med* 1852; 85-100.

Steg PG, James SK, Atar D, *et al.* ESC Guidelines of the management of acute myocardial infarction in patients presenting with ST-segment elevation. *Eur Heart J* 2012; 33:2569-619.

Stewart DJ, Hilton JD, Arnold JM, *et al.* Angiogenic gene therapy in patients with nonrevascularizable ischemic heart disease: a phase 2 randomized, controlled trial of AdVEGF(121) (AdVEGF121) versus maximum medical treatment. *Gene Ther* 2006; 13:1503-11.

Stout DA, Basu B, Webster TJ. Poly(lactic-co-glycolic acid): carbon nanofiber composites for myocardial tissue engineering applications. *Acta Biomater* 2011; 7:3101-12.

Strem BM, Zhu M, Alfonso Z, *et al.* Expression of cardiomyocytic markers on adipose tissue-derived cells in a murine model of acute myocardial injury. *Cytotherapy* 2005; 7:282-91

Sultana N, Zhang L, Yan J, *et al.* Resident c-kit(+) cells in the heart are not cardiac stem cells. *Nat Commun* 2015; 6:8701.

Sun Q, Zhang Z, Sun Z. The potential and challenges of using stem cells for cardiovascular repair and regeneration. *Genes Dis* 2014; 1:113-9.

Swammerdam J. *Biblia naturae*. 1737.

Sylva M, van der Hoff MJ, Moorman AF. Development of the human heart. *Am J Med Genet A* 2014; 164A:1347-71.

**T**akahashi K, Yamanaka S. Induction of pluripotent stem cells from mouse embryonic and adult fibroblast cultures by defined factors. *Cell* 2006; 126:663-76.



Tallini YN, Greene KS, Craven M, *et al.* c-kit expression identifies cardiovascular precursors in the neonatal heart. *Proc Natl Acad Sci U S A* 2009; 106:1808-13.

Tamama K, Sen CK, Wells A. Differentiation of bone marrow mesenchymal stem cells into the smooth muscle lineage by blocking ERK/MAPK signaling pathway. *Stem Cells Dev* 2008; 17:897-908.

Tan G, Shim W, Gu Y, *et al.* Differential effect of myocardial matrix and integrins on cardiac differentiation of human mesenchymal stem cells. *Differentiation* 2010; 79:260-71.

Tang J, Wang J, Guo L, *et al.* Mesenchymal stem cells modified with stromal cell-derived factor 1 alpha improve cardiac remodeling via paracrine activation of hepatocyte growth factor in a rat model of myocardial infarction. *Mol Cells* 2010; 29:9-19.

Tang JM, Wang JN, Zhang L, *et al.* VEGF/SDF-1 promotes cardiac stem cell mobilization and myocardial repair in the infarcted heart. *Cardiovasc Res* 2011; 91:402-11.

Tang YL, Zhao Q, Qin X, *et al.* Paracrine action enhances the effects of autologous mesenchymal stem cell transplantation on vascular regeneration in rat model of myocardial infarction. *Ann Thorac Surg* 2005; 80:229-36.

Tipnis S, Viswanathan C, Majumdar AS. Immunosuppressive properties of human umbilical cord-derived mesenchymal stem cells: role of B7-H1 and IDO. *Immunol Cell Biol* 2010; 88:795-806.

Toma C, Pittenger MF, Cahill KS, *et al.* Human mesenchymal stem cells differentiate to a cardiomyocyte phenotype in the adult murine heart. *Circulation* 2002; 105:93-8.

Tomescot A, Leschik J, Bellamy V, *et al.* Differentiation in vivo of cardiac committed human embryonic stem cells in postmyocardial infarcted rats. *Stem Cells* 2007; 25:2200-5.

Tsuchiya N, Sato S, Kigami R, *et al.* Effect of a chitosan sponge impregnated with platelet-derived growth factor on bone augmentation beyond the skeletal envelope

in rat calvaria. *J Oral Sci* 2014; 56:23-8.

Tufvesson E, Westergren-Thorsson G. Biglycan and decorin induce morphological and cytoskeletal changes involving signalling by the small GTPases RhoA and Rac1 resulting in lung fibroblast migration. *J Cell Sci* 2003; 116:4857-64.

**U**niversity of Southern California, Keck School of Medicine. Glossary of terms. Available at: <http://www.cts.usc.edu/zglossary-stent.html>. Accessed May 02, 2017.

**V**aliente-Alandi I, Schafer AE, Blaxall BC. Extracellular matrix-mediated cellular communication in the heart. *J Mol Cell Cardiol* 2016; 91:228-37.

Valina C, Pinkernell K, Song YH, *et al.* Intracoronary administration of autologous adipose tissue-derived stem cells improves left ventricular function, perfusion, and remodelling after acute myocardial infarction. *Eur Heart J* 2007; 28:2667-77.

Van Berlo JH, Kanisicak O, Maillet M, *et al.* c-kit<sup>+</sup> cells minimally contribute cardiomyocytes to the heart. *Nature* 2014; 509:337-41.

Van de Werf F. New antithrombotic agents: are they needed and what can they offer to patients with a non-ST-elevation acute coronary syndrome? *Eur Heart J* 2009; 30:1695-702.

Van Dijk A, Niessen HW, Zandieh Doulabi B, *et al.* Differentiation of human adipose-derived stem cells towards cardiomyocytes is facilitated by laminin. *Cell Tissue Res* 2008; 334:457-67.

Van Leeuwenhoek A. *Arcana naturae detecta*. 1695; 1-568.

Vandenburgh HH, Karlisch P, Farr L. Maintenance of highly contractile tissue-cultured avian skeletal myotubes in collagen gel. *In Vitro Cell Dev Biol* 1988; 24:166-74.

Vecino E, Heller JP, Veiga-Crespo P, *et al.* Influence of extracellular matrix components on the expression of integrins and regeneration of adult retinal ganglion cells. *PLoS One* 2015; 10:e0125250.

Vera Janavel GL, De Lorenzi A, Cortés C, *et al.* Effect of vascular endothelial growth factor gene transfer on infarct size, left ventricular function and myocardial perfusion in sheep after 2 months of coronary artery occlusion. *J Gene Med* 2012; 14:279-87.

Vial C, Gutiérrez J, Santander C, *et al.* Decorin interacts with connective tissue growth factor (CTGF)/CCN2 by LRR12 inhibiting its biological activity. *J Biol Chem* 2011; 286:24242-52.

Vincent SD, Buckingham ME. How to make a heart: the origin and regulation of cardiac progenitor cells. *Curr Top Dev Biol* 2010; 90:1-41.

Vinci MC, Tessitore G, Castiglioni L, *et al.* Mechanical compliance and immunological compatibility of fixative-free decellularized/cryopreserved human pericardium. *PLoS One* 2013; 8:e64769.

Vittet D, Prandini MH, Berthier R, *et al.* Embryonic stem cells differentiate in vitro to endothelial cells through successive maturation steps. *Blood* 1996; 88:3424-31.

Vracko R, Thorning D, Frederickson RG. Fate of nerve fibers in necrotic, healing, and healed rat myocardium. *Lab Invest* 1990; 63:490-501.

Vunjak-Novakovic G, Tandon N, Godier A, *et al.* Challenges in cardiac tissue engineering. *Tissue Eng Part B Rev* 2010; 16:169-87.

Vunjak-Novakovic G, Lui KO, Tandon N, *et al.* Bioengineering heart muscle: a paradigm for regenerative medicine. *Annu Rev Biomed Eng* 2011; 13:245-67.

Vunjak-Novakovic G, Eschenhagen T, Mummery C. Myocardial tissue engineering: in vitro models. *Cold Spring Harb Perspect Med* 2014; 4:a014076.

**W**aksman R, Fournadjiev J, Baffour R, *et al.* Transepicardial autologous bone marrow-derived mononuclear cell therapy in a porcine model of chronically infarcted myocardium. *Cardiovasc Radiat Med* 2004; 5:125-31.

Wall ST, Yeh CC, Tu RY, *et al.* Biomimetic matrices for myocardial stabilization and stem cell transplantation. *J Biomed Mater Res A* 2010; 95:1055-66.

Walles T, Herden T, Haverich A, *et al.* Influence of scaffold thickness and scaffold composition on bioartificial graft survival. *Biomaterials* 2003; 24:1233-9.

Wang B, Borazjani A, Tahai M, *et al.* Fabrication of cardiac patch with decellularized porcine myocardial scaffold and bone marrow mononuclear cells. *J Biomed Mater Res A* 2010a; 94:1100-10.

Wang B, Tedder ME, Perez CE, *et al.* Structural and biomechanical characterizations of porcine myocardial extracellular matrix. *J Mater Sci Mater Med* 2012a, 23:1835-47.

Wang H, Zhang X, Li Y, *et al.* Improved myocardial performance in infarcted rat heart by co-injection of basic fibroblast growth factor with temperature-responsive chitosan hydrogel. *J Heart Lung Transplant* 2010b; 29:881-7.

Wang H, Shi J, Wang Y, *et al.* Promotion of cardiac differentiation of brown adipose derived stem cells by chitosan hydrogel for repair after myocardial infarction. *Biomaterials* 2014; 35:3986-98.

Wang H, Luo X, Leighton J. Extracellular matrix and integrins in embryonic stem cell differentiation. *Biochem Insights* 2015; 8:15-21.

Wang L, Shansky J, Borselli C, *et al.* Design and fabrication of a biodegradable, covalently crosslinked shape-memory alginate scaffold for cell and growth factor delivery. *Tissue Eng Part A* 2012b; 18:2000-7.

Wang T, Jiang XJ, Tang QZ, *et al.* Bone marrow stem cells implantation with alpha-cyclodextrin/MPEG-PCL-MPEG hydrogel improves cardiac function after myocardial infarction. *Acta Biomater* 2009a; 5:2939-44.

Wang T, Wu DQ, Jiang XJ, *et al.* Novel thermosensitive hydrogel injection inhibits post-infarct ventricle remodelling. *Eur J Heart Fail* 2009b; 11:14-9.

Wang Y, Ahmad N, Wani MA, *et al.* Hepatocyte growth factor prevents ventricular remodeling and dysfunction in mice via Akt pathway and angiogenesis. *J Mol Cell Cardiol* 2004; 37:1041-52.

Wassenaar JW, Gaetani R, Garcia JJ, *et al.* Evidence for mechanisms underlying the

functional benefits of a myocardial matrix hydrogel for post-MI treatment. *J Am Coll Cardiol* 2016; 67:1074-86.

Weaver WD, Cerqueira M, Hallstrom AP, *et al.* Prehospital-initiated vs hospital-initiated thrombolytic therapy: the Myocardial Infarction Triage and Intervention Trial. *JAMA* 1993; 270:1211-6.

Weber KT. Cardiac interstitium in health and disease: the fibrillar collagen network. *J Am Coll Cardiol* 1989; 13:1637-52.

Wegner MP, Bozec L, Horton MA, *et al.* Mechanical properties of collagen fibrils. *Biophys J* 2007; 93:1255-63.

Wei HJ, Chen CH, Lee WY, *et al.* Bioengineered cardiac patch constructed from multilayered mesenchymal stem cells for myocardial repair. *Biomaterials* 2008; 29:3547-56.

Weinberger F, Mehrkens D, Friedrich FW, *et al.* Localization of Islet-1-positive cells in the healthy and infarcted adult murine heart. *Circ Res* 2012; 110:1303-10.

Weinhaus AJ, Roberts KP. Anatomy of the human heart. In: Handbook of cardiac anatomy, physiology, and devices. 2nd Edition. Minneapolis, MN: *Springer Science*, 2009:59.

Wessels A, Pérez-Pomares JM. The epicardium and epicardially derived cells (EPDCs) as cardiac stem cells. *Anat Rec A Discov Mol Cell Evol Biol* 2004; 276:43-57.

Weymann A, Loganathan S, Takahashi H, *et al.* Development and evaluation of a perfusion decellularization porcine heart model--generation of 3-dimensional myocardial neoscaffolds. *Circ J* 2011; 75:852-60.

Wilson SH, Bell MR, Rihal CS, *et al.* Infarct artery reocclusion after primary angioplasty, stent placement, and thrombolytic therapy for acute myocardial infarction. *Am Heart J* 2001; 141:704-10.

Windecker S, Bax JJ, Myat A, *et al.* Future treatment strategies in ST-segment elevation myocardial infarction. *Lancet* 2013; 382:644-57.

Wollert KC, Meyer GP, Lotz J, *et al.* Intracoronary autologous bone-marrow cell

transfer after myocardial infarction: the BOOST randomised controlled clinical trial. *Lancet* 2004; 364:141-8.

World Health Organization. The top 10 causes of death. Fact sheet N\_310. 2016. Available at: <http://www.who.int/mediacentre/factsheets/fs310/en/>. Accessed December 20, 2016.

Wright MJ, Wightman LM, Lilley C, *et al.* In vivo myocardial gene transfer: optimization, evaluation and direct comparison of gene transfer vectors. *Basic Res Cardiol* 2001; 96:227-36.

**X**

in M, Olson EN, Bassel-Duby R. Mending broken hearts: cardiac development as a basis for adult heart regeneration and repair. *Nat Rev Mol Cell Biol* 2013; 14:529-41.

Xiong Q, Hill KL, Li Q, *et al.* A fibrin patch-based enhanced delivery of human embryonic stem cell-derived vascular cell transplantation in a porcine model of postinfarction left ventricular remodeling. *Stem Cells* 2011; 29:367-75.

Xiong Q, Ye L, Zhang P, *et al.* Functional consequences of human induced pluripotent stem cell therapy: myocardial atp turnover rate in the in vivo swine heart with postinfarction remodeling. *Circulation* 2013; 127:997-1008.

Xiong Y, Zeng YS, Zeng CG, *et al.* Synaptic transmission of neural stem cells seeded in 3-dimensional PLGA scaffolds. *Biomaterials* 2009; 30:3711-22.

Xu C, Police S, Rao N, *et al.* Characterization and enrichment of cardiomyocytes derived from human embryonic stem cells. *Circ Res* 2002; 91(6):501-8.

Xu D, Nishimura T, Zheng M, *et al.* Enabling autologous human liver regeneration with differentiated adipocyte stem cells. *Cell Transplant* 2014; 23:1573-84.

Xu FJ, Wang ZH, Yang WT. Surface functionalization of polycaprolactone films via surface-initiated atom transfer radical polymerization for covalently coupling cell-adhesive biomolecules. *Biomaterials* 2010; 31:3139-47.

Xu W, Zhang X, Qian H, *et al.* Mesenchymal stem cells from adult human bone marrow

differentiate into a cardiomyocyte phenotype in vitro. *Exp Biol Med (Maywood)* 2004; 229:623-31.

**Y**amauchi H, Desgranges P, Lecerf L, *et al.* New agents for the treatment of infarcted myocardium. *FASEB J* 2000; 14:2133-4.

Yan Z, Zhuansun Y, Chen R, *et al.* Immunomodulation of mesenchymal stromal cells on regulatory T cells and its possible mechanism. *Exp Cell Res* 2014; 324:65-74.

Yang J, Shi G, Bei J, *et al.* Fabrication and surface modification of macroporous poly(L-lactic acid) and poly(L-lactic-co-glycolic acid) (70/30) cell scaffolds for human skin fibroblast cell culture. *J Biomed Mater Res* 2002; 62:438-46.

Yang M, Chen CZ, Shu YS, *et al.*, Preseeding of human vascular cells in decellularized bovine pericardium scaffold for tissue-engineered heart valve: an in vitro and in vivo feasibility study. *J Biomed Mater Res B Appl Biomater* 2012; 100:1654-61.

Yang ZJ, Chen B, Sheng Z, *et al.* Improvement of heart function in postinfarct heart failure swine models after hepatocyte growth factor gene transfer: comparison of low-, medium- and high-dose groups. *Mol Biol Rep* 2010; 37:2075-81.

Yañez R, Lamana ML, García-Castro J, *et al.* Adipose tissue-derived mesenchymal stem cells have in vivo immunosuppressive properties applicable for the control of the graft-versus-host disease. *Stem Cells* 2006; 24:2582-91.

Yao K, Huang R, Qian J, *et al.* Administration of intracoronary bone marrow mononuclear cells on chronic myocardial infarction improves diastolic function. *Heart* 2008; 94:1147-53.

Ye L, Chang YH, Xiong Q, *et al.* Cardiac repair in a porcine model of acute myocardial infarction with human induced pluripotent stem cell-derived cardiovascular cell population. *Cell Stem Cell* 2014; 15:750-61.

Ye Q, Zünd G, Benedikt P, *et al.* Fibrin gel as a three dimensional matrix in cardiovascular tissue engineering. *Eur J Cardiothorac Surg* 2000; 17:587-91.

Yeh YT, Hur SS, Chang J, *et al.* Matrix stiffness regulates endothelial cell proliferation

through septin 9. *PLoS One* 2012; 7:e46889.

Yeong WY, Sudarmadji N, Yu HY, *et al.* Porous polycaprolactone scaffold for cardiac tissue engineering fabricated by selective laser sintering. *Acta Biomater* 2010; 6:2028-34.

Yeung T, Georges PC, Flanagan LA, *et al.* Effects of substrate stiffness on cell morphology, cytoskeletal structure, and adhesion. *Cell Motil Cytoskeleton* 2005; 60:24-34.

Yoon SJ, Fang YH, Lim CH, *et al.* Regeneration of ischemic heart using hyaluronic acid-based injectable hydrogel. *J Biomed Mater Res B Appl Biomater* 2009; 91:163-71.

Yoon SJ, Hong S, Fang YH, *et al.* Differential regeneration of myocardial infarction depending on the progression of disease and the composition of biomimetic hydrogel. *J Biosci Bioeng* 2014; 118:461-8.

**Z**achary I, Morgan RD. Therapeutic angiogenesis for cardiovascular disease: biological context, challenges, prospects. *Heart* 2011; 97:181-9.

Zaruba MM, Soonpaa M, Reuter S, *et al.* Cardiomyogenic potential of C-kit(+) expressing cells derived from neonatal and adult mouse hearts. *Circulation* 2010; 121:1992-2000.

Zhang G, Nakamura Y, Wang X, *et al.* Controlled release of stromal cell-derived factor-1 alpha in situ increases c-kit + cell homing to the infarcted heart. *Tissue Eng* 2007; 13:2063-71.

Zhang J, Wilson GF, Soerens AG, *et al.* Functional cardiomyocytes derived from human induced pluripotent stem cells. *Circ Res* 2009a; 104:e30-41.

Zhang S, Sun A, Ma H, *et al.* Infarcted myocardium-like stiffness contributes to endothelial progenitor lineage commitment of bone marrow mononuclear cells. *J Cell Mol Med* 2011; 15:2245-61.

Zhang Y, He Y, Bharadwaj S, *et al.* Tissue-specific extracellular matrix coatings for the promotion of cell proliferation and maintenance of cell phenotypes. *Biomaterials*



2009b; 30:4021-8.

Zhou B, Ma Q, Rajagopal S, *et al.* Epicardial progenitors contribute to the cardiomyocyte lineage in the developing heart. *Nature* 2008; 454:109-13.

Zhou J, Chen J, Sun H, *et al.* Engineering the heart: evaluation of conductive nanomaterials for improving implant integration and cardiac function. *Sci Rep* 2014; 4:3733.

Zhou S, Chen LS, Miyauchi Y, *et al.* Mechanisms of cardiac nerve sprouting after myocardial infarction in dogs. *Circ Res* 2004; 95:76-83.

Zimmermann WH, Fink C, Kralisch D, *et al.* Three-dimensional engineered heart tissue from neonatal rat cardiac myocytes. *Biotechnol Bioeng* 2000; 68:106-14.

Zimmermann WH, Didié M, Wasmeier GH, *et al.* Cardiac grafting of engineered heart tissue in syngenic rats. *Circulation* 2002a; 106:1151-7.

Zimmermann WH, Schneiderbanger K, Schubert P, *et al.* Tissue engineering of a differentiated cardiac muscle construct. *Circ Res* 2002b; 90:223-30.

Zimmermann WH, Melnychenko I, Wasmeier G, *et al.* Engineered heart tissue grafts improve systolic and diastolic function in infarcted rat hearts. *Nat Med* 2006; 12:452-8.





